

Artificial Intelligence for Smart Energy Storage Applications

Lead Guest Editor: Nagamalai Vasimalai

Guest Editors: B Madhavan and Mohamad Hafiz Mamat





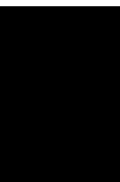
Artificial Intelligence for Smart Energy Storage Applications

International Transactions on Electrical Energy Systems

Artificial Intelligence for Smart Energy Storage Applications

Lead Guest Editor: Nagamalai Vasimalai

Guest Editors: B Madhavan and Mohamad Hafiz
Mamat



Copyright © 2023 Hindawi Limited. All rights reserved.

This is a special issue published in “International Transactions on Electrical Energy Systems.” All articles are open access articles distributed under the Creative Commons Attribution License, which permits unrestricted use, distribution, and reproduction in any medium, provided the original work is properly cited.

Associate Editors

Chitti Babu Baladhandautham , India
Antonio Bracale , Italy
Tomislav Capuder , Croatia
Chia Chi Chu , Taiwan
Gilsoo Jang , Republic of Korea
Dusmanta K. Mohanta , India
Daniela Proto, Italy
Ahmet Mete Vural , Turkey

Academic Editors

JAGABAR SATHIK M MOHAMED ALI,
India
Sobhy M. Abdelkader, United Kingdom
Johny Renoald Albert , India
Rodolfo Araneo, Italy
Enrique Rosales Asensio, Spain
Faroque Azam, India
Hamed Badihi , Finland
Ajay Kumar Bansal , India
Ajay Kumar Bansal, India
Ramesh Chand Bansal , Australia
Yukun Bao , China
Prasenjit Basak , India
Dr. CH Hussaian Basha, India
Youcef Belkhier, France
Jaouher Ben Ali, Tunisia
Sujin Bureerat , Thailand
Dhanamjayulu C , India
Murthy Cherukuri , India
Paulo Costa , Portugal
Michele De Santis , Italy
Mouloud Azzedine Denai , United Kingdom
Harsh Dhiman , India
Sheng Du , China
Youssef Errami , Morocco
Davide Falabretti , Italy
Salvatore Favuzza , Italy
Aymen Flah , Tunisia
Ci-Wei Gao , China
Samuele Grillo , Italy

Yueshi Guan, China
Zhitao Guan, China
Nitin K. Gupta , India
Reza Jalilzadeh Hamidi, USA
Santoshkumar Hampannavar , India
Tianqi Hong , USA
Wei-tzer Huang , Taiwan
Kyeon Hur, Republic of Korea
Kamran Iqbal , USA
Hamed Jafari Kaleybar, Italy
Jyotheeswara Reddy Kalvakurthi, India
Kangli Liu, China
Shaofeng Lu , China
Ibrahim Mahariq, Kuwait
Anjaneer Kumar Mishra , India
Manohar Mishra, India
Adel Oubelaid, Algeria
Dr. Narendra Babu P , India
Gayadhar Panda, India
Dr. N. Prabakaran , India
Santi A. Rizzo, Italy
Julio Rosas-Caro , Mexico
Mohammad Sadi , USA
Akshay Kumar Saha , South Africa
Lalit Chandra Saikia , India
Irfan Sami, Republic of Korea
Subrata kumar Sarker, Bangladesh
Gulshan Sharma , South Africa
Pawan Sharma, Norway
Yiming Shen , China
Dr. Arvind R. Singh , South Africa
Sudhakar babu T , India
Shafaat Ullah, Pakistan
Jesus Valdez-Resendiz , Mexico
Kusum Verma , India
Yu-Chi Wu , Taiwan
Rui Yao, China

Contents

Retracted: Application of Improved Deep Learning Method in Intelligent Power System

International Transactions on Electrical Energy Systems

Retraction (1 page), Article ID 9890682, Volume 2023 (2023)

Retracted: Optimization Technique for Renewable Energy Storage Systems for Power Quality Analysis with Connected Grid

International Transactions on Electrical Energy Systems

Retraction (1 page), Article ID 9859245, Volume 2023 (2023)

Retracted: Power Tracking and Energy Balancing of Energy Storage Systems under Unreliable Communication Network

International Transactions on Electrical Energy Systems

Retraction (1 page), Article ID 9847986, Volume 2023 (2023)

Retracted: The Construction of Smart Chinese Medicine Cloud Health Platform Based on Deep Neural Networks

International Transactions on Electrical Energy Systems

Retraction (1 page), Article ID 9847928, Volume 2023 (2023)

Retracted: Informatization of Accounting System of Electric Power Enterprises Based on Sensor Monitoring and Cloud Computing

International Transactions on Electrical Energy Systems

Retraction (1 page), Article ID 9842047, Volume 2023 (2023)

Retracted: Analysis of Dynamic Relationship between Energy Consumption and Economic Growth Based on PVAR Model

International Transactions on Electrical Energy Systems

Retraction (1 page), Article ID 9842036, Volume 2023 (2023)

Retracted: Teaching Practice of Engineering Management Course for Engineering Education Certification under Background of Artificial Intelligence

International Transactions on Electrical Energy Systems

Retraction (1 page), Article ID 9835801, Volume 2023 (2023)

Retracted: Optical Fiber Multiparameter Detection and Numerical Simulation and Characteristics of Water Quality Particulate Matter Based on Single-Photon Detection Technology

International Transactions on Electrical Energy Systems

Retraction (1 page), Article ID 9828746, Volume 2023 (2023)

Retracted: Influence of Educational Informatization Based on Machine Learning on Teaching Mode

International Transactions on Electrical Energy Systems

Retraction (1 page), Article ID 9827548, Volume 2023 (2023)

Retracted: Evaluation Method of Street Green Landscape Viewing Degree Based on Machine Learning

International Transactions on Electrical Energy Systems

Retraction (1 page), Article ID 9823196, Volume 2023 (2023)

Retracted: Hazard Trend Identification Model Based on Statistical Analysis of Abnormal Power Generation Behavior Data

International Transactions on Electrical Energy Systems
Retraction (1 page), Article ID 9812690, Volume 2023 (2023)

Retracted: Assessing the Feasibility of Cogeneration Retrofit for Heating and Electricity Demands in Marine Diesel Engines

International Transactions on Electrical Energy Systems
Retraction (1 page), Article ID 9792481, Volume 2023 (2023)

Retracted: Short-Term Load Monitoring of a Power System Based on Neural Network

International Transactions on Electrical Energy Systems
Retraction (1 page), Article ID 9790319, Volume 2023 (2023)

Retracted: Simulation of Flow-Induced Vibration and Dynamic Performance of Circular-Arc Helical Gear Pump under Background of Machine Learning

International Transactions on Electrical Energy Systems
Retraction (1 page), Article ID 9789630, Volume 2023 (2023)

Retracted: Surface Feature Prediction Modeling and Parameter Optimization for Turning TC17 Titanium Alloy

International Transactions on Electrical Energy Systems
Retraction (1 page), Article ID 9785765, Volume 2023 (2023)

Retracted: The Optimal Integration of Computer Information Technology and Energy Economic Management

International Transactions on Electrical Energy Systems
Retraction (1 page), Article ID 9785724, Volume 2023 (2023)

Retracted: Psychological Motivation of Athletes' Physical Training Based on Deep Learning Model

International Transactions on Electrical Energy Systems
Retraction (1 page), Article ID 9782507, Volume 2023 (2023)

Retracted: Evaluation of the Fluctuation Mechanism of Behavioral Financial Market Based on Edge Computing

International Transactions on Electrical Energy Systems
Retraction (1 page), Article ID 9768256, Volume 2023 (2023)

Retracted: Power Grid Intelligent Energy Dispatching Interactive System Based on Virtual Reality Technology

International Transactions on Electrical Energy Systems
Retraction (1 page), Article ID 9846942, Volume 2023 (2023)

Contents

Retracted: Mathematical Modeling Method of the Improved Genetic Algorithm for Random Power Fluctuation

International Transactions on Electrical Energy Systems
Retraction (1 page), Article ID 9898450, Volume 2023 (2023)

Retracted: Precise Positioning of Redundant Robot Motion Energy-Saving Control Based on Sensing Technology

International Transactions on Electrical Energy Systems
Retraction (1 page), Article ID 9871594, Volume 2023 (2023)

Retracted: Energy Conservation Optimization and Numerical Simulation of Urban Green Space Landscape Pattern

International Transactions on Electrical Energy Systems
Retraction (1 page), Article ID 9850849, Volume 2023 (2023)

Retracted: Modeling and Optimization of Ship Waste Heat Utilization System Based on Genetic Algorithm and Sensing

International Transactions on Electrical Energy Systems
Retraction (1 page), Article ID 9841824, Volume 2023 (2023)

Retracted: Simulation of Multisensor Energy Data Fusion Transformer Acquisition System Based on FPGA

International Transactions on Electrical Energy Systems
Retraction (1 page), Article ID 9819174, Volume 2023 (2023)

Retracted: Data Mining Algorithm for Power User Network Based on Multi-Information Fusion

International Transactions on Electrical Energy Systems
Retraction (1 page), Article ID 9760814, Volume 2023 (2023)

Retracted: Application of Computer Vision and Sensor Technology in Multivariate Assessment of Ecological Environment Carrying Capacity

International Transactions on Electrical Energy Systems
Retraction (1 page), Article ID 9891307, Volume 2023 (2023)

Retracted: State Diagnosis and Monitoring Method of Robot Electric Power Equipment Based on Data Mining

International Transactions on Electrical Energy Systems
Retraction (1 page), Article ID 9873104, Volume 2023 (2023)

Retracted: Application of Laser Scanning Technology in Digital Method

International Transactions on Electrical Energy Systems
Retraction (1 page), Article ID 9863826, Volume 2023 (2023)

Retracted: A Fault-Tolerant Structure for Nano-Power Communication Based on the Multidimensional Crossbar Switch Network

International Transactions on Electrical Energy Systems
Retraction (1 page), Article ID 9850432, Volume 2023 (2023)

Retracted: Electricity Network Security Monitoring Based on Bee Colony Algorithm

International Transactions on Electrical Energy Systems
Retraction (1 page), Article ID 9841936, Volume 2023 (2023)

Retracted: Optimal Pricing Model of Environmental Quality Index Futures from the Perspective of Green Finance

International Transactions on Electrical Energy Systems
Retraction (1 page), Article ID 9832594, Volume 2023 (2023)

Retracted: Wireless Mobile Power Communication System Based on Artificial Intelligence Algorithm

International Transactions on Electrical Energy Systems
Retraction (1 page), Article ID 9826972, Volume 2023 (2023)

Retracted: Application of Data Mining Algorithm in Electric Power Marketing Inspection Forecast Analysis

International Transactions on Electrical Energy Systems
Retraction (1 page), Article ID 9816417, Volume 2023 (2023)

Retracted: Application of Internet of Things Technology in Optimization of Electronic Assembly Process Parameters

International Transactions on Electrical Energy Systems
Retraction (1 page), Article ID 9809618, Volume 2023 (2023)

Retracted: Define Electronic Enterprise Financial Management Information Decision-Making Process Based on IoT and the ERP Model

International Transactions on Electrical Energy Systems
Retraction (1 page), Article ID 9806569, Volume 2023 (2023)

Retracted: Application of the Lagrange Equation for Intelligent Sensor Vibration Control for Power Network Monitoring

International Transactions on Electrical Energy Systems
Retraction (1 page), Article ID 9804134, Volume 2023 (2023)

Retracted: Seismic Performance and Vibration Control of Rapid Construction Environmental Protection Wall Based on Artificial Intelligence

International Transactions on Electrical Energy Systems
Retraction (1 page), Article ID 9796018, Volume 2023 (2023)

Retracted: Reconstruction and Utilization of Energy Economy Information Resources against Humanistic Background

International Transactions on Electrical Energy Systems
Retraction (1 page), Article ID 9790764, Volume 2023 (2023)

Contents

Retracted: Improved VMD-+ACO Algorithm Navigation and Positioning Technology for Robot Electric Power Inspection

International Transactions on Electrical Energy Systems
Retraction (1 page), Article ID 9787820, Volume 2023 (2023)

Retracted: Application of Big Data Technology in Environmental Pollution Control in Energy Ecological Economic Zone

International Transactions on Electrical Energy Systems
Retraction (1 page), Article ID 9784587, Volume 2023 (2023)

Retracted: Realization of Single-Phase Grounding Fault Location and Recovery Technology in Distribution Network

International Transactions on Electrical Energy Systems
Retraction (1 page), Article ID 9783795, Volume 2023 (2023)

Retracted: On-Load Electromagnetic Compatibility Test and Simulation Closed-Loop of the Electric Drive System of New Energy Vehicles

International Transactions on Electrical Energy Systems
Retraction (1 page), Article ID 9768042, Volume 2023 (2023)

Retracted: High Efficiency Compound Vacuum Oil Gas Separation Technology Based on Integrated Oil Filter of Ultra-High Voltage Transformer

International Transactions on Electrical Energy Systems
Retraction (1 page), Article ID 9764245, Volume 2023 (2023)


Retracted: Application of Big Data and Internet of Things Technology in the Management of Financial Operating Income of Electric Power Enterprises

International Transactions on Electrical Energy Systems
Retraction (1 page), Article ID 9762856, Volume 2023 (2023)


Retracted: Innovation and Entrepreneurship Coupling Based on Simultaneous Equation Model and Its Energy Economic Effect Measurement

International Transactions on Electrical Energy Systems
Retraction (1 page), Article ID 9756231, Volume 2023 (2023)


[Retracted] Assessing the Feasibility of Cogeneration Retrofit for Heating and Electricity Demands in Marine Diesel Engines

Xianglong Liu , Hao Yang, Zhao Feng, Guang Hu, and Zhi Zeng
Research Article (10 pages), Article ID 3280579, Volume 2023 (2023)

[Retracted] Optimization Technique for Renewable Energy Storage Systems for Power Quality Analysis with Connected Grid

R. Senthil Kumar, B. V. S. Acharyulu, P. K. Dhal, Richa Adlakha, Sonu Kumar, C. Saravanan, and Krishna Bikram Shah 
Research Article (7 pages), Article ID 4675421, Volume 2023 (2023)

[Retracted] Short-Term Load Monitoring of a Power System Based on Neural Network

Di Yang 

Research Article (10 pages), Article ID 4581408, Volume 2023 (2023)

[Retracted] Application of Improved Deep Learning Method in Intelligent Power System

Huijie Liu , Yang Liu , and ChengWen Xu 


Research Article (6 pages), Article ID 6788668, Volume 2022 (2022)

[Retracted] Influence of Educational Informatization Based on Machine Learning on Teaching Mode

Lei Ma  and Jian Li


Research Article (7 pages), Article ID 6180113, Volume 2022 (2022)

[Retracted] Evaluation of the Fluctuation Mechanism of Behavioral Financial Market Based on Edge Computing

Xiaoliang Yuan 

Research Article (8 pages), Article ID 2751197, Volume 2022 (2022)

[Retracted] Optical Fiber Multiparameter Detection and Numerical Simulation and Characteristics of Water Quality Particulate Matter Based on Single-Photon Detection Technology

Quan Xu , Cuiyun Gao, and Chun Zhou


Research Article (10 pages), Article ID 3170082, Volume 2022 (2022)

[Retracted] The Optimal Integration of Computer Information Technology and Energy Economic Management

Ning Zhang  and Zengxin Li 


Research Article (7 pages), Article ID 9067413, Volume 2022 (2022)

[Retracted] Analysis of Dynamic Relationship between Energy Consumption and Economic Growth Based on PVAR Model

Junyan Han 


Research Article (7 pages), Article ID 3945522, Volume 2022 (2022)

[Retracted] Teaching Practice of Engineering Management Course for Engineering Education Certification under Background of Artificial Intelligence

Dan Wang , Fengyi Han, Qi Zhao, and Yinyin Lv

Research Article (12 pages), Article ID 3106491, Volume 2022 (2022)


[Retracted] Surface Feature Prediction Modeling and Parameter Optimization for Turning TC17 Titanium Alloy

Zhibo Deng, Zhe Wang, and Xuehong Shen 

Research Article (12 pages), Article ID 2979858, Volume 2022 (2022)

Contents

[Retracted] Innovation and Entrepreneurship Coupling Based on Simultaneous Equation Model and Its Energy Economic Effect Measurement

Wei Chen 

Research Article (8 pages), Article ID 8218645, Volume 2022 (2022)

[Retracted] Simulation of Flow-Induced Vibration and Dynamic Performance of Circular-Arc Helical Gear Pump under Background of Machine Learning

Xiaoling Wei, Yongbao Feng , Xiaoxia Han, and Zhenxin He


Research Article (10 pages), Article ID 9513357, Volume 2022 (2022)

[Retracted] The Construction of Smart Chinese Medicine Cloud Health Platform Based on Deep Neural Networks

Yaofeng Miao  and Yuan Zhou


Research Article (10 pages), Article ID 6751915, Volume 2022 (2022)

[Retracted] Psychological Motivation of Athletes' Physical Training Based on Deep Learning Model

Yining Yang 


Research Article (11 pages), Article ID 1962461, Volume 2022 (2022)

[Retracted] Evaluation Method of Street Green Landscape Viewing Degree Based on Machine Learning

Tieming Wang, Mengyu Liu , and Wenhua Huang


Research Article (9 pages), Article ID 2729408, Volume 2022 (2022)

[Retracted] Informatization of Accounting System of Electric Power Enterprises Based on Sensor Monitoring and Cloud Computing

Xiaohua Tie 


Research Article (7 pages), Article ID 3506989, Volume 2022 (2022)

[Retracted] Application of the Lagrange Equation for Intelligent Sensor Vibration Control for Power Network Monitoring

Xiaojing Cheng 

Research Article (9 pages), Article ID 4616889, Volume 2022 (2022)

[Retracted] Seismic Performance and Vibration Control of Rapid Construction Environmental Protection Wall Based on Artificial Intelligence

Jie Fu , Shuangxi Zhou, Li Liu, and Mingxing Liu


Research Article (8 pages), Article ID 1385774, Volume 2022 (2022)

[Retracted] Wireless Mobile Power Communication System Based on Artificial Intelligence Algorithm

Juan Du  and Mingqi Guo 


Research Article (7 pages), Article ID 1636033, Volume 2022 (2022)

[Retracted] Application of Big Data and Internet of Things Technology in the Management of Financial Operating Income of Electric Power Enterprises

Huiling Su 


Research Article (8 pages), Article ID 6167479, Volume 2022 (2022)

[Retracted] Define Electronic Enterprise Financial Management Information Decision-Making Process Based on IoT and the ERP Model

Huiling Su 

Research Article (8 pages), Article ID 1191031, Volume 2022 (2022)

[Retracted] Application of Laser Scanning Technology in Digital Method

Fangfang Liu 






Research Article (11 pages), Article ID 2629688, Volume 2022 (2022)

[Retracted] Power Grid Intelligent Energy Dispatching Interactive System Based on Virtual Reality Technology

Wenjian Hu , Yang Yang , Baoan Liu , Siyan Guo , and Kuizhong Zhang 

Research Article (8 pages), Article ID 8008461, Volume 2022 (2022)

[Retracted] Improved VMD-+ACO Algorithm Navigation and Positioning Technology for Robot Electric Power Inspection

Yingkai Long , Mingming Du , Xiaoxiao Luo , Siquan Li , and Xiping Jiang 



Research Article (6 pages), Article ID 5467622, Volume 2022 (2022)

[Retracted] Power Tracking and Energy Balancing of Energy Storage Systems under Unreliable Communication Network

He Cai , Yaqi He , and Huanli Gao 





Research Article (9 pages), Article ID 6550925, Volume 2022 (2022)

[Retracted] Electricity Network Security Monitoring Based on Bee Colony Algorithm

Wenzhi Su  and Baolong Zhang 




Research Article (8 pages), Article ID 4533154, Volume 2022 (2022)

[Retracted] High Efficiency Compound Vacuum Oil Gas Separation Technology Based on Integrated Oil Filter of Ultra-High Voltage Transformer

Jin Guan , Xuechao Hu , Huan Liu , and Yaoguo Yang 

Research Article (6 pages), Article ID 9989686, Volume 2022 (2022)







[Retracted] On-Load Electromagnetic Compatibility Test and Simulation Closed-Loop of the Electric Drive System of New Energy Vehicles

Xinwen Luo , Weize Liu , and Jingpu Li 

Research Article (6 pages), Article ID 9256401, Volume 2022 (2022)

Contents

[Retracted] Realization of Single-Phase Grounding Fault Location and Recovery Technology in Distribution Network

Di Zhang , Haiguo Tang , Jiran Zhu , Hengyi Zhou , Zhidan Zhang , and Xingrong Song 
Research Article (10 pages), Article ID 6282843, Volume 2022 (2022)

[Retracted] Data Mining Algorithm for Power User Network Based on Multi-Information Fusion
Shutong Huang 

Research Article (6 pages), Article ID 2337460, Volume 2022 (2022)

[Retracted] Hazard Trend Identification Model Based on Statistical Analysis of Abnormal Power Generation Behavior Data

Gaojun Xu , Xusheng Qian , Xiaodong Li , and Weijiang Wu 
Research Article (7 pages), Article ID 5463109, Volume 2022 (2022)

[Retracted] Application of Computer Vision and Sensor Technology in Multivariate Assessment of Ecological Environment Carrying Capacity

Zhiguo Wang  and Wei Wang 
Research Article (8 pages), Article ID 5087610, Volume 2022 (2022)

[Retracted] Application of Big Data Technology in Environmental Pollution Control in Energy Ecological Economic Zone

Xinxue Jin  and Xinxin Jin 
Research Article (7 pages), Article ID 1569905, Volume 2022 (2022)

[Retracted] Modeling and Optimization of Ship Waste Heat Utilization System Based on Genetic Algorithm and Sensing

Long Lyu 
Research Article (8 pages), Article ID 9917212, Volume 2022 (2022)





[Retracted] State Diagnosis and Monitoring Method of Robot Electric Power Equipment Based on Data Mining

Haifeng Guo , Zhaojun Meng , Huimin Yu , Rui Chen , Ling Li , and Li Cheng 
Research Article (7 pages), Article ID 4272364, Volume 2022 (2022)


[Retracted] Application of Internet of Things Technology in Optimization of Electronic Assembly Process Parameters

Xianghui Song 
Research Article (7 pages), Article ID 2375521, Volume 2022 (2022)

[Retracted] Application of Data Mining Algorithm in Electric Power Marketing Inspection Forecast Analysis


Weijiang Wu , Gaojun Xu , Xusheng Qian , and Chengbo Chu 
Research Article (7 pages), Article ID 9229415, Volume 2022 (2022)

[Retracted] Optimal Pricing Model of Environmental Quality Index Futures from the Perspective of Green Finance

Junwen Che , Shenghe Zhou , Rui Shan , Hui Jia , and Zheng Liu 


Research Article (8 pages), Article ID 6951040, Volume 2022 (2022)

[Retracted] Mathematical Modeling Method of the Improved Genetic Algorithm for Random Power Fluctuation

Fu Zhu 

Research Article (7 pages), Article ID 1889952, Volume 2022 (2022)

[Retracted] Precise Positioning of Redundant Robot Motion Energy-Saving Control Based on Sensing Technology

Yaping Lu 


Research Article (8 pages), Article ID 6367598, Volume 2022 (2022)

[Retracted] Reconstruction and Utilization of Energy Economy Information Resources against Humanistic Background

Lan Du 



Research Article (7 pages), Article ID 2301322, Volume 2022 (2022)

[Retracted] Energy Conservation Optimization and Numerical Simulation of Urban Green Space Landscape Pattern

Lan Wang 

Research Article (7 pages), Article ID 5324854, Volume 2022 (2022)

[Retracted] A Fault-Tolerant Structure for Nano-Power Communication Based on the Multidimensional Crossbar Switch Network

Jun Luo  and Boxun Liao 

Research Article (8 pages), Article ID 4783847, Volume 2022 (2022)

[Retracted] Simulation of Multisensor Energy Data Fusion Transformer Acquisition System Based on FPGA

Lan Luan  and Dan Hu 

Research Article (7 pages), Article ID 7612674, Volume 2022 (2022)

Retraction

Retracted: Application of Improved Deep Learning Method in Intelligent Power System

International Transactions on Electrical Energy Systems

Received 28 November 2023; Accepted 28 November 2023; Published 29 November 2023

Copyright © 2023 International Transactions on Electrical Energy Systems. This is an open access article distributed under the Creative Commons Attribution License, which permits unrestricted use, distribution, and reproduction in any medium, provided the original work is properly cited.

This article has been retracted by Hindawi, as publisher, following an investigation undertaken by the publisher [1]. This investigation has uncovered evidence of systematic manipulation of the publication and peer-review process. We cannot, therefore, vouch for the reliability or integrity of this article.

Please note that this notice is intended solely to alert readers that the peer-review process of this article has been compromised.

Wiley and Hindawi regret that the usual quality checks did not identify these issues before publication and have since put additional measures in place to safeguard research integrity.

We wish to credit our Research Integrity and Research Publishing teams and anonymous and named external researchers and research integrity experts for contributing to this investigation.

The corresponding author, as the representative of all authors, has been given the opportunity to register their agreement or disagreement to this retraction. We have kept a record of any response received.

References

- [1] H. Liu, Y. Liu, and C. Xu, "Application of Improved Deep Learning Method in Intelligent Power System," *International Transactions on Electrical Energy Systems*, vol. 2022, Article ID 6788668, 6 pages, 2022.

Retraction

Retracted: Optimization Technique for Renewable Energy Storage Systems for Power Quality Analysis with Connected Grid

International Transactions on Electrical Energy Systems

Received 28 November 2023; Accepted 28 November 2023; Published 29 November 2023

Copyright © 2023 International Transactions on Electrical Energy Systems. This is an open access article distributed under the Creative Commons Attribution License, which permits unrestricted use, distribution, and reproduction in any medium, provided the original work is properly cited.

This article has been retracted by Hindawi, as publisher, following an investigation undertaken by the publisher [1]. This investigation has uncovered evidence of systematic manipulation of the publication and peer-review process. We cannot, therefore, vouch for the reliability or integrity of this article.

Please note that this notice is intended solely to alert readers that the peer-review process of this article has been compromised.

Wiley and Hindawi regret that the usual quality checks did not identify these issues before publication and have since put additional measures in place to safeguard research integrity.

We wish to credit our Research Integrity and Research Publishing teams and anonymous and named external researchers and research integrity experts for contributing to this investigation.

The corresponding author, as the representative of all authors, has been given the opportunity to register their agreement or disagreement to this retraction. We have kept a record of any response received.

References

- [1] R. Senthil Kumar, B. V. S. Acharyulu, P. K. Dhal et al., "Optimization Technique for Renewable Energy Storage Systems for Power Quality Analysis with Connected Grid," *International Transactions on Electrical Energy Systems*, vol. 2023, Article ID 4675421, 7 pages, 2023.

Retraction

Retracted: Power Tracking and Energy Balancing of Energy Storage Systems under Unreliable Communication Network

International Transactions on Electrical Energy Systems

Received 28 November 2023; Accepted 28 November 2023; Published 29 November 2023

Copyright © 2023 International Transactions on Electrical Energy Systems. This is an open access article distributed under the Creative Commons Attribution License, which permits unrestricted use, distribution, and reproduction in any medium, provided the original work is properly cited.

This article has been retracted by Hindawi, as publisher, following an investigation undertaken by the publisher [1]. This investigation has uncovered evidence of systematic manipulation of the publication and peer-review process. We cannot, therefore, vouch for the reliability or integrity of this article.

Please note that this notice is intended solely to alert readers that the peer-review process of this article has been compromised.

Wiley and Hindawi regret that the usual quality checks did not identify these issues before publication and have since put additional measures in place to safeguard research integrity.

We wish to credit our Research Integrity and Research Publishing teams and anonymous and named external researchers and research integrity experts for contributing to this investigation.

The corresponding author, as the representative of all authors, has been given the opportunity to register their agreement or disagreement to this retraction. We have kept a record of any response received.

References

- [1] H. Cai, Y. He, and H. Gao, "Power Tracking and Energy Balancing of Energy Storage Systems under Unreliable Communication Network," *International Transactions on Electrical Energy Systems*, vol. 2022, Article ID 6550925, 9 pages, 2022.

Retraction

Retracted: The Construction of Smart Chinese Medicine Cloud Health Platform Based on Deep Neural Networks

International Transactions on Electrical Energy Systems

Received 28 November 2023; Accepted 28 November 2023; Published 29 November 2023

Copyright © 2023 International Transactions on Electrical Energy Systems. This is an open access article distributed under the Creative Commons Attribution License, which permits unrestricted use, distribution, and reproduction in any medium, provided the original work is properly cited.

This article has been retracted by Hindawi, as publisher, following an investigation undertaken by the publisher [1]. This investigation has uncovered evidence of systematic manipulation of the publication and peer-review process. We cannot, therefore, vouch for the reliability or integrity of this article.

Please note that this notice is intended solely to alert readers that the peer-review process of this article has been compromised.

Wiley and Hindawi regret that the usual quality checks did not identify these issues before publication and have since put additional measures in place to safeguard research integrity.

We wish to credit our Research Integrity and Research Publishing teams and anonymous and named external researchers and research integrity experts for contributing to this investigation.

The corresponding author, as the representative of all authors, has been given the opportunity to register their agreement or disagreement to this retraction. We have kept a record of any response received.

References

- [1] Y. Miao and Y. Zhou, "The Construction of Smart Chinese Medicine Cloud Health Platform Based on Deep Neural Networks," *International Transactions on Electrical Energy Systems*, vol. 2022, Article ID 6751915, 10 pages, 2022.

Retraction

Retracted: Informatization of Accounting System of Electric Power Enterprises Based on Sensor Monitoring and Cloud Computing

International Transactions on Electrical Energy Systems

Received 28 November 2023; Accepted 28 November 2023; Published 29 November 2023

Copyright © 2023 International Transactions on Electrical Energy Systems. This is an open access article distributed under the Creative Commons Attribution License, which permits unrestricted use, distribution, and reproduction in any medium, provided the original work is properly cited.

This article has been retracted by Hindawi, as publisher, following an investigation undertaken by the publisher [1]. This investigation has uncovered evidence of systematic manipulation of the publication and peer-review process. We cannot, therefore, vouch for the reliability or integrity of this article.

Please note that this notice is intended solely to alert readers that the peer-review process of this article has been compromised.

Wiley and Hindawi regret that the usual quality checks did not identify these issues before publication and have since put additional measures in place to safeguard research integrity.

We wish to credit our Research Integrity and Research Publishing teams and anonymous and named external researchers and research integrity experts for contributing to this investigation.

The corresponding author, as the representative of all authors, has been given the opportunity to register their agreement or disagreement to this retraction. We have kept a record of any response received.

References

- [1] X. Tie, "Informatization of Accounting System of Electric Power Enterprises Based on Sensor Monitoring and Cloud Computing," *International Transactions on Electrical Energy Systems*, vol. 2022, Article ID 3506989, 7 pages, 2022.

Retraction

Retracted: Analysis of Dynamic Relationship between Energy Consumption and Economic Growth Based on PVAR Model

International Transactions on Electrical Energy Systems

Received 28 November 2023; Accepted 28 November 2023; Published 29 November 2023

Copyright © 2023 International Transactions on Electrical Energy Systems. This is an open access article distributed under the Creative Commons Attribution License, which permits unrestricted use, distribution, and reproduction in any medium, provided the original work is properly cited.

This article has been retracted by Hindawi, as publisher, following an investigation undertaken by the publisher [1]. This investigation has uncovered evidence of systematic manipulation of the publication and peer-review process. We cannot, therefore, vouch for the reliability or integrity of this article.

Please note that this notice is intended solely to alert readers that the peer-review process of this article has been compromised.

Wiley and Hindawi regret that the usual quality checks did not identify these issues before publication and have since put additional measures in place to safeguard research integrity.

We wish to credit our Research Integrity and Research Publishing teams and anonymous and named external researchers and research integrity experts for contributing to this investigation.

The corresponding author, as the representative of all authors, has been given the opportunity to register their agreement or disagreement to this retraction. We have kept a record of any response received.

References

- [1] J. Han, "Analysis of Dynamic Relationship between Energy Consumption and Economic Growth Based on PVAR Model," *International Transactions on Electrical Energy Systems*, vol. 2022, Article ID 3945522, 7 pages, 2022.

Retraction

Retracted: Teaching Practice of Engineering Management Course for Engineering Education Certification under Background of Artificial Intelligence

International Transactions on Electrical Energy Systems

Received 28 November 2023; Accepted 28 November 2023; Published 29 November 2023

Copyright © 2023 International Transactions on Electrical Energy Systems. This is an open access article distributed under the Creative Commons Attribution License, which permits unrestricted use, distribution, and reproduction in any medium, provided the original work is properly cited.

This article has been retracted by Hindawi, as publisher, following an investigation undertaken by the publisher [1]. This investigation has uncovered evidence of systematic manipulation of the publication and peer-review process. We cannot, therefore, vouch for the reliability or integrity of this article.

Please note that this notice is intended solely to alert readers that the peer-review process of this article has been compromised.

Wiley and Hindawi regret that the usual quality checks did not identify these issues before publication and have since put additional measures in place to safeguard research integrity.

We wish to credit our Research Integrity and Research Publishing teams and anonymous and named external researchers and research integrity experts for contributing to this investigation.

The corresponding author, as the representative of all authors, has been given the opportunity to register their agreement or disagreement to this retraction. We have kept a record of any response received.

References

- [1] D. Wang, F. Han, Q. Zhao, and Y. Lv, "Teaching Practice of Engineering Management Course for Engineering Education Certification under Background of Artificial Intelligence," *International Transactions on Electrical Energy Systems*, vol. 2022, Article ID 3106491, 12 pages, 2022.

Retraction

Retracted: Optical Fiber Multiparameter Detection and Numerical Simulation and Characteristics of Water Quality Particulate Matter Based on Single-Photon Detection Technology

International Transactions on Electrical Energy Systems

Received 28 November 2023; Accepted 28 November 2023; Published 29 November 2023

Copyright © 2023 International Transactions on Electrical Energy Systems. This is an open access article distributed under the Creative Commons Attribution License, which permits unrestricted use, distribution, and reproduction in any medium, provided the original work is properly cited.

This article has been retracted by Hindawi, as publisher, following an investigation undertaken by the publisher [1]. This investigation has uncovered evidence of systematic manipulation of the publication and peer-review process. We cannot, therefore, vouch for the reliability or integrity of this article.

Please note that this notice is intended solely to alert readers that the peer-review process of this article has been compromised.

Wiley and Hindawi regret that the usual quality checks did not identify these issues before publication and have since put additional measures in place to safeguard research integrity.

We wish to credit our Research Integrity and Research Publishing teams and anonymous and named external researchers and research integrity experts for contributing to this investigation.

The corresponding author, as the representative of all authors, has been given the opportunity to register their agreement or disagreement to this retraction. We have kept a record of any response received.

References

- [1] Q. Xu, C. Gao, and C. Zhou, "Optical Fiber Multiparameter Detection and Numerical Simulation and Characteristics of Water Quality Particulate Matter Based on Single-Photon Detection Technology," *International Transactions on Electrical Energy Systems*, vol. 2022, Article ID 3170082, 10 pages, 2022.

Retraction

Retracted: Influence of Educational Informatization Based on Machine Learning on Teaching Mode

International Transactions on Electrical Energy Systems

Received 28 November 2023; Accepted 28 November 2023; Published 29 November 2023

Copyright © 2023 International Transactions on Electrical Energy Systems. This is an open access article distributed under the Creative Commons Attribution License, which permits unrestricted use, distribution, and reproduction in any medium, provided the original work is properly cited.

This article has been retracted by Hindawi, as publisher, following an investigation undertaken by the publisher [1]. This investigation has uncovered evidence of systematic manipulation of the publication and peer-review process. We cannot, therefore, vouch for the reliability or integrity of this article.

Please note that this notice is intended solely to alert readers that the peer-review process of this article has been compromised.

Wiley and Hindawi regret that the usual quality checks did not identify these issues before publication and have since put additional measures in place to safeguard research integrity.

We wish to credit our Research Integrity and Research Publishing teams and anonymous and named external researchers and research integrity experts for contributing to this investigation.

The corresponding author, as the representative of all authors, has been given the opportunity to register their agreement or disagreement to this retraction. We have kept a record of any response received.

References

- [1] L. Ma and J. Li, "Influence of Educational Informatization Based on Machine Learning on Teaching Mode," *International Transactions on Electrical Energy Systems*, vol. 2022, Article ID 6180113, 7 pages, 2022.

Retraction

Retracted: Evaluation Method of Street Green Landscape Viewing Degree Based on Machine Learning

International Transactions on Electrical Energy Systems

Received 28 November 2023; Accepted 28 November 2023; Published 29 November 2023

Copyright © 2023 International Transactions on Electrical Energy Systems. This is an open access article distributed under the Creative Commons Attribution License, which permits unrestricted use, distribution, and reproduction in any medium, provided the original work is properly cited.

This article has been retracted by Hindawi, as publisher, following an investigation undertaken by the publisher [1]. This investigation has uncovered evidence of systematic manipulation of the publication and peer-review process. We cannot, therefore, vouch for the reliability or integrity of this article.

Please note that this notice is intended solely to alert readers that the peer-review process of this article has been compromised.

Wiley and Hindawi regret that the usual quality checks did not identify these issues before publication and have since put additional measures in place to safeguard research integrity.

We wish to credit our Research Integrity and Research Publishing teams and anonymous and named external researchers and research integrity experts for contributing to this investigation.

The corresponding author, as the representative of all authors, has been given the opportunity to register their agreement or disagreement to this retraction. We have kept a record of any response received.

References

- [1] T. Wang, M. Liu, and W. Huang, "Evaluation Method of Street Green Landscape Viewing Degree Based on Machine Learning," *International Transactions on Electrical Energy Systems*, vol. 2022, Article ID 2729408, 9 pages, 2022.

Retraction

Retracted: Hazard Trend Identification Model Based on Statistical Analysis of Abnormal Power Generation Behavior Data

International Transactions on Electrical Energy Systems

Received 28 November 2023; Accepted 28 November 2023; Published 29 November 2023

Copyright © 2023 International Transactions on Electrical Energy Systems. This is an open access article distributed under the Creative Commons Attribution License, which permits unrestricted use, distribution, and reproduction in any medium, provided the original work is properly cited.

This article has been retracted by Hindawi, as publisher, following an investigation undertaken by the publisher [1]. This investigation has uncovered evidence of systematic manipulation of the publication and peer-review process. We cannot, therefore, vouch for the reliability or integrity of this article.

Please note that this notice is intended solely to alert readers that the peer-review process of this article has been compromised.

Wiley and Hindawi regret that the usual quality checks did not identify these issues before publication and have since put additional measures in place to safeguard research integrity.

We wish to credit our Research Integrity and Research Publishing teams and anonymous and named external researchers and research integrity experts for contributing to this investigation.

The corresponding author, as the representative of all authors, has been given the opportunity to register their agreement or disagreement to this retraction. We have kept a record of any response received.

References

- [1] G. Xu, X. Qian, X. Li, and W. Wu, "Hazard Trend Identification Model Based on Statistical Analysis of Abnormal Power Generation Behavior Data," *International Transactions on Electrical Energy Systems*, vol. 2022, Article ID 5463109, 7 pages, 2022.

Retraction

Retracted: Assessing the Feasibility of Cogeneration Retrofit for Heating and Electricity Demands in Marine Diesel Engines

International Transactions on Electrical Energy Systems

Received 28 November 2023; Accepted 28 November 2023; Published 29 November 2023

Copyright © 2023 International Transactions on Electrical Energy Systems. This is an open access article distributed under the Creative Commons Attribution License, which permits unrestricted use, distribution, and reproduction in any medium, provided the original work is properly cited.

This article has been retracted by Hindawi, as publisher, following an investigation undertaken by the publisher [1]. This investigation has uncovered evidence of systematic manipulation of the publication and peer-review process. We cannot, therefore, vouch for the reliability or integrity of this article.

Please note that this notice is intended solely to alert readers that the peer-review process of this article has been compromised.

Wiley and Hindawi regret that the usual quality checks did not identify these issues before publication and have since put additional measures in place to safeguard research integrity.

We wish to credit our Research Integrity and Research Publishing teams and anonymous and named external researchers and research integrity experts for contributing to this investigation.

The corresponding author, as the representative of all authors, has been given the opportunity to register their agreement or disagreement to this retraction. We have kept a record of any response received.

References

- [1] X. Liu, H. Yang, Z. Feng, G. Hu, and Z. Zeng, "Assessing the Feasibility of Cogeneration Retrofit for Heating and Electricity Demands in Marine Diesel Engines," *International Transactions on Electrical Energy Systems*, vol. 2023, Article ID 3280579, 10 pages, 2023.

Retraction

Retracted: Short-Term Load Monitoring of a Power System Based on Neural Network

International Transactions on Electrical Energy Systems

Received 28 November 2023; Accepted 28 November 2023; Published 29 November 2023

Copyright © 2023 International Transactions on Electrical Energy Systems. This is an open access article distributed under the Creative Commons Attribution License, which permits unrestricted use, distribution, and reproduction in any medium, provided the original work is properly cited.

This article has been retracted by Hindawi, as publisher, following an investigation undertaken by the publisher [1]. This investigation has uncovered evidence of systematic manipulation of the publication and peer-review process. We cannot, therefore, vouch for the reliability or integrity of this article.

Please note that this notice is intended solely to alert readers that the peer-review process of this article has been compromised.

Wiley and Hindawi regret that the usual quality checks did not identify these issues before publication and have since put additional measures in place to safeguard research integrity.

We wish to credit our Research Integrity and Research Publishing teams and anonymous and named external researchers and research integrity experts for contributing to this investigation.

The corresponding author, as the representative of all authors, has been given the opportunity to register their agreement or disagreement to this retraction. We have kept a record of any response received.

References

- [1] D. Yang, "Short-Term Load Monitoring of a Power System Based on Neural Network," *International Transactions on Electrical Energy Systems*, vol. 2023, Article ID 4581408, 10 pages, 2023.

Retraction

Retracted: Simulation of Flow-Induced Vibration and Dynamic Performance of Circular-Arc Helical Gear Pump under Background of Machine Learning

International Transactions on Electrical Energy Systems

Received 28 November 2023; Accepted 28 November 2023; Published 29 November 2023

Copyright © 2023 International Transactions on Electrical Energy Systems. This is an open access article distributed under the Creative Commons Attribution License, which permits unrestricted use, distribution, and reproduction in any medium, provided the original work is properly cited.

This article has been retracted by Hindawi, as publisher, following an investigation undertaken by the publisher [1]. This investigation has uncovered evidence of systematic manipulation of the publication and peer-review process. We cannot, therefore, vouch for the reliability or integrity of this article.

Please note that this notice is intended solely to alert readers that the peer-review process of this article has been compromised.

Wiley and Hindawi regret that the usual quality checks did not identify these issues before publication and have since put additional measures in place to safeguard research integrity.

We wish to credit our Research Integrity and Research Publishing teams and anonymous and named external researchers and research integrity experts for contributing to this investigation.

The corresponding author, as the representative of all authors, has been given the opportunity to register their agreement or disagreement to this retraction. We have kept a record of any response received.

References

- [1] X. Wei, Y. Feng, X. Han, and Z. He, "Simulation of Flow-Induced Vibration and Dynamic Performance of Circular-Arc Helical Gear Pump under Background of Machine Learning," *International Transactions on Electrical Energy Systems*, vol. 2022, Article ID 9513357, 10 pages, 2022.

Retraction

Retracted: Surface Feature Prediction Modeling and Parameter Optimization for Turning TC17 Titanium Alloy

International Transactions on Electrical Energy Systems

Received 28 November 2023; Accepted 28 November 2023; Published 29 November 2023

Copyright © 2023 International Transactions on Electrical Energy Systems. This is an open access article distributed under the Creative Commons Attribution License, which permits unrestricted use, distribution, and reproduction in any medium, provided the original work is properly cited.

This article has been retracted by Hindawi, as publisher, following an investigation undertaken by the publisher [1]. This investigation has uncovered evidence of systematic manipulation of the publication and peer-review process. We cannot, therefore, vouch for the reliability or integrity of this article.

Please note that this notice is intended solely to alert readers that the peer-review process of this article has been compromised.

Wiley and Hindawi regret that the usual quality checks did not identify these issues before publication and have since put additional measures in place to safeguard research integrity.

We wish to credit our Research Integrity and Research Publishing teams and anonymous and named external researchers and research integrity experts for contributing to this investigation.

The corresponding author, as the representative of all authors, has been given the opportunity to register their agreement or disagreement to this retraction. We have kept a record of any response received.

References

- [1] Z. Deng, Z. Wang, and X. Shen, "Surface Feature Prediction Modeling and Parameter Optimization for Turning TC17 Titanium Alloy," *International Transactions on Electrical Energy Systems*, vol. 2022, Article ID 2979858, 12 pages, 2022.

Retraction

Retracted: The Optimal Integration of Computer Information Technology and Energy Economic Management

International Transactions on Electrical Energy Systems

Received 28 November 2023; Accepted 28 November 2023; Published 29 November 2023

Copyright © 2023 International Transactions on Electrical Energy Systems. This is an open access article distributed under the Creative Commons Attribution License, which permits unrestricted use, distribution, and reproduction in any medium, provided the original work is properly cited.

This article has been retracted by Hindawi, as publisher, following an investigation undertaken by the publisher [1]. This investigation has uncovered evidence of systematic manipulation of the publication and peer-review process. We cannot, therefore, vouch for the reliability or integrity of this article.

Please note that this notice is intended solely to alert readers that the peer-review process of this article has been compromised.

Wiley and Hindawi regret that the usual quality checks did not identify these issues before publication and have since put additional measures in place to safeguard research integrity.

We wish to credit our Research Integrity and Research Publishing teams and anonymous and named external researchers and research integrity experts for contributing to this investigation.

The corresponding author, as the representative of all authors, has been given the opportunity to register their agreement or disagreement to this retraction. We have kept a record of any response received.

References

- [1] N. Zhang and Z. Li, "The Optimal Integration of Computer Information Technology and Energy Economic Management," *International Transactions on Electrical Energy Systems*, vol. 2022, Article ID 9067413, 7 pages, 2022.

Retraction

Retracted: Psychological Motivation of Athletes' Physical Training Based on Deep Learning Model

International Transactions on Electrical Energy Systems

Received 28 November 2023; Accepted 28 November 2023; Published 29 November 2023

Copyright © 2023 International Transactions on Electrical Energy Systems. This is an open access article distributed under the Creative Commons Attribution License, which permits unrestricted use, distribution, and reproduction in any medium, provided the original work is properly cited.

This article has been retracted by Hindawi, as publisher, following an investigation undertaken by the publisher [1]. This investigation has uncovered evidence of systematic manipulation of the publication and peer-review process. We cannot, therefore, vouch for the reliability or integrity of this article.

Please note that this notice is intended solely to alert readers that the peer-review process of this article has been compromised.

Wiley and Hindawi regret that the usual quality checks did not identify these issues before publication and have since put additional measures in place to safeguard research integrity.

We wish to credit our Research Integrity and Research Publishing teams and anonymous and named external researchers and research integrity experts for contributing to this investigation.

The corresponding author, as the representative of all authors, has been given the opportunity to register their agreement or disagreement to this retraction. We have kept a record of any response received.

References

- [1] Y. Yang, "Psychological Motivation of Athletes' Physical Training Based on Deep Learning Model," *International Transactions on Electrical Energy Systems*, vol. 2022, Article ID 1962461, 11 pages, 2022.

Retraction

Retracted: Evaluation of the Fluctuation Mechanism of Behavioral Financial Market Based on Edge Computing

International Transactions on Electrical Energy Systems

Received 28 November 2023; Accepted 28 November 2023; Published 29 November 2023

Copyright © 2023 International Transactions on Electrical Energy Systems. This is an open access article distributed under the Creative Commons Attribution License, which permits unrestricted use, distribution, and reproduction in any medium, provided the original work is properly cited.

This article has been retracted by Hindawi, as publisher, following an investigation undertaken by the publisher [1]. This investigation has uncovered evidence of systematic manipulation of the publication and peer-review process. We cannot, therefore, vouch for the reliability or integrity of this article.

Please note that this notice is intended solely to alert readers that the peer-review process of this article has been compromised.

Wiley and Hindawi regret that the usual quality checks did not identify these issues before publication and have since put additional measures in place to safeguard research integrity.

We wish to credit our Research Integrity and Research Publishing teams and anonymous and named external researchers and research integrity experts for contributing to this investigation.

The corresponding author, as the representative of all authors, has been given the opportunity to register their agreement or disagreement to this retraction. We have kept a record of any response received.

References

- [1] X. Yuan, "Evaluation of the Fluctuation Mechanism of Behavioral Financial Market Based on Edge Computing," *International Transactions on Electrical Energy Systems*, vol. 2022, Article ID 2751197, 8 pages, 2022.

Retraction

Retracted: Power Grid Intelligent Energy Dispatching Interactive System Based on Virtual Reality Technology

International Transactions on Electrical Energy Systems

Received 10 October 2023; Accepted 10 October 2023; Published 11 October 2023

Copyright © 2023 International Transactions on Electrical Energy Systems. This is an open access article distributed under the Creative Commons Attribution License, which permits unrestricted use, distribution, and reproduction in any medium, provided the original work is properly cited.

This article has been retracted by Hindawi following an investigation undertaken by the publisher [1]. This investigation has uncovered evidence of one or more of the following indicators of systematic manipulation of the publication process:

- (1) Discrepancies in scope
- (2) Discrepancies in the description of the research reported
- (3) Discrepancies between the availability of data and the research described
- (4) Inappropriate citations
- (5) Incoherent, meaningless and/or irrelevant content included in the article
- (6) Peer-review manipulation

The presence of these indicators undermines our confidence in the integrity of the article's content and we cannot, therefore, vouch for its reliability. Please note that this notice is intended solely to alert readers that the content of this article is unreliable. We have not investigated whether authors were aware of or involved in the systematic manipulation of the publication process.

Wiley and Hindawi regrets that the usual quality checks did not identify these issues before publication and have since put additional measures in place to safeguard research integrity.

We wish to credit our own Research Integrity and Research Publishing teams and anonymous and named external researchers and research integrity experts for contributing to this investigation.

The corresponding author, as the representative of all authors, has been given the opportunity to register their agreement or disagreement to this retraction. We have kept a record of any response received.

References

- [1] W. Hu, Y. Yang, B. Liu, S. Guo, and K. Zhang, "Power Grid Intelligent Energy Dispatching Interactive System Based on Virtual Reality Technology," *International Transactions on Electrical Energy Systems*, vol. 2022, Article ID 8008461, 8 pages, 2022.

Retraction

Retracted: Mathematical Modeling Method of the Improved Genetic Algorithm for Random Power Fluctuation

International Transactions on Electrical Energy Systems

Received 3 October 2023; Accepted 3 October 2023; Published 4 October 2023

Copyright © 2023 International Transactions on Electrical Energy Systems. This is an open access article distributed under the Creative Commons Attribution License, which permits unrestricted use, distribution, and reproduction in any medium, provided the original work is properly cited.

This article has been retracted by Hindawi following an investigation undertaken by the publisher [1]. This investigation has uncovered evidence of one or more of the following indicators of systematic manipulation of the publication process:

- (1) Discrepancies in scope
- (2) Discrepancies in the description of the research reported
- (3) Discrepancies between the availability of data and the research described
- (4) Inappropriate citations
- (5) Incoherent, meaningless and/or irrelevant content included in the article
- (6) Peer-review manipulation

The presence of these indicators undermines our confidence in the integrity of the article's content and we cannot, therefore, vouch for its reliability. Please note that this notice is intended solely to alert readers that the content of this article is unreliable. We have not investigated whether authors were aware of or involved in the systematic manipulation of the publication process.

Wiley and Hindawi regrets that the usual quality checks did not identify these issues before publication and have since put additional measures in place to safeguard research integrity.

We wish to credit our own Research Integrity and Research Publishing teams and anonymous and named external researchers and research integrity experts for contributing to this investigation.

The corresponding author, as the representative of all authors, has been given the opportunity to register their agreement or disagreement to this retraction. We have kept a record of any response received.

References

- [1] F. Zhu, "Mathematical Modeling Method of the Improved Genetic Algorithm for Random Power Fluctuation," *International Transactions on Electrical Energy Systems*, vol. 2022, Article ID 1889952, 7 pages, 2022.

Retraction

Retracted: Precise Positioning of Redundant Robot Motion Energy-Saving Control Based on Sensing Technology

International Transactions on Electrical Energy Systems

Received 3 October 2023; Accepted 3 October 2023; Published 4 October 2023

Copyright © 2023 International Transactions on Electrical Energy Systems. This is an open access article distributed under the Creative Commons Attribution License, which permits unrestricted use, distribution, and reproduction in any medium, provided the original work is properly cited.

This article has been retracted by Hindawi following an investigation undertaken by the publisher [1]. This investigation has uncovered evidence of one or more of the following indicators of systematic manipulation of the publication process:

- (1) Discrepancies in scope
- (2) Discrepancies in the description of the research reported
- (3) Discrepancies between the availability of data and the research described
- (4) Inappropriate citations
- (5) Incoherent, meaningless and/or irrelevant content included in the article
- (6) Peer-review manipulation

The presence of these indicators undermines our confidence in the integrity of the article's content and we cannot, therefore, vouch for its reliability. Please note that this notice is intended solely to alert readers that the content of this article is unreliable. We have not investigated whether authors were aware of or involved in the systematic manipulation of the publication process.

Wiley and Hindawi regrets that the usual quality checks did not identify these issues before publication and have since put additional measures in place to safeguard research integrity.

We wish to credit our own Research Integrity and Research Publishing teams and anonymous and named external researchers and research integrity experts for contributing to this investigation.

The corresponding author, as the representative of all authors, has been given the opportunity to register their agreement or disagreement to this retraction. We have kept a record of any response received.

References

- [1] Y. Lu, "Precise Positioning of Redundant Robot Motion Energy-Saving Control Based on Sensing Technology," *International Transactions on Electrical Energy Systems*, vol. 2022, Article ID 6367598, 8 pages, 2022.

Retraction

Retracted: Energy Conservation Optimization and Numerical Simulation of Urban Green Space Landscape Pattern

International Transactions on Electrical Energy Systems

Received 3 October 2023; Accepted 3 October 2023; Published 4 October 2023

Copyright © 2023 International Transactions on Electrical Energy Systems. This is an open access article distributed under the Creative Commons Attribution License, which permits unrestricted use, distribution, and reproduction in any medium, provided the original work is properly cited.

This article has been retracted by Hindawi following an investigation undertaken by the publisher [1]. This investigation has uncovered evidence of one or more of the following indicators of systematic manipulation of the publication process:

- (1) Discrepancies in scope
- (2) Discrepancies in the description of the research reported
- (3) Discrepancies between the availability of data and the research described
- (4) Inappropriate citations
- (5) Incoherent, meaningless and/or irrelevant content included in the article
- (6) Peer-review manipulation

The presence of these indicators undermines our confidence in the integrity of the article's content and we cannot, therefore, vouch for its reliability. Please note that this notice is intended solely to alert readers that the content of this article is unreliable. We have not investigated whether authors were aware of or involved in the systematic manipulation of the publication process.

Wiley and Hindawi regrets that the usual quality checks did not identify these issues before publication and have since put additional measures in place to safeguard research integrity.

We wish to credit our own Research Integrity and Research Publishing teams and anonymous and named external researchers and research integrity experts for contributing to this investigation.

The corresponding author, as the representative of all authors, has been given the opportunity to register their agreement or disagreement to this retraction. We have kept a record of any response received.

References

- [1] L. Wang, "Energy Conservation Optimization and Numerical Simulation of Urban Green Space Landscape Pattern," *International Transactions on Electrical Energy Systems*, vol. 2022, Article ID 5324854, 7 pages, 2022.

Retraction

Retracted: Modeling and Optimization of Ship Waste Heat Utilization System Based on Genetic Algorithm and Sensing

International Transactions on Electrical Energy Systems

Received 3 October 2023; Accepted 3 October 2023; Published 4 October 2023

Copyright © 2023 International Transactions on Electrical Energy Systems. This is an open access article distributed under the Creative Commons Attribution License, which permits unrestricted use, distribution, and reproduction in any medium, provided the original work is properly cited.

This article has been retracted by Hindawi following an investigation undertaken by the publisher [1]. This investigation has uncovered evidence of one or more of the following indicators of systematic manipulation of the publication process:

- (1) Discrepancies in scope
- (2) Discrepancies in the description of the research reported
- (3) Discrepancies between the availability of data and the research described
- (4) Inappropriate citations
- (5) Incoherent, meaningless and/or irrelevant content included in the article
- (6) Peer-review manipulation

The presence of these indicators undermines our confidence in the integrity of the article's content and we cannot, therefore, vouch for its reliability. Please note that this notice is intended solely to alert readers that the content of this article is unreliable. We have not investigated whether authors were aware of or involved in the systematic manipulation of the publication process.

Wiley and Hindawi regrets that the usual quality checks did not identify these issues before publication and have since put additional measures in place to safeguard research integrity.

We wish to credit our own Research Integrity and Research Publishing teams and anonymous and named external researchers and research integrity experts for contributing to this investigation.

The corresponding author, as the representative of all authors, has been given the opportunity to register their agreement or disagreement to this retraction. We have kept a record of any response received.

References

- [1] L. Lyu, "Modeling and Optimization of Ship Waste Heat Utilization System Based on Genetic Algorithm and Sensing," *International Transactions on Electrical Energy Systems*, vol. 2022, Article ID 9917212, 8 pages, 2022.

Retraction

Retracted: Simulation of Multisensor Energy Data Fusion Transformer Acquisition System Based on FPGA

International Transactions on Electrical Energy Systems

Received 3 October 2023; Accepted 3 October 2023; Published 4 October 2023

Copyright © 2023 International Transactions on Electrical Energy Systems. This is an open access article distributed under the Creative Commons Attribution License, which permits unrestricted use, distribution, and reproduction in any medium, provided the original work is properly cited.

This article has been retracted by Hindawi following an investigation undertaken by the publisher [1]. This investigation has uncovered evidence of one or more of the following indicators of systematic manipulation of the publication process:

- (1) Discrepancies in scope
- (2) Discrepancies in the description of the research reported
- (3) Discrepancies between the availability of data and the research described
- (4) Inappropriate citations
- (5) Incoherent, meaningless and/or irrelevant content included in the article
- (6) Peer-review manipulation

The presence of these indicators undermines our confidence in the integrity of the article's content and we cannot, therefore, vouch for its reliability. Please note that this notice is intended solely to alert readers that the content of this article is unreliable. We have not investigated whether authors were aware of or involved in the systematic manipulation of the publication process.

Wiley and Hindawi regrets that the usual quality checks did not identify these issues before publication and have since put additional measures in place to safeguard research integrity.

We wish to credit our own Research Integrity and Research Publishing teams and anonymous and named external researchers and research integrity experts for contributing to this investigation.

The corresponding author, as the representative of all authors, has been given the opportunity to register their agreement or disagreement to this retraction. We have kept a record of any response received.

References

- [1] L. Luan and D. Hu, "Simulation of Multisensor Energy Data Fusion Transformer Acquisition System Based on FPGA," *International Transactions on Electrical Energy Systems*, vol. 2022, Article ID 7612674, 7 pages, 2022.

Retraction

Retracted: Data Mining Algorithm for Power User Network Based on Multi-Information Fusion

International Transactions on Electrical Energy Systems

Received 3 October 2023; Accepted 3 October 2023; Published 4 October 2023

Copyright © 2023 International Transactions on Electrical Energy Systems. This is an open access article distributed under the Creative Commons Attribution License, which permits unrestricted use, distribution, and reproduction in any medium, provided the original work is properly cited.

This article has been retracted by Hindawi following an investigation undertaken by the publisher [1]. This investigation has uncovered evidence of one or more of the following indicators of systematic manipulation of the publication process:

- (1) Discrepancies in scope
- (2) Discrepancies in the description of the research reported
- (3) Discrepancies between the availability of data and the research described
- (4) Inappropriate citations
- (5) Incoherent, meaningless and/or irrelevant content included in the article
- (6) Peer-review manipulation

The presence of these indicators undermines our confidence in the integrity of the article's content and we cannot, therefore, vouch for its reliability. Please note that this notice is intended solely to alert readers that the content of this article is unreliable. We have not investigated whether authors were aware of or involved in the systematic manipulation of the publication process.

Wiley and Hindawi regrets that the usual quality checks did not identify these issues before publication and have since put additional measures in place to safeguard research integrity.

We wish to credit our own Research Integrity and Research Publishing teams and anonymous and named external researchers and research integrity experts for contributing to this investigation.

The corresponding author, as the representative of all authors, has been given the opportunity to register their agreement or disagreement to this retraction. We have kept a record of any response received.

References

- [1] S. Huang, "Data Mining Algorithm for Power User Network Based on Multi-Information Fusion," *International Transactions on Electrical Energy Systems*, vol. 2022, Article ID 2337460, 6 pages, 2022.

Retraction

Retracted: Application of Computer Vision and Sensor Technology in Multivariate Assessment of Ecological Environment Carrying Capacity

International Transactions on Electrical Energy Systems

Received 19 September 2023; Accepted 19 September 2023; Published 20 September 2023

Copyright © 2023 International Transactions on Electrical Energy Systems. This is an open access article distributed under the Creative Commons Attribution License, which permits unrestricted use, distribution, and reproduction in any medium, provided the original work is properly cited.

This article has been retracted by Hindawi following an investigation undertaken by the publisher [1]. This investigation has uncovered evidence of one or more of the following indicators of systematic manipulation of the publication process:

- (1) Discrepancies in scope
- (2) Discrepancies in the description of the research reported
- (3) Discrepancies between the availability of data and the research described
- (4) Inappropriate citations
- (5) Incoherent, meaningless and/or irrelevant content included in the article
- (6) Peer-review manipulation

The presence of these indicators undermines our confidence in the integrity of the article's content and we cannot, therefore, vouch for its reliability. Please note that this notice is intended solely to alert readers that the content of this article is unreliable. We have not investigated whether authors were aware of or involved in the systematic manipulation of the publication process.

Wiley and Hindawi regrets that the usual quality checks did not identify these issues before publication and have since put additional measures in place to safeguard research integrity.

We wish to credit our own Research Integrity and Research Publishing teams and anonymous and named external researchers and research integrity experts for contributing to this investigation.

The corresponding author, as the representative of all authors, has been given the opportunity to register their agreement or disagreement to this retraction. We have kept a record of any response received.

References

- [1] Z. Wang and W. Wang, "Application of Computer Vision and Sensor Technology in Multivariate Assessment of Ecological Environment Carrying Capacity," *International Transactions on Electrical Energy Systems*, vol. 2022, Article ID 5087610, 8 pages, 2022.

Retraction

Retracted: State Diagnosis and Monitoring Method of Robot Electric Power Equipment Based on Data Mining

International Transactions on Electrical Energy Systems

Received 19 September 2023; Accepted 19 September 2023; Published 20 September 2023

Copyright © 2023 International Transactions on Electrical Energy Systems. This is an open access article distributed under the Creative Commons Attribution License, which permits unrestricted use, distribution, and reproduction in any medium, provided the original work is properly cited.

This article has been retracted by Hindawi following an investigation undertaken by the publisher [1]. This investigation has uncovered evidence of one or more of the following indicators of systematic manipulation of the publication process:

- (1) Discrepancies in scope
- (2) Discrepancies in the description of the research reported
- (3) Discrepancies between the availability of data and the research described
- (4) Inappropriate citations
- (5) Incoherent, meaningless and/or irrelevant content included in the article
- (6) Peer-review manipulation

The presence of these indicators undermines our confidence in the integrity of the article's content and we cannot, therefore, vouch for its reliability. Please note that this notice is intended solely to alert readers that the content of this article is unreliable. We have not investigated whether authors were aware of or involved in the systematic manipulation of the publication process.

Wiley and Hindawi regrets that the usual quality checks did not identify these issues before publication and have since put additional measures in place to safeguard research integrity.

We wish to credit our own Research Integrity and Research Publishing teams and anonymous and named external researchers and research integrity experts for contributing to this investigation.

The corresponding author, as the representative of all authors, has been given the opportunity to register their agreement or disagreement to this retraction. We have kept a record of any response received.

References

- [1] H. Guo, Z. Meng, H. Yu, R. Chen, L. Li, and L. Cheng, "State Diagnosis and Monitoring Method of Robot Electric Power Equipment Based on Data Mining," *International Transactions on Electrical Energy Systems*, vol. 2022, Article ID 4272364, 7 pages, 2022.

Retraction

Retracted: Application of Laser Scanning Technology in Digital Method

International Transactions on Electrical Energy Systems

Received 19 September 2023; Accepted 19 September 2023; Published 20 September 2023

Copyright © 2023 International Transactions on Electrical Energy Systems. This is an open access article distributed under the Creative Commons Attribution License, which permits unrestricted use, distribution, and reproduction in any medium, provided the original work is properly cited.

This article has been retracted by Hindawi following an investigation undertaken by the publisher [1]. This investigation has uncovered evidence of one or more of the following indicators of systematic manipulation of the publication process:

- (1) Discrepancies in scope
- (2) Discrepancies in the description of the research reported
- (3) Discrepancies between the availability of data and the research described
- (4) Inappropriate citations
- (5) Incoherent, meaningless and/or irrelevant content included in the article
- (6) Peer-review manipulation

The presence of these indicators undermines our confidence in the integrity of the article's content and we cannot, therefore, vouch for its reliability. Please note that this notice is intended solely to alert readers that the content of this article is unreliable. We have not investigated whether authors were aware of or involved in the systematic manipulation of the publication process.

Wiley and Hindawi regrets that the usual quality checks did not identify these issues before publication and have since put additional measures in place to safeguard research integrity.

We wish to credit our own Research Integrity and Research Publishing teams and anonymous and named external researchers and research integrity experts for contributing to this investigation.

The corresponding author, as the representative of all authors, has been given the opportunity to register their agreement or disagreement to this retraction. We have kept a record of any response received.

References

- [1] F. Liu, "Application of Laser Scanning Technology in Digital Method," *International Transactions on Electrical Energy Systems*, vol. 2022, Article ID 2629688, 11 pages, 2022.

Retraction

Retracted: A Fault-Tolerant Structure for Nano-Power Communication Based on the Multidimensional Crossbar Switch Network

International Transactions on Electrical Energy Systems

Received 19 September 2023; Accepted 19 September 2023; Published 20 September 2023

Copyright © 2023 International Transactions on Electrical Energy Systems. This is an open access article distributed under the Creative Commons Attribution License, which permits unrestricted use, distribution, and reproduction in any medium, provided the original work is properly cited.

This article has been retracted by Hindawi following an investigation undertaken by the publisher [1]. This investigation has uncovered evidence of one or more of the following indicators of systematic manipulation of the publication process:

- (1) Discrepancies in scope
- (2) Discrepancies in the description of the research reported
- (3) Discrepancies between the availability of data and the research described
- (4) Inappropriate citations
- (5) Incoherent, meaningless and/or irrelevant content included in the article
- (6) Peer-review manipulation

The presence of these indicators undermines our confidence in the integrity of the article's content and we cannot, therefore, vouch for its reliability. Please note that this notice is intended solely to alert readers that the content of this article is unreliable. We have not investigated whether authors were aware of or involved in the systematic manipulation of the publication process.

Wiley and Hindawi regrets that the usual quality checks did not identify these issues before publication and have since put additional measures in place to safeguard research integrity.

We wish to credit our own Research Integrity and Research Publishing teams and anonymous and named external researchers and research integrity experts for contributing to this investigation.

The corresponding author, as the representative of all authors, has been given the opportunity to register their agreement or disagreement to this retraction. We have kept a record of any response received.

References

- [1] J. Luo and B. Liao, "A Fault-Tolerant Structure for Nano-Power Communication Based on the Multidimensional Crossbar Switch Network," *International Transactions on Electrical Energy Systems*, vol. 2022, Article ID 4783847, 8 pages, 2022.

Retraction

Retracted: Electricity Network Security Monitoring Based on Bee Colony Algorithm

International Transactions on Electrical Energy Systems

Received 19 September 2023; Accepted 19 September 2023; Published 20 September 2023

Copyright © 2023 International Transactions on Electrical Energy Systems. This is an open access article distributed under the Creative Commons Attribution License, which permits unrestricted use, distribution, and reproduction in any medium, provided the original work is properly cited.

This article has been retracted by Hindawi following an investigation undertaken by the publisher [1]. This investigation has uncovered evidence of one or more of the following indicators of systematic manipulation of the publication process:

- (1) Discrepancies in scope
- (2) Discrepancies in the description of the research reported
- (3) Discrepancies between the availability of data and the research described
- (4) Inappropriate citations
- (5) Incoherent, meaningless and/or irrelevant content included in the article
- (6) Peer-review manipulation

The presence of these indicators undermines our confidence in the integrity of the article's content and we cannot, therefore, vouch for its reliability. Please note that this notice is intended solely to alert readers that the content of this article is unreliable. We have not investigated whether authors were aware of or involved in the systematic manipulation of the publication process.

Wiley and Hindawi regrets that the usual quality checks did not identify these issues before publication and have since put additional measures in place to safeguard research integrity.

We wish to credit our own Research Integrity and Research Publishing teams and anonymous and named external researchers and research integrity experts for contributing to this investigation.

The corresponding author, as the representative of all authors, has been given the opportunity to register their agreement or disagreement to this retraction. We have kept a record of any response received.

References

- [1] W. Su and B. Zhang, "Electricity Network Security Monitoring Based on Bee Colony Algorithm," *International Transactions on Electrical Energy Systems*, vol. 2022, Article ID 4533154, 8 pages, 2022.

Retraction

Retracted: Optimal Pricing Model of Environmental Quality Index Futures from the Perspective of Green Finance

International Transactions on Electrical Energy Systems

Received 19 September 2023; Accepted 19 September 2023; Published 20 September 2023

Copyright © 2023 International Transactions on Electrical Energy Systems. This is an open access article distributed under the Creative Commons Attribution License, which permits unrestricted use, distribution, and reproduction in any medium, provided the original work is properly cited.

This article has been retracted by Hindawi following an investigation undertaken by the publisher [1]. This investigation has uncovered evidence of one or more of the following indicators of systematic manipulation of the publication process:

- (1) Discrepancies in scope
- (2) Discrepancies in the description of the research reported
- (3) Discrepancies between the availability of data and the research described
- (4) Inappropriate citations
- (5) Incoherent, meaningless and/or irrelevant content included in the article
- (6) Peer-review manipulation

The presence of these indicators undermines our confidence in the integrity of the article's content and we cannot, therefore, vouch for its reliability. Please note that this notice is intended solely to alert readers that the content of this article is unreliable. We have not investigated whether authors were aware of or involved in the systematic manipulation of the publication process.

Wiley and Hindawi regrets that the usual quality checks did not identify these issues before publication and have since put additional measures in place to safeguard research integrity.

We wish to credit our own Research Integrity and Research Publishing teams and anonymous and named external researchers and research integrity experts for contributing to this investigation.

The corresponding author, as the representative of all authors, has been given the opportunity to register their agreement or disagreement to this retraction. We have kept a record of any response received.

References

- [1] J. Che, S. Zhou, R. Shan, H. Jia, and Z. Liu, "Optimal Pricing Model of Environmental Quality Index Futures from the Perspective of Green Finance," *International Transactions on Electrical Energy Systems*, vol. 2022, Article ID 6951040, 8 pages, 2022.

Retraction

Retracted: Wireless Mobile Power Communication System Based on Artificial Intelligence Algorithm

International Transactions on Electrical Energy Systems

Received 19 September 2023; Accepted 19 September 2023; Published 20 September 2023

Copyright © 2023 International Transactions on Electrical Energy Systems. This is an open access article distributed under the Creative Commons Attribution License, which permits unrestricted use, distribution, and reproduction in any medium, provided the original work is properly cited.

This article has been retracted by Hindawi following an investigation undertaken by the publisher [1]. This investigation has uncovered evidence of one or more of the following indicators of systematic manipulation of the publication process:

- (1) Discrepancies in scope
- (2) Discrepancies in the description of the research reported
- (3) Discrepancies between the availability of data and the research described
- (4) Inappropriate citations
- (5) Incoherent, meaningless and/or irrelevant content included in the article
- (6) Peer-review manipulation

The presence of these indicators undermines our confidence in the integrity of the article's content and we cannot, therefore, vouch for its reliability. Please note that this notice is intended solely to alert readers that the content of this article is unreliable. We have not investigated whether authors were aware of or involved in the systematic manipulation of the publication process.

Wiley and Hindawi regrets that the usual quality checks did not identify these issues before publication and have since put additional measures in place to safeguard research integrity.

We wish to credit our own Research Integrity and Research Publishing teams and anonymous and named external researchers and research integrity experts for contributing to this investigation.

The corresponding author, as the representative of all authors, has been given the opportunity to register their agreement or disagreement to this retraction. We have kept a record of any response received.

References

- [1] J. Du and M. Guo, "Wireless Mobile Power Communication System Based on Artificial Intelligence Algorithm," *International Transactions on Electrical Energy Systems*, vol. 2022, Article ID 1636033, 7 pages, 2022.

Retraction

Retracted: Application of Data Mining Algorithm in Electric Power Marketing Inspection Forecast Analysis

International Transactions on Electrical Energy Systems

Received 19 September 2023; Accepted 19 September 2023; Published 20 September 2023

Copyright © 2023 International Transactions on Electrical Energy Systems. This is an open access article distributed under the Creative Commons Attribution License, which permits unrestricted use, distribution, and reproduction in any medium, provided the original work is properly cited.

This article has been retracted by Hindawi following an investigation undertaken by the publisher [1]. This investigation has uncovered evidence of one or more of the following indicators of systematic manipulation of the publication process:

- (1) Discrepancies in scope
- (2) Discrepancies in the description of the research reported
- (3) Discrepancies between the availability of data and the research described
- (4) Inappropriate citations
- (5) Incoherent, meaningless and/or irrelevant content included in the article
- (6) Peer-review manipulation

The presence of these indicators undermines our confidence in the integrity of the article's content and we cannot, therefore, vouch for its reliability. Please note that this notice is intended solely to alert readers that the content of this article is unreliable. We have not investigated whether authors were aware of or involved in the systematic manipulation of the publication process.

Wiley and Hindawi regrets that the usual quality checks did not identify these issues before publication and have since put additional measures in place to safeguard research integrity.

We wish to credit our own Research Integrity and Research Publishing teams and anonymous and named external researchers and research integrity experts for contributing to this investigation.

The corresponding author, as the representative of all authors, has been given the opportunity to register their agreement or disagreement to this retraction. We have kept a record of any response received.

References

- [1] W. Wu, G. Xu, X. Qian, and C. Chu, "Application of Data Mining Algorithm in Electric Power Marketing Inspection Forecast Analysis," *International Transactions on Electrical Energy Systems*, vol. 2022, Article ID 9229415, 7 pages, 2022.

Retraction

Retracted: Application of Internet of Things Technology in Optimization of Electronic Assembly Process Parameters

International Transactions on Electrical Energy Systems

Received 19 September 2023; Accepted 19 September 2023; Published 20 September 2023

Copyright © 2023 International Transactions on Electrical Energy Systems. This is an open access article distributed under the Creative Commons Attribution License, which permits unrestricted use, distribution, and reproduction in any medium, provided the original work is properly cited.

This article has been retracted by Hindawi following an investigation undertaken by the publisher [1]. This investigation has uncovered evidence of one or more of the following indicators of systematic manipulation of the publication process:

- (1) Discrepancies in scope
- (2) Discrepancies in the description of the research reported
- (3) Discrepancies between the availability of data and the research described
- (4) Inappropriate citations
- (5) Incoherent, meaningless and/or irrelevant content included in the article
- (6) Peer-review manipulation

The presence of these indicators undermines our confidence in the integrity of the article's content and we cannot, therefore, vouch for its reliability. Please note that this notice is intended solely to alert readers that the content of this article is unreliable. We have not investigated whether authors were aware of or involved in the systematic manipulation of the publication process.

Wiley and Hindawi regrets that the usual quality checks did not identify these issues before publication and have since put additional measures in place to safeguard research integrity.

We wish to credit our own Research Integrity and Research Publishing teams and anonymous and named external researchers and research integrity experts for contributing to this investigation.

The corresponding author, as the representative of all authors, has been given the opportunity to register their agreement or disagreement to this retraction. We have kept a record of any response received.

References

- [1] X. Song, "Application of Internet of Things Technology in Optimization of Electronic Assembly Process Parameters," *International Transactions on Electrical Energy Systems*, vol. 2022, Article ID 2375521, 7 pages, 2022.

Retraction

Retracted: Define Electronic Enterprise Financial Management Information Decision-Making Process Based on IoT and the ERP Model

International Transactions on Electrical Energy Systems

Received 19 September 2023; Accepted 19 September 2023; Published 20 September 2023

Copyright © 2023 International Transactions on Electrical Energy Systems. This is an open access article distributed under the Creative Commons Attribution License, which permits unrestricted use, distribution, and reproduction in any medium, provided the original work is properly cited.

This article has been retracted by Hindawi following an investigation undertaken by the publisher [1]. This investigation has uncovered evidence of one or more of the following indicators of systematic manipulation of the publication process:

- (1) Discrepancies in scope
- (2) Discrepancies in the description of the research reported
- (3) Discrepancies between the availability of data and the research described
- (4) Inappropriate citations
- (5) Incoherent, meaningless and/or irrelevant content included in the article
- (6) Peer-review manipulation

The presence of these indicators undermines our confidence in the integrity of the article's content and we cannot, therefore, vouch for its reliability. Please note that this notice is intended solely to alert readers that the content of this article is unreliable. We have not investigated whether authors were aware of or involved in the systematic manipulation of the publication process.

Wiley and Hindawi regrets that the usual quality checks did not identify these issues before publication and have since put additional measures in place to safeguard research integrity.

We wish to credit our own Research Integrity and Research Publishing teams and anonymous and named external researchers and research integrity experts for contributing to this investigation.

The corresponding author, as the representative of all authors, has been given the opportunity to register their agreement or disagreement to this retraction. We have kept a record of any response received.

References

- [1] H. Su, "Define Electronic Enterprise Financial Management Information Decision-Making Process Based on IoT and the ERP Model," *International Transactions on Electrical Energy Systems*, vol. 2022, Article ID 1191031, 8 pages, 2022.

Retraction

Retracted: Application of the Lagrange Equation for Intelligent Sensor Vibration Control for Power Network Monitoring

International Transactions on Electrical Energy Systems

Received 19 September 2023; Accepted 19 September 2023; Published 20 September 2023

Copyright © 2023 International Transactions on Electrical Energy Systems. This is an open access article distributed under the Creative Commons Attribution License, which permits unrestricted use, distribution, and reproduction in any medium, provided the original work is properly cited.

This article has been retracted by Hindawi following an investigation undertaken by the publisher [1]. This investigation has uncovered evidence of one or more of the following indicators of systematic manipulation of the publication process:

- (1) Discrepancies in scope
- (2) Discrepancies in the description of the research reported
- (3) Discrepancies between the availability of data and the research described
- (4) Inappropriate citations
- (5) Incoherent, meaningless and/or irrelevant content included in the article
- (6) Peer-review manipulation

The presence of these indicators undermines our confidence in the integrity of the article's content and we cannot, therefore, vouch for its reliability. Please note that this notice is intended solely to alert readers that the content of this article is unreliable. We have not investigated whether authors were aware of or involved in the systematic manipulation of the publication process.

Wiley and Hindawi regrets that the usual quality checks did not identify these issues before publication and have since put additional measures in place to safeguard research integrity.

We wish to credit our own Research Integrity and Research Publishing teams and anonymous and named external researchers and research integrity experts for contributing to this investigation.

The corresponding author, as the representative of all authors, has been given the opportunity to register their agreement or disagreement to this retraction. We have kept a record of any response received.

References

- [1] X. Cheng, "Application of the Lagrange Equation for Intelligent Sensor Vibration Control for Power Network Monitoring," *International Transactions on Electrical Energy Systems*, vol. 2022, Article ID 4616889, 9 pages, 2022.

Retraction

Retracted: Seismic Performance and Vibration Control of Rapid Construction Environmental Protection Wall Based on Artificial Intelligence

International Transactions on Electrical Energy Systems

Received 19 September 2023; Accepted 19 September 2023; Published 20 September 2023

Copyright © 2023 International Transactions on Electrical Energy Systems. This is an open access article distributed under the Creative Commons Attribution License, which permits unrestricted use, distribution, and reproduction in any medium, provided the original work is properly cited.

This article has been retracted by Hindawi following an investigation undertaken by the publisher [1]. This investigation has uncovered evidence of one or more of the following indicators of systematic manipulation of the publication process:

- (1) Discrepancies in scope
- (2) Discrepancies in the description of the research reported
- (3) Discrepancies between the availability of data and the research described
- (4) Inappropriate citations
- (5) Incoherent, meaningless and/or irrelevant content included in the article
- (6) Peer-review manipulation

The presence of these indicators undermines our confidence in the integrity of the article's content and we cannot, therefore, vouch for its reliability. Please note that this notice is intended solely to alert readers that the content of this article is unreliable. We have not investigated whether authors were aware of or involved in the systematic manipulation of the publication process.

Wiley and Hindawi regrets that the usual quality checks did not identify these issues before publication and have since put additional measures in place to safeguard research integrity.

We wish to credit our own Research Integrity and Research Publishing teams and anonymous and named external researchers and research integrity experts for contributing to this investigation.

The corresponding author, as the representative of all authors, has been given the opportunity to register their agreement or disagreement to this retraction. We have kept a record of any response received.

References

- [1] J. Fu, S. Zhou, L. Liu, and M. Liu, "Seismic Performance and Vibration Control of Rapid Construction Environmental Protection Wall Based on Artificial Intelligence," *International Transactions on Electrical Energy Systems*, vol. 2022, Article ID 1385774, 8 pages, 2022.

Retraction

Retracted: Reconstruction and Utilization of Energy Economy Information Resources against Humanistic Background

International Transactions on Electrical Energy Systems

Received 19 September 2023; Accepted 19 September 2023; Published 20 September 2023

Copyright © 2023 International Transactions on Electrical Energy Systems. This is an open access article distributed under the Creative Commons Attribution License, which permits unrestricted use, distribution, and reproduction in any medium, provided the original work is properly cited.

This article has been retracted by Hindawi following an investigation undertaken by the publisher [1]. This investigation has uncovered evidence of one or more of the following indicators of systematic manipulation of the publication process:

- (1) Discrepancies in scope
- (2) Discrepancies in the description of the research reported
- (3) Discrepancies between the availability of data and the research described
- (4) Inappropriate citations
- (5) Incoherent, meaningless and/or irrelevant content included in the article
- (6) Peer-review manipulation

The presence of these indicators undermines our confidence in the integrity of the article's content and we cannot, therefore, vouch for its reliability. Please note that this notice is intended solely to alert readers that the content of this article is unreliable. We have not investigated whether authors were aware of or involved in the systematic manipulation of the publication process.

Wiley and Hindawi regrets that the usual quality checks did not identify these issues before publication and have since put additional measures in place to safeguard research integrity.

We wish to credit our own Research Integrity and Research Publishing teams and anonymous and named external researchers and research integrity experts for contributing to this investigation.

The corresponding author, as the representative of all authors, has been given the opportunity to register their agreement or disagreement to this retraction. We have kept a record of any response received.

References

- [1] L. Du, "Reconstruction and Utilization of Energy Economy Information Resources against Humanistic Background," *International Transactions on Electrical Energy Systems*, vol. 2022, Article ID 2301322, 7 pages, 2022.

Retraction

Retracted: Improved VMD-+ACO Algorithm Navigation and Positioning Technology for Robot Electric Power Inspection

International Transactions on Electrical Energy Systems

Received 19 September 2023; Accepted 19 September 2023; Published 20 September 2023

Copyright © 2023 International Transactions on Electrical Energy Systems. This is an open access article distributed under the Creative Commons Attribution License, which permits unrestricted use, distribution, and reproduction in any medium, provided the original work is properly cited.

This article has been retracted by Hindawi following an investigation undertaken by the publisher [1]. This investigation has uncovered evidence of one or more of the following indicators of systematic manipulation of the publication process:

- (1) Discrepancies in scope
- (2) Discrepancies in the description of the research reported
- (3) Discrepancies between the availability of data and the research described
- (4) Inappropriate citations
- (5) Incoherent, meaningless and/or irrelevant content included in the article
- (6) Peer-review manipulation

The presence of these indicators undermines our confidence in the integrity of the article's content and we cannot, therefore, vouch for its reliability. Please note that this notice is intended solely to alert readers that the content of this article is unreliable. We have not investigated whether authors were aware of or involved in the systematic manipulation of the publication process.

Wiley and Hindawi regrets that the usual quality checks did not identify these issues before publication and have since put additional measures in place to safeguard research integrity.

We wish to credit our own Research Integrity and Research Publishing teams and anonymous and named external researchers and research integrity experts for contributing to this investigation.

The corresponding author, as the representative of all authors, has been given the opportunity to register their agreement or disagreement to this retraction. We have kept a record of any response received.

References

- [1] Y. Long, M. Du, X. Luo, S. Li, and X. Jiang, "Improved VMD-+ACO Algorithm Navigation and Positioning Technology for Robot Electric Power Inspection," *International Transactions on Electrical Energy Systems*, vol. 2022, Article ID 5467622, 6 pages, 2022.

Retraction

Retracted: Application of Big Data Technology in Environmental Pollution Control in Energy Ecological Economic Zone

International Transactions on Electrical Energy Systems

Received 19 September 2023; Accepted 19 September 2023; Published 20 September 2023

Copyright © 2023 International Transactions on Electrical Energy Systems. This is an open access article distributed under the Creative Commons Attribution License, which permits unrestricted use, distribution, and reproduction in any medium, provided the original work is properly cited.

This article has been retracted by Hindawi following an investigation undertaken by the publisher [1]. This investigation has uncovered evidence of one or more of the following indicators of systematic manipulation of the publication process:

- (1) Discrepancies in scope
- (2) Discrepancies in the description of the research reported
- (3) Discrepancies between the availability of data and the research described
- (4) Inappropriate citations
- (5) Incoherent, meaningless and/or irrelevant content included in the article
- (6) Peer-review manipulation

The presence of these indicators undermines our confidence in the integrity of the article's content and we cannot, therefore, vouch for its reliability. Please note that this notice is intended solely to alert readers that the content of this article is unreliable. We have not investigated whether authors were aware of or involved in the systematic manipulation of the publication process.

Wiley and Hindawi regrets that the usual quality checks did not identify these issues before publication and have since put additional measures in place to safeguard research integrity.

We wish to credit our own Research Integrity and Research Publishing teams and anonymous and named external researchers and research integrity experts for contributing to this investigation.

The corresponding author, as the representative of all authors, has been given the opportunity to register their agreement or disagreement to this retraction. We have kept a record of any response received.

References

- [1] X. Jin and X. Jin, "Application of Big Data Technology in Environmental Pollution Control in Energy Ecological Economic Zone," *International Transactions on Electrical Energy Systems*, vol. 2022, Article ID 1569905, 7 pages, 2022.

Retraction

Retracted: Realization of Single-Phase Grounding Fault Location and Recovery Technology in Distribution Network

International Transactions on Electrical Energy Systems

Received 19 September 2023; Accepted 19 September 2023; Published 20 September 2023

Copyright © 2023 International Transactions on Electrical Energy Systems. This is an open access article distributed under the Creative Commons Attribution License, which permits unrestricted use, distribution, and reproduction in any medium, provided the original work is properly cited.

This article has been retracted by Hindawi following an investigation undertaken by the publisher [1]. This investigation has uncovered evidence of one or more of the following indicators of systematic manipulation of the publication process:

- (1) Discrepancies in scope
- (2) Discrepancies in the description of the research reported
- (3) Discrepancies between the availability of data and the research described
- (4) Inappropriate citations
- (5) Incoherent, meaningless and/or irrelevant content included in the article
- (6) Peer-review manipulation

The presence of these indicators undermines our confidence in the integrity of the article's content and we cannot, therefore, vouch for its reliability. Please note that this notice is intended solely to alert readers that the content of this article is unreliable. We have not investigated whether authors were aware of or involved in the systematic manipulation of the publication process.

Wiley and Hindawi regrets that the usual quality checks did not identify these issues before publication and have since put additional measures in place to safeguard research integrity.

We wish to credit our own Research Integrity and Research Publishing teams and anonymous and named external researchers and research integrity experts for contributing to this investigation.

The corresponding author, as the representative of all authors, has been given the opportunity to register their agreement or disagreement to this retraction. We have kept a record of any response received.

References

- [1] D. Zhang, H. Tang, J. Zhu, H. Zhou, Z. Zhang, and X. Song, "Realization of Single-Phase Grounding Fault Location and Recovery Technology in Distribution Network," *International Transactions on Electrical Energy Systems*, vol. 2022, Article ID 6282843, 10 pages, 2022.

Retraction

Retracted: On-Load Electromagnetic Compatibility Test and Simulation Closed-Loop of the Electric Drive System of New Energy Vehicles

International Transactions on Electrical Energy Systems

Received 19 September 2023; Accepted 19 September 2023; Published 20 September 2023

Copyright © 2023 International Transactions on Electrical Energy Systems. This is an open access article distributed under the Creative Commons Attribution License, which permits unrestricted use, distribution, and reproduction in any medium, provided the original work is properly cited.

This article has been retracted by Hindawi following an investigation undertaken by the publisher [1]. This investigation has uncovered evidence of one or more of the following indicators of systematic manipulation of the publication process:

- (1) Discrepancies in scope
- (2) Discrepancies in the description of the research reported
- (3) Discrepancies between the availability of data and the research described
- (4) Inappropriate citations
- (5) Incoherent, meaningless and/or irrelevant content included in the article
- (6) Peer-review manipulation

The presence of these indicators undermines our confidence in the integrity of the article's content and we cannot, therefore, vouch for its reliability. Please note that this notice is intended solely to alert readers that the content of this article is unreliable. We have not investigated whether authors were aware of or involved in the systematic manipulation of the publication process.

Wiley and Hindawi regrets that the usual quality checks did not identify these issues before publication and have since put additional measures in place to safeguard research integrity.

We wish to credit our own Research Integrity and Research Publishing teams and anonymous and named external researchers and research integrity experts for contributing to this investigation.

The corresponding author, as the representative of all authors, has been given the opportunity to register their agreement or disagreement to this retraction. We have kept a record of any response received.

References

- [1] X. Luo, W. Liu, and J. Li, "On-Load Electromagnetic Compatibility Test and Simulation Closed-Loop of the Electric Drive System of New Energy Vehicles," *International Transactions on Electrical Energy Systems*, vol. 2022, Article ID 9256401, 6 pages, 2022.

Retraction

Retracted: High Efficiency Compound Vacuum Oil Gas Separation Technology Based on Integrated Oil Filter of Ultra-High Voltage Transformer

International Transactions on Electrical Energy Systems

Received 19 September 2023; Accepted 19 September 2023; Published 20 September 2023

Copyright © 2023 International Transactions on Electrical Energy Systems. This is an open access article distributed under the Creative Commons Attribution License, which permits unrestricted use, distribution, and reproduction in any medium, provided the original work is properly cited.

This article has been retracted by Hindawi following an investigation undertaken by the publisher [1]. This investigation has uncovered evidence of one or more of the following indicators of systematic manipulation of the publication process:

- (1) Discrepancies in scope
- (2) Discrepancies in the description of the research reported
- (3) Discrepancies between the availability of data and the research described
- (4) Inappropriate citations
- (5) Incoherent, meaningless and/or irrelevant content included in the article
- (6) Peer-review manipulation

The presence of these indicators undermines our confidence in the integrity of the article's content and we cannot, therefore, vouch for its reliability. Please note that this notice is intended solely to alert readers that the content of this article is unreliable. We have not investigated whether authors were aware of or involved in the systematic manipulation of the publication process.

Wiley and Hindawi regrets that the usual quality checks did not identify these issues before publication and have since put additional measures in place to safeguard research integrity.

We wish to credit our own Research Integrity and Research Publishing teams and anonymous and named external researchers and research integrity experts for contributing to this investigation.

The corresponding author, as the representative of all authors, has been given the opportunity to register their agreement or disagreement to this retraction. We have kept a record of any response received.

References

- [1] J. Guan, X. Hu, H. Liu, and Y. Yang, "High Efficiency Compound Vacuum Oil Gas Separation Technology Based on Integrated Oil Filter of Ultra-High Voltage Transformer," *International Transactions on Electrical Energy Systems*, vol. 2022, Article ID 9989686, 6 pages, 2022.

Retraction

Retracted: Application of Big Data and Internet of Things Technology in the Management of Financial Operating Income of Electric Power Enterprises

International Transactions on Electrical Energy Systems

Received 19 September 2023; Accepted 19 September 2023; Published 20 September 2023

Copyright © 2023 International Transactions on Electrical Energy Systems. This is an open access article distributed under the Creative Commons Attribution License, which permits unrestricted use, distribution, and reproduction in any medium, provided the original work is properly cited.

This article has been retracted by Hindawi following an investigation undertaken by the publisher [1]. This investigation has uncovered evidence of one or more of the following indicators of systematic manipulation of the publication process:

- (1) Discrepancies in scope
- (2) Discrepancies in the description of the research reported
- (3) Discrepancies between the availability of data and the research described
- (4) Inappropriate citations
- (5) Incoherent, meaningless and/or irrelevant content included in the article
- (6) Peer-review manipulation

The presence of these indicators undermines our confidence in the integrity of the article's content and we cannot, therefore, vouch for its reliability. Please note that this notice is intended solely to alert readers that the content of this article is unreliable. We have not investigated whether authors were aware of or involved in the systematic manipulation of the publication process.

Wiley and Hindawi regrets that the usual quality checks did not identify these issues before publication and have since put additional measures in place to safeguard research integrity.

We wish to credit our own Research Integrity and Research Publishing teams and anonymous and named external researchers and research integrity experts for contributing to this investigation.

The corresponding author, as the representative of all authors, has been given the opportunity to register their agreement or disagreement to this retraction. We have kept a record of any response received.

References

- [1] H. Su, "Application of Big Data and Internet of Things Technology in the Management of Financial Operating Income of Electric Power Enterprises," *International Transactions on Electrical Energy Systems*, vol. 2022, Article ID 6167479, 8 pages, 2022.

Retraction

Retracted: Innovation and Entrepreneurship Coupling Based on Simultaneous Equation Model and Its Energy Economic Effect Measurement

International Transactions on Electrical Energy Systems

Received 19 September 2023; Accepted 19 September 2023; Published 20 September 2023

Copyright © 2023 International Transactions on Electrical Energy Systems. This is an open access article distributed under the Creative Commons Attribution License, which permits unrestricted use, distribution, and reproduction in any medium, provided the original work is properly cited.

This article has been retracted by Hindawi following an investigation undertaken by the publisher [1]. This investigation has uncovered evidence of one or more of the following indicators of systematic manipulation of the publication process:

- (1) Discrepancies in scope
- (2) Discrepancies in the description of the research reported
- (3) Discrepancies between the availability of data and the research described
- (4) Inappropriate citations
- (5) Incoherent, meaningless and/or irrelevant content included in the article
- (6) Peer-review manipulation

The presence of these indicators undermines our confidence in the integrity of the article's content and we cannot, therefore, vouch for its reliability. Please note that this notice is intended solely to alert readers that the content of this article is unreliable. We have not investigated whether authors were aware of or involved in the systematic manipulation of the publication process.

Wiley and Hindawi regrets that the usual quality checks did not identify these issues before publication and have since put additional measures in place to safeguard research integrity.

We wish to credit our own Research Integrity and Research Publishing teams and anonymous and named external researchers and research integrity experts for contributing to this investigation.

The corresponding author, as the representative of all authors, has been given the opportunity to register their agreement or disagreement to this retraction. We have kept a record of any response received.

References

- [1] W. Chen, "Innovation and Entrepreneurship Coupling Based on Simultaneous Equation Model and Its Energy Economic Effect Measurement," *International Transactions on Electrical Energy Systems*, vol. 2022, Article ID 8218645, 8 pages, 2022.

Retraction

Retracted: Assessing the Feasibility of Cogeneration Retrofit for Heating and Electricity Demands in Marine Diesel Engines

International Transactions on Electrical Energy Systems

Received 28 November 2023; Accepted 28 November 2023; Published 29 November 2023

Copyright © 2023 International Transactions on Electrical Energy Systems. This is an open access article distributed under the Creative Commons Attribution License, which permits unrestricted use, distribution, and reproduction in any medium, provided the original work is properly cited.

This article has been retracted by Hindawi, as publisher, following an investigation undertaken by the publisher [1]. This investigation has uncovered evidence of systematic manipulation of the publication and peer-review process. We cannot, therefore, vouch for the reliability or integrity of this article.

Please note that this notice is intended solely to alert readers that the peer-review process of this article has been compromised.

Wiley and Hindawi regret that the usual quality checks did not identify these issues before publication and have since put additional measures in place to safeguard research integrity.

We wish to credit our Research Integrity and Research Publishing teams and anonymous and named external researchers and research integrity experts for contributing to this investigation.

The corresponding author, as the representative of all authors, has been given the opportunity to register their agreement or disagreement to this retraction. We have kept a record of any response received.

References

- [1] X. Liu, H. Yang, Z. Feng, G. Hu, and Z. Zeng, "Assessing the Feasibility of Cogeneration Retrofit for Heating and Electricity Demands in Marine Diesel Engines," *International Transactions on Electrical Energy Systems*, vol. 2023, Article ID 3280579, 10 pages, 2023.

Research Article

Assessing the Feasibility of Cogeneration Retrofit for Heating and Electricity Demands in Marine Diesel Engines

Xianglong Liu ^{1,2}, Hao Yang,² Zhao Feng,² Guang Hu,² and Zhi Zeng²

¹Hunan Engineering Research Center of Energy Saving and Material Technology of Green and Low Carbon Building, Hunan Institute of Engineering, Xiangtan 411104, China

²Department of Building Engineering, Hunan Institute of Engineering, Xiangtan 411104, China

Correspondence should be addressed to Xianglong Liu; 20150235125@mail.sdufe.edu.cn

Received 29 July 2022; Revised 22 August 2022; Accepted 26 August 2022; Published 11 May 2023

Academic Editor: Nagamalai Vasimalai

Copyright © 2023 Xianglong Liu et al. This is an open access article distributed under the Creative Commons Attribution License, which permits unrestricted use, distribution, and reproduction in any medium, provided the original work is properly cited.

In the marine engineering industry, turbocharged diesel engines are often used to generate electricity, and hot oil can be extracted after generating electricity. However, marine diesel engine heat recovery can be distinguished from gas heat recovery for turbocharged and nonturbocharged diesel engine systems. The ideal air model Brayton cycle is used to evaluate the feasibility of turbocharged/nonturbocharged cogeneration retrofits in turbocharged diesel engine systems, and the paper is designed to evaluate the effect of pressure and temperature and cooling ratio of exergy efficiency. The results show that the performance of turbocharged and nonturbocharged work increases with increasing pressure ratio until it reaches a maximum value and decreases with increasing pressure ratio at a constant temperature. If an electric generator is selected first, the heat recovery after the turbocharger can be used to improve the contract for heating and electricity needs. While the exergy efficiency is selected priorly, cogeneration retrofit for heating and electricity demands can be used for heat recovery without the turbocharger system.

1. Introduction

Many turbocharger diesel engines are provided the power for the need of marine engineering (including FPSO (the floating production storage and offloading facility) and oil extraction platform). The extracted oil and other heat users of marine engineering should be offered huge quantity of heat. Then, the cogeneration retrofit for heating and electricity of diesel engines with and without a turbocharger is the way to solve the heat loss problem of released flue gas.

In order to use the heat loss of turbocharged and nonturbocharged diesel engines, many researchers focus on the study of the system. Many researchers focus on the ORC process to utilize engine power loss. Ma et al. designed an ORC waste heat recovery system that uses a water jacket as a preheat source and exhaust gas as an evaporative heat source to treat waste heat from special internal combustion engines. The system can increase the efficiency of the diesel engine by 14.23% when R141b is used as the working fluid. Yang et al. [2], Wang et al. [3], and Song et al. [4] have

conducted research on the dual loop ORC (DORC) of internal combustion engine waste heat recovery. The research results show that DORC can effectively improve the efficiency of internal combustion engines. It improves its economy. Mosaffa et al. [5] compared to the organic Rankine cycle, the gas recycling cycle, and the organic Rankine regeneration cycle and found that the regeneration cycle can achieve the highest efficiency, and the recycled gas achieves the highest efficiency of 39.93% whose prices increased only by 5.2%. Bombarda et al. [6] analyzed the effects of system vapor pressure, vapor temperature, and expansion on the Kalina cycle and ORC performance in a typical diesel engine operation. The results of the study show that the ORC system is suitable for heat recovery in internal combustion engines. Mago [7] and Vaja [8] discussed the effect of space reheating on ORC performance from several perspectives. The research results show that the thermal process of the recycling center can improve the thermal efficiency and energy output of the ORC system. It can also reduce the inevitable loss of the system. Menel et al. [9] proposed an ORC system using

a store-retrieval technique. The system can recover the latent heat of the superheated working water through the heat storage process. The thermal efficiency of the system is higher than the traditional ORC system and can increase by 2.25%. Yang et al. designed a dual loop organic ordered cycle (ORC) system for waste recovery in 6-cylinder diesel engines, and it has been shown that the maximum energy saving of dual-circuit ORC system efficiency (WHRE) can be conducted at 5.4%.

While the ORC system is too complex for offshore oil extraction facilities, some researchers use the turbocharger to reduce the temperature of the flue gas of diesel engines. Hopman has conducted research on diesel engine turbocharged power generation technology [11, 12]. The research results show that the use of turbocharged power generation devices can increase the fuel economy of diesel engines by 5%. Patterson et al. [13] used the power generation compound turbine technology combined with the high-speed motor to recover the energy of the low-pressure stage turbine of the two-stage supercharged diesel engine. For MAN Company, it is proposed to connect the turbocharger and the electric turbine in parallel, which reduces the gas flow from the turbocharger so that part of the exhaust gas, after leaving the cylinder of the diesel engine, goes directly to the turbocharger to work [14]. This method of power turbine can increase the output of the engine by 3–5% according to SMCR. Wärtsilä [15] created a similar electronic device that uses fuel separation before the turbocharger so that the rest of the exhaust gas, after leaving the engine cylinder, goes directly to the electrical work. Taking Wärtsilä 14RT-flex96C (maximum sustainable rated power 80080 kW) as an example, the research results show that, without reducing the engine output power, 10% of the engine exhaust gas will directly enter the power turbine without passing through the turbocharger. The power turbine can emit about 2500 kW of power under 100% CMCR working conditions, accounting for 3% of the engine output, which effectively increases the efficiency of the ship's engine. Caterpillar and John Deere proposed the use of electric compound turbines (ETC) to replace turbochargers and power turbines. Studies have shown that fuel consumption can be predicted to be reduced by 5–10% after the use of ETC devices [16, 17].

From the practical operation, the flue gas temperature is just depressed above 300°C and the remaining heat can be used with heat recovery boilers. Jayakumar et al. [18], to analyze the thermal performance, used the ideal air model Brayton cycle to remove the fan of the boiler engine to compensate for the waste due to the limited space of the coast limited compared to the design.

2. System Description and Assumptions

As shown in Figure 1, the oil is used as a fuel for diesel engines to generate power, and the waste heat is used by boilers and sent to consumers for heating in marine

engineering. First, the gas enters the turbocharger of the diesel engine to increase the air pressure. The flue gas is then discharged into the thermal boiler, and the heat obtained is used to heat the consumer. Physical description includes working fluid: working water is the best fuel; flue mass flow is the same as the air entering the furnace, and the specific heat of the working water is constant.

Brayton air cycle was used in the study of debris removal from turbo diesel engine to evaluate the feasibility of marine engineering contract, according to the work of Liu et al. [19]. Figure 2 shows the corresponding T-S diagram of the Brayton cycle with and without turbocharging [20].

2.1. Mathematical Modeling. Table 1 introduces and expounds on analyzing the devised plant from various standpoints [21].

The various standpoints are determined in Table 2.

The output power W (kW) of the system is written as

$$W = \eta_G q_m c_p [(T_3 - T_2) - (T_4 - T_1)], \quad (1)$$

where q_m and C_p are, respectively, flow mass of flue gas and the specific heat of flue gas.

The exergy of turbocharger E_T (kW) can be written as

$$\begin{aligned} E_T &= q_m C_p \eta_T (T_4 - T_6) \\ &= \frac{q_m C_p \eta_T \beta T_1 (\theta_C - 1)}{\eta_C}, \end{aligned} \quad (2)$$

where the efficiency of turbocharger η_T is 0.5.

Then, (1) can be calculated as

$$W = \eta_G q_m c_p T_1 \left[\alpha \eta_D \left(1 - \frac{1}{\theta_C \rho_{Com} \rho_R} \right) - \frac{\theta_C - 1}{\eta_C} \right], \quad (3)$$

where η_G is the efficiency of the electric generator.

The exergy of heat recovery after turbocharger is E_Q , which is given as follows:

$$\begin{aligned} E_Q &= \int_{T_5}^{T_6} q_m C_p \left(1 - \frac{T}{T_1} \right) dT \\ &= q_m C_p (T_6 - T_5) - q_m C_p T_1 \ln \left(\frac{T_6}{T_5} \right). \end{aligned} \quad (4)$$

The fuel energy (combustion processes) exergy E (kW) of the system can be written as

$$\begin{aligned} E &= q_m C_p (T_3 - T_2) \\ &= q_m C_p T_1 \left(\alpha - 1 - \frac{\theta_C - 1}{\eta_C} \right). \end{aligned} \quad (5)$$

2.2. Mathematical Model with the Turbocharger System without considering Heat Recovery. The relationship of exergy efficiency ε with the compressor pressure ratio θ_C and temperature ratio parameter α is

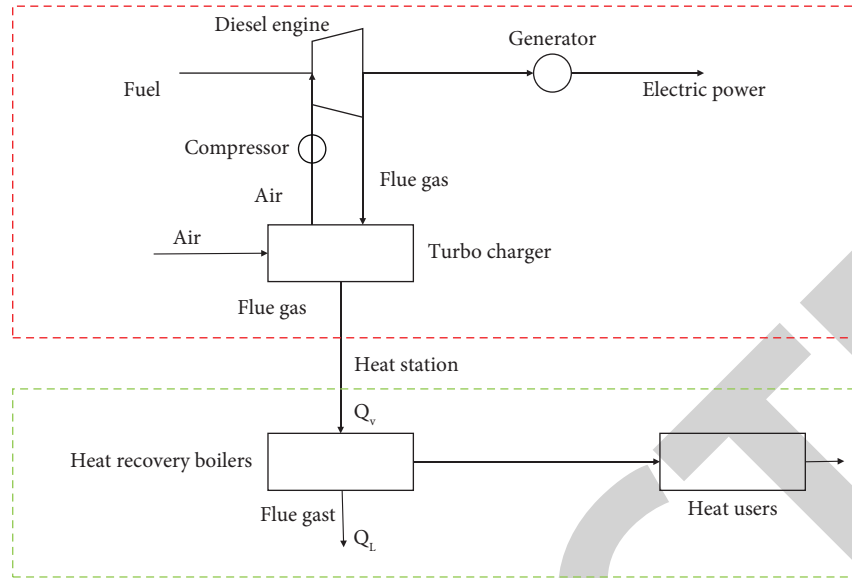


FIGURE 1: Cogeneration retrofit with a turbocharger and heat recovery boilers.

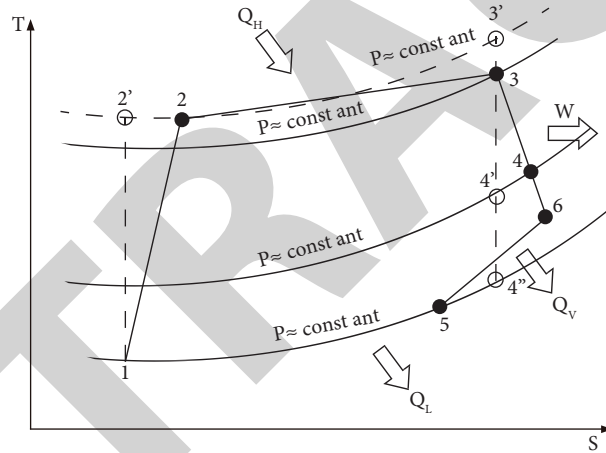


FIGURE 2: System description for turbocharger diesel engines.

TABLE 1: Thermodynamic parameters of the Brayton system.

Thermodynamic parameters	Definition	Formula
η_c	Efficiency of the compressor (%)	$\eta_c = (T_2' - T_1)/(T_2 - T_1)$
η_D	Efficiency of expansion (%)	$\eta_D = (T_3 - T_4)/(T_3' - T_4')$
ρ_{com}	The efficiency loss of the combustion process (%)	$\rho_{Com} = (p_3/p_2)^{(\gamma-1)/\gamma}$
γ	The ratio of specific heat capacity	$\rho_D = (p_6/p_4)^{(\gamma-1)/\gamma}$
ρ_D	The fluidity loss of the turbocharge process (%)	$\rho_D = (p_6/p_4)^{(\gamma-1)/\gamma}$
ρ_R	The fluidity loss of the heat recovery process (%)	$\rho_R = (p_5/p_6)^{(\gamma-1)/\gamma}$
θ_C	The compressor pressure ratio	$\theta_C = T_2'/T_1 = (p_2/p_1)^{(\gamma-1)/\gamma}$
θ_D	The expansion ratio parameter	$\theta_D = T_3/T_4' = (p_3/p_4)^{(\gamma-1)/\gamma} = \theta_C \rho_{Com} \rho_R \rho_D$
α	The temperature ratio parameter	$\alpha = T_3/T_1$
β	The turbocharger parameter	$\beta = (T_4 - T_6)/(T_2 - T_1)$

TABLE 2: The standpoint parameters at points of 1-6 as follows.

State point	P	V	T
1	P_1	v_1	T_1
2	$P_2 = (\theta_C)^{\gamma/(\gamma-1)} P_1$	$v_2 = [1 + (\theta_C - 1)/\eta_C] (\theta_C)^{-\gamma/(\gamma-1)v_1}$	$T_2 = [1 + (\theta_C - 1)/\eta_C] T_1$
3	$P_3 = (\rho_{Com} \theta_C)^{\gamma/(\gamma-1)} P_1$	$v_3 = \alpha (\rho_{Com} \theta_C)^{-\gamma/(\gamma-1)v_1}$	$T_3 = \alpha T_1$
4	$P_4 = P_1 (\rho_R \rho_D)^{-\gamma/(\gamma-1)}$	$v_4 = \alpha (\rho_R \rho_D)^{\gamma/(\gamma-1)} \{1 - \eta_D (1 - (1/\theta_C \rho_{Com} \rho_R \rho_D))\} v_1$	$T_4 = \alpha \{1 - \eta_D (1 - (1/\theta_C \rho_{Com} \rho_R \rho_D))\} T_1$
5	$P_5 = P_1$	$v_5 = \alpha_R v_1$	$T_5 = \alpha_R T_1$
6	$P_6 = (\rho_R)^{-\gamma/(\gamma-1)} P_1$	$v_6 = v_1 (\rho_R)^{\gamma/(\gamma-1)} \{ \alpha (1 - \eta_E (1 - 1/\theta_C \rho_{Com} \rho_R \rho_D)) \} T_1$	$T_6 = \alpha \{ (1 - \eta_D (1 - 1/\theta_C \rho_{Com} \rho_R \rho_D)) - \beta (\theta_C - 1)/\eta \} T_1$

$$\begin{aligned}\varepsilon &= \frac{W + E_T}{E} \\ &= \frac{\eta_{Com}\eta_G[\alpha\eta_D(1 - 1/(\theta_C\rho_{Com}\rho_R)) - \theta_C - 1/\eta_C] + \eta_T\beta(\theta_C - 1)/\eta_C}{\alpha - 1 - (\theta_C - 1/\eta_C)}.\end{aligned}\quad (6)$$

Equation (6) can be written as equation (7).

$$\varepsilon = 1 - \frac{1}{\theta_C} + \beta \frac{\theta_C - 1}{\alpha - \theta_C}.\quad (7)$$

From (7), ε is related to α and θ two parameters, then the partial derivative of ε to θ_C is written as (8) and ε to α is written as (9).

$$\frac{\partial \varepsilon}{\partial \theta_C} = \frac{1}{\theta_C^2} + \frac{\beta(\alpha - 1)}{(\alpha - \theta_C)^2},\quad (8)$$

$$\frac{\partial \varepsilon}{\partial \alpha} = \frac{-\beta(\theta_C - 1)}{(\alpha - \theta_C)^2}.\quad (9)$$

From (8) and (9), there is a nonexistent value for ε , which means ε increases with the increase of θ_C ; ε decreases with the increase of α .

2.3. Mathematical Model for the Turbocharger System with Heat Recovery after Turbocharger. The exergy efficiency ε of the Brayton cycle with heat recovery can be calculated as

$$\varepsilon = \frac{P + W + E_Q}{E}.\quad (10)$$

Equality (10) is very difficult to solve, so the maximum value can only be estimated from the actual work data and error codes, excluding heat treatment.

2.4. Thermodynamic Model for the System with Heat Recovery without Turbocharger. The exergy of heat recovery without the turbocharger is E_Q , which is given as follows:

$$\begin{aligned}E_Q &= \int_{T_5}^{T_4} q_m C_P \left(1 - \frac{T}{T_1}\right) dT \\ &= q_m C_P (T_4 - T_5) - q_m C_P T_1 \ln\left(\frac{T_4}{T_5}\right).\end{aligned}\quad (11)$$

The exergy efficiency ε of Brayton cycle with heat recovery without turbo charger can be calculated as

$$\varepsilon = \frac{P + E_Q}{E}.\quad (12)$$

2.5. Mathematical Process. The mathematical process for the cogeneration system with and without the turbocharger is written as Figure 3. The irreversible influence parameters η_C , η_E , δp_{Com} , η_{Com} , η_G , ρ_{Com} , and ρ_R of the system are defined in the process (gotten as reference). Average field atmospheric pressure and average air temperature and γ are 1.4

and are calculated by the ratio of specific heat capacity at constant pressure C_p (1.004 kJ/kg °C) to specific heat capacity at constant volume C_v (0.718 kJ/kg °C). Table 3 provides the input data required for modeling the system.

Then, α , θ_C , temperature, and pressure of standpoints 2–6 are calculated from Table 1, and the relationship of ε with θ_C and α are calculated through equations (1)–(12) of the irreversible system.

3. Results and Discussion

The effects of ratio and temperature on exergy efficiency with and without turbocharging are investigated to evaluate the feasibility of contract retrofitting in marine engineering systems under various loads. The performance is shown in Figure 4, which shows the performance of the turbodiesel engine in various products after testing the performance of the turbodiesel engine in operation.

3.1. Parameter Tests of the Turbocharger Diesel Engine. CNOOC (National Offshore Oil Corporation of China) received diesel engine certification documents from engine manufacturers after the installation of 111 FPSOs. Table 4 lists the main characteristics of FPSO diesel engines. The approved engine is a marine engineering turbocharged diesel engine, and the acceptance criteria are fully evaluated. The information is certified by BV (Bureau Veritas). According to the information about the permissible limits, the test set-up of the diesel generator is shown in Figure 4. Operating without the variable W, round temperature T1 (K), P1 (bar), working temperature P2 (bar), T4 (K), and T6 (K), etc. are considered. Table 5 shows the operating parameters of the 34025 turbocharger diesel engine.

3.2. The Exergy Efficiency for the Turbocharger System without Heat Recovery. With the irreversible parameters assumed as follows: $\eta_{Com} = 1$, $\eta_G = 1$, $\eta_D = 1$, $\eta_C = 1$, $\rho_{Com} = 1$, $\rho_R = 1$, the relationship of ε with θ_C , α , and β for the turbocharger system without flue gas heat recovery under variable loads is studied as follows.

The relationship between compressor pressure P2 (kg/cm²), fuel consumption mh (kg/h), and air temperature T4 (K) for various nonthermal generators is shown in Figure 5. To confirm the recorded data, T1 (K) and P1 (kg/cm²) are stable for most of the work. As shown in Figure 5, the exergy efficiency increases as the temperature ratio parameter increases, while the pressure ratio is constant. Moreover, irreversible parameters can only be assumed to be constant at 1. For each variable of the load, the irreversibility cannot be less than 1 and the changes are not changed slightly in the

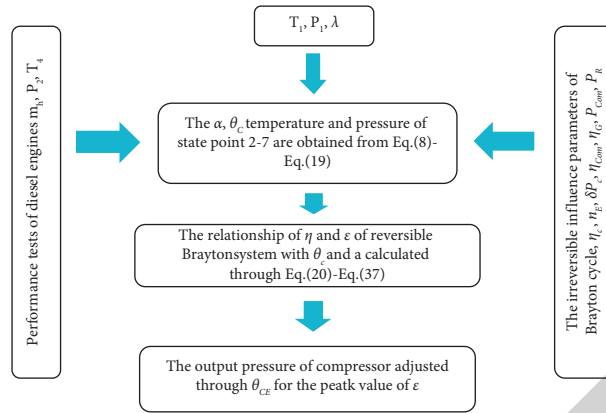


FIGURE 3: The diagram shows the development of the integrated generator in this study.

TABLE 3: Required input data for the modeling of the system.

Parameters	Values	Units
P_1	101.3	Kpa
T_1	298.15	K
γ	1.4	—
C_p	1.004	(kJ/kg °C)
C_v	0.718	(kJ/kg °C)
Q_{net}	42000	(kJ/kg)

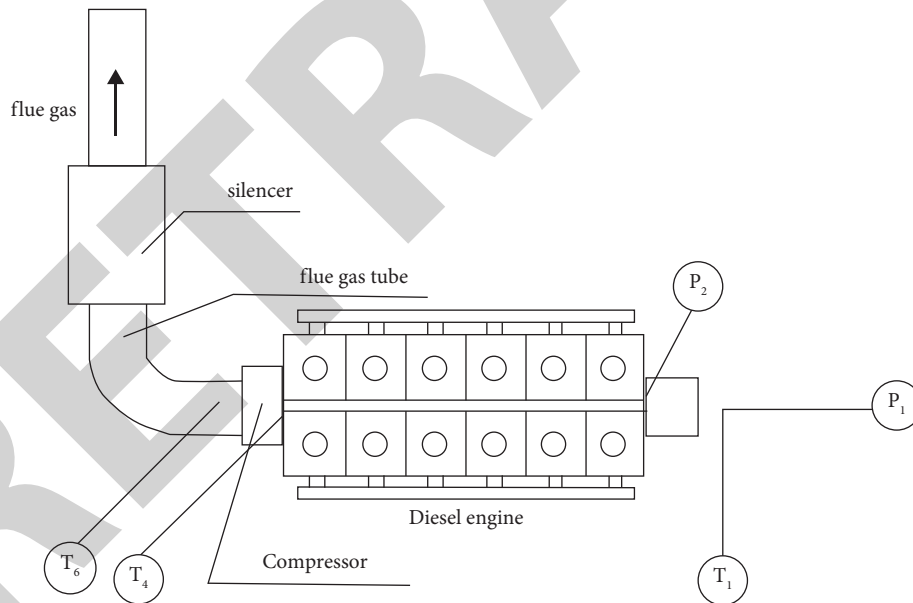


FIGURE 4: The essential operation parameters of turbocharger diesel engines.

TABLE 4: The main parameters of the diesel engine.

Parameters	Values
Model	16CM32C
Speed (rpm)	750
Cylinder bore diameter (mm)	320
Engine type	4-Stroke-cycle-diesel
Power (kW)	8000
Cylinder number	16
Fuel	Oil
Certification	BV

TABLE 5: Operating parameters of 34025 turbocharger diesel engine.

Output power, W (kW)	Load ratio (%)	T_2 (K)	T_3 (K)	q_m (kg/h)	Temperature ratio, α	T_4 (K)	T_6 (K)
8800	110	786.22	1886.71	44098.5	6.06	747.15	619.15
8000	100	761.90	1739.62	45965.8	5.61	708.15	599.15
6800	75	728.04	1603.38	45134.0	5.16	684.15	594.15
4000	50	623.46	1324.7	37760.0	4.28	658.15	620.15
2000	25	507.15	1063.6	30358.3	3.46	644.15	631.15

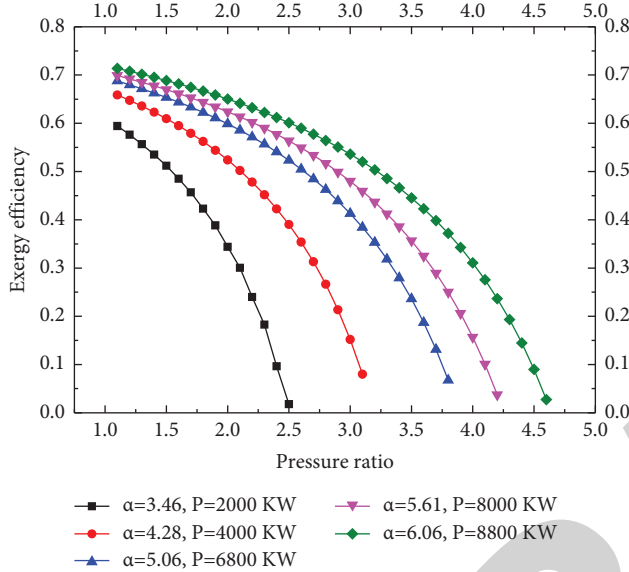


FIGURE 5: The relationship between pressure ratio and exergy efficiency without heat recovery for the turbocharger system.

variable and not influenced by engineering developments. Then, all the irreversible parameters were written on the paper: $\eta_T = 0.5\eta_D = 0.82$, $\eta_C = 0.82$, $\eta_G = 0.97$, $\rho_{Com} = 0.98$, $\rho_R = 1$ (without flue gas heat recovery).

From Figure 6, it can be seen that with the increase of the ratio, the performance of the body first increases and then decreases and the performance of the pressure ratio is higher by 2 to 3.5. Because as the pressure ratio increases, the efficiency of the compressor also increases and the efficiency of the compressor reaches the maximum, and when the pressure ratio increases, the efficiency of the compressor does not increase much, or even increase the oil consumption is increased. The exergy efficiency of the system gradually decreases, so it appears to increase first and then shows the decreasing trend. From Figure 6, compressor P_2 and maximum temperature T_3 of diesel engines can increase the combustion efficiency and the two parameters cannot be unlimitedly increased which can decrease the exergy efficiency ϵ .

3.3. The Exergy Efficiency for the Turbo System with Heat Recovery. The irreversible parameters are shown in Figures 7 and 8.

Figure 7 shows the hot gas reciprocating turbocharger system without consideration of the variable parameters, and Figure 8 shows the hot gas reciprocating the

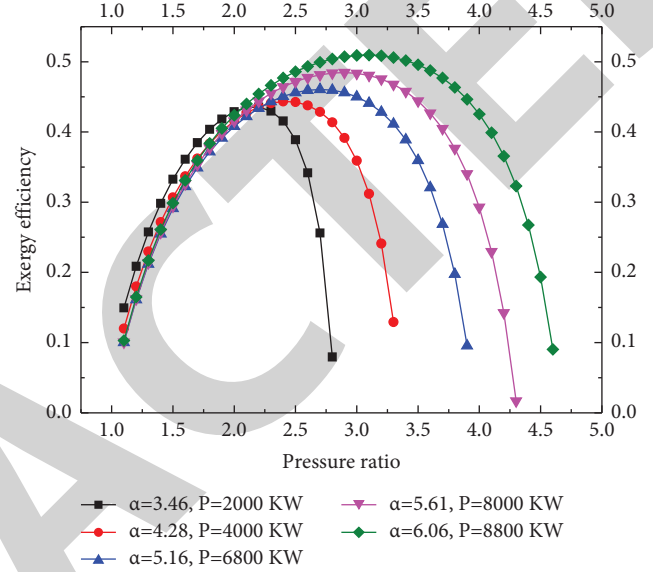


FIGURE 6: The relationship between pressure ratio and exergy efficiency without flue gas heat recovery for the turbo system considering the irreversible parameters.

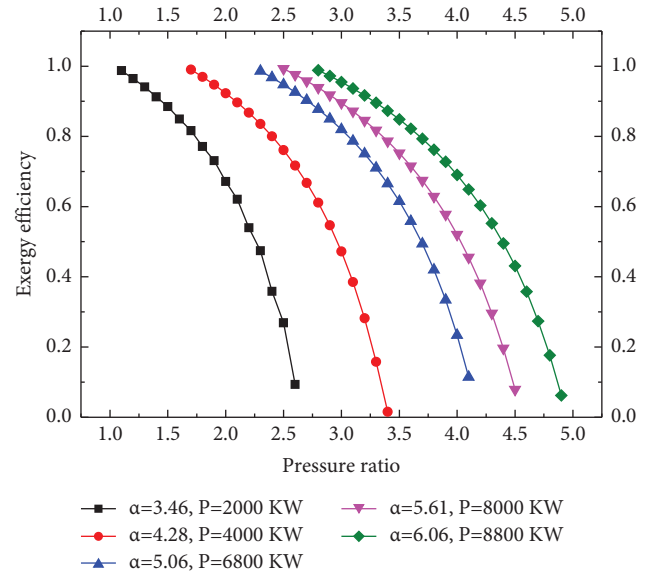


FIGURE 7: The relationship between pressure ratio and exergy efficiency with heat recovery for the turbo system.

turbocharger system with the variable parameters: ($\eta_T = 0.5\eta_D = 0.82$, $\eta_C = 0.82$, $\eta_G = 0.97$, $\rho_{Com} = 0.98$, $\rho_R = 1$). As shown in Figure 7, when the pressure ratio is constant, the

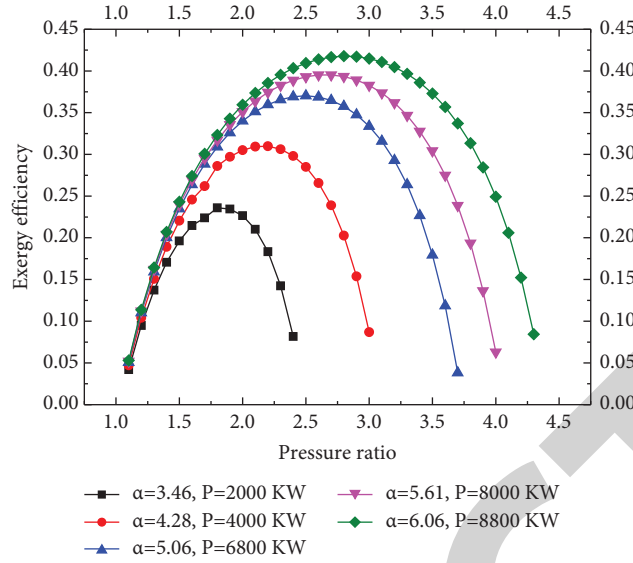


FIGURE 8: The relationship between pressure ratio and exergy efficiency with heat recovery for the turbo system considering the irreversible parameters.

TABLE 6: The θ_{CE} for different systems under variable loads.

Load ratio (%)	α	θ_{CE} (reversible)	θ_{CE} (irreversible)	θ_{CE} (with heat recovery)	θ_{CE} (irreversible, big value)
110	3.46	1.73	1.98	1.4	8.38
100	4.28	2.14	2.31	1.6	12.68
75	5.16	2.58	2.68	1.8	19.44
50	5.61	2.8	2.86	1.9	24.3
25	6.06	3.03	3.03	2.0	30.66

exergy efficiency increases as the temperature ratio parameter increases.

The parameters for the 34025 diesel engine in the real mode are 1.66, 2.02, 2.36, 2.47, and 2.54; for different products, they are 0.4585, 0.5335, 0.5932, 0.6183, and 0.6440, respectively. The peak values of flue gas heat recovery are greater than the peak values of 0.2068, 0.2033, 0.2019, 0.2015, and 0.2049. The reason for this is that the heat recovery can increase the efficiency of the turbocharging system.

The value of the Brayton variable during recovery is 1% lower than the comparison, indicating that high performance can be obtained in real work by adjusting the performance such as pressure ratio and temperature, as shown in Figure 7 and Figure 8.

The different systems under variable loads with heat recovery of the turbocharger system are summarized in Table 6 from Figures 6–8.

Then, (12) can be rewritten as

$$\theta_C = \frac{\eta_D \alpha}{(\alpha \eta_D + 1 - \alpha) \rho_{Com} \rho_R} - \sqrt{\left(\frac{\eta_D \alpha}{(\alpha \eta_D + 1 - \alpha) \rho_{Com} \rho_R} \right)^2 - \frac{\alpha \eta_D (\alpha \eta_C - \eta_C + 1)}{(\alpha \eta_D + 1 - \alpha) \rho_{Com} \rho_R}} \quad (13)$$

From Figure 8 and Table 4, the thermal efficiency analysis of the marine engineering turbocharger diesel engine is more appropriate than the energy thermal efficiency analysis. Of course, power generation is more important than heat recovery.

3.4. The Comparison of Exergy Efficiency of Heat Recovery with and without the Turbo Charger. Figure 9 shows the calculation results of the waste heat recovery efficiency

without considering the irreversible loss. Figure 9 shows that when the system only heats up again, as the pressure ratio increases, the increase is increased, the pressure is lower, the pressure ratio is higher from 1 to 1.5, and the result is better than the turbocharger. The reason for this is that the turbocharger system converts heat energy into all kinds of energy.

Figure 10 shows that when the system is only reheated, the exergy efficiency first increases and then decreases as the pressure ratio increases, but when the

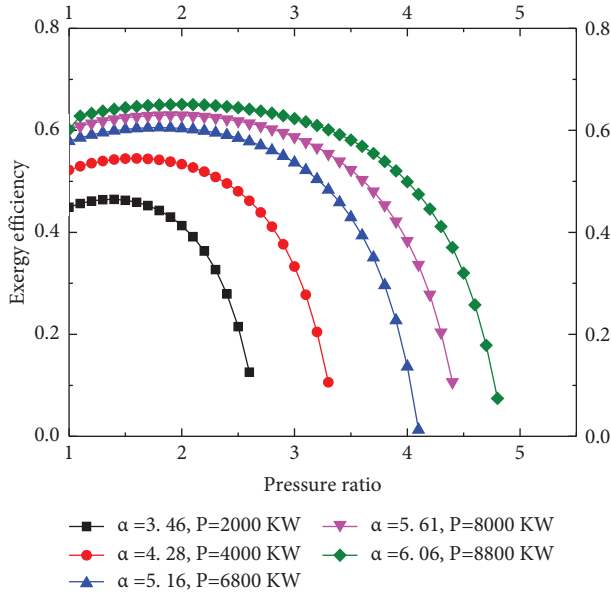


FIGURE 9: The relationship between pressure ratio and exergy efficiency with heat recovery without the turbocharger considering the irreversible parameters.

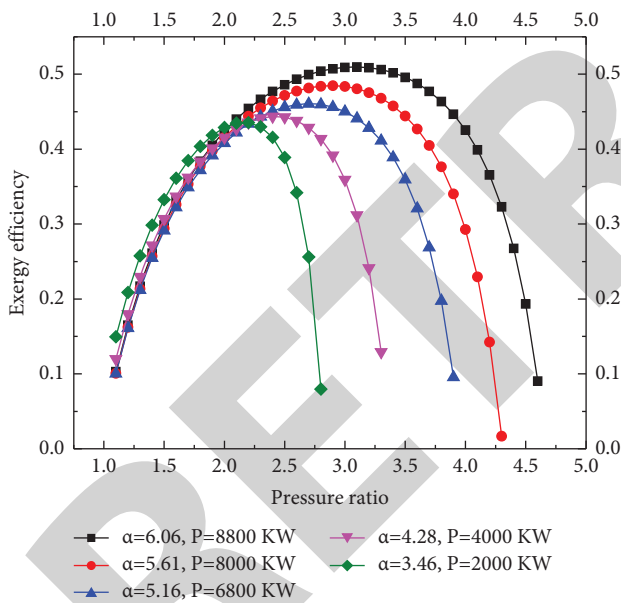


FIGURE 10: The relationship between pressure ratio and exergy efficiency with heat recovery with the turbocharger considering the irreversible parameters.

pressure ratio is moderate, the increase is small and high exergy efficiencies are 0.2 and 3.5, and it is found that when only waste heat recovery is used, its efficiency is higher than that of a compressor system.

4. Conclusions

An analysis of the Brayton system for turbocharged diesel engines has been carried out by considering the effects of local instability, system pressure ratio, and operating

temperature. For the development of marine engineering cogeneration systems and by studying turbochargers under different loads, conclusions can be drawn as follows:

- (1) Compressor P2 and the maximum temperature T3 of the diesel engine can increase the mixing efficiency, and both cannot increase, which reduces the efficiency of exergy.
- (2) It can be seen from the article that by correcting the performance parameters such as pressure ratio and temperature of the turbocharger diesel system, it can achieve high efficiency in operation really.
- (3) If a diesel engine is selected first, cogeneration can be used for heat recovery after the turbocharger for heat and electricity needs. If the use of electricity is chosen first, the use of renewable energy can be used without a turbocharger by installing cogeneration for heat and electricity needs.

Nomenclature

Q_H :	Combustion processes energy (kJ)
Q_v :	Heat recovery quantity (kJ)
Q_L :	Flue gas discharged (kJ)
η_c :	Efficiency of the compressor (kJ)
T :	Temperature (kJ)
η_D :	Efficiency of expansion (%)
ρ_{com} :	The efficiency loss of the combustion process (%)
P :	Pressure (bar)
γ :	The ratio of specific heat capacity
ρ_D :	The fluidity loss of turbo charge process (%)
ρ_R :	The fluidity loss of heat recovery process (%)
θ_C :	The compressor pressure ratio (%)
θ_D :	The expansion ratio parameter (%)
α :	The temperature ratio parameter
β :	The turbo charger parameter
α_R :	Temperature ratio parameter of heat recovery
ε :	The exergy efficiency of Brayton system (%)
W :	The output power of Brayton cycle (kW)
q_m :	Flow mass of flue gas (kg/h)
C_p :	The specific heat at of flue gas
E_T :	The exergy of the turbocharger (kW)
η_T :	The efficiency of turbo (%)
η_G :	The efficiency of the electric generator (%)
E_Q :	Exergy of heat recovery after the turbocharger (%)
E :	The fuel energy (combustion processes) exergy of the Brayton cycle (kW)
θ_{CE} :	The output pressure of compressor (kg/cm ²).

Data Availability

The data used to support the findings of this study are available from the corresponding author upon request.

Conflicts of Interest

The authors declare that they have no conflicts of interest.

Retraction

Retracted: Optimization Technique for Renewable Energy Storage Systems for Power Quality Analysis with Connected Grid

International Transactions on Electrical Energy Systems

Received 28 November 2023; Accepted 28 November 2023; Published 29 November 2023

Copyright © 2023 International Transactions on Electrical Energy Systems. This is an open access article distributed under the Creative Commons Attribution License, which permits unrestricted use, distribution, and reproduction in any medium, provided the original work is properly cited.

This article has been retracted by Hindawi, as publisher, following an investigation undertaken by the publisher [1]. This investigation has uncovered evidence of systematic manipulation of the publication and peer-review process. We cannot, therefore, vouch for the reliability or integrity of this article.

Please note that this notice is intended solely to alert readers that the peer-review process of this article has been compromised.

Wiley and Hindawi regret that the usual quality checks did not identify these issues before publication and have since put additional measures in place to safeguard research integrity.

We wish to credit our Research Integrity and Research Publishing teams and anonymous and named external researchers and research integrity experts for contributing to this investigation.

The corresponding author, as the representative of all authors, has been given the opportunity to register their agreement or disagreement to this retraction. We have kept a record of any response received.

References

- [1] R. Senthil Kumar, B. V. S. Acharyulu, P. K. Dhal et al., "Optimization Technique for Renewable Energy Storage Systems for Power Quality Analysis with Connected Grid," *International Transactions on Electrical Energy Systems*, vol. 2023, Article ID 4675421, 7 pages, 2023.

Research Article

Optimization Technique for Renewable Energy Storage Systems for Power Quality Analysis with Connected Grid

R. Senthil Kumar,¹ B. V. S. Acharyulu,² P. K. Dhal,³ Richa Adlakha,⁴ Sonu Kumar,⁵ C. Saravanan,⁶ and Krishna Bikram Shah⁷

¹Department of Electrical and Electronics Engineering, SRMIST, Kattankulathur-603203, Chengalpattu District, Tamilnadu, India

²Department of Electrical and Electronics Engineering, Lendi Institute of Engineering and Technology, Jonnada (village), Denkada Mandal, Vizianagaram 535005, Andhra Pradesh, India

³Department of Electrical and Electronics Engineering,

Vel Tech Rangarajan Dr.Sagunthala R& D Institute of Science and Technology, Chennai, Tamil Nadu 600062, India

⁴Department of Electrical and Electronics Engineering, Manav Rachna International Institute of Research and Studies, Faridabad, Haryana, India

⁵Department of Electronics and Communication Engineering, Koneru Lakshmaiah Education Foundation, K L Deemed to be University, Vaddeswaram, Guntur District, Andhra Pradesh-522302, India

⁶Department of Electrical and Electronics Engineering, J.K.K.Munirajah College of Technology, T.N.Palayam-638506, Erode Dt, TN, India

⁷Department of Computer Science and Engineering, Nepal Engineering College, Changunarayan, Bhaktapur, Nepal

Correspondence should be addressed to Krishna Bikram Shah; krishnabs@nec.edu.np

Received 22 September 2022; Revised 28 October 2022; Accepted 24 November 2022; Published 10 May 2023

Academic Editor: Nagamalai Vasimalai

Copyright © 2023 R. Senthil Kumar et al. This is an open access article distributed under the Creative Commons Attribution License, which permits unrestricted use, distribution, and reproduction in any medium, provided the original work is properly cited.

Power quality is the main problem with the power system network. Poor electricity quality may cause disruptions and financial challenges for consumers. Additionally, it could cause electronic gadgets to overheat, be damaged, or operate inadvertently. Transformers and other components of the power distribution system may also overheat and experience core saturation. This study investigates potential problems with the quality of the electricity in a photovoltaic linked power system. This paper suggests a new optimization method for day-ahead trading and control in DC microgrid power management (MG). The goal of the multiobjective optimization dispatch (MOOD) problem is to lower overall operational costs as well as the costs associated with power loss in efficient conservation systems and exhaust emission quantities such as nitrogen oxides, sulphur dioxide, and carbon dioxide. Using the weighted sum approach, the multiobjective optimization problem is reduced to a single optimization problem. The analytical hierarchy process (AHP) method is then used to calculate the weight coefficients while accounting for each objective function's preferences. Power balancing, high levels of renewable energy penetration, the most effective scheduling of battery charging and discharging, control of load curtailment, and the technical limitations of the system are all taken into account when evaluating the system's performance in both grid-connected and standalone operation modes. The ant lion optimizer (ALO) technique is taken into account to tackle MOOD, comparing the effectiveness of the proposed method to other well-known heuristic optimization techniques. The simulation's results demonstrate how effectively the proposed strategy can address the coordinated control and optimization dispatch difficulties. They also found that operating the MG system economically in grid-connected mode can save overall costs by roughly 4.70% compared to doing it in independent mode.

1. Introduction

In the aim of meeting the enormous requirement for electrical power in today's climate, hybrid renewable energy sources (or HRES) in conjunction with the grid connectivity are becoming more crucial [1–3]. This integration lessens environmental issues and the consumption of fossil fuels even further. In grid-connected systems, devices like battery energy storage systems (BESS), HRES, photovoltaic or the PV systems, and wind turbines are posing problems with the management of quality of power [4–6]. The underdeveloped or very less industrialized countries in Sub-Saharan Africa (SSA) face difficult obstacles when trying to make investments in renewable energy options because countering climate change issues brought on by excessive fossil fuel use comes with high initial costs. This is particularly true considering the region's modernisation. Nevertheless, other economic and environmental criteria are typically taken into account when constructing renewable energy systems [7–9].

Numerous environmental problems result from the production of energy using conventional techniques. One of the potential options for generating clean, effective energy is the fuel cell (FC), a novel renewable energy source. A mismatch between power generation as well as load power results in a departure from the required voltage and frequency in the power supply because renewable energy sources are unreliable [10]. A novel control method for the power flow regulation with the unified power flow controller (UPFC) in grid-connected hybrid renewable energy systems, like photovoltaic-wind, has been presented to address this issue. Distributed generation are DGs that produce power using renewable energy (DER). One of the DER systems with the highest promise is solar photovoltaic (PV), which uses just sunlight, a free and clean source of energy, to produce electricity. To avoid problems with power outages, the centralized power plant may need to boost the grid's reserve power as a result of the increased use of DER. In addition, the system may experience power quality problems as a result of the growing penetration level. Power quality is the most crucial component in power distribution systems. It is described as the utility's capacity to give customers steady, noise-free electricity. Electronic devices and parts of the electricity distribution system would be damaged by poor power quality because frequency variations would induce operation in undesirable areas. Higher DER penetration is necessary in order to produce more power. However, this also implies that there might be a load power mismatch at any time.

This paper is organized as different sections, which are literature review as Section 2, proposed work as Section 3, results and discussion as Section 4, and conclusions as Section 5.

2. Literature Review

Atom search optimization (or ASO) and a unified power flow controller (or UPQC) are recommended in conjunction with the HRES system to address these issues. A number of specialist power devices such as UPQC are used to efficiently

reduce PQ issues like voltage, current sag, swell, and total harmonic distortion. The UPQC will be driven by a fractional order PID controller using system parameters created using the ASO technique. The best results are obtained when the results are compared to the PI. The MATLAB/Simulink application is used to represent the test system [11]. This research presents an intelligent control technique for grid-connected hybrid power systems combining solar-based PV, the wind turbines along with the storage of battery power to attain the optimum power quality enhancement (OPQE). Within this suggested hybrid renewable energy sources (HRES) system, the unified power quality conditioner with active and reactive power (UPQC-PQ) is constructed with a fractional-order proportional integral derivative (FOPID) controller based on atom search optimization (ASO). The fundamental goal has been to control voltage while reducing the power loss and the total harmonic distortion (THD). The UPQC-PQ uses the ASO-based FOPID organiser to alleviate power quality (PQ) issues like sag, swell, disturbances, real and reactive power, and THD minimizations connected to voltage and current. The novel approach is presented in a variety of modes, including $PRES > 0$, $PRES = 0$, and simultaneous PQ reinforcement and RES power injection. The effectiveness of the suggested methodology is determined by comparing the results to those obtained utilizing earlier literature approaches, including PI controller, BBO, ESA, GSA, RFA, GA, and GWO. The model has now been made using the MATLAB and the Simulink work-based architecture [12]. The supply gap in Sierra Leone was addressed in [13] by using the multiobjective particle swarm optimization (MOPSO) method to size ten grid-connected hybrid cubes that were optimally distributed among photovoltaic (PV) modules, onsite wind turbines, and the biomass gasification plants with the sugarcane bags, battery energy storage systems (BESS), and the diesel generation systems as the optional power. In Kabala, which is a district in the Northern and Kenema District in Southern Sierra Leone, potential plant sites for PV, wind, and biomass were subjected to well-established methodologies for resource assessment. The ten hybrid modules underwent long-term analysis with the following goals in mind: reducing the probability of a deficient power supply, the diesel energy portion, the life span costs, and carbon dioxide (CO_2) emissions. Kabala area is the practical location for PV and the wind farm projects, according to generating capacity of 27.4 percentages and 31.7 percentages for PV and wind, respectively. The comparison of the optimal results across selected blocks for DPSP values of 0–50% identifies the most cost-effective and ecologically beneficial course of action that policymakers in Sierra Leone and the surrounding area could take in circumstances like these [13]. For the purpose of meeting the enormous requirement for electric power, hybrid renewable energy sources (HRES) connected to the grid has become far more significant. With this incorporation, the usage of fossil fuel is being progressively reduced, as are environmental issues. HRES in grid-connected systems, such as the solar (PV) systems, the wind turbines (WT), and the battery energy storage systems (BESS), are affecting the electricity quality. Black widow optimization (BWO) with distributed

power flow controller (DPFC) has been suggested as a solution to these problems in the HRES system. One of the many bespoke power devices, including DPFC, is useful in reducing PQ problems such as voltage and current sagging, swell, total harmonic disturbances, and shattered order. The BWO approach is used to create the control parameters for the DPFC, which is driven by a PID controller. The analysis produced the greatest findings when it was compared to different techniques, including PSO, BWO, and GA. Software called MATLAB/Simulink is used to simulate the test system [14]. This research suggests an effective method for managing the power flow of hybrid renewable energy systems coupled with smart grid systems. The suggested method in this case combines the MEHOTSA tabu search algorithm with the modified elephant herding optimization technique. In the suggested technique, the evaluation process is carried out to identify the appropriate control commands for such architecture as well as to create the switching pulses datasets for the standalone approach while taking into account the power disparity in between generator and the load sides. The multiobjective functions are built using the reactive and active power categories generated for the grid depending upon the source power that seems to be easily obtainable. The finished dataset is used to hasten the completion of the control operation by running the Tabu search algorithm online. The recommended technique-based modeling approach enhances the power operator's system parameters in the context of the various power flow kinds. The power flow management within the smart grid system is managed depending on the power supply and load side parameter variants by using the proposed approach. The suggested technique is also in charge of managing the energy sources to generate the required amount of electricity for the grid, making best use of both energy storage devices and renewable energy sources. Finally, the performance of the suggested model is evaluated in comparison to alternative methods using the MATLAB/Simulink platform [15]. The voltage stability of the grid-connected FC is improved in this study using boost converters, a 25-level cascaded H-bridge (CHB) multilevel inverter (MLI), and traditional PID controllers. Two PID controllers had been used to control the MLI linked to the grid for controlling the point of common coupling (PCC) voltage between the FC and the grid. The PID optimizers are tuned for dynamic processes using traditional evolutionary techniques like particle swarm optimization (PSO) and squirrel search algorithm (or SSA). An improved squirrel search algorithm (ISSA) has indeed been suggested in this study to significantly improve the convergence speed of computation and precision of the traditional methodologies used. This article's grid-connected power network was created in the MATLAB and Simulink environment. To evaluate the efficiency of the suggested controller, the systems also are subjected to a number of demanding voltage sag and swell situations. The development of the voltage profile, the enhancement of the power quality, and the shorter execution time of the suggested ISSA approaches have been featured in a full comparison with the traditional PID, PSO, SSA, and ISSA techniques. The results show how

the suggested strategy outperforms the conventional ones in the aspects of better dynamic voltage responsiveness, increased power quality, and decreased harmonics. Total harmonic distortion (THD) analysis is utilized to determine the power quality indicators. The numbers obtained validate the proposed controller's real-time implementation because they are well within the IEEE-547 indices [16]. The suggested control method combines a recurrent neural network and the binary version of the grey wolf optimization (bGWO) (RNN). The dataset of control signals for the UPFC's shunt and series converters is produced here using bGWO. The RNN approach executes and forecasts the ideal control signals of the UPFC based on the completed dataset. Similar to this, suggested control strategy reduces power losses while controlling voltage variation. The suggested model is then put into practice in the working stage of Matrix Laboratory and Simulink, and the effectiveness of the execution is evaluated using current approaches, including fuzzy logic controller, improved particle swarm optimization, and grey wolf optimization. Analysis is also done on the suggested and the existing techniques' optimal gain parameters and elapsed times. The suggested hybrid technique's optimum gain parameters, such as $K_p K_i$, are 2.5 and 150. The suggested methodology took 30.15 seconds to complete. Overall, the comparison findings show the suggested technique's superiority and prove its ability to resolve the aforementioned issues [17].

3. Proposed Work

Multiple MGs are used in the proposed architecture's design. For the purpose of measuring the power flow in a specific MG, the separate MGs are deployed with an SM. Let us say, created MMG configuration consists of six MGs, denoted as MG1, MG2, MG3, MG4, MG5, and MG6, and the six matching SMs, denoted in the form of SM1, SM2, SM3, SM4, SM5, and SM6. The utility grid (UG) and MGs are shown in Figure 1's representation of the system.

An MG is made up of RES like solar and wind energy along with battery storage. Grid-connected or island-based modes can meet consumer demand. Each MG is connected to an electricity line heading toward the UG and an information line coming from the SM. The information stream coming from SMs is getting closer to the central controller. A multiple stage unique EMS is used to carry out the suggested MMG. Predicting the MG's operating mode comes first, then managing energy in islanded mode, and ultimately, updating the MG status for precise operation mode predictions utilizing future states. The unique entities known as SMs are able to track and produce precise values of the power flow. Such parameters enable the control and administration of energy. The central controller collects the fluctuations in electricity output and consumption on each MG for use in making decisions. The MGs are operated in accordance with the central controller's judgment. On the other side, MG status is tracked in order to forecast MG state in the future. The efficient management of energy is ensured by the precise assessment of the operation mode. It is suggested to use the innovative three-stage RES-GRID to

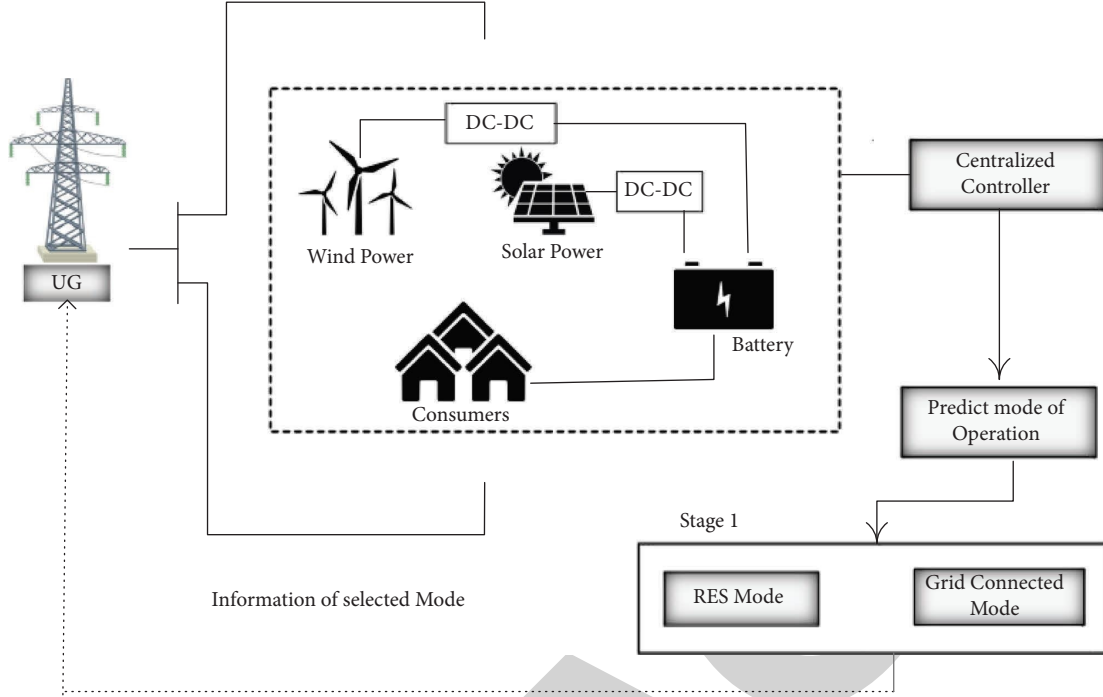


FIGURE 1: Proposed RES-GRID model.

control energy effectively through wise mode selection and power exchange. Grid-connected modes as well as islanded modes are the two categories under which operation modes in MMG are categorized. A form of operation for islands, the self-electrical sources that MG is intended to have, are utilised to meet consumer demand. Due to the usage of renewable resources, electricity generation in this mode is not constant. Renewable energy resources like wind power and the solar energy are dependent on the nature and cannot supply electricity continuously. Since it continuously and autonomously creates the same quantity of electricity, the grid-connected operation mode differs from the islanded mode. Here, the weather has a big impact on how much power MGs can generate. Neural networks (NNs) are concerned about the analysis of climatic variables nearby the MG in order to precisely anticipate the mode.

At this stage, the meteorological data for each MG is extracted, and each is assigned an operation mode. Since wind and solar power are used in this application, the corresponding weather variations include wind speed and the light intensity. Generally, the measurements of monochromatic radiation's frequency are used to quantify light intensity. Let L represent the expected light level at time t . As shifting seasons additionally have an impact on solar activity, it is anticipated that this investigation will make use of luminance measurements taken throughout the summer months. Then, perhaps the wind speed is considered for the wind turbine's renewable resource. Traditionally, height of the turbine hub is used to differentiate the wind speed. Depending on the wind turbine's elevation, the air's density varies. W should represent the wind speed at time T . Ambient limitations are incorporated into NN to determine the operating mode.

The operation of human brain neurons is mimicked in a machine learning system known as NN. The back-propagation algorithm-based NN structure is made up of the structures of the input, hidden neurons, and output neurons. The input layer's neurons are interconnected with the hidden layer's neurons, and all of the hidden layer's neurons are connected to the output layer's neurons. The suggested NN works well when dealing with difficult decision-making problems. Let links be the means by which the succeeding layers of neurons are connected, with M and N being two neurons and their individual weights being $w_{(i,j)}$. An activation function is then used to convert the information needed to calculate the weighted sum from propagation functions into an input for the subsequent layer. Thus, the input from MG_1 is given as net_{MG_1} , consider $M = \{i_1, i_2, i_3, \dots, i_n\}$. With this, propagation function is demonstrated as

$$NET_{MG_1} = F_{Pro}(O_{i1}, O_{i2}, \dots, O_{in}, W_{i1,j}, W_{i2,j}, \dots, W_{in,j}). \quad (1)$$

The proliferation purpose F_{Pro} is composed of subjective values and results from other levels and is denoted by $(o_{i1}, o_{i2}, \dots, o_{in})$. Individual neurons are multiplied by the weight $w_{i,j}$ to anticipate the weighted sum. Whenever it exceeds the threshold value, the activation function is employed to stimulate the neurons. In this case, the activation function is defined as, where I is the threshold of the i th neuron.

$$A_i(t) = F_{act}(net_i(t), A_i(t-1), \Theta_i). \quad (2)$$

F_{act} (activation function) $A_i(t-1)$ stands for the former activation state, that is, changed into $A_i(t)$, which is the new activation state, and signifies the activation function. In

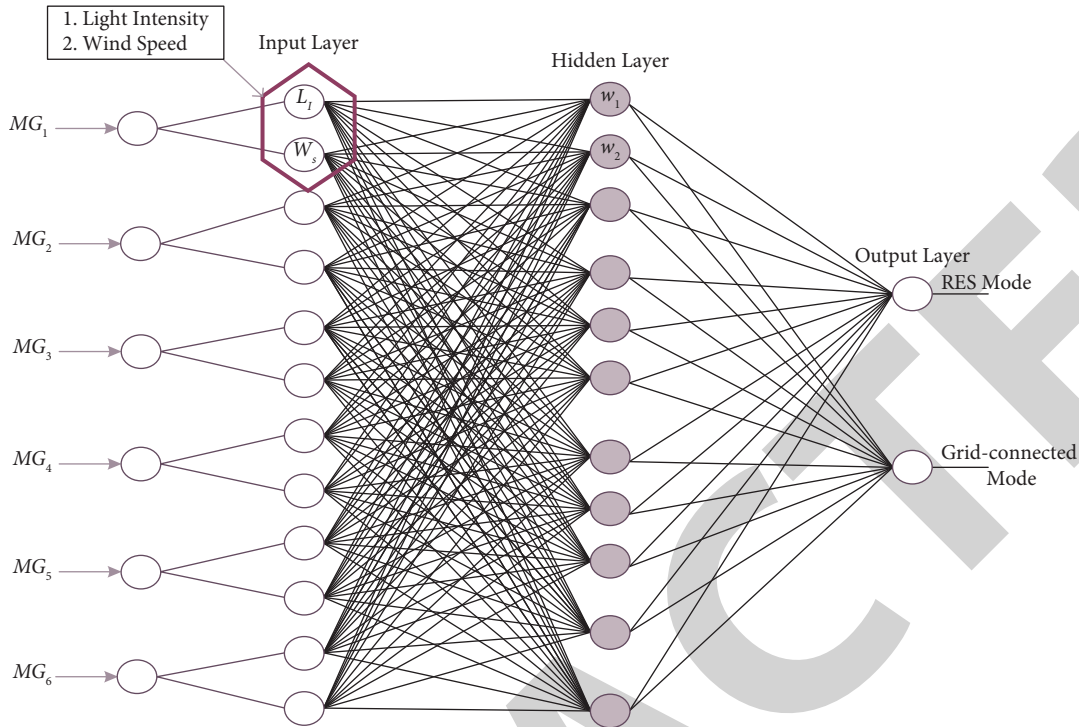


FIGURE 2: Neural network structure for mode selection.

order to improve output accuracy, the neurons in the NN are given the capacity to fine-tune the connection's standard. The operation mode of the neural network is decided upon using training samples made up of various LI as well as WS values. On the other hand, stage 3's evaluation of future state guarantees correct operation selection prediction. Given that MGs are dispersed across the environment, it is important to take into account the major RES restrictions while determining their mode of operation. Additionally, since their ability to produce power is dependent on natural resources, light intensity as well as the wind speed has to be taken into account when determining how they will operate. Poor weather conditions tend to restrict productivity, which manifests in the unmet needs of the customer. In this scenario, the MGs are run in grid-connected mode until a specific range of RES production is reached. The islanded MG is then transferred to stage 2 processing shown in Figure 2.

4. Results and Discussion

The suggested RES-GRID performance is validated in this section by creating it with the proper programming. Comparative results and the simulation environment make up this section's two subcategories. MATLAB Simulink is used to investigate the proposed RES-GRID model. This software is a graphical programming environment with a focus on creating dynamic RES networks. The three stages for processing of mode identification, energy conservation, and future state prediction in MatlabR2017b suits well for the creation of RES-GRID. Integrated on the Windows operating system is MatlabR2017b.

TABLE 1: Simulation setup.

Parameters	Specifications	
Number of PV	5	
Number of microgrids	5	
Wind mills count	5	
Simulation time	200 s	
Renewable energy capacity	Battery	150 kW
	Wind	60 kW
	PV	60 kW
External grid	200 kW	
Mode of operation	Islanded/grid-connected	

The presented RES-GRID specifications are listed in Table 1 and are taken into account in our layout. These restrictions do not stop there; the modeled RES-GRID is made up of six microgrids, each with a different load. The controller chooses their operational mode based on their production. Mode prediction, energy management, and power exchanges are used to carry out three-stage measurements based on these parameters. In island mode, energy management is focused. Figure 3 shows fluctuation rate and grid-connected mode.

Figure 4 shows about RES mode and grid-connected mode. The suggested approach also functions well in aspects of convergence rate and duration, taking less time and iterations to resolve to the global optimal solution. Additionally, it should be noted that each optimization algorithm has a maximum iteration constraint of 200 and a population restriction of $Np = 40$. In conclusion, we believe that using the ALO algorithm to resolve the overall objective function significantly reduces the overall cost and validates the

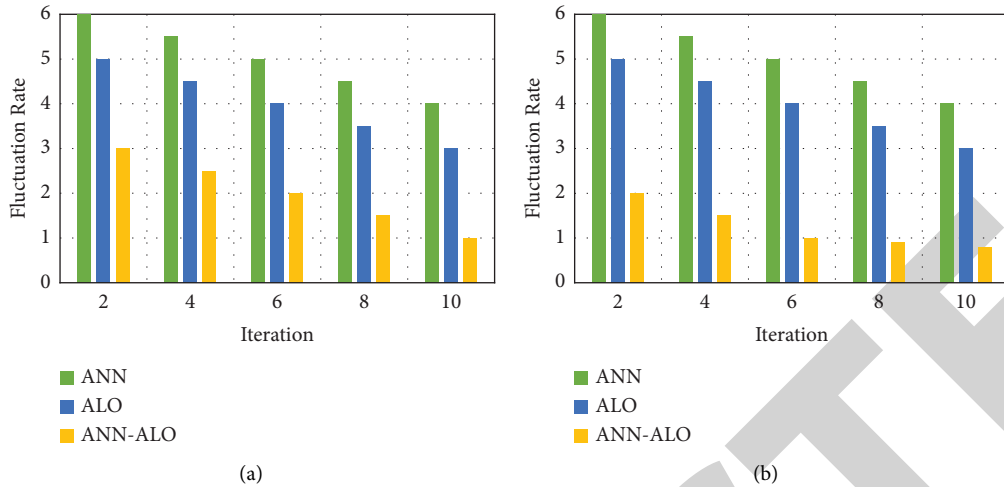


FIGURE 3: Fluctuation rate. (a) RES mode and (b) grid-connected mode.

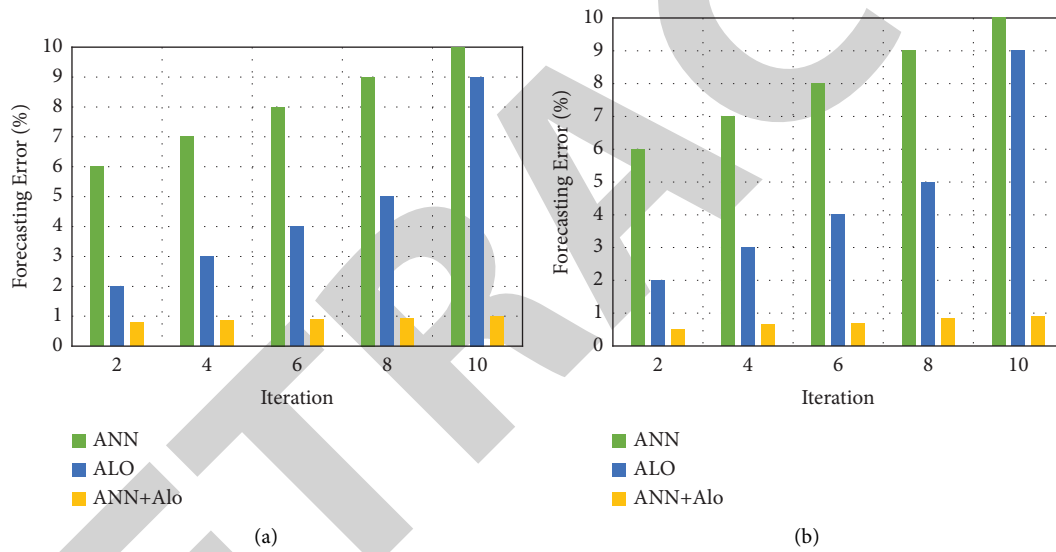


FIGURE 4: Forecasting error (%). (a) RES mode and (b) grid connected mode.

effectiveness of the strategy for managing the MOOD problem of the investigated MG.

The ant lion optimizer (ALO) algorithm, a new optimization technique, is used in this article to address a number of electrical power system issues, such as the reduction of fuel costs, the reduction of active and reactive power losses, the coordination of overcurrent relays, the improvement of the performance of brushless DC wheel motors, and the improvement of the efficiency of isolated protection transformers. The ALO algorithm gives better outcomes and convergence capability for the electrical power system problem when compared to the firefly algorithm and particle swarm optimization. Several optimization techniques were used to address problems with the electrical power supply. The recently published ant lion optimizer (ALO) algorithm is used in these studies to address power system problems. The ALO algorithm was devised in 2015 by Seyedali Mirjalili. The suggested method has a very high rate

of convergence and only needs a few parameter adjustments. As a result, it can be used to solve both restricted and unrestricted optimization techniques. When analyzing weaknesses in power systems, the ALO algorithm performs effectively. Results show how effective the suggested algorithm is by contrasting the competitive advantages of the ALO algorithm to those of other techniques.

5. Conclusion and Future Work

In this study, we introduced a unique energy management system for the day-ahead optimal power management and the control of an MG, comprising of several distributed generator types, including solar arrays, wind turbines, diesel generators, microturbines, fuel cells, and battery storage systems. The suggested EMS is built with a two-layer architecture, using an ant lion optimizer algorithm to handle the multiobjective optimization dispatch problem as well as

Retraction

Retracted: Short-Term Load Monitoring of a Power System Based on Neural Network

International Transactions on Electrical Energy Systems

Received 28 November 2023; Accepted 28 November 2023; Published 29 November 2023

Copyright © 2023 International Transactions on Electrical Energy Systems. This is an open access article distributed under the Creative Commons Attribution License, which permits unrestricted use, distribution, and reproduction in any medium, provided the original work is properly cited.

This article has been retracted by Hindawi, as publisher, following an investigation undertaken by the publisher [1]. This investigation has uncovered evidence of systematic manipulation of the publication and peer-review process. We cannot, therefore, vouch for the reliability or integrity of this article.

Please note that this notice is intended solely to alert readers that the peer-review process of this article has been compromised.

Wiley and Hindawi regret that the usual quality checks did not identify these issues before publication and have since put additional measures in place to safeguard research integrity.

We wish to credit our Research Integrity and Research Publishing teams and anonymous and named external researchers and research integrity experts for contributing to this investigation.

The corresponding author, as the representative of all authors, has been given the opportunity to register their agreement or disagreement to this retraction. We have kept a record of any response received.

References

- [1] D. Yang, "Short-Term Load Monitoring of a Power System Based on Neural Network," *International Transactions on Electrical Energy Systems*, vol. 2023, Article ID 4581408, 10 pages, 2023.

Research Article

Short-Term Load Monitoring of a Power System Based on Neural Network

Di Yang 

State Grid Hebei Marketing Service Center, Shijiazhuang, Hebei 050000, China

Correspondence should be addressed to Di Yang; 164304427@stu.cuz.edu.cn

Received 11 August 2022; Revised 23 October 2022; Accepted 24 November 2022; Published 6 April 2023

Academic Editor: Nagamalai Vasimalai

Copyright © 2023 Di Yang. This is an open access article distributed under the Creative Commons Attribution License, which permits unrestricted use, distribution, and reproduction in any medium, provided the original work is properly cited.

In order to improve the accuracy of power load forecasting, this paper proposes a neural network-based short-term monitoring method. First, the original energy load signal is decomposed by the CEEMDAN algorithm to obtain several eigenmode function components and residual components; several eigenmode function components and residual functions are fed into the NARX neural network for computational purposes. The partial hypothesis is superimposed in the following part to obtain the final short-term forecast. According to the test results, the MAPE of the CEEMDAN-NARX model is 4.753%, 3.540%, and 0.343% lower than the SVM, RNN, and NARX models, respectively, and 3.741% and 2.682% lower than CEEMDAN-SVM and CEEMDAN-RNN, respectively. The MAPE and RMSE of the CEEMDAN-NARX model are 0.765% and 101.7 MW, respectively, which are 0.468% and 45.2 MW lower than NARX models, respectively. Compared to CEEMDAN-SVM, the MAPE of CEEMDAN-NARX and CEEMDAN-RNN decreased by 0.986% and 0.692%, respectively, and the RMSE of CEEMDAN-NARX decreased by 111.5 and 65.7 MW, respectively, compared to CEEMDAN-SVM. Conclusion is that the load forecasting model based on the combination of CEEMDAN algorithm and NARX neural network can effectively connect, reduce the negative impact of noise on forecasting results, and improve forecasting accuracy.

1. Introduction

The rapid development of smart grids is important for the sustainable development of the entire business community. The successful deployment of smart grids projects has a positive impact on the energy sector. At the same time, the needs of the electricity industry for the power grid are gradually improving. The operation of the power system needs to be safe and stable in order to provide a guaranteed power environment for industrial production and residents' lives. However, there are difficulties in the phased generation, transmission, consumption, and direct storage of a large amount of electric energy in the power system, which leads to a large waste of power resources that cannot be consumed in social production and life, causing serious environmental pollution and instability of the power system. The accuracy of short-term power load forecasting can provide guarantee for the safe and stable operation of the power system and help power companies to arrange

production and distribution plans according to the actual power load, thus reducing waste. In addition, the electrical equipment shall be inspected and maintained in a planned way to provide safety guarantee for the sustainable production of electric power. Therefore, it is necessary to strengthen the load monitoring and planned distribution of electric power enterprises. Among them, short-term power system load forecasting is one of the important studies of the power system [1]. In order to achieve the accuracy and efficiency of short-term power load forecasting results, it is necessary to consider many factors that affect power load forecasting. However, in the process of power load forecasting, in addition to the internal factors that can be controlled, it will also be affected by uncontrollable external factors, resulting in inaccurate forecasting. With the rapid development of artificial intelligence technology, the neural network model has been widely used in the field of power, and more and more researchers have applied it to short-term power load forecasting. Because it has adaptive and

nonlinear adaptive ability, it can solve the power load forecasting problem under the influence of complex factors [2]. The main driving factors of power load include social production, residents' life, and meteorological factors. Due to the uncertainty of social production, life, and meteorological factors, it is necessary to consider the combination of external factors when carrying out effective, accurate, and reliable short-term power load forecasting. For example, the meteorological factor temperature, in summer and winter, human production, and life need high-energy consumption power equipment for refrigeration or heating, so the power load consumed is far greater than that in other seasons [3]. When energy load data is collected, problems such as electrical equipment failure, meter failure, and signal interference can cause abnormal or incomplete data, resulting in biased short-term energy load forecasting. Therefore, the data needs to be preprocessed. In summary, the results of short-term energy load forecasting are important for all areas of human society. However, in order to achieve accurate prediction results, it is necessary to create an effective short-term energy load forecasting model by combining artificial intelligence technology, energy load forecasting features, and load influencing factors [4]. Power load forecasting can be understood as statistical analysis of the change trend of historical power load, and the change law obtained in the analysis process can be used in the future power load forecasting research. Theoretically, power load forecasting is used to explore the balance between different forecasting methods, power load data, and power load influencing factors.

2. Literature Review

Tang et al. proposed a short-term energy load forecasting method based on support vector regression (SVR). This method uses a special selection process for automatic input model selection and an optimization mechanism for SVR superparameter optimization, which reduces operator interaction. The experimental results confirm the effectiveness of this method. In the literature, a short-term load forecasting model based on empirical mode decomposition (EEMD) and segmented particle optimization (SS-PSO) was proposed to predict ultra-short-term energy loads, with the results being effective [5]. Guo et al. proposed an improved hybrid power load forecasting method that combines the least squares algorithm, Kalman filtering algorithm, and chaotic Kalman filtering algorithm and uses different weighting methods to optimize the short-term power load forecasting model [6]. Liang uses an improved support vector machine (SVM) method, and using the nonlinear relationship between load forecasting and load impact parameters, to establish holiday and non holiday power load forecasting models, and achieves short-term power load forecasting. With the development of the Internet of things and smart meter technology, researchers have introduced deep learning based on the Internet of things to get the characteristics of the data received and accurately predict the future before load values [7]. Guo and others have proposed machine

learning-based predictive modeling. This method uses a small amount of data to estimate power consumption patterns and peak operating times. Experimental results show that this algorithm can save 0.62–2.28 percent of energy costs compared to other traditional energy estimation methods [8]. Yang et al. proposed an optimal method of speed estimation based on Gaussian process quantile regression (GPQR) and applied it to smart grid [9]. Zhou et al. proposed a nonparametric kernel regression method to estimate energy [10]. Su et al. used dynamic neural networks to predict daily energy consumption to manage production and social life and to increase the efficiency of energy systems [11]. Demirdelen et al. proposed an improved postpropagation neural network based on technology decomposition and pollination-optimization for short-term forecasting [12]. Guo et al. proposed a hierarchical neural model with a time window and used it to predict long-term energy [13]. Xie et al. proposed a hybrid forecasting model combining flight path optimization (FOA) and the general regression neural network for energy load estimation [14].

Regarding the reduction of the accuracy of power load forecasting caused by the time change of energy load and noise, this paper presents a short model of forecasting based on the combination of CEEMDAN algorithm and NARX neural network. The CEEMDAN algorithm decomposes the original power load signal into different components, which effectively suppresses noise and reduces errors, and solved the time-varying problem using NARX neural network dynamics and feedback.

3. Research Methods

3.1. Power Load Forecasting Method. The initial development period of power load forecasting technology was in the 1960s. At that time, the economic development of the world was in the initial stage, and the demand for electricity also increased, which led to the development and expansion of the entire power system, and load forecasting also got preliminary development.

Traditional forecasting methods use the collected power load time series data to find out the law of power consumption and make a guiding method for power load forecasting. Traditional prediction methods include trend extrapolation, regression analysis, and time series.

Although the classical forecasting method is simple and easy, the accuracy of forecasting is difficult to meet the requirements and theoretical research such as artificial neural network (ANN), wavelet transform (wavelet transform), fuzzy logic (FL), and combined estimates.

The short-term power load is greatly affected by economy, weather, politics, and other uncertain factors, and there are periodic changes within a year. Therefore, in short-term load forecasting, it is necessary to comprehensively consider various influencing factors and understand their periodicity. Generally speaking, the basic steps of short-term load forecasting are as follows:

First, we formulate a prediction plan according to the prediction purpose. We fully understand the content and purpose of load forecasting and analyze its nature. The load characteristics of different regions, different times, and different power grids are different.

Second, data should be collected. The main research object of power load forecasting is historical data. The selection of sample data will directly affect the effect of load forecasting. In addition, the work of sorting out data is also very important. For the missing values and abnormal values in the sample data, appropriate methods should be selected to deal with them to ensure the reliability of the data.

Third, we choose prediction methods and build prediction models. Through the analysis of historical load data, according to the advantages, disadvantages, and applicability of different load forecasting methods, we select the appropriate forecasting method and establish the model on this basis. Establishing a model is a crucial step in load forecasting. After the model is established, the optimal parameters are found by adjusting parameters.

Fourth, we take the prediction and analyze the prediction error. The prediction results are generated from the defined prediction model and the measurement model, and the error of the prediction is analyzed. The difference between the estimated value and the actual value can be taken as the final result if it is within the specified range. If the difference between the estimated value and the actual value is large, various parameters of the model are adjusted and readjusted until the forecast is achieved.

Fifth, we look into the summary and reflection. After getting the prediction results, through analyzing the prediction error and comparing the performance of various methods, this paper summarizes the success and shortcomings of load forecasting and looks forward to the next research content.

3.2. CEEMDAN Algorithm Principle

3.2.1. EMD Algorithm and Its Improved Algorithm. The Empirical Mode Decomposition (EMD) algorithm can transform linear and nonstationary systems into linear and steady-state functions (IMFS). EMD has the advantages of efficient and complete conversion, but poor conversion affects the actual decomposition of EMD. By improving the EMD algorithm, we can obtain empirical mode decomposition (EEMD) and all ensemble empirical mode decomposition (CEEMD) algorithms. The EEMD algorithm optimizes the existing problems of EMD, reduces the conversion error of the upper and lower envelopes, makes the local effect of abnormal signals, and thus changes the mode EMD, but the residual noise remains to be the signal. The CEEMD algorithm adds positive and negative white noise to the original signal and each EMD signal and finally gives the calculated result. The CEEMD algorithm can save

the calculation time and remove the noise from the IMF components. It not only solves the problem of modal aliasing but also accurately reconstructs the original signal. However, if the parameters are improperly selected, wrong components will be generated, resulting in the components that do not meet the definition of IMF components [15].

In essence, the solution process of empirical mode decomposition algorithm is a “screening” process, from which the eigenmode function with high frequency to low frequency is obtained, and finally, there is a monotonic residual sequence that can no longer be decomposed, which is also known as trend term.

IMF must meet the following two qualifications:

- (1) The number of maximum and minimum points of the whole data must be equal to or no more than the number of points passing through the origin.
- (2) The mean value of the upper and lower envelopes generated by the maximum and minimum values of the whole data is zero.

The specific stages of the EMD algorithm decomposition are as follows:

- (1) The upper and lower envelopes and the middle envelope $m_1(t)$ use the cubic spline interpolation method based on the maximum and minimum values of the original signal.
- (2) The intermediate signal is the difference between the original signal and the mean envelope to judge whether the intermediate signal meets the conditions of IMF. If the intermediate signal conforms to the assumption of eigenmode function, the first IMF component is obtained. If the limiting conditions are not met, the intermediate signal needs to continue the previous step 1 to obtain the mean envelope $m_2(t)$ and then obtain a new intermediate signal and so on; until the intermediate signal meets the conditions, it is recorded as imf_1 .
- (3) After obtaining imf_1 , we use the original signal to subtract imf_1 to obtain a new original signal and then perform the previous steps 1 and 2 on the new original signal to obtain imf_2 . We repeat steps 1–3 mentioned above until no new IMF component can be generated and the decomposition process is over.

3.2.2. CEEMDAN Algorithm. Aiming at the problems of EEMD algorithm and CEEMD algorithm, this paper uses the CEEMDAN algorithm to process power load signal. CEEMDAN is an improvement based on EMD and EEMD algorithms.

The CEEMDAN algorithm adds adaptive white noise in each decomposition stage, so that the reconstruction error tends to zero. The CEEMDAN algorithm can not only eliminate the mode aliasing in EMD by adding adaptive noise but also solve the nonstationary problem of the signal by decomposing the load signal into components of different frequencies. The steps of the CEEMDAN algorithm are as follows:

- (1) The power load signal set containing white noise is generated as follows (1):

$$x^i(t) = x(t) + w^i(t), \quad (1)$$

where $w^i(t)$ ($i = 1, 2, \dots, I$) is the noise satisfying the Gaussian distribution, and I is the total number of samples in the power load signal set [16].

- (2) We perform EMD on $x^i(t)$ to obtain the first-order component IMF_1^i of each sample and take its mean value as the first-order IMF component of $x(t)$, that is, the following formula:

$$\widetilde{\text{IMF}}_1(t) = \frac{1}{I} \sum_{i=1}^I \text{IMF}_1^i. \quad (2)$$

- (3) We calculate the first-order residual quantity and the second-order component. The expressions of the first-order residual quantity and the second-order component are, respectively, as follows :

$$r_1(t) = x(t) - \widetilde{\text{IMF}}_1(t), \quad (3)$$

$$\widetilde{\text{IMF}}_2(t) = \frac{1}{I} \sum_{i=1}^I E_1\{r_1(t) + \varepsilon_1 E_1[w^i(t)]\}, \quad (4)$$

where $E_i(\cdot)$ represents the i -order IMF component of the signal, and ε_i is the parameter controlling the white noise energy.

- (4) The expressions for calculating the k ($k = 2, 3, \dots, K$) (K is the highest order of the IMF component) order residual, the $k+1$ order IMF component, and the $k+1$ order IMF component are as follows:

$$r_k(t) = r_{k-1}(t) - \widetilde{\text{IMF}}_k(t), \quad (5)$$

$$\widetilde{\text{IMF}}_{k+1}(t) = \frac{1}{I} \sum_{i=1}^I E_1\{r_k(t) + \varepsilon_k E_k[w^i(t)]\}. \quad (6)$$

- (5) We repeat step 4 until the residual cannot be decomposed again, and the judgment standard is that the number of extreme points of the residual is at most 2. If the residual satisfies the following equation:

$$R(t) = x(t) - \sum_{k=2}^K \widetilde{\text{IMF}}_k(t), \quad (7)$$

then the original signal of power load is finally decomposed into the following formula:

$$x(t) = \sum_{k=2}^K \widetilde{\text{IMF}}_k(t) + R(t). \quad (8)$$

3.3. Training of NARX Neural Network. The NARX neural network is a dynamic neural network with memory and feedback functions, which can store historical load data and calculate it together with future load data. Therefore, the network has dynamic performance and is not easy to lose information [17]. The tasks of prediction and classification, the one-dimensional and two-dimensional prediction of highly nonlinear relations, and nonlinear classification boundaries that can be achieved by the multilayer network are completed by the nonlinear excitation function in the hidden neuron. The weight of the network controls the characteristics of the nonlinear excitation function. The training starts to adjust continuously when it contacts the weight characteristics, so that the excitation function can gradually approach the expected response, and the process of the network prediction error gradually falling below the specified error threshold is called network learning. The typical NARX neural network structure is shown in Figure 1.

The steps of network training are as follows:

- (1) We set neural network parameters. The parameters to be set include the number of training steps of neural network, transfer function f of hidden layer, transfer function g of output layer, and learning rate η .

- (2) We calculate the output of the hidden layer. The expression of the output is as follows:

$$H_j = f\left(\sum_{i=1}^n \omega_{hj} x_h(t) + \sum_{s=1}^m \omega_{sj} x_s(t) - a_j\right), j = 1, 2, \dots, l. \quad (9)$$

- (3) We calculate the output of the output layer. The expression of the output is as follows:

$$y_v = g\left(\sum_{j=1}^l H_j \omega_{jv} - B_v\right), v = 1, 2, \dots, m. \quad (10)$$

- (4) We calculate the error value. The expression of the error is as follows:

$$e = \frac{1}{2} \sum_{v=1}^m e_v^2, e_v = o_v - y_v(t). \quad (11)$$

- (5) We calculate the weight. The relevant expression is as follows:

$$\omega'_{hj} = \omega_{hj} + \eta H_j x_h(t) \sum_{v=1}^m \omega_{jv} e_v, h = 1, 2, \dots, n, \quad (12)$$

$$\omega'_{sj} = \omega_{sj} + \eta H_j y_s(t) \sum_{v=1}^m \omega_{jv} e_v, s = 1, 2, \dots, m, \quad (13)$$

$$\omega'_{jv} = \omega_{jv} + \eta H_j e_v. \quad (14)$$

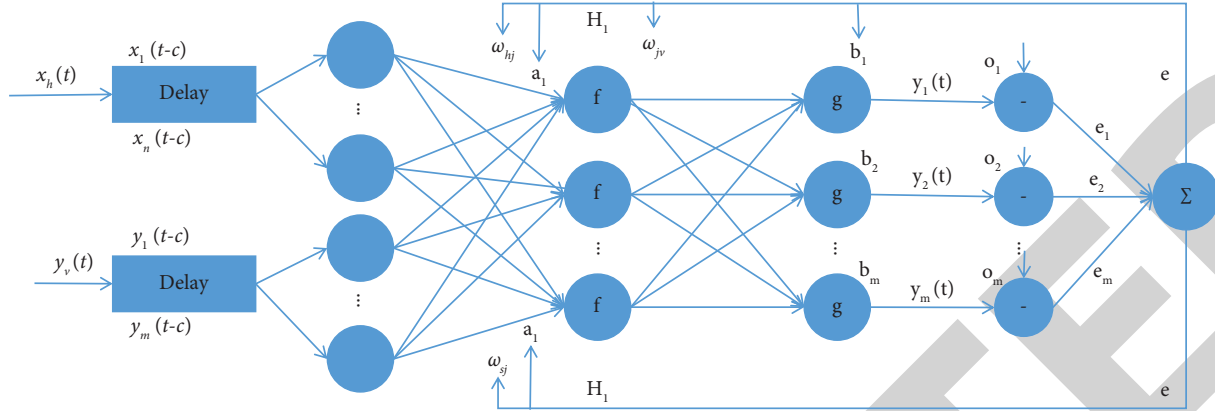


FIGURE 1: Typical NARX neural network structure.

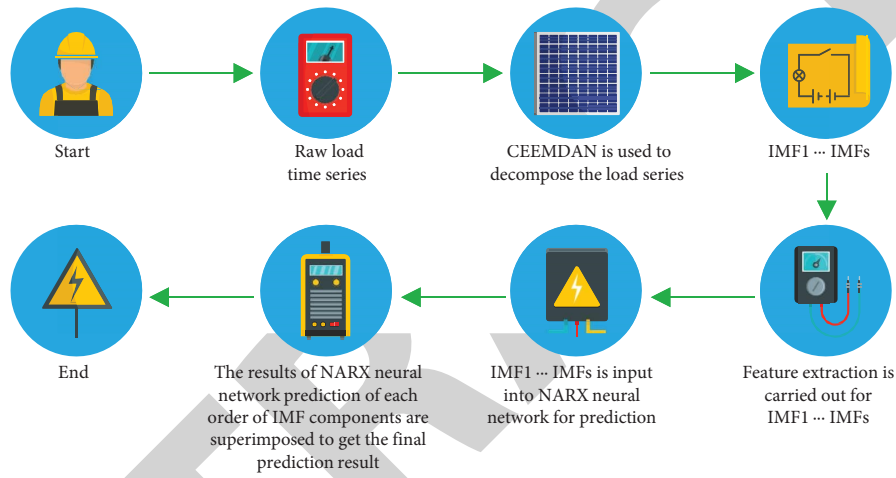


FIGURE 2: Short-term load forecasting process based on the CEEMDAN algorithm and NARX neural network.

- (6) We calculate the threshold. The relevant expression is the following formula:

$$a'_j = a_j + \eta H_j \sum_{v=1}^m \omega_{jv} e_v, \quad (15)$$

$$b'_v = b_v + e_v. \quad (16)$$

- (7) We set the number of iterations as the number of hidden layer neurons to judge whether the iteration is over, if not, we return to step 2 to continue the iteration. If the iteration ends, we complete the training.

3.4. Short Term Load Forecasting Model Based on CEEMDAN Algorithm and NARX Neural Network. NARX neural network-based CEEMDAN algorithm and short-term load prediction model CEEMDAN algorithm is used to process the initial energy load signal, obtain several species and residues, extract the sequence and characteristics of each residue, and then subtract them. The features of each order and more are fed into the NARX neural network for prediction. The NARX neural network handles feedback

efficiently, and the output is a function of the historical data and the current input. The NARX neural network is capable of feedback, delay, memory storage, and integration with historical data, so the predictive model can adapt to changes over time signal load [18]. Figure 2 shows the short bootstrap process based on CEEMDAN algorithm and NARX neural network.

Figure 2 shows that the NARX neural network parameters, the number of layers, and the latency affect the accuracy of the prediction model. The input and output process vector dimensions are set to 4 and 1, respectively, depending on the nature of the external input and prediction. The structure of the NARX network is shown in Figure 3.

4. Result Analysis

4.1. CEEMDAN Algorithm Is Used to Process the Original Signal of Power Load. The original power load signal in this paper is selected from the 88 day power load data of a city in Hebei Province, China, as shown in Figure 4. The sampling period in Figure 4 is 30 min, and the total number of samples is 4416.

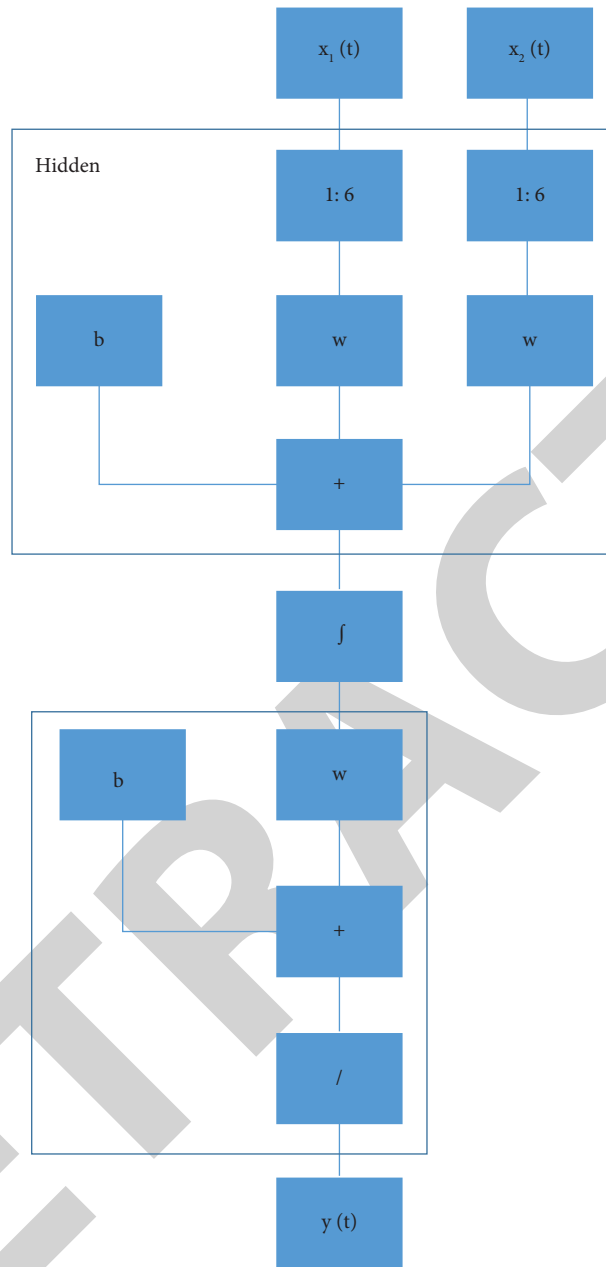


FIGURE 3: NARX network structure constructed.

Power load signals not only have linear and non-stationary problems but in an increasingly complex power environment, many factors can make power load signals unstable. Therefore, linear and nonstationary electrical load signals need to be linearized and stabilized using the CEEMDAN algorithm [19]. The energy load signal can be decomposed into IMF components and residual components in order of frequency, and the complex signal can be decomposed into a problem, and more physically meaningful frequencies that can be obtained are distinguished by

different types of linear and nonstationary between signals. The energy load signal was decomposed by the CEEMDAN algorithm, and the results are shown in Figure 5(a) and 5(b).

After the decomposition of the CEEMDAN algorithm, 11 IMF components and 1 residual component are obtained. The decomposed material and the rest are 88 days of data, from which Saturday and Sunday's data are extracted to make 12 groups of weekend's data. Data from the first holiday group is used for feature extraction. The average of 10 groups of data is used as training to estimate the final group of holiday's data

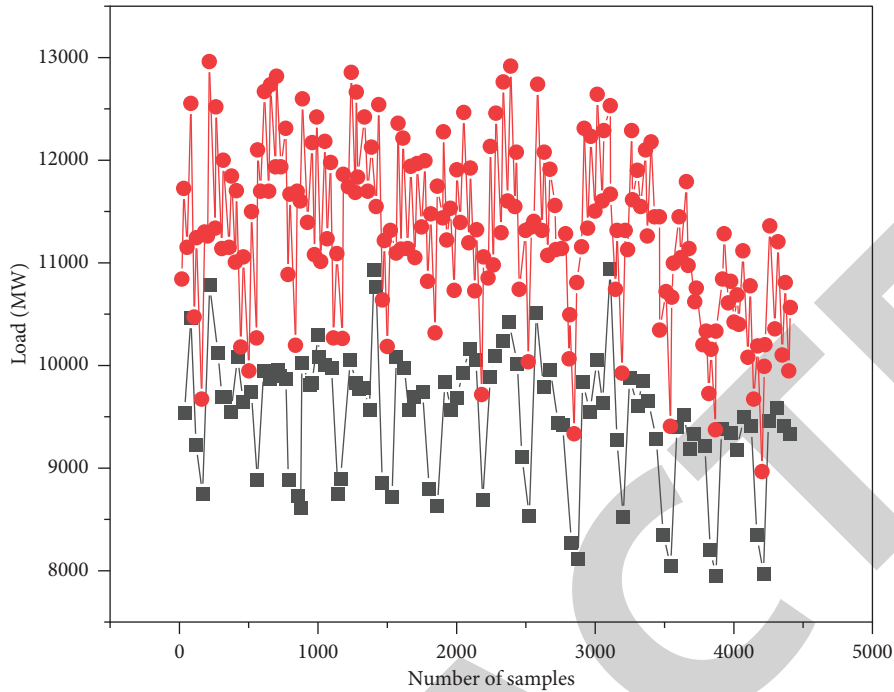


FIGURE 4: Power load of a city.

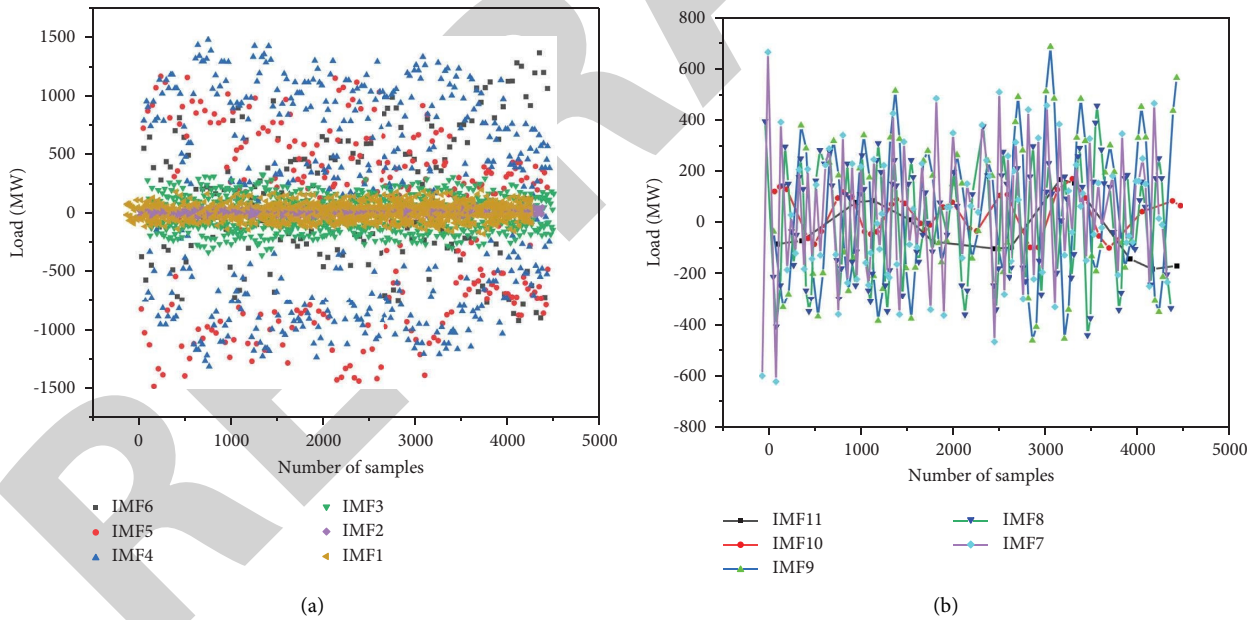


FIGURE 5: Decomposition results of the CEEMDAN algorithm. (a) Six IMF components. (b) Six IMF components and 1 residual component.

[20]. Preprocessed components and residual parts are fed into the NARX neural network for prediction, respectively, and 12 groups of data are obtained. The final short-term load estimate is obtained by overlaying 12 sets of forecast data.

The mean absolute percentage error (MAPE) and root mean square error (RMSE) are used to measure the model’s predictive performance. The formula for calculating MAPE and RMSE is as follows:

TABLE 1: MPAE and RMSE under hidden layer 3.

Delay order	5	6	7
MAPE (%)	0.788	0.805	0.776
RMSE (MW)	105.1	105.4	104.5

TABLE 2: MPAE and RMSE under hidden layer 4.

Delay order	5	6	7
MAPE (%)	0.824	0.765	0.759
RMSE (MW)	107.4	101.7	104.3

TABLE 3: MPAE and RMSE under hidden layer 5.

Delay order	5	6	7
MAPE (%)	0.751	0.823	0.778
RMSE (MW)	111.5	121.1	118.2

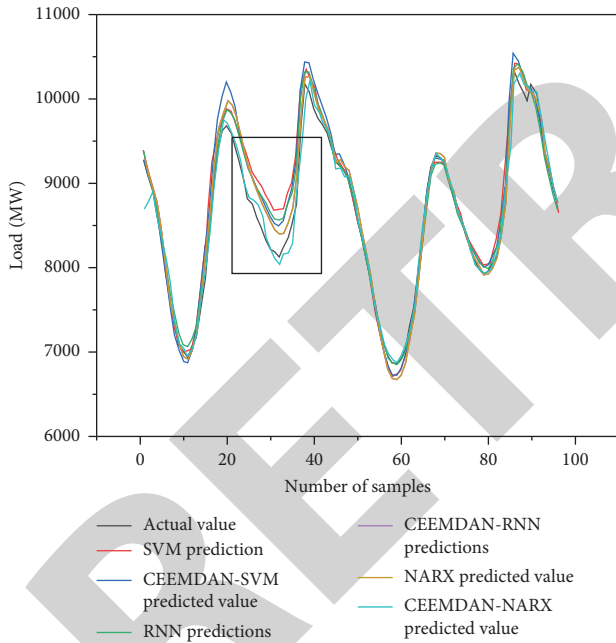


FIGURE 6: Comparison of prediction results of 6 models.

$$\text{MAPE} = \frac{1}{M} \sum_{t=1}^M \left| \frac{Y(t) - Y'(t)}{Y(t)} \right| \times 100\%, \quad (17)$$

$$\text{RMSE} = \sqrt{\frac{1}{M} \sum_{t=1}^M (Y(t) - Y'(t))^2}, \quad (18)$$

where $Y(t)$ is the actual load value at the time, $Y'(t)$ is the predicted load value at the time, and M is the predicted number of points [21].

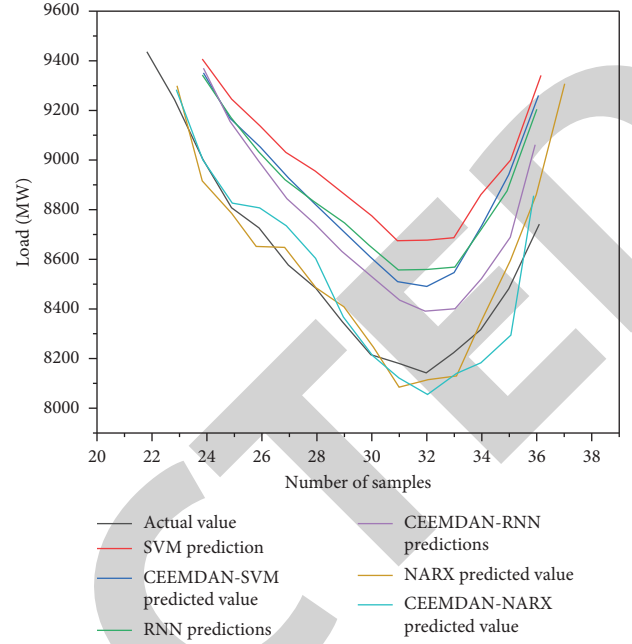


FIGURE 7: Enlarged view of the marked area in Figure 6.

TABLE 4: Evaluation indicators of each model.

Model	MAPE (%)	RMSE (MW)
SVM	2.034	231.5
CEEMDAN-SVM	1.751	213.2
RNN	1.495	179.1
CEEMDAN-RNN	1.457	167.4
NARX	1.233	146.9
CEEMDAN-NARX	0.765	101.7

TABLE 5: Evaluation indicators of local prediction of each model.

Model	MAPE (%)	RMSE (MW)
SVM	5.454	475.2
CEEMDAN-SVM	4.442	387.7
RNN	4.241	368.6
CEEMDAN-RNN	3.383	298.4
NARX	1.044	129.3
CEEMDAN-NARX	0.701	70.4

4.2. *Determining NARX Neural Network Parameters.* MPAE and RMSE in different parameter combinations are shown in Tables 1–3.

As shown in Tables 1–3, the number of hidden layers is 4 and the order delay is 6 when CEEMDAN algorithm and NARX neural network model have the best prediction performance.

4.3. *Analysis of Prediction Results.* In order to verify the validity of the proposed model, this paper presents the experimental results of three traditional power load forecasting models (SVM, RNN, and NARX) and three

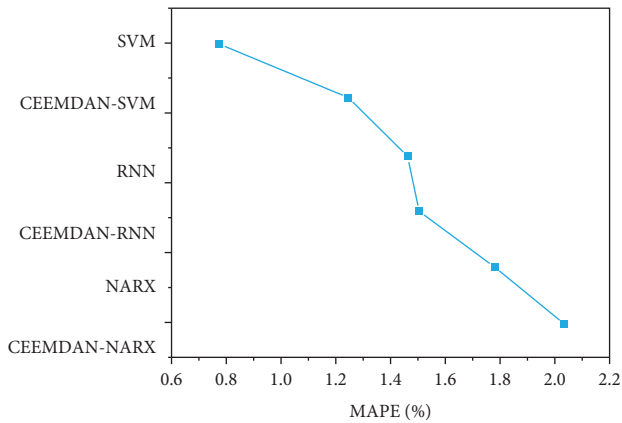


FIGURE 8: Histogram of MAPE of 6 models.

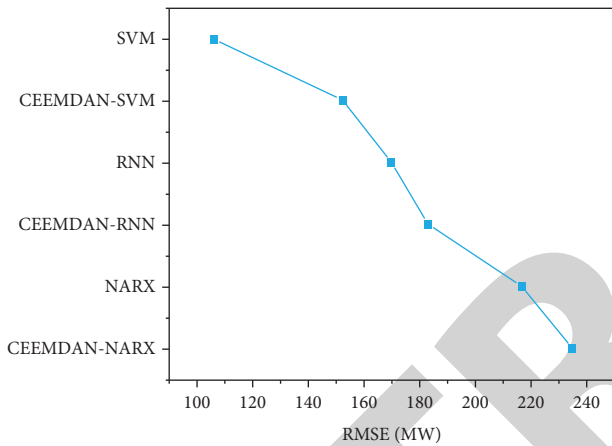


FIGURE 9: Histogram of RMSE of six models.

combined load forecasting models (CEEMDAN-SVM, CEEMDAN-RNN, and CEEMDAN-NARX). The results obtained by combining these three models with the CEEMDAN algorithm are compared [22]. A comparison of the prediction results of the six models is shown in Figure 6. Figure 7 is a magnified view of the area marked in Figure 6, where the selected area is near the electrical load cavity. Figure 7 shows that each model has a large prediction bias caused by the sudden drop in electricity load demand.

According to equations (17) and (18), the evaluation MAPE and RMSE indexes of each model can be obtained, and the results are shown in Table 4. Table 4 shows that the MAPE and RMSE of the CEEMDAN-NARX model proposed in this paper are 0.765% and 101.7 MW lower than other models, respectively. The lower the value of the evaluation index, the better the performance of the model and the more feasible the CEEMDAN-NARX model.

Table 5 shows the local prediction evaluation metrics for each model [23]. Table 5 shows that the MAPE of the CEEMDAN-NARX model is 4.753%, 3.540%, and 0.343% lower than that of the traditional bootstrapping single model SVM, RNN, and NARX, and 3.741% and 2.682% lower than the bootstrapping model combined prediction model

CEEMDAN-SVM and CEEMDAN-RNN, respectively. These data show that the prediction accuracy of the CEEMDAN-NARX model is better than the other models, even in special cases such as near the trough.

In order to more intuitively express the differences between MAPE and RMSE among the six models, the histograms of MAPE and RMSE of the six models are shown in Figures 8 and 9 respectively.

It can be seen from Figures 8 and 9 that the MAPE and RMSE values of the combined model composed of SVM, RNN, NARX, and CEEMDAN are smaller than their corresponding single model, so the prediction accuracy of the combined model composed of CEEMDAN is relatively high [24]. The MAPE and RMSE of the CEEMDAN-NARX model proposed in this paper are 0.765% and 101.7 MW, which are reduced by 0.468% and 45.2 MW, respectively, compared to the same NARX model. Compared to CEEMDAN-SVM, the MAPE of CEEMDAN-NARX and CEEMDAN-RNN are reduced by 0.986% and 0.692%, respectively. Compared to CEEMDAN-SVM, the RMSE of CEEMDAN-NARX is reduced by 111.5 and 65.7 mW, respectively.

5. Conclusion

This paper presents a short-term load monitoring of power model based on the CEEMDAN algorithm and NARX neural network. First, the CEEMDAN algorithm decomposes the original energy load signal into components and residual components, which can suppress noise, reduce the frequency of separation, and improve the degree of integration. The decomposed objects and residual objects are fed to the NARX neural network for prediction. The NARX neural network can store load history data and calculate load history together with future load data. It has dynamic performance and is not prone to data loss. The combined model was compared with existing predictive models. According to the MAPE and RMSE test result values, the prediction accuracy of the CEEMDAN-NARX model is high, indicating that the model can monitor power load capacity.

Data Availability

The data used to support the findings of this study are available from the corresponding author upon request.

Conflicts of Interest

The authors declare that there are no conflicts of interest regarding the publication of this paper.

References

- [1] D. Y. Deng, J. Li, Z. Y. Zhang, Y. F. Teng, and Q. Huang, "Short term power load forecasting based on EEMD-GRU-MLR," *Power Grid Technology*, vol. 44, no. 2, pp. 593–602, 2020.
- [2] J. Wang, R. Q. Li, S. Liu, W. S. Cao, H. Wang, and Y. Chen, "Short term load forecasting based on improved short - and

Retraction

Retracted: Application of Improved Deep Learning Method in Intelligent Power System

International Transactions on Electrical Energy Systems

Received 28 November 2023; Accepted 28 November 2023; Published 29 November 2023

Copyright © 2023 International Transactions on Electrical Energy Systems. This is an open access article distributed under the Creative Commons Attribution License, which permits unrestricted use, distribution, and reproduction in any medium, provided the original work is properly cited.

This article has been retracted by Hindawi, as publisher, following an investigation undertaken by the publisher [1]. This investigation has uncovered evidence of systematic manipulation of the publication and peer-review process. We cannot, therefore, vouch for the reliability or integrity of this article.

Please note that this notice is intended solely to alert readers that the peer-review process of this article has been compromised.

Wiley and Hindawi regret that the usual quality checks did not identify these issues before publication and have since put additional measures in place to safeguard research integrity.

We wish to credit our Research Integrity and Research Publishing teams and anonymous and named external researchers and research integrity experts for contributing to this investigation.

The corresponding author, as the representative of all authors, has been given the opportunity to register their agreement or disagreement to this retraction. We have kept a record of any response received.

References

- [1] H. Liu, Y. Liu, and C. Xu, "Application of Improved Deep Learning Method in Intelligent Power System," *International Transactions on Electrical Energy Systems*, vol. 2022, Article ID 6788668, 6 pages, 2022.

Research Article

Application of Improved Deep Learning Method in Intelligent Power System

HuiJie Liu , Yang Liu , and ChengWen Xu 

ShiJiaZhuang Institute of Railway Technology, ShiJiazhuang, Hebei 050061, China

Correspondence should be addressed to Yang Liu; 20141196@stu.sicau.edu.cn

Received 9 September 2022; Revised 3 October 2022; Accepted 10 October 2022; Published 24 November 2022

Academic Editor: Nagamalai Vasimalai

Copyright © 2022 HuiJie Liu et al. This is an open access article distributed under the Creative Commons Attribution License, which permits unrestricted use, distribution, and reproduction in any medium, provided the original work is properly cited.

In view of the inaccurate short-term power load prediction in the power system, where the smart grid cannot effectively coordinate the production, transportation, and distribution of electric energy, the authors propose the application of improved deep learning methods in intelligent power systems. The method uses the convolutional neural network to establish the energy prediction calculation model, uses CNN adaptive data features to mine characteristics, quantifies power uncertainty, uses drop regularization to optimize the deep network structure, uses the deep forest to learn the extracted data features, and builds a prediction model, in order to achieve accurate prediction of power load and solve the problem that the accuracy of existing forecasting methods decreases due to random fluctuations of power. The results showed the following: in the power load forecast results over the weekend, the random forest and the LSTM algorithm forecast results were relatively close and the RMSEs were 17.3 and 17.1, respectively, while the SVM predicted a larger RMSE error of 27.5. The authors' method predicts the best with 14.8. *Conclusion.* After verification based on actual load data, in the case of uncertain fluctuations in power load, this method can accurately predict the power load, and the accuracy is higher than that of the more popular methods at present, and it is expected to become an important technical support for solving the core problems of smart grid.

1. Introduction

With the rapid development of smart grids, this raises many concerns about the efficient use of the environment, sustainability, and energy independence; therefore, the construction of power load forecasting system has become the main purpose of power supply management. The development of smart grids has benefited from advances in information and communication technologies, which are increasingly becoming a powerful and efficient system. In this environment, research on more secure, reliable, efficient, and cost-effective smart grids has attracted extensive attention, as shown in Figure 1. At present, the daily operation and planning of the smart grid require load forecasting for users one day in advance. The accuracy of intraday forecasting models is relevant to many decisions, including gas supply planning, security measures, financial planning for power generation, and e-business planning. However, predicting the next day is a difficult task as it

depends on other factors like weather and probability. In order to achieve this, it is important to reduce the uncertainty related to the demand and to meet the requirements for the product. To achieve this goal, it is necessary to understand the characteristics of demand forecasting, and based on this, it is necessary to improve or select an optimal model for short-term load forecasting. The problem of short-term load forecasting can be considered as a time forecasting problem, that is, based on the current load forecasting load, a series of neural network models is integrated for forecasting, which further improves the accuracy of load forecasting. The neural network algorithm is only used for high-accuracy short-term energy load forecasting; the neural network algorithm only has a small number of hidden nodes, which will limit the investment properties of some casino problems in researching the network structure. This is very important in the study of machine learning algorithms. On the other hand, during short-term energy load forecasting, the peak load is considered to be an important factor affecting the

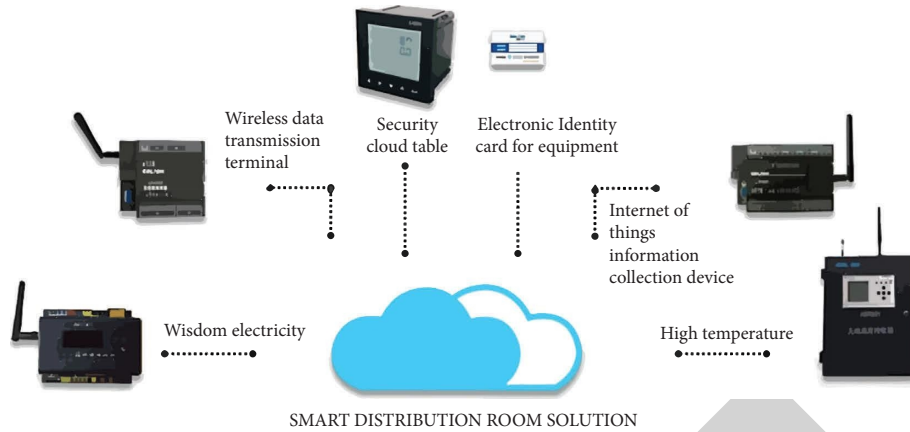


FIGURE 1: Intelligent power system.

stability of the smart grid. Despite the accuracy of the machine learning algorithm, both overestimation and trough can lead to power loss at peak loads. In some cases, the weekly maximum forecast is the short-term forecast goal because it is the most important in the short term. Power sector operations such as electricity production, safety measures, and energy conservation are based on the results of short-term peak load forecasting. Therefore, it is necessary to improve the accuracy of short-term energy load forecasting.

2. Literature Review

The origin of short-term power load forecasting is early, and many researchers have done a lot of research on power load forecasting, so there are many methods for power load forecasting, and they have achieved good results [1]. For short- and medium-term electricity, simple linear regression, multiple linear regression, nonlinear regression, the artificial neural network (ANN), and the support vector machine (SVM) among others have been used by many researchers. Linear regression was used for load forecasting. Zhang et al. combined the ant colony algorithm with gray theory; the gray ant colony neural network is established, and the feedback algorithm is added on the basis of the GM (1,1) model, after which the unique advantages of the two can be exerted, and the expected results can be obtained [2]. Chen and Chen used autoregressive modeling to develop a method based on nonlinear load regression and modified it with chaos theory, successfully reducing the influence of local extreme values on the prediction results [3]. In their report, Ngoc chose to use the Grassberger–Procaccia algorithm for short-term load prediction by chaotic dynamic reconstruction, and the least-squares regression method was used to obtain residual values relevant factor [4]. Yu Investigated a random forest model for predicting short-term energy loads, which is a multiple regression tree (CART) research [5]. Souza chose a neural fuzzy structure that can be defined as ANN (artificial neural network), which is composed of experimental data and can find the system parameters of fuzzy reasoning. Selection of a neural fuzzy model can be described as the ANN (Artificial Neural Network) with research data to find collision-free systems [6]. Lakhmiri ANN-based short-term load forecasting [6]. Lakhmiri ANN-based

short-term load forecasting models are excellent, and the most common type of the ANN is the multilayer perceptron (MLP), which uses previous load data to estimate the load curve. As we know, network structure plays an important role in neural networks, because information about the structure (including estimated time or change) is reflected in the neural network structure [7]. Liu et al. proposed an ANN-based time prediction model for home use [8].

On the basis of current research, the authors propose the application of improved deep learning methods in intelligent power systems. A new convolutional neural network-deep forest prediction method is used; first, the energy prediction calculation model is established by using the convolutional neural network, and the power uncertainty is quantified by combining it with the monte carlo algorithm. Second, the obtained uncertainty evaluation features and power distribution features are input into the deep forest to accurately predict short-term power loads [9]. The specific workflow of this method is shown in Figure 2:

Sufficient short-term power load data time series is sorted out under similar working conditions from historical data, and the deep convolutional network is fed into as training samples. The deep convolutional network utilizes multilayer convolution and pooling; the authors propose the potential laws hidden in the data that are difficult to describe or discover by analytical methods and store them in the form of graph data [10]. The authors use dropout regularization to optimize the deep network structure and realize the uncertain quantification of extracted features through the uncertain evaluation of model parameters; therefore, it is possible to consider the influence of the uncertainty of the original data on the prediction results. Finally, the authors use the deep forest to learn the extracted data features and establish a prediction model to achieve an accurate prediction of power load.

3. Methods

3.1. Deep Convolutional Networks. The deep convolutional network is a popular deep learning algorithm, which can effectively identify the spatial relationship between elements of complex matrix and extract key data features according to the theoretical basis of the deep convolutional network. The

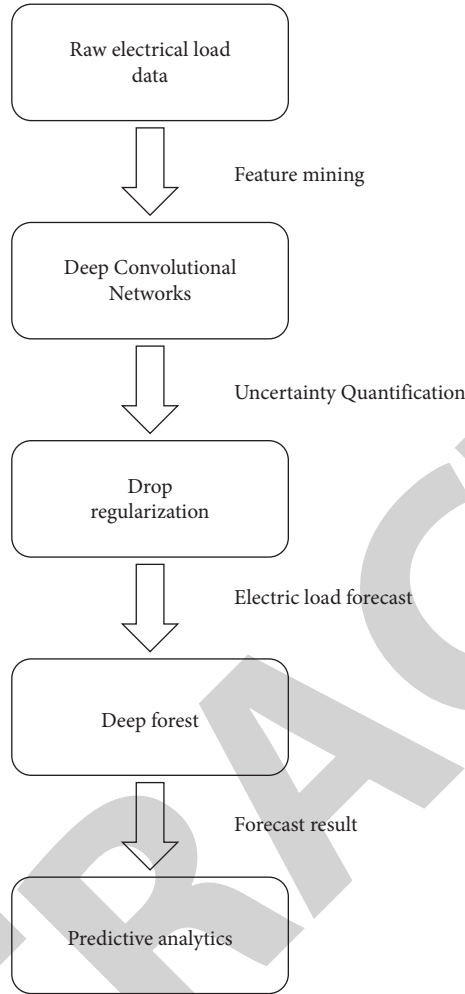


FIGURE 2: A new method for accurate prediction of power load.

CNN model developed by the authors includes an input layer, two layers (C1 and C3), two layers (P2 and P4), a fully connected layer (FC5), and an output layer (Softmax). A deep convolutional network uses a convolutional kernel to extract texture features from the input (image) matrix, and the convolution process descends the feature map, reduces the map dimension, and extracts local features. After two folds and merge layers, the original image features can be extracted. After that, the fully connected layer (FC5) is a high-level process to show the characteristics of different groups. The output method uses the Softmax function to give the result of the distribution [11]. To achieve this, a deep process is added between the second integration layer and all connected processes for later processing. In this way, the effectiveness of deep convolutional network training will become clearer, the extraction of sensitive feature information will be more accurate, and it will provide a basis for future predictions.

3.2. Monte Carlo—Discard Regularization. In order to measure the uncertainty of the parameters of the deep convolutional network model, the authors adopt a Monte Carlo dropout regularization (Monta Carlo-dropout

regularization) algorithm, using the Monte Carlo uncertainty estimation capability to quantify the uncertainty of the model parameters; this indirectly reflects the hidden uncertainty of the power load data, making the final prediction result accurate and reliable [12].

In general, a deep convolutional network can be represented by a function $f^w(x)$, where x is the network input and w is the network weight. The output of the network after training is $y = f^w(x)$. The prediction for the new sample x^* is $y^* = f^w(x^*)$. In order to measure the uncertainty of the network, the calculation process of the Monte Carlo-drop regularization is as follows: first, use the new data x^* to test the trained convolutional network and randomly discard the intermediate layer neurons N times with a fixed probability p while calculating the prediction to obtain a set of predicted value vectors $y^*1 y^*2 \cdots y^*N$. From this, the uncertainty of the network prediction can be evaluated as follows:

$$\text{Var}[f^w(x^*)] = \frac{1}{N} \sum_{i=1}^N (y_i^* - \bar{y}^*)^2, \quad (1)$$

$$e = \sqrt{\text{Var}[f^w(x^*)]}.$$

In the formula, $\text{Var}[f^w(x^*)]$ is the variance of N times Monte Carlo forecast, \bar{y}^* is the average value of N times Monte Carlo forecast, and e is the forecast uncertainty. In this way, using Monte Carlo dropout, the prediction uncertainty can be evaluated, and the evaluation results can be sent to the subsequent prediction model for learning and memory; in this way, the new data will be adaptively compensated for the influence of uncertainty, and the prediction results will be accurate and stable.

3.3. Deep Forest. The deep forest (gcForest) is a method for deep exploration of random forests. In a random forest, a subset of data sets L is first generated by bootstrapping them using the first data set x . Then, each subdataset is used to create a decision tree, and all subdatasets form a forest containing L decision trees. Finally, each decision tree is generated, and the final outcome of the random forest is determined by a voting or averaging strategy. Deep forest implements the entire decision tree as a random forest, and class classification probabilities are generated by calculating the percentage of different classes in the report [13]. Therefore, the yield of a deep forest is defined as the result of the distribution of all trees identified in the forest. Deep learning techniques are used in deep forests using multivariate analysis (MGS) and cascade forests. The goal of MGS is to extract useful information from an input image as follows: first, each grayscale image ($M \times M$ matrix; M is the size of the image) is printed by a sliding window (window size k) to generate a subimage S . Each subgraph is a $k \times k$ matrix. If the slip is j , then $S = [(M-k)/j + 1] \times 2$. Then, when training all random forests simultaneously, using each small image, the output vector of each forest has points C and corresponds to the result of the class letter C for information. The output vectors of the two training forest models are combined into $2C$ key feature vectors for each subimage. Therefore, for each grayscale image, both forest models generate a feature matrix of dimension $S \times 2C$. Finally, collect each column of the feature matrix to obtain a $2 \times S \times C$ visual probability vector based on the MGS output of each gray image. A multislide window can be used to scan grayscale images so that output vectors can be generated for each grayscale image. In this study, we use a sliding window with grayscale image size $M=28$, sliding window size $k=26$, and sliding window size $j=1$, so the number of images is sub $S=9$. The cascade forest is the baseline. The deep forest is used to implement deep learning strategies. It accepts a vector of MGS results and outputs the final distribution. A matte forest has a multilayer structure, each layer has two random forests and two random forests [14]. Similar to the MGS forest, each sampled random forest in the cascade forest produces a result vector of C elements, so the output length of each layer is $4C$. The number of layers is determined during training, and learning is verified using cross-validation at each layer. For each grayscale image, the input to the first layer is the MGS probability $P(=S \times 2C)$. Then, the output of the first layer (i.e., $4C$ probability elements) is combined with the original P probability elements, and a new vector (i.e., $4C + P$ probability elements) is

generated as input to the second layer. Similar connections are repeated to form the input vectors of the following layers up to the last layer. The results of the four forest models in the last layer are averaged to create the final result for class C . For the deep forest, the maximum of the final result is used [15]. Because the number of layers in the cascade forest is determined adaptively based on the training performance, the complexity of the model can be adjusted to multivariate data, which is more efficient than deep neural networks. Therefore, the authors' energy load forecasting plan can flexibly process different sets of data, adapt to changes in the data set, and produce stable and reliable accurate predictions.

4. Results and Discussion

One key smart grid technology is efficient energy management and demand-side implementation. Among them, short-term energy load forecasting is of particular importance. In order to solve this problem, the authors propose to use deep learning techniques in the power of intelligence and a new method of deep learning taking into account the uncertainty of prediction. To analyze the effectiveness of the method, the historical data of the energy load of the power plant over a period of time was analyzed [16]. The power grid continuously records the complete power load data in 2021; due to the large amount of data, Figure 3 only shows the complete power load historical data for two days. It can be seen from the data curve that the original power load data show obvious fluctuations, indicating that there are many uncertainties in the power load during the operation of the power grid, so that the data curve does not show useful laws or trends.

Furthermore, the authors conducted a detailed analysis of the historical data in order to grasp the characteristics of the data in advance and analyze the frequency of power load fluctuations, especially the influence of different time periods and seasons on power load fluctuations, so as to provide ideas for the analysis of historical data. Through careful analysis of the historical data, it is found that the distribution of the power load curve on weekends (Saturday and Sunday) at each time point is relatively similar; on weekdays (Monday to Friday), due to the complex and changeable power demand, the distribution of the power load curve at different time points is more random, and there is no regular probability distribution; therefore, it is more difficult to predict on weekends than on weekdays. In addition, through the analysis, it is also found that the curve fluctuations of the data are more frequent in summer than in other seasons, showing more complex uncertainties, thus bringing more adverse effects on power load forecasting. In order to quantitatively analyze the fluctuation of the power curve of the power grid in 2021 on weekdays, weekends, and summer, the variance calculation of the data in these three time periods is carried out, and the results are shown in Table 1 [17].

From the calculation results in Table 1, it can be seen that the power fluctuation degree of the historical data is for weekends, weekdays, summer, and other time periods. It is

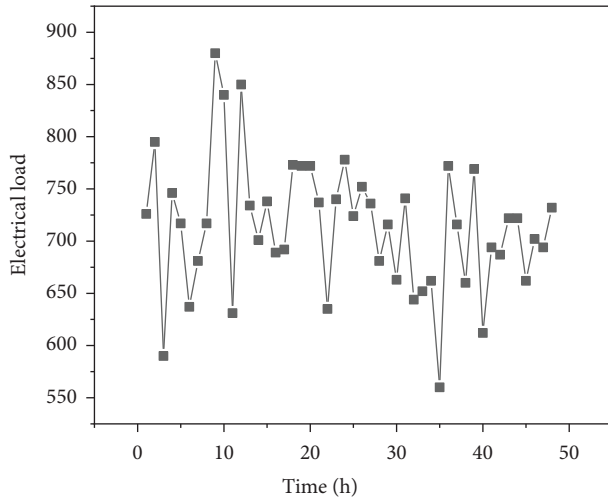


FIGURE 3: Two-day power load historical data.

TABLE 1: Power load fluctuation variance.

Period	Volatility variance/(MVh)
Weekend	2719.1
Working day	3554.3
Summer	4652.7

foreseeable that due to the uncertainty brought about by fluctuations, the difficulty of forecasting is in the weekends, working days, summer, and other time periods. However, if the uncertainty of power load fluctuations can be well controlled, the prediction accuracy in different time periods can be reduced, and stable and accurate power load prediction results can be output. In order to verify this academic point of view, the historical data were predicted for different time periods. In order to test the prediction accuracy, two metrics, the root mean square error (RMSE), and the mean absolute percentage error (MAPE) [18] were used. The results are shown in Tables 2–4. Among them, the more popular methods such as LSTM, SVM, and random forest are compared. Table 2 shows the predicted results of power load on working days. In the analysis, the complete power load data of the grid for 100 consecutive working days (excluding weekends) were selected [19]. From the prediction results, the prediction results of random forest and the LSTM algorithm are relatively close, more accurate than the SVM but not as good as the authors' method. This is because the author's method analyzes the uncertainty of the model, and the network will adaptively compensate for the effects of random power fluctuations.

Table 3 shows the forecast results of the power load for the weekend. The complete power load data of the grid for 100 consecutive weekends (excluding weekdays) were selected for the analysis. From the predicted results, the prediction results of random forest and LSTM algorithms are relatively close, with RMSE of 17.3 and 17.1, respectively, while the SVM prediction has a larger RMSE error of 27.5; The authors' method predicts the best with 14.8. This is

TABLE 2: Workday power load forecast results.

Method of prediction	Prediction accuracy	
	RMSE	MAPE
SVM	26.1	0.025
Random forest	19.5	0.023
LSTM	19.3	0.023
Method	17.2	0.021

TABLE 3: Weekend power load forecast results.

Method of prediction	Prediction accuracy	
	RMSE	MAPE
SVM	27.5	0.026
Random forest	17.3	0.022
LSTM	17.1	0.022
Method	14.8	0.020

TABLE 4: Three-month power load forecast results in summer.

Method of prediction	Prediction accuracy	
	RMSE	MAPE
SVM	35.1	0.033
Random forest	27.8	0.027
LSTM	27.5	0.026
Method	18.3	0.022

because the authors' method can utilize the adaptive ability of the deep forest to sample size, so this method adjusts the forest parameters according to the actual sample size, in order to achieve accurate predictions for different samples [20].

Table 4 specifically analyzes the power load forecast results for the three months in summer. Due to the large fluctuations in electricity consumption in summer, the resulting uncertainty also increases. From the prediction results, the RMSE predicted by the random forest and LSTM algorithms are 27.8 and 27.5, respectively, and the SVM prediction RMSE error is 35.1. The prediction effect RMSE of the authors' method is 18.3. It can be seen that the power fluctuation has a great influence on the prediction accuracy, but the authors' method can still accurately predict the power load. It can be seen that the authors' method is a reasonable and effective power load forecasting method.

5. Conclusion

Aiming at the key problem of accurate prediction of power load in the current smart grid system, the authors propose the application of the improved deep learning method in the intelligent power system, which can solve the problem that the accuracy of existing prediction methods is reduced due to random fluctuation of power. The actual power data analysis results show that due to the uncertainty evaluation based on discarding regularization, the proposed deep learning method can accurately predict the power load in the case of large power fluctuations, and the accuracy is higher than that of the more popular methods. Therefore, given the

Retraction

Retracted: Influence of Educational Informatization Based on Machine Learning on Teaching Mode

International Transactions on Electrical Energy Systems

Received 28 November 2023; Accepted 28 November 2023; Published 29 November 2023

Copyright © 2023 International Transactions on Electrical Energy Systems. This is an open access article distributed under the Creative Commons Attribution License, which permits unrestricted use, distribution, and reproduction in any medium, provided the original work is properly cited.

This article has been retracted by Hindawi, as publisher, following an investigation undertaken by the publisher [1]. This investigation has uncovered evidence of systematic manipulation of the publication and peer-review process. We cannot, therefore, vouch for the reliability or integrity of this article.

Please note that this notice is intended solely to alert readers that the peer-review process of this article has been compromised.

Wiley and Hindawi regret that the usual quality checks did not identify these issues before publication and have since put additional measures in place to safeguard research integrity.

We wish to credit our Research Integrity and Research Publishing teams and anonymous and named external researchers and research integrity experts for contributing to this investigation.

The corresponding author, as the representative of all authors, has been given the opportunity to register their agreement or disagreement to this retraction. We have kept a record of any response received.

References

- [1] L. Ma and J. Li, "Influence of Educational Informatization Based on Machine Learning on Teaching Mode," *International Transactions on Electrical Energy Systems*, vol. 2022, Article ID 6180113, 7 pages, 2022.

Research Article

Influence of Educational Informatization Based on Machine Learning on Teaching Mode

Lei Ma¹ and Jian Li²

¹*School of Humanities and Education, Nanchang University of Technology, Nanchang, Jiangxi, China*

²*School of Aerospace, Nanchang University of Technology, Nanchang, Jiangxi, China*

Correspondence should be addressed to Lei Ma; malei@nut.edu.cn

Received 26 August 2022; Revised 20 September 2022; Accepted 28 September 2022; Published 11 October 2022

Academic Editor: Nagamalai Vasimalai

Copyright © 2022 Lei Ma and Jian Li. This is an open access article distributed under the Creative Commons Attribution License, which permits unrestricted use, distribution, and reproduction in any medium, provided the original work is properly cited.

In recent years, with the rapid progress of educational information techniques, the application of computer teaching methods in school education has also shown a constantly changing trend. How to change the traditional classroom structure, improve the teachers' information literacy, build a new information-based teaching format, and promote the integration of information technique and pedagogy have become an important topic of the current educational research study. Machine learning is a key technology in artificial intelligence and is widely used in various fields. The core of educational informatization is to carry out personalized learning, and the main auxiliary technology of personalized learning is machine learning. So, this article studied the influence of machine learning-based educational informatization on the teaching mode. Through the investigation and research methods, this article found that the educational informatization teaching mode based on machine learning is helpful to improve students' autonomous learning ability, comprehensive ability, and learning effect. In the information-based teaching mode, the learning effect reached a maximum of about 90, with an average increase of 12, which showed that the educational information-based teaching mode based on machine learning is feasible.

1. Introduction

In the wake of the go-ahead of the message age and technique, machine learning has also been applied in various fields. Humans' understanding of teaching mode has measured up a split-new height within a definite space of continuous go-ahead education, and more attention is paid to the effective request of the educational message teaching pattern, thereby promoting the development of the scientific teaching pattern. Numerous research reports showed that message-based teaching pattern based on machine learning is of great implication to classroom teaching. Therefore, the discussion on the message teaching pattern based on machine learning has become a top priority.

Now more and more educators are committed to the related research on the teaching mode of educational informatization [1]. Miao analyzed the teaching effect of the informatization teaching mode and proposed and constructed the informatization teaching mode based on the

network course [2]. Xu introduced the concept, characteristics, and teaching process of the information-based teaching mode and analyzed the teaching consequences [3–7]. The abovementioned research studies described the relevant content of the educational informatization teaching pattern, and the influence of the informatization teaching pattern on education is far-reaching.

Because machine learning has been applied in different fields; many scholars have also studied it. Segovia studied the work of machine learning on methods for dealing with datasets containing large amounts of irrelevant information, especially the problem of selecting relevant features and selecting relevant examples [8]. Ha studied the progress made in both empirical and theoretical work in machine learning and proposed a general framework for different approaches [9]. Cai used machine learning algorithms to train classifiers and to decode stimuli, mental states, behaviors, and other variables of interest from data, so as to show that the data contain information about them [10]. Park proposed a new

heuristic for machine learning feature detection [11]. Hiroi employed three machine learning methods including Naive Bayes, maximum entropy classification, and support vector machines and found that the performance of the three machine learning methods on sentiment classification is inferior to the classification of traditional topics [12]. Kumar believed that automated data is provided by machine learning [13]. Saltepe provided a comprehensive and independent introduction to the field of machine learning that combined breadth and in-depth coverage. He provided necessary background material on topics such as probability, optimization, and linear algebra and discussed recent developments in the field [14]. The application of machine learning to education is to better help learners, teachers, etc., to better carry out learning, teaching, and other work.

In order to better promote the development of education, this article studied the impact of educational informatization based on machine learning on the teaching mode. Through research, it has been found that students preferred the informatization teaching mode, and the educational informatization teaching mode based on machine learning can help improve the comprehensive ability and learning effect of students.

2. Information-Based Teaching Mode Based on Machine Learning

2.1. An Overview of Machine Learning. Machine learning is a section of artificial intelligence [15–17]. Machine learning is a science in the field of artificial intelligence, and its main research is how to use artificial intelligence to improve the performance of specific algorithms in powerful learning. Computers learn patterns and techniques from data to apply to the task of making predictions on new data.

From an algorithmic point of view, traditional machine learning algorithms can be mainly divided into two categories, namely, supervised learning and unsupervised learning. The specific meanings are as follows:

- (1) Urge learning: assuming that there are several data inputs and corresponding outputs; the goal is to learn a mapping effect so that the performance can predict the export of new data samples. The classic problems are classification problems and regression problems.
- (2) Unsupervised learning: assuming that only some data are input without any relevant supervision and guidance; the purpose is to develop the hidden performance and data hidden in the data. The classic problems are clustering problems and data dimensionality reduction problems.

The computer learns from the data and gradually explores the laws and patterns in order to perform prediction tasks on the new data, as shown in Figure 1.

2.2. Data Mining Based on Machine Learning. The machine learning model has successfully combined the knowledge of probability theory and has obtained good results. Data

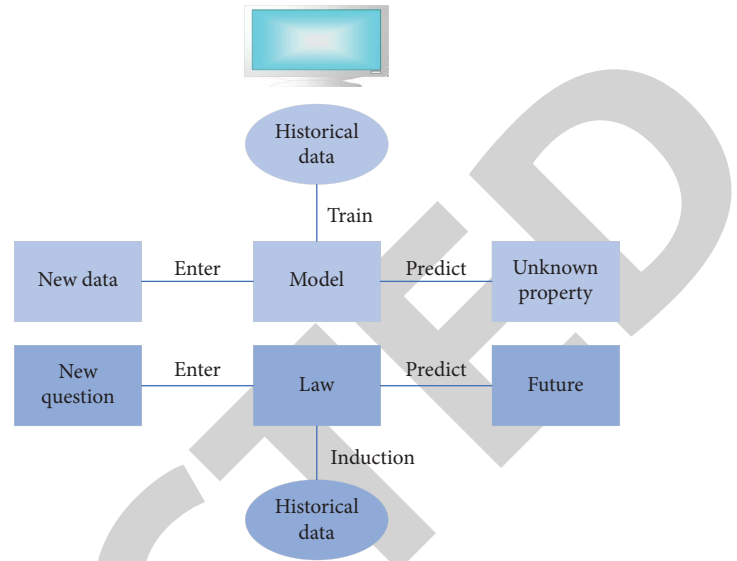


FIGURE 1: Machine learning algorithms.

mining technology belongs to the probability distribution process of random variables and is a category attribute of machine learning. Data mining is an integration and classification tool for applied cognitive analysis, so data mining techniques can be classified as technical optimization problems.

Generally speaking, the types of tasks can be divided into narrative data mining and forecasting data excavation. The type of description depends on the general features stored in the database. The types of predictions are mainly in view of the interpretation of the data collected to aid guesswork. The first task of data excavation is to identify the info patterns that need to be extracted (belonging to mining tasks). In the actual application process, the knowledge model meets the requirements of its users, and they must have the opportunity to extract each other. It is especially important that the functions of the data mining software should be enriched, and the types of samples extracted should be more extensive.

Based on the function of data excavation, it can be divided into the following aspects:

- (1) Concept description: the summary method has a rich basic data. The summary set description should be as simple and clear as possible. It describes a concept that can be obtained by using the extracted conceptual data structure and data distribution (or a combination of the above methods).
- (2) Association analysis: studying and extracting unusual grouping rules in data; the rules are used to represent the relationship between data or attributes of objects. At present, the research on data mining association rules has achieved results, and there are many kinds of algorithms, and their efficiency levels are high, and their scope of application is also expanding.
- (3) Classification and prediction: it is a specific knowledge analysis mode for classification and prediction. Obviously, the role of a classifier is to

extract mathematical models that can describe and classify data, thereby deriving data types that are currently unrecognized by machines. Classification is generally used to infer data that is currently unknown.

The steps of data excavation can be classified into problem identification, data collection and prioritization, data excavation algorithm performance, and result assessment. The data mining process is shown in Figure 2.

By using known data, it becomes clear which data are included in knowledge analysis. Depending on the data, for a given mining target, the appropriate dataset is selected from the data source. The data mining process is to solve the problem of knowledge extraction and the issue of data format differences in the operation terrace.

2.3. Data Mining Process of Machine Learning in Smart Learning. Smart education is the development of extensive integration of information technology and advanced educational concepts. Smart education has the characteristics of adaptive mode, cognitive perception, active work promotion, resource planning and organization, collaboration, and adaptability to differences. Today's smart education is in view of students' big data, and artificial intelligence needs to be used to deeply mine these data to discover potential knowledge and strategies. The application of data mining technology in the field of education has also opened the curtain for the application of machine learning in the field of education. Machine learning is mainly used to develop and mine data science, however, it is also used to create a better learning environment through machine learning, create favorable conditions for teachers to conduct effective training, and allow students to personalize their learning. Therefore, the correct and effective use of machine learning is an effective way to realize wisdom education. Educational data is discovered and interpreted through big data excavation, and the specific process is shown in Figure 3.

In the wisdom education system under the big data surroundings, there would be much big data info. However, not all the information is useful. At this time, it is essential to filter the data to find the target data. Target data cannot be directly used for data mining and processing and also need to be prechecked and transformed into data that can be measured by data models to measure and inform power. Simultaneously, the transformed data demand has to be tested to ensure that the data are authentic and reliable.

2.4. Teaching Mode of Education Informatization. Education informatization is the process of collecting information as a basic element of the education system and making extensive use of information technology in the field of education to promote educational innovation. In the procedure of educational informatization, it is essential to pay attention to the detailed analysis of the educational system from the perspective of information, and based on this, it is important to effectively apply these information

techniques to education. The main features of the educational message include multimedia teaching materials, resource globalization, and management automation. There are many teaching modes of educational informatization, among which the most representative ones are the learning mode of throwing mistakes, the mode of scaffolding teaching, and the mode of multimedia network teaching. The teaching mode of educational informatization is shown in Figure 4.

3. Educational Informatization Algorithm Based on Machine Learning

Machine learning-based educational informatization algorithms must select appropriate knowledge analysis tools or algorithms to mine the largest amount of data, and data mining operations must be meticulous, including automatic prediction of data, opinion, and bias detection. Then, the appropriate knowledge analysis algorithm is used to establish the data mining method pattern. The main knowledge analysis algorithms include Naive Bayes and support vector machine.

3.1. Naive Bayes Algorithm. The Naive Bayes algorithm is a classification model mainly based on the Bayes' theorem, first proposed by Maron, and it is one of the most commonly used classification methods in statistics. "Naive" refers to the assumption that the contribution of feature items to determining which category the text belongs to is independent of each other, that is, the feature items in the text are independent of each other. The basic idea is that each database sample without a class label is represented by a feature vector $Y = \{x_1, x_2, \dots, x_m\}$. x_m is an attribute, and the unknown samples are assigned and calculated by Naive Bayes classification, which is represented by the formula

$$F(A) = \max\{q(f_1|A), q(f_2|A), \dots, q(f_n|A)\}. \quad (1)$$

According to the Bayes' theorem, we get

$$q(f|A) = \frac{q(A|f)q(f)}{q(A)}. \quad (2)$$

If an unknown data sample A is given, and all classes are constant, and properties are relatively independent, then the characteristic class is expressed as

$$F(A) = \text{amg}_{f \in F} \max q(f) * \prod_{i=1}^m q_i. \quad (3)$$

If $q(f)$ is the parameter attribute estimation, then its calculation formula is

$$q(f) = \frac{M(f)}{M}, \quad (4)$$

$$M(f) = \sum_{i=1}^M \delta(f_h, f),$$

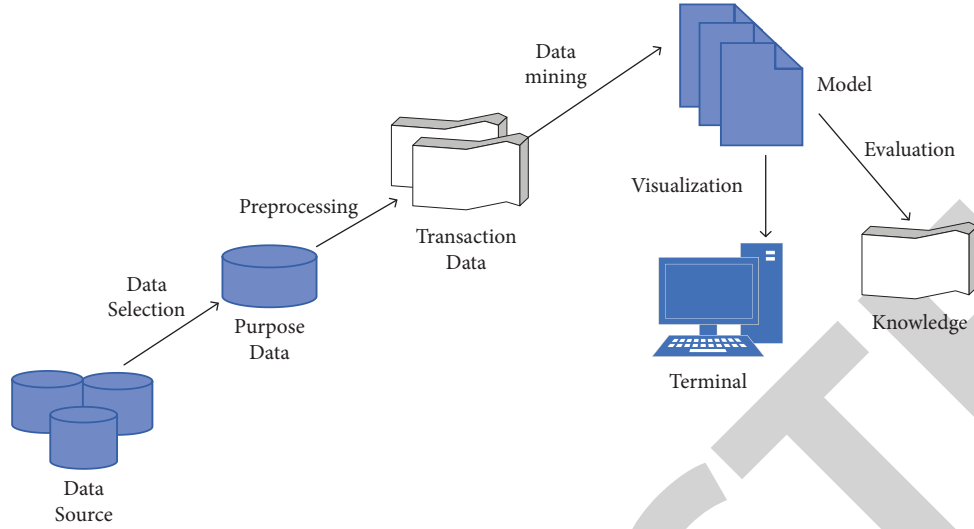


FIGURE 2: Data mining process.

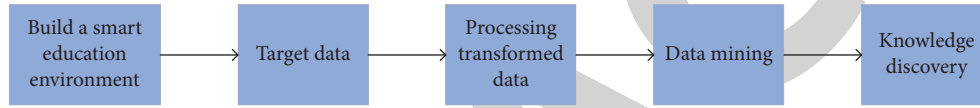


FIGURE 3: Data mining process of machine learning in smart learning.

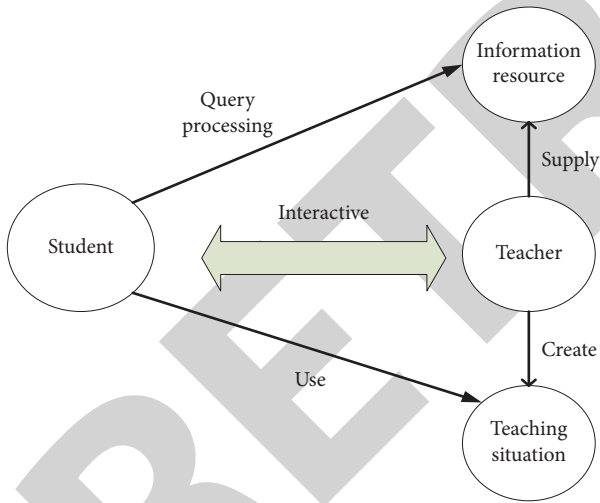


FIGURE 4: Teaching mode of educational informatization.

$q(x_i, f)$ is the conditional probability. When the attribute of x_i is variable, then the calculation formula of the conditional probability is

$$q(x_i, f) = \frac{M(x_i|f)}{M(f)}, \quad (5)$$

$$M(x_i, f) = \sum_{i=1}^M (\delta x_i, x) \delta(f_h, f),$$

$M(f)$ is the number of samples belonging to the class. M is the sum number of data samples, and δ defines a new binary function. If the parameters are the same, it is 1, and if the

parameters are different, it is 0. When the characteristic attribute is a continuous value, usually assuming that its value is normally distributed, which is expressed by the formula

$$g(a, \beta, \vartheta) = \frac{1}{\sqrt{2\pi}} e^{-(a-1)/2x^2}, \quad (6)$$

$$q(x_i|f) = g(x_i, \beta_i, \vartheta_i).$$

Since the mean and standard deviation of the distribution of each category of items in the research sample have been calculated, then the required estimates can be obtained by substituting the above formula.

Bayesian network is based on probability estimation, which can effectively deal with uncertainty and volatility, while fully considering the correlation between attributes. Bayesian models are generally limited by their number of nodes and the complexity of relationships between nodes, and it is difficult to classify high-dimensional datasets with many feature items.

3.2. Support Vector Machine Theory. Support vector machine (SVM) is a new technology in the field of data mining classification. It is a small statistical model based on the principle of structural risk reduction and the VC theory. SVM has good learning and generalization capabilities and it is a machine learning algorithm based on big data.

In a two-dimensional line space, the general form of the linear discriminant function is $g(a) = v \cdot a + y$, then the class label prediction of the sample can be expressed as

$$\begin{aligned} b &= v \cdot q + y(q + y > 0), \\ b &= -v \cdot q + y(q + y < -1). \end{aligned} \quad (7)$$

The above formula can be unified and generalized into a more compact formula as shown:

$$b_i [(v \cdot a_i) + y] - 1 = 0, \quad i = 1, 2, 3, \dots, n. \quad (8)$$

The support vector machine requires the largest classification interval, which is actually equivalent to minimizing the objective function, and it is expressed as

$$f(v) = \frac{\|v\|^2}{2}. \quad (9)$$

The learning task of SVM can also formally describe the constrained optimization problem.

$$\min_v \frac{\|v\|^2}{2} = b_i (v \cdot a_i) - 1. \quad (10)$$

Since the objective function is quadratic and the constraints on parameters w and b are linear, so this problem is a convex programming problem and can be solved by transforming it into a Lagrangian problem. The optimal solution of equation (9) is the saddle point of the Lagrangian function, which can be defined as follows:

$$K_q(v, y, b) = \frac{\|v\|^2}{2} - \sum_{i=1}^k b_i (b_i (v \cdot a_i) + y) - 1. \quad (11)$$

Among them, b_i is the Lagrange multiplier, since the gradient of v at the saddle point is 0, so we get

$$\frac{\partial K}{\partial v} = v - \sum_{i=1}^k b_i a_i, \quad (12)$$

$$\frac{\partial K_q}{\partial y} = \sum_{i=1}^k b_i a_i.$$

One way to solve inequality constraints is to convert them into a set of equality constraint bases. Ensuring that the Lagrangian multipliers are not negative and that after their transformation, the optimal solution still satisfies the formula, we get

$$b_i (b_i (v \cdot a_i) + y) - 1 = 0. \quad (13)$$

It can be seen from the abovementioned formula that only after the training instance satisfies the optimal solution, the Lagrangian multiplier is 0, that is, only the coefficient b_i of the support vector is not zero, so it can be expressed as

$$v = \sum_{CW} b_i a_i. \quad (14)$$

Advantages of support vector machine (SVM): a support classifier is a new algorithm based on machine learning, which has good learning ability and general ability, and even if the discriminant function is obtained from a limited dataset, it can still produce a small error on

the test set. SVM is essentially a convex quadratic optimization problem, and the optimal solution found can be guaranteed to be the global optimal solution. In terms of text, most of them are multidimensional and sparse text objects. Support vector technology has a strong mathematical theoretical foundation, which can be used for high-dimensional data, and it can also be used to solve nonlinear problems as well. It can be seen that the support vector machine algorithm has strong application potential in text classification.

4. Experimental Results of the Influence of Educational Informatization on Teaching Mode Based on Machine Learning

At present, many schools have introduced the teaching mode of education informatization, and they are loved by students and have good results. However, the information-based teaching model is still in its infancy. This study adopted the survey and research method to analyze and study the educational information-based teaching model.

4.1. Recognition Contrast. In order to more clearly and objectively comprehend the practical effects of the information-based teaching pattern in schools, a random survey of 100 people in a school is conducted to focus on their recognition of the information-based teaching pattern. The recognition degree is divided into very like, relatively like, general, dislike, and very dislike, as shown in Figure 5.

From the bar chart in Figure 5, it can be clearly seen that more than 80% of the students agreed with the information-based teaching model and preferred this teaching model. 52.3% of the students preferred the information-based teaching model, accounting for the total number of participants in the survey. Only a small number of students did not like the message-based teaching pattern, which may be due to the low level of understanding of the message-based teaching pattern. These data showed that students generally prefer the message-based teaching pattern and reflected that the feasibility of implementing a message-based teaching pattern in the teaching pattern.

4.2. Comparison of Different Teaching Modes in terms of Self-Existent Learning Capability. The common teaching pattern and the message-based teaching pattern were compared, and the tests were repeated 6 times, as shown in Figure 6.

Figure 6 studied the comparison between the ordinary teaching pattern and the information-based teaching pattern on self-existent learning capability. It can be clearly seen from the figure that the information-based teaching pattern cultivates students' self-existent learning capability which is significantly higher than that of the ordinary teaching pattern. The self-existent learning capability of the ordinary teaching pattern fluctuated around 60 times, while the self-existent learning capability under

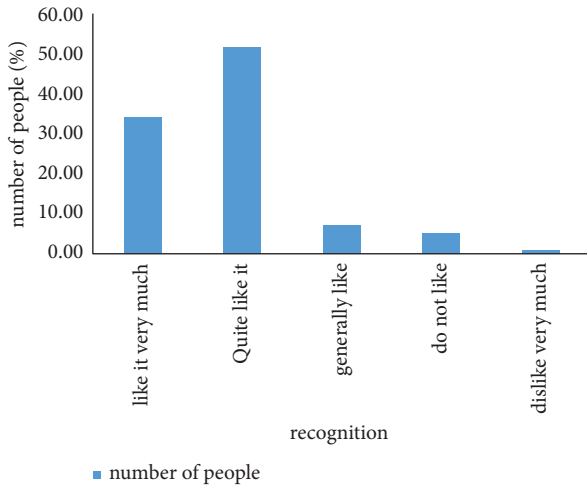


FIGURE 5: Recognition of the information-based teaching model.

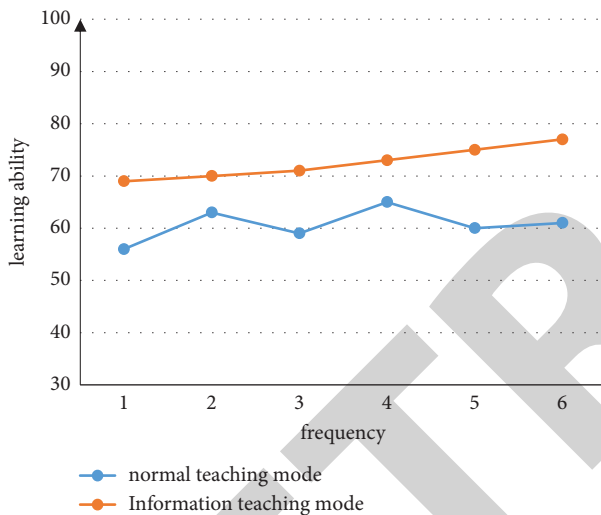


FIGURE 6: Comparison of different teaching modes in autonomous learning ability.

the information-based teaching pattern was on the rise. The self-existent learning capability under the information-based teaching pattern was around 77, which showed that the information-based teaching mode was more conducive to the cultivation of students' self-existent learning capability.

4.3. Comparison of Different Teaching Modes in Comprehensive Ability Training. In the process of students' learning, we should pay attention in guiding students to combine theory with practice and pay attention to the cultivation of students' comprehensive ability. In order to have a clearer understanding of which teaching mode is more suitable for the cultivation of students' comprehensive ability, the common teaching pattern and the message-based teaching pattern were compared, and the tests were repeated 6 times, as shown in Figure 7.

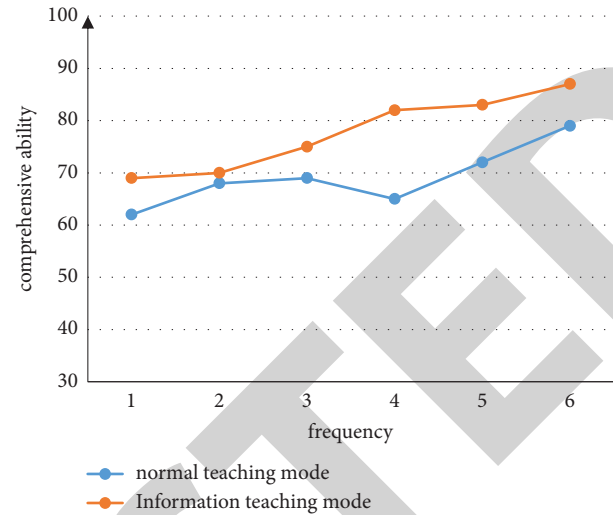


FIGURE 7: Comparison of different teaching modes in comprehensive ability training.

TABLE 1: Comparison of different teaching methods in terms of learning effect.

	Normal teaching mode	Information teaching mode
1	72	83
2	77	79
3	75	85
4	69	87
5	70	89
6	78	90

In Figure 7, under the general teaching mode, the highest comprehensive ability was around 79, and the lowest was around 62. The comprehensive ability under the information-based teaching mode showed a gradual upward trend, and the highest comprehensive ability reached about 87.

4.4. Comparison of Unequal Teaching Pattern in terms of Learning Effect. The ultimate purpose of using the information-based teaching mode is to improve the students' learning ability, and the learning effect is the performance of the learning ability. A survey is conducted on the 6 academic achievements of a school, and the learning effect under the two teaching modes is investigated. The specific outcome is shown in Table 1.

To study the learning sequel of the two teaching modes more intuitively, this study drew the survey results into Figure 8.

It can be clearly seen from the line chart in Figure 8 that the teaching influence under the common methods was about 78, and the learning influence under the message-based teaching pattern was about 90. On the whole, the learning influence under the message-based teaching pattern was higher than the learning influence under the ordinary teaching pattern and the average improvement was 12. It

Retraction

Retracted: Evaluation of the Fluctuation Mechanism of Behavioral Financial Market Based on Edge Computing

International Transactions on Electrical Energy Systems

Received 28 November 2023; Accepted 28 November 2023; Published 29 November 2023

Copyright © 2023 International Transactions on Electrical Energy Systems. This is an open access article distributed under the Creative Commons Attribution License, which permits unrestricted use, distribution, and reproduction in any medium, provided the original work is properly cited.

This article has been retracted by Hindawi, as publisher, following an investigation undertaken by the publisher [1]. This investigation has uncovered evidence of systematic manipulation of the publication and peer-review process. We cannot, therefore, vouch for the reliability or integrity of this article.

Please note that this notice is intended solely to alert readers that the peer-review process of this article has been compromised.

Wiley and Hindawi regret that the usual quality checks did not identify these issues before publication and have since put additional measures in place to safeguard research integrity.

We wish to credit our Research Integrity and Research Publishing teams and anonymous and named external researchers and research integrity experts for contributing to this investigation.

The corresponding author, as the representative of all authors, has been given the opportunity to register their agreement or disagreement to this retraction. We have kept a record of any response received.

References

- [1] X. Yuan, "Evaluation of the Fluctuation Mechanism of Behavioral Financial Market Based on Edge Computing," *International Transactions on Electrical Energy Systems*, vol. 2022, Article ID 2751197, 8 pages, 2022.

Research Article

Evaluation of the Fluctuation Mechanism of Behavioral Financial Market Based on Edge Computing

Xiaoliang Yuan 

School of Accounting and Finance, Zhejiang Technical Institute of Economics, Hangzhou 310018, Zhejiang, China

Correspondence should be addressed to Xiaoliang Yuan; 270051@zjtie.edu.cn

Received 18 August 2022; Revised 7 September 2022; Accepted 19 September 2022; Published 11 October 2022

Academic Editor: Nagamalai Vasimalai

Copyright © 2022 Xiaoliang Yuan. This is an open access article distributed under the Creative Commons Attribution License, which permits unrestricted use, distribution, and reproduction in any medium, provided the original work is properly cited.

The global economy is growing faster and faster. Behavioral finance is a transformation of financial theory. Over the past decade, this shift has had strong repercussions in academia, challenging the dominance of traditional finance and forming its own theoretical system. With the development of the stock market, traditional financial theories and behavioral financial theories continue to converge, and traditional financial theories based on investor rationality and efficient market assumptions are subject to unprecedented conjectures. Financial markets are affected by subjective factors such as people's behaviors and emotions. Investors always make decisions based on bounded rationality, cognitive deficits, and, ultimately, rationality. In order to avoid the complex and unpredictable risks of financial markets and understand their changing laws, the analysis of the characteristics of financial instability is conducive to understanding the nature and internal principles of financial markets. Analysis of the volatility characteristics of financial markets must give priority to the analysis of financial chronological order. Financial time series are characterized by differences in financial markets, which are indeterminate orders, and the analysis of their fluctuations becomes crucial for stimulating the microstructure of financial behavior markets. Therefore, in order to give full play to the role of edge computing and promote the controllability of behavioral financial market volatility, this paper used the calculation task load model algorithm, time slot length optimization algorithm, asymmetric thick-tail random fluctuation, and volatility analysis application algorithm to study the subject of how to learn to reduce financial market volatility, summarizing and discussing the experiment. The research results showed that the behavioral financial market volatility mechanism based on edge computing constructed in this paper improved the predictability of financial market volatility by 15%.

1. Introduction

The scale of the financial market and market entities have expanded rapidly. At the same time, with the continuous expansion of the opening of the financial market to the outside world and with the rapid development of financial markets, the volatility of financial risk can be difficult to detect. Financial investments, as a product of our times, are influenced by human behavior, psychological emotions, and other subjective factors. Investors have always made decisions and other issues with a limited degree of rationality. It is of great value to establish a more controllable behavioral financial market. Therefore, the behavioral financial market studied in this paper is of practical value.

Based on research into behavioral finance and the psychology of human decision-making, this paper examined the impact of investors' investment decisions on behavioral financial markets. In the research of the behavioral financial market, many scholars have invested research. Chen W believed that investors' mentality is related to the short-term interaction of financial stocks such as the Shanghai Composite Index, Shenzhen Stock Exchange and Shenwan, and used the time difference correlation coefficient to judge the medium and long-term correlation of each variable [1]. The Colasante A study found that age and geographic location were important determinants of risk-taking in all regions. Furthermore, risk attitudes in both financial and nonfinancial environments are associated with higher levels of risk aversion in nonfinancial environments [2]. Grling et al.

explored how social comparison and competitive motivation explain high risk in fund management. Experiments on asset markets demonstrated this when performance depended on ranking-based incentives [3]. Ferri investigated whether traders behave differently under higher time pressure (fast conditions) versus lower time pressures (slow conditions). Compared with the “fast” condition, the “slow” condition suppressed market price fluctuations and significantly reduced the spread between limit orders and orders, thereby improving payment fairness [4]. The findings of Brenner L showed that Robo-advisory firms appear to be a good option when it comes to finding investment advice, especially for investors who are concerned about possible conflicts of interest [5]. Morone et al. studied the impact of the quality and quantity of trader information on the distribution of benefits in the laboratory financial market. The results lead us to conclude that signal accuracy is important to justify a nonuniform distribution. Furthermore, subjects were overconfident in their signal quality, which created an “additional” difference as signal quality improved [6]. Chauhan Y understood that more financially literate investors recognize the value of financial advice and have a higher willingness to pay. These investors are also less likely to consult a financial advisor if the advisory fee exceeds the investor’s maximum WTP (willingness to pay) [7].

Scholars have carried out a lot of research on the analysis of the behavioral financial market volatility mechanism, but they all directly use data collection and information technology. There are few theories about the use of volatility mechanism analysis to promote the development of behavioral financial markets. Therefore, this paper conducted an in-depth study of how behavioral financial markets utilize volatility mechanism analysis. In order to make the function of the behavioral financial market come into play, many scholars have carried out research on edge computing. Wang et al. proposed a real-time method to estimate the antenna surface of a large-aperture reflector by calculating the antenna panel position based on an edge sensor [8]. Yang et al. used application functions and edge computing algorithms to efficiently compute and reduce the computational tasks of individual edge nodes to achieve balanced task allocation and scheduling, effectively improving the operability and security of the IoT smart substation auxiliary system [9]. Tafrishi et al. designed a new type of filter that simplifies object detection, tracking, display, and more. The existing boundary-based algorithms and tracking algorithms can provide appropriate automatic control for mobile robots, but many algorithms suffer from complex calculations due to their over-reliance on a large number of road signs [10]. For real-time monitoring, Dong et al. implemented boundary calculation of noise monitoring. The goal was to better detect chemical machinery and equipment by monitoring noise pollution. Through mathematical modeling, noise pollution monitoring of chemical machinery and equipment was carried out on the basis of boundary calculation and compared with conventional noise pollution monitoring [11]. Meng et al. proposed a miner state monitor based on long-term memory network edge counting and random forest degradation decision-making, which can

understand the physical condition and working state of miners in real-time and provide a coal mine with guarantees for the health and safety of miners [12]. Du et al. proposed an optimization model for high-end computing confidence evaluation based on graph theory, aiming at the problems of limited equipment resources in the high-end computing environment and ignoring computing load and confidence path iteration in existing confidence models [13]. For high-end computing environments, Song and Bai proposed a dynamic backlight adjustment mechanism for smartphones, which can effectively reduce the power consumption of smartphones while providing visual effects [14]. Although scholars have carried out more research on edge computing, few of their research results are directly related to the behavioral financial market, and edge computing has a short development time, so there are often some problems in actual development and application. In order to address these issues, this paper investigated edge computing for the development of behavioral financial markets.

Due to the current behavioral finance, investors’ rational decision-making methods are limited. At the same time, problems such as cognitive bias and limited rationality have also appeared, and behavioral finance has become more and more volatile in the financial market. In addition, the current research also has the problem that the research system is not systematic enough, the research content is empty, as well as the research object is marginalized. Faced with this situation, this paper used edge computing technology, time slot length optimization algorithm, volatility analysis, and asymmetric thick-tail stochastic volatility model to study behavioral financial market volatility so as to improve the accuracy of behavioral financial market volatility.

2. Behavioral Financial Market Volatility Mechanism Model Based on Edge Computing

2.1. Edge Computing Logic Model. Edge computing is to integrate basic network, computing, storage and application functions into an open platform to achieve the purpose of nearby services [15, 16]. Its applications are all deployed at the edge to improve the responsiveness of network services for real-time business, application intelligence, security and privacy needs. Edge computing is between physical entities and industrial connections or at the top of physical entities. However, cloud computing can still access the historical data of edge computing. Its structure is shown in Figure 1:

As can be seen from Figure 1, the edge computing model is composed of three parts: cloud, edge, and terminal. All three layers can provide resources and services for applications. As the development of IoT applications has led to a large increase in terminal devices, the terminal resources of the IoT are limited, and remote cloud services are often required to provide services to users. If all device data is transmitted to the cloud center for unified processing and then returned to the device, it would inevitably cause great loss and damage to the network connection and data center and also easily overload the cloud core, blocking services and affecting the experience of end-user devices. By providing computing services close to users, the network and resource

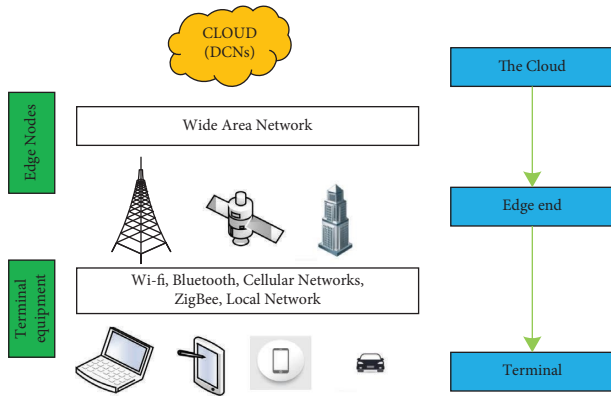


FIGURE 1: Logic structure diagram of the edge calculation.

load of the cloud center can be effectively reduced. Edge computing is not to replace cloud computing but to expand cloud computing and provide a better computing platform for the Internet of Things.

2.2. Behavioral Finance Model. Behavioral finance is a borderline subject that intersects finance, psychology, behavior, sociology and other disciplines and strives to reveal the irrational behavior and decision-making laws of financial markets. It explains, studies and predicts the development of financial markets from the perspective of the specific behavior and psychology of individuals [17, 18]. By analyzing the deviation and inconsistency of the market behavior of financial market entities, it is possible to discover the business philosophy and decision-making behavior characteristics of different market entities in different environments, and try to create a model that accurately reflects real decisions, so that the behavior of market participants and market behavior becomes a model that describes the situation, as shown in Figure 2:

As can be seen from Figure 2, when the price rises, investors' risk aversion decreases, and the decrease in risk aversion leads to an increase in the price, and the exaggerated reaction intensifies. In the case of falling prices, investors' risk aversion has been strengthened, sending prices further lower. The exaggerated response also intensified. Clearly, from two perspectives, changes in risk aversion can lead to overreactions that can be explained by biased expectations. Second, risk aversion to change in time-measured cumulative markets is a positive rate term during high price periods and a disutility term during low price periods. That is, when prices rise, the risk of change increases utility. The total gain is greater than the gain from wealth growth just because of rising prices, and there is an additional positive gain. Likewise, during price declines, risk aversion to change reduces utility, and the overall benefit of the reduction is greater than the reduction in utility, so a reduction in value results in a reduction in resources with no additional benefit. When prices rise, investors feel less risky and feel more rewarded than purely rational investors. Likewise, when prices fall, investors feel riskier and believe they have more to lose than purely rational investors.

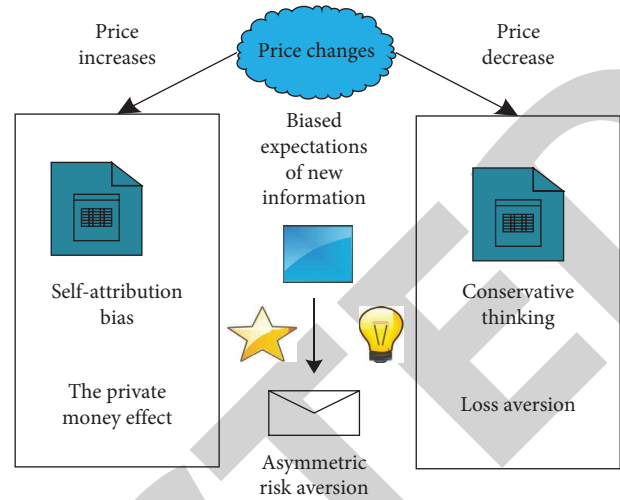


FIGURE 2: A descriptive model of behavioral finance.

Clearly, the role of biased expectations reinforces the role of variable loss aversion in explaining rising market phenomena. In conclusion, the combined effect of variable risk aversion and biased expectations is a phenomenon that reinforces discrete accumulation and cross-sectional models.

2.3. Fluctuation Mechanism Model. In the financial market, the volatility mechanism mainly refers to the standard deviation of the change value of a financial instrument in a specific time frame and is often used to quantify the risk and uncertainty of a financial instrument. It is commonly used to express the movement of stock prices [19].

The most important of these is the fundamental trend of the stock, that is, the situation in which the stock price rises or falls across the board. For investors, if the underlying trend continues to rise, a bull market will form. If it falls, a bear market is formed. The second direction of stock movement is called the secondary trend of stock prices. Because the secondary tendency tends to go in the opposite direction of the primary tendency and restricts it to some extent, it is also called the adjustment of the stock price.

Typically, in both trends, the following features are present: long-term investors are interested in the underlying trend in stock prices, with the aim of buying stocks and selling them in time before a bull market begins [20]. There would be some short-term speculators who would pay more attention to the corrective direction of the stock price in order to make short-term profits. The specific financial market volatility model is shown in Figure 3:

As can be seen from Figure 3, there are roughly two kinds of fluctuations in the behavioral financial market: first, when the stock is undervalued, it directly or indirectly increases the demand for the stock, which in turn stimulates leveraged purchases. Therefore, the increase in the leverage ratio of the stock market results in an increase in the stock price; the second is that when stocks are overvalued, there would be two results: (1) it would directly increase the supply, resulting in a decrease in the leverage ratio of the stock market and a drop in the stock price; (2) there would

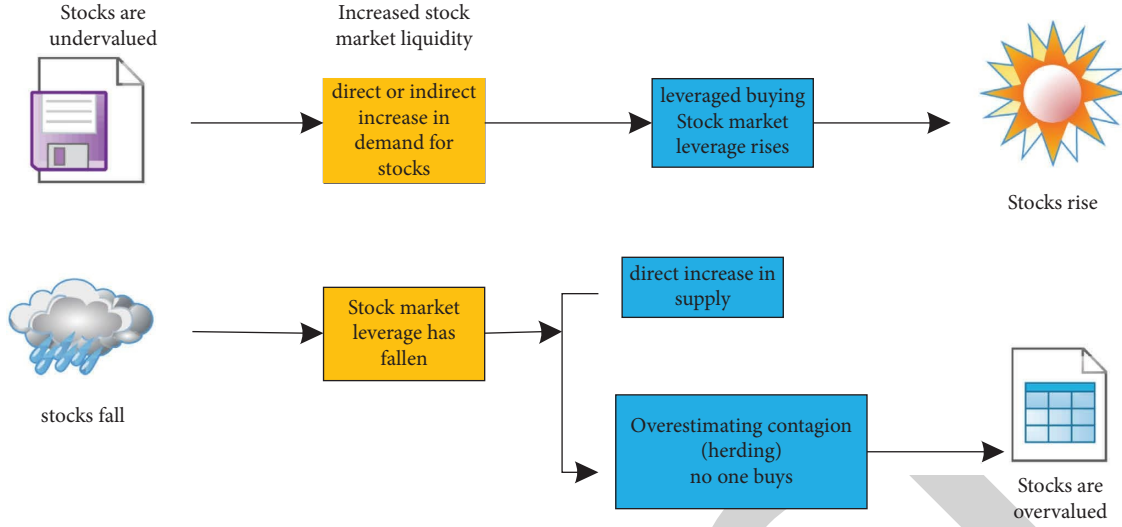


FIGURE 3: Model of the fluctuation mechanism.

be a herd effect due to the contagion of overvalued signals, resulting in a situation where no one takes the order. This situation can also lead to lower stock market leverage and, therefore, lower stock prices.

3. Algorithm Utilization of Behavioral Financial Market Volatility Mechanism Based on Edge Computing

3.1. Computing Task Load Model Algorithm. The computational task load model algorithm combines power consumption and delay factors into one. The load can meet the individual needs of different users, and the relevant factors can be flexibly adjusted [21].

According to the above analysis, the time t required to complete the execution of all computing tasks is

$$t = \max\{t_{loc}^{N_1}, t_{ser}^{N_2}\}, N_1 + N_2 = N. \quad (1)$$

The energy e required to complete all tasks is

$$e = e_{loc}^{N_1} + e_{ser}^{N_2}, N_1 + N_2 = N. \quad (2)$$

The overall load of the system is assumed to be expressed as K :

$$K = \lambda^t t + \lambda^e e. \quad (3)$$

Among them, the coefficients λ^t and λ^e represent the weights of computing task delay and energy consumption when offloading decision-making, respectively. The two coefficients satisfy the following relationship:

$$\begin{cases} \lambda^t + \lambda^e = 1, \\ \lambda^t \geq 0, \\ \lambda^e \geq 0. \end{cases} \quad (4)$$

When λ^t is larger, it means that the user at this time is more concerned about the delay of the calculation and is more sensitive to the delay; when the value of λ^e becomes

larger, it means that the power of the mobile phone of the mobile phone is reduced, so more consideration needs to be given to the power consumption of computing work to improve the battery life of the mobile phone. In this way, the mobile phone user can appropriately determine the weighting factor according to his own situation at the time.

Thus, the goal is to optimize the load P

$$P = \min k. \quad (5)$$

3.2. Time Slot Length Optimization Algorithm. The time slot length is the main factor in reducing the transmission delay of data distribution. Assuming that the data object to be delivered and transmitted contains N data packets in the network, the slot length is represented by the ability to send N data packets in one transmission. The expected delay can be estimated by using the following formula:

$$D_{\text{overall}} = D_{\text{firstArr}} + D_{\text{prop}}. \quad (6)$$

Among them, D_{firstArr} represents the delay when the first batch of n data packets reaches the last hop and D_{prop} represents the transmission delay of transmitting the remaining batches of data packets. D_{firstArr} is obtained by the following formula:

$$D_{\text{firstArr}} = h\tau \frac{n}{q}. \quad (7)$$

Among them, τ is the time required to transmit a single packet lock and q is the average link quality, and n/q is the expected number of transmissions.

Considering the situation of multiple pipelines, when the first batch of data packets reaches the node of the h hop, the second batch of data packets has already reached the node of the $(h-3)$ hop. At this time, D_{prop} represents the following:

$$D_{\text{prop}} = 3 \cdot \frac{n}{q} \left(\frac{N}{n} - 1 \right). \quad (8)$$

Combining the formula, the desired data distribution transmission delay can be calculated by using the time slot length n , so the optimal time slot length n can be obtained by solving the following formula:

$$\begin{aligned} D_{\text{overall}}(n) &= 0, \\ D_{\text{firstall}}(n) &= 0. \end{aligned} \quad (9)$$

3.3. Volatility Analysis. Volatility is related to the range of possible returns for holding a stock and the probability of it occurring. The more volatile a stock is, the wider the range of its possible outcomes and the greater the probability that returns would be at the edge of the range. A portfolio is assumed to be composed of x securities. σ_m ($m = 1, 2, 3, \dots, x$) represents the standard deviation of each security, and W_n ($n = 1, 2, 3, \dots, x$) represents the weight of different securities in the portfolio, then

$$\sigma^2 = \sum_{m=1}^x \sum_{n=1}^x w_m w_n \text{cov}(r_m r_n). \quad (10)$$

Among them, $\text{cov}(r_m r_n)$ ($m, n = 1, 2, 3, \dots, x$) is the covariance of security m and security n . When r_m and r_n are discrete random variables, there are

$$\left\{ \begin{aligned} \text{cov}(r_m, r_n) &= E((r_m - E(r_m))(r_n - E(r_n))) \\ &= \sum_{k=1}^x (r_{mk} - E r_{mk})(r_{nk} - E r_n). \end{aligned} \right. \quad (11)$$

When r_m and r_n are continuous random variables, there are

$$\text{cov}(r_m r_n) = \int_{-\infty}^{+\infty} \int_{-\infty}^{+\infty} (r_m - E(r_m))(r_n - E(r_n)) f(r_m, r_n) dr_m dr_n. \quad (12)$$

The following formula is derived from the standard deviation

$$\sigma^2 = \sum_{m=1}^x \sum_{n=1}^x w_m w_n \rho_{mn} \sigma_m \sigma_n. \quad (13)$$

The matrix form is expressed as

$$\sigma^2 = [W_1 \dots W_x] \begin{bmatrix} \sigma_1^2 & \sigma_{12} & \dots & \sigma_{1x} \\ \dots & \dots & \dots & \dots \\ \sigma_{m1} & \sigma_{m2} & \dots & \sigma_m^2 \end{bmatrix} \begin{bmatrix} W_1 \\ \dots \\ W_m \end{bmatrix}. \quad (14)$$

Among them, σ_{mn} is the covariance of r_m and r_n .

Others are the same as above. Through the above analysis, it can be seen that there are two parts of the risk or variance of the portfolio products: one is the systematic risk that cannot be eliminated, and the other is the unsystematic risk that can be eliminated.

3.4. Asymmetric Thick-Tailed Random Fluctuations. The asymmetric thick-tailed SV (Schedule Variance) is derived from the standard model. If the observation error of the

standard model has a thick-tailed probability distribution, and the perturbation term of the observation formula is related to the perturbation term of the wave equation, a thick-tailed asymmetric model is obtained. Its specific expression is as follows:

$$r_t = \beta +_0 \sum_{i=1}^p \beta_i r_{t-i} + e^{z_t/2} \varepsilon_t z_{t+1} = \mu + a(z_t - \mu) + \delta_{\eta_t} \eta_t. \quad (15)$$

Among them, $\varepsilon_t \sim dt(0, 1, \omega)$, $\eta_t \sim dN(0, 1)$, and $\text{cov}(\varepsilon_t, \eta_t) = \rho$.

It can be verified that the above transformation is effective, and a transformation is made to ε_t in the new model again, and the parameter m is introduced to satisfy a normal distribution with a mean of 0 and a variance of 1.

There are

$$\varepsilon_t = \gamma \sqrt{1 + \rho^2} + \rho_t. \quad (16)$$

Therefore, there are

$$\text{corr}(\gamma_t, \eta_t) = E((\gamma_t)) \eta_t. \quad (17)$$

Formula (17) is brought in, so the transformed model is

$$r_t = \beta_0 + \sum_{i=1}^p \beta_i r_{t-1} + \lambda_t e^{z_t/2} (\gamma \sqrt{1 - \rho^2} + \rho \eta_t). \quad (18)$$

4. Evaluation of the Fluctuation Mechanism of Behavioral Financial Market Based on Edge Computing

4.1. Research Purpose. This paper uses a computational task load model algorithm, time slot length optimization, volatility analysis, and asymmetric thick-tail stochastic volatility model to study the behavioral financial market volatility mechanism to prove that edge computing has obvious support and guidance for behavioral financial market volatility.

4.2. Research Design. This paper takes the typical herd behavior and loss aversion behavior in the commercial bank credit market as an example to conduct an empirical study on it. It is helpful to explore the significant degree of influence of commercial banks' credit behavior on commercial banks and the research on the analysis of behavioral financial market fluctuation mechanism.

5. Simulation Experiment of Behavioral Financial Market Volatility Mechanism

5.1. Analysis of the Balance of Nonperforming Loans in Commercial Finance. The NPL ratio is determined to check for herding among commercial banks and refers to the tendency of investors to ignore their own valuable private information and follow the decision-making style of the majority in the market. Since the data of different loan balances cannot be directly obtained, the data of different loan balances are obtained according to the relationship

between the nonperforming loan balance and the nonperforming loan ratio. It is mainly an empirical study on data selection and processing of sheep herds in four types of commercial banks: rural, large, urban and stock. Taking 2014–2017 as an example, Figure 4 shows the balance of nonperforming loans.

As can be seen from Figure 4, nonperforming loans in four industries were on the rise from 2014–2017. Large commercial banks had the largest share of nonperforming loans in 2015–2016. Large commercial banks doubled from 300 shares in 2015 to 600 shares in 2016, and joint-stock transaction banks increased from 85 shares to 210 shares. City commercial banks increased from 75 shares to 150 shares, and rural commercial banks increased the least, with only 65 shares.

5.2. Analysis of the Proportion of Nonperforming Loans in Commercial Finance. The monthly ratio of nonperforming loans of banks is an important indicator to measure the safety of bank credit assets. The greater the proportion of nonperforming assets, the higher the ratio of total loans that cannot be repaid; the lower the proportion of nonperforming assets, the less the total amount owed by financial institutions.

The proportion of the nonperforming loan balance of the four types of commercial banks is shown in Figure 5.

As can be seen from Figure 5, large commercial banks dropped from 73% to 50%, with an average proportion of 61.75%; joint-stock commercial banks increased from 13% to 17%, with an average proportion of 18.25%; city commercial banks increased from 8% to 19%, with an average proportion of 13.75%; rural commercial banks increased from 7% to 10%, with an average proportion of about 8.8%. In 2014–2015, large commercial banks accounted for more nonperforming loan balances than the other three banks combined, and rural commercial banks accounted for the smallest quarterly nonperforming loan balance. However, with the continuous change in time, the proportion of the quarterly nonperforming loan balance of large commercial banks continued to decline, and the proportion of the other three types of commercial banks showed an upward trend, among which the proportion of rural commercial banks increased the most rapidly.

5.3. Analysis of Nonperforming Loan Ratio of Commercial Finance. The nonperforming loan ratio refers to the proportion of bad debts in financial institutions. Nonperforming loans are five types of loans, normal loans, prospect loans, concern loans, doubtful loans and losses, all of which are called nonperforming loans.

The nonperforming loan ratios of the four types of commercial banks are shown in Figure 6.

From Figure 6, it can be seen that from 2014 to 2017, commercial banks showed a trend of first falling and then rising. Among the four types of banks, rural commercial banks have the highest nonperforming loan ratio, and joint-stock commercial banks have the lowest nonperforming loan ratio at the beginning. However, by 2015, city

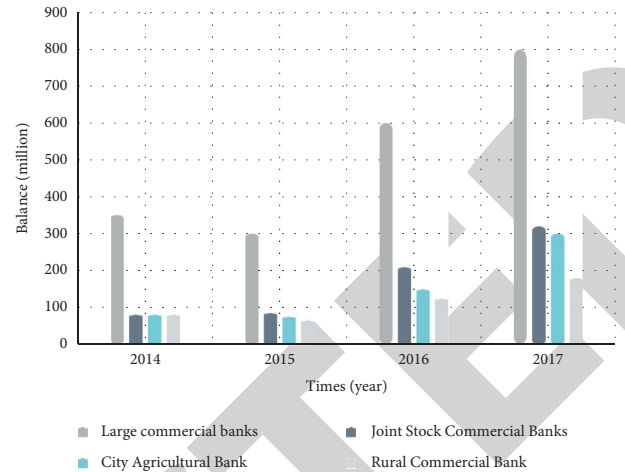


FIGURE 4: The quarterly nonperforming loan balance of commercial banks.

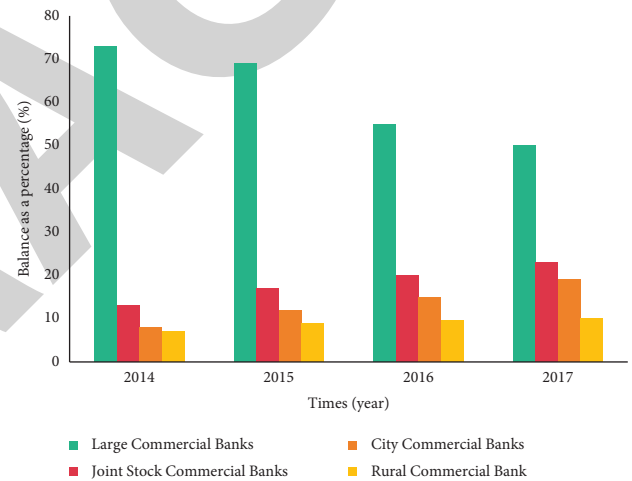


FIGURE 5: Trend chart of outstanding nonperforming loans of all banks.

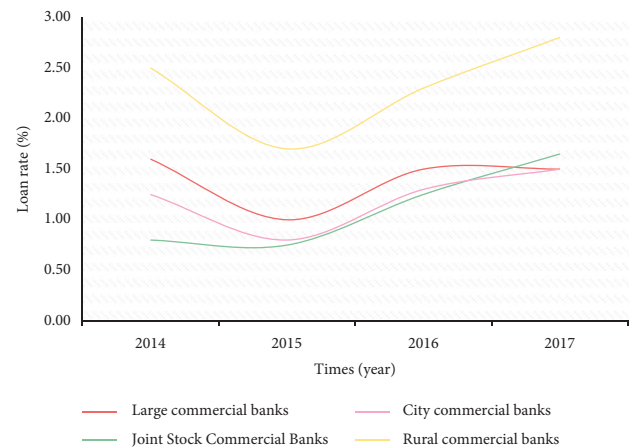


FIGURE 6: Quarterly nonperforming loan ratio of commercial banks.

commercial banks became the lowest. As calculated from Figure 6, the quarterly NPL ratio of large commercial banks averaged 1.4%; the average quarterly nonperforming loan ratio of joint-stock banks was 1.11%; the average quarterly nonperforming loan ratio of urban commercial banks was 1.21%; the average quarterly nonperforming loan ratio of rural commercial banks was 2.325%.

Therefore, the balance of nonperforming loans, the ratio of nonperforming loans and the sum of various loans of joint-stock commercial banks, city commercial banks and rural commercial banks always show the same upward or downward trend as the data of large commercial banks. Therefore, there is herding behavior among these four commercials and financial markets.

5.4. Analysis of Edge Computing. The rapid development of global smartphones has promoted the development of mobile terminals and edge computing. For the Internet of Things, the breakthrough of edge computing technology means that many controls can be completed directly at the local edge computing layer without going through the cloud. This would greatly improve the efficiency of data processing and reduce the data load. Because it is closer to the user, it is also possible to react more quickly to the user, thereby handling demands at the edge. The edge computing benchmark architecture in the Edge Computing Consortium includes aspects such as devices, networks, data, and applications. Platform providers mainly provide hardware and software infrastructure in terms of network interconnection, computing power, data storage, and application.

In addition to the commonly used computational task offloading algorithms for performance analysis, the proposed algorithm is compared with the following algorithms:

- (1) Local execution: all computing tasks are executed locally without task unloading
- (2) Execution on the cloud: all computing tasks are offloaded to the cloud for execution, not locally
- (3) Greedy Unloading: when the task is unloaded, the greedy strategy is used

The selection of parameters is shown in Table 1:

If the current local CPU (Central Processing Unit) is idle, it would be executed locally. When the launcher is inactive, the task would be transferred to the cloud for execution; referring to the required parameters in Table 1, Figure 7 shows a graph of the average task latency for each method with different numbers of computational tasks.

From Figure 7, it can be seen that the local execution has the highest latency, which indicates that task offloading can reduce the task execution time. The average latency of local execution, on-cloud execution, and federated task offloading increases with the number of tasks, and on-cloud execution tends to grow much faster than federated task offloading because all on-cloud tasks are executed in the cloud. When there are too many tasks, the task waiting time also increases rapidly, and in order to unload common tasks, some tasks are executed locally. It is equivalent to executing some tasks in parallel, reducing the task delay. At the same time, it can

TABLE 1: Reference table to the relevant parameters of edge calculation.

Id	Symbol	Value	Meaning
1	N	20	Number of tasks to be performed
2	P_{cup}	0.5 W	The computational power of the local CPU
3	p_{tu}	2W	Mobile devices transmit power
4	f_{ico}	1GHz	The computing power of mobile devices
5	ω	1MHz	Channel bandwidth

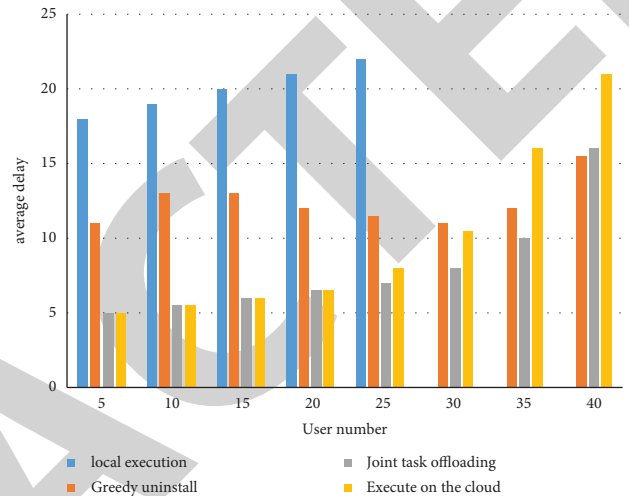


FIGURE 7: Average latency under different task numbers.

be seen that when the number of tasks is less than a certain value, the delays of cloud execution and joint task offloading are very close. Because when there are few tasks, most tasks are offloaded to the server for execution, and as the number gradually increases, only some tasks are scheduled to be executed locally. The obvious difference is the greedy implementation, where the average latency first increases, then decreases, and then continues to increase. This is because, in the beginning, for cloud execution and offloading of shared tasks, the local CPU (central processing unit) is idle. Therefore, greedy execution puts a large part of the task on local execution. However, the latency of local execution should be much larger than that of cloud execution, so the average total latency is initially increased; because the execution speed on the cloud is faster, more tasks would be arranged to be offloaded to the cloud for execution, which would reduce the overall average delay; however, the rewards for offloading tasks are also limited. The average total latency also increases when there are more tasks. The behavioral financial market volatility mechanism combined with edge computing improved the predictability of financial market volatility by 15%.

6. Conclusion

Due to the current behavioral finance, investors' rational decision-making methods were limited, and problems such as cognitive bias and limited rationality also appeared, and behavioral finance fluctuated more and more in the financial market. In addition, the current research also had some

Retraction

Retracted: Optical Fiber Multiparameter Detection and Numerical Simulation and Characteristics of Water Quality Particulate Matter Based on Single-Photon Detection Technology

International Transactions on Electrical Energy Systems

Received 28 November 2023; Accepted 28 November 2023; Published 29 November 2023

Copyright © 2023 International Transactions on Electrical Energy Systems. This is an open access article distributed under the Creative Commons Attribution License, which permits unrestricted use, distribution, and reproduction in any medium, provided the original work is properly cited.

This article has been retracted by Hindawi, as publisher, following an investigation undertaken by the publisher [1]. This investigation has uncovered evidence of systematic manipulation of the publication and peer-review process. We cannot, therefore, vouch for the reliability or integrity of this article.

Please note that this notice is intended solely to alert readers that the peer-review process of this article has been compromised.

Wiley and Hindawi regret that the usual quality checks did not identify these issues before publication and have since put additional measures in place to safeguard research integrity.

We wish to credit our Research Integrity and Research Publishing teams and anonymous and named external researchers and research integrity experts for contributing to this investigation.

The corresponding author, as the representative of all authors, has been given the opportunity to register their agreement or disagreement to this retraction. We have kept a record of any response received.

References

- [1] Q. Xu, C. Gao, and C. Zhou, "Optical Fiber Multiparameter Detection and Numerical Simulation and Characteristics of Water Quality Particulate Matter Based on Single-Photon Detection Technology," *International Transactions on Electrical Energy Systems*, vol. 2022, Article ID 3170082, 10 pages, 2022.

Research Article

Optical Fiber Multiparameter Detection and Numerical Simulation and Characteristics of Water Quality Particulate Matter Based on Single-Photon Detection Technology

Quan Xu ^{1,2}, Cuiyun Gao,^{1,2} and Chun Zhou¹

¹School of Electronic and Information Engineering, Anhui Jianzhu University, Hefei 230601, Anhui, China

²Power Quality Analysis and Load Detection Technology Laboratory, Anhui Jianzhu University, Hefei 230601, Anhui, China

Correspondence should be addressed to Quan Xu; xuquan@ahjzu.edu.cn

Received 25 August 2022; Revised 15 September 2022; Accepted 22 September 2022; Published 10 October 2022

Academic Editor: Nagamalai Vasimalai

Copyright © 2022 Quan Xu et al. This is an open access article distributed under the Creative Commons Attribution License, which permits unrestricted use, distribution, and reproduction in any medium, provided the original work is properly cited.

Water quality testing is of great significance for daily water use or water use in high precision manufacturing. The use of single-photon detection technology to detect water particles is one of the important methods of physical water quality detection. However, the current water quality particle detection technology needs to be improved in the range and accuracy of turbidity detection. The paper aims to use single-photon detection technology to design a fiber optic turbidity detection system to solve the current problems of small turbidity detection range and low accuracy in a large range. In response to this, this paper has made an in-depth understanding of single-photon detection technology and designed two sets of detection schemes using the performance of photons. The first set is the transmission optical fiber turbidity detection, which can effectively detect the ultralow turbidity range and a wide range of water quality particles. The second set is a scattering optical fiber turbidity detection system, which can effectively detect water particles in the low and medium turbidity range. In this paper, the two systems were integrated into a whole system, so the results of the two detection methods can also be compared, and the detected turbidity can be obtained more accurately. The experimental results showed that for the transmission optical fiber turbidity detection system, the detection effect of the system was the best under the incident light intensity of 11 μm , and the fitting value was 0.99; for the scattering optical fiber turbidity detection system, the detection effect of the system was the best under the incident light intensity of 4 μm , and the fitting value was 0.99.

1. Introduction

Water is one of the most precious resources that nature bestows on mankind. It is indispensable in life and plays an important role in agriculture, industry, and economic development. However, water is also a scarce resource for mankind. In areas with extreme water scarcity, even human survival is a problem, for example, China's water resources. China is a country with a mild water shortage. Due to China's large population, the distribution of water resources is uneven. With the Yangtze River as the boundary, the south has nearly 80% of freshwater resources. Therefore, more perfect measures must be taken for protecting water resources. In this regard, wastewater treatment is a major and sustainable way to protect water resources. It is a powerful measure for the

efficient use of water resources to treat and reuse the sewage produced by humans. However, whether the treated sewage can meet the standard, whether it can be reused, and where it can be applied are all issues that need to be considered. The most important of these issues is water quality testing. By using single-photon technology to detect water quality particles, it is possible to judge the water quality and then detect whether the water quality meets the standard and whether it can be reused. Therefore, from this aspect, it is necessary to use single-photon technology to design a fiber optic turbidity detection system to detect water quality treatment.

Single-photon technology is widely used in ranging, turbidity detection, and other places. Many scholars have conducted research on single-photon technology. Passig detected single vessel plumes from distances of several kilometers by

single particle mass spectrometry. He analyzed the metal content of individual particles preserved during atmospheric transport, which led to a dramatic increase in the accuracy of detection [1]. Jia designed and fabricated silicon carbide microdisks and experimentally characterized their multimode resonances in air and water [2]. To effectively assess the health risks of cyanobacterial blooms, MD Graham devised an early warning system. The system was capable of rapidly detecting species of interest and determining whether their cellular concentrations exceeded the recommended guidelines [3]. Sultana proposed a new approach to rainwater harvesting. He first conducted multiparameter detection of water quality particulate matter and collected it after confirming that it was drinkable, which solved the drinking water problem in some water deficient areas [4]. Asbach studied the performance of the water-based personal condensation particle counter PUFPC100 when sampling a variety of different test aerosols [5]. Many scholars have conducted research on the application of single-photon technology in industry and biomedicine, and the research results have also been very satisfactory. However, their research only focused on the existing performance of single-photon technology and did not improve or develop new applications of single-photon technology.

For water quality testing, scholars have been carrying out research for a long time. Huffaker presented a new platform for stand-alone absorbing and multiplying photodiodes. Out of the 4400 nanowires that make up a photodiode, each event was confined to one nanowire, and the platform was used for single-photon detection [6]. Deng designed and developed a photodiode-based high dynamic range photodetection module, which simplifies system operation and can easily detect various incident light intensities [7]. To cope with the large error in light intensity measurement in extreme cases, Zhou improved the UV (ultraviolet) single-photon detection technology and designed a high performance UV photodiode with a diameter of $300\ \mu\text{m}$ [8]. Silver demonstrated an upconversion-based multiplexing scheme for single-photon detection using a waveguide with multiple phase-matched peaks [9]. Ren combined dual-comb-based laser ranging technology with time-correlated single-photon counting technology to make single-photon measurements more precise. He also demonstrated its feasibility for precise laser ranging under photons [10]. However, their water quality detection methods are still stuck in the traditional light absorption law detection method, which has a small detection range and low precision.

The innovations of this paper are as follows: (1) the single-photon detection technology was improved so that the single-photon detection technology can be better applied to the detection of water particles. (2) An optical fiber turbidity detection system of the transmission type and scattering type was designed, which greatly improved the range and accuracy of turbidity detection.

2. Optical Fiber Water Quality Particle Detection

2.1. Optical Fiber Detection Technology. Optical fibers are often used as broadband transmission media in daily use.

Due to the silica material of optical fibers, the light source can be totally reflected in the structure [11, 12]. Optical fiber now has a strong application in electronic technology. Since the transmission of light inside the fiber is total reflection, the transmission loss of the signal in the fiber is much lower than the loss in the conduction of the wire. Additionally, since the main raw material for optical fiber production is silicon, which is very abundant on Earth and easy to mine, the price is very cheap. All of these have prompted many optical fibers to be used in daily production and life. The schematic diagram of fiber structure and propagation is shown in Figure 1.

In 1977, optical fiber sensing technology was discovered and gradually began to be applied in various fields. With the rapid popularization of Internet construction, optical fiber communication technology has developed rapidly [13, 14]. Optical fiber sensing technology has also developed various properties, such as temperature, humidity, speed, sound field, and magnetic field. Optical fiber as a medium can pass light waves with ultralow loss. Optical fiber sensing technology transmits external signals in the form of light waves through optical fibers [15, 16]. Since the transmission of light waves in the optical fiber is less affected by the outside world, optical fiber sensing technology is a relatively stable sensing technology. The emergence of optical fiber sensors has enabled many water quality detection equipment to develop toward strong adaptability, compactness, portability, and intelligence. The physical map of optical fiber and optical cable is shown in Figure 2.

2.2. Principle of Detection of Particulate Matter in Water Quality

2.2.1. Lambert –Beer Transmission Law. Transmission and reflection occur when a wave propagates from one medium to a different medium and when there are discontinuities in the medium through which the wave propagates. In optics, there are many materials to which Lambert Beer's law of transmission can be applied. It is suitable for all electromagnetic radiation and light-absorbing material measurements, including gases, liquids, and solids, and even the microscopic world of molecules, atoms, and ions. The use of the transmission law can shine brightly in quantitative measurements. The basic principle of using the Lambert–Beer transmission law is to test water quality particulate matter and to use the degree of light loss to judge the abundance of water quality particulate matter. When the photons are emitted from a light source, in the turbid water, some particles would reflect, refract, and absorb the irradiated light, which causes the light to be hindered in the process of propagation. As long as the direction of light propagation and the intensity of light are well controlled, and when the change characteristics of the weakening of light energy are detected and numerically simulated, the particle concentration of water quality can be obtained [17, 18].

Light travels through the medium. Since the medium has certain obstacles to the transmission of light, the output light

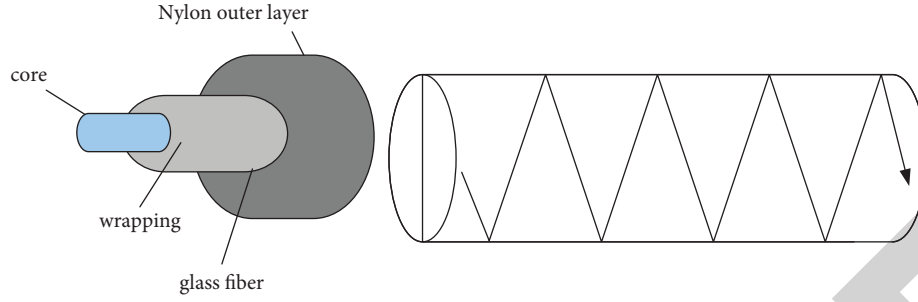


FIGURE 1: Optical fiber structure and transmission mode.

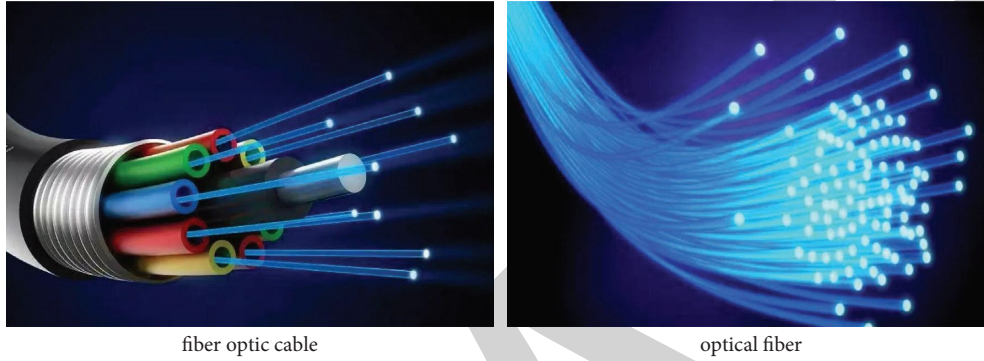


FIGURE 2: Optical cable and optical fiber.

would have a certain loss. According to the Lambert–Beer transmission law, the farther the light travels, the greater the loss of light [19, 20]. It is assumed that the medium in Figure 3 is uniform, and then, this process can be expressed by the following formulas.

$$d_I = \alpha I d_x, \quad (1)$$

$$\int_{I_o}^{I_t} \frac{d_I}{I} = \int_0^l \alpha d_x, \quad (2)$$

$$I_t = I_o e^{-\alpha l}. \quad (3)$$

Among them, l is the distance of light penetration; I_o, I_t are the intensity of the incident light and outgoing light, respectively; d_I, d_x are the loss of light and the dielectric layer. The incident light I_o causes loss after passing through the dielectric layer d_x . The fact that α must be negative can be obtained by using the knowledge of integration as shown in formula (2).

It can be seen that the above formulas are aimed at a solid substance with a homogeneous medium. The internal structure of solid matter is relatively stable, and the attenuation of light is proportional to the transmission distance and would not be affected by other factors [21]. However, if the solid is replaced by a liquid substance, the above formulas cannot directly denote the attenuation coefficient of light. This is due to the fact that in liquid substances, molecular motion is more active, and the propagation of photons cannot be well controlled [22]. Therefore, the weakening process of light is not only related to the distance

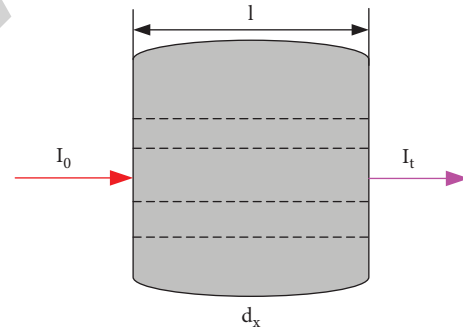


FIGURE 3: Propagation of light in a medium.

but also to the concentration or type of the liquid itself. To detect the transmission relationship of the liquid, (4) and (5) can be combined:

$$\alpha = \beta C \Rightarrow I_t = I_o e^{-\beta C l}, \quad (4)$$

$$I_t = I_o e^{kT}. \quad (5)$$

From the above derivation, it can be found that different media would lead to different relationships between the intensity of incident light and outgoing light, and two factors cause the energy difference between the intensity of transmitted light and the intensity of incident light. These two factors are the distance transmitted and the medium transmitted, respectively. However, both are the same as changing the transmittance of light by changing the loss of light. Therefore, in the detection technology, as long as the

change law of light is used, the turbidity of liquid can be detected (that is, the value of the small particles in liquid). Next, two methods of liquid detection are introduced.

2.2.2. Scattering Turbidity Detection. The phenomenon of light scattering can be understood as the phenomenon that when a beam of light passes through a medium with inhomogeneous optical properties, light is observed in other directions than the incident light, that is, the phenomenon in which the direction of the incident light changes during the transmission process. Light scattering is very common in nature, and even in a beautiful landscape, as shown in Figure 4.

In scattering turbidity detection, scattering phenomena in nature are also used. In detection, a string of parallel lights is first input into the sample to be tested. At this time, the propagation of light would cause changes [23]. When the particulate matter in the solution is so small that it is smaller than the wavelength of the incident light, the scattered light intensity can be expressed as follows:

$$I_R = \mu \cdot \eta \cdot I_0, \quad (6)$$

$$\mu = \frac{K_R N V^2}{\lambda^4}, \quad (7)$$

$$\eta = \left(\frac{n_1^2 - n_2^2}{n_1^2 + 2n_2^2} \right)^2. \quad (8)$$

The scattered light intensity consists of three parts, namely, the incident light I_0 , the refractive index η , and the refraction process μ . Among them, λ is the initial light wavelength; N and V are the particle number and volume of the liquid to be tested, respectively; K_R is the Rayleigh scattering coefficient, this coefficient is fixed in liquid detection. n_1, n_2 are the refractive indices of the particles.

In the detection process, since the liquid to be tested does not change frequently, it can be assumed that V and λ remain unchanged, then K_R is proportional to N . Formula (6) can be expressed as follows:

$$I_R = K' I_0 N, \quad (9)$$

$$K' = \frac{\mu}{N} \cdot \eta. \quad (10)$$

Among them, K' becomes a constant value, which can be used as a new refractive index.

When the particulate matter in the solution is larger than the wavelength of the incident light, the scattered light intensity can be expressed as follows:

$$I_M = K_M A N I_0. \quad (11)$$

The difference from Formula (9) is that when the particle diameter is larger, the refractive index changes. K_M is Mie scattering, which can better simulate the scattering characteristics of large particles, such as smoke and haze. A is the surface area of the particle. When the particles are larger, the concentration is larger and the

scattered light intensity is larger, so that (11) can be simplified as follows:

$$I_S = K N I_0. \quad (12)$$

At this time, N is no longer the number of particles per unit volume but the concentration. K is the index of refraction after finishing.

2.2.3. Transmission Turbidity Detection. The process of light transmission is always accompanied by the process of absorption and loss of light energy. The traditional transmission turbidity detection method is also proposed by using the law of the energy attenuation change characteristics in the transmission process. The scattering-type detection is used to judge the intensity of the refracted light, while the transmission type is used to judge the transmitted light intensity, which focuses on the loss of light during the propagation process. Therefore, the intensity of light cannot be used as a criterion for evaluation during detection. What is used here is the energy of light. According to the glass duality of light, the photon energy collected after the incident light passes through the medium can be measured.

$$E = h\nu, \quad (13)$$

$$\nu = \frac{c}{\lambda}. \quad (14)$$

Formula (13) and (14) are basic formulae in optics, where h is Planck's constant. ν is the frequency of light, which can also be obtained by dividing the speed of light c by the wavelength λ .

In a certain period of time Δt , the stable incident light transmission power used in the experiment can be expressed as follows:

$$P_t = \frac{(nM_t)h\nu/\lambda}{\eta\Delta t}, \quad (15)$$

Among them, M_t represents the photon pulse signal and η here represents the efficiency value of photon detection.

When using transmittance to detect liquid turbidity, there are two situations. When liquid is relatively pure, the transmission of light would hardly be hindered, which can be represented by a linear relationship. When turbidity is high, the transmission of light can only be expressed in exponential form. Specifically, it is necessary to set a threshold value to determine the turbidity of liquid. When turbidity is less than the threshold value, a linear relationship is used to express it so that the measurement can be performed quickly, and the lower limit of turbidity during detection is further improved. After referring to a large amount of literature, 0.1 NTU (turbidity unit) is used as the threshold. When the turbidity T is less than 0.1 NTU, the calculation formula is (16); when the turbidity T is greater than 0.1 NTU, the calculation formula is (17).

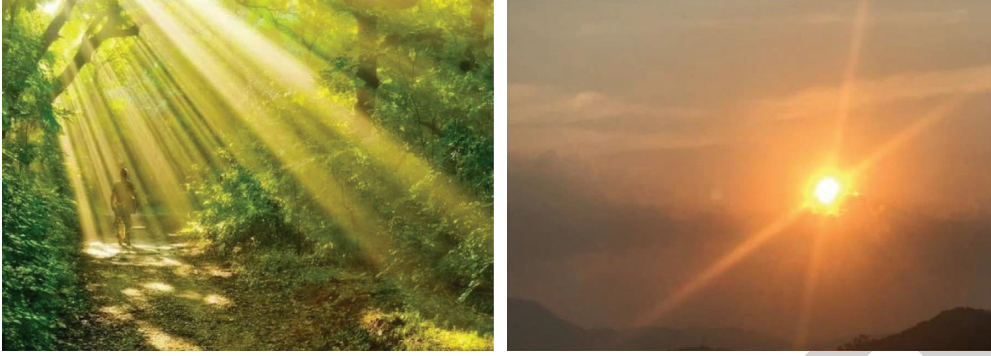


FIGURE 4: Light scattering phenomenon.

$$M = K'' \cdot T + C_1, \quad (16)$$

$$M = K'' \cdot \sum_{n=0}^{\infty} \frac{T^n}{n!} + C. \quad (17)$$

Among them, K'' is the conversion coefficient, which can be obtained jointly by the transmission power and the law of refraction. Due to space constraints, the calculation is not detailed here. C, C_1 are constants.

2.3. Design and Construction of the Optical Fiber Detection System

2.3.1. Overall Design of the System. Based on the optical fiber single-photon detection technology, a system is designed for the transmission turbidity detection method and the scattering turbidity detection method introduced above, which makes the counting more convenient and the presented data more intuitive. To improve the measurement lower limit and stability of the detection system, the structure of the optical fiber probe is improved in this paper. Optical elements such as a new condenser lens and reflector are added to the probe port, which makes the entire optical fiber optical path structure more compact and stable and provides the possibility of finally realizing a wide dynamic measurement range and a portable structure. Figure 5 shows the overall structure of the system. The difference between the transmission type and the scattering-type detection methods is mainly present in the calculation method, and the difference in hardware is not very large. Therefore, the scattering-type turbidity detection system is described in detail. In Figure 5, with a fixed laser as the light source and a steady state laser emission, the power can be adjusted. The optical fiber attenuator can adjust the light intensity appropriately to achieve the effect of controlling the variable. The sample cell is used as the test storage location and is surrounded by metal material. The incoming direction of the fiber is adjusted by using the fiber collimator, which can ensure that the light beam can pass through the container accurately. Afterward, the measurement of the scattered light intensity and the photon energy is performed by the single-photon detection module. Finally, it is counted by using a photon counter, and the data results are further processed by using

the computer and presented in a visual way. In terms of hardware selection, due to the high clock frequency of FPGA and a small internal delay, all control logic is completed by hardware, which is fast and efficient. Simultaneously, it has a very powerful hardware description language and simulation tools, which are convenient for checking the correctness of the results. The advantages of the field-programmable gate array (FPGA) in high-speed signal acquisition and processing are utilized, and the acquired pulse signals are processed on FPGA, which greatly improves the data processing efficiency.

The physical system is assembled based on the overall design architecture of the system and the desirability and cost-effectiveness of materials. The main hardware choices are shown in Table 1.

In the system test, the standard solution of formazin is used to detect turbidity. Formazin standard solution is often used in optical experiments because the formazin standard solution is stable and not easy to deteriorate, and it is also convenient to store. Additionally, the method for preparing the standard solution of formazin is relatively simple, and the materials are easy to obtain. In preparation, typically 25.0 ml of water is added to a 2.5 g urotropine sample to allow complete fusion, and then, 1.0 g of hydrazine sulfate is added to the urotropine aqueous solution. Finally, the mixture solution is diluted with water to 100 ml. After standing for a period of time, a standard formazin standard turbidity solution is prepared, and the turbidity of the solution is 400 NTU. It must be shaken well before use. In the experiment of this paper, the standard solution of formazin purchased from the laboratory was directly used for the test to avoid more errors in the experiment due to the errors caused by the preparation of the standard solution.

3. Turbidity Detection System Test Results

First, a multipoint measurement experiment with a wide turbidity range was carried out using the built-in measuring device. This paper was mainly carried out in three aspects: the preparation before the experiment, the result of the experiment, and the analysis of the result of the experiment. For the transmission detection technique, samples with 0–1000 NTU turbidity were tested herein and samples with 0–1 NTU turbidity were analyzed. For scattering detection,

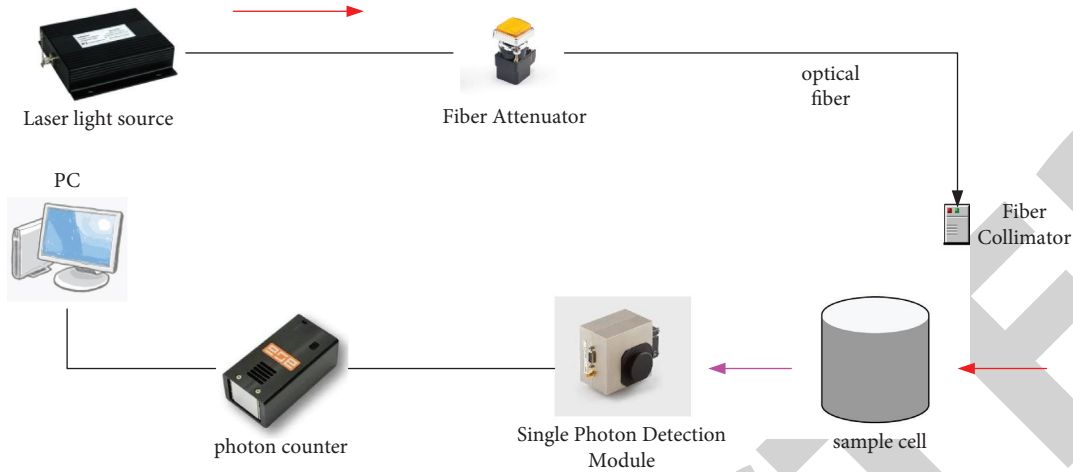


FIGURE 5: Schematic diagram of the fiber optic turbidity detection system.

TABLE 1: Hardware selection.

Serial number	Hardware	Product source
1	852 nm steady state laser	Thorlabs, DBR852S
2	Fiber attenuator	Thorlabs, VOA850-APC
3	Single-photon detector	PerkinElmer, SPCM-AQRH
4	Bandpass filter	Thorlabs, FB850-10

samples with a turbidity of 10–150 NTU were tested and compared with commercial Hach turbidity.

3.1. Test of the Transmission Fiber Inspection System. The designed transmission optical fiber detection system was tested. In the test, in order to highlight the advantages of the large detection range of the transmission turbidity detection system, samples of 0–1000 NTU were tested. In addition, in order to prove the effectiveness of the system, the light sources with multiple light intensities were also tested. The test results are shown in Figure 6.

In order to avoid adjusting the working state of the laser and obtain a wider dynamic measurement range as much as possible under a certain power, an optimal light intensity value should be sought for the system. Therefore, the influence of the variation of the light intensity of the light source on the measurement results of the system was discussed. In Figure 6, the abscissa represents the turbidity of the standard solution of formazin and the ordinate represents the photon count. Photon counting is adopted by the data acquisition module FPGA in the system. In order to reduce the error as much as possible, the photon counting period was particularly set to 1 ms, and the average value was used to represent the counting value of the system. From the data in Figure 6, there was an obvious exponential relationship between the photon count and the change in turbidity under different light intensities. The higher the turbidity, the lower the photon counts. When the turbidity

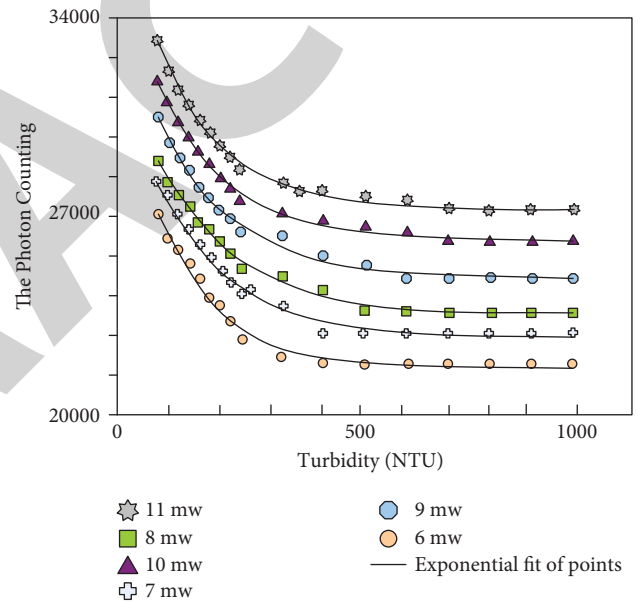


FIGURE 6: Measurement results under different light intensities.

reached 500 NTU, the photon counts did not change as the turbidity increased.

From the fitted curve, the system photon count values were on the curve, which indicated that the fitting was good. In Table 2, the fitting situation was calculated by using SPSS software. When the light intensity of the light source was 6–11 mw, the fitting indexes were 0.97, 0.97, 0.98, 0.98, 0.99, and 0.99, respectively. It can also be seen from the fitting index that the fitting index values were all greater than 0.8, and it can be considered that the fitting is excellent. This also proves that the transmission optical fiber turbidity measurement system designed in this paper has good performance for turbidity detection. However, it can also be found that with the increase of the light intensity in the light source, the fitting index also increased from 0.97 to 0.99, which shows that an appropriate increase in the light intensity can improve the testing effect of the system. The transmission

TABLE 2: Fitting degree of the transmission system under different light intensities.

Serial number	Incident light intensity (wm)	Fitted value
1	6	0.97
2	7	0.97
3	8	0.98
4	9	0.98
5	10	0.99
6	11	0.99

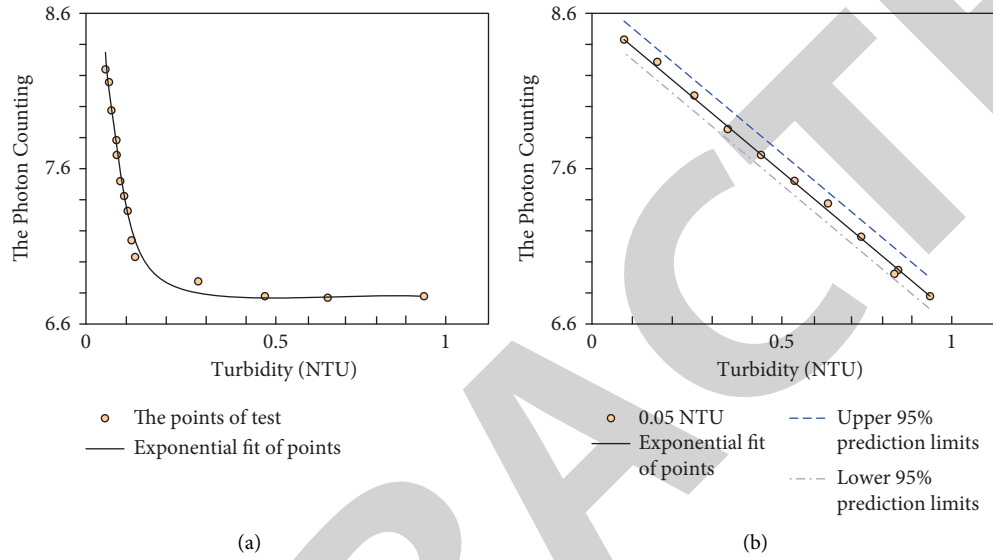


FIGURE 7: System results for low turbidity range measurements. (a) Low turbidity range measurement results. (b) Ultralow turbidity range measurement results.

detection system designed in this paper was not suitable for matching the strong light source. When the light source is very strong, the penetration of photons could damage parts of the instrument. Therefore, as far as the test results are concerned, when the light intensity was 11 mW, the detection effect of the system was the best.

In water quality testing, often low turbidity aqueous solutions need to be tested more. In a solution with low turbidity, it is almost transparent to the naked eye, and the number of particles in it would not affect the viewing of the naked eye. Therefore, it is of great significance for water quality detection to have a better detection effect on low turbidity solutions. In this regard, the transmissive system was further tested. The low turbidity range of 0-1 NTU and the ultralow turbidity range of 0-0.1 were tested, and the results are shown in Figure 7.

In Figure 7(a), at low concentrations, a similar trend to the large range is shown; both showed an exponential trend with a fit index of 0.98. In Figure 7(b), at ultralow concentrations, the light counts and turbidity showed a linear trend, and the fitting index was 0.99. Additionally, to reduce errors, multiple experiments were carried out for ultralow turbidity, and the upper and lower confidence intervals of the experimental data are also marked in Figure 7(b). It can be seen that the system tests showed two different trends at low turbidity, which was also consistent with the principle

presented in the method of the introduction section. It was linear below the 0.1 NTU threshold and exponential above 0.1 NTU.

3.2. Test of the Scattering Fiber Detection System. In the sample cell, a clean glass bottle with good sealing performance was placed, and a small amount of formazin standard turbidity solution was added. In the experiment, 15 groups of samples with turbidity ranging from 10 NTU to 150 NTU were tested. Each turbidity sample was tested 5 times, and the average value represented the test value of the system. The result is shown in Figure 8.

In Figure 8, the abscissa represents the standard liquid turbidity and the ordinate represents the photon count. It can be seen that the photon counts of the scattering system showed a linear trend with the change in turbidity. The photon counts were distributed around the fitted line, and the values on both sides of the fitted line were the same. This showed that the photon count of scattered light in the 90° direction increased gradually with the increase of the turbidity value and was proportional to it. After calculation, the fitted value reached 0.99. This showed that in the system, as long as the photon count of scattered light in the 90° direction can be accurately measured, the solution turbidity can be reversed.

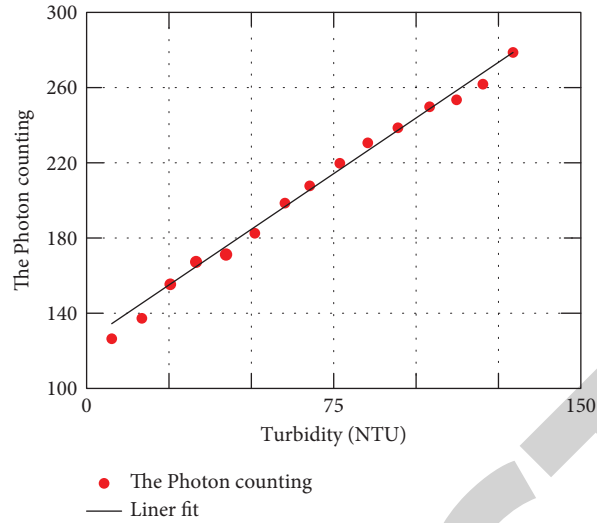


FIGURE 8: Scattered turbidity measurement results.

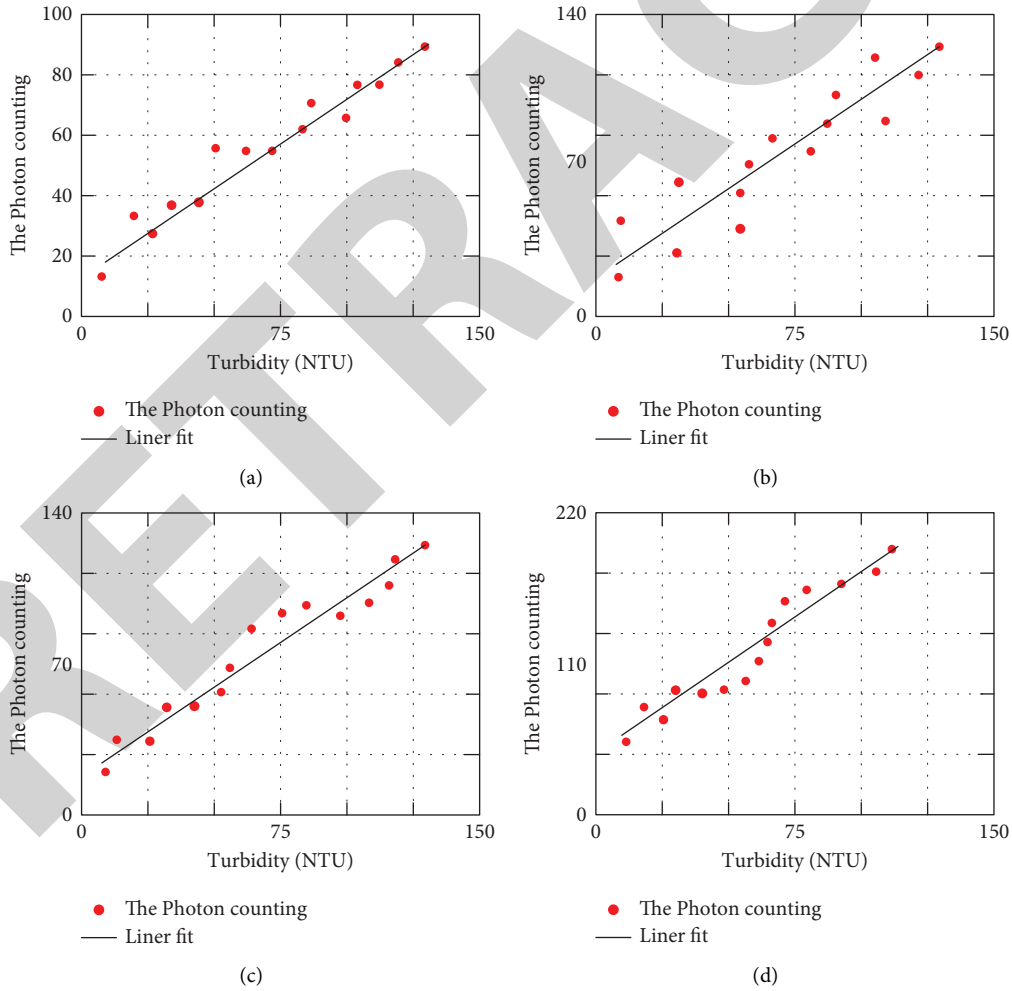


FIGURE 9: Influence of different incident light intensity values on the measurement results. (a) 1 wm. (b) 2 wm. (c) 3 wm. (d) 4 wm.

Scattering detection technology is more suitable for measuring medium and low turbidity because in the solution of high turbidity, the light would be scattered many times on

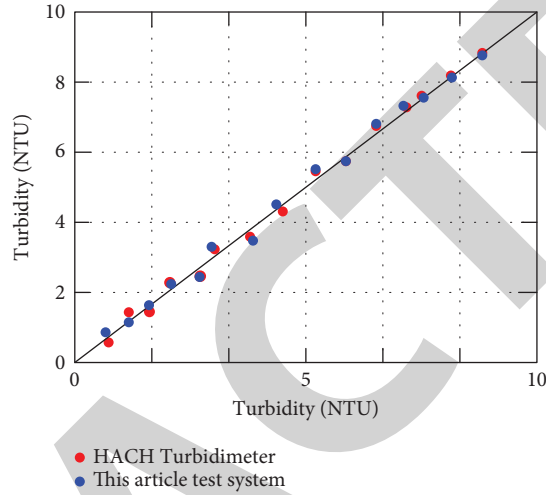
the large particles, which greatly increases the error of the test. It is precisely the process of scattering that would affect the accuracy, so it is necessary to test the influence of the

TABLE 3: Fitting degree of the scattering system under different light intensities.

Serial number	Incident light intensity (wm)	Fitted value
1	1	0.94
2	2	0.96
3	3	0.98
4	4	0.99



(a)



(b)

FIGURE 10: Comparison between the system in this paper and the turbidimeter. (a) HACH turbidimeter physical diagram. (b) HACH turbidimeter physical diagram.

light source intensity on the test accuracy. The test results are shown in Figure 9. Figures 9(a)–9(d), respectively, show the test results when the light intensity is 1 μm , 2 μm , 3 μm , and 4 μm .

By comparing the four groups of different incident light intensities as shown in Figure 9, it can be found that different incident light intensities would affect the degree of fitting between turbidity and photon counts. The fit values of the four groups of light intensities are shown in Table 3.

Table 3 shows that as the light intensity increased, the fitting degree also increased gradually. When the incident light was 4 μm , the fitting value was the highest, which was 0.99. This showed that the most suitable incident light intensity of the scattering turbidity detection system in this paper was 4 μm .

In order to further prove the accuracy of the system in this paper, the system in this paper was compared with more mature commercial turbidimeters in the experiment. The Hach 2100 Q turbidimeter was chosen for this article because of its wide measurement range and high accuracy. The comparison with the system in this paper can further illustrate the effectiveness of the system in this paper. In the experiment, the sample solution of 0–10 NTU was tested in this paper, and the test results are shown in Figure 10.

Figure 10(a) shows the actual picture of the commercial turbidimeter used in this paper, and Figure 10(b) shows a comparison result graph. In Figure 10(b), the blue dots are the test results of the scattering system in this paper, the red dots are the test results of the HACH turbidimeter, and the

black solid line is the diagonal line, which represents the standard test result. The abscissa represents the true turbidity of the formazin standard solution, and the ordinate represents the detected turbidity. It can be seen from Figure 10(b) that the test results of the system in this paper had a high similarity with the test results of the HACH turbidimeter; the overall difference was not more than 2%, and both were near the diagonal. This also showed that the performance of the system in this paper was comparable to that of the more commonly used commercial turbidimeters in the market.

4. Conclusions

In this paper, a turbidity detection system was designed in detail, and the numerical simulation and parameter inspection of water quality particle detection were analyzed. To obtain a large-scale turbidity detection effect, a transmission fiber turbidity detection system based on single-photon technology was designed. The result was that the detection effect could be higher in the range of 0–1000 NTU. To test the accuracy, this paper also designed a scattering optical fiber turbidity detection system, which had a high detection accuracy at low and medium concentrations. After experimental verification, the system designed in this paper was similar to the results of the current commercial HACH turbidimeter, which showed that the system designed in this paper was more effective in turbidity detection. However, there are some flaws in this paper that deserve to be

Retraction

Retracted: The Optimal Integration of Computer Information Technology and Energy Economic Management

International Transactions on Electrical Energy Systems

Received 28 November 2023; Accepted 28 November 2023; Published 29 November 2023

Copyright © 2023 International Transactions on Electrical Energy Systems. This is an open access article distributed under the Creative Commons Attribution License, which permits unrestricted use, distribution, and reproduction in any medium, provided the original work is properly cited.

This article has been retracted by Hindawi, as publisher, following an investigation undertaken by the publisher [1]. This investigation has uncovered evidence of systematic manipulation of the publication and peer-review process. We cannot, therefore, vouch for the reliability or integrity of this article.

Please note that this notice is intended solely to alert readers that the peer-review process of this article has been compromised.

Wiley and Hindawi regret that the usual quality checks did not identify these issues before publication and have since put additional measures in place to safeguard research integrity.

We wish to credit our Research Integrity and Research Publishing teams and anonymous and named external researchers and research integrity experts for contributing to this investigation.

The corresponding author, as the representative of all authors, has been given the opportunity to register their agreement or disagreement to this retraction. We have kept a record of any response received.

References

- [1] N. Zhang and Z. Li, "The Optimal Integration of Computer Information Technology and Energy Economic Management," *International Transactions on Electrical Energy Systems*, vol. 2022, Article ID 9067413, 7 pages, 2022.

Research Article

The Optimal Integration of Computer Information Technology and Energy Economic Management

Ning Zhang  and Zengxin Li 

Economics Department, Qinhuangdao Vocational and Technical College, Qinhuangdao, Hebei 066102, China

Correspondence should be addressed to Zengxin Li; 20141117@stu.sicau.edu.cn

Received 3 September 2022; Revised 23 September 2022; Accepted 28 September 2022; Published 10 October 2022

Academic Editor: Nagamalai Vasimalai

Copyright © 2022 Ning Zhang and Zengxin Li. This is an open access article distributed under the Creative Commons Attribution License, which permits unrestricted use, distribution, and reproduction in any medium, provided the original work is properly cited.

The author proposes a method combining entropy weight method and TOPSIS method with computer information technology in order to save energy with maximum efficiency and improve efficiency. The author constructs the optimal integration of computer information technology and enterprise economic management. Managers use computer information technology to analyze data and problems more accurately and have stronger control ability. The noncooperative game model of gender warfare game and smart pig game are used to simulate negotiation and cooperation in reality, which is conducive to the formulation of cooperation mechanisms and the flexibility of negotiation to promote the realization of regional energy cooperation. Finally, combined with computer information technology, a comprehensive evaluation model of the energy economic system is constructed by using the entropy weight method and the TOPSIS method. The authors used a paired t test for the three evaluation results to examine whether their evaluation results were significantly different. Experimental results show that the correlation coefficient between method 1, method 2, and method 3 are both 0.984, and the correlation coefficient between method 2 and method 3 is 0.974, and the results are all significant. *Conclusion.* The method can effectively improve the efficiency and effectiveness of energy economy, and the detection results are better.

1. Introduction

With the widespread use of computer information technology in the world, enterprises also make full use of computer information technology in energy economic management, which meets the requirements of the development of the times and keeps pace with the development of the times. In the information age, the use of computer information technology in the energy economic management of enterprises will have more prominent advantages, which will not only bring new opportunities to the enterprise itself but also achieve a leading position in the economic market. It can also bring a series of conveniences to enterprises, thereby providing economic benefits for enterprises. The use of computer information technology is a means and method for enterprises to carry out economic management. With the help of computer information technology, the effectiveness of economic management can be improved. The issue of energy has received increasing

attention. Energy is the material basis for the survival and development of human society. Throughout the history of human social development, every major advancement in human social civilization has been accompanied by the improvement and replacement of energy. The development and utilization of energy has greatly promoted the development of the world economy and human society. In the next 20 years, the gap between energy supply and demand will continue to expand. The main reasons are uneven distribution of resources leads to increased difficulty in development; low energy efficiency leads to serious waste of resources; and unreasonable energy consumption structure leads to aggravation of environmental pollution, as shown in Figure 1 [1]. So far, the overemphasis on economic growth indicators and the sustainable production capacity of energy, and the neglect of economic growth mode and environmental pollution problems are still serious. The sustainable development mode of energy economy deserves further study [2]. Solving this problem in this big

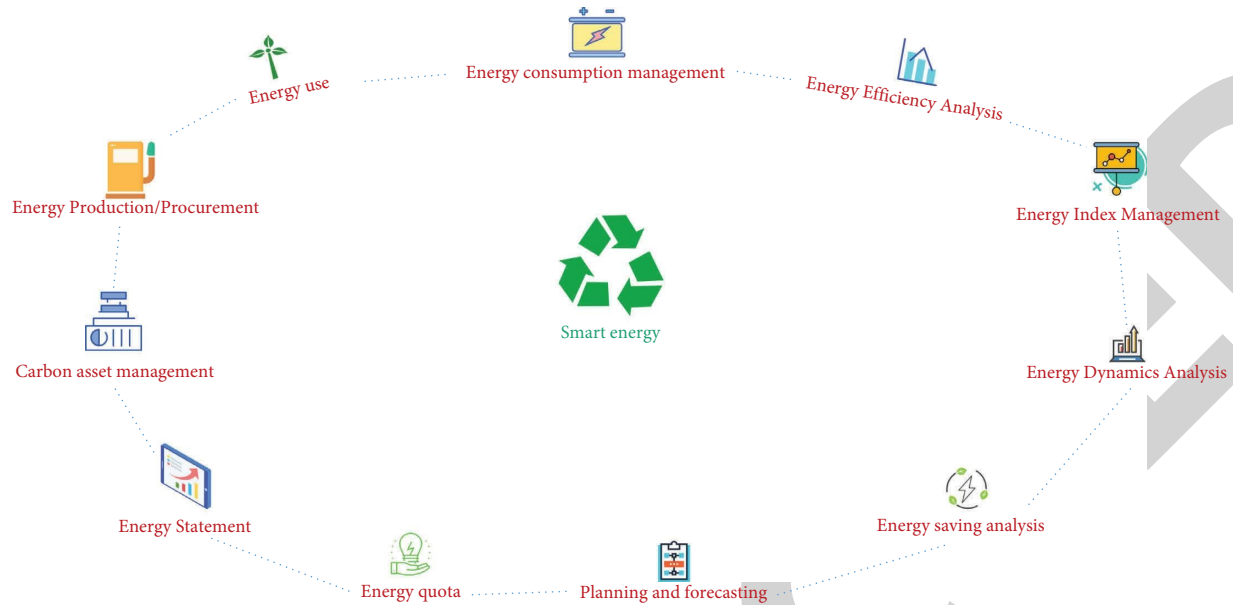


FIGURE 1: Energy economic management.

environment can save energy with maximum efficiency. Energy saving is a long-term strategic policy for my country's economic development. On the basis of ensuring energy supply, enterprise energy work, through intensive planning and taking safety measures to obtain the maximum reduction of production costs, in order to better serve the business goals of the enterprise. It should be said that it is the purpose of enterprise energy work, which plays an important role in the sustainable and healthy development of the economy and the improvement of people's living standards. Research on energy economy is of great significance to the development of human society [3].

2. Literature Review

Karimi used a historical deductive approach to propose an explicit energy economic growth model, drawing the conclusion that the current socioeconomic model is unsustainable and energy security critical [4]. Ldn used sample data from a certain region, the causal relationship between GDP and total energy consumption and consumption of various energy sources (coal, oil, natural gas, and electricity) was analyzed separately by using cointegration techniques. It is found that there is no cointegration relationship between GDP and these, but there is a two-way Granger causality relationship with total energy consumption, coal, and electricity, respectively. There is a one-way Granger causality from GDP to oil and natural gas to GDP [5]. Zhou examined the relationship between per capita energy consumption and per capita GDP in 11 oil-exporting countries using panel unit root and cointegration techniques. The results show that there is a one-way Granger causality between economic growth and energy consumption [6]. Carrasco et al. introduced energy variables into the C-D production function. The results from the research on the relationship between economic growth and energy consumption show that economic development is inseparable from energy [7]. The

results of the empirical study by Han et al. show that, in the short term, there is a fluctuating relationship between energy consumption and GDP, but in the long run, there is a stable equilibrium relationship between energy consumption and economic growth, and there is a one-way causal relationship from energy consumption to economic growth [8]. Guo et al. showed that through the cointegration analysis of energy consumption and economic growth, there is a long-term equilibrium relationship between them, and the past economic growth mainly relied on energy consumption [9]. A study of an economy by Hyland et al. shows that: The ecological index of economic growth is between the "national standard value" and the "warning value," and the health of the economic growth pattern during this period is relatively poor [10]. Through the research of Granger causality test, cointegration test, and error correction model, Jayakumar et al. show that there is a significant one-way Granger causality between economic growth and energy consumption, and there is a long-term equilibrium relationship between the two [11]. In view of the above problems, the author proposes a method to construct a comprehensive evaluation model for the energy economic system using the entropy weight method which is the TOPSIS method and the combination of the two methods in combination with computer technology. The sustainable development capacity shows an increasing trend, while the coordination capacity first increases and then weakens, specifically, it gradually shifts from moderate sustainable development capability and coordination capability to moderate sustainable development capability and strong coordination capability, and transitions to a state where both sustainable development capability and coordination capability are strong. In order to take into account the improvement of system coordination; make overall planning for the coordinated development of energy, economy, population, and environment, and then continuously promote the sustainable development of energy economy.

3. Methods

3.1. Optimal Integration of Computer Information Technology and Enterprise Economic Management. Computer information technology brings advanced ideas and methods to enterprise economic management. In the economic management of enterprises, it is necessary to have advanced ideas and management methods in order to be one step ahead of other enterprises in the market. Therefore, it is necessary to use computer information technology. Management software in computer information technology is the carrier of management ideas and management models. For example, customer management software can provide enterprises with scientific product and service evaluation methods; human resource management software can bring a convenient performance appraisal system to the enterprise; and financial management software makes the analysis methods of management accounting convenient to apply. This management software brings advanced ideas and methods to enterprise economic management [12]. Computer information technology promotes the establishment of modern management methods in enterprise economic management. Traditional economic management methods have been unable to promote the development of enterprises, and we must actively use computer information technology to promote enterprises to gradually move towards the era of e-commerce [13]. For example, various application software in e-commerce solutions help enterprises to carry out online transactions such as online ordering, distribution, and settlement; there are also ERP software based on supply chain, which can realize the business interaction between enterprises, suppliers, and customers. Use computer information technology to improve the effectiveness of economic management. Traditional economic management methods make many management functions stay in time and delay development, and real-time control in the event and precontroller in advance appear to be more difficult. When the enterprise is carrying out economic management, the implementation of manufacturing management software can eliminate the lack of planned production and achieve zero inventory. The use of ERP software in economic management can effectively arrange and dispatch funds, reduce unnecessary cash reserves, and reduce financial expenses. The system software can make various management reports available at any time. Computer information technology helps enterprise economic managers to break through the limitations of their ability. At present, the use of computer information technology in enterprise economic management can help managers implement various management requirements, achieve management goals that could not be achieved in the past, and expand management space. Managers can use financial software to have more precise financial control capabilities: Using data warehouses, managers will have stronger data memory capabilities [14]. Therefore, managers use computer information technology to analyze data and problems more accurately and have stronger control ability.

3.2. Analysis of Abnormal Energy Consumption Data. The energy management system needs to collect and store a large amount of energy consumption data of the supervised objects, classify the data according to the energy consumption

objects such as buildings, departments, and pipelines, and display it to the system users. Faced with such a large amount of data, it is difficult for us to effectively find unreasonable energy consumption or abnormal energy consumption in the energy consumption system, and it is almost impossible to find various problems in the system at the equipment, design, or operation level. Through computer information processing technology, the establishment of an energy consumption data model provides us with a higher tool for energy consumption analysis and diagnosis. Modern building energy efficiency systems help system users deal with these massive data through two tools: alarm and warning mechanisms and data presentation software [15]. Today, in most building energy-saving systems, the normal operation of the abnormal energy consumption alarm function completely depends on the user selecting the corresponding limit or threshold value for the energy consumption alarm and warning through the man-machine interface. This is a very difficult task for the user: If the threshold is set too tight, there will be a lot of false positives in the system; if the threshold is set too loosely, the system will not be able to discover all the abnormal energy usage and the damage to the system and equipment behind it. Data presentation software can help users analyze and diagnose problems, but such untargeted operations often take a lot of time.

3.2.1. Data Mining. The energy management system takes energy informatization and intelligence as the core goal and is fully developed around the intelligence of energy information collection, information processing, information display and push, and energy regulation and control [16]. Intelligent information collection is the key technology of campus energy management system, the intelligent information collection equipment in the system needs to have the characteristics of self-organizing network, self-diagnosis, self-repair, uninterrupted operation, high stability, and high reliability and can automatically collect energy information in the campus, reduce the human input in information collection, and improve the accuracy and reliability of collection. The intelligent information processing can analyze and process the information by the system central server or rely on the powerful processing capability of cloud computing, and provide a strong data guarantee for decision-making [17].

3.2.2. Economic Subsystem. The economic subsystem belongs to the power subsystem. In the system, future economic growth is determined by the economic growth rate and the economic aggregate in the base period, and affects energy consumption through three industries, it affects the total population through per capita GDP and, at the same time, excessive economic growth will have adverse effects on the environment [18]. The flow of the economic subsystem is shown in Figure 2.

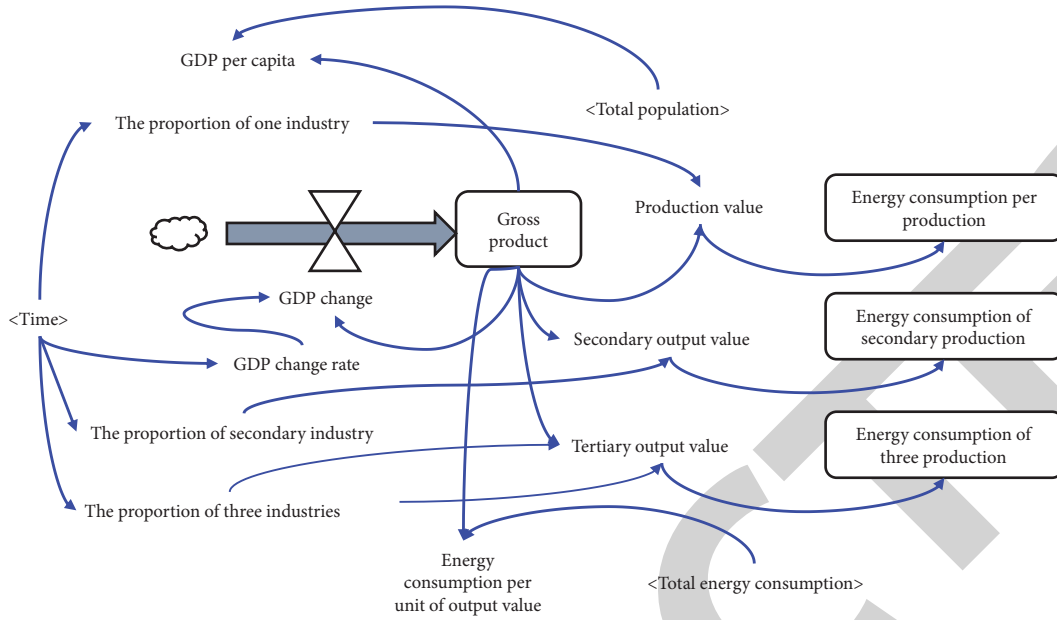


FIGURE 2: Flow chart of the economic subsystem.

3.3. Comprehensive Evaluation Model Based on the Entropy Weight Method. At present, there are many methods for evaluating sustainable development index systems at home and abroad, such as the principal component analysis method, the grey relational analysis method, and attribute reduction method of rough set. The established models include the fuzzy comprehensive evaluation model, the multidimensional grey evaluation model, and the regression analysis joint integration model [19]. The methods for determining the weights of evaluation indicators can be divided into two types: objective assignment and subjective assignment. Among them, the subjective evaluation methods mainly include AHP, Delphi, and other methods. Most of these methods are qualitative analysis and are greatly affected by human factors, so the evaluation results are likely to be distorted; The objective assignment method mainly includes factor analysis method, principal component analysis method, entropy value method, and other methods. These methods determine the weight by the degree of difference and mutual relationship between the index data, therefore, errors caused by subjective factors are avoided. The author uses information entropy to determine the weight of the sustainable evaluation index of the energy economy.

3.3.1. Principle of Entropy Weight Method. Entropy was originally a thermodynamic concept, and now it has been widely used in engineering technology, social economy, and other fields. The entropy weight method is an objective evaluation method based on the principle of entropy, which can effectively avoid the deviation caused by human factors [20]. The information entropy describes the relative magnitude of the change of the index value through the rate of change of the sample data and thus obtains the weight of the index. The faster the index value changes relative to the ideal

value, the smaller its information entropy will be, and on the contrary, the greater the utility, the greater the weight. Therefore, the weight determined by the entropy method represents the relative rate of change of the indicator, and the relative level of the indicator is represented by the degree of progress after normalization of the sample data. The final evaluation value is their product, which well reflects the combination of the development speed and relative speed of the index. To sum up, the entropy method avoids the influence of human factors on the weight of indicators, making the selection of weights more scientific. Assuming that there are m evaluation indicators and n evaluation samples in the evaluation index system, the set of all sample indicators is: $S = \{s_1, s_2, \dots, s_n\}$, each subsample can be described as: $s_i = \{C_{i1}, C_{i2}, \dots, C_{im}\}$. The initial data matrix C of the indicator is: $C = \{c_{ij}\}_{n \times m}$, $i = 1, 2, \dots, n$; $j = 1, 2, \dots, m$, among them, c_{ij} is the value of the j th evaluation index in the i th year. Since, the numerical dimensions of the evaluation indicators may be different and cannot be compared with each other, the author first standardized the initial data matrix C . The indicators are divided into reverse polarity, positive polarity, and moderate polarity. If the ideal value of the index C_j is C_j^* , the smaller the C_{ij}^* of the reverse polarity index is, the better, the greater the positive polarity index, the better, and the moderate polarity index is the best. Assuming $M_j = \max\{c_j\}$ and $m_j = \min\{c_j\}$, the ideal value of the reverse indicator is $C_{ij}^* = m_j/c_{ij}$, and the ideal value of the positive indicator is $C_{ij}^* = c_{ij}/M_j$. Note that the normalized value of C_{ij}^* is y_{ij} , as shown in the following formula:

$$y_{ij} = \frac{C_{ij}^*}{\sum_{i=1}^n C_{ij}^*}, \quad y_{ij} \in (0, 1). \quad (1)$$

Therefore, the initial data matrix C of the indicator can be expressed as the following formula after normalization.

TABLE 1: Degree grading on the interval [0, 1].

B_1	System Sustainability Status
$B_1 \in [0, 0.3)$	Very poor
$B_1 \in [0.3, 0.5)$	Poor
$B_1 \in [0.5, 0.7)$	Moderate
$B_1 \in [0.7, 0.9)$	Strong
$B_1 \in [0.9, 1)$	Very strong

$$Y = \{y_{ij}\}_{n \times m}. \quad (2)$$

Due to the normalization of the initial data, the evaluation value of sustainability is between 0 and 1. The closer the calculated index evaluation value is to 1, the greater the influence of the index on the system sustainable development capability of the sample; and vice versa. The author classifies the sustainable development capability according to the classification standard of correlation degree in statistics, as shown in Table 1.

The index of system coordination ability is mainly used to examine the coordination status among the four subsystems of energy, the economy, the environment, and population. Their coordination relationship shows that the values of their respective development levels should be balanced. That is, the more coordinated the relationship between them is, the closer the values of their respective development levels are; otherwise, the deviation of the development level value will be larger.

3.4. Principle of TOPSIS Method

3.4.1. TOPSIS Method. The technique for order preference by similarity to ideal solution, referred to as TOPSIS) is a sorting method that approximates the ideal solution. It is one of the methods to establish a preference relationship with positive and negative ideal solutions as a reference, and to deal with the sorting and selection of multiobjective decision-making problems. The basic idea is the virtual optimal solution (also called the positive ideal solution, that is, the optimal value of each indicator) and the worst solution (also called negative ideal solution; that is, the worst value of each indicator). The relative closeness of the solution to the solution in the target space. In order to measure the degree to which a solution is close to the positive ideal solution and far away from the negative ideal solution, use the value of relative closeness (0–1) to determine the order of the schemes. The greater the relative closeness, the better the scheme, and vice versa. The research steps of the TOPSIS method are shown in Figure 3. As can be seen from Figure 3, the steps of the TOPSIS method research: first, in order to eliminate the influence of different measurement units, it is necessary to normalize the indicators; second, multiple alternatives are found by normalizing the processed raw data matrix.

The TOPSIS method is a comprehensive distance evaluation method for multiattribute decision-making schemes. Its advantages are that by normalizing the original data, eliminates the influence of different dimensions, uses the

original data information to sort the results, and quantitatively reflects the pros and cons of different evaluation schemes. Moreover, there are no strict requirements on sample size, data distribution, and the number of indicators. Different indicators can be combined for comprehensive evaluation. It has the characteristics of small calculation amount, intuitive geometric meaning, wide application range, and small information distortion. The comprehensive evaluation index system of sustainable development of the energy economy is a complex system with 39 indicators. The TOPSIS method can directly, clearly, and accurately reflect the state of sustainable development of the energy economy.

3.4.2. Smart Pig Game Model. The smart pig game is a proposed noncooperative game model. Suppose there is a big pig and a small pig in the pig sty. The two parts of the pig sty have a pig trough and a button, respectively. The button is used to control the supply of pig food. Pressing the button will bring 10 units of pig food into the trough, but whoever presses the button will need to pay the cost of 2 units. If the big pig arrives first, it will eat 9 units of pig food, while the little pig can only eat 1 unit. When both arrive at the same time, the big pig will eat 7 units and the little pig will eat 3 units. If the little pig comes first, the big pig will eat 6 units and the little pig will eat 4 units. By calculating the cost and benefit, the payment matrix of the big pig and the little pig can be obtained as shown in Table 2.

It can be seen that in the smart pig game, whether the big pig chooses to act or wait, the best choice for the little pig is to wait. Given the choice of strategy that the little pig is waiting for, the optimal choice for the big pig can only be action. Therefore, the Nash equilibrium of this game is that the big pig moves and the little pig waits, and each gets 4 units of net profit. The enlightenment of the game of smart pigs is that more work does not necessarily mean more, and less work does not necessarily mean less, which confirms the free-rider behavior in public goods cooperation. The significance of the smart pig game for regional energy cooperation is that in the process of energy cooperation, some countries will take the free-rider strategy choice without paying the corresponding cost, which is not conducive to the development of regional energy cooperation; therefore, strengthening the negotiation and implementing the principle of differentiated treatment will contribute to the realization of regional energy cooperation.

3.4.3. Gender War Game Model. Gender warfare game is a cooperative game model. Suppose a couple has only one TV at home. The husband likes to watch football games and the wife likes to watch soap operas. If both parties agree to watch football games, then the husband gets 2 units of utility and the wife gets 1 unit of effect; if both parties agree to watch soap operas, the wife gets 2 units of effect and the husband gets 1 unit of the effect; if the two sides disagree, the result can only be ignored by everyone, and each can only get 0 units of utility. The payment proofs of both parties are shown in Table 3.

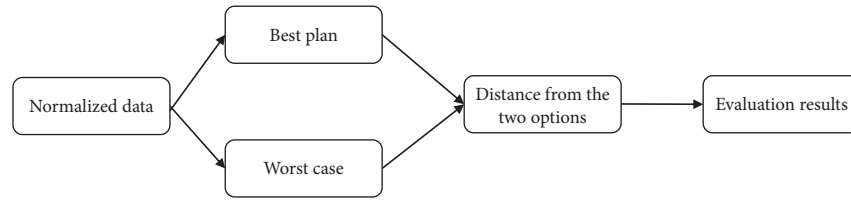


FIGURE 3: The steps of the TOPSIS study.

TABLE 2: Smart pig game matrix.

		Piggy	
		Action	Wait
Big pig	Action	5; 1	4; 4
	Wait	9; -1	0; 0

TABLE 3: Gender war game matrix.

		Wife	
		Football game	Soap opera
Husband	Football game	2; 1	0; 0
	Soap opera	0; 0	1; 2

It can be seen that there are two equilibrium outcomes in the gender war game, both sides of the game will prefer an equilibrium, for example, the husband prefers football games, while the wife prefers soap operas. However, an equilibrium result will still occur, because both parties will gain more profit if they reach an agreement than if they disagree. The emergence of an equilibrium outcome will depend on the importance of the position of both parties in the family, the skills of negotiation, and the choice of taking turns calling the shots. The significance of the gender war game for regional energy cooperation lies in the flexibility of cooperation mechanism formulation and negotiation. There is also the dilemma of joint risk avoidance in regional energy cooperation, which leads to the breakdown of cooperation, however, noncooperation is not beneficial to both parties, which makes the emergence of equilibrium results possible. The emergence of the two equilibrium results means that the strength of both parties, the negotiation process and the availability of information in regional energy cooperation will determine the direction of the equilibrium results, formulating agreements, and establishing compensation mechanisms, will make cooperation more stable, so as to facilitate the realization of regional energy cooperation.

4. Results and Discussion

We refer to the entropy weight method as method 1, the TOPSIS method as method 2, and the entropy weight TOPSIS method as method 3. The results of the three evaluation methods for the development level of energy economy are basically the same, and the only difference is the magnitude of the value, which is due to the difference in data processing methods. To further investigate their differences, the authors used a paired t test on the three evaluation results to examine whether their evaluation

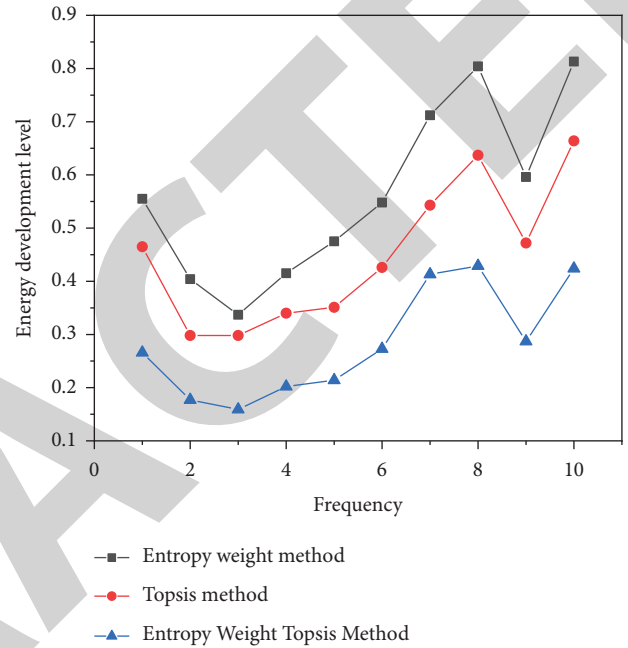


FIGURE 4: Comparison of energy development level results.

results were significantly different, and the results showed the correlation coefficients between method 1, method 2, and method 3 are both 0.984, and the correlation coefficient between method 2 and method 3 is 0.974, and the results are all significant. Since the correlation coefficient is between $[0, 1]$, the larger the value, the more consistent the results of the two methods are, as shown in Figure 4. Therefore, the evaluation results of the three methods on the energy development level are basically the same.

The ability of sustainable development shows an increasing trend, while the ability of coordination first increases and then decreases. Specifically speaking, firstly, sustainable development capacity and coordination capacity are relatively moderate. Then, gradually turn to sustainable development ability moderate and strong coordination ability. Finally, it has transitioned to a state of strong sustainable development capacity and coordination.

5. Conclusion

The author analyzes the composition of the comprehensive evaluation index system for the sustainable development of the energy economy and uses the entropy weight method, the TOPSIS method and the combination of the two methods in combination with computer technology to

Retraction

Retracted: Analysis of Dynamic Relationship between Energy Consumption and Economic Growth Based on PVAR Model

International Transactions on Electrical Energy Systems

Received 28 November 2023; Accepted 28 November 2023; Published 29 November 2023

Copyright © 2023 International Transactions on Electrical Energy Systems. This is an open access article distributed under the Creative Commons Attribution License, which permits unrestricted use, distribution, and reproduction in any medium, provided the original work is properly cited.

This article has been retracted by Hindawi, as publisher, following an investigation undertaken by the publisher [1]. This investigation has uncovered evidence of systematic manipulation of the publication and peer-review process. We cannot, therefore, vouch for the reliability or integrity of this article.

Please note that this notice is intended solely to alert readers that the peer-review process of this article has been compromised.

Wiley and Hindawi regret that the usual quality checks did not identify these issues before publication and have since put additional measures in place to safeguard research integrity.

We wish to credit our Research Integrity and Research Publishing teams and anonymous and named external researchers and research integrity experts for contributing to this investigation.

The corresponding author, as the representative of all authors, has been given the opportunity to register their agreement or disagreement to this retraction. We have kept a record of any response received.

References

- [1] J. Han, "Analysis of Dynamic Relationship between Energy Consumption and Economic Growth Based on PVAR Model," *International Transactions on Electrical Energy Systems*, vol. 2022, Article ID 3945522, 7 pages, 2022.

Research Article

Analysis of Dynamic Relationship between Energy Consumption and Economic Growth Based on PVAR Model

Junyan Han 

Department of Legal Technology, Hainan Vocational College of Political Science and Law, Haikou 570100, Hainan, China

Correspondence should be addressed to Junyan Han; 20141128@stu.sicau.edu.cn

Received 5 September 2022; Revised 25 September 2022; Accepted 28 September 2022; Published 7 October 2022

Academic Editor: Nagamalai Vasimalai

Copyright © 2022 Junyan Han. This is an open access article distributed under the Creative Commons Attribution License, which permits unrestricted use, distribution, and reproduction in any medium, provided the original work is properly cited.

In order to analyze the relationship between energy consumption and economic growth dynamics, the author proposes a dynamic analysis technology of energy consumption and economic growth based on the PVAR model. This technology uses the PVAR method to compare and quantitatively describe the relationship between economic growth and energy consumption in developed and developing countries from 1990 to 2009, using impulse response functions and variance decomposition analysis methods; study the similarities and differences between total energy consumption and various fossil energy consumption and the dynamic impact of economic development, and finally establish a PVAR model for analysis. Experimental results show that: in the forecast of variance analysis, the impact explanatory power of the total energy consumption of developing countries on the fluctuation of economic growth reaches 8.85070. However, the contribution of total energy consumption in developed countries to economic growth is insufficient. The explanatory power of economic growth in developed countries to total energy consumption is 15.58070, while that in developing country is 29.28070, both of which are greater than the explanatory power of their respective total energy consumption on economic growth. *Conclusion.* The technology based on the PVAR model can effectively meet the needs of analyzing the dynamic relationship between energy consumption and economic growth.

1. Introduction

With the rapid development of the global economy, energy and economic issues have gradually become a hot issue of general concern in the international community. Since human beings entered the industrial age, energy, especially fossil energy, has become one of the important factors related to the future development direction and development level of the entire world economy.

Energy is an indispensable material resource for the survival and development of human society and an important strategic material related to a country's economic lifeline. The healthy development of the energy system has become an important material basis for sustainable social and economic development. However, problems such as insufficient supply of energy, especially fossil energy, deviation of energy structure, and low energy efficiency have become the bottleneck of the economic development of all countries in the world. Energy consumption promotes

economic growth, and economic growth promotes the large-scale development and utilization of energy, at the same time, energy is also a restrictive factor, with the rapid development of the economy, it is bound to face the contradiction between increasing energy demand and energy scarcity. Since the oil crisis in the 1970s, the causal relationship between energy consumption and economic growth has been studied, and whether economic development is ahead of energy consumption or whether energy consumption promotes economic growth, it has always been an issue of interest to economists and policy analysts. As their relationship directly affects the formulation of government energy policy. If energy consumption is the cause of economic growth, then energy shortages will hinder economic growth; if economic growth is the cause of energy consumption growth, it means that economic growth is not strongly dependent on energy, and the implementation of energy reserve policies will have little effect on the economy. However, the relationship between energy consumption and

economic growth has long been a contentious issue. At different times and in different countries, different testing methods often lead to different conclusions.

Correctly handling and understanding the relationship between energy consumption and economic growth is very important for long-term social and economic planning, energy development strategies, and the formulation of relevant laws and regulations, and can provide some help for building a safe and sustainable energy future [1].

2. Literature Review

Over the past half-century, the panel data model (PVAR model) has made great progress. The PVAR model has become an important branch of econometrics, related theories such as panel data unit root test theory, panel data cointegration theory, panel data causality test, mixed panel data model, static panel data model, dynamic panel data model, spatial panel data model, panel data error correction model, panel data vector autoregressive model, rotating panel data model, and so on are becoming more and more mature. It has become a common research direction for scholars to discuss macro and microeconomic issues of various countries with panel data. With the maturity of the PVAR model, a lot of achievements have been made in the application of the model. The research results in the last three years abroad include Khalid applies the PVAR model to study which factors affect the growth process of French manufacturing enterprises [2]. Yurtkuran used the PVAR model to study the effect of rising house prices on household consumption in South Africa [3]. Xu using the PVAR model to study the impact of renewable and nonrenewable energy sources on economic growth and carbon dioxide emissions in Europe and Eurasian countries [4]. Panwar discussed the relationship between terrorist attacks and public spending in Europe using the PVAR model [5]. Kuang used the PVAR model to analyze the loan supply of euro area countries during the global financial crisis [6]. Moldovan Used the PVAR model to study the relationship between the threat of terrorism and economic growth in developing countries [7]. Emir used the PVAR model to analyze the relationship between income growth and energy consumption [8]. Horobet used the PVAR model to discuss the relationship between monetary policy, asset prices, and the macroeconomic environment in 17 OECD countries [9]. Popa used the PVAR model to study the output relationship between the global oil sector and the nonoil sector [10]. Sun used the PVAR model to study the dynamic relationship between the income gap between the eastern and western regions of Germany and the regional labor market and labor transfer [11]. Shabani used the PVAR model to study the labor income problem of US residents [12]. Umarov applies the PVAR model to the problem of bank risk in EU countries [13].

In response to the above problems, the author uses the panel data vector autoregression (PVAR) method, where all variables are assumed to be endogenous, which shows the interaction between the variables; analyze the relationship between oil, natural gas, and coal individual energy

consumption and economic growth, and the relationship between total energy consumption and economic growth; At the same time, the impact of each shock can be differentiated to obtain the impact of the impulse response excluding the impact of other factors, and to better analyze the relationship between energy consumption and economic growth variable decomposition. A PVAR model is used to further determine the magnitude of the effect and to measure the contribution of each effect to the variation in the endogenous variables. As shown in Figure 1.

3. Research Methods

3.1. Energy Consumption Theory. Energy consumption refers to the energy used for production and living. Per capita energy consumption is an important indicator for measuring the economic development of a country and the standard of living of the people. The higher the consumption of energy per person, the greater the product of the country and the rich. In developing countries, changes in energy consumption are closely related to the process of industrialization. With the development of the economy, the energy consumption in the early and middle industrialization period will generally increase slowly, and the economic development will move to the postindustrial stage, there have been major changes in business development, and efforts. Electricity consumption has started to decrease.

3.2. Economic Growth Theory. Economic growth is a term used by economists and journalists and refers to the growth of a country's GDP in a year compared to previous years. Broadly speaking, the meaning of economic growth is the expansion of the productive resources of the economy in the production of goods and services necessary for the survival of its members in a period (for example, the expansion of the supply curve outside). Productivity growth is determined by the country's natural resources, real capital formation, efficiency, human capital formation, skill level, and development of the organizational environment. Therefore, the growth of the economy determines the expansion and improvement of the range of production.

3.3. Analysis of Correlation Changes between Economic Growth and Energy Consumption. Generally speaking, energy consumption will promote economic development, the greater the energy consumption, the higher the labor productivity, with the improvement of labor productivity, the total social wealth is also increasing, the economy is developing rapidly, and the amount of energy required for production and life will also increase accordingly, therefore, there is a spiral upward momentum between energy and the economy. As can be seen from Figure 2, from 1971 to 2010, GDP increased from 3.20024 E+12 USD to 6.31952 E+13 USD. Correspondingly, the total energy consumption has also grown steadily, from 5500032.48 kilotons of oil equivalent to 12324301.2 kilotons of oil equivalent. In general, energy consumption growth is slower than GDP growth, but GDP is more volatile.

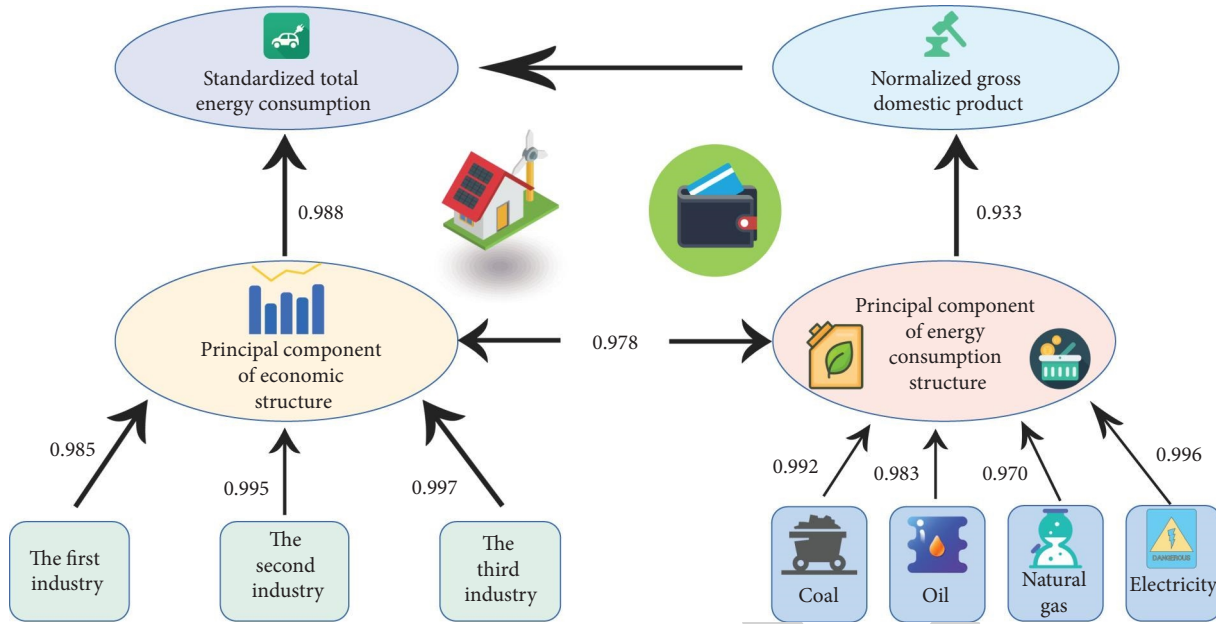


FIGURE 1: Relationship between energy consumption and economic growth based on the PVAR model.

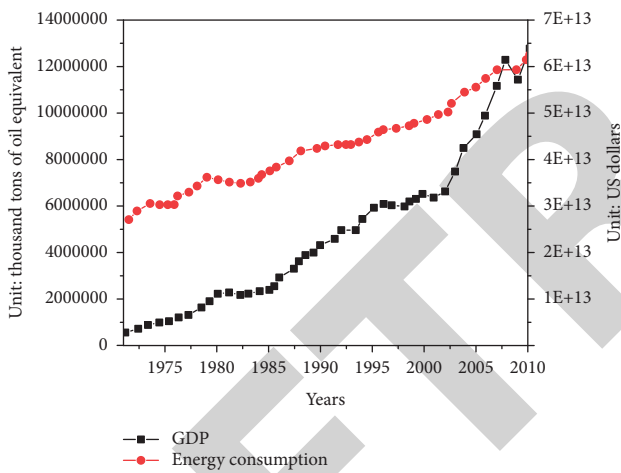


FIGURE 2: Trend chart of world GDP and total energy consumption from 1971 to 2007.

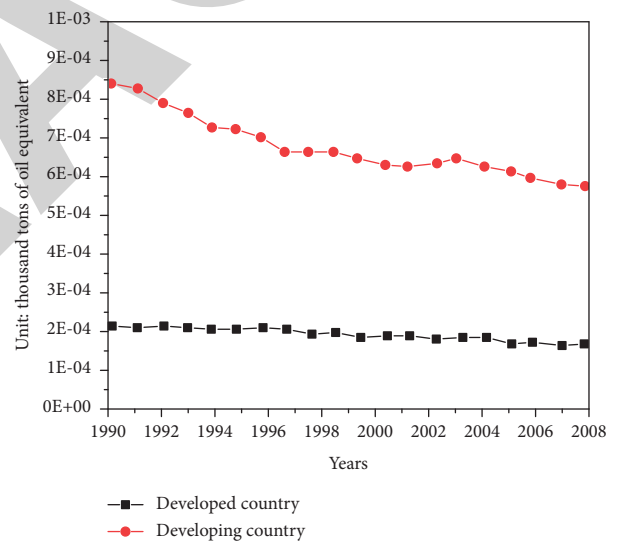


FIGURE 3: Trend chart of energy consumption intensity from 1990 to 2008.

The change in energy consumption intensity can be seen from Figure 3, both developed and developing countries show a downward trend year by year. The energy consumption intensity of developed countries was at a relatively low level in 1990, it can be seen that the energy utilization efficiency is relatively high, so the energy consumption intensity declines relatively slowly. In developing countries, the energy consumption intensity is relatively high, and the lowest value from 1990 to 2008 was much higher than the highest value in developed countries.

The change of the elastic coefficient of energy consumption can be seen from Figure 4 that the elastic coefficient of energy consumption fluctuates up and down, which is very unstable and does not show an obvious change law, among them, the fluctuation range of the energy consumption elasticity coefficient of developed countries is

larger than that of developing countries, and the energy consumption elasticity coefficients of the two are high and low. In 2008, energy consumption in developed countries experienced a large negative growth relative to the economy, and the energy consumption elasticity coefficient was large.

3.4. Theoretical Basis of PVAR Model

3.4.1. Introduction to PVAR Model. The characteristics of the PVAR model are that it combines the characteristics of the traditional time series VAR model and the panel data model. A multivariate dynamic system model is established, which provides a flexible analysis framework for the analysis of multivariate system dynamics, more and more problems

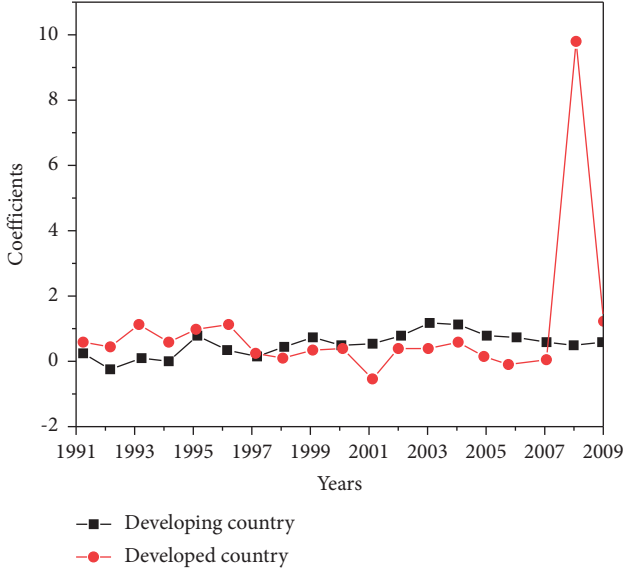


FIGURE 4: Trend chart of energy consumption elasticity coefficient from 1991 to 2009.

in reality can be discussed by establishing panel vector autoregressive models.

Zhang did pioneering work on the study of the PVAR model and proposed the problem of building a vector autoregressive model on panel data, but in the equation model, he makes a very strong assumption: by making the observation in the first period equal to the life of the individual unit in the first period, the restriction on the length of the lag is avoided, that is, there is a correspondence such as $m(t) = t - 1$ between the length of the lag period m and the period t , but in fact, it is often difficult to observe the entire lifespan of each economic unit, which requires some assumptions to be made based on the existing observation data to determine the relationship between the time series X and Y [14, 15].

Ameen analyzed that when N is relatively large and T is small in panel data, and the time series has a unit root and cointegration relationship, how to effectively estimate the parameters of random effects and fixed effects in panel vector autoregressive models, here, Liu given that the individuals in the panel data are independent, the analysis shows that generalized distance estimation (GMM) and quasi-maximum likelihood estimation QML() will fail, extended generalized distance estimation (extended GMM) and QML estimation can avoid this situation, and QML estimation shows better characteristics [16, 17].

The constructed model is shown in the following formula:

$$w_{i,t} = (I_m - \Phi)u_i + \Phi w_{i,t-1} + \varepsilon_{i,t}. \quad (1)$$

$w_{i,t}$ is a $m \times 1$ -dimensional random variable, $i = 1, 2, \dots, N$; $t = 1, 2, \dots, T$; Φ is the $m \times m$ -dimensional cross-sectional coefficient matrix; u_i is the $m \times 1$ -dimensional vector individual fixed effects; $\varepsilon_{i,t}$ is a random interference term, and several assumptions are given in the paper [18].

The general model of the panel vector autoregressive model can be expressed as follows:

$$Y_{i,t} = \gamma_0 + \sum_{k=1}^m \Phi_{t,k} Y_{i,t-k} + \sum_{j=1}^m \Psi_{t,j} X_{i,t-j} + \gamma_i + u_{i,t}. \quad (2)$$

$i = 1, 2, \dots, N$; $t = 1, 2, \dots, T$; $Y_{i,t}$ is the $M \times 1$ vector of the M observable variables of the cross-section individual i at time t , $X_{i,t}$ is the $M \times 1$ vector of the observable deterministic strict exogenous variable, $\Psi_{i,j}$ is the coefficient matrix to be estimated for $M \times M$, γ_i is the M unobservable individual fixed effect matrix of individual i , and $u_{i,t}$ is the random error term [19].

In practical use, there are situations where the coefficient matrix of lagged endogenous and exogenous variables is time invariant, as shown in the following formula:

$$Y_{i,t} = \gamma_0 + \sum_{k=1}^m \Phi_k Y_{i,t-k} + \sum_{j=1}^m \Psi_j X_{i,t-j} + \gamma_i + u_{i,t}. \quad (3)$$

$i = 1, 2, \dots, N$; $t = 1, 2, \dots, T$; Moreover, the estimation method and assumption of equation (3) can be easily extended to equation (2), therefore, for the convenience of discussion, the following analysis is aimed at equation (3).

3.4.2. Assumptions of the PVAR Model

Assumption 1. For any number of individuals N and epoch length T , $Y_{1,t}, Y_{2,t}, \dots, Y_{NT}$ are both observable variables.

Assumption 2. For arbitrary $i = 1, \dots, N$; $t = 1, \dots, T$, $u_{i,t}$ is an independent and identically distributed random variable whose random error term satisfies zero expectation and whose covariance matrix is Ω , namely, $u_{i,t} \sim i.i.d(0, \Omega)$.

Assumption 3. When $s < t$, Y_i , X_i and γ_i are orthogonal to the random error term, as shown in equation:

$$E[Y_{i,s} u_{i,t}] = E[X_{i,s} u_{i,t}] = E[\gamma_i u_{i,t}] = 0, \quad (s < t). \quad (4)$$

3.4.3. Identification of PVAR Model. The so-called model validation includes estimates and parameters in the model, such as coefficients and lags. The first difference can be obtained, as shown in the following equation:

$$\Delta Y_{i,t} = \Delta \sum_{k=1}^m \Phi_k Y_{i,t-k} + \Delta \sum_{j=1}^m \Psi_j X_{i,t-j} + \Delta u_{i,t}. \quad (5)$$

From assumption 3, when $s < t - 1$, it is shown in the following formula:

$$E[\Delta Y_{i,s} u_{i,t}] = E[\Delta X_{i,s} u_{i,t}] = 0, \quad (s < t - 1). \quad (6)$$

Suppose $y_{i,t}^j$ is the j th variable in the economic variable vector $Y_{i,t}$, then the first-order difference model of $y_{i,t}^j$ is a vector, as shown in the following formula:

$$\Delta y_{i,t}^j = \sum_{k=1}^m \phi_k^j \Delta Y_{i,t-k} + \sum_{l=1}^m \psi_l^j \Delta X_{i,t-l} + v_{i,t}^j. \quad (7)$$

Among them, $v_{i,t}^j$ is the random error term of the single-equation first-order difference model whose endogenous variable is $y_{i,t}^j$, namely $v_{i,t}^j = \Delta u_{i,t}^j$; vectors $\phi_l^j = (\phi_{1,l}^j, \phi_{2,l}^j, \dots, \phi_{m,l}^j)$ and $\psi_l^j = (\psi_{1,l}^j, \psi_{2,l}^j, \dots, \psi_{m,l}^j)$ ($l = 1, 2, \dots, p$).

Therefore, by the orthogonal condition of hypothesis 3, model (7) has an instrumental variable vector as shown in the following formula:

$$Z_{i,j} = [1, \Delta Y'_{i,t-2}, \Delta Y'_{i,t-3}, \dots, \Delta Y'_{i,2}, \Delta X'_{i,t-2}, X'_{i,t-3}, \dots, \Delta X'_{i,2}]. \quad (8)$$

That is, the number of instrumental variables in equation (7) is $2t - 3$.

Since the identifiable condition of equation (7) is that the number of instrumental variables is at least the number of variables on the right side of equation (8), therefore, equation (8) is recognizable when $2t - 3 \geq 2m + 3$, that is, when $t \geq m + 3$. Therefore, the identifiable condition of the panel vector autoregressive model (3) is $T \geq m + 3$ [20].

But for equation (5), due to differential transformation, there will be $(T - m - 2)2(m + 1)$ parameters to be estimated in the model, and $(T - m - 2)2(m + 1) + 1$ parameters to be estimated if the constant term is included. Therefore, when considering the constant term, it is necessary to satisfy $(T - m - 2)2(m + 1) + 1 \geq 2(m + 3)$, among them, $2(m + 3)$ is the number of variables in formula (5), that is, if the $T \geq 2m + 3$ rule is satisfied, formula (5) can be fully identified, and m all represent the number of lag periods.

4. Analysis of Results

4.1. Impulse Response Analysis. The impulse response function describes the influence of the orthogonal innovation of a variable in the model on each variable in the system, through the dynamic response of each variable to the shock; the impact of each shock factor on other factors can be specifically analyzed [21].

The author gave the variables a shock with a standard deviation size and obtained the relevant impulse response function graph. The 5% confidence interval was obtained from 500 Monte Carlo simulations. In the figure, the horizontal axis represents the time of response to the shock, and the vertical axis represents the degree of response of each variable to the shock of the endogenous variable. Ignoring personal responses turns into shock. The middle curve represents the response curve, and the two side curves represent the reliability of the two different models [3].

Figure 5 clearly shows the dynamic impact of the GDP and total energy consumption of developed and developing countries. It can be seen that in developed countries, with an orthogonal innovation of GDP, the total energy consumption increased slightly in the first period, decreased rapidly in the second period, and then gradually returned to a balanced state. Conversely, in the face of an orthogonal innovation in total energy consumption, the response of GDP is positive in

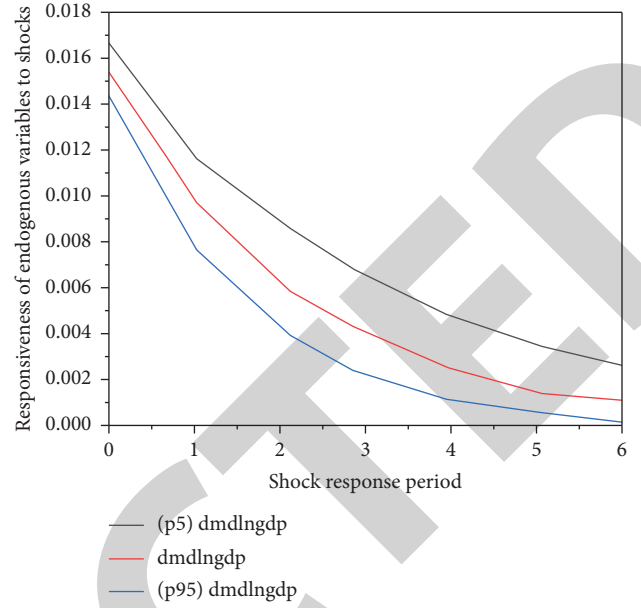


FIGURE 5: Impulse response plot of total energy consumption and real GDP.

the six lag periods, however, the effect is small, first increasing significantly, then, decreasing significantly, and then, gradually returning to the equilibrium state [22].

For developed countries, with an orthogonal innovation of oil and coal consumption, the GDP first rises and then falls and tends to converge, the impact caused by oil consumption fluctuates more, and the impact of natural gas consumption on GDP is small, the impact is not significant [23]. Generally speaking, the consumption of the three types of fossil energy in developed countries has a positive impact on the GDP, but the effect is small. The above results combined with the basic regression results show that, the total energy consumption of developed countries has a positive effect on economic growth and this effect is delayed, economic development generally depends on the total energy consumption for a long time, energy, as a necessary factor of production, has a nonnegligible impact on economic development. However, economic growth has a positive effect on total energy consumption, and this effect is lagged, indicating that economic growth has a greater effect. The long-term effects and relationship between total energy consumption and economic changes on total energy consumption. Overall, energy consumption and business growth are strengthening but not equal.

4.2. Variance Decomposition. Variance decomposition provides information about the significance of each negative effect that contributes to the sample variance. The panel model variance decomposition is used to describe the magnitude of the effect, thereby measuring the contribution of each shock to the change in the endogenous variable [24].

The results of variance analysis are shown in Tables 1 and 2, the fluctuation of each variable mainly comes from itself. The equation analysis results of oil, natural gas, coal

TABLE 1: Variance decomposition results of total energy consumption and real GDP.

Period S	Developed countries			Developing country		
		Dmdlngdp	Dmdlntec		Dmlngdp2	Dmdlntec2
10	Dmdlngdp	0.96513	0.03487	Dmdlngdp2	0.91146	0.08854
10	Dmdlntec	0.15581	0.84419	Dmdlntec2	0.29281	0.70719
20	Dmdlngdp	0.96513	0.03487	Dmdlngdp2	0.90759	0.09241
20	Dmdlntec	0.15583	0.84417	Dmdlntec2	0.29285	0.70715
30	Dmdlngdp	0.96513	0.03487	Dmdlngdp2	0.90655	0.09345
30	Dmdlntec	0.15583	0.84417	Dmdlntec2	0.29288	0.70712

TABLE 2: Variance decomposition results of oil, natural gas, coal consumption, and real GDP.

Period S	Developed countries					Developing country				
		Dmdlngdp	Dmlncc	Dmdlnoc	Dmdlngc		Dmdlngdp2	Dmlncc2	Dmdlnoc2	Dmdlngc2
10	Dmdlngdp	0.9769	0.0085	0.0113	0.0031	Dmdlngdp2	0.9161	0.0175	0.0588	0.007
10	Dmlncc	0.0865	0.9110	0.0006	0.0017	Dmlncc2	0.0837	0.8822	0.0300	0.0039
10	Dmdlnoc	0.1230	0.0101	0.8662	0.0006	Dmdlnoc2	0.4329	0.0012	0.5646	0.0011
10	Dmdlngc	0.0349	0.0145	0.0127	0.9378	Dmdlngc2	0.0410	0.0013	0.0342	0.9233
20	Dmdlngdp	0.9764	0.0081	0.0114	0.0040	Dmdlngdp2	0.9115	0.0183	0.0615	0.0085
20	Dmlncc	0.0879	0.9096	0.0006	0.0017	Dmlncc2	0.1119	0.8169	0.0666	0.0043
20	Dmdlnoc	0.1231	0.0102	0.8659	0.0006	Dmdlnoc2	0.4925	0.0047	0.4979	0.0047
20	Dmdlngc	0.0349	0.0145	0.0127	0.9377	Dmdlngc2	0.0575	0.0016	0.0549	0.8858
30	Dmdlngdp	0.9764	0.0081	0.0114	0.0040	Dmdlngdp2	0.9072	0.0185	0.0652	0.0088
30	Dmlncc	0.0880	0.9096	0.0006	0.0017	Dmlncc2	0.1510	0.7280	0.1160	0.0048
30	Dmdlnoc	0.1231	0.0102	0.8659	0.0006	Dmdlnoc2	0.4849	0.0066	0.5016	0.0067
30	Dmdlngc	0.0349	0.0145	0.0127	0.9377	Dmdlngc2	0.0827	0.0020	0.0835	0.8316

consumption, and real GDP in developing countries have great changes in different forecast periods, the explanatory power of oil, natural gas and coal on economic growth has gradually increased, indicating that the influence of these variables in developing countries has a lag. However, the variables of other systems have little effect on the results of equation analysis in different forecast periods, indicating that after 10 forecast periods, the system has been basically stable.

In the 10th forecast, fluctuations in energy consumption and economic growth are explained as follows: the explanatory power of the total energy consumption of developing countries to the fluctuation of economic growth reaches 8.85%, while the contribution of total energy consumption of developed countries to economic growth is insufficient; the explanatory power of economic growth in developed countries to total energy consumption is 15.58%, and that in developing countries is 29.28%, both of which are greater than the explanatory power of their respective total energy consumption to economic growth, there is also a similar relationship between the three fossil energy sources and economic growth, indicating that the interaction between economic fluctuations and energy consumption is unequal; the explanatory power of oil consumption for economic growth in developing countries is relatively high, while the explanatory power of natural gas consumption for economic growth is relatively low.

5. Conclusions

The author proposes technical research on the dynamic relationship analysis between energy consumption and economic growth based on the PVAR model. This

technology uses the PVAR method to compare and quantitatively describe the relationship between economic growth and energy consumption in developed and developing countries from 1990 to 2009, using impulse response functions and variance decomposition analysis methods; study the similarities and differences between total energy consumption and various fossil energy consumption and the dynamic impact of economic development, and finally, establish a PVAR model for analysis. It is proved that the technology based on the PVAR model can effectively meet the needs of analyzing the dynamic relationship between energy consumption and economic growth.

Data Availability

The data used to support the findings of this study are available from the corresponding author upon request.

Conflicts of Interest

The authors declare that they have no conflicts of interest.

References

- [1] C. Zhang, X. Wu, and S. Peng, "Research on relationship between energy saving and emission reduction efficiency and economic development of Guangdong," *IOP Conference Series: Earth and Environmental Science*, vol. 680, no. 1, Article ID 012112, 2021.
- [2] Y. Khalid, M. Wu, A. Silaen et al., "Oxygen enrichment combustion to reduce fossil energy consumption and emissions in hot rolling steel production," *Journal of Cleaner Production*, vol. 320, no. 8, Article ID 128714, 2021.

Retraction

Retracted: Teaching Practice of Engineering Management Course for Engineering Education Certification under Background of Artificial Intelligence

International Transactions on Electrical Energy Systems

Received 28 November 2023; Accepted 28 November 2023; Published 29 November 2023

Copyright © 2023 International Transactions on Electrical Energy Systems. This is an open access article distributed under the Creative Commons Attribution License, which permits unrestricted use, distribution, and reproduction in any medium, provided the original work is properly cited.

This article has been retracted by Hindawi, as publisher, following an investigation undertaken by the publisher [1]. This investigation has uncovered evidence of systematic manipulation of the publication and peer-review process. We cannot, therefore, vouch for the reliability or integrity of this article.

Please note that this notice is intended solely to alert readers that the peer-review process of this article has been compromised.

Wiley and Hindawi regret that the usual quality checks did not identify these issues before publication and have since put additional measures in place to safeguard research integrity.

We wish to credit our Research Integrity and Research Publishing teams and anonymous and named external researchers and research integrity experts for contributing to this investigation.


The corresponding author, as the representative of all authors, has been given the opportunity to register their agreement or disagreement to this retraction. We have kept a record of any response received.

References

- [1] D. Wang, F. Han, Q. Zhao, and Y. Lv, "Teaching Practice of Engineering Management Course for Engineering Education Certification under Background of Artificial Intelligence," *International Transactions on Electrical Energy Systems*, vol. 2022, Article ID 3106491, 12 pages, 2022.

Research Article

Teaching Practice of Engineering Management Course for Engineering Education Certification under Background of Artificial Intelligence

Dan Wang ¹, Fengyi Han,² Qi Zhao,³ and Yinyin Lv¹

¹Education Quality Supervising and Evaluation Center, Changchun Institute of Technology, Changchun 130012, Jilin, China

²Bim School of Technology and Industry, Changchun Institute of Technology, Changchun 130012, Jilin, China

³School of Energy and Power, Changchun Institute of Technology, Changchun 130012, Jilin, China

Correspondence should be addressed to Dan Wang; wangdan@ccit.edu.cn

Received 19 August 2022; Revised 5 September 2022; Accepted 21 September 2022; Published 6 October 2022

Academic Editor: Nagamalai Vasimalai

Copyright © 2022 Dan Wang et al. This is an open access article distributed under the Creative Commons Attribution License, which permits unrestricted use, distribution, and reproduction in any medium, provided the original work is properly cited.

With the advancement of China's industrial construction, the field of engineering management has also attracted more attention. However, China's engineering management major is currently in a growing stage due to the issue of the opening years, and the teaching and practice setting of each course is also in an immature stage, which makes China's engineering management majors present more and more problems. The truancy rate has been increasing year by year, the students' dominant position in the class has become objectified, and their trust in teachers has decreased. Students' learning shows the characteristics of individualization and diversity. Higher requirements are put forward for teachers' teaching quality, and schools lack an effective supervision mechanism. In order to solve these problems better, it is imperative to reform and innovate the course teaching of engineering management majors. The core of engineering education accreditation is to confirm that engineering graduates meet established quality standards recognized by the industry. It is a unique method to test whether the course teaching of engineering management majors is qualified and attracts many scholars to discuss it. Engineering education accreditation has attracted many scholars to discuss it because it is a unique means to test the qualifications of engineering management students' course teaching. This study was based on an in-depth exploration of the teaching practice of engineering management courses and combines artificial intelligence with an engineering education certification. Through the research and analysis of colleges and universities, the research finally showed that the engineering management professional course teaching of engineering education certification under the background of artificial intelligence can promote the attendance of students in school by about 20%. The achievement of course teaching objectives has increased by about 13% and the comprehensive ability level of graduates has increased by about 8%. It improved the overall level of students and the teaching quality and efficiency of engineering management courses and also promoted the development of college education so that today's engineering management graduates can better meet the needs of today's society.

1. Introduction

With the development of China's market economy, the traditional mode and method in the field of engineering management today is the general contracting mode of engineering, that is, the integrated mode of design, procurement, and construction. After the project decision-making stage, starting from the design, and after bidding, the engineering company is entrusted to carry out general

contracting for design, procurement, and construction. This model has been difficult to meet the needs of the rapid development of the current construction industry. A more complete and effective method has become an urgent need for the implementation of the whole process management of engineering projects. However, due to the late establishment of engineering management majors in colleges and universities, the engineering management major curriculum system has been continuously explored and improved. In

today's boom in artificial intelligence, artificial intelligence + education have also attracted many scholars to study it. At the same time, engineering education certification, as an important way of college education and teaching reform, is highly praised by many scholars. Therefore, we have reason to believe that the teaching practice of engineering management courses based on engineering education certification under the background of artificial intelligence is conducive to promoting the development of engineering management teaching in colleges and universities and the training of engineering management talents. Finally, it would meet the needs of the current engineering management field for compound talents who understand technology and management and have both economic and legal backgrounds.

For the analysis of the teaching practice of engineering management courses of engineering education certification under the background of artificial intelligence, various scholars have carried out research on it at different levels. Dong mainly studied the reform of digital image processing courses under engineering education certification. He showed that the three core concepts certified by engineering education can be applied to the teaching reform of digital image processing, and the teaching effect can be significantly improved through this teaching reform [1]. Wang and Fan mainly studied the concept and practice of engineering education certification for mechanical majors in local colleges and universities. His introduction to the background, requirements, and procedures of engineering education professional program certification showed the necessity and urgency of engineering education professional program certification in general colleges and universities [2]. Zhang and Huang mainly studied the international comparison of environmental engineering professional degree education accreditation. They systematically sorted out and analyzed the content of the professional certification standards for environmental engineering education, certification procedures, and the relationship between certification and engineer qualifications [3]. Jia et al. mainly studied the continuous improvement strategy of automation majors under the background of engineering education certification. They analyzed the development status and future orientation of the automation major, indicating that the engineering education certification is conducive to promoting the functionalization of engineering and the internationalization of the construction of automation majors. It pointed out the direction for the future development of the automation profession [4]. The research of these scholars is limited. Their research focuses on the importance of professional accreditation in engineering education and accreditation standards. The research direction tends to be more specific to the analysis of the importance of engineering education professional certification, but the analysis of its teaching practice is rarely involved and discussed. Therefore, some scholars have turned their research direction to the current hot artificial intelligence and conducted in-depth research on it. Ehsan et al. research on how AI context affected perceptions of AI explanations and their hands-on work has taken an important step forward in

advancing human-centered multivariate interpretable AI discourses [5]. Li et al. mainly studied the spoken English teaching system based on virtual reality under the background of artificial intelligence and demonstrated the spoken English training system based on artificial intelligence and virtual reality technology. He made oral English teaching meet the requirements of the times, and it can improve the efficiency of oral English training [6]. Rongpeng et al. mainly studied the fusion of cellular networks and AI and speculated that AI-enhanced 5G cellular networks would make the acclaimed ICT a reality [7]. Hassabis et al. mainly studied neuroscience-inspired artificial intelligence and showed that recent advances in artificial intelligence would be the key to driving future research in both neuroscience and artificial intelligence [8]. From these scholars' research on artificial intelligence, it can be seen that the application field of artificial intelligence is extremely extensive and has achieved very good results, and it is mostly used in manufacturing, financial industry, transportation, and other fields and has achieved very good results in medicine, and there is also some research on its use in the field of education. There is very little research on the teaching practice analysis of engineering management courses for engineering education certification under artificial intelligence. This means that the teaching practice analysis of engineering management courses for engineering education certification under the background of artificial intelligence is a relatively new field, which needs to be explored and studied.

Based on the in-depth research on engineering education certification under the background of artificial intelligence, the research showed that engineering education certification under the background of artificial intelligence was conducive to promoting the improvement of the teaching quality and efficiency of engineering management courses. For today's colleges and universities, engineering education certification programs are also extremely necessary, which can promote the development of college education and have practical significance for the construction of colleges and universities today.

2. Teaching of Engineering Education Accredited Engineering Management Courses

In order to explore the teaching of engineering management courses for engineering education certification in the context of artificial intelligence, it is first necessary to introduce its related concepts and information.

2.1. Project Management. The teaching of project management is as follows.

2.1.1. Overview of Engineering Management Major. In the United States, engineering management is called "construction engineering management" [9]. It is generally affiliated with the School of Engineering, and its teaching focuses on the whole process of engineering projects,

including design, budgeting, procurement, construction, operation, and maintenance, and has a bachelor's degree in engineering management. China's engineering management undergraduate colleges are mostly based on business schools, management departments, and engineering colleges [10]. Because foreign universities do not have a unified professional direction, the differences between universities also show their own characteristics, showing more diversified characteristics. In the engineering management courses of foreign universities, engineering technology courses account for a large proportion, more than half, of which the proportion of practice and internship is also large, and the curriculum system pays more attention to the combination with future professional qualifications. Under the guidance of the Ministry of Education, the engineering management major in China cultivates certain basic knowledge in management, economics, civil engineering technology, and law. It is a senior compound talent who can manage the whole process in the field of world engineering project construction. From the perspective of curriculum design and talent training methods, the engineering management major mainly covers four professional subjects including management, finance, technology, and law. The curriculum design mainly includes public basic courses, professional basic courses, and subject-oriented basic courses. It is interspersed with curriculum design, practical education, and practice inside and outside the school, and finally, it carries out a graduation design (or thesis). In contrast, the engineering management majors in many Chinese universities either fail to establish their advantages or have no obvious characteristic advantages. Most of the talent training projects are based on classroom teaching, and teachers have few scientific research projects, and it is even difficult to create a platform for undergraduates to experiment and learn.

2.1.2. Construction of Engineering Management Courses. The curriculum is the core of teaching and the key to cultivating students, and the establishment of a curriculum and the establishment of a knowledge system is the specific embodiment of the educational purpose of students [11]. In order to promote the development of engineering management majors, we can start from four aspects, and through a series of effective measures, the teaching quality of engineering management majors can be continuously improved [12]. First, it can optimize the knowledge structure and build a "broad, fine, and rich" curriculum system. Schools should optimize the curriculum system and knowledge structure as a whole and attach importance to practice and innovation. Public basic courses and some basic courses can be set up by subject categories, while professional basic courses and professional courses can be carried out according to different fields. Second, the investment in education funds can be increased, and the reform of curriculum and teaching content can be promoted. Universities should vigorously promote the reform of curriculum and teaching content, explore the cultivation of knowledge and ability, reconstruct the curriculum system, update teaching content, and build a

series of courses. Third, it is necessary to strengthen teacher incentives and strengthen teacher training. In terms of teacher team building, it is necessary to strengthen the training of teachers in public courses and basic courses. In the promotion of professional titles, "teaching and research sections" can be set up and guided by excellent teachers. Fourth, we can strengthen technical support and strictly review the quality of submitted materials. Schools can set up a separate server on the "Quality Course" website to ensure the normal operation of the website and teaching videos.

2.1.3. Teaching Reform of Engineering Management Major Courses. With the rapid development of China's engineering construction industry, undergraduate education in engineering management has also been a good reference. However, compared with similar majors, the engineering management major is set up for a shorter period of time, and the degree of professional development is not high. The teaching of engineering management major is not perfect enough, the understanding and positioning of engineering management major are not accurate enough, and there are some problems in professional direction, curriculum system setting, and direction. It is necessary not only to meet the requirements of professional certification and evaluation but also to maintain the professional characteristics of the faculty of the Department of Engineering Management. In addition to improving the curriculum, sand table simulation, simulation software, etc., it also needs to reform the curriculum and graduation thesis.

It not only enables students to have a better understanding of applied professional knowledge but also integrates the knowledge they have learned, thereby enhancing their scientific research and innovation capabilities. Due to the advantages of qualitative and quantitative methods (short time, low cost, more practical, and quantitative analysis method is to establish mathematical model based on statistical data, which is more scientific), the dissertations of graduates majoring in engineering management are carried out from both quantitative and qualitative aspects, which are proposed for practical problems. On the whole, students feel that the graduation project can integrate the knowledge and skills learned in school so that they can better grasp and apply what they have learned, thereby enhancing their problem-solving ability and teamwork ability.

With the reform of graduation design, course content can also be adjusted accordingly. Based on the national excellent course "Project Cost Planning and Control," combined with the design of the existing courses, a relatively complete project cost management system has been constructed. The promulgation of the curriculum design reform plan has certain reference significance for other disciplines on the basis of modularization, clustering, and other fields. At the same time, it can also promote the improvement of students' practical ability.

2.1.4. Importance of Teaching Reform of Engineering Management Courses. Facing the complex and changing international economic environment, it is necessary to cultivate

better management talents. In the new century, in the context of economic globalization, engineering management is an important leader in the construction industry. In recent years, China's engineering management major has gradually formed a school-running concept centered on research-based undergraduate education so that its advantages in discipline and scientific research have been fully utilized. It is necessary to adhere to the student-oriented approach and focus on cultivating students' international vision and thinking ability. With high-level projects and horizontal projects serving to teach, the teaching content is more abundant and the teaching quality is improved. It is necessary to pay attention to the basics, focus on practice, focus on engineering and scientific research, and strengthen students' innovative consciousness and practical ability [13].

2.2. Engineering Education Certification. The teaching of engineering education certification is as follows.

2.2.1. Overview of Engineering Education Accreditation. Engineering Education Accreditation (also known as Engineering Education Professional Accreditation or Professional Accreditation) is a special accreditation for the engineering and technical education community [14]. It is relative to the accreditation of ordinary schools. Different from the general accreditation of schools, engineering professional accreditation mainly provides quality assurance for engineering professionals trained by higher education institutions to practice in the professional field. It is generally a professional accreditation by professional committees and engineering training institutions for engineering majors offered through higher education institutions offering certificate programs. It is a major part of the accreditation of engineering higher education. The Engineering Education Professional Accreditation is designed to enhance the training of engineering personnel in higher education organizations to meet the basic needs of the professional world. It is a professional accreditation carried out by professional accreditation organizations such as engineering associations for engineering majors provided by higher education organizations that submit applications for accreditation. In nature, engineering education certification is a qualification evaluation, not a merit evaluation because it is a test of whether engineering educators meet minimum standards of quality. The main purpose of the professional certification of engineering teachers is to evaluate the qualification of engineering personnel to meet the specified quality standards. At the same time, it is necessary to provide quality assurance for Chinese engineering personnel to go to the international engineering education field. It improves the continuous improvement of China's engineering teaching system, thereby improving the service quality of China's engineering teachers.

2.2.2. Features of Engineering Education Certification. With China's formal accession to the "Washington Accord," professional certification work in China has become

increasingly popular. To ensure its smooth implementation, China's engineering education practice has established a relatively complete quality assurance system. Under the guidance of result-oriented teaching ideas, the school adheres to the student-oriented, with training objectives, graduation requirements, and curriculum system quality assurance as the core under the guidance of the seven standards of the "Engineering Education Accreditation Standards." It provides perfect guarantee measures for engineering education practice and forms a relatively complete professional education quality guarantee system, which has distinct characteristics and practical effects [15]. First, it is necessary to stipulate that vocational education should have a certain basis. Clear target requirements enable engineering education to be implemented. Judging from the actual work in China, engineering education has clear regulations in terms of training objectives, curriculum systems, and graduation requirements. Under such demands, the practice of engineering education has a clearer direction. Second, a sound evaluation system ensures the quality of personnel training. Under the environment of certification, engineering education itself has a relatively complete evaluation system, and a relatively complete evaluation system has been carried out in terms of training objectives, curriculum system, and graduation conditions. Especially for the whole teaching link of engineering education, it has established a relatively complete quality evaluation system. This assessment includes both internal and external assessments within the school. Third, through the perfect certification process, the smooth progress of the certificate is guaranteed. China's engineering education certification system has a complete certification process and clear norms, which have a certain guiding role in improving the teaching quality of higher vocational colleges.

2.3. Artificial Intelligence. The teaching of artificial intelligence is as follows.

2.3.1. Overview of Artificial Intelligence. Artificial intelligence (artificial intelligence is abbreviated as AI) [16]. Although artificial intelligence contains intelligence, it is not really intelligent and has no real body. Artificial intelligence generally relies on computers to build artificial intelligence to simulate human perception, learning, reasoning, and other abilities. Some scholars say that artificial intelligence relies on machines to do things that require human intelligence. Some scholars also said that the most important thing about artificial intelligence is that it can not only allow machines to imitate humans but also make machines surpass the capabilities of humans, thereby helping humans to do tasks that require brainpower and intelligence. Some scholars believe that artificial intelligence is a discipline that allows computers to express human intelligence by completing various tasks. From the viewpoints of these scholars, it can be seen that the essence of artificial intelligence is to rely on computers to imitate human intelligence so that it can help people perform part of their mental work. These remarks clearly show that, for artificial intelligence, most

people think that it is the product of human technology and the embodiment of human intelligence. Although it can perform some intellectual activities in place of human beings, it cannot surpass human beings. The artificial intelligence mentioned in this study is more of all kinds of intelligent devices and applications created based on artificial intelligence.

Traditional AI problems (or goals) include reasoning, knowledge representation, planning, learning, natural language processing, perceiving, moving, and controlling objects. Ordinary intelligence is a long-term goal in this regard. Methods include statistics, computational intelligence, and traditional symbolic intelligence. Artificial intelligence uses many tools, such as search and mathematical optimization, neural networks, statistics, probability, and economics. In terms of artificial intelligence, it involves computers, information engineering, mathematics, psychology, linguistics, philosophy, and many other aspects. The specific structure of artificial intelligence is shown in Figure 1.

2.3.2. System Classification of Artificial Intelligence. There are three types of AI: analytical, human-inspired, and human-like AI [17]. Analytical AI has only the characteristics that match its cognitive intelligence. On this basis, from the perspective of cognition, the past experience is used to provide a reference for future policy formulation. Artificial intelligence is created by humans and contains intelligence. In addition to cognitive factors, it is also necessary to understand human emotion and incorporate it into decision-making. Humanized AI exhibits various abilities (such as cognitive, emotional, and social intelligence), and it is consciously aware of itself when communicating with others.

2.3.3. Artificial Intelligence Algorithms. Artificial intelligence is generally algorithm-centric. An algorithm is a set of clear instructions, performed by a set of mechanical computers. Complex algorithms are often based on other simpler algorithms. Many AI algorithms can be learned from data; they can improve themselves by learning new heuristics (strategies and “rules of thumb”), or they can write other algorithms themselves. The “learners” described below, such as Bayesian networks, decision trees, and nearest neighbors, can theoretically learn arbitrarily close functions, including mathematical functions that best describe the world. So, students can take every possible hypothesis into account and compare them to the data to get the full knowledge. In fact, it is impossible to take all possibilities into account, which is a kind of “combinatorial explosion,” that is, the time required to solve a problem increases exponentially. Much of the research on artificial intelligence is about how to identify and avoid thinking about possibilities that are unlikely to bring benefits. On this basis, the study would introduce an artificial intelligence-based clustering analysis method.

2.3.4. Basic Principle of Cluster. Cluster analysis is one of the most commonly used methods in data mining, which can

find unknown objects in a database [18]. The principle of this classification is “like things cluster together.” It groups individuals or data objects that meet similar criteria into groups based on the similarity between individuals or data objects. People or data that do not meet the same conditions are divided into different groups, and each group formed by group processing is called a class [19]. The specific cluster analysis process is shown in Figure 2.

The above description expresses the clustering problem by a mathematical formula and can be expressed as follows.

Assuming that the given dataset is $A = \{a_n | n = 1, 2, \dots, m\}$, a_n represents the data object; according to the approximation of each data object between the data, the data of each dataset can be divided into L groups, and let it satisfy

$$\begin{aligned} C_i | i &= \{1, 2, \dots, l\}, \\ C_i &\subseteq A, \\ C_n \cap C_i &= \emptyset, \\ \bigcup_{n=1}^l C_n &= A. \end{aligned} \quad (1)$$

This process is clustering; among them, $C_n (n = 1, 2, \dots, n)$ is cluster (class).

It can also be said that the input in the cluster analysis can be expressed by ordinal pairs (b, d) or (b, f) .

Among them, b is a group of samples and d, f is the standard of similarity or dissimilarity between cluster samples.

Since the output partition of cluster analysis can be expressed as

$$b = (H_1, H_2, \dots, H_L), \quad (2)$$

among them, $H_L (l = 1, 2, \dots, P)$ is a subset of b .

The specific formula is expressed as

$$\begin{aligned} H_1 \cup H_2 \cup \dots \cup H_l &= B, \\ H_n \cap H_i &= \emptyset, \quad n \neq i, \end{aligned} \quad (3)$$

where H_1, H_2, \dots, H_L is the class.

For example, the center of a class is a node in a multidimensional space, which can represent a class by a set of nodes, or a class by its features.

2.3.5. Cluster Algorithm. Types of data structures in cluster analysis: define g variables to represent j objects. The relational representation of this data structure can be expressed by the $j \times g$ matrix, which can be expressed as

$$\begin{bmatrix} b_{11} & \dots & b_{1y} & \dots & b_{1g} \\ \vdots & \vdots & \vdots & \vdots & \vdots \\ \cdot b_{n1} & \dots & b_{ny} & \dots & b_{ng} \\ \vdots & \vdots & \vdots & \vdots & \vdots \\ b_{j1} & \dots & b_{jy} & \dots & b_{jg} \end{bmatrix}. \quad (4)$$

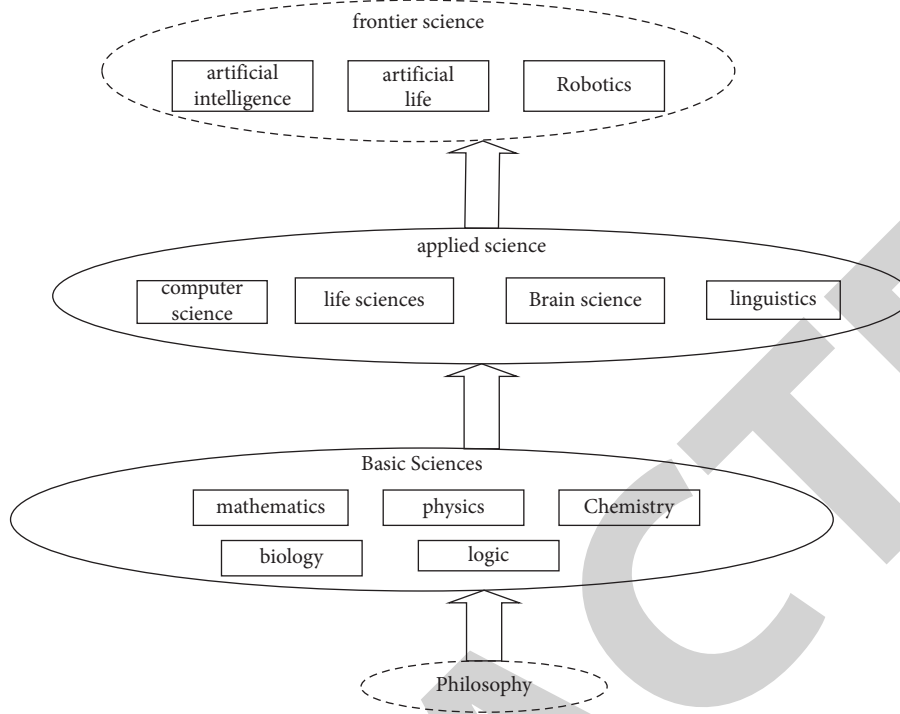


FIGURE 1: Schematic structure of artificial intelligence.

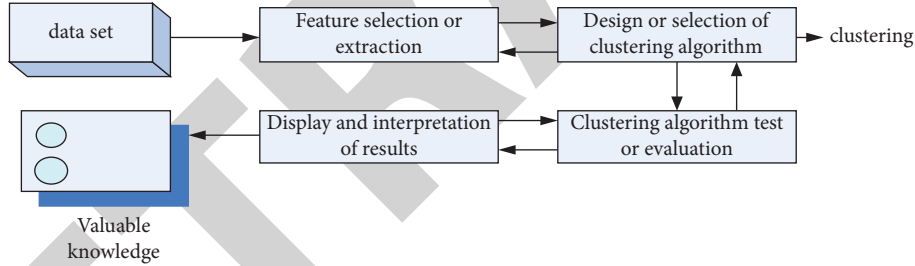


FIGURE 2: Cluster analysis flowchart.

Similarity measure: the basic concept of cluster analysis (considering the similarity between individuals and data objects, it classifies individuals and data objects that meet the similarity criteria into sets. It reclassifies individuals or data objects that do not meet the similarity criteria into different groups) can be obtained that the main feature of the measurement cluster is “similarity” [20]. The similarity within the class is the highest, and the similarity between the classes is the lowest. When the dissimilarity $t(k, k')$ is used to represent two similar samples k and k' , the value of $t(k, k')$ would be large. Once the two are not similar, the value of $t(k, k')$ would be smaller, and the metric of EE and similarity is reflexive, which is expressed as

$$\forall k' k \subset k \forall k', \quad k \in K. \quad (5)$$

In general, the similarity metric for clustering algorithms can be normalized as

$$0 \leq t(k, k') \leq 1 \quad \forall k', \quad k \in K. \quad (6)$$

Under normal circumstances, the selection of the dissimilarity index is higher than the similarity index. Thus, the dissimilarity measure can be expressed by the following formula:

$$d(k', k), \forall k', \quad k \in K. \quad (7)$$

Usually, the variables of the objects discussed are continuous intervals, so the dissimilarity can also be called distance. When k and k' are similar, the distance $d(k, k')$ would be small. Once they are not similar, the $d(k, k')$ distance would be larger.

Here, there are several formulas commonly used to define distances, and this study only introduces the formulas related to defining distances.

Manhattan distance:

$$d(n, i) = |k_{n1} - s_{i1}| + |k_{n2} - k_{i2}| + \dots + |k_{nx} - k_{ix}|, \quad (8)$$

where $d(n, i)$ is the distance from the data object n to the data object i and $(k_{n1}, k_{n2}, \dots, k_{nx})$, $(k_{i1}, k_{i2}, \dots, k_{ix})$ is the x attributes of data object n to data object i , respectively.

Euclidean distance:

$$d(n, i) = \sqrt{|k_{n1} - k_{i1}|^2 + |k_{n2} - k_{i2}|^2 + \dots + |k_{nx} - k_{ix}|^2}. \quad (9)$$

Minka's distance:

$$d(n, i) = (|k_{n1} - k_{i1}|^p + |k_{n2} - k_{i2}|^p + \dots + |k_{nx} - k_{ix}|^p)^{1/p}, \quad (10)$$

where p is a positive integer.

When p is 1, Minka's distance is the Manhattan distance; when p is 2, Minka's distance is the Euclidean distance.

The clustering algorithm, as a common type of artificial intelligence algorithm, is also one of the most widely used computing methods today. In business, clustering can help market analysts to distinguish different consumer groups from consumer databases. It can also be used as a standalone tool to discover some deep information distributed in the database. At the same time, cluster analysis can also be used as a preprocessing step for other analysis algorithms in data mining algorithms. It has achieved remarkable results in many fields. This section introduces the concepts, principles, and related technologies of clustering algorithms and focuses on describing the relevant formulas of clustering algorithms. It provides an empirical theoretical basis for the analysis of the teaching practice of engineering management courses of engineering education certification based on artificial intelligence background and clustering algorithm analysis [21, 22].

3. Course Teaching under Engineering Education Certification

In order to study the application of an engineering management major in an artificial intelligence environment, this paper studies the practice of an engineering management major [23, 24].

In order to analyze the teaching practice of engineering management courses based on engineering education certification in the context of artificial intelligence, we designed an experiment to empirically explore this. In order to better understand and grasp the current teaching situation of engineering management majors, this study conducts a survey on 2018–2021 undergraduates majoring in engineering management from the aspects of survey content, survey method, and survey scope based on statistical principles [25].

3.1. Objects and Survey Content. This research mainly selects two local colleges and universities with the same teacher rankings, School A and School B. School A uses the traditional engineering education certification course teaching method to teach students courses. School B conducts course teaching with the teaching method of engineering education certification under the background of artificial intelligence. We conducted research on students from both schools. The

content of the questionnaire consists of three parts. The first part is the age, gender, and grade of the subjects. The second part is the investigation content. The third part is the work performance of college graduates under the two teaching modes and the evaluation of graduates by employers. The survey contents include attendance rate, teaching method recognition, classroom teaching satisfaction, and class attendance rate.

A survey of student attendance was conducted to understand the attendance of engineering management students, as well as reasons for absenteeism and learning attitudes. The survey of teaching identity is to clarify students' understanding of teachers' teaching methods and whether teachers can stimulate students' interest in learning. The goal of the classroom teaching satisfaction survey is to comprehensively evaluate the quality of teachers' educational services, including the reasons for their satisfaction and dissatisfaction, and ways to improve their expectations. Therefore, this survey requires both "learning" and "teaching" in order to comprehensively and effectively reflect the current teaching status of engineering management majors.

3.2. Statistics of Survey Results. The two schools each distributed 300 copies of the questionnaire: school A returned 278 copies, school B returned 282 copies, school A had 15 invalid questionnaires, and school B had 6 invalid questionnaires. The effective rate of the questionnaire in school A was 87.67%, and the effective rate of the questionnaire in school B was 92%. Among the 278 questionnaires, 188 were boys and 90 were girls in school A; 189 were boys and 93 were girls in 282 schools in B. The specific survey sample numbers of students of different grades and the distribution of sample numbers are shown in Tables 1 and 2.

3.2.1. Student Truancy Behavior. After in-depth calculation and data analysis of the questionnaire, it can be known that there are great differences among the research subjects of different age groups in the student's class attendance rate, classroom teaching identity, and classroom satisfaction. Figure 3 is a comparison chart of whether students from the two schools have skipped classes.

As can be seen from Figure 3, there are only 48 students who do not skip classes in School A, accounting for only about 17% of the students surveyed. This shows that there are many truancy behaviors among students in school A who use traditional teaching methods. Although most students only skip classes occasionally, it can also show from the side that skipping classes has become a common phenomenon. To a certain extent, it can reflect that there are problems in the traditional course teaching of engineering management majors. In school B, 101 students did not skip classes with the teaching method under the background of artificial intelligence, accounting for about 36% of the students surveyed. School B students skip classes less frequently, and only a few skip classes more frequently. This shows that the attendance rate of students in school B is much higher than that of school A in engineering management major.

TABLE 1: Gender distribution of samples.

School	Gender	Number	Proportion (%)	Total samples
A	Sample number of boys	188	67.62	278
	Sample number of girls	90	32.38	
B	Sample number of boys	189	67.02	282
	Sample number of girls	93	32.98	

TABLE 2: Sample grade distribution.

School	Grade	Freshman	Sophomore	Junior	Senior	Total samples
A	Number of samples	66	70	65	77	278
	Proportion (%)	23.74	25.18	23.38	27.70	100
B	Number of samples	73	70	64	75	282
	Proportion (%)	25.88	24.82	22.70	26.60	100

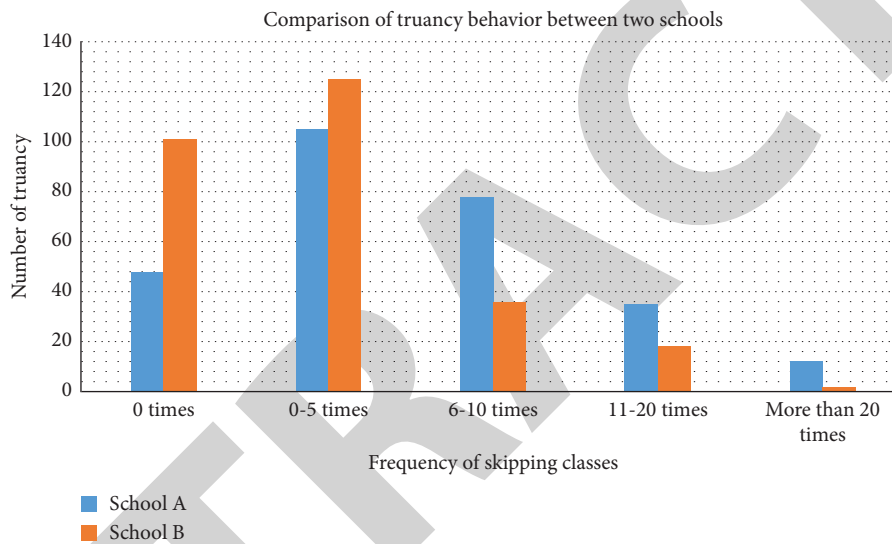


FIGURE 3: Comparison of truancy frequency between school A and school B.

In view of the fact that the attendance rate of students in school A is much lower than that in school B, we have investigated the truancy behavior of students in school A and the reasons why students in school B do not skip class. The specific results are shown in Tables 3 and Table 4.

From Table 3, it can be seen that most of the reasons why students in school A choose to skip classes are because they think that they cannot learn anything in the course or the teaching methods of the teachers do not like it. These two kinds of students account for 32.01% and 32.37% of the total, respectively. This means that most of the school A students do not like the courses and teaching methods of the major. To a certain extent, this reflects the learning attitude of traditional engineering management students and the problems existing in the course teaching field.

It can be seen from Table 4 that most of the reasons why students in school B do not skip classes believe that knowledge is useful to them, the teaching method is interesting, and the teaching content is novel. These three types of students account for 26.6%, 26.95%, and 26.24% of the

total, respectively, which show that the students of school B are more satisfied with the teaching method of the engineering management major of engineering education certification under the improved artificial intelligence background. In this course teaching mode, the attendance rate of students has increased by about 20%, and the attendance rate of students has been greatly improved. Teaching method identity and classroom teaching satisfaction are high. Students can really learn knowledge, be attracted by the courses, meet the needs of students, and ultimately develop engineering management students to a higher quality.

3.2.2. Test Situation of Students' Professional Courses. In order to analyze the learning situation of the students in the two universities, this study evaluates the achievement of the course teaching objectives of the third-year students majoring in engineering management in the two universities, that is, the course achievement test. This study evaluates the professional courses of each student participating in the survey and uses the course scores to

TABLE 3: Investigation on the causes of students' truancy in school A.

Reason	Number of people	Percentage (%)	Cumulative percentage (%)
Cannot learn anything	89	32.01	32.01
Do not like teachers	18	6.47	38.48
Dislike teaching methods	90	32.37	70.85
The teaching content is too old	50	17.99	88.84
Too inefficient	18	6.47	95.31
Other	13	4.69	100
Total	278	100	100

TABLE 4: Investigation of students' nontruancy behavior in school B.

Reason	Number of people	Percentage (%)	Cumulative percentage (%)
Knowledge is useful to oneself	75	26.60	26.60
Interesting teaching methods	76	26.95	53.55
Get good results	42	14.90	68.45
Novel teaching content	74	26.24	94.69
Other	15	5.31	100
Total	282	100	100

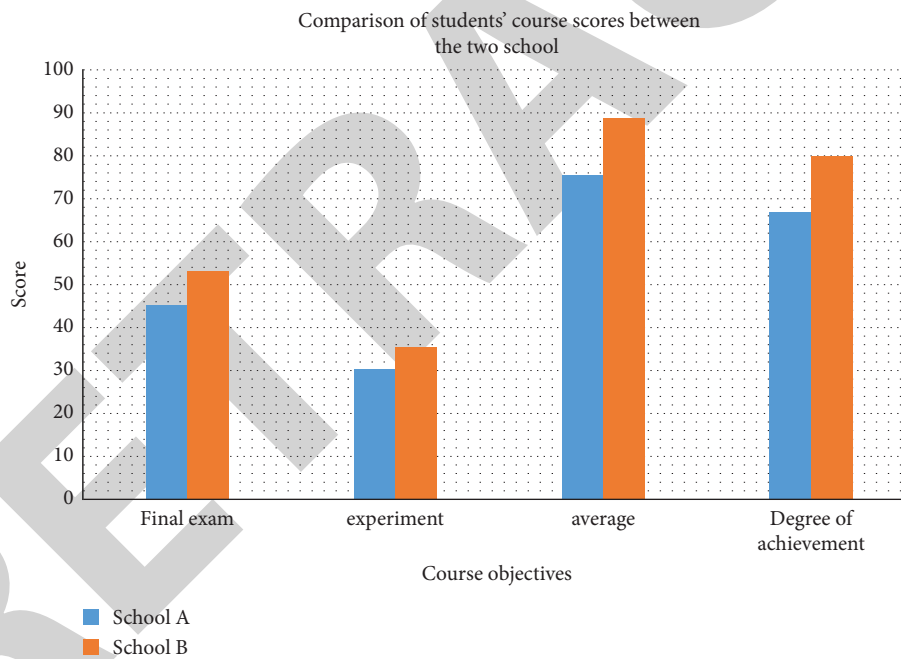


FIGURE 4: Comparison of professional courses of students in the two universities.

analyze the achievement of professional courses for students in the two schools under the two methods. The specific situation is shown in Figure 4.

It can be seen from Figure 4 that the students of school A are lower than the students of school B in terms of final grades of professional courses, in-class experiments, or overall average scores. This means that, for students majoring in engineering management, the curriculum mastery of students in school A is much lower than that of students in school B. For the final degree of achievement of the course objectives, there are only 67 students in School A. The number of students in school B is 80. The overall

mastery of the teaching knowledge of the course is improved by 13% in school B compared with school A. This shows that the engineering management course teaching of engineering education certification under the background of artificial intelligence is beneficial to students to better grasp the knowledge learned in the semester.

3.2.3. Unit's Evaluation of School's Graduate Internship Students. In addition to the statistical analysis of students' attendance and the achievement of course teaching, the last survey we chose is the unit's evaluation of the internship-

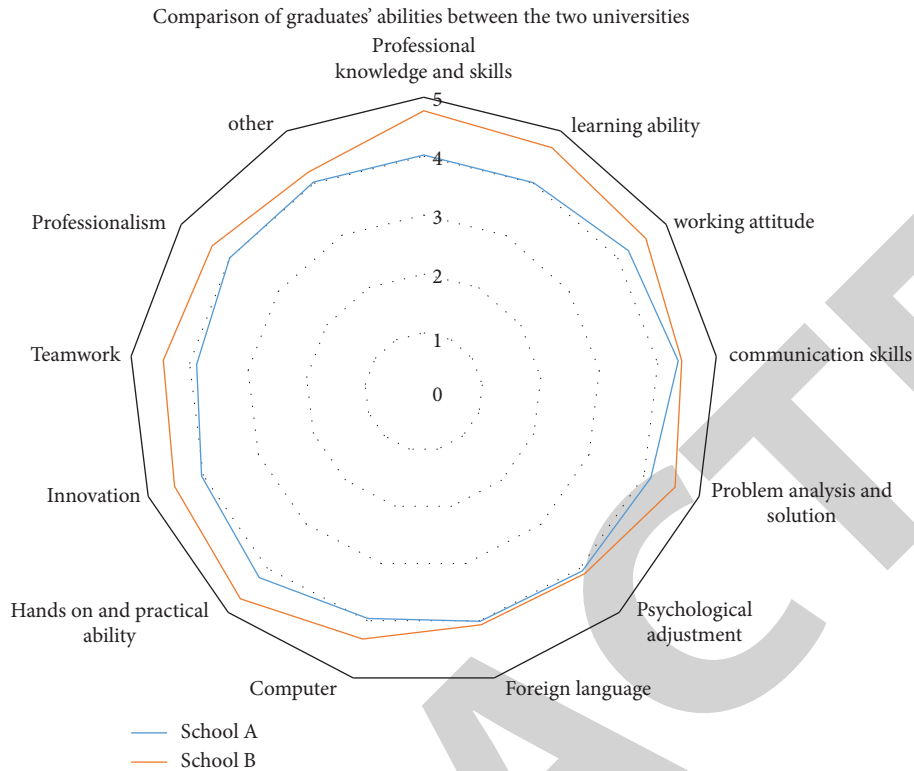


FIGURE 5: Evaluation of the unit on the internship of graduates from the two universities.

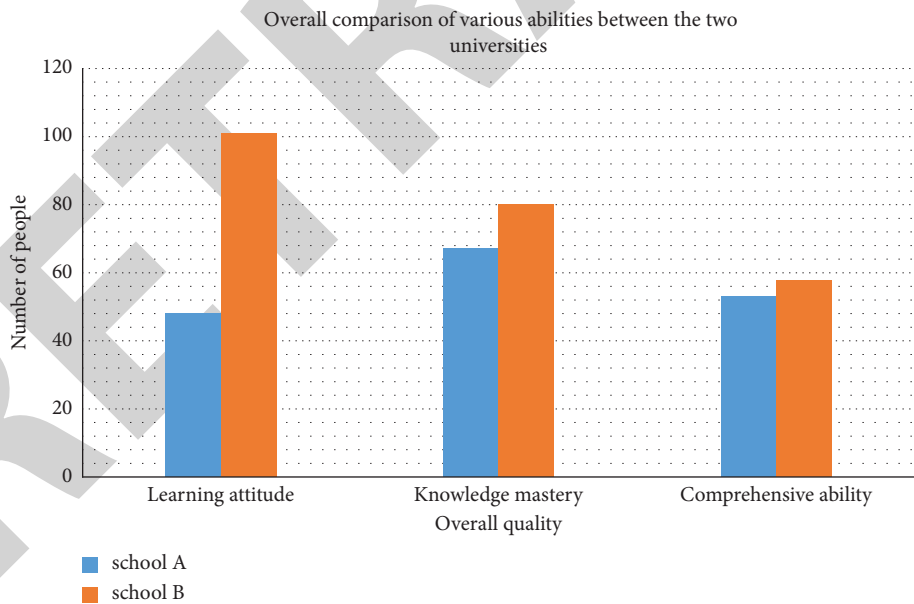


FIGURE 6: Learning ability comparison.

related situation of senior graduates. The specific evaluation situation is shown in Figure 5.

It can be seen from Figure 5 that there is still a big difference in the evaluation of various abilities of the graduates of the two schools. The evaluation of the senior students of school A is basically around 4 by the employing unit; the evaluation of senior students of school B is basically

above 4, and some are about to approach 5. This shows that the overall ability level and quality of students in school B are better than those in school A. Only in terms of foreign language level and communication skills, the overall situation of students in the two schools is similar. In terms of professional knowledge and skills, willingness to learn, innovation ability, and teamwork ability, the students of

school B are much higher than the students of school A by about 0.5 points. This shows that the teaching of engineering management courses based on engineering education certification in the context of artificial intelligence is helping to improve students' abilities, which means that students can better adapt to social needs when they graduate and face work.

It can be seen from the above that, compared with school A based on traditional engineering management courses, the students of school B based on the background of artificial intelligence would have more outstanding abilities in all aspects. The details are shown in Figure 6.

It can be seen from Figure 6 that students in school B have a better learning attitude than students in school A, and the student attendance rate has increased by about 20 points. For the mastery of course teaching knowledge, the students of school B are also better than those of school A, and the degree of achievement of the teaching standard of the course has increased by about 13 points. As for the comprehensive ability level of the students after graduation, the students of school B have improved by about 8 points compared with the students of school A. This shows that engineering management students certified in engineering teaching under the background of artificial intelligence are at a higher overall level than students under the original traditional course teaching. It can not only promote the improvement of the teaching quality and efficiency of engineering management courses but also promote the development of college education and can also better meet the needs of today's engineering management for compound talents.

4. Conclusion

At the same time, the development of the market economy has promoted the development of China's engineering management, and at the same time, it has put forward higher requirements for talents in engineering management. This study focuses on the teaching practice of engineering management professional courses for engineering education certification under the background of artificial intelligence. First, a brief description of the research background of the study, then a brief overview of the previous research by scholars, and then an overview of the related concepts and algorithms of the study are given. Finally, through experimental investigation and analysis, the research shows that the teaching practice of engineering management professional courses of engineering teaching certification under the background of artificial intelligence is more favorable and more in line with the current development needs. It can promote the improvement of the teaching quality and efficiency of engineering management courses and, at the same time, make the current engineering management graduates more in line with the needs of the current engineering management field for compound talents. However, there are still shortcomings in this study. This research is relatively lacking at the microlevel. Therefore, future research can pay more attention to the microlevel and focus on the specific teaching curriculum design and implementation. At the same time, the improvement of the engineering

management profession in the future is the general trend, which can be achieved by establishing a sound institutional system. In particular, a more in-depth discussion on the division of personnel responsibilities in the curriculum reform would become an important direction for the reform of continuing education in the future.

Data Availability

No data were used to support the findings of the study.

Conflicts of Interest

The authors state that there are no conflicts of interest.

Acknowledgments

This work was supported by the research topic of planning subject for the 13th five-year plan of Jilin Province Education Sciences (ZD19045), Higher Education Teaching Reform of Jilin Province (JLZT204520190725155032), and Jilin Province Science and Technology Development Plan Project (20220508143RC).

References

- [1] J. Dong, "Discussion on curriculum reform of digital image processing under the certification of engineering education," *Open Journal of Social Sciences*, vol. 10, no. 1, pp. 8–12, 2022.
- [2] H. Wang and X. Fan, "Conception and practice of engineering education certification for mechanical majors in local colleges and universities," *Journal of Higher Education*, vol. 8, no. 5, pp. 227–230, 2017.
- [3] Y. Zhang and Y. Huang, "International comparison of professional degree education certification in environmental engineering," *IOP Conference Series: Materials Science and Engineering*, vol. 562, no. 1, pp. 012104–012114, 2019.
- [4] H. M. Jia, J. W. Zhang, and W. U. Di, "Research on continuous improvement strategies of automation specialty under background of engineering education certification," *Sci-tech Innovation and Productivity*, vol. 18, no. 9, pp. 119–123, 2018.
- [5] U. Ehsan, S. Passi, and Q. V. Liao, "The who in explainable AI: how AI background shapes perceptions of AI explanations," vol. 256, no. 8, pp. 248–249, 2021.
- [6] X. Li, Y. Xie, and T. Liu, "Research on oral english teaching system based on VR in the background of AI," *Journal of Physics: Conference Series*, vol. 1550, no. 2, pp. 022031–31, 2020.
- [7] R. Rongpeng, Z. Zhao, X. Zhou et al., "Intelligent 5G: when cellular networks meet artificial intelligence," *IEEE Wireless Communications*, vol. 24, no. 5, pp. 175–183, 2017.
- [8] D. Hassabis, D. Kumaran, C. Summerfield, and M. Botvinick, "Neuroscience-inspired artificial intelligence," *Neuron*, vol. 95, no. 2, pp. 245–258, 2017.
- [9] T. Han, "RETRACTED: research on the teaching reform path of operational research course of engineering management major based on computer technology," *Journal of Physics: Conference Series*, vol. 1744, no. 3, pp. 032238–38, 2021.
- [10] K. Georgousoglou, Y. Mouzakitis, and E. D. Adamides, "On the contribution of risk management plans to municipal solid waste management: evidence from a major Greek municipality," *IOP Conference Series: Earth and Environmental Science*, vol. 899, no. 1, pp. 012071–12117, 2021.

Retraction

Retracted: Surface Feature Prediction Modeling and Parameter Optimization for Turning TC17 Titanium Alloy

International Transactions on Electrical Energy Systems

Received 28 November 2023; Accepted 28 November 2023; Published 29 November 2023

Copyright © 2023 International Transactions on Electrical Energy Systems. This is an open access article distributed under the Creative Commons Attribution License, which permits unrestricted use, distribution, and reproduction in any medium, provided the original work is properly cited.

This article has been retracted by Hindawi, as publisher, following an investigation undertaken by the publisher [1]. This investigation has uncovered evidence of systematic manipulation of the publication and peer-review process. We cannot, therefore, vouch for the reliability or integrity of this article.

Please note that this notice is intended solely to alert readers that the peer-review process of this article has been compromised.

Wiley and Hindawi regret that the usual quality checks did not identify these issues before publication and have since put additional measures in place to safeguard research integrity.

We wish to credit our Research Integrity and Research Publishing teams and anonymous and named external researchers and research integrity experts for contributing to this investigation.


The corresponding author, as the representative of all authors, has been given the opportunity to register their agreement or disagreement to this retraction. We have kept a record of any response received.

References

- [1] Z. Deng, Z. Wang, and X. Shen, "Surface Feature Prediction Modeling and Parameter Optimization for Turning TC17 Titanium Alloy," *International Transactions on Electrical Energy Systems*, vol. 2022, Article ID 2979858, 12 pages, 2022.

Research Article

Surface Feature Prediction Modeling and Parameter Optimization for Turning TC17 Titanium Alloy

Zhibo Deng,¹ Zhe Wang,² and Xuehong Shen³ 

¹Party and Government Office, Xi'an Aeronautical Polytechnic Institute, Xi'an 710089, Shaanxi, China

²Aviation Manufacturing Engineering School, Xi'an Aeronautical Polytechnic Institute, Xi'an 710089, Shaanxi, China

³School of Mechanical Engineering, Northwestern Polytechnical University, Xi'an 710072, Shaanxi, China

Correspondence should be addressed to Xuehong Shen; xhs@mail.nwpu.edu.cn

Received 18 August 2022; Revised 5 September 2022; Accepted 7 September 2022; Published 5 October 2022

Academic Editor: Nagamalai Vasimalai

Copyright © 2022 Zhibo Deng et al. This is an open access article distributed under the Creative Commons Attribution License, which permits unrestricted use, distribution, and reproduction in any medium, provided the original work is properly cited.

Surface integrity has a very significant effect on surface roughness and surface microhardness. These are the main characteristics of surface integrity. The present study investigated the influence of the cutting depth (a_p), the cutting speed (v_c), and the feed rate (f) on the surface roughness (Ra) and surface microhardness (HV) in turning TC17 titanium alloy. Data obtained from the Box-Behnken design experiments were used to develop the response surface methodology (RSM) and artificial neural network (ANN) models. Through analysis of variance (ANOVA), the relative effects of each cutting parameter on the responses have been determined. To examine the interaction effects of cutting parameters, 3D surface plots were generated. The desirability function approach (DFA) was used to optimize cutting parameters to achieve the lowest surface roughness and highest surface microhardness. The results show that ANN response prediction models have higher prediction accuracy and lower error than RSM prediction models. The optimization parameters are 60 m/min cutting speed, 0.06 mm/r feed rate, and 0.2 mm cutting depth for the minimum surface roughness and maximum surface microhardness with a maximum error of 2.83%.

1. Introduction

Titanium alloy materials have lots of advantages of high strength, good toughness, and high adaptability to forging temperature and are widely used in the manufacture of aerospace parts [1]. However, in the titanium alloy cutting process, the heat and force actions are prone to drastic changes, and the chips are very easy to adhere for causing significant tool wear [2, 3], which makes it difficult to control the concerning characteristics. It is indispensable to study the surface roughness and microhardness of titanium alloy cutting. Many professionals have conducted a large number of research on the cutting of titanium alloy materials. Mersni et al. [4] analyzed the influence of cutting speed, depth of cut, and feed per tooth on the three-dimensional surface roughness using Taguchi's method and optimized the best cutting parameters to obtain the best machining workpiece's surface. Kumar et al. [5] employed multiresponse grey relational analysis (GRA) technology to optimize process

parameters and observed the influence of cutting parameters on the surface roughness and material removal rate through the main effect diagram. Kiswanto et al. [6] used a cemented carbide tool with a diameter of 1 mm to conduct a milling experiment by changing the spindle speed and feed rate in high-speed cutting under the condition of a fixed cutting depth to measure the surface roughness under different variable combinations. They discovered that a slower cutting speed and feed rate are better for improving surface processing quality. Thirumalai et al. [7] established the quadratic regression empirical prediction model of surface roughness and cutting temperature of turning titanium alloy. Applying signal-to-noise ratio (SNR), the proportion of cutting speed on surface roughness is 38%, and the feed rate is 25%. The most important factor affecting cutting temperature is cutting speed, and the least influential factor is cutting depth. Samin et al. [8] employed Taguchi's experimental design method to carry out Ti6Al4V turning experiments. The analysis showed that the feed rate and the

TABLE 1: Chemical composition of TC17.

Element	Wt. (%)	Element	Wt. (%)
Al	5.23	Fe	0.3
Sn	1.97	C	0.05
Zr	1.9	N	0.05
Mo	4.06	H	0.01
Cr	4.04	O	0.12
Ti	Balance		

cutting depth are the most relevant parameters that affect surface roughness and cutting force. Through the turning experiments with different tool radius, Mazid et al. [9] obtained the optimized parameter range of surface roughness from $0.5\ \mu\text{m}$ to $1\ \mu\text{m}$ based on a cutting speed of 60–250 m/min, the feed speed 0.1 mm/r and the cutting depth 0.5 mm. Matras et al. [10] put forward that the influence of cutting speed on surface roughness can be ignored, and it takes the minimum surface roughness as the objective to optimize the process parameters. Seung et al. [11] analyzed the impact of machining tools on the machinability of titanium alloy. The consequences show that the dynamic range of cutting force and surface roughness of coated cemented carbide tool and cermet tool is larger than cemented carbide tool, and the influencing factors of tool life are tool material, cutting speed, and feed. By studying the influence of tool microstructure on chip morphology, cutting force, surface state, and surface roughness, Qian et al. [12] analyzed and summarized the test data and found that the key factor to improve the machinability of TC21 titanium alloy was the microstructure. Besides, scholars pay attention to the tool wear because the material is easy to stick to the tool in the process of titanium alloy. Aramcharoen [13] found that low-temperature cooling can reduce friction between the tool and the chip, improve production efficiency and tool life, and create a thinner secondary deformation zone. Taking 0.1 mm as the tool wear limit, Priarone et al. [14] proposed that low-temperature cooling can extend the tool life of uncoated cemented carbide tools by 2 minutes, CBN tools about 7.2 minutes, and PCD tools with different grain sizes by 14 minutes compared with traditional oil cooling and low-temperature cooling. With the emergence of new processing methods, Che-Haron [15] carried out the cutting experiments of Ti-6Al-2Sn-4Zr-6Mo with different grain sizes ($1.0\ \mu\text{m}$ and $0.68\ \mu\text{m}$) uncoated cemented carbide tools to describe that the main forms of tool wear are excessive cutting. Furthermore, it is stated that the finer the grain size, the longer is the tool life. Muhammad et al. [16] used unified Ti6Al4V turning experiments to analyze tool wear and energy distributions to evaluate the tool wear rate and energy generated by different cutting conditions. Due to the large contact length and high chip compression ratio, serious tool wear and a large energy zone appear in high-speed cutting.

At present, the research on titanium alloy mainly focuses on Ti6Al4V. Compared with others, the TC17 has bigger yield strength, smaller elongation, and lower elasticity modulus. The research on TC17 titanium alloy is still relatively very lacking. Therefore, it is necessary to study the surface roughness and surface microhardness of turning

TABLE 2: Material properties of TC17.

Material properties	Value
Elastic modulus	112 (GPa)
Tensile strength	1960 (MPa)
Yield strength	1890 (MPa)
Density	$4.55\ (\text{g}/\text{cm}^3)$
Hardness	41 (HRC)
Elastic modulus	112 (GPa)
Tensile strength	1960 (MPa)

TABLE 3: Chosen parameters and levels.

Code	Experimental factors	Units	Levels		
			1	2	3
A	Cutting speed	m/min	30	60	90
B	Feed rate	mm/r	0.06	0.12	0.18
C	Cutting depth	mm	0.1	0.2	0.3

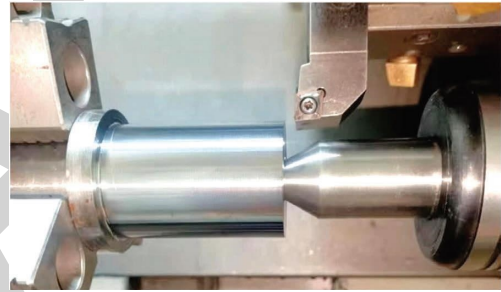


FIGURE 1: The experimental conditions.

TC17. The results can conduct the selection of cutting parameters according to the application requirements.

2. Experimental Conditions and Methods

The experimental material is titanium alloy TC17, which is an $\alpha+\beta$ dual-phase alloy rich in α phase. Its chemical composition is depicted in Table 1, and its fundamental material properties are presented in Table 2 [17, 18]. The experimental piece is $\Phi 60\ \text{mm} \times 280\ \text{mm}$ bar material. The tool model is a hard alloy tool YG6, with a rake angle of 6° , and a relief angle of 10° . In order to reduce the cutting temperature, a large amount of cutting fluid with a cooling effect should be poured into the cutting area. Because the thermal conductivity of titanium alloy is low, which is only 1/7 of steel and 1/6 of aluminum, the heat can't be quickly transferred with the chips in the machining process. When turning and cutting titanium alloys, emulsions or water-soluble cutting fluids with extreme pressure additives are often used, which is not easy to reach the ignition temperature. It is better not to use gaseous coolant in titanium alloy processing, so as to avoid toxic substances and hydrogen embrittlement and also prevent high-temperature stress corrosion cracking of titanium alloy. In this experiment, the emulsion is selected for cooling. According to the actual processing conditions. To reduce the interference of other nonconcerned factors on the reliability of the

TABLE 4: The response surface experimental results.

No.	Cutting speed v_c (m/min)	Feed rate f (mm/r)	Cutting depth a_p (mm)	Surface roughness Ra (μm)	Surface microhardness HV
1	60	0.12	0.2	1.36	455
2	30	0.06	0.3	0.79	435
3	60	0.12	0.2	1.28	460
4	90	0.06	0.1	0.7	438
5	30	0.06	0.1	0.68	440
6	90	0.18	0.3	2.51	449
7	60	0.18	0.2	2.17	450
8	60	0.06	0.2	0.74	456
9	90	0.18	0.1	1.81	412
10	60	0.12	0.1	1.35	440
11	60	0.12	0.2	1.32	458
12	60	0.12	0.2	1.2	449
13	90	0.06	0.3	0.83	421
14	30	0.12	0.2	1.58	426
15	90	0.12	0.2	1.37	420
16	30	0.18	0.3	2.32	480
17	60	0.12	0.2	1.45	452
18	60	0.12	0.3	1.53	468
19	60	0.12	0.2	1.21	448
20	30	0.18	0.1	2.27	426

TABLE 5: Analysis of variance for Ra .

Source	DF	Adj SS	Adj MS	F-value	P-value	C. (%)	Signif
Model	9	5.74	0.64	45.52	<0.0001	97.62	YES
A	1	0.018	0.018	1.26	0.288	0.31	
B	1	5.39	5.39	384.57	<0.0001	91.67	
C	1	0.14	0.14	9.77	0.0108	2.38	
AB	1	0.014	0.014	0.97	0.3475	0.24	
AC	1	0.056	0.056	4.01	0.0732	0.95	
BC	1	0.033	0.033	2.32	0.1586	0.56	
A ²	1	0.014	0.014	1.01	0.338	0.24	
B ²	1	7.38E-03	7.38E-03	0.53	0.4845	0.13	
C ²	1	3.73E-03	3.73E-03	0.27	0.6172	0.06	
Error	10	0.14	0.014				
Total	19	5.88					

experimental results, each set of experiments adopts a new blade. Using the Box-Behnken design experimental program [19], which is shown in Table 3, to plan the experiment with cutting speed, feed, and cutting depth as experimental factors with three levels defined for each factor.

The length of processing for each set of parameters is 10 millimeters. Figure 1 illustrates the experimental conditions. The experimental results are surface roughness (Ra) and surface microhardness (HV), which were measured using the conventional surface roughness tester TR240 and the digital display Micro Vickers hardness tester HV-50, respectively. To reduce measurement error, the average of three measurements is applied to each result. Table 4 represents the precise experimental arrangement and measurement data.

3. Prediction Model and Influence Law

3.1. Analysis of Variance (ANOVA). Analysis of variance (ANOVA) is one method for assessing the significance of input factors on response variables. In addition, it is a

TABLE 6: Analysis of variance for HV.

Source	DF	Adj SS	Adj MS	F-value	P-value	C. (%)	Signif
Model	9	5300.78	588.98	15.51	<0.0001	93.31	YES
A	1	448.9	448.9	11.82	0.0064	7.90	
B	1	72.9	72.9	1.92	0.196	1.28	
C	1	940.9	940.9	24.78	0.0006	16.56	
AB	1	105.12	105.12	2.77	0.1271	1.85	
AC	1	105.12	105.12	2.77	0.1271	1.85	
BC	1	1596.13	1596.13	42.03	<0.0001	28.10	
A ²	1	1750.14	1750.14	46.08	<0.0001	30.81	
B ²	1	62.64	62.64	1.65	0.228	1.10	
C ²	1	91.64	91.64	2.41	0.1514	1.61	
Error	10						
Total	19						

convenient and swift solution process that is widely accepted and utilized. Table 5 are the results of ANOVA for surface roughness (Ra). In Table 5, the P-Value does not exceed 0.05, which indicates that the influence of the input

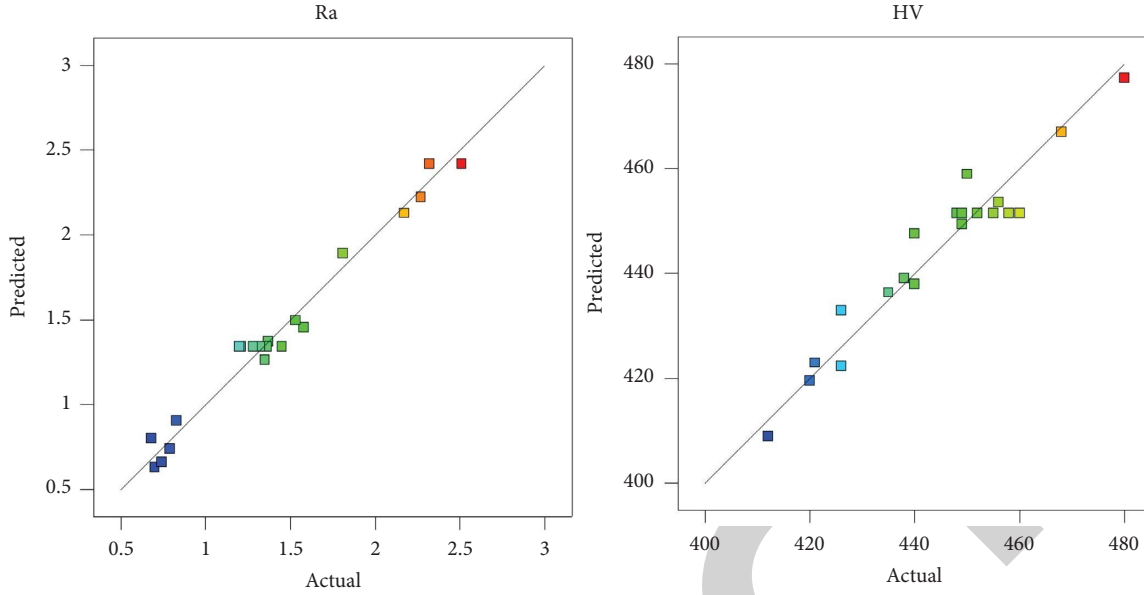


FIGURE 2: Comparison of prediction models for Ra and HV .

parameters is established, and the cutting parameters play a key role in surface roughness. The A , B , and C input parameters expend percentages for surface roughness (Ra) are 0.31%, 91.67%, and 2.38% respectively. It indicates that B has the principal influence on the surface roughness (Ra), shortly followed by C . The P -Value of A to surface roughness (Ra) is greater than 0.05, indicating that it can be ignored.

For the surface microhardness (HV), the ANOVA results are shown in Table 6. Through analysis, the percentage contributions of process parameters for A , B , and C were defined as (7.90%, 1.28%, and 16.56%), respectively. It shows that C with 16.56% contributions occupies the first position in influencing surface microhardness (HV). The next factor is A with 7.90% contributions. For the low contribution of B (1.28%), it shows that B has no significant influence on the surface microhardness (HV).

3.2. Response Surface Method(RSM) Modeling Development

3.2.1. Regression Analysis. Regression analysis is based on a large number of test data analysis results, using mathematical methods to establish the relationship model between input variables and output variables. It can be used to predict the value of the variable and is widely used in industrial production and science research. The response surface method (RSM) is a test method that considers interference factors and is accepted by the public [20, 21]. The regression model obtained through experimental design can be expressed as in the following Equation:

$$y = \beta_0 + \sum_{i=1}^m \beta_i x_i + \sum_{i=1}^m \beta_{ii} x_i^2 + \sum_{i < j} \beta_{ij} x_i x_j, \quad (1)$$

where, β_0 is the constant term, β_i is the linear effect of x_i , β_{ii} is the second-order effect of x_i , β_{ij} is the interactive effect between x_i and x_j , and x_i and x_j are the input and response variables, respectively.

Equations (2) and (3) can be used to calculate prediction models for surface roughness (Ra) and surface microhardness (HV) (3).

$$\begin{aligned} Ra = & 0.792 - 0.01v_c + 8.02f - 3.25a_p \\ & - 0.02v_c f + 0.02v_c a_p + 10.06f a_p \\ & + 0.00007v_c^2 + 14.39f^2 + 3.68a_p^2 \end{aligned} \quad (2)$$

$$R^2 = 0.9762,$$

$$\begin{aligned} HV = & 408.86 + 3.62v_c - 623.18f - 343.90a_p \\ & - 2.01v_c f - 1.21v_c a_p + 2354.16f a_p \\ & - 0.02v_c^2 + 1325.75f^2 + 577.27a_p^2 \end{aligned} \quad (3)$$

$$R^2 = 0.9331.$$

The correlation coefficients R^2 of the regression equations that advanced for the predictive surface roughness and surface microhardness were computed as $R^2 = 98\%$ and $R^2 = 93\%$, respectively. Figure 2 depicts a comparison of experimental results and predicted values obtained from regression equations. Most of the true values are scattered on the predicted value, and a small part of the true values are scattered on both sides of the predicted value, indicating that the model fits well with the actual results. As a result, the regression model can estimate the surface feature, including Ra and HV .

3.2.2. Surface Plot in 3D. Figure 3 shows the variation of Ra with the interaction of machining process factors. The cutting depth in Figure 3(a) is 0.2 mm. The surface roughness increases linearly as the feed rate (f) increases

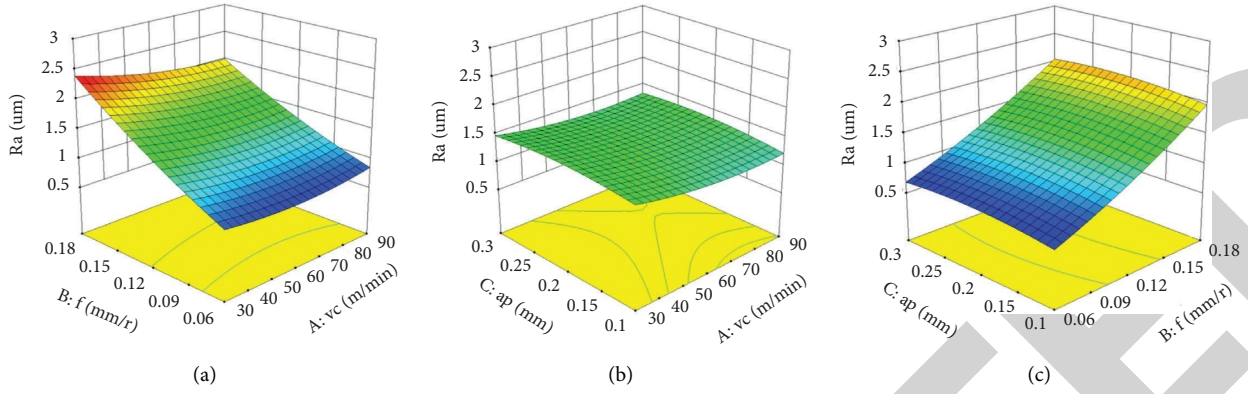


FIGURE 3: The influence of the machining factor on R_a . (a) Interaction of f and v_c on R_a , (b) interaction of a_p and v_c on R_a , and (c) interaction of a_p and f on R_a .

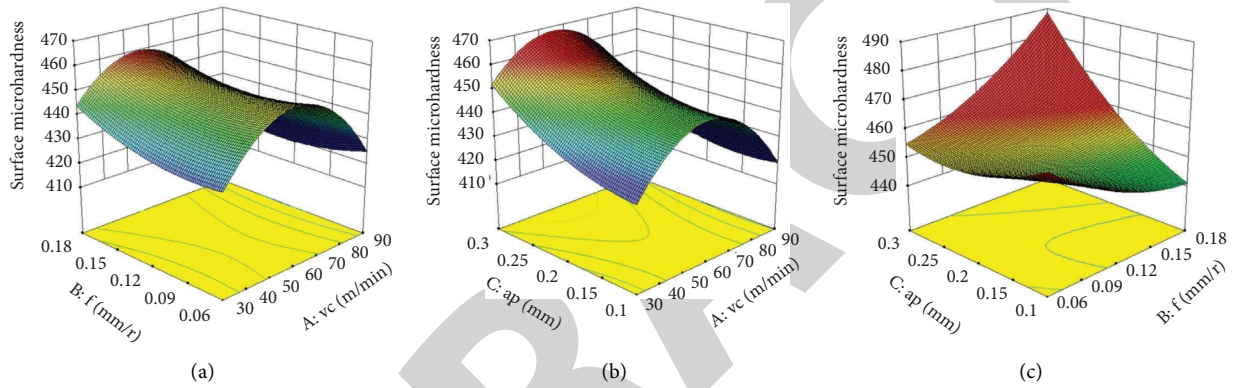


FIGURE 4: The influence of cutting parameters on HV . (a) The influence of f and v_c on HV . (b) The influence of a_p and v_c on HV . (c) The influence of a_p and f on HV .

from 0.06 mm/r to 0.18 mm/r. The effect of cutting speed on the R_a is less than the feed rate. The roughness is at its worst state level when the feed rate and cutting speed are both set to low levels.

The interaction of cutting speed and cutting depth on R_a is illustrated in Figure 3(b). In this analysis, the feed rate is selected by 0.12 mm/r, and the fluctuation range of R_a is from 1.2 to 1.6 μm . It has been discovered that both the cutting depth and the cutting speed have some very slight effects on the R_a . The R_a response surface graph of the cutting depth and feed rate at a cutting speed of 60 m/min is shown in Figure 3(c). In contrast, R_a is susceptible to feed rate fluctuations and less susceptible to cutting depth. The R_a reaches the maximum value of 2.4 μm with the machining parameter factor cutting speed which is 60 m/min, the feed rate is 0.18 mm/r, and the cutting depth is 0.3 mm.

The 3D plot of milling parameters on surface microhardness (HV) was presented in Figure 4. In Figure 4(a), while the feed goes up from the initial value of 0.06 mm/r to 0.18 mm/r, the maximum surface microhardness is obtained at $v_c = 70$ m/min. Figure 4(b) demonstrates that the surface microhardness rises with increasing cutting depth. Figure 4(c) demonstrates that the cutting depth continuously increases from 0.1 to 0.3 mm, while the microhardness decreases. The maximum microhardness value can be

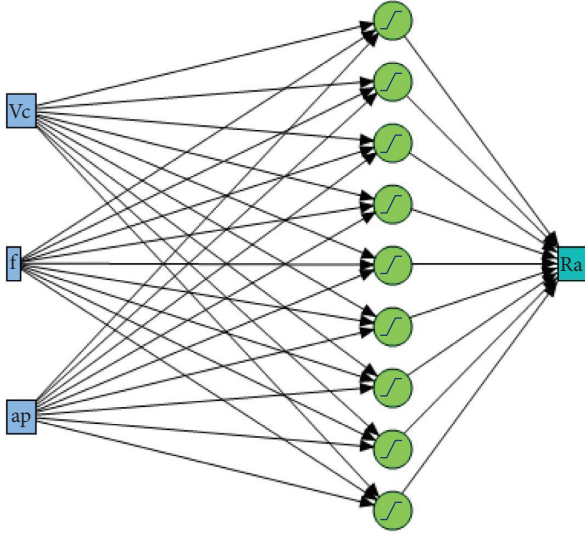
obtained under the condition of large feed and large cutting depth, up to nearly 490 HV . It can be seen from the interaction depicted and contour diagram of the comprehensive response surface that microhardness is sensitive to feed rate and cutting depth, which is consistent with the coefficient reflection of the established model.

4. Artificial Neural Network (ANN)

Compared with the regression analysis, the artificial neural network (ANN) does not need to specify the mathematical model in advance, which avoids the shortcomings of the curve fitting method and improves the prediction modeling accuracy. ANN is widely used in prediction, classification, and other research due to its self-learning and self-adaptive advantages in processing random data and nonlinear data. Maheshwera et al. [22] used regression analysis and artificial neural network models to predict the R_a of AISI 52100 steel during hard turning. The difference between the calculated values of the model and the experimental results is particularly small. Using the ANN, Abbas et al. [23] successfully predicted the surface roughness of AZ61 magnesium alloy final turning with an accuracy of 1.35%. For the drilling process, Kolesnyk et al. [24] selected ANN to research CFRP/Ti alloy material and analyzed the cutting heat

TABLE 7: Performance of ANN structure of Ra .

Inp_Hid_Oup	Root mean square error (RMSE)	Coefficient of determination (R^2)
3-5-1	0.0508	0.9871
3-6-1	0.0886	0.9607
3-7-1	0.0881	0.9611
3-8-1	0.0504	0.9873
3-9-1	0.0171	0.9999
3-10-1	0.0818	0.9665

FIGURE 5: The optimal network structure for Ra .

generated in the drilling process and the surface quality of the workpiece after drilling. The results show that ANN can be used to identify the drilling parameter-hole quality relationship. Sangwan et al. [25] and Kumar and Chauhan [26] proposed a method combining ANN and genetic algorithm to optimize the turning machining factors. It can be seen

from the above research works that using the ANN model to examine the nonlinear relationship between the virtual machining parameters and the machining performance is effective in predicting the actual machining process.

The structure of the neural network can be defined as 3- H -1, which stands for three input parameters (cutting speed, feed rate, and cutting depth) with H number of hidden layer nodes and one response (surface roughness or surface microhardness). The excitation function of the neural network adopts the hyperbolic tangent function (TanH) [27], which transforms values to be between -1 and 1 and its expression is given in the following Equation:

$$\text{TanH} = \frac{e^{2x} - 1}{e^{2x} + 1} \quad (4)$$

4.1. Application of ANN to Model (Ra). According to Table 7, some ANN structures were tested. Figure 5 depicts the best network topology, which is 3-9-1 based on a smaller RMSE and a higher R^2 . It is made up of three input layer nodes, nine hidden layer nodes, and one output layer node with a linear transfer function.

The mathematical model for surface roughness (Ra) derived by the ANN approach is shown in the following Equation with $R^2 = 99.99\%$:

$$\begin{aligned} Ra = & 1.9478 - 0.4451 * H1 + 1.7919 * H2 - 1.5120 * H3 + 3.1112 * H4 \\ & - 0.4457 * H5 + 0.5689 * H6 + 0.7477 * H7 + 3.1521 * H8 - 0.47247 * H9, \end{aligned} \quad (5)$$

where,

$$\begin{aligned} H1 &= \text{TanH}(3.4307 + -6.5460 * ap + 8.7363 * f + -0.04552 * Vc), \\ H2 &= \text{TanH}(1.4897 + 1.6920 * ap + -15.8407 * f + 0.0022 * Vc), \\ H3 &= \text{TanH}(-3.6149 + 8.3069 * ap + 6.0278 * f + 0.01098 * Vc), \\ H4 &= \text{TanH}(-2.59039 + 7.2156 * ap + 3.4107 * f + 0.0076 * Vc), \\ H5 &= \text{TanH}(3.5705 - 2.3971 * ap + -15.6305 * f + -0.02977 * Vc), \\ H6 &= \text{TanH}(-2.8044 + 0.1261 * ap + 7.1547 * f + 0.0197 * Vc), \\ H7 &= \text{TanH}(-0.5712 + -3.5080 * ap + 10.1420 * f + 0.01147 * Vc), \\ H8 &= \text{TanH}(1.7555 + -2.8133 * ap + -5.9964 * f + -0.0103 * Vc), \\ H9 &= \text{TanH}(-3.9836 - 1.9689 * ap + 20.2767 * f + 0.03528 * Vc), \end{aligned} \quad (6)$$

4.2. *Application of ANN to Model (HV)*. In the same way, the test results of the several ANN architectures of *HV* are shown in Table 8. The architecture chosen is 3-10-1 (Figure 6) with the highest R^2 and the lowest RMSE.

The mathematical model obtained by the ANN method for the surface microhardness (*HV*) is expressed in the following Equation with $R^2 = 99.23\%$:

TABLE 8: Performance of ANN structure of HV.

Inp_Hid_Oup	RMSE	R^2
3-5-1	11.3270	0.6309
3-6-1	103005	0.6947
3-7-1	2.3532	0.9840
3-8-1	10.2615	0.6970
3-9-1	2.3882	0.9835
3-10-1	1.6329	0.9923

$$\begin{aligned}
 HV = & 425.8282 + 25.4849 * H1 + 1.8094 * H10 + 298.8565 * H2 \\
 & + 41.14935 * H3 - 22.76606 * H4 - 122.02144 * H5 \\
 & - 19.6225 * H6 - 158.3730 * H7 - 38.6868 * H8 - 136.0233 * H9,
 \end{aligned} \tag{7}$$

where,

$$\begin{aligned}
 H1 &= \text{TanH}(3.3995 - 8.1659 * ap - 3.0219 * f - 0.0270 * Vc), \\
 H2 &= \text{TanH}(-2.7765 + 5.2553 * ap + 3.6597 * f + 0.0102 * Vc), \\
 H3 &= \text{TanH}(1.8557 + 3.7416 * ap - 17.2210 * f - 0.0135 * Vc), \\
 H4 &= \text{TanH}(2.2312 - 11.05189 * ap - 1.0593 * f - 0.0057 * Vc), \\
 H5 &= \text{TanH}(-3.4709 + 7.0627 * ap - 3.4015 * f + 0.02637 * Vc), \\
 H6 &= \text{TanH}(-6.0225 + 8.4248 * ap + 25.9316 * f + 0.02868 * Vc), \\
 H7 &= \text{TanH}(-3.2211 + 3.0372 * ap + 7.5765 * f + 0.01766 * Vc), \\
 H8 &= \text{TanH}(5.2797 - 3.4336 * ap - 24.5623 * f - 0.02859 * Vc), \\
 H9 &= \text{TanH}(0.17486 + 2.9591 * ap - 1.5697 * f - 0.0149 * Vc), \\
 H10 &= \text{TanH}(-2.6185 + 1.1293 * ap + 16.5582 * f + 0.01407 * Vc).
 \end{aligned} \tag{8}$$

Table 9 and Figures 7 and 8 are the comparison of experimental and estimated by RSM and ANN, and the absolute percentage error (Δ) is calculated using the following Equation [22]:

$$\Delta = \left| \frac{y_{\text{exp}} - y_{\text{pred}}}{y_{\text{exp}}} \right| \times 100\%. \tag{9}$$

For RSM and ANN, the maximum test errors for surface roughness are about 30.02% and 11.78%, respectively. The mean absolute percentage error between RSM and experimental values can be seen as 9.50%, whereas the same value is only 3.48% with the ANN model. In surface microhardness, the same maximum test errors for RSM and ANN are revealed as 15.84% and 3.22%, respectively. The mean absolute percentage

errors between experimental and estimated by RSM and ANN are found to be 7.36% and 0.85%. Actual values and anticipated values for ANN and RSM are shown in Figures 7 and 8. Thus, it can be seen that ANN is closer to the test results than RSM, showing a better fitting effect.

5. Optimization with DFA

One of the most popular approaches for manufacturing's multiple response process optimizations is the desire function approach (DFA) [28, 29]. A typical way is the desirability approach, which allocates a "score" to a collection of replies and selects factor settings that maximizes that score. To find out the maximum and minimum of the target goal, the desirability can be defined from the following Equations:

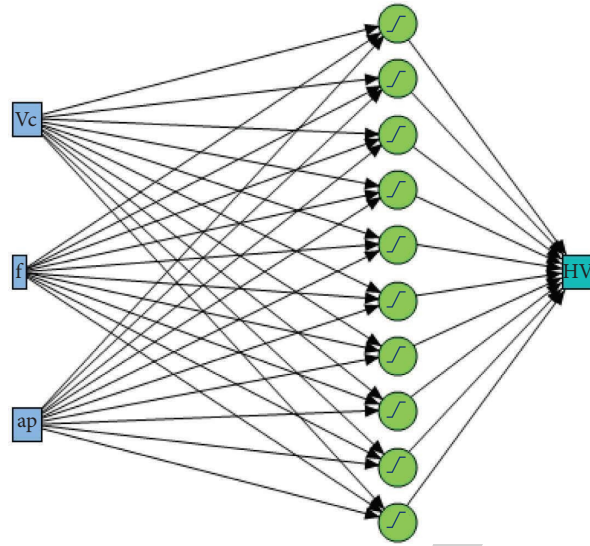


FIGURE 6: The optimal network structure for HV.

TABLE 9: Comparison of the measured and predicted value.

No.	R_a (μm) exp	Surface roughness (R_a)				HV (%) exp	Surface microhardness (HV)			
		RSM pred	ANN pred	Error (%) (RSM)	Error (%) (ANN)		RSM pred	ANN pred	Error (%) (RSM)	Error (%) (ANN)
1	1.36	1.4483	1.3414	6.49	1.37	455	480.1878	455.8414	5.54	0.18
2	0.79	0.7693	0.7919	2.62	0.24	435	443.4931	434.5498	1.95	0.10
3	1.28	1.4483	1.3414	13.15	4.80	460	480.1878	455.8414	4.39	0.90
4	0.7	0.8362	0.7289	19.45	4.12	438	503.8056	437.634	15.02	0.08
5	0.68	0.8842	0.6828	30.02	0.41	440	445.1016	439.8475	1.16	0.03
6	2.51	2.4843	2.6508	1.02	5.61	449	514.1188	447.0804	14.50	0.43
7	2.17	2.2372	1.9451	3.10	10.37	450	487.6745	461.8817	8.37	2.64
8	0.74	0.7629	0.7444	3.10	0.60	456	482.2466	455.3319	5.76	0.15
9	1.81	2.1177	1.8151	17.00	0.28	412	473.7475	410.6579	14.99	0.33
10	1.35	1.4221	1.3597	5.34	0.72	440	476.2698	454.162	8.24	3.22
11	1.32	1.4483	1.3414	9.72	1.62	458	480.1878	455.8414	4.84	0.47
12	1.2	1.4483	1.3414	20.69	11.78	449	480.1878	455.8414	6.95	1.52
13	0.83	0.9613	0.8347	15.82	0.57	421	487.6771	418.8745	15.84	0.50
14	1.58	1.5113	1.5847	4.35	0.30	426	440.0838	434.1304	3.31	1.91
15	1.37	1.5113	1.3815	10.31	0.84	420	484.2918	418.2745	15.31	0.41
16	2.32	2.4363	2.3226	5.01	0.11	480	484.4068	479.3656	0.92	0.13
17	1.45	1.4483	1.3414	0.12	7.49	452	480.1878	455.8414	6.24	0.85
18	1.53	1.5480	1.4374	1.17	6.05	468	495.6513	462.1011	5.91	1.26
19	1.21	1.4483	1.3414	19.69	10.86	448	480.1878	455.8414	7.18	1.75
20	2.27	2.3097	2.3047	1.75	1.53	426	429.5155	425.728	0.83	0.06
Average				9.50	3.48				7.36	0.85

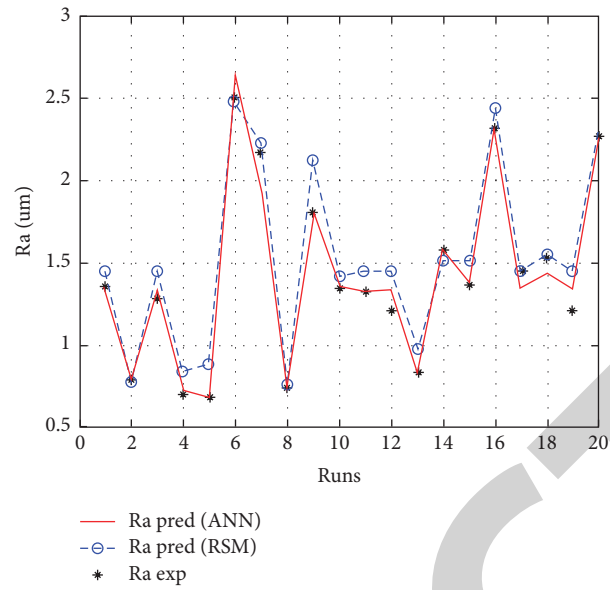
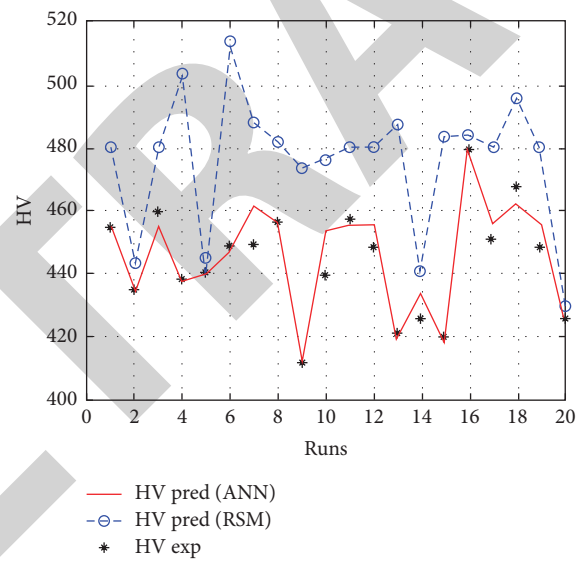
FIGURE 7: Experimental, RSM, and ANN predicted results for Ra .FIGURE 8: Experimental, RSM, and ANN predicted results for HV .

TABLE 10: Expectation assessment for Ra and HV .

Runs.	ANN predicted value ($y_{i,p}$)		Individual desirability (d_i)		Composite desirability (Des_{comb}) (%)	Rank
	Ra	HV	Ra (%)	HV (%)		
1	1.3414	455.8414	0.6654	0.6576	0.6615	3
2	0.7919	434.5498	0.9446	0.3477	0.5731	12
3	1.3414	455.8414	0.6654	0.6576	0.6615	3
4	0.7289	437.6340	0.9766	0.3926	0.6192	11
5	0.6828	439.8475	1.0000	0.4248	0.6518	9
6	2.6508	447.0804	0.0000	0.5301	0.0000	19
7	1.9451	461.8817	0.3586	0.7455	0.5171	13
8	0.7444	455.3319	0.9687	0.6502	0.7936	1
9	1.8151	410.6579	0.4246	0.0000	0.0000	19
10	1.3597	454.1620	0.6560	0.6332	0.6445	10
11	1.3414	455.8414	0.6654	0.6576	0.6615	3
12	1.3414	455.8414	0.6654	0.6576	0.6615	3
13	0.8347	418.8745	0.9228	0.1196	0.3322	16
14	1.5847	434.1304	0.5417	0.3416	0.4302	14
15	1.3815	418.2745	0.6450	0.1109	0.2674	17
16	2.3226	479.3656	0.1668	1.0000	0.4084	15
17	1.3414	455.8414	0.6654	0.6576	0.6615	3
18	1.4374	462.1011	0.6166	0.7487	0.6795	2
19	1.3414	455.8414	0.6654	0.6576	0.6615	3
20	2.3047	425.7280	0.1759	0.2193	0.1964	18

TABLE 11: Confirmation of optimization results.

Responses	Predicted ($v_{c2-f1-a_p2}$)	Experimental ($v_{c2-f1-a_p2}$)	Error (%)
Ra (μm)	0.7444	0.751	0.89
HV	455.3319	468.2	2.83

desirability. It is expected that the individual desirability of surface roughness is smaller the better and surface microhardness is larger the better, which were calculated by Equations (10) and (11) respectively. Table 10 shows the evaluated individual and composite desirability, as well as their rank for (Ra) and (HV). The optimization parameters are $v_{c2-f1-a_p2}$, which are cutting speed = 60 m/min, feed rate = 0.06 mm/r, and cutting depth = 0.2 mm with estimated $Ra = 0.7444\mu\text{m}$ and surface microhardness $HV = 455.3319$.

$$d_i = \begin{cases} 0, & \text{if } y_{i,p} \leq y_{i,p,\min} \\ \frac{y_{i,p,\max} - y_{i,p}}{y_{i,p,\max} - y_{i,p,\min}}, & \text{if } y_{i,p,\min} \leq y_{i,p} \leq y_{i,p,\max} \\ 1, & \text{if } y_{i,p} \geq y_{i,p,\max} \end{cases} \quad (10)$$

$$d_i = \begin{cases} 0, & \text{if } y_{i,p} \leq y_{i,p,\min} \\ \frac{y_{i,p} - y_{i,p,\min}}{y_{i,p,\max} - y_{i,p,\min}}, & \text{if } y_{i,p,\min} \leq y_{i,p} \leq y_{i,p,\max} \\ 1, & \text{if } y_{i,p} \geq y_{i,p,\max} \end{cases} \quad (11)$$

$$Des_{comb} = \left(\prod_{i=1}^n d_i \right)^{(1/n)}, \quad (12)$$

where, d_i is the individual desirability and $y_{i,p}$ is the response, $y_{i,p,\max}$ and $y_{i,p,\min}$ are the max and the min values of the response. n is the number of responses. Des_{comb} is the composite desirability, which gets all goals combined into one desirability function.

According to the previous analysis, ANN models with reliable predictability are used to evaluate individual

6. Confirmation Test

To verify the reliability of the optimization results, the optimized parameters of $v_{c2-f1-a_p2}$ were selected for the confirmation experiment (seen in Table 11). The surface roughness and surface microhardness obtained by the test were $0.751\mu\text{m}$ and 468.2 . The error rates are about 0.89% and 2.83% between the predicted and experimental, which can prove the reliability of the optimization results.

7. Conclusions

In this paper, the predicted models of surface roughness and surface microhardness are established using RSM and ANN techniques in the TC17 turning experiment based on the Box-Behnken design, and the following conclusions can be obtained:

- (1) From the ANOVA analysis, feed rate with 91.67% contributions has the most important influence on the surface roughness (Ra) and cutting depth with 16.56% contributions occupies the first position in influencing the quality of surface microhardness (HV).

- (2) The ANN prediction models of surface roughness ($R^2 = 99.99\%$) and surface microhardness ($R^2 = 99.23\%$) have higher prediction accuracy and small error than the RSM prediction models of surface roughness ($R^2 = 97.62\%$) and surface microhardness ($R^2 = 93.31\%$).
- (3) The mean absolute percentage errors for Ra and HV between experimental and estimated by ANN can be only 3.48% and 0.85%, which are smaller than 9.50% and 7.36% estimated by RSM.
- (4) The optimization parameters with minimum surface roughness and maximize surface microhardness are cutting speed 60 m/min, feed rate 0.06 mm/r, and cutting depth 0.2 mm, which were obtained with the DFA technique. In the confirmed experiment, the errors of Ra and HV between ANN predicted and the experiment are 0.89% and 2.83%.

Data Availability

The data of this paper can be obtained through the e-mail to the authors.

Conflicts of Interest

The authors declare that they have no conflicts of interest.

Authors' Contributions

Z. D. and Z. W. performed data curation; Z. W. and X. S. performed investigation; Z. W. developed the methodology; Z. W. wrote the original draft; Z. D. and X. S. reviewed and edited the study. All authors have read and agreed to the published version of the manuscript.

Acknowledgments

This study was supported by Natural Science Basic Research Program of Shaanxi (Program No. 2022JM-304) and Scientific Research Program Funded by Education Department of Shaanxi Provincial Government (Program No. 22JK0428).

References

- [1] M. Rahman, Y. S. Wong, and A. R. Zareena, "Machinability of titanium alloys," *JSME International Journal Series C*, vol. 46, no. 1, pp. 107–115, 2003.
- [2] T. Liang, Z. Dinghua, and Y. Changfeng, "Effect of high-speed milling parameters on surface metamorphic layer of TC17 titanium alloy," *Journal of Aeronautical Materials*, vol. 37, pp. 75–81, 2017.
- [3] L. Liyun, W. Jinfang, and T. Zhibiao, "Study on the roughness of the machined surface and wear mechanism of the cutter in dry cutting aluminum alloy with YG8 cemented carbide," *Technology and Test*, vol. 6, pp. 120–123, 2018.
- [4] W. Mersni, M. Boujelbene, S. B. Salem, and A. S. Alghamdi, "Optimization of the surface roughness in ball end milling of titanium alloy Ti-6Al-4V using the Taguchi Method," *Procedia Manufacturing*, vol. 20, pp. 271–276, 2018.
- [5] R. Kumar, S. Roy, P. Gunjan, A. Sahoo, D. D. Sarkar, and R. K. Das, "Analysis of MRR and surface roughness in machining Ti-6Al-4V ELI titanium alloy using EDM process," *Procedia Manufacturing*, vol. 20, pp. 358–364, 2018.
- [6] G. Kiswanto, A. Mandala, M. Azmi, and T. J. Ko, "The effects of cutting parameters to the surface roughness in high speed cutting of micro-milling titanium alloy Ti-6Al-4V," *Key Engineering Materials*, vol. 846, pp. 133–138, 2020.
- [7] R. Thirumalai, K. Techato, M. Chandrasekaran, K. Venkatapathy, and M. Seenivasan, "Experimental investigation during turning process of titanium material for surface roughness," *Materials Today Proceedings*, vol. 45, pp. 1423–1426, 2021.
- [8] R. Samin, M. Z. Nuawi, and S. M. Haris, "Optimization of the surface roughness for titanium Ti6Al4V in turning process using Taguchi method," *Test Engineering and Management*, vol. 83, pp. 1072–1078, 2020.
- [9] A. M. Mazid, M. S. Hasan, and K. B. Ahsan, "An investigation on optimum process parameters in terms of surface roughness for turning titanium alloy Ti-6Al-4V using coated carbide," *International Journal of Engineering Materials and Manufacture*, vol. 4, pp. 137–145, 2019.
- [10] A. Matras, W. Zbala, and M. Machno, "Research and method of roughness prediction of a curvilinear surface after titanium alloy turning," *Materials*, vol. 12, pp. 1–14, 2019.
- [11] H. Y. Seung, H. L. Jeong, and H. O. Sung, "A study on cutting characteristics in turning operations of titanium alloy used in automobile," *International Journal of Precision Engineering and Manufacturing*, vol. 20, pp. 209–216, 2019.
- [12] X. Qian, X. Duan, and J. Zou, "Effects of different tool microstructures on the precision turning of titanium alloy TC21," *International Journal of Advanced Manufacturing Technology*, vol. 106, no. 11–12, pp. 5519–5526, 2020.
- [13] A. Aramcharoen, "Influence of cryogenic cooling on tool wear and chip formation in turning of titanium alloy," *Procedia CIRP*, vol. 46, pp. 83–86, 2016.
- [14] P. C. Priarone, F. Klocke, M. G. Faga, D. Lung, and L. Settineri, "Tool life and surface integrity when turning titanium aluminides with PCD tools under conventional wet cutting and cryogenic cooling," *International Journal of Advanced Manufacturing Technology*, vol. 85, no. 1–4, pp. 807–816, 2016.
- [15] C. H. Che-Haron, "Tool life and surface integrity in turning titanium alloy," *Journal of Materials Processing Technology*, vol. 118, no. 1–3, pp. 231–237, 2001.
- [16] Y. Muhammad, H. I. Syed, A. K. Jaffery, and K. Mushtaq, "Development and analysis of tool wear and energy consumption maps for turning of titanium alloy (Ti6Al4V)," *Journal of Manufacturing Processes*, vol. 62, pp. 613–622, 2021.
- [17] X. Shen, D. Zhang, C. Yao, L. Tan, and H. Yao, "Formation mechanism of surface metamorphic layer and influence rule on milling TC17 titanium alloy," *International Journal of Advanced Manufacturing Technology*, vol. 6, pp. 1–18, 2021.
- [18] X. Shen, D. Zhang, and L. Tan, "Effects of cutter path orientations on milling force, temperature, and surface integrity when ball end milling of TC17 alloy," *Proceedings of the Institution of Mechanical Engineers-Part B: Journal of Engineering Manufacture*, vol. 7, Article ID 095440542097107, 2020.
- [19] L. Zhanqiang and A. Xin, "Investigation of wear lifespan of cutting tools in high-speed machining," *Tool Engineering*, vol. 12, pp. 3–7, 2001.

Retraction

Retracted: Innovation and Entrepreneurship Coupling Based on Simultaneous Equation Model and Its Energy Economic Effect Measurement

International Transactions on Electrical Energy Systems

Received 19 September 2023; Accepted 19 September 2023; Published 20 September 2023

Copyright © 2023 International Transactions on Electrical Energy Systems. This is an open access article distributed under the Creative Commons Attribution License, which permits unrestricted use, distribution, and reproduction in any medium, provided the original work is properly cited.

This article has been retracted by Hindawi following an investigation undertaken by the publisher [1]. This investigation has uncovered evidence of one or more of the following indicators of systematic manipulation of the publication process:

- (1) Discrepancies in scope
- (2) Discrepancies in the description of the research reported
- (3) Discrepancies between the availability of data and the research described
- (4) Inappropriate citations
- (5) Incoherent, meaningless and/or irrelevant content included in the article
- (6) Peer-review manipulation

The presence of these indicators undermines our confidence in the integrity of the article's content and we cannot, therefore, vouch for its reliability. Please note that this notice is intended solely to alert readers that the content of this article is unreliable. We have not investigated whether authors were aware of or involved in the systematic manipulation of the publication process.

Wiley and Hindawi regrets that the usual quality checks did not identify these issues before publication and have since put additional measures in place to safeguard research integrity.

We wish to credit our own Research Integrity and Research Publishing teams and anonymous and named external researchers and research integrity experts for contributing to this investigation.

The corresponding author, as the representative of all authors, has been given the opportunity to register their agreement or disagreement to this retraction. We have kept a record of any response received.

References

- [1] W. Chen, "Innovation and Entrepreneurship Coupling Based on Simultaneous Equation Model and Its Energy Economic Effect Measurement," *International Transactions on Electrical Energy Systems*, vol. 2022, Article ID 8218645, 8 pages, 2022.

Research Article

Innovation and Entrepreneurship Coupling Based on Simultaneous Equation Model and Its Energy Economic Effect Measurement

Wei Chen 

Xi'an International University, Xi'an 710077, Shaanxi, China

Correspondence should be addressed to Wei Chen; 100070@yzpc.edu.cn

Received 26 August 2022; Revised 14 September 2022; Accepted 22 September 2022; Published 5 October 2022

Academic Editor: Nagamalai Vasimalai

Copyright © 2022 Wei Chen. This is an open access article distributed under the Creative Commons Attribution License, which permits unrestricted use, distribution, and reproduction in any medium, provided the original work is properly cited.

In order to quantitatively analyze the synergistic relationship between the digital economy and high-quality development, the author proposes a measure of the coupling and coordination of China's digital economy and high-quality development. Based on the data of 271 prefecture-level and above cities in China from 2016 to 2021, the coupling coordination degree model is used to examine the coupling relationship between the digital economy and high-quality development. The result shows that China's digital economy and high-quality development are highly coupled, with an average coupling value of 0.9227. *Conclusion.* This study reveals the characteristics and facts of the coupling and coordination relationship between China's digital economy and high-quality development and provides useful policy inspiration for the central and regional formulation of differentiated digital economy development policies and high-quality development strategies.

1. Introduction

Since the revolution, China's economic development has been strong and healthy, contributing to the country's economy and modern development, and contributing to the improvement of the comprehensive national strength. With the release of "Made in China 2025" in May 2015, it is said that the business industry has taken an important position in the national economy, and the manufacturing industry has passed to carry out important economic activities in the country. As the world's second largest economy, China has become active on the international stage, and China's economic development is also the emergence of deep economic ties by examining economic agglomeration levels and spatial patterns. It is important to understand more about the practice of Chinese production. In 2017, the report of the 19th National Congress of China's economy pointed out that China's economy has moved from the stage of rapid growth to the stage of good growth, and also talked about the importance of good growth. After the revolution, high investment, development, and spending a lot of money on the development of the economy have achieved success and

created many problems, and the old model is increasing. In the new situation, the development should be changed from general expansion to qualitative development [1]. Now, the Chinese people want a better life, and it is necessary to support this growth with good economic development. The successful development of China's economy has pointed out such issues as the direction and path of the country's further economic development, the meaning of development quality, the state of development, and the difference in level. It is worth having a deep discussion about the good development in different areas of my country. The point of connection is to break the boundaries of the central system, remove the limitations of the central system, and reconnect and integrate various things. The cooperation network has three characteristics: One is that the systems are independent of each other. Another thing is that the systems manage communication and connection at the same time. The third is the interaction and influence of the body and various parts of the body [2]. Industrial agglomeration and high-quality economic development are two independent systems, and as a result of their relationship, a large integrated system of industrial agglomeration and high-quality economic

development grow up. Connections are of different types based on different distribution systems. According to the development of the system, it can be divided into good connections and bad connections. According to the development time of the system, it can be divided into static connections and dynamic connections. Depending on the nature of the system, it can be divided into homogeneous connections and heterogeneous connections. According to the influence of the system, it can be divided into isotype bindings and other isotype bindings, as shown in Figure 1.

2. Literature Review

From the perspective of a specific region, Li, X. introduced the economic-ecological environment effect coupling coordination degree model into the microscopic research field of “geopark,” more objectively reflecting the sustainable development level of the Geopark [3]. Jt and Yl analyzed the sustainable development capability and industrial efficiency of Xixi National Wetland Park by constructing comprehensive indicators of ecological environment and economy, and then explored the effective mode of resource protection in Xixi Park [4]. From an inter-provincial perspective, Kilambi constructed a comprehensive evaluation index system for ecological sustainability and high-quality economic development with the province as the research unit, and then comprehensively analyzed the coupling and interactive development relationship between the two systems [5]. Wen deeply investigated the coupling and coordination effect of green technology innovation and industrial transformation and upgrading in 28 provinces in China [6]. Zhang presented a revised model to evaluate the cooperation and integration of three major systems: “economic development-economic economy-ecological environment” in 31 provinces of China [7]. From the perspective of the river basin, Ravisankar, P. analyzed the spatial pattern and spatio-temporal coupling characteristics of ecological environment and high-quality development level in the Yellow River Basin, and the research conclusions provided a useful reference for the coordinated development of the two systems [8]. Forbes, D. L., drew on the sensitivities, resilience, and stress theory to explore the coupling and coordination relationship between ecological environmental vulnerability and economic poverty in poor areas [9]. Through the integration of the connection model and the level of the problem model, an in-depth analysis of the combination and process of water efficiency and economic development can be done [10]. In terms of urbanization and the ecological environment, Fazekas theoretically explores the nonlinear relationship between urbanization and the ecological environment and aims to provide theoretical support for the sustainable development of mega-city agglomerations [11]. Li introduced the concept of “connectivity cube” to explain the connection between the process and the dynamic change of urban and ecological environment [12]. Luo in an in-depth discussion of spatio-temporal evolution characteristics of urbanization and ecological resilience in the Pearl River Delta using a connectivity model provides a scientific

approach to realize cooperation and sustainable development of urbanization and ecological resilience [13].

From the perspective of system theory, this paper comprehensively investigates the coordinated interaction between China's digital economy and high-quality development. Taking Chinese urban data as research samples, this paper analyzes the regional differences and spatial effects of the coupling and coordination between digital economy and high-quality development in China.

3. Research Methods

3.1. Measurement of Coupling Coordination Degree. The degree of coordination of the connection is the degree of interaction between two or more systems, including the degree of connection and the degree of integration, and the degree of connection indicates the degree of cooperation between machines, the higher the degree of connection, the stronger cooperation. Relationship between systems cooperation refers to the degree of interaction between subsystems, and the higher the cooperation, the stronger the system power [14]. The level of connection of the joint together with the level of connection and the level of cooperation, which can describe the level of development and coordination of systems. The author uses an integration model to evaluate the integration of digital economy and economic growth in 271 cities at the provincial and higher levels in China. The levels of joint degree integration are explained in the following.

3.1.1. Standardization of Index Data. Consider k_{xi} and k_{yi} are the original values of the i -th indicator of the digital economic system and the high-quality development system, respectively, the value of i is $1, 2, \dots, n$, and k'_{xi} is the standardized index data. The following formula is obtained, as shown in

$$\left\{ \begin{array}{l} k'_{xi} = \frac{k_{xi} - \min(k_{xi})}{\max(k_{xi}) - \min(k_{xi})}, \\ \text{when } k_{xi} \text{ is a positive indicator,} \\ k'_{xi} = \frac{\max(k_{xi}) - k_{xi}}{\max(k_{xi}) - \min(k_{xi})}, \\ \text{when } k_{xi} \text{ is a negative indicator.} \end{array} \right. \quad (1)$$

3.1.2. Comprehensive Development Level of Computing Subsystem. Let w_{xi} and w_{yi} be the weights of the i -th index of the digital economic system and the high-quality development system, respectively, and the information entropy is used to determine the weight. The following formula is obtained, as shown in

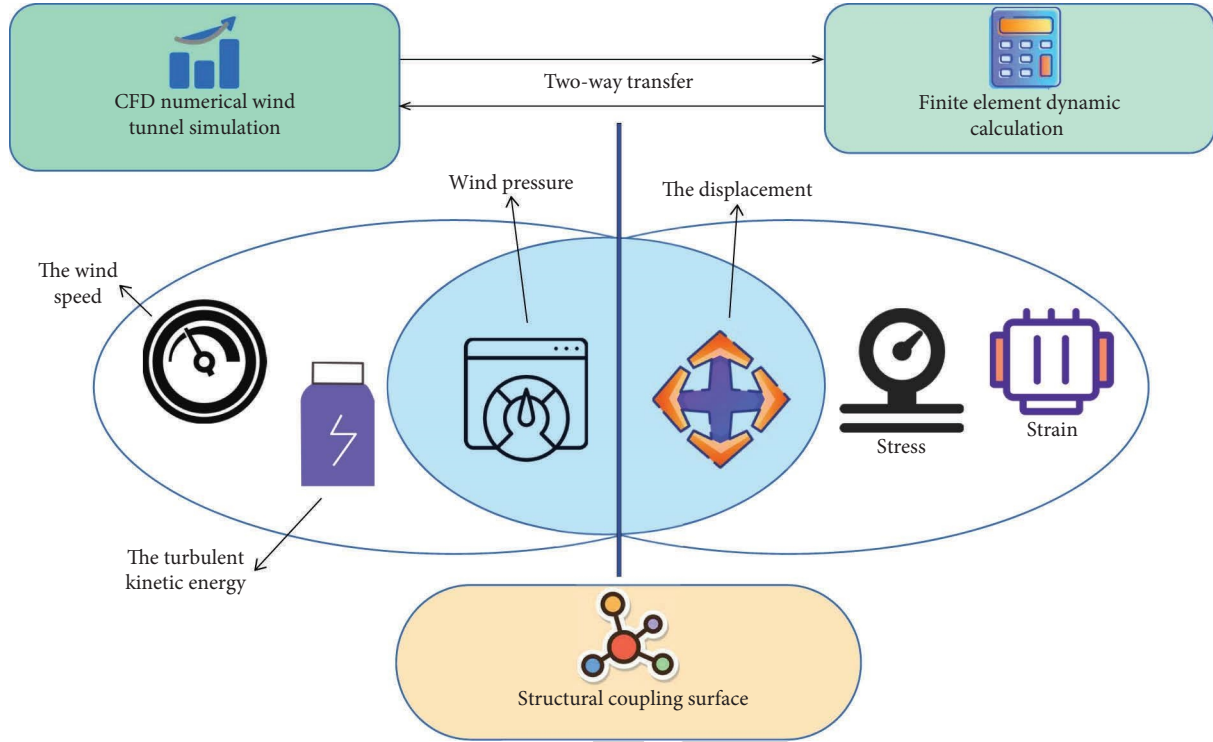


FIGURE 1: The innovation and entrepreneurship coupling of the simultaneous equation model.

$$\begin{cases} U_x = \sum_{i=1}^n k_{xi}' \times w_{xi}, \\ U_y = \sum_{i=1}^n k_{yi}' \times w_{yi}. \end{cases} \quad (2)$$

$$\begin{cases} D_{xy} = (C_{xy} \times T_{xy})^{1/2}, \\ T_{xy} = \alpha U_x + \beta U_y. \end{cases} \quad (5)$$

3.1.3. *Calculation of the Coupling Degree and Coupling Coordination Degree.* The following formula is obtained, as shown in

$$C = n \left[\frac{U_1 U_2 \cdots U_L}{(U_1 + U_2 + \cdots + U_L)^L} \right]^{1/L}. \quad (3)$$

Among them, C represents the coupling degree between subsystems, and its value range is $[0, 1]$, and L represents the number of subsystems. When $L = 2$, the following formula is obtained, as shown in

$$C_{xy} = 2 \left[\frac{U_x U_y}{(U_x + U_y)^2} \right]^{1/2}. \quad (4)$$

Among them, it represents the connection between digital marketing and quality improvement. The level of connectivity can only represent the interaction between digital economy and positive development [15]. To realize the hierarchical model of integration to accurately measure the relationship and relationship between digital marketing and the strategic development process. The standard level of integration is obtained by the formula given by

Among them, D_{xy} represents the coupling coordination value of the digital economy and high-quality development, and the value range is $[0, 1]$, U_x and U_y are the comprehensive scores of the digital economy and high-quality development, respectively, and α and β are the undetermined coefficients, respectively.

3.2. Indicator Selection, Data Description, and Coupling Type Division

3.2.1. *Selection Indicator and Information.* According to the reality of China's economic development, the development to be happy shows the real need for a new development strategy, including the availability of information in the city, and creating a multi-level assessment that includes six secondary economic indicators: growth, innovation potential, design, environmental quality, open development, and the quality of life of residents [16]. The specific parameters and their explanations are shown in Table 1. The sources of the indicators are "China Urban Statistical Yearbook," "China Science and Technology Statistical Yearbook," "China Regional Economic Statistical Yearbook," and development of digital accounting. The data were jointly provided by Peking University's Digital Finance Research Center and Ant Financial Group. Excluding province-level cities with large missing data, 1,626 sample surveys from 271 provinces and cities in China were completed between 2016 and 2021, as shown in Table 1.

TABLE 1: Indicator system of digital economy and high-quality development.

	Subsystem	Criterion layer	Indicator layer	Indicator properties	
Digital economy and high-quality development coupling coordination system	Digital economy system	Internet penetration	Internet users per 100 people	+	
		Internet-related practitioners	Proportion of employees in computer services and software	+	
		Internet related output	Total telecom services per capita	+	
		Number of mobile Internet users	Number of mobile phone users per 100 people	+	
		Digital financial inclusion development	China digital financial inclusion index	+	
		Economic growth	GDP growth rate	+	
	High-quality development system	Creativity	Industrial structure	Investment in science and technology	+
				Advanced industrial structure	+
		Environmental quality	Open development	Proportion of producer services PM2.5	-
				The actual amount of foreign capital used in the current year	+
		Living standard of residents		Education expenditure per capita (yuan/person)	+
				Number of hospital beds per capita (pieces per 10,000 people)	+

3.2.2. *Model and Type Distribution of Connection Coordination Evaluation.* According to Zhang Xu et al., the integration of subsystems is divided into four types: low integration, medium integration, high integration, large integration, and special distribution models are shown in Table 2.

4. Results Analysis

4.1. *Overall Features.* Using panel data from 271 provinces and cities in China from 2016 to 2021, according to the joint model developed by the author, social and economic relations Digital marketing and growth are measured. Table 3 shows the level of development of the digital economy and the level of growth of the development quality [17]. Table 3 represents the comparison between the scores of digital marketing and quality improvement, which is used to measure the practice or business level of digital marketing compared to quality improvement, if the ratio more than 1, it means that the digital economy is ahead of good development; If the ratio is less than 1, it means that the digital market lags behind the growth rate; If the ratio is equal to 1, it means that both are developing at the same time [18]. Table 3 is used to measure the relationship between digital economy and sustainable development, and it refers to the connection between digital economy and sustainable development. The development will have a good relationship between the two.

Table 3 shows that China's digital economy and economic growth have a positive relationship, with an average correlation of 0.9227, indicating a positive relationship between digital economy and economic development; the relationship grow well and is increasing year by year. Digital marketing and development have always been mutually exclusive and collaborative, but the level of cooperation and

collaboration has increased year by year during the survey period; from the reports, it is said that both digital marketing and development gradually support and reinforce each other. The digital economy is still falling below the growth rate, but at the same time, it is seen that the gap between the digital economy and the growth rate is gradually narrowing, and continue to develop connections and links between digital marketing and quality improvement.

4.2. *Characteristics of Seven Regions.* Table 4 and Figure 2 show the main characteristics of cooperation and collaboration between the digital economy and the development quality in China's seven regions from 2016 to 2021. Digital economy and the development quality of South China and Northwest China are the development level. In the region, the level of the first level of connection and collaboration has increased from 0.3274 to 0.3074 in 2016 to 0.3878 and 0.3834 in 2021, all of which are medium connection types. The relationship between digital economy and economic growth in East China and North China is in the second stage at the regional level, increasing from 0.3137 to 0.3152 in 2016 to 0.3762 and 0.3754 in 2021 – type of binding medium. The relationship between digital economy and economic growth in the Northeast and Southwest regions is in the third stage at the regional level, increasing from 0.3112 to 0.2657 in 2016 to 0.3638 and 0.3501 in 2021, at the middle level half of the right tie. Central China's cooperation between digital economy and growth is the lowest among the seven regions, from 0.2628 in 2016 to 0.3293 in 2021, changing from low cooperation to high cooperation.

To further analyze the reasons for the lack of connection and cooperation between the digital economy and the positive development of the regions, Table 5 reports descriptive statistics on the composite scores of digital economy and quality development for the seven regions during

TABLE 2: The distribution of types of collaboration and the connection between digital marketing and sustainable development.

Coordination value	$1 \leq D \leq 0.2$	$0.4 < D \leq 0.6$	$0.4 < D \leq 0.7$	$0.9 < D \leq 1.1$
Basic type	Low-coupling coordination	Moderately coupled coordination	Highly coupled coordination	Extremely coupled coordination

TABLE 3: The general characteristics of cooperation and collaboration between the digital economy and sustainable development.

years	U_x	U_y	U_x/U_y	C_{xy}	D_{xy}	Coupling coordination type
2016	0.0697	0.1432	0.4877	0.8943	0.3018	Moderately coupled coordination
2017	0.0766	0.1498	0.5102	0.9011	0.3125	Moderately coupled coordination
2021	0.0823	0.1606	0.5114	0.9082	0.3256	Moderately coupled coordination
2019	0.0907	0.1703	0.5328	0.9237	0.3411	Moderately coupled coordination
2020	0.1014	0.1685	0.6026	0.9481	0.3507	Moderately coupled coordination
2021	0.1152	0.1755	0.6556	0.9605	0.3665	Moderately coupled coordination

TABLE 4: Degree of collaboration and cooperation between digital economy and sustainable development in seven regions in China.

Years	North-east area	Huadong region	North China	Central China	South China	Southwest region	North-west region
2016	0.3112	0.3137	0.3152	0.2628	0.3274	0.2657	0.3074
2017	0.3151	0.3226	0.3257	0.2761	0.3405	0.2815	0.3202
2021	0.3225	0.3354	0.3386	0.2897	0.3511	0.3024	0.3338
2019	0.3412	0.3524	0.3545	0.3089	0.3594	0.3172	0.3428
2020	0.3513	0.3632	0.3631	0.3105	0.3695	0.3317	0.3593
2021	0.3638	0.3762	0.3754	0.3293	0.3878	0.3501	0.3834
Average value	0.3343	0.3438	0.3455	0.2963	0.3561	0.3082	0.3412
Sample size	205	469	199	253	223	181	101

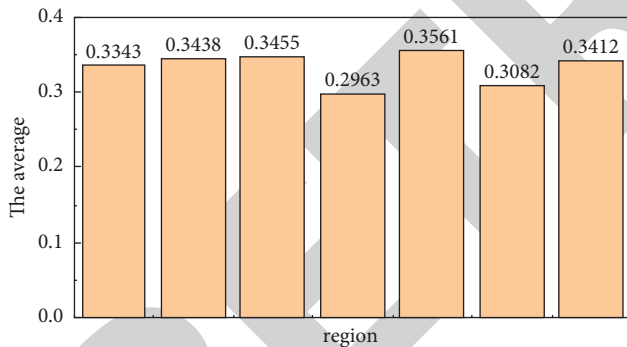


FIGURE 2: Average value of coupling coordination between digital economy and high-quality development in seven regions of China.

the observation period. Table 5 shows that regional disparities in the digital economy are greater than positive growth rates. The highest average digital marketing score is 0.1294, the lowest is 0.0631, and the highest is 2.05 times. The highest average score for good construction is 0.1778, the lowest is 0.1354, and the highest is 1.31 times lower [19]. It can be seen that the big difference in the level of digital economy between the regions is the main reason for the discrepancy between the link between digital economy and economic growth, and the relationship links between digital marketing mix scores and growth. In Central China, the least is the link between digital marketing and sustainable development; South China is the only region with an average score of more than 0.10 in the digital economy score, and it is

the first of the seven regions in terms of the quality of digital economy and the average of cooperation and collaboration.

In general, the cooperation and integration of the digital economy and the development of the seven regions are all central and integrated, and all the cooperation and cooperation is not very high. Although there is a positive relationship between the digital economy and growth, because of the short term of the digital economy and the integration of the digital economy and the traditional economy, great business and social relations have never existed. Digital economy and high-quality development have not established a mature and stable interactive development relationship. From the point of view of time, the integration and integration of all areas of the digital economy and the development of the quality are increasing, indicating the growth of the digital economy and it penetrates into business and people. The positive interaction between the digital economy and the positive development will be improved. From the point of view of regional comparison, the author believes that the relationship between digital economy and positive development in the northwest, which has a poor economy, is likely associated with the relative return of digital marketing. In 2021, the ratio score of digital economy and development quality is 0.6131 in Northwest China, 0.5548 in Central China, 0.5747 in Southwest China, and the score of digital economy in Northwest is high. China's economy is far from Central China and Southwest China in the high-quality development system, and the degree of synchronization between the digital economy and the development quality of

TABLE 5: Descriptive statistics of comprehensive scores of digital economy and high-quality development in seven regions.

Area	Digital economy			Area	High-quality development		
	Average value	Maximum value	Minimum		Average value	Maximum value	Minimum
Central China	0.0631	0.2086	0.0186	Central China	0.1354	0.3637	0.0698
Southwest	0.0665	0.2293	0.0137	Southwest	0.1538	0.3347	0.0872
Northeast	0.0757	0.1952	0.0216	East China	0.1603	0.6015	0.0784
Northwest	0.0866	0.2805	0.0255	South China	0.1678	0.7193	0.0755
North China	0.0897	0.3337	0.0344	Northeast	0.1721	0.2807	0.1025
East China	0.0996	0.4966	0.0173	Northwest	0.1764	0.3263	0.0994
South China	0.1294	0.7198	0.0212	North China	0.1778	0.6642	0.0746

Northwest China is more than that of Central China and Southwest China. But in the long run, government departments should support the development of digital economy in economically developed regions such as southern, northern, and eastern China. The government should take the lead in implementing the construction of digital China in the region and explore the role of digital economy in promoting high-quality development and the law of interactive development between the two.

4.3. Urban Hierarchical Characteristics. Overall, 271 sample cities are divided into different cities, and the degree of integration is connected to different levels of different cities, and the results are shown in Table 6. For the first city, the cooperation between the digital economy and high cities – The improvement is the highest, from 0.6134 in 2016 to 0.6688 in 2021, the cooperation relationship is normal in high-level collaboration, and high-level. Of continuous integration [20]. The cooperation between the digital economy and the cooperation efficiency of the first new city has increased from 0.4267 in 2016 to 0.4963 in 2021, which is the cooperation average, and it is approximately 0.4963 in 2021, which achieved a very good management style, but there is still a big difference compared to the first-tier cities. The relationship between digital economy and the development quality of secondary cities has increased from 0.3756 in 2016 to 0.4433 in 2021, and the average integration and cooperation has increased to 0.4433 in 2021 during the survey period. Lower than the first-tier city and the new first-tier city, but far ahead of the third-tier city. For third-, fourth-, and fifth-tier cities, the general result of social interaction is that the third-tier city is larger than the fourth-tier city, and the fourth-tier city is smaller. In the fifth city, the difference in the degree of connection rules is very small, and they have moved from low connection rules to medium connection rules during the observation period.

Cooperation and coordination of China's digital economy and development have a great impact on cities at different stages, and the integration of cities in the first stage is more as new first-tier cities and second-tier cities. The integration of the second cities is more than the third, fourth-, and fifth cities. The coupling degree of digital economy and high-quality development in third-tier, fourth-tier, and fifth-tier cities is at a low level. On the one hand, the economic structure of third-tier and fourth-tier cities is mainly based on primary and secondary industries,

which deviates from the purpose of high-quality development to a certain extent. There is little cooperation and integration between the digital economy and the successful development of the third, fourth, and fifth cities. Secondary production deviates to any extent from the goal of good growth. On the other hand, digital marketing is high technology and requires not only some business needs but also requires a lot of investment and expertise at the first stage, which meet the needs of developing digital businesses. The low level of digital economy and quality development have created a low level of coordination and integration between third and fourth level cities. The digital economy is a product of economic growth that has reached a certain level, and the third-, fourth-, and fifth-tier cities cannot support the costs and risks of digital business; so at this stage, we must seize the opportunity to control the country's production. We must put business development first.

4.4. Typical Analysis of the Yangtze River Basin and the Yellow River Basin. According to the purpose of the research, sample data of 19 and 29 states and cities that flow from the Yellow River Basin and the Blue River Basin have been taken to measure, and measure the number of businesses and highways growing well between the Yellow River Basin and the Blue River. Table 7 shows the relationship between the basin and the two, and the results. During the survey, the score of the digital economy and development quality of the Blue River Basin was higher than that of the Yellow River Basin. The average score of digital economy and development quality of the Blue River Basin is 0.1002 and 0.1807, and the Yellow River Basin is 0.0905 and 0.1588. Looking at how much the digital business lags behind the positive development, the average of the digital business for positive development is 0.5503. Less than 0.5697 in the Yellow River basin. The connection and integration of the digital economy and the development of the quality of the Blue River Basin and the Yellow River Basin are in the form of medium integration, and the medium of integration of the Blue River Basin is 0.3544, which is higher than 0.3382. First, in the Yellow River Basin, 34.48 percent of the 10 cities with two or more levels are located in the Blue River Basin, while there are only three cities with two or more levels in the Yellow River Basin. 15.78%. As the economic level of the cities flowing through the Blue River Basin is higher than that of the Yellow River Basin, the Blue River Basin has the basis for

TABLE 6: Coupling and coordination degree of digital economy and high-quality development in cities of different levels.

Years	First-tier cities	New first-tier cities	Second-tier cities	Third-tier city	Fourth-tier cities	Fifth-tier cities
2016	0.6134	0.4267	0.3756	0.2857	0.2742	0.2745
2017	0.6228	0.4476	0.3837	0.2971	0.2862	0.2824
2018	0.6287	0.4723	0.3951	0.3094	0.2975	0.2958
2019	0.6507	0.4756	0.4133	0.3244	0.3128	0.3127
2020	0.6452	0.4846	0.4275	0.3335	0.3213	0.3232
2021	0.6688	0.4963	0.4433	0.3508	0.3344	0.3414
Average value	0.6384	0.4672	0.4064	0.3168	0.3043	0.3051
Sample size	25	91	181	415	482	439

TABLE 7: Coupling and coordination characteristics of digital economy and high-quality development in the Yangtze and Yellow River basins.

years	U_x	U_y	U_x/U_y	Coupling coordination	U_x	U_y	U_x/U_y	Coupling coordination
2016	0.0756	0.1593	0.4744	0.3190	0.0708	0.1435	0.4937	0.3107
2017	0.0803	0.1647	0.4876	0.3282	0.0756	0.1564	0.4835	0.3218
2018	0.0927	0.1794	0.5165	0.3477	0.0849	0.1608	0.5276	0.3343
2019	0.1042	0.1932	0.5391	0.3655	0.0946	0.1604	0.5905	0.3445
2020	0.1194	0.1895	0.3604	0.3762	0.0994	0.1632	0.6091	0.3505
2021	0.1298	0.1986	0.6528	0.3897	0.1174	0.1685	0.6963	0.3667
Average value	0.1002	0.1807	0.5503	0.3544	0.0905	0.1588	0.5697	0.3382
Sample size			175				115	

the development of emerging industries such as innovation and business. In Yellow River basin, digital printing is more than marketing. In the river basin and the Ocean River, economic development, sustainable development, and protection of the ecological environment should be the main points of development.

5. Conclusion

The author created a digital economy and development performance evaluation system based on data from 271 provinces and cities in China from 2016 to 2021, based on the scores of the digital economy and the development quality are calculated and obtained. In the digital economy, the level of cooperation and integration between the government and the development quality is calculated. Time-series trends and differences in the connections and integration of digital economy and development quality from the perspective of seven regions, cities at different levels, and red rivers and the Yellow River basin were introduced. On the other hand, the author's research supports the results of research on the interaction between digital marketing and positive development. On the other hand, it shows the nature and reality of the relationship between China's digital economy and development from different angles, and provides policy inspiration for the government central and regional to create different policies for the development of digital economy good construction.

Data Availability

The data used to support the findings of this study are available from the author upon request.

Conflicts of Interest

The author declares no conflicts of interest.

Acknowledgments

The study was supported by Shaanxi Soft Science Research Plan Project, under No. : 2019KRM169.

References

- [1] Y. Ding, H. Zhang, and S. Tang, "How does the digital economy affect the domestic value-added rate of Chinese exports?" *Journal of Global Information Management*, vol. 29, no. 5, pp. 71–85, 2021.
- [2] S. Sultana, S. Akter, E. Kyriazis, and S. F. Wamba, "Architecting and developing big data-driven innovation (ddi) in the digital economy," *Journal of Global Information Management*, vol. 29, no. 3, pp. 165–187, 2021.
- [3] L. Xiwen, D. Xu, and S. Shiyu, "Research on the internal control problems faced by the financial sharing center in the digital economy era1—an example of financial sharing center of h co. ltd," *Procedia Computer Science*, vol. 187, no. 9, pp. 158–163, 2021.
- [4] J. Tian and Y. Liu, "Research on total factor productivity measurement and influencing factors of digital economy enterprises," *Procedia Computer Science*, vol. 187, pp. 390–395, 2021.
- [5] Y. N. Liu and T. Y. Zhang, "Research framework of college students' financing mode in innovation and entrepreneurship in jilin province," *DEStech Transactions on Economics Business and Management*, vol. 1, 2021.
- [6] S. Tan, "Construction of multi-dimensional dynamic innovation and entrepreneurship platform for college students

Retraction

Retracted: Simulation of Flow-Induced Vibration and Dynamic Performance of Circular-Arc Helical Gear Pump under Background of Machine Learning

International Transactions on Electrical Energy Systems

Received 28 November 2023; Accepted 28 November 2023; Published 29 November 2023

Copyright © 2023 International Transactions on Electrical Energy Systems. This is an open access article distributed under the Creative Commons Attribution License, which permits unrestricted use, distribution, and reproduction in any medium, provided the original work is properly cited.

This article has been retracted by Hindawi, as publisher, following an investigation undertaken by the publisher [1]. This investigation has uncovered evidence of systematic manipulation of the publication and peer-review process. We cannot, therefore, vouch for the reliability or integrity of this article.

Please note that this notice is intended solely to alert readers that the peer-review process of this article has been compromised.

Wiley and Hindawi regret that the usual quality checks did not identify these issues before publication and have since put additional measures in place to safeguard research integrity.

We wish to credit our Research Integrity and Research Publishing teams and anonymous and named external researchers and research integrity experts for contributing to this investigation.

The corresponding author, as the representative of all authors, has been given the opportunity to register their agreement or disagreement to this retraction. We have kept a record of any response received.

References

- [1] X. Wei, Y. Feng, X. Han, and Z. He, "Simulation of Flow-Induced Vibration and Dynamic Performance of Circular-Arc Helical Gear Pump under Background of Machine Learning," *International Transactions on Electrical Energy Systems*, vol. 2022, Article ID 9513357, 10 pages, 2022.

Research Article

Simulation of Flow-Induced Vibration and Dynamic Performance of Circular-Arc Helical Gear Pump under Background of Machine Learning

Xiaoling Wei, Yongbao Feng , Xiaoxia Han, and Zhenxin He

Department of Missile Engineering, PLA Rocket Force University of Engineering, Xi'an 710025, Shaanxi, China

Correspondence should be addressed to Yongbao Feng; fyb1213@sina.com

Received 25 August 2022; Revised 16 September 2022; Accepted 21 September 2022; Published 4 October 2022

Academic Editor: Nagamalai Vasimalai

Copyright © 2022 Xiaoling Wei et al. This is an open access article distributed under the Creative Commons Attribution License, which permits unrestricted use, distribution, and reproduction in any medium, provided the original work is properly cited.

At present, with the continuous development and great improvement of mechanical manufacturing, processing, and assembly technology, mechanical flow-induced vibration (FIV) with a relatively concentrated frequency domain can be controlled by active and passive noise reduction methods. However, whether it is active noise reduction or passive noise reduction, they all focus on how to suppress the transmission of sound waves and cannot solve the problems of flow leakage, obvious temperature rise, and noise excitation from the root cause. Therefore, it is necessary to determine the location of the primary and secondary excitation sound sources of FIV, the identification of true and false sounds, and the characteristic relationship between flow and noise. This provides a theoretical basis and engineering application direction for the mechanism of noise reduction of FIV. The numerical calculation part of the acoustics in this paper is solved by the hybrid method, and the flow field is discretely calculated by the large eddy simulation (LES) module in the Fluent software. When the calculated flow field is stable, the velocity field of one impeller rotation period is selected to be output as the iterative value of the sound field and imported into ACTRAN for Fourier transform. Then, the sound field calculation is carried out, and the result of the spatial and temporal variation of the sound field is finally obtained. Through experiments, it was found that when the load of the gear pump is 8 MPa, the volumetric efficiency of the optimized circular-arc helical gear pump of the sliding bearing was improved by about 4%. When the rotation speed is 2100 r/min, the arc helical gear pump reduced the surface temperature rise by 2.5°C. This verified that the optimized performance of the sliding bearing in the arc helical gear pump is significantly improved. Through the theoretical model of the temperature rise of the sliding bearing, the phenomenon that the surface temperature of the prototype gear pump was not significantly increased with the loading in the low pressure region is explained.

1. Introduction

A pump is a device that can convert mechanical energy into pumping fluid energy. Usually, the motor drives the impeller to rotate through the rotation of the pump shaft, and the fluid generates energy after the impeller rotates to do work, so as to meet the conveying conditions required by the user. The pump acts as an energy conversion and fluid delivery device. It is widely used in all walks of life, such as in daily life, or in agriculture, industry, and military fields. According to statistics, the power consumption of pumps accounts for more than 15% of the total power generation. When the fluid medium is transported, due to the influence

of the fluid viscosity, there are many complex flow structures in the flow field of the centrifugal pump at the same time. For example, in the region of the impeller outlet near the trailing edge of the blade, a “low energy zone” would appear on the back of the blade. The flow through this side is stable and is referred to as a “wake” structure. In the face of the “high pressure area,” the flow is unstable, called “jet” structure, which increases the velocity gradient and intensifies the fluid energy exchange, thereby affecting the mainstream flow. Therefore, if a violent and unstable flow occurs in the internal flow field and the flow deviates from the design condition, it is easy to cause high-decibel noise and large-scale vibration, thereby shortening the service life of the

pump and aggravating noise pollution. In the early days, due to the limitation of computer design level, it was difficult for researchers to perform direct numerical simulation of complex three-dimensional flow. This largely relies on experimental or analytical methods to study flow-induced noise production. Therefore, in order to meet the needs of increasing the bearing life of the industrial system, this paper analyzes the FIV phenomenon of the arc helical gear pump and builds a performance test model of the arc helical gear pump. Through the gear pump temperature rise test experiment, the influence law of load and rotational speed on the gear pump temperature rise is proposed. It proves that the arc helical gear pump can run smoothly under high pressure and high speed compared with other ordinary gear pumps.

The innovation of this paper is that a dynamic performance simulation method of arc helical gear pump is proposed, which provides a new way for the simulation of the gear pump model. This method improves the mechanical efficiency by optimizing the gear pump bearing, which can also increase the service life of the pump. It reduces costs for the use of factory pumps.

2. Related Work

With the expansion of computing power and the improvement and development of machine learning (ML) theory, it has gradually been applied to various leading areas. Buczak and Guven investigated the application of machine learning to analyze network intrusion detection. A short tutorial description of each method was presented [1]. Zhou et al. provided directions for identifying relevant opportunities and challenges for the various stages of ML and components of MLBiD [2]. Kavakiotis et al. conducted a systematic review of the application of machine learning, data mining techniques, and tools in the field of diabetes research, resulting in predictions and diagnosis [3]. It can be seen that machine learning is widely used in network security, industrial machinery, medical, and other fields.

FIV is a common problem in energy systems, so in order to reduce the loss caused by FIV, many scholars have conducted related research. For example, Merzari et al. discussed the use of computational fluid dynamics code Nek5000 coupled with structural code Diablo to simulate flow and associated FIV in a helical coil heat exchanger [4]. Xu et al. studied the dynamic response of smooth cylinders placed either upstream or downstream of a tandem cylinder to improve the understanding of the FIV behavior of a dual tandem cylinder system [5]. Quen et al. conducted experiments on low mass ratio flexible cylinders with two and three initial helical blades. The cylinder can freely vibrate in the in-line and transverse flow directions at subcritical Reynolds numbers [6]. Ren et al. conducted an experimental study of FIV on flexible pipes fitted with spiral slats. The results showed that the suppression efficiency and fatigue damage reduction rate of oscillatory flow are not as ideal as steady flow [7]. Xu et al. conducted an experimental study of two identical elastically mounted cylinders in series in a surface water channel. It was concluded that when the

deceleration speed does not exceed 12.0, when $T/D = 2.57$, 3.57, and 4.57, the flow characteristics of the upstream cylinder are similar to that of the single cylinder [8]. In general, their engineering estimation method mainly obtains the parameters in the empirical formula through data regression and considers less structural factors. Although verified by experiments, it is still difficult to guide the FIV design of hydraulic machinery.

3. Simulation of FIV Sliding Bearing in Arc Helical Gear Pump

3.1. Experiment Bench Data Acquisition System. The overall idea and principle of the test software part of the arc helical gear wheel pump in this paper are shown in Figure 1.

It can be seen from Figure 1 that the software part measures the temperature, flow, pressure, speed, and other properties by the sensor and converts it into an analog signal. The data acquisition card is input to the host computer according to the corresponding channel, and the signal acquisition and conversion are completed through software processing [9]. In this paper, LabVIEW software is used for programming to complete the acquisition and result display of temperature, flow, pressure, and rotational speed signals, which can display images or export data.

3.2. Simulation Model of Internal Flow Field of Gear Pump. To carry out simulation analysis, it is necessary to clarify the idea of simulation calculation, conduct a large number of practical calculations, record, analyze, and compare the condition settings and calculation results of each calculation. The simulation calculation of the pressure field is carried out first, and after a certain number of steps are relatively stable, the energy model is turned on, and the simulation calculation of the temperature field is carried out, which is easier to ensure the calculation convergence and stable and smooth progress. The high-pressure high-speed miniaturized helical gear pump designed in this paper has a design speed of 10000 r/min and a pressure of 25 MPa. This paper analyzes the dynamic performance of the internal flow field of a high-pressure high-speed miniaturized arc helical gear pump. 2D simulation cannot simulate axial leakage and pressure. Therefore, the results of the 3D simulation are closer to the true value than the 2D simulation results [10]. In view of the problem of high temperature rise during the operation of the prototype, it is necessary to analyze the influence of the internal fluid of the gear pump on the temperature rise, as shown in Figure 2.

Figure 2 is a flow chart of analyzing the gear pump using Fluent software. In order for the experiment to make the simulation analysis accurate and smooth, it is necessary to clarify the idea of simulation calculation, carry out a large number of practical calculations, record, analyze, and compare the condition settings and calculation results of each calculation [11–13]. The simulation calculation of the pressure field is carried out first, and after a certain number of steps are relatively stable, the energy model is opened, and the simulation calculation of the temperature field is carried

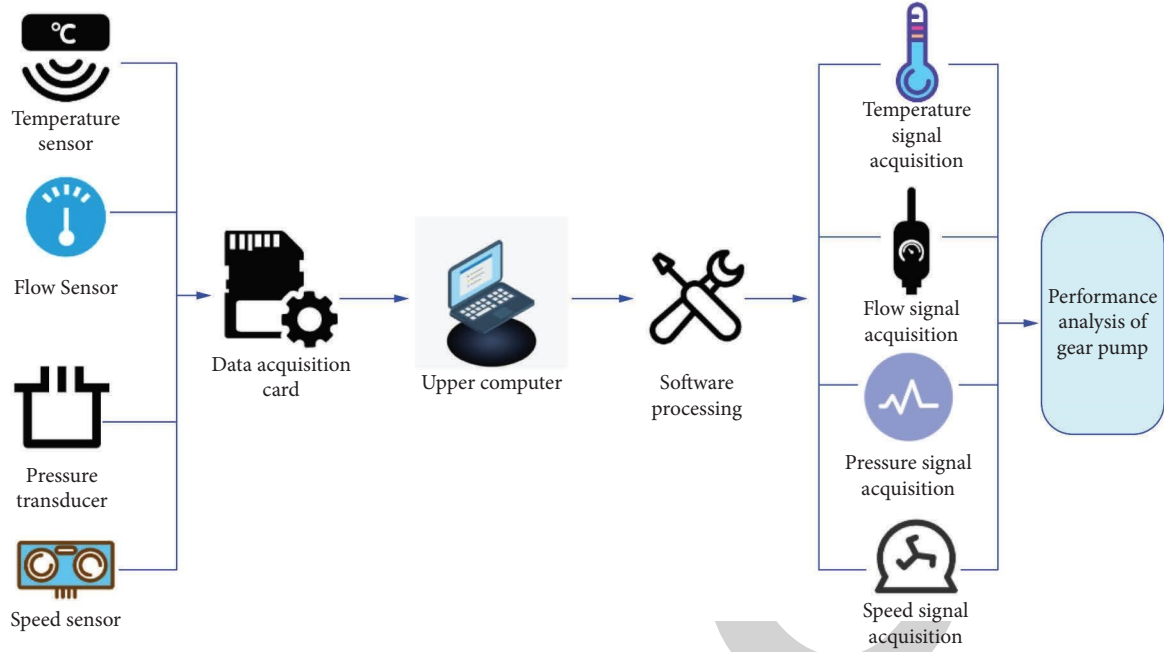


FIGURE 1: Schematic diagram of the experimental bench software.

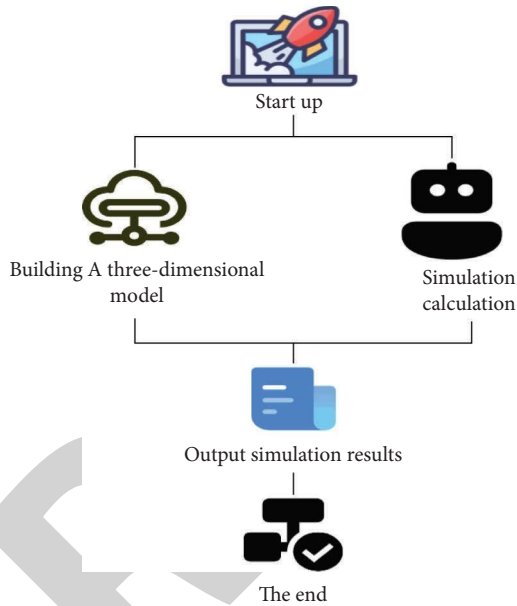


FIGURE 2: Flow diagram of fluent analysis gear pump flow field.

out. It is easier to ensure the calculation convergence and stable and smooth progress.

3.3. Construction of FIV Model. FIV is the flow-acoustic coupling caused by the unsteady flow of fluid. The sound generation process is very complex, including a quadrupole source in which turbulent fluid participates in sound generation, and a dipole source generated by fluid-structure coupling excitation after the fluid hits the solid wall [14, 15]. Therefore, in the process of numerical simulation, it is

necessary to comprehensively consider the actual flow situation and the relevant principles of computational fluid dynamics and select a suitable numerical model to simulate the internal flow field. Compared with direct numerical simulation (DNS) and Reynolds time-averaged simulation (RNS), large eddy simulation is in between. It neither has high requirements on spatial and temporal resolution like DNS nor can it only provide average information of turbulence like RNS, resulting in insufficient description of the flow field. This section mainly introduces the governing equations of large eddy simulation.

The N-S equation for the incompressible constant viscosity coefficient is

$$\frac{\partial u_i}{\partial t} + \frac{\partial u_i u_j}{\partial x_j} = -\frac{1}{\rho} \frac{\partial p}{\partial x_i} + \frac{\partial (\nu \cdot 2S_{ij})}{\partial x_j} \quad (1)$$

In the formula, the stretch rate tensor is

$$S_{ij} = \frac{1}{2} \left(\frac{\partial u_i}{\partial x_j} + \frac{\partial u_j}{\partial x_i} \right) \quad (2)$$

The subscripts $i, j = 1, 2, 3$ and u_i represent the velocity components associated with x_i , ρ is the fluid density, and ν is the fluid's kinematic viscosity coefficient.

In the large eddy simulation, the large and small vortex systems are distinguished by filtering [16]. Assuming that $f(x, t)$ is the instantaneous variable of flow, in the physical space-time domain, the large-scale eddy can be expressed as

$$\bar{f}(x, t) = \int_D \bar{G}(x, x', \Delta) f(x', t) dx' \quad (3)$$

In the formula, D is the computational domain of the flow field, x' and x represent the vectors before and after filtering, respectively, and G represents the filter function.

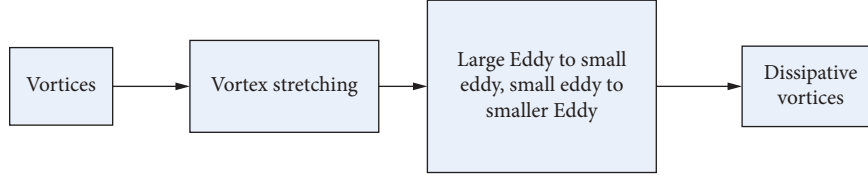


FIGURE 3: Cascade process of fluid energy.

The commonly used filter function \bar{G} is divided into two categories: uniform filter and nonuniform filter [17, 18]. However, when carrying out the numerical simulation of wall turbulence, the normal grid in the near-wall area must be densified according to the proportional rules. Considering the two factors of calculation efficiency and accuracy, a nonuniform box filter is generally used [19], and its expression is

$$\bar{G}(\eta) = \begin{cases} \frac{1}{\Delta}, & |\Delta| \leq \frac{\Delta}{2}, \\ 0, & |\Delta| > \frac{\Delta}{2}. \end{cases} \quad (4)$$

In the formula, Δ is the scale of the filter, which can be understood as the scale requirement for the grid during numerical simulation. The difference between any grid nodes is

$$\eta = x_i - x_i'. \quad (5)$$

According to the above definition, the large-scale vortex $\bar{f}(x, t)$ is the average volume of the tetrahedron or hexahedron with x_i as the central node.

The filtered equation and the incompressible N-S equation are

$$\frac{\partial \bar{u}_i}{\partial x_i} = 0, \quad (6)$$

$$\frac{\partial \bar{u}_i}{\partial t} + \frac{\partial u_i \bar{u}_j}{\partial x_j} = -\frac{1}{\rho} \frac{\partial \bar{P}}{\partial x_i} + \nu \frac{\partial^2 \bar{u}_i}{\partial x_j^2} - \frac{\partial \tau_{ij}^s}{\partial x_j}. \quad (7)$$

\bar{u}_i is the average velocity after filtering, and $\tau_{ij}^s = \overline{u_i u_j} - \bar{u}_i \bar{u}_j$ is the Reynolds stress at the sublattice scale.

The subgrid Reynolds stress τ_{ij}^s represents the interaction relationship between large and small scale vortices, and the cascade process of its turbulent energy is shown in Figure 3.

In order to explore the role of Reynolds stress in the cascade process, the Reynolds stress can be decomposed into

$$\tau_{ij} = L_{ij} + C_{ij} + R_{ij}. \quad (8)$$

Among them, L_{ij} is the Leonard stress term, C_{ij} is the cross stress term, and R_{ij} is the sublattice Reynolds stress, which represents the energy transfer of vortex systems of different sizes. Its mathematical derivation for the τ_{ij}^s modeling method is as follows.

Assuming that the generation and dissipation rates of turbulence are in equilibrium, the τ_{ij}^s is decomposed as

$$\tau_{ij}^s - \frac{1}{3} \delta_{ij} \tau_{kk} = 2\nu_T \bar{S}_{ij}. \quad (9)$$

In the formula, ν_T is the eddy viscosity coefficient of the sublattice scale; in order to satisfy the continuity equation of incompressible fluid, k exists if and only when $i = j$; δ_{ij} is the Kronecker number, and then,

$$\delta = \begin{cases} 0, & (i \neq j), \\ 1, & (i = j). \end{cases} \quad (10)$$

\bar{S}_{ij} is the strain tensor at the Reynolds scale, and then,

$$\bar{S}_{ij} = \frac{1}{2} \left(\frac{\partial \bar{u}_i}{\partial x_j} + \frac{\partial \bar{u}_j}{\partial x_i} \right). \quad (11)$$

Since ν_T is an unknown coefficient about the flow field function, it is necessary to continue to seek a method for modeling the eddy-viscous coefficient [20]. Therefore, ν_T is a function of the velocity scale and length scale of the vortex, and the formula of the turbulent molecular viscosity coefficient is

$$\nu_T = C_D k_s \frac{1}{2} \Delta. \quad (12)$$

C_D is the coefficient, k_s is the turbulent pulsation kinetic energy, and Δ is the filter width.

As mentioned above, the dissipation term σ_s of turbulent energy, on the one hand, needs to be balanced with the dissipation rate, as follows:

$$2\nu_T \bar{S}_{ij} \bar{S}_{ij} = \sigma_s. \quad (13)$$

On the other hand, the dissipation term σ_s is related to the vortex scale and can be written as

$$\sigma_s = \frac{C_E k_s^{3/2}}{\Delta}. \quad (14)$$

Simultaneously, Formulas (12), (13), and (14) can be obtained:

$$2C_D k_s^{1/2} \Delta \bar{S}_{ij} \bar{S}_{ij} = \frac{C_E k_s^{3/2}}{\Delta}. \quad (15)$$

Then,

$$k_s = 2 \frac{C_D \Delta^2 \bar{S}_{ij} \bar{S}_{ij}}{C_E}. \quad (16)$$

Substitute into Formula (12) to get:

$$v_T = C_D \Delta \sqrt{\frac{C_D}{C_E} \Delta} \sqrt{2\bar{S}_{ij}\bar{S}_{ij}}. \quad (17)$$

Then,

$$v_T = (C_S \Delta)^2 \sqrt{2\bar{S}_{ij}\bar{S}_{ij}}. \quad (18)$$

Among them, C_S is a dimensionless constant. In summary, the modeling results of the sublattice stress τ_{ij}^s are

$$\tau_{ij}^s - \frac{1}{3}\delta_{ij}\tau_{kk} = 2v_T\bar{S}_{ij} = 2(C_S\Delta)^2 \sqrt{2\bar{S}_{ij}\bar{S}_{ij}}. \quad (19)$$

So far, the numerical equation of the large eddy simulation is obtained. In the process of simulating the flow field with LES, the appropriate sublattice model and fixed solution conditions are selected according to the specific situation, so as to obtain more realistic simulation results [21].

3.4. Simulation Calculation Results of the Flow Field of Sliding Bearing in Gear Pump. The theoretical radial leakage model and the theoretical end leakage model contain a dynamic viscosity term; that is, the flow leakage is related to the viscosity properties of the selected hydraulic oil. In fact, the fluid viscosity is also affected by temperature, and the viscosity would change due to the change in temperature. The effect of temperature needs to be added to refine the original leak model [22, 23]. At the same time, the fluid studied in this paper is an incompressible fluid, and its density remains constant and does not change with temperature. During operation, the pump body deforms, and the deformation of the pump body would affect the leakage to a certain extent. Moreover, under the condition of high pressure and high speed, if the strength of the pump body is insufficient, it would cause cracks or even burst.

The relationship between kinematic viscosity and temperature is generally expressed by the Walser equation:

$$\log \log(v + a) = b - c \log T. \quad (20)$$

In the Formula, a , b , and c are constants related to the oil, and $a = 0.6$, b , and c are obtained by bringing the viscosity of the oil at two different temperatures into Formula (20). The hydraulic oil used in the gear pump experiment is generally #32 lubricating oil. The viscosity values at different temperatures are shown in Table 1. From the simulation results of the pump body deformation, it takes as many points as possible on the pump inner wall to check the position and its deformation and interpolates to fit the relationship between the circumferential position of the pump inner wall and the deformation. The gap between the tooth tip and the inner wall of the pump at a certain point is the sum of the determined radial gap and the deformation of the pump body at the position of the point, and the corresponding leakage is calculated according to different temperatures.

Taking the selection of #32 lubricating oil as an example, it is found from the calculation in Table 1 that the density of the lubricating oil is 850 kg/m^3 . The effect of temperature on its density is negligible, which is consistent with the theoretical setting.

TABLE 1: #32 Oil temperature–viscosity data.

Temperature (°C)	Dynamic viscosity	Motion viscosity
22.8	83.29	97.97
32.4	46.32	54.48
40.6	28.63	33.66
50.3	20.11	23.67
61.3	14.11	16.58

4. Experiment of Circular Helical Gear Pump

4.1. Influence of Oil Inlet Pressure on Internal Flow Field of Sliding Bearing. This section analyzes the influence of the rated pressure of the oil inlet on the internal flow field characteristics of the sliding bearing when the eccentricity is fixed. For the internal flow field of the sliding bearing, the rotational speed is 10000 r/min. When the rated pressure of the oil inlet is 5 MPa, 10 MPa, 15 MPa, 20 MPa, 25 MPa, 30 MPa, and 35 MPa, respectively, the simulation analysis is carried out.

The correctness of the simulation results and the average flow rate obtained from the simulation of the tooth circular-arc wheel pump at the same speed with different loads and the same load with different speeds in the next rotation cycle are compared with the flow value obtained by theoretical calculation, as shown in Tables 2 and 3.

It can be seen from the data in Tables 2 and 3 that the flow value obtained by the simulation calculation is close to and slightly smaller than the theoretical flow rate, and the simulation calculation of the internal flow field of the gear pump is correct.

In order to more intuitively express the influence of the rated pressure of the oil inlet on the radial force balance ability, this paper mainly analyzes the difference between the pressure of the static pressure groove and the rated pressure of the oil inlet, as shown in Figure 4.

As can be seen from Figure 4(a), the greater the inlet pressure, the greater the pressure drop in the static pressure groove. When the rated pressure of the oil inlet is 35 MPa, the pressure drop of the static pressure tank reaches 9.7 MPa. The two sliding bearings can offset 49.52% of the radial force for the driven wheel with larger radial force, and when the oil inlet pressure is 5 MPa, it can offset 63.02%. It can be seen from Figure 4(b) that the greater the rated pressure of the oil inlet, the greater the radial force on the sliding bearing. As a result, the wear of the sliding bearing is more serious, the higher the temperature of the sliding bearing, the more serious the wear at the relative position of the oil inlet. When the rated pressure of the oil inlet is 5 MPa, the average temperature rise is about 16.012°C , and when the rated pressure of the oil inlet is 35 MPa, the average temperature rise reaches 23.85°C .

4.2. Improvement of Sliding Bearing in Gear Pump. During the actual operation of the high-performance small arc gear pump, due to its high pressure and high speed, the gear pump is small in volume, and the sealing area is small, and the sealing problem may also cause leakage. The front end cover of the gear pump is sealed with an O-ring to prevent leakage between the end face of the front end cover

TABLE 2: Comparison of simulated flow and theoretical flow with different loads.

Load (MPa)	No leakage theoretical flow (L/min)	There is leakage theoretical flow (L/min)	Simulation traffic (L/min)
5	20.0172	19.6012	19.3807
15	20.0172	19.2499	19.0127
20	20.0172	19.0023	18.9935
25	20.0172	18.9238	18.001

TABLE 3: Comparison of simulated flow and theoretical flow at different speeds.

Rotational speed (r/min)	No leakage theoretical flow (L/min)	There is leakage theoretical flow (L/min)	Simulation traffic (L/min)
4000	8.00684	7.2657	7.0723
10000	20.0172	19.2489	19.0129
12000	24.0206	22.9274	22.6507

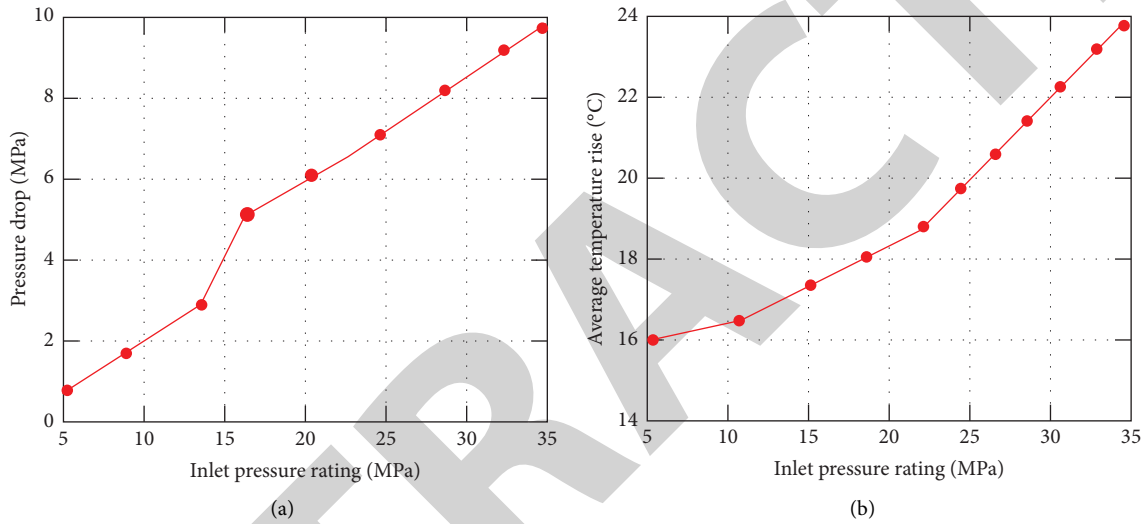


FIGURE 4: Influence of oil inlet pressure on pressure drop in static pressure tank and average bearing temperature rise (a). Influence of oil inlet pressure on pressure drop in static pressure groove (b). Influence of oil inlet pressure on average bearing temperature rise.

and the pump body, and an oil seal is installed at the through hole to prevent leakage between the drive gear shaft and the end cover. Setting the rated pressure of the internal flow field of the sliding bearing to 25 MPa, when the rotation speed is 10000 r/min, simulation analysis is carried out for different oil inlet position angles, and the influence of oil inlet position angles on the pressure and temperature rise of the static pressure tank is discussed. The location of the oil inlet with the most positive impact on the overall performance is determined, which takes into account the structural characteristics of the plain bearing, and the range of the position angle is selected from the angle between the oil inlet and the horizontal direction of 40° to 70° , as shown in Figure 5.

As can be seen in Figure 5(a), the position angle of the oil inlet increases, and the pressure of the static pressure tank decreases, and this would lead to a worsening effect of balancing the radial force, but the effect is not very large. When the position angle is 40° , the pressure of the hydrostatic groove is 17.8 MPa, and the two sliding bearings can offset 51.92% of the radial force for the driven wheel with a larger radial force. When the position angle is 70° , the pressure of the hydrostatic groove is 17.24 MPa, which can offset 50.31% of the radial force. As shown in Figure 5(b),

under the combined influence of the dynamic pressure, eccentricity, and static pressure groove pressure generated during the operation of the sliding bearing, as the oil inlet position angle increases, the temperature rise of the fluid inside the sliding bearing first decreases and then increases. It reaches a minimum value at 47° . Therefore, through the comprehensive conclusion, it is more appropriate to select 47° for the position angle of the oil inlet of the sliding bearing.

In order to more accurately analyze the influence of the oil inlet diameter on the flow field performance of the sliding bearing, from 1.25 mm to 3.85 mm, simulation analysis is carried out for every 2 mm increase, as shown in Figure 6.

As can be seen from Figure 6(a), the diameter of the oil inlet increases, and the width of the oil passage increases. The increase in the amount of high-pressure oil feed increases the pressure of the hydrostatic groove, so the effect of balancing the radial force in the hydrostatic groove becomes better, but the increase in the pressure of the hydrostatic groove tends to slow down. When the diameter of the oil inlet is 1.25 mm, the pressure of the static pressure groove is 8.79 MPa, and the two sliding bearings can only offset 25.78% of the radial force for the driven wheel with a large radial force. When the diameter is 3.85 mm, the pressure of the hydrostatic groove

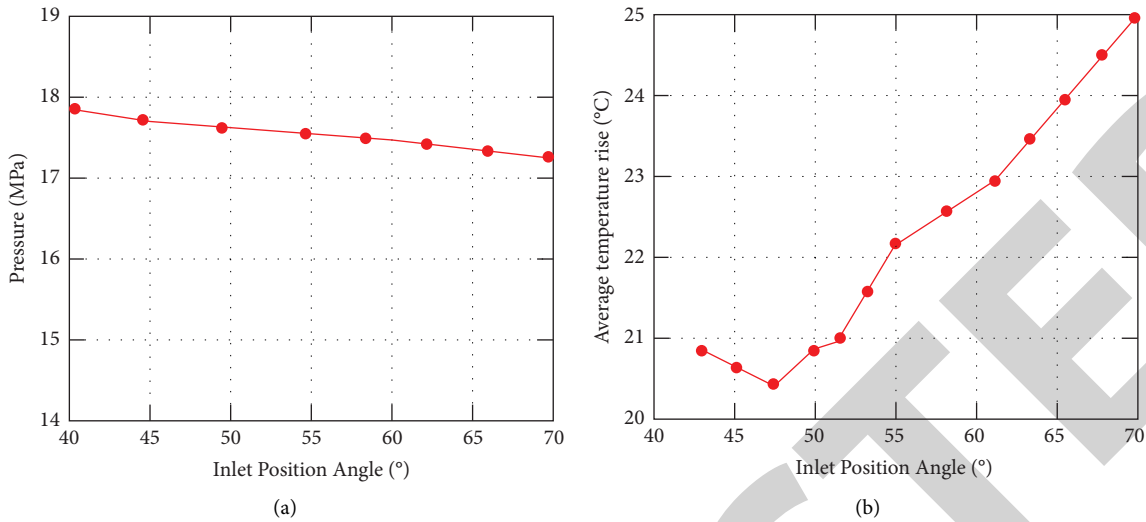


FIGURE 5: The influence of the position angle of the oil inlet on the pressure and temperature rise of the static pressure tank (a). Effect on static pressure tank pressure (b). Effect on average temperature rise.

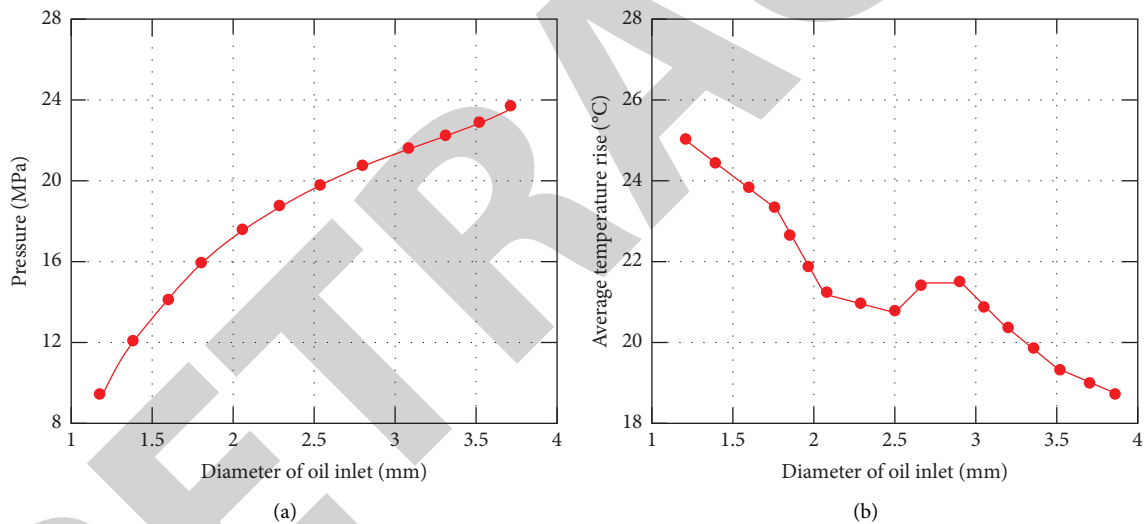


FIGURE 6: Influence of inlet diameter on pressure and temperature rise in hydrostatic tank (a). Effect on static pressure tank pressure (b). Effect on average temperature rise.

is 23.8 MPa, which can offset 67.50% of the radial force. It can be seen from Figure 6(b) that the diameter of the oil inlet increases, the high pressure oil pours in a lot, and the pressure on the gear shaft increases, which would lead to an increase in the eccentricity. The maximum temperature rise of the sliding bearing oil film increases, and a large influx of hydraulic oil would also take away a lot of heat. Therefore, the average temperature rise shows an overall trend of decreasing but fluctuates from 2.1 mm to 3.1 mm. When the diameter of the oil inlet is 1.25 mm, the average temperature rise is 25.5°C, and when the diameter is 3.85 mm, the average temperature rise is 18.5°C. As far as the overall trend is concerned, the increase in the diameter of the oil inlet has a positive effect on reducing the pressure drop in the static pressure tank and reducing the temperature rise. However, if

the diameter of the oil inlet is too large, the flow rate of the sliding bearing would increase greatly, which would increase the leakage of the gear pump, and taking into account the average temperature rise between 2.4 mm and 3.1 mm, the final choice for the diameter of the oil inlet is 2.4 mm.

4.3. Temperature Test Experiment of Arc Helical Gear Pump.

In order to study the temperature rise characteristics of the arc helical gear pump during operation, it avoids the viscosity of the lubricating oil overheating caused by the operation of the arc helical gear pump under high pressure and high speed conditions. It leads to problems such as serious wear and increased leakage, and to analyze the influence of the sliding bearing optimization on the temperature rise

characteristics of the gear pump, the experimental test and analysis of the temperature rise characteristics of the gear pump were carried out.

4.3.1. Influence of Sliding Bearing Optimization on Temperature Rise of Gear Pump Prototype. When the sliding bearings in the gear pump prototype are, respectively, without hydrostatic grooves, before optimization, and after optimization, they run for 600s under the condition of speed of 2100r/min and load of 8 MPa. The relationship between the surface temperature rise of the gear pump and the operating time was obtained. After each experimental operation, it needs to be stopped for 30 minutes to wait for the gear pump prototype and hydraulic oil to cool down. After the test, it was found that the temperature rise at the T2 position was the highest, so the relationship between the temperature rise of T2 and the time was plotted, as shown in Figure 7.

It can be seen from Figure 7 that the optimization of the sliding bearing has an obvious effect on the improvement of the temperature rise of the gear pump. It runs for 600s under the working conditions of the speed of 2100r/min and the load of 8 MPa. The surface temperature rise of the gear pump with optimized sliding bearings is reduced by about 2.5°C. Compared with the ordinary plain bearing without hydrostatic groove, the surface temperature rise of the gear pump prototype with the optimized plain bearing is reduced by about 12°C. In general, the optimized sliding bearing has significant advantages in reducing the temperature rise of high-performance small arc helical gear pumps. It also proves that the optimization of the sliding bearing is the key to improving the temperature rise of the gear pump.

4.3.2. The Influence of the Optimized Sliding Bearing on the Flow Rate of the Gear Pump Prototype. By analyzing the leakage phenomenon of the gear pump after the optimization of the arc helical gear bearing, in order to test the accuracy of the hydraulic oil temperature rise and the pump flow leakage model, the flow characteristics of the gear pump were analyzed, and the flow characteristics of the gear pump were experimentally tested and analyzed. When the sliding bearings in the gear pump prototype are the sliding bearings before optimization and the sliding bearings after optimization, the relationship between the speed and flow of the gear pump prototype is tested when the load is 8 MPa, as shown in Figure 8. In the measurement range, with the increase of rotational speed, the flow rate of the gear pump increases, which is linear.

It can be seen from Figure 8 that the optimized sliding bearing reduces the flow leakage of the gear pump. This advantage is not obvious when the speed is lower than 2500r/min. With the increase of rotational speed, it can be seen that the volumetric efficiency of the optimized sliding bearing gear pump is significantly higher than that of the gear pump before optimization. It can be obtained by calculation that when the arc gear pump runs under the working condition of the load of 10 MPa, within the tested speed range, the volumetric efficiency of the gear pump is the highest at 15000r/min, reaching 64.43%. The volumetric

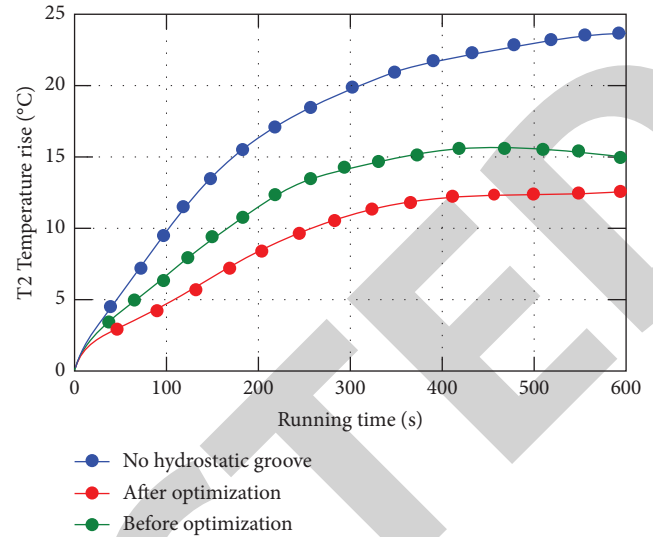


FIGURE 7: Temperature rise of gear pump with different plain bearings installed.

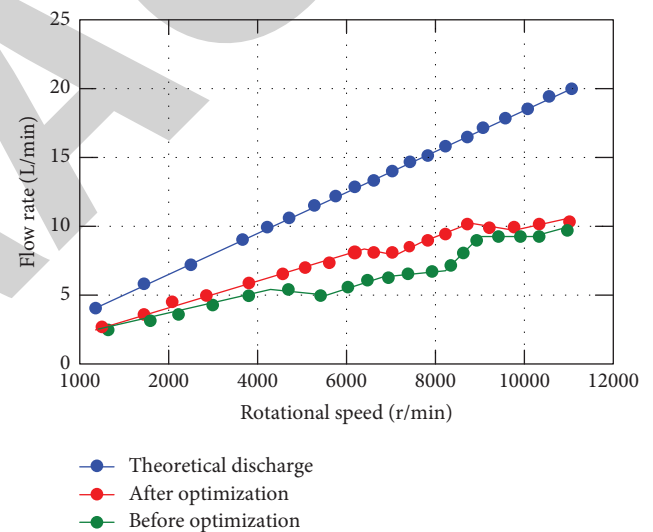


FIGURE 8: Flow rate of gear pump at different speeds before and after sliding bearing optimization.

efficiency is also relatively low when the rotational speed is low, and the volumetric efficiency of the gear pump is 53.71% at 1100r/min. The higher the rotation speed, the higher the volumetric efficiency; that is, the higher the rotation speed, the smaller the leakage, and the higher the volumetric efficiency. Before the optimization of the sliding bearing, the volumetric efficiency of the gear pump was at least 49.81% at 1700r/min and 60.16% at 15000r/min. Overall, the volumetric efficiency of the gear pump increases after the sliding bearing is optimized. The volumetric efficiency of the gear pump is the ratio of the actual flow to the theoretical flow.

4.3.3. Comparison of Theoretical Flow and Actual Flow. The leakage model is compared with the actual leakage through flow experiments to verify the correctness of the

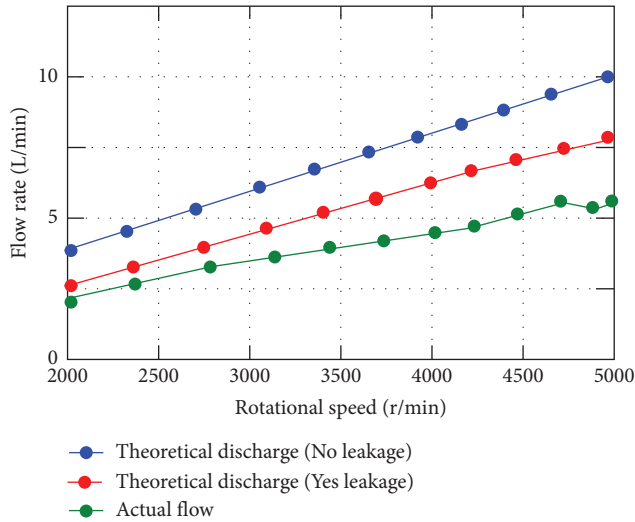


FIGURE 9: Theoretical and actual flow at different speeds.

theoretical leakage model. According to the temperature rise of different speeds obtained from the simulation, the load and other related parameters of the sliding bearing calculated by the simulation are brought into the program. When the load is 8 MPa, the relationship between the flow rates at different speeds of the gear pump prototype is tested, as shown in Figure 9.

It can be seen from Figure 9 that the flow calculation results of the theoretical model including leakage are closer to the actual flow, but there is still a certain gap. Due to the wear of the gear pump when it is running at high pressure and high speed, the leakage is aggravated. At the same time, the wear and tear generated during the actual loading operation make the temperature of the hydraulic oil rise greatly, which is also the reason for the large amount of leakage. The lower the rotational speed, the smaller the difference between the theoretical flow with leakage and the actual flow. The existing formula is more suitable for low speed. For high-speed operation, the basic leakage theoretical model can be further studied.

4.3.4. The Influence of Load on the Flow Rate of the Gear Pump Prototype. When the rotational speed of the arc helical gear pump is 5700 r/min, 6000 r/min, and 6300 r/min, respectively, it starts loading from no-load and collects the flow signal of the gear pump within the load range from 5.8 MPa to 14.8 MPa. The test results of the gear pump flow experiment are shown in Figure 10.

In Figure 10, as the load of the gear pump increases, the flow rate of the gear pump shows an overall trend of decreasing. Since the theoretical flow rate of the gear pump is constant at the same speed, the higher the load, the lower the volumetric efficiency. The higher the load, the larger the leakage, and the lower the volumetric efficiency. The accuracy of the flow leakage model and the simulation calculation of the dynamic performance of the internal flow field of the gear pump are verified.

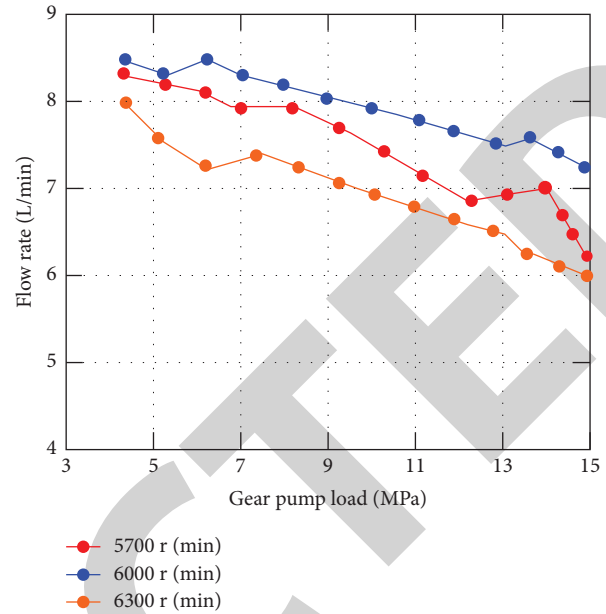


FIGURE 10: Effect of gear pump load on flow at different speeds.

5. Conclusion

In this paper, based on the background of machine learning, the three-dimensional flow field simulation and sound field source simulation of the flow field in the arc helical gear pump are carried out. The difference in the flow in the pump under different working conditions is analyzed, and the dynamic performance simulation of the gear pump is deeply studied. Aiming at the flow leakage problem of the arc helical gear pump, a flow leakage model of the gear pump is established. It solves the problem of obvious temperature rise of the sliding bearing in the gear pump and serious wear caused by the large radial force. Through experimental analysis, the surface temperature rise of the gear pump optimized by the sliding bearing is reduced by about 2.5°C when the speed is 2100 r/min for 600 s. Compared with ordinary plain bearings, the surface temperature rise is reduced by about 12°C. It is concluded that the optimization of the sliding bearing has an obvious improvement effect on the temperature rise of the gear pump. It proves that the arc helical gear pump can run smoothly under high pressure and high speed compared with other ordinary gear pumps. The application of the proposed helical gear pump simulation method in this paper is relatively shallow in research and analysis, and it still needs to be further improved. It is also possible to try to simulate various errors in the processing of the gear pump. In view of the leakage problem of the helical gear pump, the sealing materials and methods of the gear pump under high pressure conditions are studied, the compensation method of the gear pump is improved, and the leakage problem at high pressure and high speed is improved. Through simulation and experiment, it is found that the optimization of sliding bearing has a significant effect on reducing temperature rise and balancing radial force, so the sliding bearing in gear pump needs to be further optimized.

Retraction

Retracted: The Construction of Smart Chinese Medicine Cloud Health Platform Based on Deep Neural Networks

International Transactions on Electrical Energy Systems

Received 28 November 2023; Accepted 28 November 2023; Published 29 November 2023

Copyright © 2023 International Transactions on Electrical Energy Systems. This is an open access article distributed under the Creative Commons Attribution License, which permits unrestricted use, distribution, and reproduction in any medium, provided the original work is properly cited.

This article has been retracted by Hindawi, as publisher, following an investigation undertaken by the publisher [1]. This investigation has uncovered evidence of systematic manipulation of the publication and peer-review process. We cannot, therefore, vouch for the reliability or integrity of this article.

Please note that this notice is intended solely to alert readers that the peer-review process of this article has been compromised.

Wiley and Hindawi regret that the usual quality checks did not identify these issues before publication and have since put additional measures in place to safeguard research integrity.

We wish to credit our Research Integrity and Research Publishing teams and anonymous and named external researchers and research integrity experts for contributing to this investigation.

The corresponding author, as the representative of all authors, has been given the opportunity to register their agreement or disagreement to this retraction. We have kept a record of any response received.

References

- [1] Y. Miao and Y. Zhou, "The Construction of Smart Chinese Medicine Cloud Health Platform Based on Deep Neural Networks," *International Transactions on Electrical Energy Systems*, vol. 2022, Article ID 6751915, 10 pages, 2022.

Research Article

The Construction of Smart Chinese Medicine Cloud Health Platform Based on Deep Neural Networks

Yaofeng Miao  and Yuan Zhou

Engineering College, Xi'an International University, Xi'an 710077, Shaanxi, China

Correspondence should be addressed to Yaofeng Miao; miaoyaofeng2022@163.com

Received 20 August 2022; Revised 7 September 2022; Accepted 19 September 2022; Published 3 October 2022

Academic Editor: Nagamalai Vasimalai

Copyright © 2022 Yaofeng Miao and Yuan Zhou. This is an open access article distributed under the Creative Commons Attribution License, which permits unrestricted use, distribution, and reproduction in any medium, provided the original work is properly cited.

In order to improve the efficiency of doctors' diagnosis and treatment, the state has built a Chinese medicine cloud health platform. However, most medical institutions currently use internal networks, and the technical standards and specifications are not uniform. Some information is not compatible and patient information cannot be shared. Therefore, the construction of a smart traditional Chinese medicine (TCM) cloud health platform based on deep neural networks has become a current research hotspot. The research results show that the deep neural network technology has a theoretical basis and feasibility in the smart Chinese medicine cloud health platform. Combining with deep neural network technology, a cloud-based Chinese medicine cloud health system has been developed through big data analysis technology. Through the investigation and research method, this paper found that the smart Chinese medicine cloud health platform based on deep neural networks was more popular with citizens, which could improve the quality and efficiency of management. The average management quality of a smart TCM health cloud platform based on deep neural networks was 81.1, and the average management quality of a common TCM cloud health platform was 75. The efficiency of the smart Chinese medicine cloud health platform based on deep neural networks was relatively stable, with an average of 84%. The efficiency of the general TCM cloud health platform fluctuated significantly and was relatively unstable, with an average of 73.5%. The efficiency of the smart Chinese medicine cloud health platform was 10.5% higher than that of the ordinary Chinese medicine cloud health platform. This shows that the construction of the intelligent Chinese medicine cloud health platform under the deep neural network is relatively successful.

1. Introduction

In recent years, the development of deep neural network algorithms has gradually adapted to reality. The technology is also becoming more and more mature, which provides an effective way for the construction of a smart Chinese medicine cloud health platform. Due to people's bad habits of life and diet, changes in disease types and other factors have had a huge negative impact on people's health. People's health needs have shifted from traditional curative to preventive. Therefore, the introduction of deep neural networks into the construction of a smart Chinese medicine cloud health platform has become a top priority.

In order to make the research on the construction of a smart Chinese medicine cloud health platform based on deep neural networks more scientific and rigorous, many

researchers have invested in the research. Fan believed in developing intelligent medical systems so that medical care could process changes in chemical and physiological states in real time [1]. Raja's research discovered an early form of "smart medicine" that has been used in space to assess nutrition [2]. Based on the research on the development strategy of TCM informatization, combined with the current cloud computing development model, Xu analyzed the advantages of TCM informatization under cloud computing environment and how to use cloud computing technology to realize TCM informatization [3]. Zaszczynska A believed that the traditional Chinese medicine health cloud could combine the standardization of traditional Chinese medicine with big data and artificial intelligence [4]. Based on the urgent needs of the aging population for TCM health cloud and health care services, Jin constructively studied the TCM

health cloud service platform and its architecture design [5]. Singh analyzed the key technologies of the TCM health cloud platform, and then proposed the design and application of the TCM health cloud in healthcare services [6]. Liu combined the wisdom of traditional Chinese medicine with the Internet and big data. The real-time health status of the elderly was dynamically tracked and queried, which provided timely, effective, and targeted health care services for the elderly [7]. It can be seen that the research results on the TCM cloud health platform have been very rich. However, the research results on the construction of a smart TCM cloud health platform based on deep neural networks are very rare. In order to solve this problem, this paper combines the two to conduct research.

Many researchers are working on algorithms for learning deep neural network architectures. Foad discussed some modifications and extensions to convolutional and fully connected layer accelerators for deep learning networks [8]. Guo described activation encodings that were considered invalid, encodings with different memory overhead and energy properties [9]. Suk proposed to use some degree of indirection when accessing activations from memory to reduce their memory footprint by storing only valid activations [10]. Banerjee proposed a modified organization of activation programs that were considered ineffective when their detections could be obtained from memory. It was different from the original design where they were detected in the output of the previous layer [11]. Khodayar described the use of low-dimensional vector representations of sentence acoustics to control the output of a feedforward deep neural network text-to-speech system sentence by sentence [12]. Ji believed that the vector representations of sentences in the training corpus were learned together with other parameters of the model during network training [13]. Wang argued that deep neural networks were trained frame-by-frame, but the standard frame-level input parameters representing language features were complemented by features from projection layers. These parameters were jointly optimized with standard network weights [14]. In order to better study the TCM cloud health platform, this paper introduced the deep neural network into the construction of the TCM cloud health platform.

With the help of deep neural network technology, traditional Chinese medicine has finally formed a health management platform based on traditional Chinese medicine. This paper studied the construction of a smart TCM cloud health platform based on deep neural networks. Through research, it is found that the smart Chinese medicine cloud health platform based on the deep neural network is more popular among citizens, which can improve the quality and efficiency of platform management.

2. Smart TCM Cloud Health Platform Based on Deep Neural Network

2.1. Development of Neural Network. The development of neural networks includes perceptrons, multilayer perceptrons, deep neural networks, and convolutional neural networks.

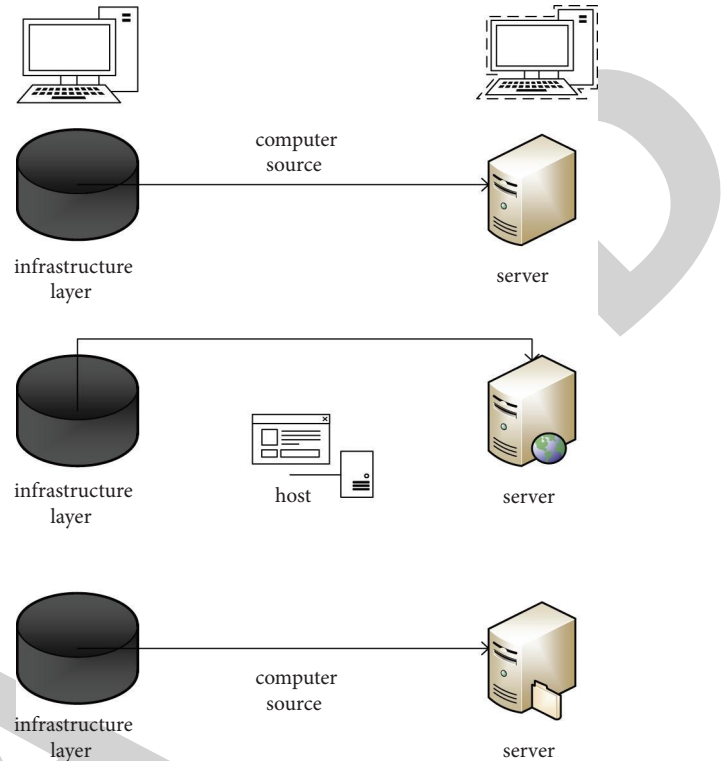


FIGURE 1: Network architecture based on deep neural network algorithms.

2.1.1. Perceptron. Neural network technology originated in the 1950s and 1960s when it was called a perceptron with an input layer, an output layer, and a hidden layer [15]. The input feature vector is transformed to the output layer through the hidden layer, and the classification result is obtained at the output layer.

2.1.2. Multilayer Perceptron. A multilayer perceptron, as the name suggests, is a perceptron with multiple hidden layers. Multilayer perceptrons can discard the original sequence of discrete transfer functions and use continuous functions to model neuron responses to stimuli. The continuous BP algorithm is used in the learning algorithm, which is now called the neural network [16]. Multilayer perceptrons solve previously unsimulated loopholes. At the same time, more layers make the network more capable of describing complex situations in the real world.

2.1.3. Deep Neural Network. The pretraining methods are used to reduce the local optimal solution problem. The hidden layer is pushed to 7 layers, and the neural network has a real “deep”, thus kicking off the deep learning craze. Structurally, there is no difference between a fully connected deep neural network and a multilayer perceptron [17].

2.1.4. Convolutional Neural Network. In a fully connected system, the lower layer neurons and all upper layer neurons can establish connections. The biggest problem is the scaling

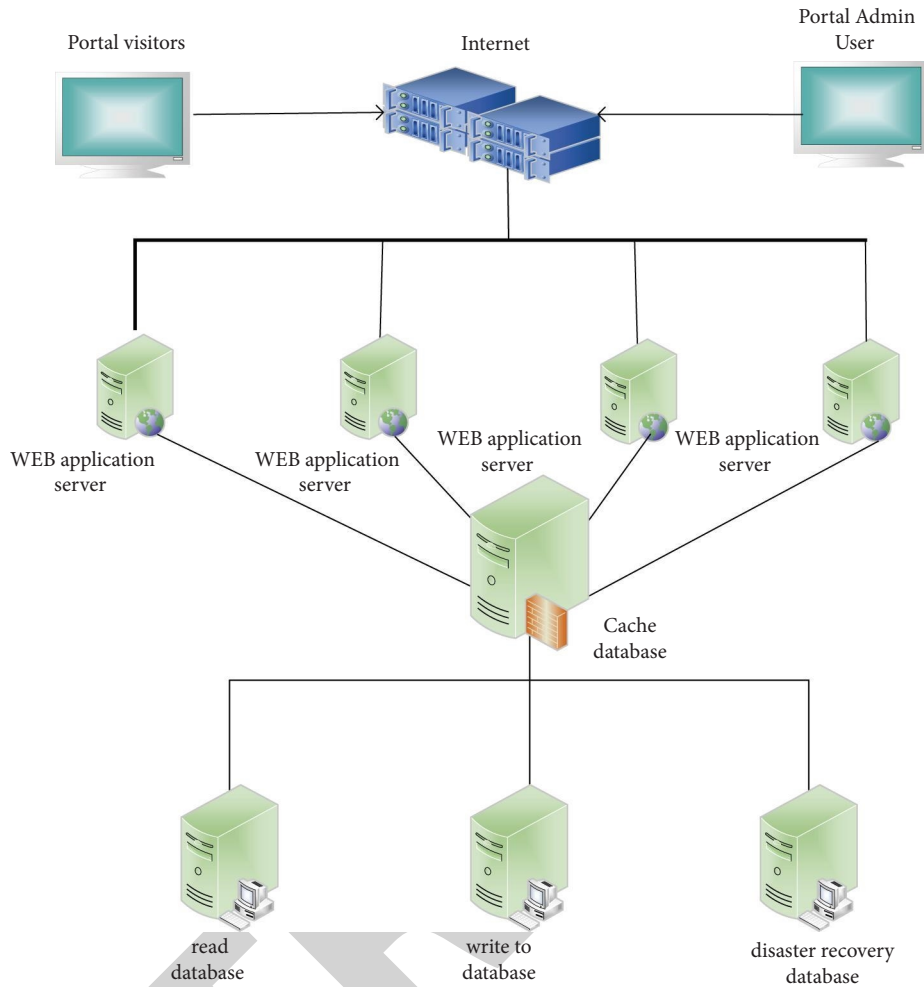


FIGURE 2: Traditional Chinese medicine cloud health platform architecture.

of the number of parameters [18]. Not all neurons in the upper and lower layers can be directly connected; they must go through “convolution” as an intermediary. The same convolution kernel is distributed in all images, and the images maintain the original positional relationship after the displacement operation. Following the same idea of using local information in the context of speech, neural networks can also be used for speech recognition. In a fully connected network or a deep neural network, the signals of neurons in each layer can be passed to the upper layers. Each time the sample is processed independently, it is also called a relay neural network. Specifically, as shown in Figure 1.

2.2. Architecture of TCM Cloud Health Platform. The traditional Chinese medicine cloud health platform is a family-based health management platform that can effectively realize the docking of cloud application platforms such as electronic medical records and information systems. The TCM cloud health platform can effectively manage personal and family health files for ordinary users and record the physical data of individuals and family members [19, 20]. It is also able to search for hospitals and clinics online and select the right doctor for an appointment or online

consultation. Moreover, it can also self-diagnose healthily and inquire about the electronic medical records of individuals and family members. At the same time, it can interact with other ordinary users or doctors in the area, or send prescriptions to pharmacies to buy drugs online [21]. As a result, a new business model of “doctor-patient company” is formed, as shown in Figure 2.

2.3. Main Functions of the TCM Cloud Health Platform. The TCM cloud platform can provide four types of users, namely ordinary users, doctors, enterprises, and platform management.

Among them, ordinary users have applications such as finding personal health records, managing family health records, finding hospitals and doctors online, obtaining hospital and doctor information, online appointment registration, online consultation, online doctor communication, and online drug purchases. It is also possible to score doctors or send pennants [22, 23].

Doctor users can obtain patient registration information and consultation information online. They are able to interact with patients online, post updates, publications, release patented medicines, and analyze revenue statistics.

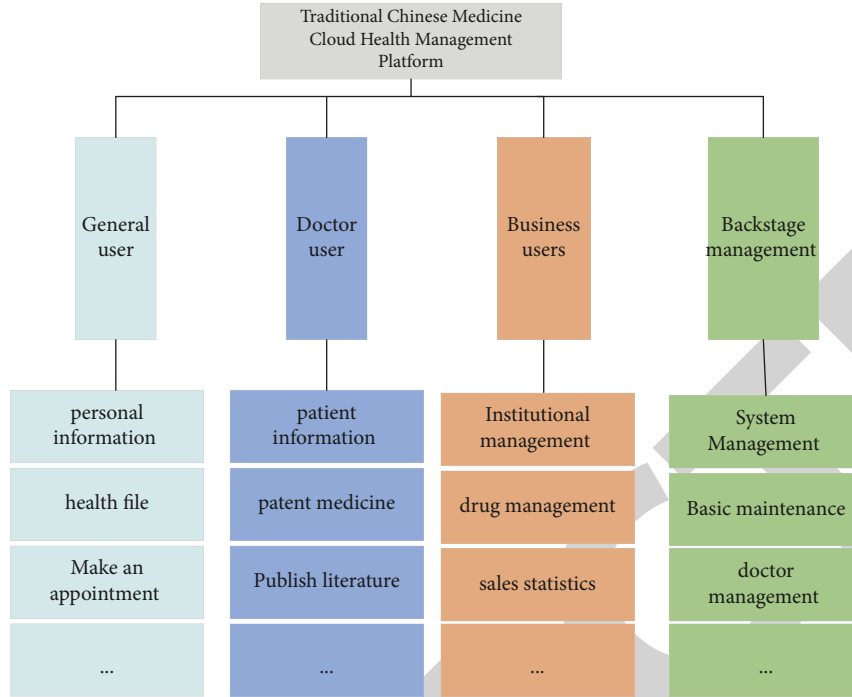


FIGURE 3: Main functions of TCM cloud health platform.

Finally, combined with the doctor's workstation, they diagnose diseases for patients, identify diseases, do electronic medical record storage, health file storage, and so on. At the same time, the doctor's diagnosis and treatment plan system includes patient diagnosis, disease identification, treatment and Western medicine prescription, viewing medical records, printing medical records, searching treatment records, and symptom comparison analysis.

Enterprise users can build their own online stores on the platform, publish drug information online, manage drug inventory, and conduct statistical analysis of sales data. The online and offline O2O business model is then realized.

Platform management is to manage each subplatform. Specifically, as shown in Figure 3.

3. Applications of Deep Neural Network Algorithms in Smart Chinese Medicine Cloud Health Platform

Deep neural networks originated from neuroscience techniques. In recent years, this technology has achieved successful breakthroughs in many fields of artificial intelligence. Deep neural networks are also known as deep learning. Since current deep networks mainly use convolutional structures, deep neural network algorithms are sometimes also referred to as deep learning algorithms.

Deep neural networks (DNN) are the foundation of many artificial intelligences at present, and DNN has achieved breakthrough success in speech recognition, image recognition, etc. Feedforward artificial neural networks (CNN) have been widely used in the computer field. In traditional nonlinear networks, object extraction and object selection are first performed on the image, and then the

network is output. CNN is an end-to-end network that directly takes raw images as network input and automatically performs feature training. Taking the recognition task as an example, CNN integrates the extraction feature selection and classification, and the final matched category is output.

The CNN network structure is mainly composed of three types of layers: convolutional layers, pooling layers, and fully connected layers. The specific structure of the CNN network is shown in Figure 4.

Compared with traditional neural networks, CNN has the characteristics of local coverage and density distribution. The connections between neurons are local connections instead of full connections, and the connection weights of neurons between layers are shared by parameters. This feature greatly reduces the weight value parameters and computational density of neural connections, thereby reducing the computational cost complexity, and makes it possible to study the training of deep convolutional networks.

3.1. Convolutional Layer. The convolutional layer is the most important structure in the CNN network, and the convolutional layer generally contains a convolution kernel. Features are extracted from the convolution kernel, and multiple feature maps are output by inputting a two-dimensional image, which is expressed as follows:

$$b_m^k = f_k \left\{ \sum_{n \in m} b_n^{k-1} * \bar{\omega}_{n,m} + y_n^k \right\}. \quad (1)$$

Among them, b_m^k represents the m -th feature vector of the k layer, and the output feature size is expressed as follows:

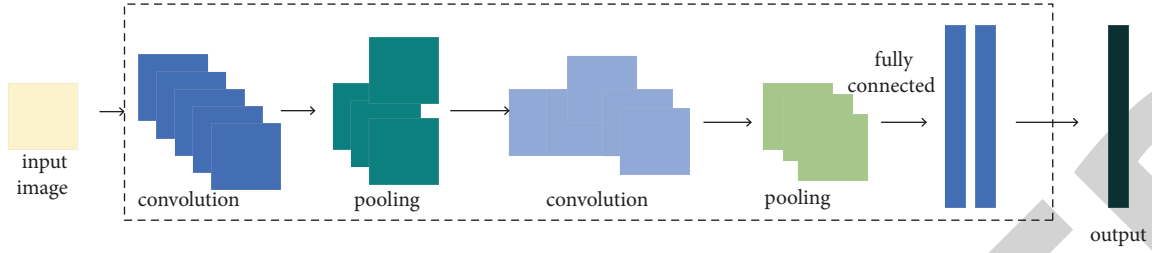


FIGURE 4: The CNN network structure.

$$k_{out} = \left\lfloor \frac{k_{in} + 2q - l}{c} \right\rfloor - 1. \quad (2)$$

3.2. Pooling Layer. This architecture can make it easier to import some parts of the transformation, with some translational fixity. After going through the pooling layer, the resulting value is related to the general statistical features of the input region but not to the position of a single feature, which is expressed by the Formula:

$$b_k = \left[\max(a^1), \max(a^2), K \max(a^l) \right]_m. \quad (3)$$

Among them, m_{\max} represents the feature vector of the weight context.

3.3. Fully Connected Layer. Each fully connected neuron is connected to all the neurons in the previous layer. Therefore, the amount of parameters is huge, and the last layer or layers of CNN are fully connected layers.

The output formula of neurons in the fully connected layer is shown as follows:

$$b_m^k = f_k \left\{ \sum_{n=1}^{k-1} b_n^{k-1} * \bar{\omega}_{n,m} \right\} + y_n^k. \quad (4)$$

3.4. Activation Function. The results of convolutional layers and fully connected layers generally need to go through an activation function. The functions in the convolutional and fully connected layers are linear function operations. In order to make the network nonlinear and increase the fitting ability of the network to handle complex functions, it is also necessary to add an activation function after the convolution and fully connected layers to perform nonarbitrary transformations.

The activation function usually has three distribution curves, which are expressed by the Formulas:

$$\begin{aligned} f(x) &= \frac{1}{1 + e^{-bx}}, \\ f(x) &= \frac{e^{bx} - e^{-bx}}{e^{bx} + e^{-bx}}, \\ f(x) &= \max(b, 0). \end{aligned} \quad (5)$$

In the process of training a neural network, a decay function is used in the forward pass to calculate the difference between the predicted value and the actual symbol. In backpropagation, the decay function is used to update the weight by taking the partial derivative of the parameter (weight). The calculation formulas are expressed as follows:

$$s_h^k = \sum_l v_l^k b_l^{k-1} + y, \quad (6)$$

$$b_l^k = \frac{o^2}{\sum_l o^2}. \quad (7)$$

When the sum of the outputs of all neurons in the layer l is equal to 1, that is

$$\sum_{h=1}^l b_h^k = 1. \quad (8)$$

When the formula does not consider the regular term, the calculation formula is shown as follows:

$$C = \frac{1}{n} \left[\sum_{i=1}^n \sum_{h=1}^l 1(n \in 1) \right]. \quad (9)$$

3.5. Stochastic Gradient Descent Function. It can be seen from calculus that when w changes to a small increment, the increment of the loss function can be completely expressed by calculus, which is expressed as follows:

$$\Delta C = \frac{\partial C}{\partial w_1} \Delta w_1 + \frac{\partial C}{\partial w_2} \Delta w_2 + \dots + \Delta w_i. \quad (10)$$

ΔC can be expressed as follows:

$$\Delta C = \left(\frac{\partial C}{\partial w_i} \right) \Delta w_i. \quad (11)$$

If the formula is expressed as follows:

$$\Delta w = \eta \Delta C. \quad (12)$$

Then the formula is obtained

$$\Delta C = -\eta \|\nabla C\|^m. \quad (13)$$

Since ΔC is also called the gradient of the loss function C , this method is also called gradient descent. By replacing w with the bias of the weight v in the deep neural network, the

update function of the weight bias can be obtained, which is expressed as follows:

$$v = v - \eta \frac{\partial C}{\partial v}, \quad (14)$$

$$y = y - \eta \frac{\partial C}{\partial Y}. \quad (15)$$

However, the sample sets for training deep neural networks tend to be very large. If all samples are input during training, the calculation of the average can take a lot of time, which makes the results very slow. When all samples are used up, one training iteration is completed. Then, the second iteration is started in the same way, and so on, until the loss function converges, which is expressed by the Formulas

$$\nabla C = \frac{1}{n} \sum_{i=1}^n \Delta C - \frac{1}{M} \sum_{i=1}^M \Delta C, \quad (16)$$

$$e_h^i = \sum_{i=1}^n \frac{1}{m} \Delta C. \quad (17)$$

The algorithm takes into account the change period of the parameters, so a higher convergence speed can be obtained under the stochastic gradient algorithm.

$$\Delta v = \sum_m \eta \frac{\partial C}{\partial M}. \quad (18)$$

When training a convolutional neural network with gradient descent, the partial derivatives of the weighted objective function need to be calculated. The algorithm that calculates the part of the objective function relative to the weighted input, studies the regression formula of the convolutional layer and the fully connected layer through the statistical graph and then studies how the accumulation layer receives and releases.

4. Construction Characteristics of TCM Cloud Health Management Platform

According to the core links and management characteristics of TCM health management, a TCM cloud health management platform is built, as follows:

- (1) Acquisition of health status parameters: Four diagnostic instruments and an electronic nose are used to understand and collect application information related to traditional Chinese medicine. The research and development of the application can more effectively ensure the objectivity and integrity of the four diagnostic research information. The data collected by wearable devices are real-time and dynamic and can be included in the collection range. Biochemical and genetic indicators in parametric chemical analysis that can be obtained by the deep neural network technology are part of microscopic

parameters and are also important factors in determining health status.

- (2) Arrangement of health files: The obtained parameter information is uniformly entered and stored in the health and medical management information system. Everyone receives a unique file archive. A health file includes an individual's general condition, including current health conditions, medical history, lifestyle, family history, recent donor visits, laboratory tests, and many health risks in work and life. Health risk factor data can be monitored and collected in real time. By running on this data in real-time, a huge amount of data can be obtained. The big data technology can be transmitted and stored in the cloud to form a personal health database, which provides targeted prevention information and guidance for everyone.
- (3) Health status assessment: The collected parameter attributes are based on the identification of status genes. Through data mining technology, machine learning, artificial neural network, and other information processing systems, an algorithm model that conforms to the thinking of traditional Chinese medicine is established, and a path from parameters to state judgment is developed and formed.
- (4) Risk warning and intervention adjustment: Chronic lifestyle disease is a long-term accumulation process that combines many health risk factors. Health risk factors are added to the health record, and long-term, comprehensive, and dynamic care for these risk factors is undertaken. Through massive data models, individual and group health risks can be assessed and risk prediction warnings are made.
- (5) TCM health manager: TCM is the core of the TCM health management platform. In addition to collecting information, operating systems, etc., it also plays the task of managing platform objects (control objects) to communicate with each other. Health lectures are issued for individual guidance of multidisease and high-risk groups, and the purpose is to monitor the whole process and all-round health.

At present, the basic structure of the traditional Chinese medicine health management system based on the overall, dynamic, and personalized has been developed. The system has preliminarily realized: macro, medium, and micro health status indication parameters collection; human-machine combined semiautomatic three-level diagnosis of TCM syndrome elements, syndrome types, and diseases; automatic optimization and fuzzy matching of self-help intervention programs such as medicated diet, diet therapy, and ointment; generation of personalized health status assessment and intervention reports and other functions. With the continuous improvement and development of theory and technology, TCM health management plays a greater role in human health.

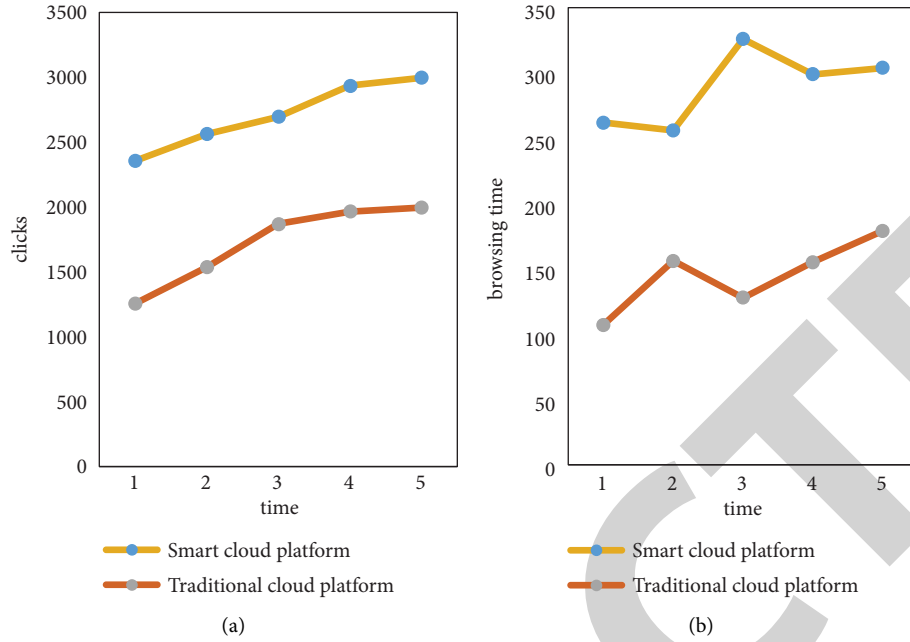


FIGURE 5: Comparison of clicks and browsing time of TCM cloud health platform. (a) Comparison of platform clicks. (b) Platform browsing time comparison.

5. Experiments Related to the Construction of a Smart Chinese Medicine Cloud Health Platform Based on Deep Neural Network

5.1. Comparison of Clicks and Browsing Time of TCM Cloud Health Platform. The smart Chinese medicine cloud health platform based on the deep neural network conducts a 6-week click comparison in the background. It is compared with the traditional Chinese medicine cloud health platform, and the changes in the number of clicks and browsing time of the two are observed. The results are shown in Figure 5.

In Figure 5, Figure 5(a) is the test result of platform clicks, and Figure 5(b) is the test result of browsing duration. In Figure 5(a), the clicks of the smart TCM health cloud platform based on the deep neural network were significantly higher than that of the ordinary TCM health platform. The number of hits of the smart Chinese medicine health cloud platform based on a deep neural network was basically more than 2200, and there was a clear upward trend. The number of hits on the ordinary Chinese medicine health platform increased from 1256 to 1996, but it was still significantly lower than that of the smart Chinese medicine health cloud platform based on the deep neural network. In Figure 5(b), it can be clearly seen that the browsing time of the smart Chinese medicine health cloud platform based on the deep neural network was higher than that of the ordinary Chinese medicine health platform. The total browsing time of the smart Chinese medicine health cloud platform based on a deep neural network was 1447 minutes. The total browsing time of the general Chinese medicine health platform was 725 minutes. To sum up, the smart Chinese medicine health cloud platform based on a deep neural network is more popular.

5.2. Platform Registration Test. Signups for both platforms were statistically tested to see how the two platforms differed in weekly signups over a 6-week period. The test statistics only record users who have registered with real names and browsed for more than 15 minutes, and those who browsed for less than 15 minutes are not recorded. The test results are shown in Figure 6.

In Figure 6, Figure 6(a) is the statistical result of the registered number of the smart Chinese medicine health cloud platform based on the deep neural network. Figure 6(b) shows the statistical results of the number of registrants of the general TCM health platform. In Figure 6(a), the total number of registrations for the six weeks was 1180, and the highest week 5 reached 286 registrations. The minimum number of sign-ups was week 1, with 127 sign-ups. In Figure 6(b), the number of registrations was significantly less than that of the deep neural network-based smart Chinese medicine health cloud platform. The total number of registrations for 6 weeks was 486, and the highest was only 102 registrations. This showed that the smart Chinese medicine health cloud platform based on a deep neural network was more attractive to people.

5.3. Comparison of Platform Satisfaction. In order to more clearly test whether the smart Chinese medicine health cloud platform based on the deep neural network can make the citizens more satisfied, 8 citizens who have used the two platforms were randomly searched for satisfaction scores, with a full score of 10. The survey results are shown in Table 1.

In order to more intuitively study the degree of public preference, this paper draws the survey results as shown in Figure 7.

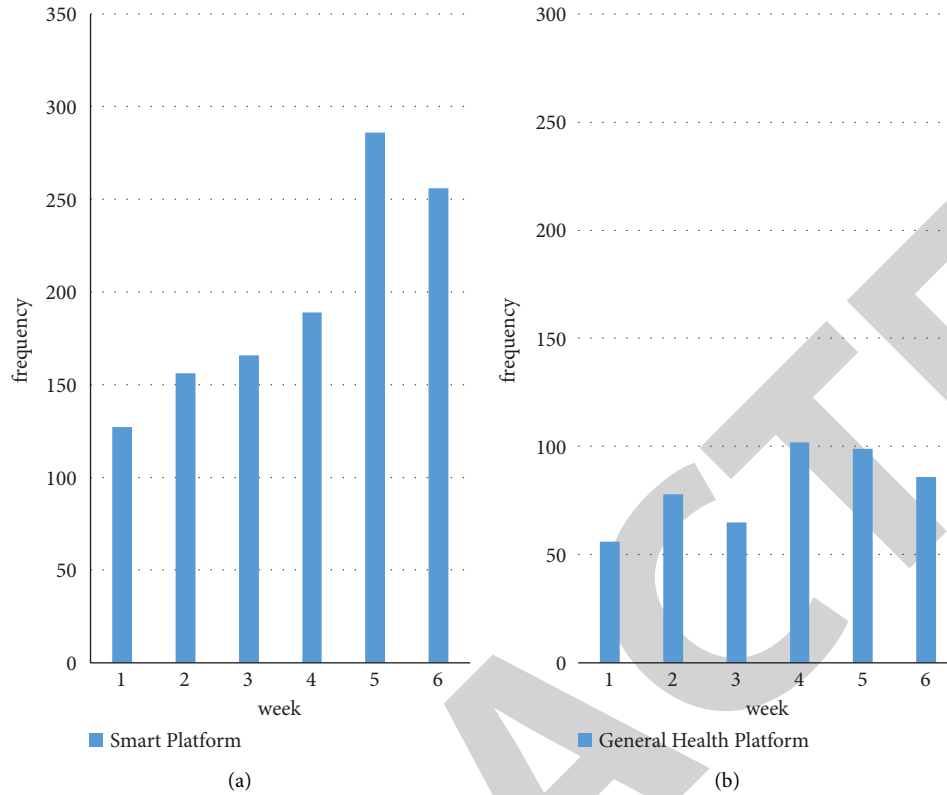


FIGURE 6: Comparison of registered numbers of TCM health platforms. (a) Number of registered smart health platforms. (b) General health platform registrations.

In Figure 7, Figure 7(a) is the statistics of citizens' scores, and Figure 7(b) is the comparison of the satisfaction of the two groups of platforms. In Figure 7(a), citizens scored the highest at 8.5 and the lowest at 6.9. Combined with Figure 7(b), the satisfaction rate increased from 52% to 85%, and the satisfaction rate increased by 33%. In Figure 7(b), the citizen's highest score was 8.1, and the lowest score was 6.3. To sum up, the construction of the smart Chinese medicine health cloud platform based on a deep neural network is still more popular among citizens.

5.4. Comparison of Platform Management Quality and Efficiency. During the experiment of the two groups of platforms, the most important improvement of management quality and efficiency is to observe the comparison of management quality and efficiency of the two groups of platforms within 6 weeks. The statistical results are shown in Figure 8.

In Figure 8, Figure 8(a) is the comparison result of the management quality of the two groups of TCM cloud health platforms. Figure 8(b) is a comparison of the efficiency of the two groups of TCM cloud health platforms. As can be seen from Figure 8(a), the management quality of the smart TCM cloud health platform from the 3rd to the 6th week showed a linear upward trend, reaching a maximum of 88. There were still fluctuations in the first and second weeks and management needed to be strengthened. The average management quality of the

TABLE 1: Satisfaction scores of the two platforms.

	Smart health TCM platform	General health TCM platform
1	6.1	6.9
2	7.2	6.3
3	8.1	7.2
4	8.4	7.5
5	7.9	7.4
6	7.8	7.0
7	8.2	8.1
8	8.5	8.1

smart Chinese medicine health cloud platform based on a deep neural network was 81.1. The management quality of the general TCM cloud health platform showed an upward trend from the first week to the fourth week. However, from the fifth week onwards, the management quality was unstable, the highest was 80, the lowest was 69, and the average management quality was 75. It can be seen from Figure 8(b) that the efficiency of the smart TCM health cloud platform based on the deep neural network was significantly higher than that of the ordinary TCM cloud health platform. The efficiency of the smart Chinese medicine cloud health platform was relatively stable, with an average of 84%. The efficiency of the general TCM cloud health platform fluctuated significantly and was relatively unstable, with an average of 73.5%. The efficiency of the smart Chinese medicine cloud health

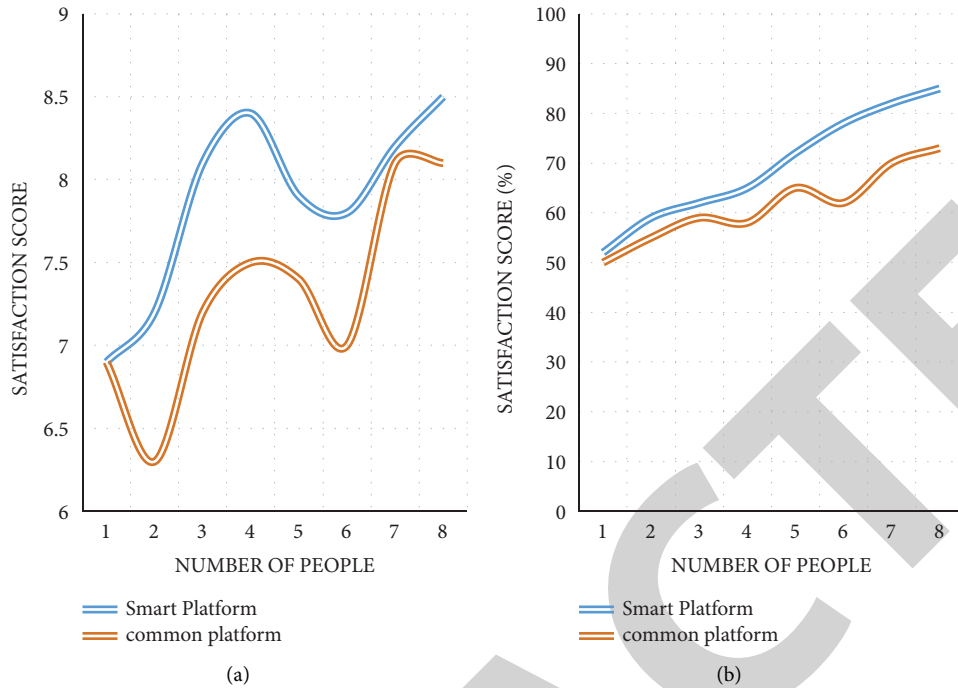


FIGURE 7: Comparison of satisfaction of TCM health platform between two groups. (a) Satisfaction scores of the two platforms. (b) Satisfaction comparison between the two platforms.

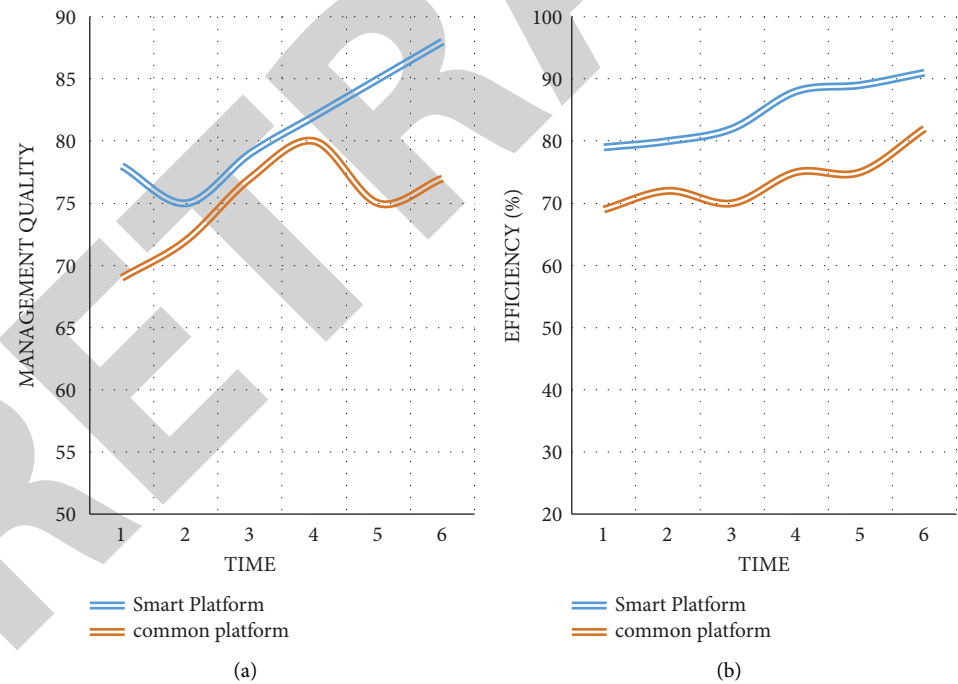


FIGURE 8: Comparison of platform management quality and efficiency. (a) Platform management quality (b) Platform efficiency.

platform was 10.5% higher than that of the ordinary Chinese medicine cloud health platform. This showed that the construction of the intelligent Chinese medicine health cloud platform based on a deep neural network was relatively successful.

6. Conclusion

With the rapid change in society, the improvement of living standards, and better living conditions, people gradually pay more and more attention to the concept of self-care. There is

Retraction

Retracted: Psychological Motivation of Athletes' Physical Training Based on Deep Learning Model

International Transactions on Electrical Energy Systems

Received 28 November 2023; Accepted 28 November 2023; Published 29 November 2023

Copyright © 2023 International Transactions on Electrical Energy Systems. This is an open access article distributed under the Creative Commons Attribution License, which permits unrestricted use, distribution, and reproduction in any medium, provided the original work is properly cited.

This article has been retracted by Hindawi, as publisher, following an investigation undertaken by the publisher [1]. This investigation has uncovered evidence of systematic manipulation of the publication and peer-review process. We cannot, therefore, vouch for the reliability or integrity of this article.

Please note that this notice is intended solely to alert readers that the peer-review process of this article has been compromised.

Wiley and Hindawi regret that the usual quality checks did not identify these issues before publication and have since put additional measures in place to safeguard research integrity.

We wish to credit our Research Integrity and Research Publishing teams and anonymous and named external researchers and research integrity experts for contributing to this investigation.

The corresponding author, as the representative of all authors, has been given the opportunity to register their agreement or disagreement to this retraction. We have kept a record of any response received.

References

- [1] Y. Yang, "Psychological Motivation of Athletes' Physical Training Based on Deep Learning Model," *International Transactions on Electrical Energy Systems*, vol. 2022, Article ID 1962461, 11 pages, 2022.

Research Article

Psychological Motivation of Athletes' Physical Training Based on Deep Learning Model

Yining Yang ^{1,2}

¹Fujian Polytechnic Normal University, Fuqing, Fujian 350300, China

²Cavite State University, Manila 0900, Philippines

Correspondence should be addressed to Yining Yang; 3221010157@stu.cpu.edu.cn

Received 15 August 2022; Revised 8 September 2022; Accepted 21 September 2022; Published 3 October 2022

Academic Editor: Nagamalai Vasimalai

Copyright © 2022 Yining Yang. This is an open access article distributed under the Creative Commons Attribution License, which permits unrestricted use, distribution, and reproduction in any medium, provided the original work is properly cited.

In the field of sports training, two methods of physical and psychological monitoring are usually used to monitor the training process. Physiological index monitoring can objectively reflect the physical function of athletes, and there are many monitoring constraints. Psychological indicators can subjectively reflect the athlete's own state, and the monitoring is simple and easy. This paper mainly used the subjective perception of effort (RPE) and the profile of mood state (POMS) scales to track and monitor 20 nonprofessional athletes in a university track and field team. Based on the change of the same training volume, the change law and relationship between RPE and POMS, and the change law and relationship between RPE, POMS, heart rate, and blood pressure were analyzed. Finally, it was concluded that the athletes are feeling more and more about the amount of training, and the minimum value $P < 0.01$ showed a very significant difference, reflecting that the increase of training volume has a significant impact on the t -test value. The training volume has an impact on both the positive and negative dimensions of POMS, but the negative dimension reflects the training volume more clearly. There was a linear relationship between RPE and POMS subscales. RPE was not significantly correlated with positive emotions but positively correlated with negative emotions and TMD. The change trend was the same and the RPE grade increases; the blood pressure and systolic blood pressure also increased accordingly, and vice versa. The POMS negative dimension and TMD were the same as changes in blood pressure increase or decrease, and TMD was not related to heart rate. Scientific training has a large impact on the training of nonprofessional athletes, and whether the training volume is reasonable or not directly affects the qualitative change of athletes' physical functions. Therefore, it is particularly important to monitor the physiological and psychological indicators of nonprofessional athletes. The improvement of sports performance is the goal, and the improvement of physical function is the guarantee.

1. Introduction

The change of training volume not only has an impact on the physical indicators of athletes, but also has a corresponding impact on psychology. RPE is a person's subjective feeling, and POMS is a person's state of mind. Both of them can reflect the size of the training volume and have been applied in a large number of experiments. Different from the application of heart rate and blood pressure, it is rare to use the two for psychological monitoring and study changes in a period of time, and it lacks the aspect of monitoring the subjective factors of athletes themselves. Increasing the continuous time monitoring of the athlete's psychological level makes great theoretical sense. At present, there are

many studies on subjective effort perception and mood state profiles in the field of sports in China, but they are mainly used as means and tools for experimental research. It is mainly used in only one experiment and reflects the subjective feeling of effort and state of mind of the subjects at all times. The amount of training in sports training is one of the elements in formulating a training plan, and it is also the fundamental content of the implementation of the training plan. Scientific arrangement of training volume is the basic guarantee for the improvement of athletes' athletic performance.

Physical training can improve the physical fitness of athletes. Chronic dietary protein deficiency significantly alters the composition and content of polyunsaturated

fatty acids in tissues and body fluids. Aneta et al. believed that the nutritional factor that may reduce the negative impact of protein malnutrition is vitamin B2 because of its greater impact on lipid metabolism [1]. The purpose of the study by Grier et al. was to determine the effect of physical activity and physical fitness on the risk of running-related injuries in physically active young adults. Data on personal characteristics, PT, military fitness test scores, and injuries were collected through questionnaires [2]. The purpose of the LCBC study was to analyze morphological and functional changes in recruits following 12 weeks of physical activity. The exercise program includes running, strength, agility, and flexibility exercises. Finally, descriptive statistical processing was performed using mean, standard deviation, difference, and percentage [3]. Couto et al. believed that iodinated contrast media is the main cause of acute kidney injury in hospitals, and contrast media-induced acute kidney injury (CI-AKI) referred to the decline in renal function caused using iodinated contrast media. This was increasingly common in populations with risk factors [4]. Although all above believe that physical training is necessary, no specific experimental process is shown.

Deep learning is an important category in machine learning. Litjens et al. believed that convolutional learning networks with deep learning algorithms are rapidly gaining popularity as a method of medical image analysis. They reviewed the applications of deep learning in tasks, such as image classification, object detection, segmentation, and alignment, and provide an overview of the research in each application area [5]. Deep learning is rapidly becoming the state of the art, leading to improved performance in various medical applications. Shen et al. introduced the basics of deep learning methods and reviewed successful experiences in image alignment, anatomical and cellular structure detection, tissue segmentation, computer-aided diagnosis, and disease prediction [6, 7]. Oshea and Hoydis presented and discussed several new applications of deep learning at the physical level. They would develop a fundamentally new approach to designing communication systems as a holistic reconstruction project. The aim was to jointly optimize the transmitter and receiver elements in a single process [8]. The above scholars have relatively thorough research on deep learning, but they have not studied a certain aspect in a targeted manner.

Psychological monitoring and physiological monitoring are two necessary means to monitor training, but for nonprofessional athletes, physiological monitoring is very difficult to implement. In psychological monitoring, a paper psychological scale can be used to complete the monitoring of athletes. The psychological state has the characteristics of recall, and the monitoring time point is more flexible. Therefore, in the process of monitoring nonprofessional athletes, it is particularly important to find the relationship between psychological indicators and physiological indicators so that the two can complement each other. The innovation of this study is to determine the law and relationship between psychology and physiology by using the training volume as a medium.

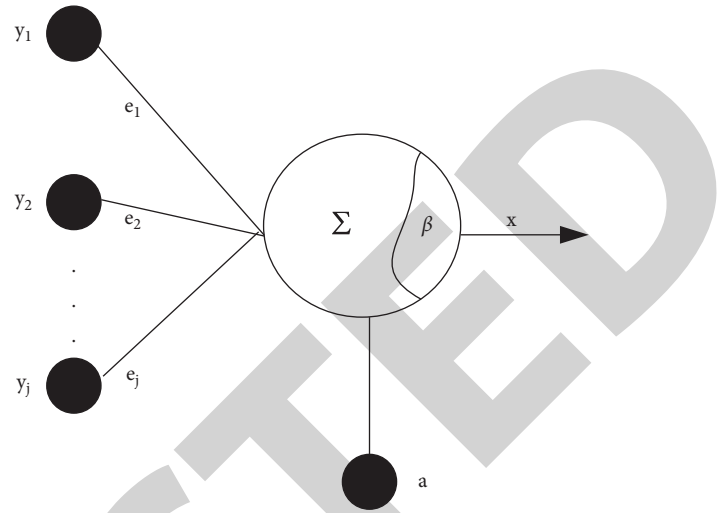


FIGURE 1: Perceptron cell model.

2. Human Motion State Recognition Based on Deep Learning

2.1. Classical Neural Networks. Various neural network structures can classify motion states, and their accuracy is the key to judge whether the network model can be applied in practice. Figure 1 shows the perceptron unit model, which is the basis of a type of artificial neural network [9].

Formula (1) shows the final result of the output, where y_j is the input of the j th perceptron and e_j is the connection weight of the j th neuron. It is a real constant; a is an offset to better control the output result [10]. β is the threshold, when the sum of the inputs needs to exceed a certain value, there would be a data output, and β is the condition used to judge whether the excitation is reached.

$$g = h \left(\sum_{j=1}^m (e_j y_j + a) - \beta \right). \quad (1)$$

Common activation functions include Sigmoid, Tanh, and ReLU, as shown in Figure 2.

It can be seen from Figure 2(a) that the sigmoid function maps the input value to the output value and compresses it between 0 and 1. In recent years, the sigmoid function has been used less and less, mainly because it has a great influence on the descending gradient of the function. The other is the ReLU function, whose graph is shown in Figure 2(b), and its Chinese meaning is the modified linear unit. Its mathematical definition formula is shown in formula (2). Compared with the sigmoid function and the Tanh function, the gradient descent obtained by the ReLU function converges faster [11].

$$h(y) = \max(0, y). \quad (2)$$

2.2. Convolutional Neural Networks. The convolutional neural network is also the first network structure to be successfully trained with multiple layers, which can share the

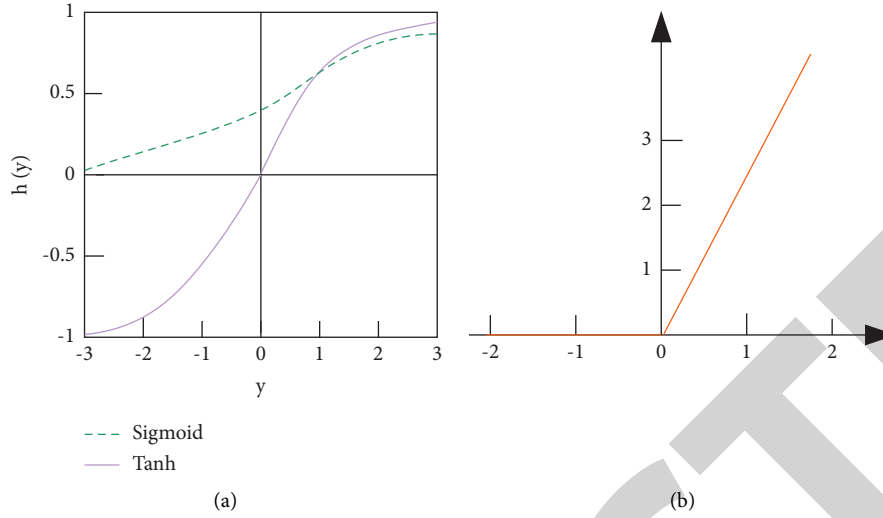


FIGURE 2: Three function images. (a) Sigmoid-Tanh function image. (b) ReLU function image.

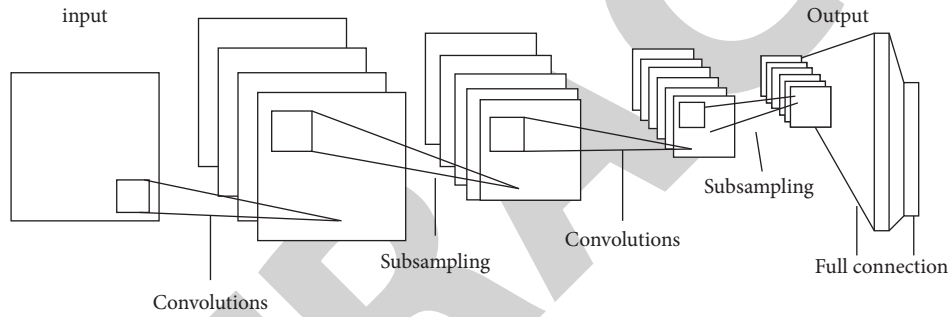


FIGURE 3: Convolutional neural network architecture.

number of parameters learned by using the spatial structure. Thus, the learning efficiency of the backpropagation algorithm is improved, and the complexity of the algorithm is reduced. Figure 3 shows the general structure of a convolutional neural network. There is no explicit requirement on the order of convolution and clustering, it can continue after the first convolution layer, or clustering can be done.

Of course, convolutional neural network also needs the support of mathematical theory, Formulas (3) and (4) show its learning process.

$$d_j = \alpha \left(\sum_{j=0}^m e_j * y_j + a \right), \quad (3)$$

$$q_j = \max(d_j). \quad (4)$$

Among them, e_j represents the weight of the j th layer, y_j represents the input of the j th layer, a represents the bias term, q_j represents the output of the j th layer, and α represents the activation function.

2.3. LSTM Neural Network. RNN performs well in signal processing, audio processing, and natural language processing, especially for time series data processing. Each

neuron can save the previous input information through internal components [12]. The structure diagram of RNN is shown in Figure 4; Figure 4(a) is the structure diagram of the RNN neural network, and Figure 4(b) is a schematic diagram of the expanded RNN neural network.

The gate structure and operation process of LSTM are shown in formulas (5)–(10). Formula (5) calculates the j_r of the value of the input gate at time r , and formula (6) calculates the memory state of the LSTM unit at time r .

$$j_r = \alpha_j (e_j \cdot [f_{r-1}, y_r] + a_j), \quad (5)$$

$$G_r = \alpha_d (e_d \cdot [f_{r-1}, y_r] + a_d). \quad (6)$$

The following formula calculates the h_r of the forget gate value at time r :

$$h_r = \alpha_h (e_h \cdot [f_{r-1}, y_r] + a_h). \quad (7)$$

The following formula calculates the D_r of the new state value of the state information at time r :

$$D_r = h_r * D_{r-1} + j_r * G_r. \quad (8)$$

Formulas (9) and (10) calculate the output values u_r and f_r of output gate and hidden layer information at time r .

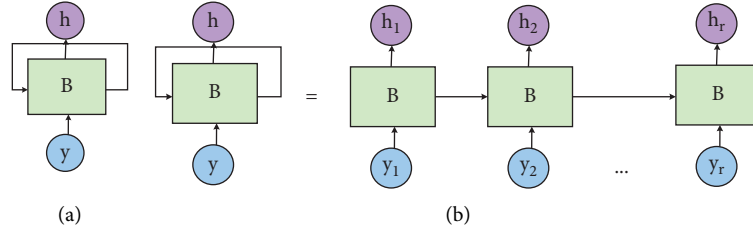


FIGURE 4: Structure diagram of RNN. (a) RNN neural network structure. (b) Schematic diagram of RNN neural network expansion.

$$u_r = \alpha_u(e_u \cdot [f_{r-1}, y_r] + a_u), \quad (9)$$

$$f_r = u_r * \alpha_r(D_r). \quad (10)$$

Among them, D_r represents the state of information transfer, f is the value of the hidden layer, α represents the activation function, and a represents the bias term.

2.4. Bi-LSTM Neural Network. Bi-LSTM, like LSTM, is also a variant of RNN. It is a bidirectional RNN neural network. This structure allows the information in the neural network to be used more effectively. The calculation process in two directions is shown in formula (11) and formula (12).

$$\overrightarrow{\text{forward}}_r = h(N_h Y_r + W_h \overrightarrow{f}_{r-1} + \vec{a}), \quad (11)$$

$$\overleftarrow{\text{backward}}_r = h(N_a Y_r + W_a \overleftarrow{f}_{r-1} + \vec{a}), \quad (12)$$

$$\text{output}_r = k\left(N\left[\overrightarrow{\text{forward}}_r, V_h + \vec{g}; \overleftarrow{\text{backward}}_r, V_a + \vec{g}\right] + d\right). \quad (13)$$

Among them, W , N is the weight matrix; a is the bias term; \rightarrow and \leftarrow represent the forward and backward transfer directions of the neural network, respectively, and h represents the activation function. Formula (13) represents the output result, V represents the weight matrix; g and d represent the bias term. N represents the joint function; k represents the new activation function; the value of $output_r$ is the score result, which is the score of a certain class. Since the LSTM unit is a variant of the RNN unit, one can directly replace the RNN unit with an LSTM, and the same is true for bidirectional RNN [13].

2.5. Bi-GRU Neural Network. In the bidirectional RNN neural network, for each neural network unit structure selection, this paper proposes two types, one is LSTM, and the other is GRU. The unit structure of the GRU is shown in Figure 5.

Formulas (14)–(17) show the calculation process of GRU. The process of taking a linear sum between the existing state and the newly computed state is similar to an LSTM cell. However, the GRU does not have any mechanism to control how exposed its state is, and the entire state is displayed every time.

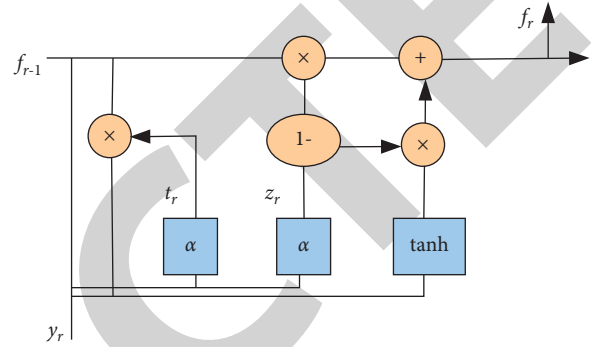


FIGURE 5: GRU neural network unit structure.

$$z_r = \alpha(e_z \cdot [f_{r-1}, y_r]), \quad (14)$$

$$t_r = \alpha(e_t \cdot [f_{r-1}, y_r]), \quad (15)$$

$$\tilde{f}_r = \tanh(e \cdot [t_r * f_{r-1}, y_r]), \quad (16)$$

$$f_r = (1 - z_r) * f_{r-1} + z_r * \tilde{f}_r. \quad (17)$$

e represents the weight, and t_r represents a set of reset gate values.

After using various neural networks to extract features, the next step is to classify the data, and the following formula is the softmax function.

$$q = \operatorname{argmax}_d q(x = d|y) = \operatorname{argmax}_d \frac{\exp(\text{output}_r)}{\sum_{g=1}^g \text{output}_r}, \quad (18)$$

where d is the class label, y is the sample feature, x is the label variable, g is the total number of classes, and $output_r$ is the output of each layer. It can be seen from this that softmax classification is a probability-based classification result [14]. The final result of softmax is the probability of identifying a certain data as each class in the current data, and the sum of the probability of classification results for a piece of data is added to 1.

There are two forms of regular expressions, $L1$ and $L2$ regular expressions, as shown in the following formulas for details.

$$D = D_0 + \frac{\eta}{n} \sum_e |e|, \quad (19)$$

$$D = D_0 + \frac{\eta}{2n} \sum_e e^2. \quad (20)$$

When using $L1$ regularization, the weight is reduced to 0 by a constant, and $L2$ is reduced by an amount proportional to e .

3. Psychological Analysis Based on Physical Fitness Training of Athletes

3.1. Objects and Methods

3.1.1. Research Objects. This paper selects 20 members of a university track and field team, namely, 10 boys and 10 girls.

3.1.2. Research Methods

Measurement Methods. RPE: the subjective feeling of effort directly monitors the subjects' subjective feelings. POMS: Mood Profiles can monitor the mood state of subjects over a period of time. Heart rate: the most sensitive indicator of training intensity; it is simple and easy to implement. Blood pressure: it monitors blood pressure changes before and after training to reflect training volume.

3.1.3. Measurement Steps

- (1) Psychological monitoring of RPE and POMS for 12 weeks was carried out on 20 athletes using RPE scale and POMS scale.
- (2) RPE is monitored every day from the beginning of training. The specific time of the test is to be completed within 10 minutes after the end of the training every day. The test is completed by me throughout the whole process.
- (3) POMS is monitored weekly from the 1st week to the 8th week of training; the test is carried out before the start of the next training week, and every Wednesday and Saturday from the 9th week to the 12th week. The scales were distributed by me half an hour before training on the day of monitoring. The athletes fill in the form based on their first feelings, and then they receive the scale and archive it.
- (4) Heart rate and blood pressure were monitored every Wednesday and Saturday from the 9th week to the 12th week. The heart rate and blood pressure test time are to complete two monitorings within 10 minutes before and after training.
- (5) Weeks 9 to 12 are 4 weeks before the competition. The main purpose of increasing the number of monitorings in the 4 weeks before the competition is to fully grasp the psychological and physiological changes of the athletes throughout the training week through the monitoring in the middle and end of the last 4 training weeks.
- (6) Sports performance is tested monthly, the training plan is formulated according to the monthly plan, and the 1-month plan is 4 weeks.
- (7) During the monitoring period, no psychological and physiological intervention is required.

3.1.4. Mathematical Statistics. Using SPSS19.0 statistical software as a data statistical tool, the RPE and POMS of different training cycles were compared. The F -test was used to conduct an overall test on the psychological and physiological indicators of male and female athletes. t -test was used to compare the differences of RPE values from weeks 1 to 12. Differences were compared between the four subscale values, total and TMD values of POMS in weeks 1–12; heart rate was compared between weeks 9 and 12. Differences in blood pressure changes were compared between weeks 9 and 12; differences in RPE values were compared between weeks 9 and 12. Differences were compared between the four subscale values and total and TMD values of POMS tested in weeks 9–12. Pearson's coefficient was used to analyze the regularity of heart rate variability, RPE, and POMS in weeks 9–12. The regularity analysis of blood pressure changes, RPE, and POMS in the 9th to 12th weeks was carried out in the experiment. Regularity analysis was performed on the four subscale values and total and TMD values of RPE and POMS from 1 to 12 weeks.

3.2. Results

3.2.1. Difference Test of Psychological Indicators. Table 1 is the test table for the differences of POMS components and RPE of male and female athletes.

As can be seen from Table 1, the differences between the four subscale values of POMS, the total score, the TMD value, and the RPE value of 10 boys and 10 girls in the untrained state were tested respectively. Among them, stress, fatigue, and total score in POMS were $P < 0.05$. Therefore, in the data analysis, the total score of stress, fatigue, and POMS cannot be compared for the overall value of 20 subjects. Other values can be analyzed and compared for a population [15].

3.2.2. Comparison of Differences in RPE Grades from Weeks 1 to 12. Table 2 is the test table of the difference before and after RPE measurement.

As can be seen from Table 2, by comparing the difference between the weekly measurement value of RPE and the measurement value on March 31, there was a significant difference in the weekly measurement value from April 18 to June 7 ($P < 0.01$). This shows that when the training volume increases, the subjective feeling of athletes is obvious, and some subjects have the highest value of 17 (very difficult), and the impact of training volume increase on individual subjects may reach the limit [16]. There was no significant difference in the other weeks, indicating that the athletes have adapted to the training volume.

3.2.3. Comparison of the Correlation between RPE and POMS in Weeks 1–12. Table 3 shows the correlation statistics between RPE and POMS subscales.

It can be seen from Table 3 that the correlation between RPE and POMS subscales is compared, and RPE is strongly correlated with depression and panic ($0.6 < r < 0.8$). There was a

TABLE 1: Difference test table of POMS components and RPE for male and female athletes.

Index	Male M ± SD	Female M ± SD	F	P	
POMS	Nervous	2.33 ± 1.85	5.50 ± 3.71	0.211	0.021
	Fatigue	3.22 ± 2.13	4.00 ± 3.90	0.175	0.012
	Energy	10.67 ± 5.87	12.00 ± 3.98	1.819	0.222
	Panic	2.56 ± 1.95	4.38 ± 3.31	0.287	0.051
	Total score	30.33 ± 7.53	47.00 ± 18.29	0.166	0.010
	TMD	97.00 ± 17.59	106.50 ± 18.89	0.680	0.299
RPE	11.44 ± 0.84	11.67 ± 1.1	0.778	0.365	

TABLE 2: Difference test table before and after RPE measurement.

Date	RPE M ± SD	t	P
3.31	11.52 ± 0.95		
4.18	12.96 ± 1.05	5.469	0.310
5.6	13.29 ± 1.73	5.149	0.000
5.21	13.33 ± 1.37	5.599	0.000
6.7	11.96 ± 0.67	1.589	0.000
6.21	11.11 ± 0.85	-1.809	0.078
7.5	11.94 ± 0.68	1.341	0.188

TABLE 3: Statistical table of correlation between RPE and POMS subscales (Pearson's coefficient r).

	Anger	Depression	Energy	Panic	Mood	TMD	RPE
Anger		0.41	0.31	0.56	0.43	0.50	0.31
Depression			0.43	0.76	0.49	0.78	0.65
Energy				0.26	0.70	0.20	0.12
Panic					0.35	0.68	0.60
Mood						0.18	0.11
TMD							0.58

TABLE 4: Test table for differences in heart rate and blood pressure between male and female athletes.

6.14	Male M ± SD	Female M ± SD	F	P
Heart rate before training	77.90 ± 11.03	73.42 ± 8.79	2.057	0.196
Heart rate after training	104.90 ± 14.68	102.43 ± 10.88	1.424	0.344
Systolic blood pressure before training	124.90 ± 14.47	119.86 ± 8.86	2.822	0.109
Diastolic blood pressure before training	84.20 ± 15.38	74.00 ± 6.13	4.766	0.035
Systolic blood pressure after training	126.70 ± 17.72	122.28 ± 8.37	9.737	0.005
Diastolic blood pressure after training	77.90 ± 10.04	79.43 ± 4.56	4.502	0.040

moderate correlation with TMD of $0.4 < r < 0.6$, a weak correlation with anger of $0.2 < r < 0.4$, and a very weak correlation with energy and mood of $0 < r < 0.2$. The correlation between TMD and POMS subscales was compared. Among them, TMD was strongly correlated with depression and panic ($0.6 < r < 0.8$), moderately correlated with anger ($0.4 < r < 0.6$), and weakly correlated with energy and mood ($0.2 < r < 0.4$). The rest of the subscales are highly correlated with the same attribute and generally less correlated among different attributes [17].

3.2.4. Values and Comparison of Indicators in Weeks 10–12

(1) *Difference Test of Heart Rate and Blood Pressure.* Table 4 is a test table about the difference in heart rate and blood pressure between male and female athletes.

It can be seen from Table 4 that the difference test is carried out through the physiological indicators of male and female athletes. Among them, the diastolic blood pressure before training, systolic blood pressure after training, and diastolic blood pressure after training $P < 0.05$ cannot be used as a regular analysis of the overall data of men and women. Other groups of data can be compared as a whole.

(2) *Comparison of Heart Rate Differences in Weeks 10–12.* Figure 6 is a comparison chart of changes in heart rate before and after training. As shown in Figure 6(a), the weekly measurement of heart rate before training was compared with the measurement value on June 14, and there was no significant difference. The average was about 79 times/min, showing a downward-up-down trend, and the change range was small.

As shown in Figure 6(b), the weekly measurement of heart rate after training was compared with the

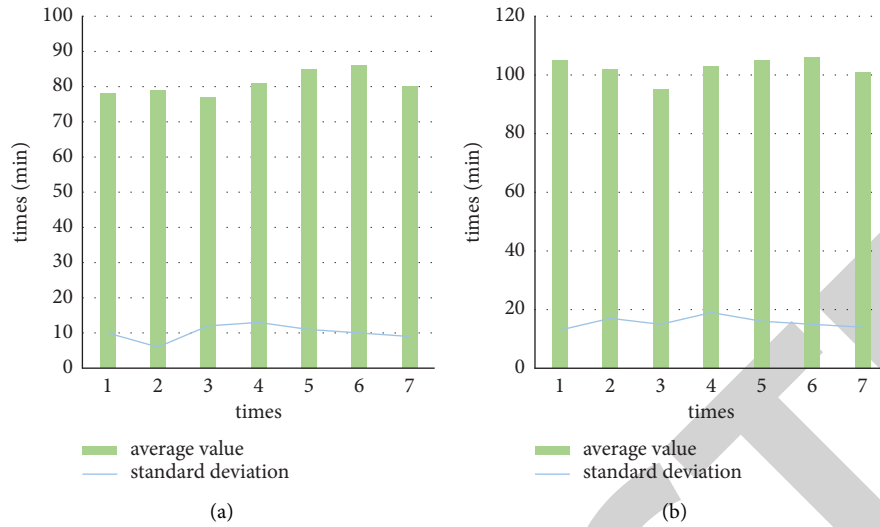


FIGURE 6: Comparison of heart rate changes before and after training. (a) Change trend of heart rate before training in weeks 10-12. (b) Change trend of heart rate after training in weeks 10-12.

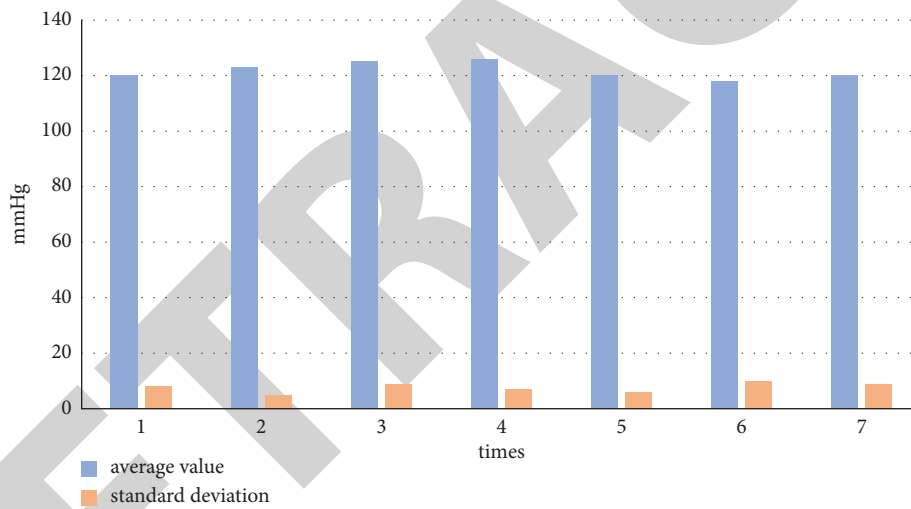


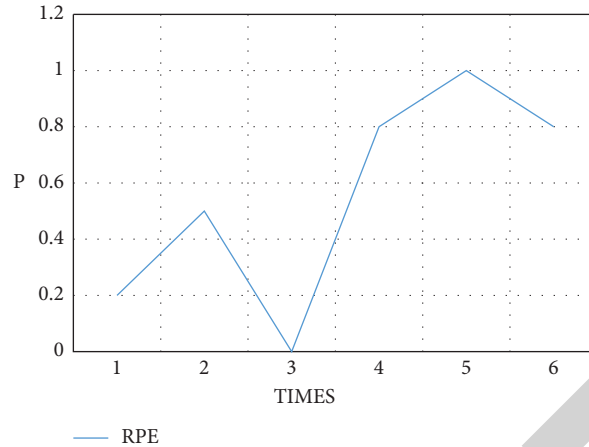
FIGURE 7: Trend of systolic blood pressure before training in weeks 10-12.

measurement value on June 14, and there was a significant difference on June 21 ($P < 0.05$). There was no significant difference in the rest, and the average value was around 104 times/min, showing a downward-up-down trend with a small change.

(3) *Comparison of Blood Pressure Differences in Weeks 10-12.* Figure 7 is the trend chart of systolic blood pressure before training in weeks 10-12. The weekly measurement of systolic blood pressure before training was compared with the measurement value on June 14, and there was no significant difference. The overall value was within the normal range, but the individual data fluctuated greatly, and the blood pressure value of the throwing athletes was higher. The systolic blood pressure before training showed an increasing-decreasing trend [18].

(4) *Comparison of RPE Grade Differences in Weeks 10-12.* Figure 8 is a graph of the change trend of the P value of RPE from weeks 10 to 12, and the weekly measured values of RPE are compared with the measured values on June 14th. The significant difference on June 25 was $P < 0.01$, indicating that the impact of training volume on RPE became greater, and there was no significant difference at other times.

(5) *Comparison of the Correlation between Psychological Indicators and Physiological Indicators.* As shown in Table 5, the correlation analysis is carried out through psychological indicators and physiological indicators. The positive and negative values only represent the size of the determined basic indicators, and the absolute value of the numerical value represents the degree of correlation. Among them, heart rate before training was strongly correlated with TMD

FIGURE 8: Trend of P value of RPE in weeks 10–12.TABLE 5: Statistical table of correlation between physiological indicators and psychological indicators in the 10th to 12th weeks (Pearson's coefficient r).

	Anger	Depression	Energy	Panic	Mood	TMD	RPE
Heart rate before training	0.53	0.53	-0.60	0.15	0.42	0.62	-0.14
Heart rate after training	-0.39	-0.01	0.08	0.09	-0.52	-0.15	-0.16
Systolic blood pressure before training	0.79	-0.53	0.09	-0.51	-0.55	-0.52	0.61

($0.6 < r < 0.8$), and systolic blood pressure before training was strongly correlated with RPE and anger ($0.6 < r < 0.8$). There was a moderate correlation between heart rate and anger, depression, and energy before training ($0.4 < r < 0.6$) and a moderate correlation between heart rate and emotion after training ($0.4 < r < 0.6$). Pretraining systolic blood pressure was moderately correlated with depression, panic, mood, and TMD ($0.4 < r < 0.6$).

3.2.5. Comparison of the Influence of Training Volume on Sports Performance in Weeks 1–12. Sports performance is an objective indicator that reflects the training effect of athletes, and it can also reflect the changes in the physical function of athletes after training for a certain period of time. Physical performance changes with the amount of training in each phase of the training program. When evaluating the impact of training volume on the subscales of RPE and POMS, the impact of changes in an athlete's physical function on changes in athletic performance should be considered [19].

The sports performances of 4 athletes were randomly selected, 1 for men's 100 m, 1 for men's 400 m, and 2 for women's 400 m. Sports performance improved with the increase of training volume in the first eight weeks but did not decrease with the decrease of training volume in the last four weeks. It shows that with the continuous deepening of sports training, the physical function of athletes has improved, and the sports performance has also made breakthroughs. The results are shown in Table 6.

The results in March are the sports results before training, the results in May and June are the sports results in training, and the results in July are the results of participating in the Provincial University Games. The first three

TABLE 6: Statistical table of changes in sports performance of 4 athletes.

Project	3.31	5.26	6.28	7.20
Men's 100 m	11''45	11''36	11''40	11''21
Men's 400 m	56''21	53''92	54''50	53'' 67
Women's 400 m (1)	1'13''60	1'11''67	1'09'' 80	1'09''65
Women's good 400 m (2)	1'22''50	1'21''00	1'14''50	1'12''20

results are hand-timed, and those of the Provincial University are electronic-timed.

3.3. Data and Discussion

3.3.1. Analysis of the Regularity of Training Volume and RPE and POMS in Weeks 1–12. The training program is based on a 4-week 1-month cycle. The first 4 weeks are the intervention period, the training volume is moderate and the intensity is medium and small, the weekly training load changes are small, and the weekly training content is similar. The purpose is to allow the athlete to develop their own adaptation to the training. The second 4 weeks is the strengthening period, the training volume is large and the intensity is large, the weekly training load changes greatly, and the training content is similar. The purpose is to improve the performance of the athletes; the third 4 weeks is the maintenance period, the training volume is reduced to the middle, and the intensity is moderate, and the weekly training load changes are moderate. The purpose of training is to keep the athlete in physical condition to participate in the competition. Therefore, the trend in overall training volume is medium-high-medium-high. The training

schedule is designed to fluctuate in training volume within each monthly cycle of training to prevent overfatigue. There are also changes in the training volume in the weekly training plan to ensure that the athletes are in the best physical and psychological state [20].

(1) Analysis of Training Volume and RPE Law in Weeks 1–12. Variations in training volume are performed strictly in accordance with the arrangements of the training plan. It can be seen from the change trend of the average value and standard deviation of RPE that the value of the first 4 weeks from the beginning of training gradually increased and then decreased, and the highest value was around 12. This shows that the athletes themselves feel that the training volume is gradually increasing, but the training volume is not large. In the second 4 weeks, the value has been kept at around 13.5, and the athletes themselves feel that the training volume has always maintained a certain height, but there is tension and relaxation. There is a gradual adaptation process. In the last 4 weeks, the value decreased significantly but maintained a certain level of about 11.5. The athletes felt that the training volume was reduced and maintained a certain level. The change trend of the average RPE is basically the same as the change trend of the training volume in the training plan, and the change of the training volume can affect the change of the average RPE.

Beginning in the first 4 weeks of training, the t -test value is a process from high to bottom, and the decline is very obvious. The athletes are feeling more and more about the amount of training, and the minimum value $P < 0.01$ shows a very significant difference, reflecting that the increasing process of training volume has a significant impact on the t -test value. The second 4-week t -test value was a process of steady and then rising, and the steady value was always less than 0.01. Athletes have a very large degree of perception of training volume, reflecting that the process of continuous large training volume has a more significant impact on the t -test value. The third 4-week t -test value was a process of increasing and then decreasing, but there was no difference in the value, and the impact of training volume on the t -test value became smaller. The change of training amount in the training plan reflects the change of t -test value, and there is an inherent law between the change of training amount and the change of t -test value.

From the above comparison, it can be seen that the change of training amount can have an impact on the change rule of the average value of the RPE grade and the change trend of the t -test value [21]. The change law of the influence of training amount on the t -test value can better reflect the overall change law of RPE, and the degree of reflection is obvious, and the numerical expression is comprehensive, but the change range is general.

The reflection of RPE is subjective, and it can directly reflect the athlete's tolerance to a certain training volume. At the beginning of training, although the training volume is not large, the general reactions of athletes are relatively strong. This is due to the fact that during the transitional stage from no training to training, the stimulation of the training volume to the athlete is very obvious, so the RPE level would change significantly. In the mid-term stage,

when the training volume is the largest, the value of RPE is generally high but tends to be stable. It shows that athletes have adaptability to training, and the increase of training volume is also the process of athletes improving their own abilities. Athletes' physical function is at a high level, and this stage is also the fastest stage of sports performance improvement. In the early stage of the game, the RPE is also in a stable state. Although the training volume is larger than that at the beginning, the RPE level is similar to it. This also shows that the athletes have adapted to the current training volume, the level of physical function has improved, and the feeling of the increase in training volume is not obvious.

(2) Analysis of Training Volume and POMS Law in Weeks 1–12. The positive dimension of POMS can reflect the athlete's enthusiasm for training, and the change of training volume has an obvious effect on the change of the positive dimension. At the beginning of the training, the overall value was very low and the range of changes was large, while the value was higher and more stable when the training volume increased in the mid-term, and the decrease in the value in the early stage of the game was also very stable. This shows that changes in training volume can cause changes in the positive dimension. However, athletes' attitude towards training is proactive. From no training to excessive training, the athlete's initiative declines rapidly, and oppositional emotions appear, which recover after a period of adaptation.

The negative dimension of POMS is the main indicator reflecting the mental fatigue of athletes, and it is also the main factor of TMD change. The value of negative dimension is generally high when the training volume is not large in the early stage of training. In the middle of the training, the training volume is the largest, but the negative dimension value decreases slightly, and the change range is small and stable. It can be seen that from no training to overtraining is the most prone to fatigue stage. The fatigue response is not obvious when the training volume is the largest, and the influence of the training volume before the competition on the mental state of the athletes is not a decisive factor. The stress of the game is the main factor, which has a great influence on the performance of the game.

(3) RPE and POMS Relationship in Weeks 1–12. Changes in training volume can affect the values of each subscale of RPE and POMS, and the changes in the mean and standard deviation of the two have the same place. The change trend of RPE is almost the same as that of POMS negative sentiment and TMD and partly the same as that of positive sentiment. Although changes in values can be found in the trends, they do not fully reflect the overall values. Therefore, the t -test values of each subscale of RPE and POMS were used to compare the relationship between the two. Through the comparative analysis of the relationship between the subscales of RPE and POMS, the relationship between the two is very close. Using the relationship between the RPE and the negative dimension subscale at various stages of training can directly show the impact of training volume on athletes. Changes in RPE values can reflect changes in the negative dimension of POMS.

3.3.2. *Analysis of the Regularity of Training Volume and Physiological Indicators and Psychological Indicators in the 10th to 12th Weeks.* The last 4 weeks are 4 weeks before the competition, and the training volume is medium to high in the training plan, but the training volume is different every week. The arrangement is a small amount of training before a large one. The main purpose is to keep the athletes in the state to cope with the competition, maintain their personal best results, and be able to further improve.

(1) *Analysis of Training Volume, Heart Rate, and Blood Pressure in Weeks 10–12.* From the mean and standard deviation of the data, it can be seen that the heart rate before training is a process of increasing and decreasing slowly, and the athletes' basal heart rate fluctuates. After training, the heart rate is also a process of increasing and decreasing slowly, and the recovery of the athlete's heart rate is slower. Systolic blood pressure increases and then decreases before training. The average values of the above physiological indicators can reflect the changes in training volume.

It can be seen from the overall *t*-test value that the heart rate first decreased and then increased before training, and the heart rate increased and decreased after training. The change trend of the two in the second two weeks was clearly opposite, indicating that the training volume played a great role in the change of heart rate. The systolic blood pressure decreased before training and then gradually increased, indicating that the impact of training volume on blood pressure is also more significant. The degree of change is as follows: heart rate after training > heart rate before training > systolic blood pressure before training.

The change of heart rate before and after each training can objectively explain the change of the athlete's physical function and reflect the athlete's physiological fatigue state. The heart rate changes before and after training hours are synchronous, and the changes in heart rate before and after training become larger, and vice versa. When the training volume is large, the two change in opposite directions; one becomes larger and the other becomes smaller. This also shows that there is a large gap between the heart rate changes before and after each training, and the heart rate changes when the training volume is small, and the body recovers quickly. When the training volume is large, the heart rate change increases and the body recovers slowly.

Blood pressure is another physiological indicator that effectively reflects the changes of athletes' physical functions, and the impact of training volume on blood pressure is also significant. The change trend of systolic blood pressure before training is the same, indicating that the physical function is in good condition and recovers quickly without fatigue. When the training volume is large, the trend of systolic blood pressure before training is opposite, which means that the recovery of body function is slow and prone to fatigue.

(2) *Analysis of Training Volume and RPE Law in Weeks 10–12.* The training volume also changed in the last 4 weeks, showing a trend of more and then less. The change trend of the mean and standard deviation of RPE can be seen from

the influence degree of training volume, and the change range is small. In the case of medium and high training volume, the RPE of athletes did not change significantly, indicating that most athletes have adapted to the current training volume.

The *t*-test value changed from a small fluctuation in the tenth week to a large fluctuation in the last two weeks, and the change trend was obvious and the change range was large. This can clearly reflect the size of the training volume, which is proportional to the same trend as the training volume. The main factor is that the value of the basic index is too large, but it does not affect the comparison of the change law.

The prematch RPE changes closely with the training volume. The reason for the small change is that after the physical function of the athlete is improved, the response to the stimulation of the training volume is not so strong, which indicates that the athletic ability of the athlete is also improved.

(3) *Analysis of Training Volume and POMS Law in Weeks 10–12.* The effect of training volume on POMS value can be seen such that the average value of each subscale of negative emotion in the last 4 weeks is too large. In particular, the average value of TMD is obvious, the average value of positive emotion is small, and the standard deviation changes greatly. It shows that the athletes' state of mind tends to be fatigued in the last 4 weeks and further indicates that the main factor affecting the athletes' state of mind is the stress of competition when the training volume is not the largest.

The overall change trend of the *t*-test value of each subscale of POMS and TMD was the same, which was a process of recovery from insignificant to significant, but the change of positive emotion was small. This shows that the athletes maintain a good positive state, and the negative emotions and TMD change greatly. This shows that the precompetition mood reflects the training volume mainly from negative emotions. The change range of each subscale is as follows: panic > depression > TMD > anger > energy > mood.

4. Conclusion

Psychological monitoring and physiological monitoring are two necessary means of monitoring training. Based on the scientific arrangement of training volume, this study conducted a 12-week psychological monitoring on 20 athletes and analyzed the changes in RPE, POMS, heart rate, and blood pressure during the entire training process. Through comparative analysis, it is concluded that the RPE grade can clearly reflect the impact of training volume on athletes. Only when the physical function of the athlete is not significantly improved, can it accurately reflect the athlete's tolerance to the regular changes in training volume. The *t*-test value is a process from high to bottom, and the decline is very obvious. The athletes are feeling more and more about the amount of training, and the minimum value $P < 0.01$ shows a very significant difference, reflecting that the

Retraction

Retracted: Evaluation Method of Street Green Landscape Viewing Degree Based on Machine Learning

International Transactions on Electrical Energy Systems

Received 28 November 2023; Accepted 28 November 2023; Published 29 November 2023

Copyright © 2023 International Transactions on Electrical Energy Systems. This is an open access article distributed under the Creative Commons Attribution License, which permits unrestricted use, distribution, and reproduction in any medium, provided the original work is properly cited.

This article has been retracted by Hindawi, as publisher, following an investigation undertaken by the publisher [1]. This investigation has uncovered evidence of systematic manipulation of the publication and peer-review process. We cannot, therefore, vouch for the reliability or integrity of this article.

Please note that this notice is intended solely to alert readers that the peer-review process of this article has been compromised.

Wiley and Hindawi regret that the usual quality checks did not identify these issues before publication and have since put additional measures in place to safeguard research integrity.

We wish to credit our Research Integrity and Research Publishing teams and anonymous and named external researchers and research integrity experts for contributing to this investigation.

The corresponding author, as the representative of all authors, has been given the opportunity to register their agreement or disagreement to this retraction. We have kept a record of any response received.

References

- [1] T. Wang, M. Liu, and W. Huang, "Evaluation Method of Street Green Landscape Viewing Degree Based on Machine Learning," *International Transactions on Electrical Energy Systems*, vol. 2022, Article ID 2729408, 9 pages, 2022.

Research Article

Evaluation Method of Street Green Landscape Viewing Degree Based on Machine Learning

Tieming Wang,¹ Mengyu Liu²,^{ORCID} and Wenhua Huang³

¹Hualu Engineering & Technology Co., Ltd., Xi'an 710065, Shaanxi, China

²School of Computing and Artificial Intelligence, Southwestern University of Finance and Economics, Chengdu 611130, Sichuan, China

³School of Design, Xianyang Normal University, Xianyang 712000, Shaanxi, China

Correspondence should be addressed to Mengyu Liu; 2019225029947@stu.scu.edu.cn

Received 23 August 2022; Revised 9 September 2022; Accepted 19 September 2022; Published 30 September 2022

Academic Editor: Nagamalai Vasimalai

Copyright © 2022 Tieming Wang et al. This is an open access article distributed under the Creative Commons Attribution License, which permits unrestricted use, distribution, and reproduction in any medium, provided the original work is properly cited.

Urban streetscape is a complex and multifaceted landscape system, which is an important part of urban public space system. With the acceleration of the urbanization process, the connotation of street landscape is becoming more and more abundant. It not only has natural and social attributes but also bears the function of protecting the urban ecological environment. However, in recent years, due to the dramatic increase in the size of the urban population, more and more problems have appeared in urban road landscape. To this end, relevant government departments continue to update the design of urban streets and accelerate the construction of urban street landscapes, but urban streets still have problems in terms of function and environment. The viewing degree of street green landscape is also less and less in line with people's aesthetic needs, which is difficult to meet people's life and spiritual needs. In order to change this situation, this paper combined machine learning with the evaluation method of street green landscape viewing degree and conducted experiments on it based on machine learning. The experimental results showed that the evaluation method of street green landscape viewing degree based on machine learning not only made the city more beautiful but also improved the ecological environment of the city. The air quality of the city was improved by 20.96%, which was supported and loved by the general public.

1. Introduction

In recent years, the government has vigorously promoted the creation of ecological cities, one of which is the green road. However, with the acceleration of urbanization, many planning and design efforts have gone wrong. In addition, the evaluation method of street green landscape viewing degree has not been updated, so the traditional evaluation method is still used for street landscape viewing degree, which is very unfavorable to the design and construction of street landscape. In order to solve these problems, this paper studied the evaluation method of street green landscape viewing degree based on machine learning.

The research on the evaluation method of street green landscape viewing degree has been very rich, and many experts and scholars have carried out research on it: In order

to improve the quality level of the campus green space landscape and obtain the satisfaction of the green space landscape, Xiang proposed to use the comprehensive evaluation method to construct five levels of urban greening based on the analysis of the current situation of urban greening and used seven evaluation factors to evaluate the green space landscape. [1]. Xunfan took six residential areas as the research objects and used the analytic hierarchy process to establish the evaluation index system of plant landscape in residential areas from the aspects of aesthetic effect, ecological function, leisure service, etc, as well as used the judgment matrix to calculate the index weight [2]. The evaluation criteria of traditional urban park landscape evaluation methods are mostly flood control effect and commercial demand, and the index evaluation is not comprehensive. Therefore, Shi et al. introduced the analytic

hierarchy process to evaluate the urban park landscape and analyzed the evaluation methods of urban landscape and urban park landscape, as well as selected infrastructure, landscape aesthetic level, natural ecology, and social culture as the evaluation indicators of urban park landscape [3]. In order to improve the visual landscape quality of urban road greening, Li and Weng used the analytic hierarchy process to conduct a comprehensive evaluation of greening landscape aesthetics on the greening landscape of an urban street to achieve the weight of each evaluation factor. It was calculated that in the defined standard layer, the most important factor was the art of color matching [4]. As resource conservation, environmental protection and people's health have been paid attention to by the whole society, green building of high-rise buildings has become an irresistible trend. In order to accurately evaluate the green construction evaluation level of high-rise buildings, Tang and Chen used the cloud model to achieve qualitative and quantitative conversion and established a comprehensive evaluation level by drawing a comprehensive cloud map [5]. Considering the characteristics of ordinary highways without intermediate zones, in order to better evaluate the greening level of highways and study the greening landscape of highway roads, Yuan et al. used the literature review and comprehensive analysis method to establish a comprehensive evaluation model through the analysis of the highway greening function and further verified the reliability of the evaluation index system [6]. In order to explore the impact of ecological environment evaluation methods on the overall planning environment of towns, Chong et al. used the comprehensive evaluation method to evaluate the carrying capacity of regional ecology and analyzed the pattern changes of regional landscapes by using landscape ecology [7]. It can be seen that the research results on the evaluation method of street green landscape viewing degree have been very mature.

In recent years, due to the rapid development of machine learning and the wider application of machine learning, many people have studied it: Raissi and Karniadakis proposed a new paradigm for learning partial differential formulas from data and introduced hidden physical models. They were essentially data-efficient learning machines capable of expressing fundamental physical laws using non-linear partial differential formulas, which could be applied to learn partial differential formulas and discover problems in system identification or data-driven [8]. State-of-the-art light and electron microscopes are capable of acquiring large image datasets, but quantitative evaluation of data often involves manual annotation of structures of interest and this process is time-consuming. To overcome this problem, Ignacio investigated a new machine learning tool that could train a classifier and automatically segment the remaining data [9]. Machine learning is a technique used to identify patterns that can be applied to medical images. Although it is a powerful tool that can aid in medical diagnosis, it can also be misused. To solve this problem, Erickson et al. used machine learning algorithms to systematically learn and analyze image features to classify images [10]. To quantitatively investigate how machine learning models leak



FIGURE 1: Schematic diagram of green streets.

information from individual data records, Shokri et al. performed membership inference on the target model and used the machine-learned inference model to identify the prediction difference between the trained and untrained inputs by the target model [11]. To meet people's needs, next-generation wireless networks must support ultrareliable, low-latency communications, and provide real-time, intelligent management to many Internet of Things devices in a highly dynamic environment. In this context, Chen et al. provided a comprehensive tutorial and introduced the main concepts of machine learning, especially the potential application of artificial neural networks in wireless communication [12]. Currently, methods for predicting cardiovascular risk fail to determine whether some people would benefit from preventive treatment. To solve this problem, Weng et al. was committed to investigating whether machine learning could improve the accuracy of cardiovascular risk prediction by exploiting the complex interactions among risk factors [13]. In order to enhance the resilience of machine learning, Bhagoji A N proposed and studied strategies that combined various data transformations, and reduced dimensionality by analyzing "anti-whitening," as well as evaluated and demonstrated the feasibility of linear transformation of data as a defense mechanism during the classification and training phases [14]. It can be seen from this that the research results on machine learning are very mature, and there are people studying it in various aspects.

It can be seen from this that the research results on machine learning and the evaluation method of street green landscape viewing degree have been very rich, but few people have combined them for research, which has led to a very lack of research in this area. In order to enrich the research content in this area and provide a more practical and effective reference for the evaluation method of street green landscape viewing degree, this paper studied the evaluation method of street green landscape viewing degree based on machine learning.

2. Evaluation Method of Street Green Landscape Viewing Degree Based on Machine Learning

2.1. The Concept of Green Street. At present, the definition of green street is as follows. Green street refers to the street in the urban landscape that conforms to the principles of landscape ecology, which can provide urban residents with a

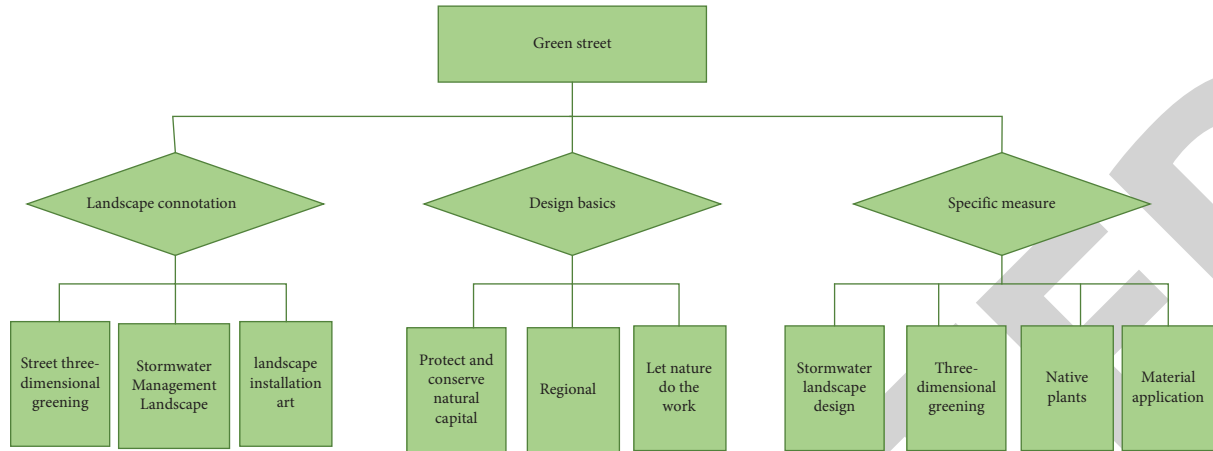


FIGURE 2: Landscape connotation, design principles, and specific measures of green streets.

streetscape for living and leisure. It also has special environmental benefits compared to traditional streets [15]. Figure 1 is a schematic diagram of a green street. As shown in Figure 2, the connotation of green street landscape is centered on the rainwater management landscape, which includes street greening, landscape installation art, and other landscape connotations. The basic principles of green street construction include preservation and conservation of natural capital, regionality, and natural work. The specific methods include urban rainwater landscape design, three-dimensional greening, native plants, and material application.



FIGURE 3: Plan of Pudong activity city.

2.2. The Function of Green Street. The green street has many special functions such as urban sediment and flood management, air purification, temperature regulation, dust and noise avoidance, and energy conservation. It is an important part of the urban ecosystem and the integration of ecology, function, and aesthetics in a street pattern adapted to the landscape. Green streets not only contain the natural, social, and human nature of streets in the traditional sense but also play a role in protecting the urban ecological environment. The traditional street design just beautifies and embellishes the urban environment, while the green street conforms to the current trend of sustainable development and low-carbon development, which is a “green” street with real practical value [16]. Figure 3 shows the plan of an event city in Pudong, whose green streets are a combination of ecology, function, and aesthetics. A green street is also a functional aggregate, with multiple functions such as urban transportation, regional characteristics representing the city, and urban stormwater management. As shown in Figure 4, in the reconstruction and design of green streets, it is necessary to take the hydrological core and take the green street itself as a link of ecology, region, and humanities so as to form a very stable composite ecosystem.

2.3. The Importance of Streetscape. Streetscape is a key factor in the external image of a city and is the basic structure of urban planning and planning. Urban streets are not only

roads for urban traffic but also important spaces for residents’ activities [17]. The types and scales of urban streetscapes are diverse, and the behavior of observers is also quite different. As shown in Figure 5, urban streets as public spaces can add convenience and fun to people’s lives. As the goal of urban street development, green street has the characteristics of multidisciplinary and multi-influencing factors. A scientific evaluation system is needed to determine the development degree of green street. Therefore, based on machine learning, this paper develops a method for evaluating the viewing degree of street green landscape, which plays a role in evaluating and monitoring the development of urban green streets, and can effectively promote the sustainable development of urban green streets [18].

2.4. The Role of Machine Learning in Street Landscape Assessment. In the field of streetscape assessment, traditional intelligent technology requires manual design of operating rules, while machine learning technology has a strong learning ability, which can capture hidden rules and predict unknown data. The streetscape assessment work is to find out the law of its change through the analysis of the site condition and then to intervene and guide it through the method of planning and design so as to make it develop in a specific direction. Therefore, machine learning has great

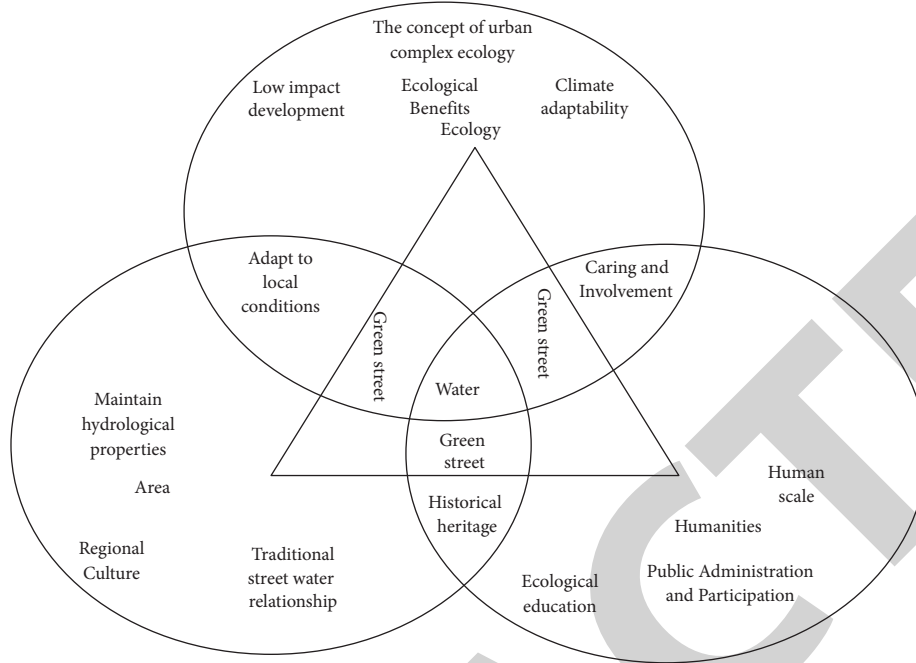


FIGURE 4: Functions of green streets.



FIGURE 5: Schematic diagram of urban green streets.

potential in the field of street landscape evaluation [19]. As shown in Figure 6, machine learning analyzes all aspects of the site and makes appropriate planning to build a beautiful streetscape. In addition, machine learning is a method that is good at inducing rules from a large amount of data and can solve various problems in different road landscape planning and design. As shown in Figure 7, according to the three stages such as information extraction, analysis and evaluation, and planning and design in the workflow of street landscape planning and design, the application methods of machine learning in street landscape can be divided into site information extraction, landscape analysis and evaluation, and self-generating system based on deep learning.

3. Application of Machine Learning Algorithms in Viewing Methods

3.1. Support Vector Machine Algorithm. Support vector machine is an algorithm used for classification in machine learning. In recent years, the development of support vector machines is very rapid, and the theoretical system is

constantly improved, as well as it also plays its unique advantages in dealing with various problems. In addition, support vector machines continue to expand their application fields, and function fitting is applied to many fields in machine learning, which opens the door for the rapid development of support vector machines. Today, this algorithm has also been successfully applied in many fields [20].

In the case of meeting the needs of data classification, the support vector machine classifies the data set and finds the best classification hyperplane so as to achieve the optimization of the linear classification of the data. In the two-dimensional data space, if the sample group can be divided by a linear function, it can be called linearly divisible. At this time, the classification linear function can be expressed as

$$f(a) = w^n a + x, \quad (1)$$

where a represents the sample vector, w represents the normal vector of the sample vector, and x represents the offset constant.

In the sample set, each training sample contains an input vector a_i and a classification label s_i ($i = 1, 2, 3, \dots, N$; N is the number of samples). The i th training sample can be denoted as $D_i = (a_i, s_i)$. In this way, the distance ς_i between the sample point and a certain hyperplane can be obtained by

$$\varsigma_i = s_i (w^n a_i + x) = |f(a_i)|. \quad (2)$$

By normalizing Formula (2), the Euclidean distance between the sample point and the hyperplane can be obtained as

$$\varsigma_i = \frac{1}{\|w\|} |f(a_i)|. \quad (3)$$



FIGURE 6: Schematic diagram of site planning.

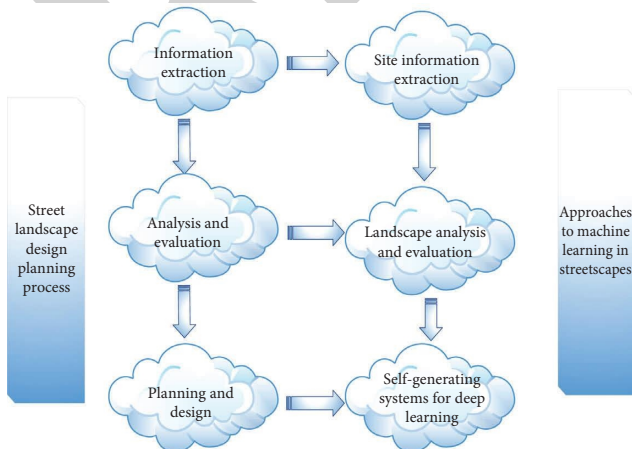


FIGURE 7: Application of machine learning in streetscape.

The minimum distance between each sample point is set to 1; thus, the geometric distance between hyperplanes can be expressed as $2/\|w\|$, and the geometric distance and $\|w\|$ are inversely proportional. If the hyperplane geometric spacing is maximized, then $\|w\|$ must be minimized, which is equivalent to minimizing $\|w\|^2/2$. Since the minimum interval between sample points is 1, there is the following formula:

$$s_i (w^n a_i + x) - 1 \geq 0. \tag{4}$$

Therefore, the solution of the optimal hyperplane can be equivalent to minimize $\|w\|^2/2$ under the constraints of Formula (4). It is worth noting that in a real case, the sample set may have an outlier. Due to the existence of outliers, the classification hyperplane cannot reasonably divide the

samples, which has an adverse effect on the classification hyperplane. At this time, a slack variable $\{\vartheta_i\}_{i=1}^N$ needs to be introduced to reflect the degree of deviation between the sample points and the ideal classification conditions. When $0 < \vartheta \leq 1$, the sample point classification is on the correct side of the classification hyperplane; when $\vartheta > 1$, the sample point classification is on the wrong side of the classification hyperplane. In this way, if the target sample set $\{(a_i, x_i)\}_{i=1}^N$ is an indivisible problem, its optimal principle can be transformed into

$$\min \frac{\|w\|^2}{2} + C \sum_{i=1}^N \vartheta_i, \quad (5)$$

$$\begin{cases} s_i(w^n a_i + x) \geq 1 - \vartheta_i \\ (i = 1, 2, \dots, N; \vartheta_i \geq 0) \end{cases},$$

where, C is the penalty coefficient, which is a parameter representing the degree of penalty for misclassification and can be determined by empirical value or grid optimization. If C is too large, it is easy to cause overfitting; if C is too small, it may lead to a decrease in fitting accuracy.

3.2. Principal Component Analysis Algorithm. Principal component analysis is a data dimensionality reduction method based on machine learning, and it can transform large amounts of data into smaller ones. At the same time, it can also reflect the information of the original data to the greatest extent. The principal component analysis method can not only reduce the dimension of the data but also can effectively solve the problem that some indicators cannot accurately reflect the data.

3.2.1. Principal Component Analysis Model. g is set as the data matrix, and x is the variable index. Each row of the data matrix represents an observation, and each column represents a variable indicator. Among them, there are p variables g_1, g_2, \dots, g_p , and the linear combination of these variables is shown in Formulas (6)–(8):

$$F_1 = x_{11}g_1 + x_{12}g_2 + \dots + x_{1p}g_p, \quad (6)$$

$$F_2 = x_{21}g_1 + x_{22}g_2 + \dots + x_{2p}g_p, \quad (7)$$

$$F_3 = x_{p1}g_1 + x_{p2}g_2 + \dots + x_{pp}g_p, \quad (8)$$

where, if p comprehensive indicators F_1, F_2, \dots, F_p are obtained, the above matrix transformation must meet the following conditions:

$$x'_i = (x_{i1}, x_{i2}, \dots, x_{ip}), \quad (9)$$

$$x'_i x_{ip} = 1, \quad (10)$$

$$x_{i1}^2 + x_{i2}^2 + x_{ip}^2, \quad (i = 1, 2, \dots, p). \quad (11)$$

3.2.2. Basic Steps of Principal Component Analysis. The general steps of principal component analysis are as follows:

- ① The covariance matrix Σ of the original data is calculated.
- ② The solution of the eigenvalue of matrix Σ is $m_1 \geq m_2 \geq \dots \geq m_p > 0$, and the corresponding unit eigenvector is x_1, x_2, \dots, x_p . The i th principal component is $F_i = x'_i g$, and the variance of the i th principal component is $m_i, i = 1, 2, \dots, p$.
- ③ Finally, the variance contribution rate of each principal component is calculated as

$$\vartheta_i = \frac{m_i}{\sum_{j=1}^p m_j}, \quad i = 1, 2, \dots, p. \quad (12)$$

The size of the variance contribution rate of each principal component reflects the size of the original information contained in the component, and the principal component's representation of the size of the confidence is gradually weakened. Finally, the cumulative variance contribution rate of the variance of the first n principal components is calculated as

$$\varpi_n = \frac{\sum_{i=1}^n m_i}{\sum_{j=1}^p m_j}, \quad n < p. \quad (13)$$

Among them, it is ideal when the cumulative variance contribution rate reaches more than 85%. At this time, the original p variables can be replaced by n principal components.

- ④ The score calculation of the sample on the n principal components is observed by

$$F_i = x_{i1}g_1 + x_{i2}g_2 + \dots + x_{ip}g_p, \quad i = 1, 2, \dots, m. \quad (14)$$

If the above four steps are satisfied, the principal component analysis can be performed by converting the original p dimensional data into the reduced n dimensional data.

4. Experimental of the Evaluation Method of Street Green Landscape Viewing Degree Based on Machine Learning

4.1. Experimental Method. In order to conduct a more detailed and effective study on the evaluation method of street green landscape viewing degree based on machine learning, this paper conducts experiments on the evaluation method of street green landscape viewing degree based on machine learning. This experiment selects two cities, A and B, both of which have relatively developed economic levels and complete infrastructure. However, the traditional evaluation method of street green landscape viewing degree is still adopted in the local area, which leads to the low viewing degree of street green landscape. There is little green vegetation in the street, which is not only uncharacteristic but also lacks cultural heritage. In addition, the planning of

TABLE 1: Citizens' awareness of machine learning and the support for this experiment.

Reply Number of people in the project	Do you know anything about machine learning?	Are you satisfied with the current green landscape sign of the street?	Do you think this experiment can make a difference to the streetscape?	Do you support this experiment in your city?
Yes	82	64	135	132
No	112	128	56	42
Uncertain	6	8	9	26

streetscape is also very unreasonable, which has affected the daily traffic of citizens. Every rainy season would always affect the drainage of rainwater, resulting in a large amount of water on the ground. It not only reduces the viewing degree of the street green landscape but also creates inconvenience to the daily life of citizens. This experiment plans to conduct a one-year experiment on the evaluation method of street green landscape viewing degree based on machine learning in city A, and city B also retains the traditional street green landscape viewing degree evaluation method. After the experiment, the air quality, traffic convenience, and citizens' satisfaction with the two cities are compared. Before the experiment is carried out, a questionnaire is also conducted on 200 citizens of city A to understand their cognition of machine learning and the support for this experiment so as to ensure that the experiment can be carried out smoothly, and the results of the survey are shown in Table 1.

As can be seen from Table 1, although more than half of the people have no understanding of machine learning, more than half of the people are very dissatisfied with the current design of the green landscape of urban streets. They hope that there would be a new way to measure the viewability of street green landscape to change the status quo, so nearly two-thirds of the people support this experiment and believe that this experiment can improve the green landscape viewing of the city streets. Therefore, the experiment is carried out very smoothly.

4.2. Analysis of Experimental Data. In order to compare the experimental results after the experiment, relevant data such as air quality, traffic convenience, and citizens' satisfaction with the city are also collected in cities A and B before the experiment. It is assumed that the city's air quality, transportation convenience, and citizens' satisfaction with the city are scored out of 100 points. The higher the score, the better the air quality, and the more convenient the transportation is, as well as the higher the citizens' satisfaction with the city. Figure 8 shows the air quality, traffic convenience, and citizens' satisfaction with the cities in cities A and B before the experiment.

As shown in Figure 8, the air quality, traffic convenience, and citizens' satisfaction with the city are basically the same in these two cities. The air quality just passes the pass line, and the convenience of transportation is not high, only more than 50 points. This would inevitably lead to citizens' dissatisfaction with the city, so citizens' satisfaction with the city is also very low, and a new evaluation method of street green landscape viewing is urgently needed to change this status quo.

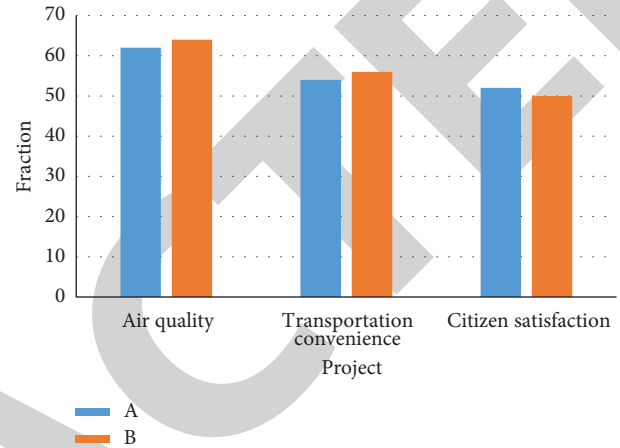


FIGURE 8: The air quality, accessibility, and satisfaction of citizens in city A and B.

4.3. Analysis of Experimental Results. After a year of experimentation on the evaluation method of street green landscape viewing based on machine learning in city A, great changes have taken place in city A. Compared with before, the green vegetation of the street has not only increased a lot, but also combined with the cultural characteristics of the place, which is very literary. In addition, the green landscape of the street is designed according to the city's topography and transportation facilities, so it is very neatly arranged without affecting the city's transportation system and drainage system and also highly useable. Therefore, the air quality and transportation convenience of city A have been greatly improved, and citizens' satisfaction with the city has naturally increased. However, city B, which still uses the traditional evaluation method of street green landscape viewing degree has not changed much compared to before. During the experiment, this paper also collects data on changes in air quality and traffic convenience, and the satisfaction of citizens with the city each month in the two cities, and the changes are shown in Figures 9–11.

From Figures 9–11, it can be seen that the air quality of city A, which has carried out the experiment of the evaluation method of street green landscape viewing based on machine learning, has improved a lot in this year compared to the previous year. In the next few months, it has stabilized at about 75 points, which is about 20.96% higher than before the experiment. In addition, this method combines the streetscape with the city's topography and road conditions, so the city's traffic is much more convenient than before, which greatly facilitates citizens' travel activities. Due to the improvement of the city's air quality and traffic, as well as the

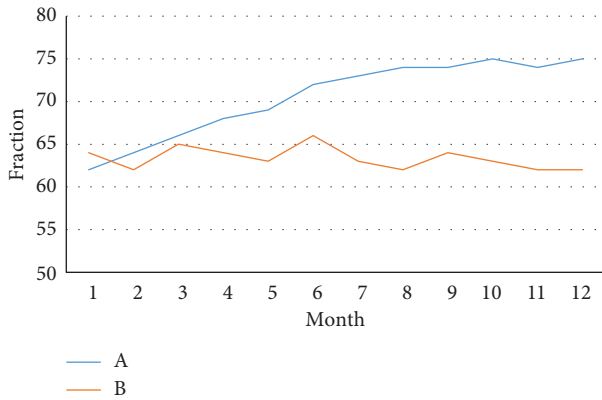


FIGURE 9: Changes in air quality in two cities A and B each month.

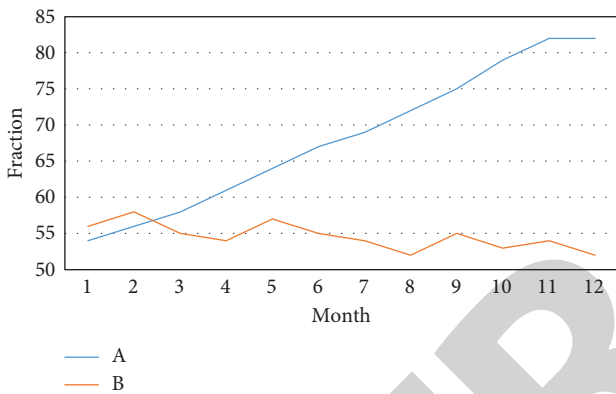


FIGURE 10: Changes in the monthly traffic convenience of the two cities in A and B.

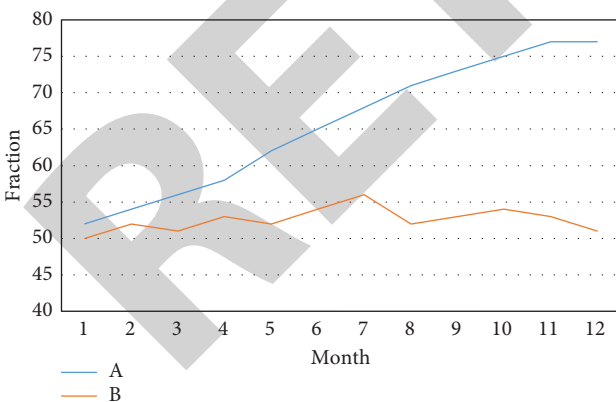


FIGURE 11: Changes in the monthly satisfaction of citizens in the two cities A and B.

street green landscape viewing, the city’s residents are naturally more satisfied with the city than before. However, the air quality, traffic convenience, and citizens’ satisfaction in city B, which are still using the traditional evaluation method of street green landscape viewing, fluctuate only slightly and not improve much.

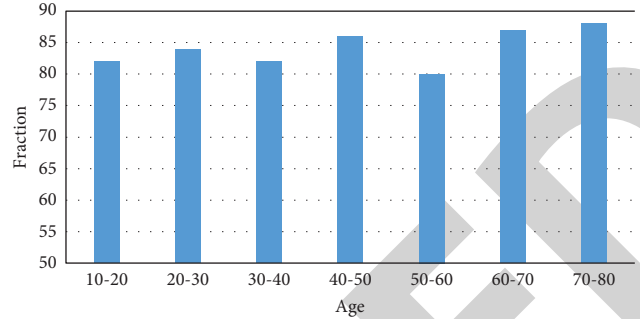


FIGURE 12: The scoring results of this experiment at different ages in city A.

5. Experiment Summary of Landscape Viewing Degree Evaluation Method Based on Machine Learning

In order to further ensure whether the evaluation method of street green landscape viewing degree based on machine learning is accepted by people and whether it is practical, after the end of this experiment, people of all ages in city A would be asked to rate this experiment. The full score is 100 points, and the average of the scores of each age stage is taken, as well as the scoring results are shown in Figure 12.

As shown in Figure 12, this experiment is liked by citizens of all ages, and their scores are basically above 80. It can be seen that the evaluation method of street green landscape viewing degree based on machine learning has strong practicability. The introduction of machine learning, an intelligent exploratory data analysis method driven by data, can not only provide new solutions and method support for street green landscape design but also supply a practical diagnosis for the current situation and problems of the personality representation of the streetscape and provide targeted and operable guidance for the realization of the streetscape’s characteristics from the inside out.

6. Conclusions

Since street green landscape is an important part of urban ecology and urban landscape, the scientific evaluation of street green landscape viewing degree has always been a frontier direction pursued by academia. In recent years, machine learning has been gradually applied to the analysis and evaluation of street green landscape, and some results have been achieved at this stage. However, the evaluation method of street green landscape viewing degree based on machine learning has not been widely used and popularized, and the method is not perfect at the technical level, so the current urban street green landscape is still unsatisfactory. To make the city more comfortable and beautiful, people from all walks of life need to work together to promote the use of machine learning-based street green landscape viewing evaluation methods and technology updates.

Retraction

Retracted: Informatization of Accounting System of Electric Power Enterprises Based on Sensor Monitoring and Cloud Computing

International Transactions on Electrical Energy Systems

Received 28 November 2023; Accepted 28 November 2023; Published 29 November 2023

Copyright © 2023 International Transactions on Electrical Energy Systems. This is an open access article distributed under the Creative Commons Attribution License, which permits unrestricted use, distribution, and reproduction in any medium, provided the original work is properly cited.

This article has been retracted by Hindawi, as publisher, following an investigation undertaken by the publisher [1]. This investigation has uncovered evidence of systematic manipulation of the publication and peer-review process. We cannot, therefore, vouch for the reliability or integrity of this article.

Please note that this notice is intended solely to alert readers that the peer-review process of this article has been compromised.

Wiley and Hindawi regret that the usual quality checks did not identify these issues before publication and have since put additional measures in place to safeguard research integrity.

We wish to credit our Research Integrity and Research Publishing teams and anonymous and named external researchers and research integrity experts for contributing to this investigation.

The corresponding author, as the representative of all authors, has been given the opportunity to register their agreement or disagreement to this retraction. We have kept a record of any response received.

References

- [1] X. Tie, "Informatization of Accounting System of Electric Power Enterprises Based on Sensor Monitoring and Cloud Computing," *International Transactions on Electrical Energy Systems*, vol. 2022, Article ID 3506989, 7 pages, 2022.

Research Article

Informatization of Accounting System of Electric Power Enterprises Based on Sensor Monitoring and Cloud Computing

Xiaohua Tie 

Xi'an International University Business School, Xi'an, Shaanxi 710077, China

Correspondence should be addressed to Xiaohua Tie; 1519640429@st.usst.edu.cn

Received 26 August 2022; Revised 10 September 2022; Accepted 22 September 2022; Published 29 September 2022

Academic Editor: Nagamalai Vasimalai

Copyright © 2022 Xiaohua Tie. This is an open access article distributed under the Creative Commons Attribution License, which permits unrestricted use, distribution, and reproduction in any medium, provided the original work is properly cited.

In order to promote, restrict, regulate, and balance the accounting work of electric power enterprises, the author proposes an electric power enterprise accounting system based on sensor monitoring and cloud computing. Through the method of integrating information technology on the basis of accounting computerization, through a sensor and modular design analysis, an accounting information management system model is formed. The accounting information management system based on cloud computing combines accounting and management functions. The system test results show that the accounting information management system is in a state of 480 concurrent users, the average response time of a data query is 4.3 seconds, and the average response time of a data access is 5.1 seconds. The average value of the execution data scale per second is 103.52. *Conclusion.* In order to further improve the accounting software of electric power enterprises, develop management accounting software, and effectively perform the functions of management accounting.

1. Introduction

Accounting uses results as the main point of measurement; the main goal is to improve the business; it uses special methods for companies and organizations; and it is an action that includes complete, continuous, and business management of organizations and other organizations. Registration, management, financial reporting, forecasting, decision-making, monitoring, and analysis, as well as social and business development, are part of the importance of business management. With the advent of the information age, traditional accounting has changed from manual book-keeping, manual calculation, and manual verification to using computers to carry out corresponding work. However, these tasks are transferred from traditional manual to computer calculation, and only the part that needs manual calculation is handed over to the computer. The operation process, data entry, statistical methods, and other processes still require a lot of manual participation [1]. On this basis, accounting information technology is also based on the computer, but humans are used to calculate the target information and enterprise entities, and the actual operation

process and work platform are still carried out in traditional accounting. In fact, in this accounting informatization process, the use of computers only stays with “computing.” With the continuous popularization of computers, the functions are becoming more and more powerful, involving all aspects of society, and its main functions are developing towards informatization and intelligence, its main function can not only stay on “calculation,” but can use various computer software, the manual tedious work is transformed into the operation of the computer [2]. Through the computer, the data are not only calculated but also various statistics and analyses are carried out to maximize the use of various functions of the computer. Accounting informatization mainly combines accounting and information technology. With the advent of the information society, corporate finance will cater to the trend of informatization, relying on computers to process increasingly complex corporate financial information flows and incorporating corporate management into the informatization system. When the network and communication means are highly developed and electronic equipment and mobile equipment are constantly updated, the foundation of accounting

informatization exists in a wide range of hardware and software environments. Information-based accounting can provide information to enterprise leaders in the network environment, increase the competitiveness of enterprises, and solve the “island” phenomenon in computerized accounting at the network level. Through the analysis and calculation of a large amount of information, it provides decision support for enterprise management. Existing enterprises mainly use accounting computerization to realize the main financial management and some accounting software to realize the overall audit of the enterprise, but in general, the accounting information standard has not been reached [3]. In accounting informatization, through information technology, network systems, and communication systems, general manual business processes are transformed into a series of software executions and protocol interactions on hardware such as computers, mobile devices, networks, and communications, and business processing is automated.

2. Literature Review

Scouse et al. and others conducted in-depth research on the formal meaning of cloud computing and its advantages and disadvantages and believed that the technical level and scientific theoretical basis of cloud computing development are the reasons for ensuring that cloud computing can be used in enterprises and achieve good results [4]. Hein et al. and others propose to serve the public with software, hardware, and postmaintenance, which can establish a new business management model and provide good development conditions for enterprises [5]. Jpc et al. and others conducted a study on the needs of enterprises in cloud computing, including a comprehensive analysis of enterprise data information, enterprise capital flow, management methods, etc., and sorted out a perfect evaluation method after the analysis [6]. Zhang et al. obtained the importance of cloud computing for future accounting information construction according to the theoretical research of reality, classified small and medium-sized enterprises by means of qualitative and quantitative cooperation, and then obtained the characteristics of various types of small and medium-sized enterprises. Then, according to various characteristics, find out the matching method of cloud computing technology and effective risk management [7]. Lv and Li have developed a cloud computing technology based on the service differential agreement, using the service differential agreement as the basic, according to the feedback questions put forward by users, in order to evaluate different levels of service for cloud computing providers. It is used as a reference for new companies when choosing cloud computing [8]. Arcos-Aviles et al. and others have studied different usage patterns of cloud computing in their paper, and based on the research results, they have drawn up corresponding executable programs [9]. Liu, C. et al., the study of small and medium enterprises, found that because the development of accounting information requires a lot of investment due to capital, management, and other problems, small and medium enterprises have difficulty creating and creating financial information, but because cloud computing can

effectively manage investment costs, small and medium enterprises will often use cloud computing when creating financial information [10].

System testing is a process of comprehensive verification of the system by organically combining the design elements, operating environment, and external conditions (such as the network) of the accounting information system of electric power enterprises. Verification includes determining whether the system functions meet the usage requirements, whether the system performance meets the function needs, etc. Through system testing, it is possible to find out where the actual effect does not match the expected effect as early as possible, so as to carry out targeted repair and improvement and do the final check for the final realization of the system.

3. Research Methods

3.1. Overall Design of Accounting Information Management System

3.1.1. System Construction Background. The design of the accounting information management system should be based on the perspective of development, adapt to the development of the times and the requirements of scientific financial management, recognize the responsibility and mission of accounting work, and be guided by the scientific concept of development, get rid of the shackles of the traditional financial management model, adopt reform and innovative management measures, change the extensive development thinking of extension and expansion, and promote the safe and stable progress of financial work.

3.1.2. System Design Concept. Establishing and implementing an accounting information management system that combines modern information technology and computer technology. Information mainly refers to accounting information resources, and computer technology mainly focuses on accounting information processing, referred to as information processing processor, which is the core part of the information management system [11, 12]. An accounting information system is a human-computer interaction management information system using modern information processing technology. Its application meets the requirements of enterprise accounting management and can effectively solve the problems encountered in accounting and management. The information is collected, stored, processed, analyzed, transmitted, and fed back through three parts: people, computer technology equipment, and operating procedures. Through the accounting information management system, a decision-making system can be established to help managers solve some diverse problems, including plan monitoring, budgeting, and cost management, in order to provide support for the leadership to formulate corporate development strategies. Therefore, the design of an accounting information management system mainly includes three modules. As shown in Figure 1.

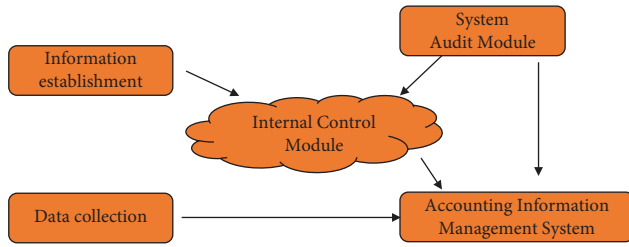


FIGURE 1: The module of accounting information management system.

3.2. Detailed System Design and Implementation

3.2.1. Advantages of Accounting Information Management System

(1) *Informatization.* The accounting information management system is a management system constructed by using modern computer technology as a platform for building the foundation of information technology.

(2) *Open up.* With the development of the Internet, the accounting information management system has a high degree of automation in information processing and effectively realizes resource sharing. Through the system, relevant systems inside and outside the enterprise can exchange real-time data and obtain information from each other [13].

(3) *Intelligent.* The design of the system is mainly through the application system combined with human, computer, network, and software programs, which not only have the function of accounting but also have the function of control and management. It has the characteristics of intelligence and humanization.

(4) *Diversification.* Through the exchange of information between internal and external enterprises, the collection of information is diversified, the information channels are wide, and the amount of information is increased.

3.2.2. Detailed Design

(1) *System hardware architecture.* The hardware architecture of the accounting information management system needs to include several parts, such as a server, a client, a browser, etc., as shown in Figure 2.

(2) *System UI page design.* In order to ensure the safety and efficiency of the management of financial information and to provide good services for accounting operations, it is necessary to create a clear and understandable UI operation interface, as shown in Figure 3.

3.2.3. Detailed Design of the Application

(1) *Internal control module.* To improve internal control, when developing internal control for accounting, you must start with three things: data management, income and expenditure data, and customer management. [14].

- (1) Basic data management mainly responsible for the collection and recording of sales, daily reports, accounting risks, and other information in accounting.
- (2) Supervision of revenue and expenditure information collect data from relevant business systems and conduct analysis and processing to supervise and evaluate accounting revenue and expenditure.
- (3) User information management record and analyze the performance of accounting staff to select, deal with violations, and ensure that accounting internal control management falls within the timeliness.

(2) *System audit module.* For the effective implementation of the internal control system, it is necessary to carry out an internal audit of the management system to achieve the safe and effective application of the system. After the traditional business control activities of enterprises are gradually embedded in computer programs, the effectiveness of business information will depend on the reliability of the information system, and the reliability of the information system will depend on the control and execution of the information system. Therefore, the accounting information management system should not only formulate the internal control system but also review the implementation of the internal control system through auditing activities, where relevant problems in the control system can be found, and timely improvement can make the information management system play the biggest role in the enterprise operation [15]. Information system audits mainly include auditing information technology management control; auditing data centers and data communication; auditing the system development process; and auditing system operation and maintenance. Information system auditing can ensure the effective operation of the internal control mechanism and achieve the ultimate goal of enterprise management informatization.

(3) *Network delay.* In order to prevent the influence of network changes on data transmission, network QoS management technology is introduced, and real-time monitoring is used to lay a good foundation for diffusion control. To control the network delay, you need to add a timestamp to the protocol and two fields to each packet: last received time (LRT) and current sent time (CST). After receiving a packet, the receiver calculates the local transmission time of the packet based on the LRT and SCT of the packet. At the same time, according to the last time reserved by the receiver (LST) and the time when the message is received, the delay of the receiver time can be reduced, and the packet network performance is slowed down. When B-end replies to A, it is shown as follows:

$$\begin{aligned} \text{LRT} &= TB + \Delta t_1, \\ \text{CST} &= TB + \Delta t_1 + \Delta t_2, \end{aligned} \quad (1)$$

when end A receives the message from end B, its local is

$$\text{LRT} = TA + \Delta t_1, \quad (2)$$

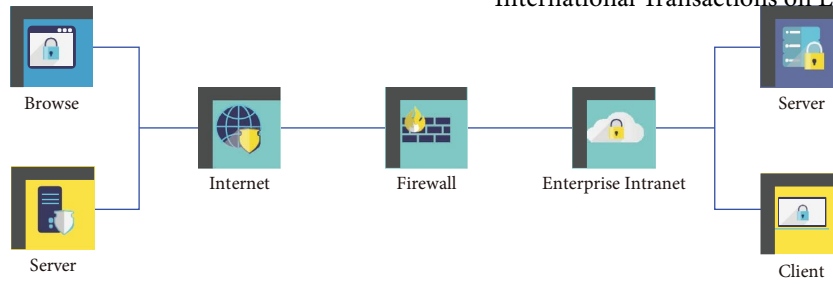


FIGURE 2: System hardware architecture diagram.

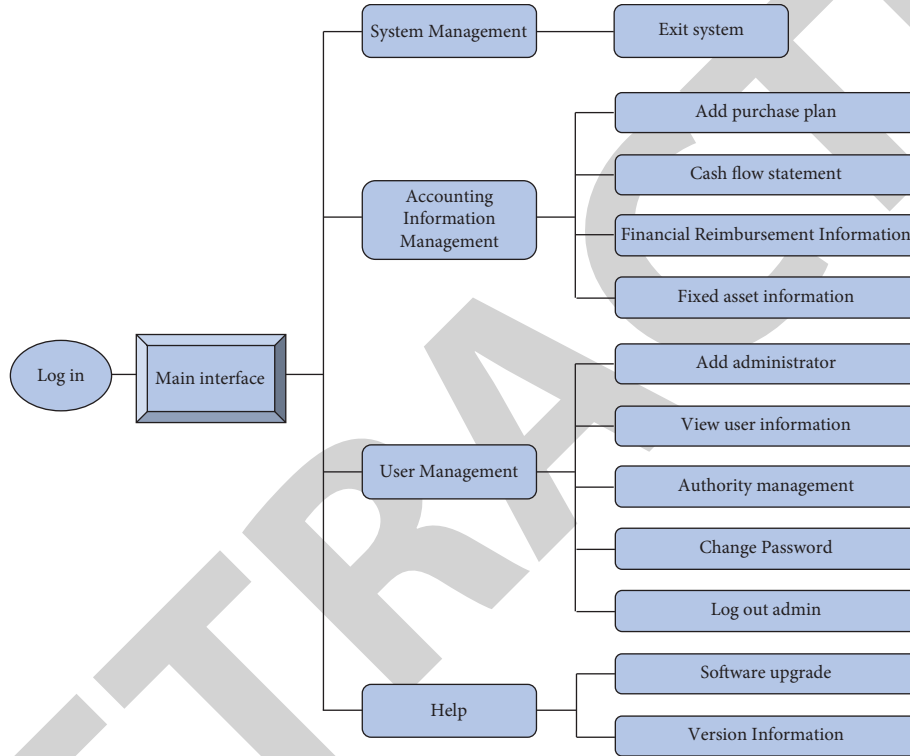


FIGURE 3: System UI page design.

and its current time is

$$CT = TA + \Delta t1 + \Delta t2 + \Delta t3. \quad (3)$$

At this time, the two-way delay of packet sending can be calculated as follows:

$$CT - LST = (CST - LRT). \quad (4)$$

3.3. Example Application of Accounting Information Management. Haier Group uses the accounting information management system to carry out daily clearing of daily operating benefits, dynamically display the daily work budget, actuality, and gap, and make a correction plan to make sure the goal is achieved. In today's increasingly developed informatization, Haier Group adopts the business philosophy of Rendanheyi, which has comprehensively improved the closed-loop optimization of Haier Nissin and the quality of employees. Through the

accounting information management system, Haier Group conducts budget and analysis of annual revenue and expenditure, scenario application, rolling forecast, etc., comprehensively runs through the cost budget of sales, production, procurement, and other businesses, pre-estimates the business results of the activity plan, and makes effective adjustments according to the plan to achieve strategic goals. Collect and analyze enterprise sales information data, risk information data, and daily report data through the internal control system. Use the income and expenditure supervision system to supervise and control the income and expenditure management system, income and expenditure status, etc. [16]. Carry out further implementation of the user's information report and the implementation of the system. The use of an information management system brings convenience to Haier Group's business operations, solves problems and inconsistencies in accounting, and contributes to

business development. The practice has proven that the system is safe and reliable, and it is worth supporting it in the work of the business.

4. Results Analysis

4.1. Test Environment. The introduction of the test environment of the accounting information management system is divided into two parts: hardware and software, as shown in Tables 1 and 2, respectively.

4.1.1. Hardware Configuration. The test hardware configuration of this research system should include servers and clients. Three rack servers and one client are arranged here; the main parameters are shown in Table 1.

4.1.2. Software Configuration. The test software configuration of this research system is based on hardware equipment, and the main parameters are shown in Table 2.

4.2. Test Method. The purpose of the accounting information management system test in this study is to eliminate potential problems in the operation of the system. The main tests are as follows:

- (1) Test whether user system login, function access, etc. Meet the expected design security goals, one is whether authorized user access is normal; the other is whether illegal user access is blocked [17].
- (2) Test whether the operation of the functional modules of the system meets the expected design and operation goals, such as basic operations such as additions, deletions, and changes, and data normative judgments.
- (3) Test whether the data backup capability of the system based on the simulated environment meets the expected design reliability goals, one is whether the system automatically completes data backup in real time; the other is whether the damaged data of the system can be repaired and whether the repair time is short [18].
- (4) Test whether the access capability of the system database meets the expected design efficiency goal, such as whether the access result can be quickly obtained by entering the access order number.
- (5) Test whether the operation of the system function modules meets the expected design logic goals, such as payroll accounting, report analysis, system settings, etc.
- (6) Test whether the system data storage and invocation meet the expected design accuracy goals, such as data reading accuracy.
- (7) Make sure that the performance of the system based on the use of multiple sources can meet the requirements of design elements, such as response time and energy efficiency.

In order to determine the architecture and operation of the data management system as a whole, this section only introduces various test methods and describes their use in the management of the evidence.

4.2.1. Integration Test. This test is mainly to access the communication business between each module of the system and its completion. It is used to ensure correct data transfer between different modules [14, 19]. Carry out a specific integration test on the system through the communication of the capital revenue and expenditure function, payroll accounting function, and report management function of the accounting information management system.

4.2.2. Effectiveness Test. This test is used to confirm whether the actual performance of the system meets the expectations of developers or customers and how well it fits or matches. The author chose the Heihe test method to carry out specific verification and confirmation of the main modules of the system [20]. This system is designed and developed for the convenience of enterprise financial management workers, so operations such as report querying and processing in the system require fast operation speed and strong operability.

4.2.3. System Test. This test is to consider the comprehensive performance of the system from the perspective of the overall situation and results; it needs to rely on a certain test environment to obtain an overall test report about the system.

4.3. System Performance Test. As mentioned above, performance measurement, based on the use of high-level access points, evaluates the performance according to the desired design goals, such as time responsiveness and high performance. To complete the results of the physical performance evaluation, it can be seen that the data management system must meet the following requirements: response time for many users at the same time is less than 5 seconds. The main contents of performance testing include the selection of testing tools and the writing of test scripts.

The author of the data management uses EVEREST software to simulate the performance and gradually increases the number of users at the same time to bring the upper limit of the physical resistance and the response time approaches this limit.

The operation process of the performance test of the accounting information management system in this study is briefly described as follows: install EVEREST software, and then write and run different system operating performance test script languages; here, the unit of concurrent user pressure growth is defined as 30/second, and the average value is taken according to the test results, and the corresponding data recording is performed using the system's

TABLE 1: System test hardware configuration.

Parameter/host	Application server	Web server	Database server	Client computer
Processor	Xeon xeon-silver	Xeon xeon-silver	Xeon xeon-bronze	Intel i5
Memory capacity	16G	32 G	8T	16 G
Hard drive capacity	2 * 1T	3 * 2T	1T	512 G
Support system	WindowsServer	WindowsServer	WindowsServer	windows8

TABLE 2: System test software configuration.

Host	System	Software
Application server	WindowsServer2012withSP2	SQLServer2012; IIS7.0
Web server	WindowsServer2012	IIS7.0; NETFramework2.0
Database server	WindowsServer2012	SQLServer2012
Client computer	Windows8	InternetExplorer8.0; MicrosoftVisualStudio TeamFoundation

TABLE 3: System stress test.

Concurrent users	Query data average response time (seconds)	Save data average response time (seconds)	Minimum	The maximum value of data executed per second
30	1.2	1.3	31	51
70	1.5	2.0	46	67
120	2.2	2.6	64	82
200	2.7	3.1	74	94
290	3.5	3.7	88	105
350	3.7	4.6	97	124
480	4.3	5.1	103	138

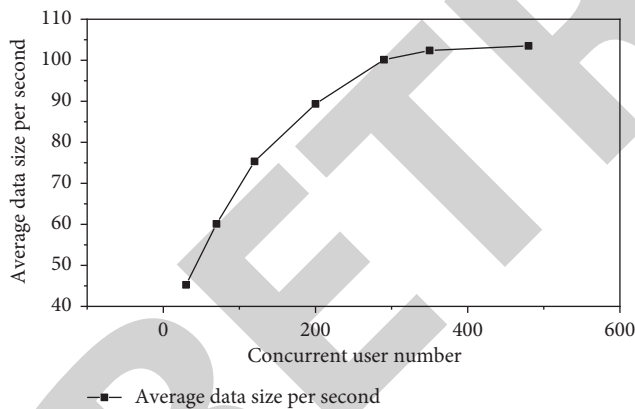


FIGURE 4: Average values under different concurrent users.

own tools [21]. The results of the performance test of the accounting information management system are shown in Table 3 and Figure 4 [22].

According to the data in Table 3 and Figure 4, the accounting information management system has 480 concurrent users, the average response time of an information query is 4.3, and the average response time of input data is 5.1 [23]. The average number of datasets processed per second is 103.52. Therefore, the results of performance evaluation are based on the desired goals and can be considered as indicators suitable for the business needs of enterprises [24].

5. Conclusion

Information management mode has changed the working mode of traditional enterprise management; through the process, financial management, cost management, income management, and expenditure of funds can be effectively managed, which reduces the investment of enterprises. With the continuous development of Internet technology and the emergence of cloud computing platforms, enterprise data management will be transformed to a cloud computing platform, and the biggest difference will be creating enterprise financial information management in the cloud environment. The author introduces the testing part of the accounting information management system, tests hardware conditions and software conditions through reasonable configuration, selects testing methods such as integration testing and effectiveness testing, and briefly describes the testing content. Finally, the test results are displayed in the functional test case table and the performance test data result in table, respectively. The results show that the accounting information management system has achieved the expected design goals.

Data Availability

The data used to support the findings of this study are available from the corresponding author upon request.

Conflicts of Interest

The author declares that there are no conflicts of interest.

Retraction

Retracted: Application of the Lagrange Equation for Intelligent Sensor Vibration Control for Power Network Monitoring

International Transactions on Electrical Energy Systems

Received 19 September 2023; Accepted 19 September 2023; Published 20 September 2023

Copyright © 2023 International Transactions on Electrical Energy Systems. This is an open access article distributed under the Creative Commons Attribution License, which permits unrestricted use, distribution, and reproduction in any medium, provided the original work is properly cited.

This article has been retracted by Hindawi following an investigation undertaken by the publisher [1]. This investigation has uncovered evidence of one or more of the following indicators of systematic manipulation of the publication process:

- (1) Discrepancies in scope
- (2) Discrepancies in the description of the research reported
- (3) Discrepancies between the availability of data and the research described
- (4) Inappropriate citations
- (5) Incoherent, meaningless and/or irrelevant content included in the article
- (6) Peer-review manipulation

The presence of these indicators undermines our confidence in the integrity of the article's content and we cannot, therefore, vouch for its reliability. Please note that this notice is intended solely to alert readers that the content of this article is unreliable. We have not investigated whether authors were aware of or involved in the systematic manipulation of the publication process.

Wiley and Hindawi regrets that the usual quality checks did not identify these issues before publication and have since put additional measures in place to safeguard research integrity.

We wish to credit our own Research Integrity and Research Publishing teams and anonymous and named external researchers and research integrity experts for contributing to this investigation.

The corresponding author, as the representative of all authors, has been given the opportunity to register their agreement or disagreement to this retraction. We have kept a record of any response received.

References

- [1] X. Cheng, "Application of the Lagrange Equation for Intelligent Sensor Vibration Control for Power Network Monitoring," *International Transactions on Electrical Energy Systems*, vol. 2022, Article ID 4616889, 9 pages, 2022.

Research Article

Application of the Lagrange Equation for Intelligent Sensor Vibration Control for Power Network Monitoring

Xiaojing Cheng 

School of Mathematics and Computer Science, Shaanxi University of Technology, Hanzhong 723001, Shaanxi, China

Correspondence should be addressed to Xiaojing Cheng; 20141296@stu.sicau.edu.cn

Received 14 July 2022; Revised 26 August 2022; Accepted 5 September 2022; Published 29 September 2022

Academic Editor: Nagamalai Vasimalai

Copyright © 2022 Xiaojing Cheng. This is an open access article distributed under the Creative Commons Attribution License, which permits unrestricted use, distribution, and reproduction in any medium, provided the original work is properly cited.

Objective. In order to control the vibration of the beam structure more effectively and improve the safety and availability of the beam structure, an application study of the Lagrange equation for vibration control of smart sensors for power grid monitoring is proposed. The vibration of the beam structure, the displacement of the beam structure under the excitation of seismic acceleration, the response analytical electrical formula, and the displacement response formula of the beam structure under the action of the kinematic force are deduced. The optimal parameters of the beam-TMDI system are given, and the parameter sensitivity analysis is carried out. Then, the control effect of the TMDI system is studied by numerical analysis, and the vibration reduction effect of the TMDI system and the tuned mass damper (TMD) system is compared. Experimental results show that when the mass ratio μ of the TMDI system and the TMD system are both set to a fixed value of 0.005, and the parameter β of the TMDI system is set to 0, namely $\beta = b = 0$, at this time, the TMDI system degenerates into a TMD system. The TMD natural frequency is 14.179 rad/s and the damping ratio is 0.0432 by the DH optimization method, while the TMD natural frequency is 14.1812 rad/s, and the damping ratio is 0.0436 by the augmented Lagrangian optimization algorithm. **Conclusion.** The vibration displacement response spectrum of a beam structure obtained by the frequency domain method can effectively reflect electricity in the displacement response of a beam structure. The parameters that minimize the vibration response of the beam structure can be accurately obtained by using the augmented Lagrangian parameter optimization method. The sensitivity of the TMDI system is controlled by the inertial device, and the inertial device has a significant impact on its robustness. The vibration reduction performance of the TMDI system is obviously better than in the conventional TMD systems.

1. Introduction

With the rapid economic development and the continuous progress of science and technology in various countries in the world, the structural systems of high-rise buildings are also constantly developing. The continuous development of concrete and steel has promoted electricity and the diversity and rationality of building structural systems, from the multistorey frame structure system to the emergence of high-rise and super high-rise buildings, which all reflect the perfect combination of social needs and technological progress in electricity. High-rise and super high-rise structures are moving towards a more integrated and intelligent direction. In the late 1960s, with the continuous development and improvement of the lateral force resistance

system, the height of high-rise buildings continued to increase. A super high-rise building structural system evolved from the beam-type transfer storey structure and giant building structural system came into being [1].

My country is in the most active seismic zone and is one of the most earthquake-prone countries. Earthquake disasters have two characteristics: suddenness and destructiveness. Previous earthquake disasters have caused incalculable loss of life and property in my country [2]. Research on the vibration control of building structural systems, combining the unique two-level structure of giant structures with structural vibration control technology, and the emergence of a new type of giant vibration reduction system, can not only reduce the impact of earthquake damage but also solve the problem of difficult earthquake

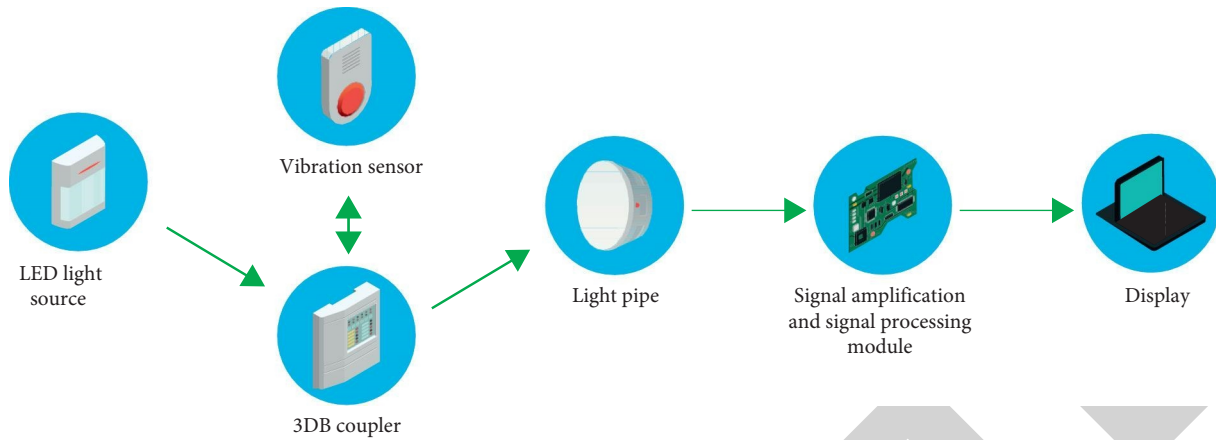


FIGURE 1: The intelligent sensor of the Lagrange dynamics equation.

resistance of high-rise structures to a certain extent, which is of great significance for engineering earthquake resistance [3].

Engineering structure vibration reduction control technology refers to the addition of control devices (or a certain mechanism, substructure, and external force) to some parts of the engineering structure, such as vibration isolation bearings, tuning mass blocks, energy dissipation supports, and others, used to change or adjust the dynamic parameters of the structure. The structural response of the structural system under the action of an earthquake or wind load is controlled within a certain range in order to ensure the safety and normal use of the structure. The related theories, technologies, and methods are collectively referred to as “engineering structure vibration reduction control”, as shown in Figure 1.

2. Literature Review

Refani et al. studied an L-shaped composite beam structure, considered the nonlinear models of the in-plane vibration and out-of-plane vibration of the L-shaped composite beam structure, and derived all nonlinear motion equations, including second-order nonlinearity [4]. Khosravi et al. studied the natural frequency and global mode shape of the L-shaped composite beam structure and obtained them by the global modal method and compared with the results calculated by the finite element method. The effectiveness of this method for solving L-shaped composite beams is illustrated [5]. Chen et al. used the global modal method to study the U-shaped composite beam structure, obtained the frequency equation of the U-shaped beam structure, and obtained the natural frequency and global mode of the system [6]. Ebrahimi-Mamaghani derived the governing equations of the plane motion of the Z-shaped composite beam structure and the boundary conditions of the system by using the Hamilton’s principle and theoretically obtained the natural frequency of the Z-shaped composite beam structure and the modal mode shape of the analytical form [7]. Tk et al. considered the bending and torsional deformation of the rod and the bending deformation of the beam. The bending and torsional motion of the T-beam were

dynamically modeled by using the global modal idea, and the characteristic equations and dynamic equations of the system were obtained [8]. Kheiri used piezoelectric sheets to control the bending vibration of the beam and used piezoelectric rings to control the torsional vibration of the rod and obtained a good control effect [9]. Chen et al. fixed active vibration control of beam structures at one end and stressed at one end by piezoelectric actuators. Based on the Euler–Bernoulli beam theory, the governing equations of the system are derived [10]. Wei et al. concluded that based on the robust control method, the vibration control problem of a piezoelectric smart beam structure was analyzed [11].

Therefore, the author proposes to use the TMDI system to control the vibration electricity of the beam structure under the action of seismic acceleration and moving force, respectively. Firstly, the mechanical analysis model under the action of seismic acceleration and moving force is established; secondly, the combination of the virtual excitation method and the Fourier transform method is used. The displacement response spectrum of the beam structure under seismic acceleration excitation is deduced, and the vibration displacement response spectrum of the beam structure under moving load is deduced by the Fourier transform. Then, on this basis, the TMDI optimal parameters that minimize the vibration response of the beam structure are obtained by using the augmented Lagrangian optimization algorithm. Finally, through an example analysis, the sensitivity of the optimal parameters of the TMDI system under the action of seismic acceleration and moving load of the beam structure in the frequency domain, the influence of the inertial device on the robustness of the TMDI system, as well as the superiority of the TMDI system are compared to the TMD system.

3. Research Methods

3.1. Frequency Domain Response of Beam-TMDI System under Random Load Excitation

3.1.1. Vibration under Seismic Acceleration. For a simply supported beam with a span of L , and a TMDI vibration reduction system is set in the middle of the span, the motion

equation of the beam-TMDI system under the excitation of seismic acceleration $\ddot{x}_g(t)$ can be expressed as in the following equations:

$$[M]\{\ddot{y}\} + [C]\{\dot{y}\} + [K]\{y\} = -[M][E]\ddot{x}_g(t) + F_T, \quad (1)$$

$$F_T = D_d[c_d(\dot{x}_d - \dot{y}) + k_d(x_d - y)], \quad (2)$$

$$(b + m_d)\ddot{x}_d + c_d(x_d - \dot{y}) + k_d(x_d - y) = -m_d\ddot{x}_g(t). \quad (3)$$

Here, $[M]$ is the mass matrix; $[C]$ is the damping matrix; $[K]$ is the stiffness matrix; $E = [1, 1, \dots, 1]$; $\{y\}$ is the displacement of the beam structure relative to the ground, namely $\{y\} = \{y_1, y_2, \dots, y_j\}^T$; F_T is the reaction force of the TMDI system to the simply supported beam; m_d , k_d , c_d , and b are the mass parameters of TMDI, spring stiffness, damping, and inertial mass parameters, respectively; x_d is the vertical displacement of the mass block of the TMDI system; and $D_d = [0, \dots, 0, 1, 0, \dots, 0]$ [12, 13]. Using the mode shape decomposition method of the structural equation of motion, the vertical displacement $y(x, t)$ of a simply supported beam at a time x and position t can be expressed as a linear combination of beam mode shapes, that is shown in the following formula:

$$y(x, t) = \sum_{j=1}^q u_j(t)\phi_j(x), \quad (4)$$

$$\ddot{u}_j + 2\xi_j\omega_j\dot{u}_j + \omega_j^2\tilde{u}_j = -\gamma_j\sqrt{S_{\ddot{x}_g}(\omega)}e^{i\omega t} + \frac{\phi_j(L/2)}{m_j}\left\{c_d\left(\dot{x}_d - \phi_j\left(\frac{L}{2}\right)\dot{\tilde{u}}_j\right) + k_d\left(x_d - \phi_j\left(\frac{L}{2}\right)\tilde{u}_j\right)\right\}. \quad (7)$$

Here, ω_j , ξ_j , and m_j are the j th-order frequency, damping ratio, and mode mass of the structure, respectively; $\gamma_j = [\phi]^T[M][E]/[\phi]^T[M][\phi]$. For the convenience of calculation, the parameter $\alpha_j = m_d\phi_j(L/2)/m_j$, $v_s = x_d - \phi_j(L/2)\tilde{u}_j$, $\dot{v}_s = \dot{x}_d - \phi_j(L/2)\dot{\tilde{u}}_j$ is defined.

Formula (7) can be simplified to the following formula:

$$\ddot{u}_j + 2\xi_j\omega_j\dot{u}_j + \omega_j^2\tilde{u}_j = -\gamma_j\sqrt{S_{\ddot{x}_g}(\omega)}e^{i\omega t} + \alpha_j(2\xi_d\omega_d\dot{v}_s + \omega_d^2v_s), \quad (8)$$

where ω_d is the frequency of the TMDI damper; $\xi_d = c_d/2m_d\omega_d$ is the damping ratio of the TMDI damper [14]. Assuming $b/m_d = \Theta$, the equation of motion (3) of TMDI can be further simplified as follows:

$$(\Theta + 1)\ddot{x}_d + \ddot{x}_g + 2\omega_d\xi_d\dot{v}_s + \omega_d^2v_s = 0. \quad (9)$$

Simultaneously formula (8) and formula (9) can be written in the matrix form as follows:

$$\hat{M}_j\ddot{\tilde{y}}_j + \hat{C}_j\dot{\tilde{y}}_j + \hat{K}_j\tilde{y}_j = \hat{F}_j. \quad (10)$$

where $\phi_j(x)$ is the first mode shape of the beam, and for a simply supported beam of equal section, the mode shape function is $\phi_j(x) = \sin(j\pi x/L)$; $u_j(t)$ is the generalized coordinate corresponding to the j -th mode of the simply supported beam [13]. The virtual acceleration excitation is constructed using the known self-spectrum as follows:

$$\ddot{\tilde{x}}_g(t) = \sqrt{S_{\ddot{x}_g}(\omega)}e^{i\omega t}. \quad (5)$$

Multiplying equation (1) on the left by $[\phi]^T$, then substituting equations (4) and (5) into equation (1) and using the orthogonality of mode shapes, the following equation can be obtained:

$$[\bar{M}]\{\ddot{\tilde{u}}\} + [\bar{C}]\{\dot{\tilde{u}}\} + [\bar{K}]\{\tilde{u}\} = -[\phi]^T[M][E]\sqrt{S_{\ddot{x}_g}(\omega)}e^{i\omega t} + [\phi]^TF_T. \quad (6)$$

In the formula, the symbol $\tilde{\cdot}$ is a virtual quantity; $[\bar{M}] = [\phi]^T[M][\phi]$; $[\bar{C}] = [\phi]^T[C][\phi]$; $[\bar{K}] = [\phi]^T[K][\phi]$; F_T is the reaction force of the TMDI system to the simply supported beam; then equation (6) is decomposed into mutually independent single degree-of-freedom equations, as shown in the following equation:

In the formula, $\tilde{y}_j = [\tilde{u}_j, v_s]^T$; $\hat{F}_j = [-\gamma_j\sqrt{S_{\ddot{x}_g}(\omega)}e^{i\omega t}, -\ddot{\tilde{x}}_g]^T$;

$$\hat{M}_j = \begin{bmatrix} 1 & 0 \\ (\Theta + 1)\phi_j(L/2) & \Theta + 1 \end{bmatrix}; \hat{K}_j = \begin{bmatrix} \omega_j^2 & -\alpha_j\omega_d^2 \\ 0 & \omega_d^2 \end{bmatrix};$$

$$\hat{C}_j = \begin{bmatrix} 2\xi_j\omega_j & -2\alpha_j\xi_d\omega_d \\ 0 & 2\omega_d\xi_d \end{bmatrix}.$$

Perform the Fourier transform on equation (10) to get the following equation:

$$\tilde{Y}_j(\omega) = (-\omega^2\hat{M}_j + i\omega\hat{C}_j + \hat{K}_j)^{-1}\tilde{F}_j(\omega). \quad (11)$$

Equation (11) can also be written as

$$\begin{Bmatrix} \tilde{u}_j(\omega) \\ v_s \end{Bmatrix} = \begin{bmatrix} H_j(\omega) & H_{js}(\omega) \\ H_{sj}(\omega) & H_s(\omega) \end{bmatrix} \begin{Bmatrix} -\gamma_j\sqrt{S_{\ddot{x}_g}(\omega)} \\ -\sqrt{S_{\ddot{x}_g}(\omega)} \end{Bmatrix}. \quad (12)$$

Then, the j th-order modal response component of the simply supported beam is shown in the following equation:

$$\tilde{u}_j(\omega) = -H_j(\omega)\gamma_j\sqrt{S_{\ddot{x}_g}(\omega)} - H_{jj}(\omega)\sqrt{S_{\ddot{x}_g}(\omega)} = H(\omega) \cdot \sqrt{S_{\ddot{x}_g}(\omega)}. \quad (13)$$

In the following formula, the transfer function $H(\omega)$ is expressed as

$$H(\omega) = \frac{-\gamma_j - (i\omega 2\alpha_j \xi_d \omega_d + \alpha_j \omega_d^2) X^{-1}}{-\omega^2 + i\omega 2\xi_j \omega_j + \omega_j^2 - X^{-1} \omega^2 (\Theta + 1) \phi_j(L/2) (i\omega 2\alpha_j \xi_d \omega_d + \alpha_j \omega_d^2)}. \quad (14)$$

In the formula, $X = -\omega^2 (\Theta + 1) + i\omega 2\xi_d \omega_d + \omega_d^2$. Then, the displacement response spectrum of the simply supported beam in the frequency domain under seismic acceleration excitation is given in the following formula:

$$\tilde{Y}(\omega) = \sum_{j=1}^q \tilde{u}_j(\omega) \phi_j(x) = \sum_{i=1}^q H(\omega) \phi_j(x) \sqrt{S_{\ddot{x}_g}(\omega)}. \quad (15)$$

For the first-order mode shape of the simply supported beam, the mid-span vibration displacement response spectrum $\tilde{Y}_1(\omega)$ of the simply supported beam considering the TMDI system under seismic acceleration excitation is given in the following formula:

$$\tilde{Y}_1(\omega) = \frac{-\gamma_1 - [m_d \phi_1(L/2)/m_1 \xi_d \omega_d + m_d \phi_1(L/2)/m_1 \omega_d^2] X^{-1} \cdot \phi_1(L/2) \cdot \sqrt{S_{\ddot{x}_g}(\omega)}}{-\omega^2 + i\omega 2\xi_1 \omega_1 + \omega_1^2 - X^{-1} \omega^2 (b/m_d + 1) \phi_1(L/2) [m_d \phi_1(L/2)/m_1 \xi_d \omega_d + m_d \phi_1(L/2)/m_1 \omega_d^2]}. \quad (16)$$

$$\ddot{u}_j(t) + 2\xi_j \omega_j \dot{u}_j(t) + \omega_j^2 u_j(t) = [F_{bj}(t) + F_{Tj}(t)], \quad (17)$$

3.1.2. Vibration under Moving Loads. When the vibration response of a simply supported beam under the excitation of a moving load is controlled by TMDI, it is assumed that the moving concentrated force p_0 moves at a uniform velocity v on the simply supported beam with a span, and the equation of motion of a standard single degree-of-freedom system with mode shape coordinates as variables is established, it is shown in the following formula:

where, $u_j(t)$ is the generalized coordinate corresponding to the j -th mode of the simply supported beam; $F_{bj}(t)$ is the j -th mode load of the moving concentrated force; and $F_{Tj}(t)$ is the j -th mode force of the TMDI, and the expressions are as follows:

$$F_{bj}(t) = \frac{1}{m_j} p_0 \sin \frac{j\pi vt}{L}, \quad (18)$$

$$\begin{aligned} F_{Tj}(t) &= \frac{1}{m_j} \phi_j\left(\frac{L}{2}\right) \left\{ k_d \left[x_d - \phi_j\left(\frac{L}{2}\right) u_j(t) \right] + c_d \left[\dot{x}_d - \phi_j(L/2) \dot{u}_j(t) \right] \right\}, \\ &= \frac{m_d}{m_j} \phi_j(L/2) \left\{ \omega_d^2 \left[x_d - \phi_j(L/2) u_j(t) \right] + 2\xi_d \omega_d \left[\dot{x}_d - \phi_j(L/2) \dot{u}_j(t) \right] \right\}. \end{aligned} \quad (19)$$

For the convenience of calculation, the following parameters are defined:

$$\begin{aligned}\alpha_j &= \phi_j\left(\frac{L}{2}\right)\frac{m_d}{m_j}, \varepsilon_j = \frac{b}{m_j}, \\ v_j &= x_d - \phi_j\left(\frac{L}{2}\right)u_j(t), \dot{v}_j = \dot{x}_d - \phi_j\left(\frac{L}{2}\right)\dot{u}_j(t), \\ \ddot{v}_j &= \ddot{x}_d - \phi_j\left(\frac{L}{2}\right)\ddot{u}_j.\end{aligned}\quad (20)$$

Formula (19) can be simplified to the following formula:

$$F_{T_j}(t) = \alpha_j(\omega_d^2 v_j + 2\xi_d \omega_d \dot{v}_j). \quad (21)$$

And because of $F_{T_j}(t) = -\phi_j(L/2)(m_d + b)\ddot{x}_d/m_j$, the following formula can be deduced.

$$\varepsilon_j[\ddot{v}_j + \phi_j(L/2)\ddot{u}_j] + \omega_d^2 v_j + 2\xi_d \omega_d \dot{v}_j = 0. \quad (22)$$

Simultaneously from formula (19), formula (21), and formula (22), the equation system is written in the matrix form as shown in the following formula:

$$\widehat{M}_j \ddot{y}_j + \widehat{C}_j \dot{y}_j + \widehat{K}_j y_j = \widehat{F}_j. \quad (23)$$

Fourier transform is performed on the above equation to obtain equation

$$Y_j(\omega) = (-\omega^2 \widehat{M}_j + i\omega \widehat{C}_j + \widehat{K}_j)^{-1} \widehat{F}_j(\omega). \quad (24)$$

Then, the j th-order modal response of the simply supported beam is

$$u_j(\omega) = H_j(\omega) F_{b_j}(\omega). \quad (25)$$

The expression of the transfer function $H_j(\omega)$ is the following formula:

$$H_j(\omega) = \left[-\omega^2 + 2i\omega\xi_j\omega_j + \omega_j^2 - \omega^2\varepsilon_j\phi_j(L/2)X^{-1}(2\xi_d\omega_d i\omega + \alpha_j\omega_d^2)^{-1} \right], \quad (26)$$

where $X = -\omega^2\varepsilon_j + 2\xi_d\omega_d i\omega + \omega_d^2$; $F_{b_j}(\omega)$ is the Fourier transform of the j -th mode load; and $\widehat{F}_{b_j}(t)$ of the moving concentrated force, which is given in the following formula:

$$F_{b_j}(\omega) = \frac{1}{m_j} p_0 \frac{j\pi\nu/L}{\omega^2 - (j\pi\nu/L)^2} \left[(-1)^j e^{-i\omega(L/\nu)} - 1 \right]. \quad (27)$$

Then, the vibration displacement response spectrum $Y(\omega)$ of the simply supported beam under the excitation of the moving force is as follows:

$$Y_1(\omega) = \frac{1/m_1 p_0 \left[(-2\pi L/\nu) - (\pi)^2 \right]^{-1} \cdot \cos(\omega L/2\nu) \cdot e^{-1(\omega L/2\nu)} \cdot \phi_1(L/2)}{-\omega^2 + i\omega 2\xi_1\omega_1 + \omega_1^2 - \omega^2 (b/m_d)\phi_1(L/2)X^{-1} \left[2\xi_d\omega_d i\omega + \phi_1(L/2) \cdot m_d/m_1\omega_d^2 \right]}. \quad (29)$$

3.2. Optimal TMDI System. In order to minimize the vibration response of a simply supported beam, the parameters of the TMDI must be optimized. For the convenience of calculation, define two parameters μ and β , where $\mu = m_d/m_1$ is the ratio of the TMDI mass m_d to the first-order mode mass m_1 of the simply supported beam. $\beta = b/m_1$ is the

mass parameter b of the inertial device, and the first-order of the simply supported beam, is the ratio of mode shape to mass m_1 [15]. In the present study, the parameters of TMDI are μ , β , ω_d , and ξ_d where ξ_d is the natural circular frequency and damping ratio of the TMDI system, respectively [16].

The design of the optimal TMDI parameters includes two steps: first, select the appropriate mass ratio μ and β . Second, find the optimal ω_d and ξ_d based on μ and β . In order to obtain the optimal ω_d and ξ_d , the author proposes to

TABLE 1: Simply supported beam parameters.

Parameter	Beam length L/m	Bending stiffness of section $EI/(N \cdot m^2)$	Mass per unit length $m/(kg \cdot m^{-1})$	Damping ratio ξ_1	First-order natural frequency $\omega_1/(rad \cdot s^{-1})$
Numerical value	20	1×10^9	3000	0.025	14.25

use the augmented Lagrange multiplier method for analysis. The augmented Lagrangian multiplier method is a method combining the penalty function outlier method on the basis of the Lagrangian multiplier method [17]. The author adopts the method of MATLAB programming to realize the purpose of finding the optimal parameters.

3.2.1. Optimization of Beam-TMDI System under Seismic Acceleration Excitation

$$\min \bar{y}(\omega) = H_1(\omega) \cdot \phi_1(x) \cdot \sqrt{S_{\ddot{x}_g}(\omega)}, \quad (30)$$

$$s.t. h(\omega) = \max \bar{y}_1(\omega) - \max \bar{y}_2(\omega) = 0. \quad (31)$$

In formulas (30) and (31), $H_1(\omega)$ is the frequency response function; $h(\omega)$ is the constraint condition;

$\max \bar{y}_1(\omega)$ is the maximum value of $\bar{y}_1(\omega)$ in the interval $0, \omega_1$; $\max \bar{y}_2(\omega)$ is the maximum value of $\bar{y}_2(\omega)$; and ω_0 is a certain frequency value and $\omega_0 > \omega_1$

The augmented Lagrangian function of the optimization problem is shown in the following formula:

$$L(\omega, \lambda, \delta) = \bar{y}(\omega) + \lambda h(\omega) + \frac{\delta}{2} h^2(\omega), \quad (32)$$

where λ is the initial Lagrange multiplier and δ is the positive penalty coefficient.

3.2.2. Optimization of Beam-TMDI System for Moving Force Excitation

$$\min y(\omega) = H_1(\omega) \cdot \phi_1(x) \cdot F_{b1}(\omega), \quad (33)$$

$$s.t. h(\omega) = \max y_1(\omega) - \max y_2(\omega) = 0, \quad (34)$$

$$L(\omega, \lambda, \delta) = y(\omega) + \lambda h(\omega) + \frac{\delta}{2} h^2(\omega). \quad (35)$$

In formulas (33)–(35), $\max y_1(\omega)$ is the maximum value of $y_1(\omega)$ in the interval $(0, \omega_1)$; $\max y_2(\omega)$ is the maximum value of $y_2(\omega)$ in the interval (ω_1, ω_0) .

4. Analysis of Results

Taking a simply supported beam as an example, the effectiveness of the TMDI control system under two different types of loads is studied. The parameters of the beam are shown in Table 1. The seismic acceleration spectrum adopts the Kanai–Tajimi spectrum, and its parameters are $\omega_g = 15.54 rad/s$, $\xi_g = 0.8523$, and $S_0 = 0.0143$. The magnitude of the moving force and the moving speed are $p_0 = 6000 kN$ and $v = 60 m/s$, respectively.

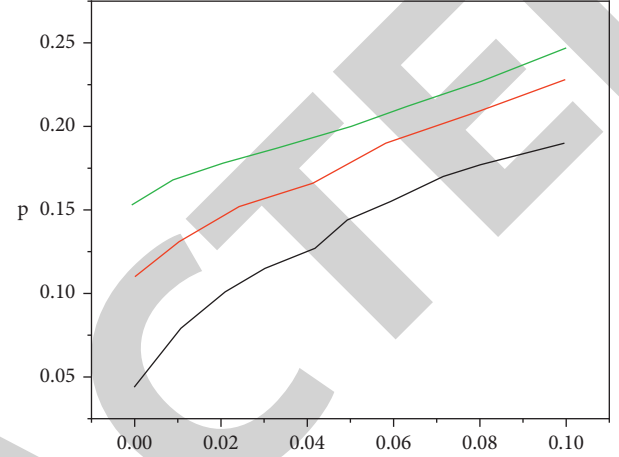


FIGURE 2: The influence of mass ratios μ and β on the optimal damping ratio of TMDI.

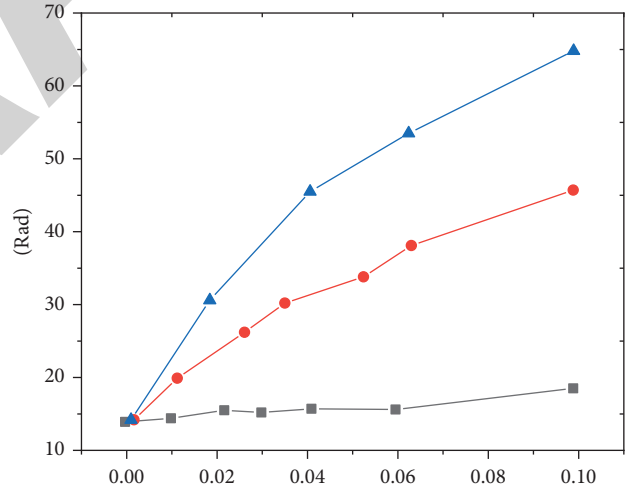


FIGURE 3: The influence of mass ratios μ and β on the optimal frequency of TMDI.

4.1. Optimal TMDI Parameters. Similar to the traditional tuned mass damper TMD, in order to optimize the damping performance of the TMDI system, parameter optimization must be carried out [18]. For different mass ratios μ and parameters β , the authors used the augmented Lagrangian optimization algorithm to optimize the TMDI damping ratio ξ_d and frequency ω_d , the optimal damping ratio ξ_d and the optimal frequency ω_d , respectively, as shown in Figures 2 and 3. As the mass ratio increases, the optimal damping ratio ξ_d of the TMDI system also increases, while the optimal frequency ω_d decreases [19]. At present, the inertial device of TMDI can amplify the physical mass of the damper by 60

times to 200 times through the setting of the parameter β [20].

It is worth noting that the TMDI system has different characteristics from the traditional TMD system. The optimal frequency of the traditional TMD system is close to the first-order natural frequency of the structure, while the optimal natural circular frequency ω_d of the TMDI system obtained by the author is much larger than the first-order natural frequency of the structure. For example, when the mass ratios are $\mu = 0.005$ and $\beta = 0.03$, the optimal damping ratio and natural circle frequency of the TMDI damper obtained by the augmented Lagrangian optimization algorithm are $\xi_d = 0.1154$ and $\omega_d = 37.5199\text{rad/s}$, respectively. The first-order natural circular frequency of the known structure is $\omega_1 = 14.25\text{rad/s}$, and it is obvious that ω_d is much larger than ω_1 . The optimal TMDI frequency values obtained by many scholars have similar characteristics.

4.2. Parameter Sensitivity Analysis. When the TMDI system adopts the optimal frequency and damping ratio, its vibration reduction performance is optimal, and the acquisition of these parameters is only related to the characteristics of the structure itself. But there are some uncertain factors in the actual structure, so it is necessary to carry out the robustness analysis of the TMDI system. Due to space limitations, the effect of the variation of design parameters ω_d and ξ_d on the maximum displacement response of the beam-TMDI system for different mass ratios μ and β under the action of moving force is shown [21]. The 3D surface exhibits a long and narrow shape, which means that the disturbance has a significant effect on the control performance. Changing the TMDI frequency can significantly change the control effect, while changing the TMDI damping ratio has little effect on the system control performance. In other words, the beam-TMDI system control performance is more sensitive to frequency. When the mass ratio μ increases, the variation range of the maximum displacement response is smaller, which indicates that the robustness of the system is stronger when the μ value increases, which is consistent with the TMD system ($\beta = 0$). In addition, when the mass ratio μ is the same, the width of the concave surface becomes wider as the β value becomes larger [22].

4.3. Simply Supported Beams—Effectiveness of the TMDI System. In order to study whether the simply supported beam is excited by seismic acceleration and moving force, whether installing the TMDI system at the mid-span position can effectively control the vibration response of the beam structure, first, set the mass ratio μ of the TMDI system to a certain value of 0.005, and β to 0.01, 0.03, and 0.05, respectively. Then, the optimal parameters of the TMDI system are obtained by the augmented Lagrangian optimization algorithm, and the frequency domain response analysis of the simply supported beam structure under seismic acceleration and moving force excitation is carried out. In addition, when the mass ratio μ is constant and as the mass ratio β increases, the control effect of the TMDI system

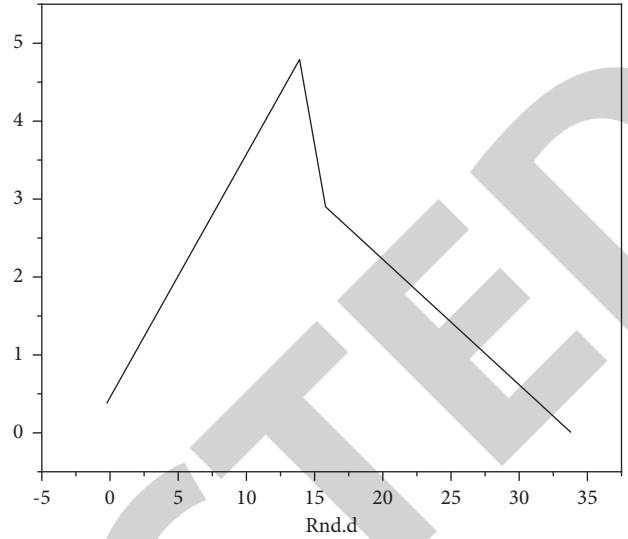


FIGURE 4: Comparison of vibration reduction performances of TMDI and TMD systems under seismic acceleration.

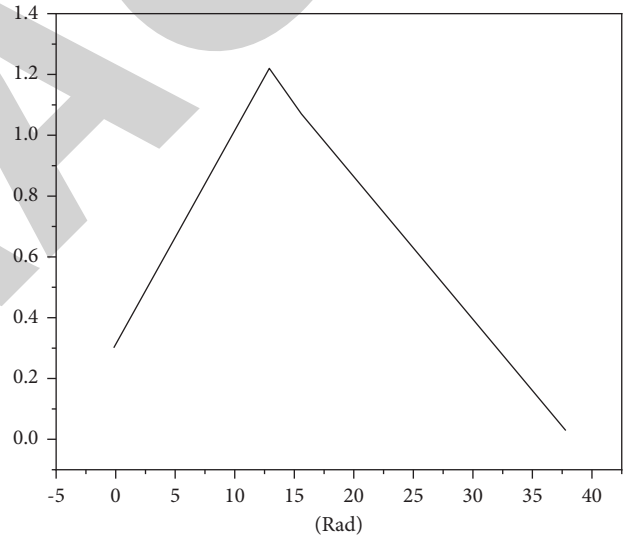


FIGURE 5: Comparison of vibration reduction performances of TMDI and TMD systems under moving force.

is better. Therefore, installing a TMDI system in the mid-span of a simply supported beam can significantly reduce its displacement response [23].

4.4. Performance Comparison of TMDI and TMD Systems. In order to effectively carry out comparative analysis, the mass ratio μ of the TMDI system and the TMD system is set to a fixed value of 0.005, and the parameter β of the TMDI system is set to 0, that is, $\beta = b = 0$, at this time, the TMDI system degenerates into a TMD system. The vibration reduction effects of the optimal TMD parameters obtained by these two optimization methods are shown in Figures 4 and 5, which are in complete agreement. This also verifies the correctness of the augmented Lagrangian optimization algorithm [24].

In order to further analyze the superiority of the TMDI system, the parameter β is set to 0.03. After parameter optimization based on the augmented Lagrangian optimization algorithm, the displacement responses in the frequency domain under the action of seismic acceleration and moving force, respectively, are obtained, as shown in Figure 4 and shown in the solid line part of Figure 5. The vibration reduction performance of the TMDI system is obviously better than that of the TMD system.

5. Conclusion

Based on the analysis results, the following conclusions are drawn:

- (1) When the mass ratio remains unchanged, the vibration reduction performance electricity of the beam-TMDI system increases with the increase in the mass ratio.
- (2) The vibration reduction performance of the TMDI system is more sensitive to the TMDI frequency value, while the damping ratio has less influence on its control effect.
- (3) When the mass ratio is small, the robustness of the TMDI system is mainly controlled by the inertial device, and the inertial device has an obvious influence on its robustness.
- (4) When using TMDI to control the vibration response electricity of the simply supported beam structure under the excitation of seismic acceleration and moving force, its vibration reduction effect is obviously better than that of the simply supported beam structure under TMD control, especially when the mass ratio is smaller than μ .

Data Availability

The data used to support the findings of this study are available from the author upon request.

Conflicts of Interest

The author declares no conflicts of interest.

Acknowledgments

The study was supported by Foundation of "Shaanxi Educational of Committee," under Project No. 11JK0514.

References

- [1] A. Taale, C. E. Ventura, and J. Marti, "On the feasibility of iot-based smart meters for earthquake early warning," *Earthquake Spectra*, vol. 37, no. 3, pp. 2066–2083, 2021.
- [2] T. Kishida, D. S. Park, R. L. Sousa, R. Armstrong, and Y. J. Byon, "Modulus reductions of dam embankment materials based on downhole array time series," *Earthquake Spectra*, vol. 36, no. 1, pp. 400–421, 2020.
- [3] G. Lanzano and L. Luzi, "A ground motion model for volcanic areas in Italy," *Bulletin of Earthquake Engineering*, vol. 18, no. 1, pp. 57–76, 2020.
- [4] A. N. Refani, Y. Tajunnisa, K. Yudoprasetyo, F. Ghifari, and D. I. Wahyudi, "Evaluation of structure performance under seismic load with non-linear time history on high-rise building affected by kendeng fault earthquake simulation," *Key Engineering Materials*, vol. 879, pp. 232–242, 2021.
- [5] F. Khosravi, S. A. Hosseini, and A. Tounsi, "Forced axial vibration of a single-walled carbon nanotube embedded in elastic medium under various moving forces," *Journal of Nano Research*, vol. 63, pp. 112–133, 2020.
- [6] H. Y. Chen, H. Ding, S. H. Li, and L. Q. Chen, "The scheme to determine the convergence term of the galerkin method for dynamic analysis of sandwich plates on nonlinear foundations," *Acta Mechanica Solida Sinica*, vol. 34, no. 1, pp. 1–11, 2021.
- [7] A. Ebrahimi-Mamaghani, A. Hs, and B. Mr, "On the vibrations of axially graded Rayleigh beams under a moving load," *Applied Mathematical Modelling*, vol. 84, pp. 554–570, 2020.
- [8] A. Tk, A. Ab, and A. Rk, "Optimization of multilayer rail substrate under moving load, using metamaterials," *Procedia Computer Science*, vol. 176, pp. 3399–3406, 2020.
- [9] F. Kheiri, "A multistage recursive approach in time- and frequency-domain for thermal analysis of thermochromic glazing and thermostatic control systems in buildings," *Solar Energy*, vol. 208, pp. 814–829, 2020.
- [10] Y. Chen, J. Xu, Y. Gao, L. Lin, J. Cao, and H. Ma, "Analysis and design of phase-shift pulse-frequency-modulated full-bridge LLC resonant converter," *IEEE Transactions on Industrial Electronics*, vol. 67, no. 2, pp. 1092–1102, 2020.
- [11] Y. Wei, Q. Luo, and A. Mantooth, "Comprehensive comparisons between frequency-domain analysis and time-domain analysis for LLC resonant converter," *IET Power Electronics*, vol. 13, no. 9, pp. 1735–1745, 2020.
- [12] T. Chen, Y. Zhu, X. X. Xi, H. Huan, and W. Ding, "Process parameter optimization and surface integrity evolution in the high-speed grinding of tial intermetallics based on grey relational analysis method," *International Journal of Advanced Manufacturing Technology*, vol. 117, no. 9–10, pp. 2895–2908, 2021.
- [13] K. Nagai, K. Nagato, T. Osa et al., "Parameter optimization in the drying process of catalyst ink for pefc electrode films with few cracks," *ECS Transactions*, vol. 104, no. 9, pp. 17–23, 2021.
- [14] X. Chen, X. Gao, X. Lin, J. Liu, and L. Le, "A novel method for rapidly calculating explosion dynamic displacement response of reticulated shell structure based on influence surfaces," *Advances in Structural Engineering*, vol. 23, no. 6, pp. 1098–1113, 2020.
- [15] Y. R. Lee, H. S. Kim, and J. W. Kang, "Seismic response control performance evaluation of tuned mass dampers for a retractable-roof spatial structure," *International Journal of Steel Structures*, vol. 21, no. 1, pp. 213–224, 2021.
- [16] W. H. Xu, Q. N. Zhang, W. C. Ma, and E. H. Wang, "Response of two unequal-diameter flexible cylinders in a side-by-side arrangement: characteristics of fiv," *China Ocean Engineering*, vol. 34, no. 4, pp. 475–487, 2020.
- [17] P. S. Phani and W. C. Oliver, "Critical examination of experimental data on strain bursts (pop-in) during spherical indentation," *Journal of Materials Research*, vol. 35, no. 8, pp. 1028–1036, 2020.
- [18] H. Vargas, J. Ramirez, and H. Arguello, "Admm-based l1-l1 optimization algorithm for robust sparse channel estimation

Retraction

Retracted: Seismic Performance and Vibration Control of Rapid Construction Environmental Protection Wall Based on Artificial Intelligence

International Transactions on Electrical Energy Systems

Received 19 September 2023; Accepted 19 September 2023; Published 20 September 2023

Copyright © 2023 International Transactions on Electrical Energy Systems. This is an open access article distributed under the Creative Commons Attribution License, which permits unrestricted use, distribution, and reproduction in any medium, provided the original work is properly cited.

This article has been retracted by Hindawi following an investigation undertaken by the publisher [1]. This investigation has uncovered evidence of one or more of the following indicators of systematic manipulation of the publication process:

- (1) Discrepancies in scope
- (2) Discrepancies in the description of the research reported
- (3) Discrepancies between the availability of data and the research described
- (4) Inappropriate citations
- (5) Incoherent, meaningless and/or irrelevant content included in the article
- (6) Peer-review manipulation

The presence of these indicators undermines our confidence in the integrity of the article's content and we cannot, therefore, vouch for its reliability. Please note that this notice is intended solely to alert readers that the content of this article is unreliable. We have not investigated whether authors were aware of or involved in the systematic manipulation of the publication process.

Wiley and Hindawi regrets that the usual quality checks did not identify these issues before publication and have since put additional measures in place to safeguard research integrity.

We wish to credit our own Research Integrity and Research Publishing teams and anonymous and named external researchers and research integrity experts for contributing to this investigation.


The corresponding author, as the representative of all authors, has been given the opportunity to register their agreement or disagreement to this retraction. We have kept a record of any response received.

References

- [1] J. Fu, S. Zhou, L. Liu, and M. Liu, "Seismic Performance and Vibration Control of Rapid Construction Environmental Protection Wall Based on Artificial Intelligence," *International Transactions on Electrical Energy Systems*, vol. 2022, Article ID 1385774, 8 pages, 2022.

Research Article

Seismic Performance and Vibration Control of Rapid Construction Environmental Protection Wall Based on Artificial Intelligence

Jie Fu ^{1,2}, Shuangxi Zhou,^{1,2} Li Liu,² and Mingxing Liu^{1,2}

¹Jiangxi Key Laboratory of Disaster Prevention-mitigation and Emergency Management, East China Jiaotong University, Nanchang 330013, Jiangxi, China

²School of Civil Engineering and Architecture, East China Jiaotong University, Nanchang 330013, Jiangxi, China

Correspondence should be addressed to Jie Fu; 2928@ecjtu.edu.cn

Received 18 August 2022; Revised 5 September 2022; Accepted 17 September 2022; Published 29 September 2022

Academic Editor: Nagamalai Vasimalai

Copyright © 2022 Jie Fu et al. This is an open access article distributed under the Creative Commons Attribution License, which permits unrestricted use, distribution, and reproduction in any medium, provided the original work is properly cited.

With the continuous increase in building types, people's demand for buildings is increasing. In addition to focusing on the work of the building itself, high requirements are also placed on the safety, stability, and durability of the building. Especially in other earthquake-prone areas, it is even more necessary to strengthen seismic isolation research to reduce vibration. Rapid construction of environmental protection walls pays attention to environmental protection and efficiency during construction, which can effectively solve problems in the construction process, but the seismic resistance of rapid construction environmental protection walls is unknown. Therefore, this paper used artificial intelligence technology to study the seismic performance of rapid construction environmental protection walls and analyzed its vibration control. This paper firstly established the seismic performance analysis model of the environmental protection wall, used the finite element method to construct the environmental protection wall model, and then used the artificial intelligence algorithm to analyze the seismic performance of the rapid construction environmental protection wall. The experimental results showed that the peak load of the rapid construction environmental protection wall was about 250 KN, and the seismic performance was good.

1. Introduction

In the design of the seismic isolation layer of the building structure, the design work is generally completed in the way of the superstructure, the intermediate isolation layer, and the substructure. The design mode of the seismic isolation layer can better improve the use efficiency of the superstructure, avoid the abnormality of the superstructure, and ensure that it can still maintain a good elastic effect after the earthquake's destructive force. In addition, in the process of seismic isolation layer design, its strength should be comprehensively analyzed in combination with relevant parameters such as building structure, construction area environment, and geological conditions. It is necessary to ensure that the seismic energy would not have a bad effect on the overall application effect of the structure. The research

on the seismic performance and vibration control of building walls can maintain the comprehensive application quality of building structures and reduce safety hazards and economic losses, so it is very necessary to test the seismic performance of building walls.

At present, there are many studies on the seismic performance and vibration control of buildings. Varum gave a detailed description of the seismic performance of buildings in Nepal [1]. Sabermahany and Attarnejad compared the seismic response of shallow hyperbolic shell raft foundations supported by steel flexural structures with those of these structures supported by piled raft foundations [2]. Bento and Simoes summarized the research status of seismic performance evaluation of buildings [3]. Sovester and Adiyanto investigated the performance of a reinforced concrete school building in Sabah that suffered multiple earthquakes [4].

Verma and Ram conducted a review of building standard guidelines that were important in preventing various types of damage typical of seismic conditions [5]. Although there are many studies on the seismic performance and vibration control of buildings, there are few studies on the seismic performance of rapid construction environmental protection walls.

Artificial intelligence has been used in construction. Roslon used artificial intelligence and hyper-heuristic algorithms to select materials and techniques during construction in a way that improves project parameters [6]. Liang et al. used artificial intelligence to predict internal heat gain in ventilation and air conditioning [7]. Zhi used blockchain and artificial intelligence to build smart cities [8]. Abioye et al. revealed AI applications, examined AI technologies in use, and identified opportunities and challenges for AI applications in the construction industry [9]. Hooda et al. studied how artificial intelligence and its various principles can be integrated with the emerging field of structural engineering [10]. Although artificial intelligence has many applications in construction, it has not been used to detect the seismic performance of buildings.

This paper used artificial intelligence technology to study the seismic performance of rapid construction of environmental protection walls. In this paper, finite element analysis software was used to establish the seismic performance analysis model of the environmental protection wall, and then artificial intelligence technology was used to identify the seismic performance of the wall, and the vibration control method is analyzed. In the experimental part, experiments were carried out on the wall from five aspects: load-displacement relationship, stiffness degradation curve, plastic rotation angle, shear deformation angle in the core area of nodes, and interstory displacement ductility coefficient to study its seismic performance.

2. Model of Seismic Performance of Environmental Protection Wall

The research object of this paper is the problem of computational fracture methods because the failure limit is a process of energy change as the crack evolves and propagates. At the same time, due to the appearance of cracks, the material is in a state of failure and the area shows non-uniformity. The finite element program ANSYS has a powerful function of calculating crack structures, so this program is used for finite element calculation and analysis of walls [11].

The local element failure method was developed based on the principle of continuous failure mechanism. If the element that reaches the critical damage value looks like a crack, the whole process of cracking and fracturing can be analyzed with clear physical meaning.

ANSYS software integrates the Solid65 rigid body 3D model mainly used for concrete, which is convenient for users to calculate the final concrete proportion. The Solid65 tool itself has two parts. One part is based on the Solid45 eight-point entity combination, which takes into account the properties of concrete, adding a concrete failure model and a

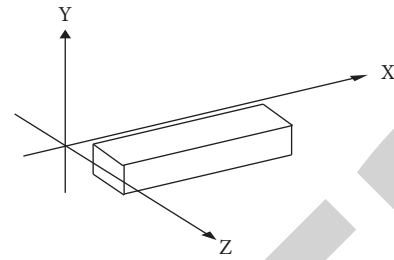


FIGURE 1: The Link8 space rod unit.

distribution model under triaxial stress. The other part is a model consisting of diffuse rebar elements. In the model, the material, position, angle, and reinforcement ratio of the reinforcement are set by entering actual parameters. Since the discrete model is used in this paper, there is no need to reinterpret the diffusion coefficient element [12].

Another important feature of the Solid65 material is the propagation crack model. Due to the high tensile strength of the material, concrete members in many cases suffer from cracks, which cause sudden changes in local stress and stiffness. In finite element analysis, there are three main methods for dealing with cracks. It includes comparing individual cracks with element boundaries, comparing distributed cracks with internal relationships, and modifying element design functions to construct basic element models.

2.1. The Type of Unit Used

2.1.1. Rod Unit. Rebar analysis in ANSYS usually adopts 2-node 3d bar elements such as Link1, Link8, Link180, beam element Beam188, and pipe element Pipe20. In this paper, the Link8 rod unit is selected, which only bears axial tension and compression and has no correction time. It has 3 directions and can be used to study various mechanical problems such as elasticity, plasticity, creep, expansion, and large deformation [13]. The Link8 pole module is shown in Figure 1.

2.1.2. Brittle Material Element (Solid65). At the loading and support points of the part, to avoid a single concentration of pressure, causing undue breakage, and difficult integration, it needs to increase the required size or add soft spots. The elastic pad uses Solid45 material, and by defining a large elastic modulus, a force or constraint is applied to the elastic pad, and the pressure is transmitted through the elastic pad. The brittle material unit is shown in Figure 2.

Due to the complex design of the computational model, there are many applications. In order to facilitate the step-by-step densification of the spatial cell grid and have a strong realization in the design, the cell type shown in Figure 2(c) is adopted in this paper.

2.1.3. Concrete Unit (Solid92). Concrete elements are used to model reinforced concrete materials. Solid92 is a ten-node tetrahedron model with high precision. The ten-node tetrahedron element has a strong correlation with the shape,

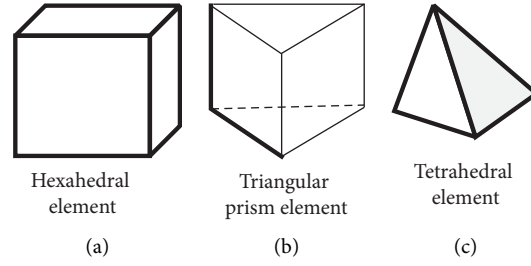


FIGURE 2: The brittle material unit (a) is a hexahedral unit, (b) is a triangular prism unit, and (c) is a tetrahedral unit.

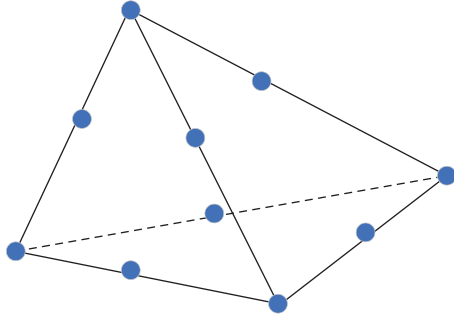


FIGURE 3: The ten-node tetrahedral element.

which is convenient for the gradual refinement of the space grid [14]. The ten-node tetrahedral element is shown in Figure 3.

2.2. Finite Element Mesh Division. There are two methods of meshing, one is the method of defining nodes and creating elements. One is to create an instance of the instance, and after the instance is created, the network is directly mapped to the instance. This paper adopts the latter method. After a model is created, there are two ways to mesh it: a free mesh method and a regular mesh method. The free grid method has a good way of adapting to complex boundaries, while the regular grid method has high requirements on the geometric boundaries of the model. Or it can be said that if the normal meshing method is used, the model needs to take special treatment [15]. This article would use the free meshing method.

2.3. Determination of Wall Analysis Model. The three solid parameters of the relevant material are described below [16].

2.3.1. Wall Tie Bars. The steel bar (a typical elastic-plastic material) can be simulated by imitating the plastic steel bar model, and the $\Phi 6$ -type tension bar is subjected to a uniaxial tensile test on the universal testing machine, and the simplified stress-strain curve is obtained.

2.3.2. Reinforced Concrete Components. Reinforced concrete members are composite elastic-plastic materials. If this is converted to a homogeneous material, the material parameters in the elastic plane can be calculated exactly as follows:

$$E = \frac{E_1 V_1 + E_2 V_2}{V_1 + V_2}. \quad (1)$$

In the formula, E_1 is the elastic modulus of the steel bar and V_1 is the total volume of the steel bar in the member. E_2 is the elastic modulus of concrete and V_2 is the volume of concrete.

Similarly, the yield stress of the same member should also be calculated equivalently as follows:

$$\sigma_s = \frac{\sigma_1 V_1 + \sigma_2 V_2}{V_1 + V_2}, \quad (2)$$

σ_1 is the yield stress of steel bars and σ_2 is the yield stress of concrete.

After a component enters the plastic stage, it can be considered to satisfy the following rules:

$$\sigma = A \varepsilon^{1/4}. \quad (3)$$

The stress-strain curve of reinforced concrete can be calculated.

2.3.3. Masonry. The masonry conforms to the law of elastic-brittle deformation. The strength of the block measured by the test is 13 MPa, and the strength of the mortar is 7 MPa. The formula for the compressive strength of masonry is

$$f_m = 0.78 \sqrt{f_1 (1 + 0.07 f_2)}. \quad (4)$$

The formula for tensile strength of masonry is as follows:

$$f_{t,m} = K_3 \sqrt{f_2}. \quad (5)$$

Among them, $K_3 = 0.141$.

3. Recognition of Vibration Pattern of Environmental Protection Wall Based on Artificial Intelligence

The intelligent pattern recognition system utilizes the motion signals of different patterns collected at the beginning and uses the network architecture for deep machine learning. It can continuously associate with different motion patterns, and then detect motion patterns in different situations and send messages to the outside world. The method can be used in intelligent motion detection and fault diagnosis and early warning systems to ensure the safe

operation of equipment [17]. It prevents and reduces the occurrence of major accidents. In this paper, by building an intelligent vibration detection system, combined with deep machine learning, it can judge different movement patterns, identify memory and learn more information, and then conduct early warning tests.

3.1. Theoretical Basis of Vibration Pattern Recognition. In this paper, the single-arm optical fiber transmission detection method is adopted. Circulators, fiber probes, reflectors, and other experimental samples were used in the experiments, and the wave Formula of the new optical fiber electromagnetic waveguide is the Maxwell1 Formula. The identification is essentially the solution of the Maxwell1 Formulas [18].

$$\begin{aligned}\nabla \times E &= -\frac{\partial B}{\partial t}, \\ \nabla \times H &= \frac{\partial D}{\partial t} + J, \\ \nabla \times D &= \rho, \\ \nabla \times B &= 0.\end{aligned}\quad (6)$$

Among them, D , B , J , ρ can be expressed as follows:

$$\begin{aligned}D &= \varepsilon E = \varepsilon_0 \varepsilon_r E, \\ B &= \mu H = \mu_0 \mu_r H, \\ J &= 0, \\ \rho &= 0.\end{aligned}\quad (7)$$

The electric field strength is represented by E , the magnetic field strength is represented by H , and the electric displacement is represented by D . The magnetic induction intensity is represented by B , the current density is represented by J , the charge density is represented by ρ , the vacuum permittivity is represented by ε_0 , and the relative permittivity is represented by ε_r .

According to Maxwell's Formulas, the electromagnetic field continuity conditions at the interface of the medium can be obtained as follows:

$$\begin{aligned}n \times (E_1 - E_2) &= 0, \\ n \times (H_1 - H_2) &= 0, \\ n \times (\mu_1 H_1 - \mu_2 H_2) &= 0, \\ n \times (\varepsilon_1 H_1 - \varepsilon_2 H_2) &= 0.\end{aligned}\quad (8)$$

The normal unit vector of the interface is denoted by n , and the permeability is the scalar constant μ .

3.2. The Method of Vibration Pattern Recognition. Specific considerations for finite element analysis are as follows:

The first step determines the field, the second step selects the translation function, and the third step determines the eigenvalues. The fourth step is to create a finite element Formula system, the fifth step is to solve the finite factor

Formulas, and the sixth step is further computational processing [19].

The first step in determining the field is to divide the field into small regions of different shapes, such as 6-sided, 4-sided, and 3-sided. The second step is to choose the interpolation function by function type and then compute the domain scale to solve for the subdomain terms. The third step is to define the eigenvalues, coefficient matrices, interpolation functions, subdomain geometry, and properties of the different problems. The fourth step is to generate the finite element Formula of the system. Specifically, the field value at the node is calculated by computer simulation. In the calculation, a linear Formula system must be generated first. The fifth step in solving the finite element Formulas is to solve the system of linear Formulas and the value of the unknown domain and finally use the interpolation function to solve the value of any point in the domain.

4. Recognition of Vibration Pattern of Environmental Protection Wall Based on Artificial Intelligence

4.1. Active Control Technology. Generally speaking, active control is a vibration reduction control technology that uses other external forces to effectively control the vibration reduction of buildings by using different external vibration reduction control forces. Its working principle consists of four factors [20]:

- (1) Sensors can be used to monitor the external shock and dynamic response of the building structure.
- (2) The target data can be transferred to the computer.
- (3) The energy to be used can be calculated using a calculation method defined by a computer program.
- (4) The energy that can effectively control the system can be generated according to the external energy source.

4.2. Semiactive Control Technology. Generally speaking, semiactive control is the use of control technology to automatically adjust the parameters in the building system to achieve the purpose of effective vibration reduction. This control mode can be effectively accomplished with only a weak current and in the semi-intermediate control technique, switches are used for effective control. The operating state of the system is effectively controlled by various functions on the switch, thus changing the dynamic performance of the building structure to a certain extent.

At present, the typical semiactive control technology devices are variable damping systems, variable stiffness systems, controllable friction system, and parameter active adjustment of the mass damping system.

4.3. Passive Control Technology. Generally, in the vibration control of building structures, passive control generally refers to a technology that does not rely on external forces to control vibration. It adds subsystems to specific areas of the building structure to effectively improve the dynamic characteristics of

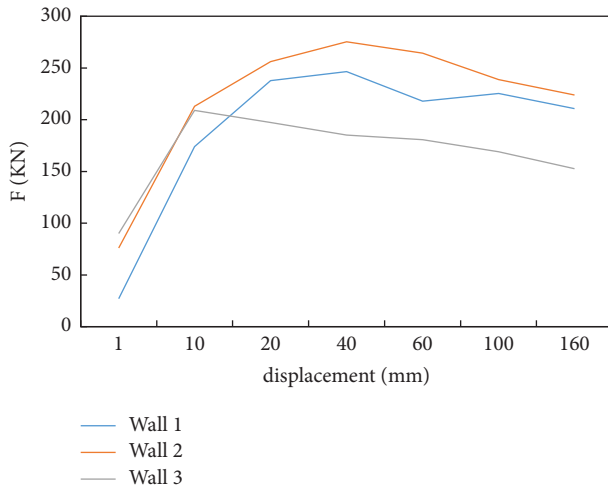


FIGURE 4: The wall load-displacement curve.

the structure itself. It is either set through a series of characteristics of the structure itself on the structural components. This passive control technology of vibration is a popular technology at present, and many passive controls have been perfected and widely used in practical applications.

4.4. Hybrid Control Technology. Hybrid control technology combines active and passive control. Combining the advantages of the two, it can not only destroy a large amount of seismic energy through the control device but also use the active control device to verify the control effect. Therefore, it is very important to use hybrid control in the design process. A general hybrid control device mainly includes a damping energy release device and a hybrid control combination of an active control hybrid device, active control, and a basic isolation device.

4.5. Comprehensive Analysis of Four Technologies. In general, the active control technology is the best among the four technologies, but due to the larger building volume and the need for more external power sources, the algorithm of the control device and system is also very complex, and this technology is less applicable than the other three technologies. Passive control technology has become the most widely used and fastest-growing technology due to its advantages of good vibration reduction, low cost, and easy implementation. The semiactive control technology is between active control and passive control. Compared with active control, it has high control accuracy and relatively low cost and has broad application prospects. The hybrid control technology is the product of multiple control technologies, which combines the advantages of all control technologies, so its development prospect is definitely broader than other control technologies [21].

5. Experimental Results of Wall Seismic Performance

Three types of quick-construction environmentally friendly walls commonly used in the market are selected and named

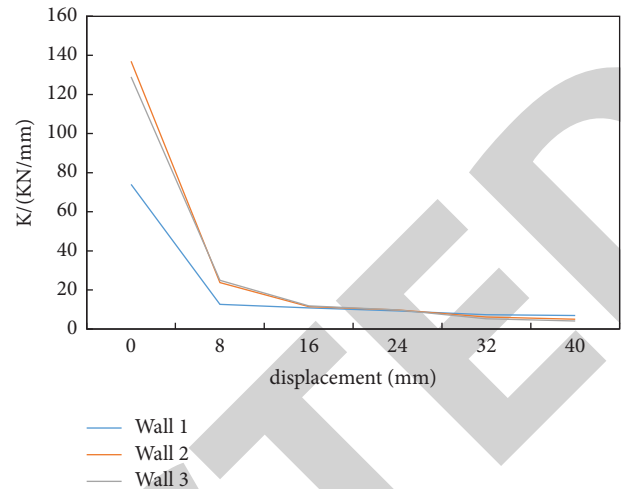


FIGURE 5: Wall stiffness degradation curve.

wall 1, wall 2, and wall 3. In this paper, the seismic performance of the wall is studied from five aspects: load-displacement relationship, stiffness degradation curve, plastic rotation angle, shear deformation angle of node core area, and interstory displacement ductility coefficient.

5.1. Load-Displacement Curve. The load-displacement curves of the three kinds of walls are shown in Figure 4.

Wall 1 reaches the initial crack state when the load is 40 kN and reaches the yield state when the load is 241.5 kN. When the load is 246.5 kN, the wall load reaches its peak value, and when the load decreases to 210.6 kN, the displacement of wall 1 reaches the limit. Wall 2 reaches the initial crack state when the load is 116 kN and reaches the yield state when the load is 219.4 kN. When the load is 275.3 kN, the load of wall 2 reaches its peak value, and when the load decreases to 223.9 kN, the displacement of wall 2 reaches the limit. When the load is 93 kN, wall 3 reaches the initial crack state, and when the load is 184.7 kN, it reaches the yield state. When the load is 209 kN, the load of wall 3 reaches its peak value, and when the load decreases by 152.7 kN, the displacement of wall 3 reaches the limit.

It can be seen from the data that in the initial stage of test loading, the curve shows a straight upward trend, and the stiffness of wall 1, wall 2, and wall 3 is not much different. When cracks appear in the wall, the structural stiffness decreases significantly, but the stiffness of wall 3 decreases the most. After the structure enters the yield state, loads of wall 1 and wall 2 continue to increase with the increase of displacement, but a load of wall 3 quickly reaches the peak value. Compared with wall 3, the descending section of the load-displacement curve of wall 1 and wall 2 is gentler.

On the whole, the peak load of the rapid construction environmental protection wall is about 250 kN.

5.2. Stiffness Degradation Curve. The three kinds of wall stiffness degradation curves are shown in Figure 5.

When there is no crack in the wall, the stiffness of the three kinds of walls is 74 kN/mm, 137 kN/mm, and 129 kN/mm.

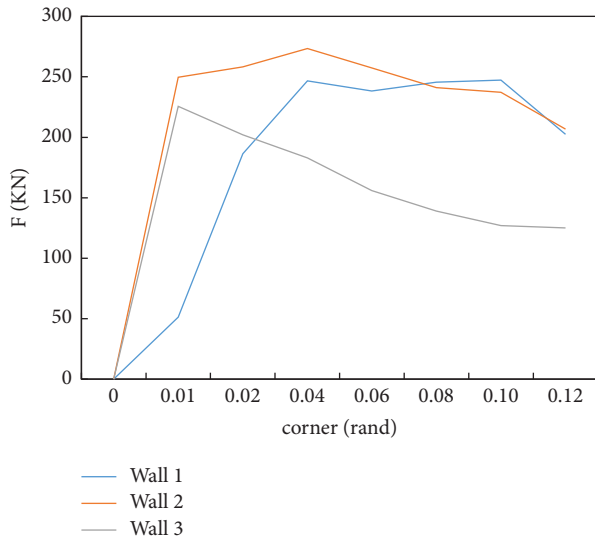


FIGURE 6: The relationship between load and plastic rotation angle.

mm respectively. When the wall crack is 8 mm, the stiffness of wall 1 is 12.6 KN/mm, the stiffness of wall 2 is 23.7 KN/mm, and the stiffness of wall 3 is 24.9 KN/mm. At this stage, the stiffness of the wall decreases sharply. When the wall crack is 16 mm, the stiffness of wall 1 is 10.8 KN/mm, the stiffness of wall 2 is 11.5 KN/mm, and the stiffness of wall 3 is 11.9 KN/mm, and then the stiffness of the wall decreases slowly.

In the early stage of test loading, cracks appeared in the wall and gradually expanded, resulting in a rapid decrease in the ability of the structure to resist horizontal loads and a rapid rate of stiffness degradation. In the later stage of loading, the stiffness degradation curve tends to be flat, indicating that after the wall is fully cracked and damaged, most of them quit work, and the structural stiffness is mainly provided by the frame. The stiffness degradation curves of wall 2 and wall 3 are similar. Compared with wall 2 and wall 3, the stiffness of wall 1 is relatively small, especially in the early stage of loading.

5.3. Plastic Corner. The relationship between load F and the plastic rotation angle is shown in Figure 6.

When the plastic rotation angle is 0.01rand, the load of wall 1 is about 50 KN, and the load of wall 2 and wall 3 is about 250 KN. When the plastic rotation angle is 0.02rand, the load of wall 1 and wall 3 is about 200 KN, and the load of wall 2 is about 250 KN. Then, with the gradual increase of the plastic corner of the wall, loads of wall 1 and wall 2 increase slowly and then gradually decrease, and a load of wall 3 decreases rapidly. When the plastic corner of the wall is 0.12rand, the load of wall 1 and wall 2 is about 200 KN, and a load of wall 3 is 125 KN.

5.4. Shear Deformation Angle in the Core Area of the Node. The relationship between the load F and the shear deformation angle γ in the core area is shown in Figure 7.

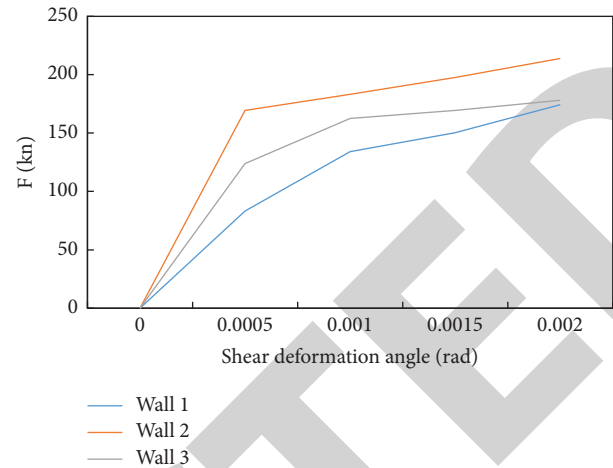


FIGURE 7: The relationship curve of the shear deformation angle of the core area.

TABLE 1: Wall interlayer displacement ductility coefficient.

Wall	Interlayer displacement ductility coefficient
Wall 1	7.4
Wall 2	11.3
Wall 3	8.1

When the wall load is small, the shear deformation angle in the core area of the wall node is very small, only 1/11 to 1/7 of the final shear deformation angle. When a large number of cracks at the column end develop and extend, the shear deformation angle begins to increase significantly, especially after the plastic hinge appears at the column end, and the shear deformation angle increases most significantly. Under the same horizontal load, the shear deformation angles of the core area of the node are wall 2, wall 3, and wall 1 in descending order.

5.5. Interlayer Displacement Ductility Coefficient. The relationship between the displacement ductility coefficients of the three kinds of walls is shown in Table 1.

The interlayer displacement ductility coefficient of wall 1 is 7.4, the interlayer displacement ductility coefficient of wall 2 is 11.3, and the interlayer displacement ductility coefficient of wall 3 is 8.1.

6. Results of Seismic Performance of Rapid Construction Environmental Protection Wall

This paper uses a machine learning algorithm to analyze the seismic performance of rapid construction environmental protection wall and discusses the vibration control method of rapid construction environmental protection walls. The research results are as follows:

- (1) In this paper, the finite element program ANSYS is used to construct the 3D model of the wall, and the element types such as rod element, brittle material element, and concrete element are introduced, and

the tetrahedral element structure is selected as the element type. Then, it builds the wall models and uses the regular mesh method to divide the finite element mesh.

- (2) This paper uses the deep learning method to construct an intelligent pattern recognition system, introduces the theoretical basis of vibration pattern recognition, and introduces the steps of vibration model recognition in detail.
- (3) This paper introduces the vibration control method for the rapid construction of environmental protection walls. It includes active control technology, semiactive control technology, passive control technology, and hybrid control technology, analyzes the control principles, and advantages and disadvantages of the four technologies.
- (4) In the experimental part, this paper selects 3 kinds of rapid construction environmental protection walls on the market. The wall is tested from five aspects: load-displacement relationship, stiffness degradation curve, plastic rotation angle, shear deformation angle of node core area, and interstory displacement ductility coefficient. This paper studies the seismic performance of rapid construction environmental protection walls. For the load-displacement relationship, the peak load of the three kinds of rapid construction environmental protection walls is about 250 KN. For the stiffness degradation curve, in the initial stage of loading, the stiffness degradation rate of the rapid construction environmental protection wall is faster, and with the gradual increase of the load, the stiffness degradation of the wall gradually slows down.

7. Conclusion

This paper uses the finite element method to establish a finite element model for the rapid construction of environmental protection walls and uses artificial intelligence technology to calculate the seismic performance of the wall. In the experiment part, the load-displacement relationship, stiffness degradation curve, plastic rotation angle, shear deformation angle of node core area, and interstory displacement ductility coefficient of rapid construction environmental protection wall were measured. The experimental results show that the rapid construction environmental protection wall has high load capacity and good seismic performance.

Data Availability

No data were used to support this study.

Conflicts of Interest

The authors declare that they have no conflicts of interest.

Authors' Contributions

All authors have seen the manuscript and approved to submit to your journal.

Acknowledgments

This work was supported by the National Natural Science Foundation of China (51968022) and Academic and Technical Leaders of Major Disciplines in Jiangxi Province (20213BCJL22039).

References

- [1] H. Varum, "Seismic performance of buildings in Nepal after the gorkha earthquake," *Impacts and Insights of the Gorkha Earthquake*, vol. 2018, no. 6, pp. 47–63, 2018.
- [2] H. Sabermahany and R. Attarnejad, "Seismic performance of buildings supported by a shallow doubly-curved shell raft foundation," *Structures*, vol. 36, no. 2, pp. 619–634, 2022.
- [3] R. Bento and A. Simoes, "Seismic performance assessment of buildings," *Buildings*, vol. 11, no. 10, pp. 440–453, 2021.
- [4] H. H. Sovester and M. I. Adiyanto, "Seismic performance of reinforced concrete school buildings in sabah," *Malaysian Academic Library Institutional Repository*, vol. 64, no. 8, pp. 148–152, 2017.
- [5] I. Verma and S. Ram, "Effect of irregularities on seismic performance of buildings," *A Review*, vol. 2020, no. 7, pp. 351–369, 2020.
- [6] J. Roslon, "Materials and technology selection for construction projects supported with the use of artificial intelligence," *Materials*, vol. 15, no. 4, pp. 1282–1283, 2022.
- [7] R. Liang, W. Ding, Y. Zandi, A. Rahimi, S. Pourkhorshidi, and M. A. Khadimallah, "Buildings' internal heat gains prediction using artificial intelligence methods," *Energy and Buildings*, vol. 258, no. 7, pp. 111794–112726, 2022.
- [8] Q. Zhi, "The integration of blockchain and artificial intelligence for a smart city," *Academic Journal of Computing & Information Science*, vol. 4, no. 8, pp. 45–63, 2021.
- [9] S. O. Abioye, L. O. Oyedele, L. Akanbi et al., "Artificial intelligence in the construction industry: a review of present status, opportunities and future challenges," *Journal of Building Engineering*, vol. 44, no. 12, pp. 103299–104127, 2021.
- [10] Y. Hooda, P. Kuhar, K. Sharma, and N. K. Verma, "Emerging applications of artificial intelligence in structural engineering and construction industry," in *International Conference on Mechatronics and Artificial Intelligence (ICMAI) 2021*, Gurgaon, India, 27 February 2021.
- [11] W. He, X. He, and C. Sun, "Vibration control of an industrial moving strip in the presence of input deadzone," *IEEE Transactions on Industrial Electronics*, vol. 64, no. 6, pp. 4680–4689, 2017.
- [12] G. Park, "Vibration control using a variable coil-based friction damper," in *Proceedings Volume 10164, Active and Passive Smart Structures and Integrated Systems 2017*, no. 9, pp. 101–105, Portland, OR, USA, 2017.
- [13] C. U. Dogruer and A. K. Pirsoltan, "Active vibration control of a single-stage spur gearbox," *Mechanical Systems and Signal Processing*, vol. 85, no. 2, pp. 429–444, 2017.
- [14] Z. Lu, Z. Wang, Y. Zhou, and X. Lu, "Nonlinear dissipative devices in structural vibration control: a review," *Journal of Sound and Vibration*, vol. 423, no. 3, pp. 18–49, 2018.
- [15] "Draeos," *Deep Learning: Neural-Inspired Artificial Intelligence*, vol. 2017, no. 5, pp. 1308–1320, 2017.
- [16] S. Elias, "Effect of SSI on vibration control of structures with tuned vibration absorbers," *Shock and Vibration*, vol. 2019, Article ID 7463031, 12 pages, 2019.
- [17] R. Atassi and R. Atassi, "Geological landslide disaster monitoring based on wireless network technology," *International*

Retraction

Retracted: Wireless Mobile Power Communication System Based on Artificial Intelligence Algorithm

International Transactions on Electrical Energy Systems

Received 19 September 2023; Accepted 19 September 2023; Published 20 September 2023

Copyright © 2023 International Transactions on Electrical Energy Systems. This is an open access article distributed under the Creative Commons Attribution License, which permits unrestricted use, distribution, and reproduction in any medium, provided the original work is properly cited.

This article has been retracted by Hindawi following an investigation undertaken by the publisher [1]. This investigation has uncovered evidence of one or more of the following indicators of systematic manipulation of the publication process:

- (1) Discrepancies in scope
- (2) Discrepancies in the description of the research reported
- (3) Discrepancies between the availability of data and the research described
- (4) Inappropriate citations
- (5) Incoherent, meaningless and/or irrelevant content included in the article
- (6) Peer-review manipulation

The presence of these indicators undermines our confidence in the integrity of the article's content and we cannot, therefore, vouch for its reliability. Please note that this notice is intended solely to alert readers that the content of this article is unreliable. We have not investigated whether authors were aware of or involved in the systematic manipulation of the publication process.

Wiley and Hindawi regrets that the usual quality checks did not identify these issues before publication and have since put additional measures in place to safeguard research integrity.

We wish to credit our own Research Integrity and Research Publishing teams and anonymous and named external researchers and research integrity experts for contributing to this investigation.

The corresponding author, as the representative of all authors, has been given the opportunity to register their agreement or disagreement to this retraction. We have kept a record of any response received.

References

- [1] J. Du and M. Guo, "Wireless Mobile Power Communication System Based on Artificial Intelligence Algorithm," *International Transactions on Electrical Energy Systems*, vol. 2022, Article ID 1636033, 7 pages, 2022.

Research Article

Wireless Mobile Power Communication System Based on Artificial Intelligence Algorithm

Juan Du  and Mingqi Guo 

Yellow River Conservancy Technical Institute, Kaifeng, Henan 475004, China

Correspondence should be addressed to Juan Du; 202003408@stu.ncwu.edu.cn

Received 30 June 2022; Revised 25 July 2022; Accepted 29 August 2022; Published 20 September 2022

Academic Editor: Nagamalai Vasimalai

Copyright © 2022 Juan Du and Mingqi Guo. This is an open access article distributed under the Creative Commons Attribution License, which permits unrestricted use, distribution, and reproduction in any medium, provided the original work is properly cited.

In order to solve the problems of low-risk assessment accuracy and long time-consuming assessment of current wireless mobile communication systems, a wireless mobile communication system based on artificial intelligence algorithms is proposed. First, the research status of risk assessment of wireless mobile communication system at home and abroad is analyzed, and the risk assessment index system of wireless mobile communication system is established; then, the learning samples are collected according to the risk assessment index system of wireless mobile communication system, and artificial intelligence algorithm is used to optimize the neural network. Build the wireless mobile communication system risk assessment model; finally, carry out the wireless mobile communication system risk assessment simulation comparison test. The experimental results show that the accuracy rate of the risk assessment of the wireless mobile communication system by the artificial intelligence algorithm is over 95%, and the assessment error is smaller than in other models. The risk assessment time of the wireless mobile communication system is significantly reduced, the real-time performance is better, and it has a higher practical application value.

1. Introduction

With the development of the communication industry, the number of wireless users is increasing day by day. Now, the penetration rate of mobile phones has reached 64.4 units/100 people. Data show that the total number of mobile phone users in Beijing exceeded 25 million in 2011, an increase of 21.0% over 2010. The number of fixed telephone users in Beijing decreased by 0.2% over last year to 8.839 million [1]. The total number of mobile phone users was 25.76 million, an increase of 21.0% over last year. Users increasingly rely on wireless communication and are sensitive to voice quality and network coverage. Complaints about voice quality, wireless coverage, and other technical aspects are also increasing.

Wireless network refers to any form of radio computer network, which is combined with telecommunication network, and can communicate with each other between network nodes without cables. According to the coverage of the network, it can be divided into wireless body area

network, wireless personal network, wireless local area network, wireless metropolitan area network, and wireless wide area network. Wireless personal networks and wireless LANs are the most exposed in daily life. Wireless networks formed by connecting several devices in a small range, such as Bluetooth devices, belong to wireless personal networks. The wireless network used to complete data exchange between network nodes or access the Internet in an area composed of wireless AP devices belongs to wireless LAN. Due to the rapid development and mutual promotion of wireless networks and mobile devices, wireless network coverage has been basically realized in public places and corporate offices [2]. Akpe, M. A. and others believe that wireless network terminal equipment and wired network terminal equipment have different characteristics, and wired network equipment will not be physically contacted by users or intruders, while the physical equipment of wireless network is likely to be contacted, so there may be intruders deploy fake APs. The computing power of wireless network terminal

equipment is usually weak, and it is easier to lose and damage than wired network terminal equipment [3]. The use of the wireless network has greatly improved the efficiency of the office and information transmission, but at the same time, due to the openness of the wireless network, its security is fragile and vulnerable to monitoring or attack. Therefore, how to implement an effective security protection mechanism for wireless networks and enhance the security of wireless networks is an important issue facing wireless networks.

Huang, H. and others used the complex network to study the secondary derivative coupling law of disasters and constructed the dynamic network model and unconventional event chain model [4]. T d ü Zenli and others proposed the risk assessment model and calculation method for the wide area measurement system (WAMS) communication backbone network, calculated the probability of risk events by using the reliability analysis method, and built a comparison judgment matrix by using the analytic hierarchy process for reference to realize the quantitative calculation of the risk impact value, so as to obtain the comprehensive risk value of the communication backbone network [5]. Shang, Y. and others proposed a risk evaluation method combining the complex network theory and the risk characteristics of the power communication network. According to the edge importance, the threats and losses caused to the network after failure are considered. According to the typical structure and communication service characteristics of power communication network, the average service risk and service risk balance are used as the network reliability evaluation indicators. Balance is used as the evaluation index of network reliability. The failure probability between different levels of power communication network is analyzed, and the risk analysis model is established [6]. On the whole, at present, the risk assessment of urban public security in the special environment is still based on the risk assessment of a single disaster in various industries. There are few studies on the spatio-temporal risk interaction between special environment (such as major activities) and urban operation, especially the coupling of multidisaster and multiscale risks; in addition, the risk assessment process lacks the updating mechanism of the risk assessment method based on the special environment and is still in the qualitative and quantitative assessment stage. There is also a certain gap between the standardized research on risk assessment and emergency management and foreign countries [7, 8].

On the basis of this research, this paper proposes a research method of wireless mobile communication system based on an artificial intelligence algorithm. Aiming at the parameter optimization problem of BP neural network applied in the risk assessment of wireless mobile communication system, a risk assessment model of wireless mobile communication system based on artificial intelligence algorithm is designed, and the risk assessment model of wireless mobile communication system is compared with other wireless mobile communication system risk assessment models. The experimental results show that the risk assessment time of the wireless mobile communication

system is significantly reduced, the real-time performance is better, and it has a higher practical application value.

2. Research Methods

2.1. Relevant Theories

2.1.1. BP Neural Network. The back-propagation algorithm is referred to as the BP algorithm, and the multilayer feedforward neural network using the BP algorithm is called the BP neural network. BP algorithm, also known as the negative gradient algorithm, adopts supervised delta learning. Its principle is to modify the connection weight between neurons in the network in the direction of gradient descent, so as to minimize the sum of square errors of network output to achieve the expected learning results. When the BP algorithm is used, the sigmoid function which can be continuously differentiable is often selected as the activation function in the neural network. Compared with a single neural network, the BP network composes simple nonlinear functions to realize highly nonlinear mapping of learning objectives. Therefore, BP neural network is widely used in nonlinear modeling in the fields of pattern recognition and adaptive control [9].

The internal calculation and learning of the BP neural network can generally be divided into two steps with different directions: the forward propagation of information and the reverse adjustment of error. The first is the forward propagation of information; that is, the information is propagated through the input layer to the hidden layer and finally output by the output layer. At this time, if the actual output is the same as the expected output, the learning and training are over, and the results are given; if it does not conform to the expected value, the error signal will return in the same way. By sequentially adjusting the weights of the release process and the hidden process, the error problem can be reduced in the negative gradient direction; that is, the error can be reduced by weight processing. After the above process, the final output of the network will gradually reach the expected output. Suppose that the input data of the BP neural network are $X = (X_1, X_2, \dots, X_n)^T$, n represents the number of nodes of neurons in the input layer, the corresponding output data are $O = (O_1, O_2, \dots, O_m)^T$, m represents the number of nodes of neurons in the output layer, and W_{ij} and W_{jk} are the connection weights of the hidden layer and the output layer, respectively. For the input component X_i of layer i , the corresponding outputs of the hidden layer and the output layer can be expressed as the following formula:

$$Y_o = f(X_i W). \quad (1)$$

The training steps of the BP neural network are as follows:

- (1) The weights W_{ij} and W_{jk} are initialized randomly. Their values must not be the same. The range is usually $(-1.0, 1.0)$. For sample (X_p, Y_p) , the output value is O_p .

- (2) Calculate the error between O_p and Y_p , and adjust the weight matrix according to the error. For the p -th sample, the following formula (2) can be obtained:

$$E_p = \left(\frac{1}{2}\right) \sum_{j=1}^m (y_{pj} - o_{pj})^2. \quad (2)$$

The neural network error calculation formula of all models is as follows (3):

$$\begin{aligned} W_{jk} &= W_{jk} + \Delta W_{jk}, \\ &= W_{jk} + \alpha O(1.0 - O_k)(Y_k - O_k)O_j, \end{aligned} \quad (4)$$

$$\begin{aligned} W_{ij} &= W_{ij} + \Delta W_{ij}, \\ &= W_{ij} + \alpha O_j(1.0 - O_j)O_i \cdot \sum_{k_1=1}^h \sum_{k_2=1}^m W_{k_1 k_2} O_{j+1, k_2} (1.0 - O_{j+1, k_2})(Y_{j+1, k_2} - O_{j+1, k_2}), \end{aligned} \quad (5)$$

where α is the learning rate.

When the traditional BP algorithm adjusts the connection weight, it only operates according to the negative gradient direction at time K . When there is a large change in the learning and training process, the conventional BP algorithm is difficult to stabilize in a short time. As can be seen from the above formula, after adding the momentum term, the network can be adjusted according to the gradient value at time k and time $k-1$ at the same time, so that the network can converge better. In the process of learning, whether the learning rate is too large or too small, it is not conducive to training. However, the formula of learning rate cannot be deduced theoretically, so the learning rate is generally selected by empirical value, which will lead to the instability of the convergence rate. For this reason, a variable step size factor can be introduced to take the learning rate as a function of a certain variable. For example, the learning rate can change with the change in error gradient. At the beginning of training, it can be larger to increase the convergence speed. When the training tends to be stable, η can be smaller to maintain stability.

The selection of some activation functions may cause the gradient to disappear. When each node in a multilayer neural network uses sigmoid function as activation function, the gradient will be multiplied by a value less than 0.25 every time, and it passes through a sigmoid layer in the error backpropagation phase of BP learning. In order to solve the drawback of gradient disappearance, researchers proposed a method to change the activation function into an improved nonlinear function such as Relu. Take the Relu function as an example. When the parameter is greater than 0, the value of the Relu function is 0. When the parameter is less than 0, the output value of the Relu function is equal to the input value. The first values W_{ij} and W_{jk} of the traditional BP neural network are randomly determined, which makes the operation of the BP neural network unstable and cannot be

$$E = \sum_{l=1}^s E_{pl}, \quad (3)$$

where s is the number of samples.

The process of reducing E can be thought of as an optimization problem. The weight matrix is processed by the steepest descent method: the following models (4) and (5) are used.

solved effectively. Therefore, this paper introduces the particle swarm optimization algorithm into the intelligent algorithm to optimize the value between W_{ij} and W_{jk} [10, 11].

2.1.2. Artificial Intelligence Algorithm. The position vector of the i -th particle is $x_i = (x_{i1}, x_{i2}, \dots, x_{iD})$, which represents a set of initial values of W_{ij} and W_{jk} , as well as a velocity vector $v_i = (v_{i1}, v_{i2}, \dots, v_{iD})$. The particles adjust the flight direction by tracking the optimal position of individuals and groups, as shown in the following formulas:

$$v_{id}(t+1) = \omega v_{id}(t) + c_1 r_1 (p_{id} - x_{id}(t)) + c_2 r_2 (p_{gd} - x_{id}(t)), \quad (6)$$

$$x_{id}(t+1) = x_{id}(t) + v_{id}(t+1), \quad (7)$$

where t is the number of iterations; ω is the inertia weight [12].

2.2. Risk Assessment of Wireless Mobile Phone Communication Based on Intelligent Algorithm

2.2.1. Risk Evaluation Index and Risk Level Setting of Wireless Mobile Power Communication System. The development of wireless mobile communication risks is based on the principles of research, usability, and functionality due to the increased risk of wireless mobile communication. First, the wireless mobile power communication system risk evaluation indicators are divided into two categories: artificial risk indicator system and technical risk indicator system [9, 13]. The technical risk indicator system is divided into hardware facilities, physical environment and guarantee, software facilities, and other risk subindicator systems, which can be subdivided into specific risk indicators. The human risk indicator system only includes the risk subindicator system

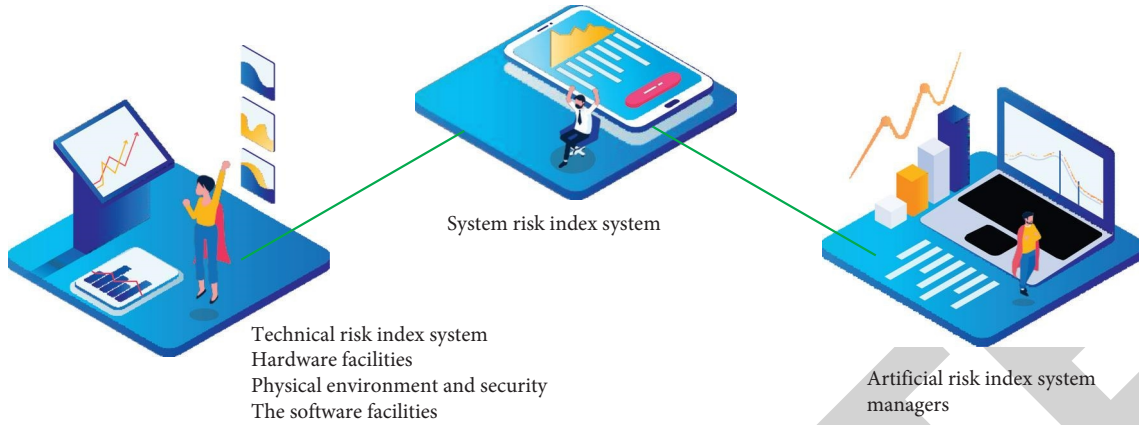


FIGURE 1: Hierarchical indicator structure.

of the manager, which can be refined. The established hierarchical indicator structure is shown in Figure 1.

According to the risk assessment specification for wireless mobile power communication system, the risk level can be set to level 5. The specific values and descriptions are shown in Table 1 [14].

2.2.2. Risk Assessment Steps of Wireless Mobile Power Communication System Based on Intelligent Algorithm

- (1) According to the principles of scientificity, applicability, and operability, the risk indicators of the wireless mobile power communication system are selected
- (2) Collect the corresponding wireless mobile power communication system risk assessment data according to the wireless mobile power communication system risk indicators
- (3) Mark the risk level of wireless mobile power communication system by relevant experts [15]
- (4) Since some indicators need to be quantified and some indicators need to be discretized, the corresponding pretreatment is performed on the indicators, and then, the preprocessed values are scaled, as shown in the following formula:

$$x'_i = \frac{(x_i - \max)}{(\max - \min)}, \quad (8)$$

where max and min, respectively, represent the maximum and minimum values of risk indicators of wireless mobile power communication system [16]

- (5) Select some data to develop a training model for wireless mobile phone communication risk assessment, access the BP neural network, and activate the influence of the BP neural network, such as minimum error training and maximum algebraic training
- (6) The intelligent particle swarm optimization algorithm is used to determine the initial connection of the BP neural network

- (7) According to the initial connection weights and related parameters, the neural network is forward learning and error back propagation, and the weights are continuously adjusted through the gradient descent algorithm to make the training error meet the preset minimum training error range

- (8) The risk assessment model of wireless mobile power communication system is established through the above steps, and the specific process is shown in Figure 2 [17]

2.3. Simulation Test

2.3.1. Risk Assessment Data Source of Wireless Mobile Power Communication System. In order to measure the performance of the wireless mobile power communication system risk measurement model based on the intelligent algorithm developed in this paper, the real-time nature of the wireless mobile communication risk data source culture is selected as the research material [18, 19]. Due to space limitations, only the risk cost of mobile communication is shown in Figure 3.

By analyzing the original value of wireless communication risk in Figure 3, it can be seen that the risk of mobile communication is different and has strong randomness, but there are also some constant changes. Finally, 50 pieces of data were selected as evidence, and additional data were used as training models for wireless communication risk assessment [20].

3. Result Analysis

3.1. Analysis of Risk Assessment Results of Wireless Mobile Power Communication System Based on this Model. The particle swarm optimization algorithm is used to determine the initial connection of the BP neural network, and then, the wireless communication risk assessment is performed on the receiving model, as shown in Figure 4 [21].

By analyzing the wireless communication risk assessment in Figure 4, it can be seen that the communication risk assessment of this form of mobile phone wireless model is very small and can be ignored. The evaluation results of

TABLE 1: Risk level of wireless mobile power communication system.

Wireless mobile communication system risk level number	Level	Value	Specific description
1	Very low	0~0.1	No impact
2	Low	0.1~0.3	Little impact
3	Middle	0.3~0.6	There is a certain impact, but the degree of impact is small
4	High	0.6~0.9	Have a great impact
5	Very high	0.9~1	Have a very serious impact

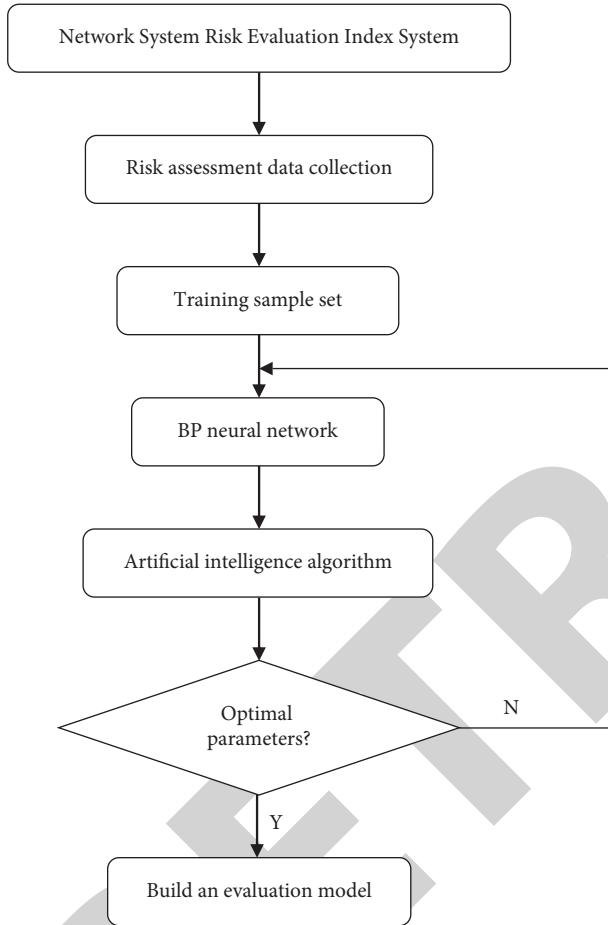


FIGURE 2: Risk assessment training process of wireless mobile power communication system.

wireless mobile power communication system risk measurement are accurate and reliable. It is a measure of risk to wireless mobile communication performance.

3.2. Performance Comparison with Classical Wireless Mobile Power Communication System Risk Assessment Model. In order to measure the effectiveness of the risk measurement of mobile communication models based on intelligent algorithms, grayscale, group analysis, and BP neural network models are used to conduct comparative experiments under the same setting data and the same simulation environment. The correct rate of risk assessment and training time of wireless mobile communication system were counted. The specific testing and training times are shown in Table 2.

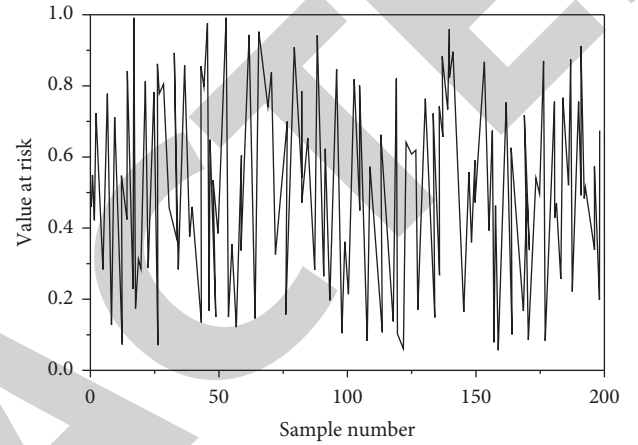


FIGURE 3: Risk value of wireless mobile power communication system risk assessment.

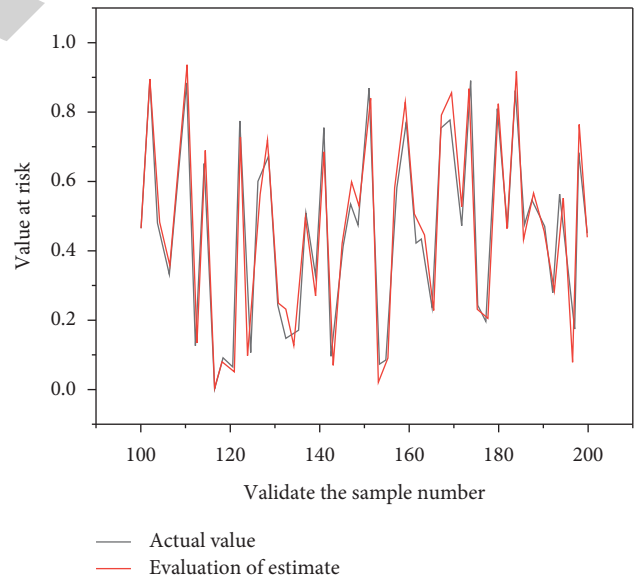


FIGURE 4: Risk assessment results of wireless mobile power communication system based on this model.

It can be seen from Table 2 that the accuracy of the wireless mobile communication risk measurement model based on the intelligent algorithm in this paper is above 95%, while the accuracy of the classic wireless mobile power communication system risk measurement standard is lower

TABLE 2: Comparison of risk assessment results of wireless mobile power communication system with classical model.

Risk assessment model of wireless mobile communication system	Evaluation accuracy rate/%	Training time/s
Gray model	88.84	11.51
Cluster analysis	86.62	12.27
Standard BP neural network	92.15	7.72
Paper model	95.67	4.67

than 95%. And the research time of this model is shorter than that of the classic wireless mobile power communication system risk measurement model, which improves the risk measurement speed of the wireless mobile power communication system [22, 23]. Therefore, the risk assessment results of wireless mobile communication system based on this model are more ideal.

4. Conclusion

The security of wireless mobile communication system is a hot research topic at present. In order to solve the problems existing in the risk assessment of the current wireless mobile communication system, a risk assessment model of wireless mobile communication system based on an artificial intelligence algorithm is designed. The results show that the accuracy rate of the risk assessment of the wireless mobile communication system by the artificial intelligence algorithm is more than 95%, and the training speed of the risk assessment of the wireless mobile communication system is fast. Evaluate modeling tools. In the era of rapid and dense information transfer, the communication network acts as a dynamic network. Due to uneven distribution of traffic density, tight frequency resources, suboptimal, and constantly changing network configuration, the service quality of the existing network is likely to be unsatisfactory. Reasonably adjust the parameters of the network, so that the network can reach the best operating state, and realize the guarantee of network quality in daily life.

Data Availability

The data used to support the findings of this study are available from the corresponding author upon request.

Conflicts of Interest

The authors declare that they have no conflicts of interest.

References

- [1] J. Zumbach, A. Oster, A. Rademacher, and U. Koglin, "Reliability and validity of behavior observation coding systems in child maltreatment risk evaluation: a systematic review," *Journal of Child and Family Studies*, vol. 31, no. 2, pp. 545–562, 2022.
- [2] N. V. Ustinova and L. S. Namazova-Baranova, "Role of pediatrician in early risk evaluation, diagnosis and management of children with autism spectrum disorders," *Вопросы современной Педиатрии*, vol. 20, no. 2, pp. 18–23, 2021.
- [3] M. A. Akpe, P. U. Ubuja, and S. E. Ivara, "Health risk evaluation of selected heavy metals in infant nutrition formula in cross river state, Nigeria," *Journal of Applied Sciences & Environmental Management*, vol. 25, no. 3, pp. 419–423, 2021.
- [4] H. Huang, Z. Q. Xu, J. X. Yan, X. G. Zhao, and D. L. Wang, "Characteristics of heavy metal pollution and ecological risk evaluation of indoor dust from urban and rural areas in taiyuan city during the heating season," *Huan jing ke xue*, vol. 42, no. 5, pp. 2143–2152, 2021.
- [5] Düzenci, H. Aslan, M. Eser, N. G. Somak, F. Bulucu, and K. Saglam, "Pulse wave velocity and esc score (european society of cardiology systematic coronary risk evaluation)," *Kocaeli Medical Journal*, vol. 10, no. 1, pp. 13–17, 2021.
- [6] Y. Shang, Y. Li, Z. Wang, X. Sun, and F. Zhang, "Risk evaluation of human corneal stromal lenticles from smile for reuse," *Journal of Refractive Surgery*, vol. 37, no. 1, pp. 32–40, 2021.
- [7] B. Wu, W. Qiu, W. Huang, G. Meng, J. Huang, and S. Xu, "Dynamic risk evaluation method for collapse disasters of drill-and-blast tunnels: a case study," *Mathematical Biosciences and Engineering*, vol. 19, no. 1, pp. 309–330, 2022.
- [8] D. Blokh, I. Stambler, J. Gitarts, E. Pinco, and E. H. Mizrahi, "Information-theoretical analysis of blood biomarkers for age-related hip fracture risk evaluation," *Applied Medical Informatics*, vol. 43, no. 1, pp. 14–23, 2021.
- [9] A. Graewingholt and P. G. Rossi, "Retrospective analysis of the effect on interval cancer rate of adding an artificial intelligence algorithm to the reading process for two-dimensional full-field digital mammography," *Journal of Medical Screening*, vol. 28, no. 3, pp. 369–371, 2021.
- [10] L. Huo, J. Zhu, P. K. Singh, and P. A. Pavlovich, "Research on qr image code recognition system based on artificial intelligence algorithm," *Journal of Intelligent Systems*, vol. 30, no. 1, pp. 855–867, 2021.
- [11] G. Deng and Y. Fu, "Fuzzy rule based classification method of surrounding rock stability of coal roadway using artificial intelligence algorithm," *Journal of Intelligent and Fuzzy Systems*, vol. 40, no. 4, pp. 8163–8171, 2021.
- [12] L. Hailong, "Role of artificial intelligence algorithm for taekwondo teaching effect evaluation model," *Journal of Intelligent and Fuzzy Systems*, vol. 40, no. 2, pp. 3239–3250, 2021.
- [13] A. Nn, B. Sy, and C. Eg, "A risk assessment model for stroke in the early post-transplant period in adult cardiac allograft recipients: a unos database analysis-sciencedirect," *Transplantation Proceedings*, vol. 53, no. 10, pp. 3039–3044, 2021.
- [14] C. R. Ferreira, M. de Bastos, M. L. Diniz et al., "Inter-observer reliability of a risk assessment model for venous thromboembolism in acutely-ill medical hospitalized patients: results from a prospective cohort study," *Phlebology*, vol. 36, no. 10, pp. 827–834, 2021.
- [15] O. Halytskyi, M. Polenkova, O. Fedirets, O. Brezhnieva-Yermolenko, and S. Hanzhiuk, "Mathematical risk assessment model for biodiesel production projects in Ukraine agriculture," *Financial and Credit Activity Problems of Theory and Practice*, vol. 2, no. 37, pp. 280–286, 2021.
- [16] C. Duan and J. Luo, "Mobile communication network optimization system based on artificial intelligence," *Wireless Communications and Mobile Computing*, vol. 2021, Article ID 9999873, 5 pages, 2021.
- [17] Y. Feng, R. Zheng, Y. Fu et al., "Assessing the thrombosis risk of peripherally inserted central catheters in cancer patients using caprini risk assessment model: a prospective cohort

Retraction

Retracted: Application of Big Data and Internet of Things Technology in the Management of Financial Operating Income of Electric Power Enterprises

International Transactions on Electrical Energy Systems

Received 19 September 2023; Accepted 19 September 2023; Published 20 September 2023

Copyright © 2023 International Transactions on Electrical Energy Systems. This is an open access article distributed under the Creative Commons Attribution License, which permits unrestricted use, distribution, and reproduction in any medium, provided the original work is properly cited.

This article has been retracted by Hindawi following an investigation undertaken by the publisher [1]. This investigation has uncovered evidence of one or more of the following indicators of systematic manipulation of the publication process:

- (1) Discrepancies in scope
- (2) Discrepancies in the description of the research reported
- (3) Discrepancies between the availability of data and the research described
- (4) Inappropriate citations
- (5) Incoherent, meaningless and/or irrelevant content included in the article
- (6) Peer-review manipulation

The presence of these indicators undermines our confidence in the integrity of the article's content and we cannot, therefore, vouch for its reliability. Please note that this notice is intended solely to alert readers that the content of this article is unreliable. We have not investigated whether authors were aware of or involved in the systematic manipulation of the publication process.

Wiley and Hindawi regrets that the usual quality checks did not identify these issues before publication and have since put additional measures in place to safeguard research integrity.

We wish to credit our own Research Integrity and Research Publishing teams and anonymous and named external researchers and research integrity experts for contributing to this investigation.

The corresponding author, as the representative of all authors, has been given the opportunity to register their agreement or disagreement to this retraction. We have kept a record of any response received.

References

- [1] H. Su, "Application of Big Data and Internet of Things Technology in the Management of Financial Operating Income of Electric Power Enterprises," *International Transactions on Electrical Energy Systems*, vol. 2022, Article ID 6167479, 8 pages, 2022.

Research Article

Application of Big Data and Internet of Things Technology in the Management of Financial Operating Income of Electric Power Enterprises

Huiling Su 

School of Economics and Management, Pingdingshan Polytechnic College, Pingdingshan, Henan 467001, China

Correspondence should be addressed to Huiling Su; 201701360147@lzpcc.edu.cn

Received 7 August 2022; Revised 27 August 2022; Accepted 5 September 2022; Published 19 September 2022

Academic Editor: Nagamalai Vasimalai

Copyright © 2022 Huiling Su. This is an open access article distributed under the Creative Commons Attribution License, which permits unrestricted use, distribution, and reproduction in any medium, provided the original work is properly cited.

Aim. In order to effectively integrate and rationally allocate the complex information flow of people, finance, and materials in the daily operation of the enterprise and improve the daily operation efficiency and management effect of the enterprise, the author proposes a method for the application of big data and Internet of Things technology in the management of financial operating income of electric power enterprises. The method specifically includes an overview of the relevant theories of financial management based on ERP and an analysis of the needs of a power company's financial management system based on ERP so as to construct an evaluation index system for the financial management system. The experimental results show that the return on assets of the experimental enterprises has increased from 27.48% in 2015 to 55.18% in 2019, an increase of 27.7%, and the profitability has been continuously enhanced. In 2019, the company achieved a net profit of 392 million yuan, an increase of about 4 times compared with the previous 77 million yuan in 2015. *Conclusion.* The application can further optimize the allocation of various resources of the enterprise and ensure the effective implementation of the long-term strategy and management goals of the enterprise on the basis of realizing the management needs of the enterprise.

1. Introduction

As an important economic lifeline of my country's national economy, the power industry is a reliable guarantee for healthy economic development, social harmony, and stability. Financial management has always been the main activity and basic content of the daily operation of an enterprise, and it is a strong guarantee for the long-term development and normal operation of an enterprise [1]. At present, the financial management informatization construction that is being widely implemented in electric power enterprises is to realize the integration strategy of financial management through informatization construction—by building a financial information management system that is harmonious and unified with business—implementing the “three-in-one” financial management goals of scientific management, orderly management, and fine management. This further improve the asset operation efficiency and asset disposal efficiency of electric power

enterprises, ensure the safety of assets and reliable supply of funds for electric power enterprises, promote the sustainable and healthy development of the economic activities of power enterprises, and ultimately, it will improve the management support for the value enhancement of power enterprises and the realization of strategic goals [2]. Financial management is one of the core businesses of electric power enterprises, from this perspective, the financial informatization of electric power enterprises should be promoted as a whole. Only by realizing the integrated group finance and business can the group's financial resources be optimally allocated. Objectively speaking, this is an inevitable requirement for the financial informationization of group enterprises. ERP takes IT as the carrier to realize the revolutionary upgrade of the informationization, coordination, and intelligent management of the enterprise business activities [3]. In this way, with “financial management” as the link, the complex information flow of human, financial, and materials in the daily operation of the

enterprise can be effectively integrated and reasonably allocated, and the daily operational efficiency and management effectiveness of the enterprise can be improved. A computer management system with standardized operation methods and refined management objectives can also be improved. The core of the ERP system is the long-term strategy and management objectives of the enterprise. The development objectives are the management needs and business contents of the enterprise. The basis of implementation lies in the management level and resource status of the enterprise. Therefore, an ERP system from a strategic point of view through information management means it further optimizes the allocation of various resources of the enterprise on the basis of realizing the needs of enterprise management, in order to ensure the effective implementation of the long-term strategy and management objectives of the enterprise [4].

2. Literature Review

The power grid company announced the smart grid plan for the first time, that is, the comprehensive construction of a strong grid with a UHV grid as the backbone and coordinated development of power grids at all levels as the basis, and a strong smart grid characterized by informatization, automation, and interaction [5]. In the report on the development of modern power grids, the Energy Administration summarizes the seven characteristics of smart grids: it has the ability to self-repair, stimulate the initiative of users to participate in the operation of the power grid, the security ability to resist attacks, the high quality of electric power, accommodate various forms of power generation and storage, prosper the power market, optimize equipment operation, and reduce power grid operating costs [6]. Eladl and others believed that the effective combination of smart grid and Internet of Things technology can improve the stability of the power system and the efficiency of energy use and achieve sustainable energy development [7]. Rk et al. pointed out that the application requirements of the smart grid for the Internet of Things are very clear, for example, in the field of power generation, the Internet of Things can be used for unit monitoring, distributed power plant monitoring, plant area monitoring, pollutant and gas emission monitoring, and energy consumption monitoring, and pumped storage monitoring. It also has a wide range of application requirements in transmission line monitoring, tower protection, intelligent substation, state detection, and so on. [8]. Oikonomou and Parvania pointed out that all aspects of the smart grid need the technical support of the Internet of Things, and most of the business of the smart grid is related to the Internet of Things [9]. From the grid connection of renewable energy in the power generation link to the real-time monitoring of the operating status of the unit; from online monitoring of transmission lines to power production management, safety assessment, and supervision; from smart meters and electricity consumption information collection to three-meter reading and interactive marketing; and from the intelligent electricity consumption and intelligent community to multinet network integration all need the support of Internet of Things technology [10].

Lorenzo et al. believed that the smart grid is actually loading sensors into the existing power network, through technical means such as RFID technology and local area network. The purpose of remote control of the power grid is achieved, and the structure optimization of the power grid is realized [11]. That is to say, the smart grid is actually the application of IoT technology on the grid. Selva et al. analyzed the application status of IoT in smart grids, the basic architecture of the Internet of Things for smart grid applications is introduced, and the application of the Internet of Things in smart grids is introduced in detail [12]. On the basis of this research, the author proposes a method to explore the application of big data and Internet of Things technology in the management of financial operating income of power enterprises. Based on the research on the application of ERP systems in the financial management of electric power enterprises, this paper introduces the background and significance of ERP financial management research, the core management ideas of ERP, and the core position of ERP financial management in enterprises [13]. Combined with the development stage of electric power enterprises, the development process of ERP financial management is summarized. The authors comprehensively analyze the characteristics of ERP financial management in electric power enterprises and its role in improving the level of financial management. At the same time, the present situation of the implementation of ERP financial management system in a certain electric power is studied and analyzed, and the more advanced domestic ERP financial management technology and methods are used for reference, in view of the current problems in business integration, budget management, and project whole-process management. The research is carried out, and the methods and countermeasures to solve the problems are explored, hoping to provide a certain reference for comprehensively improving the financial management level of power enterprises.

3. Methods

3.1. Overview of ERP Financial Management-Related Theories

3.1.1. Definition of ERP. The definition of ERP standard comes from its original English meaning, that is, enterprise resource planning [14]. It is a system for effectively sharing and utilizing enterprises resources, through the comprehensive and effective information transmission of the information system, the procurement, storage, production, and sales of resources in the enterprise, as well as human, financial, materials, and other aspects are reasonably allocated and utilized so as to achieve the improvement of enterprise business efficiency. Essentially, ERP is an information system and a tool. ERP integrates some advanced management ideas and contents in the system design, which can help enterprises to improve their management level. The development process is shown in Figure 1.

3.1.2. The Role of ERP in Enterprise Financial Management

- (1) The ERP system makes the organizational structure of the enterprise flat and the information communication reasonable. The financial management

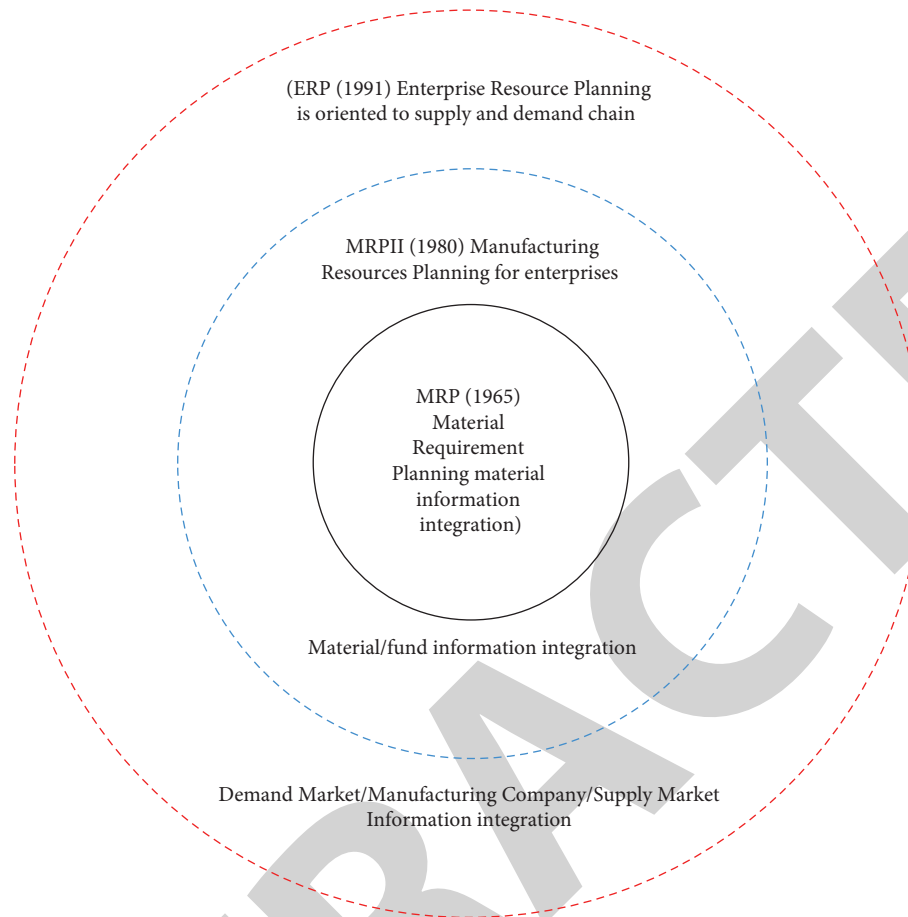


FIGURE 1: The development process of ERP.

personnel of the enterprise can support the intelligent system through the decision-making in the ERP system, fully understand and master the operating conditions of the enterprise, accurately analyze and formulate the development direction of the enterprise, and effectively control and reduce the operating costs of the enterprise. At the same time, the middle managers of the enterprise can arrange the corresponding purchase plan, production plan, sales plan, and capital plan through the ERP system. The grassroots managers of the enterprise can issue daily work orders through the operation of the ERP system. Enterprises successfully implementing ERP can also manage the supply chain well, cooperate with suppliers and distributors, improve work efficiency, and greatly enhance the competitive advantage of the entire supply chain.

- (2) The effect of the ERP project after the implementation is not only reflected in the improvement of work efficiency but also in the awareness and concept of employees to keep up with the management model of modern enterprises and to be able to look at work and solve problems from different perspectives in the past. The upgrade and development of enterprises have laid a solid foundation. The

main factor affecting the accuracy of the basic data of the company's manufacturing system is the awareness of cost management of all employees, which is caused by extensive management. In the future, it is necessary to further cultivate the awareness of refined management, at the same time, it is necessary to improve the means of measurement. With the expansion of enterprise scale, manual data collection cannot be accurate, and manual statistics often make mistakes in the case of large output [15]. The biggest advantage of ERP is to establish an integrated and transparent enterprise management system to ensure the accuracy of the original data and to control the real situation of the enterprise so as to optimize resources, respond quickly, and flexibly produce.

3.2. Demand Analysis of a Power Company's Financial Management System Based on ERP

3.2.1. The Overall Plan of a Company's ERP Implementation.

The power company's ERP implementation goal is to complete the implementation of the ERP system for project management, material management, and financial management and ultimately achieve 100% coverage of the ERP system in the company's projects, materials, finance, and

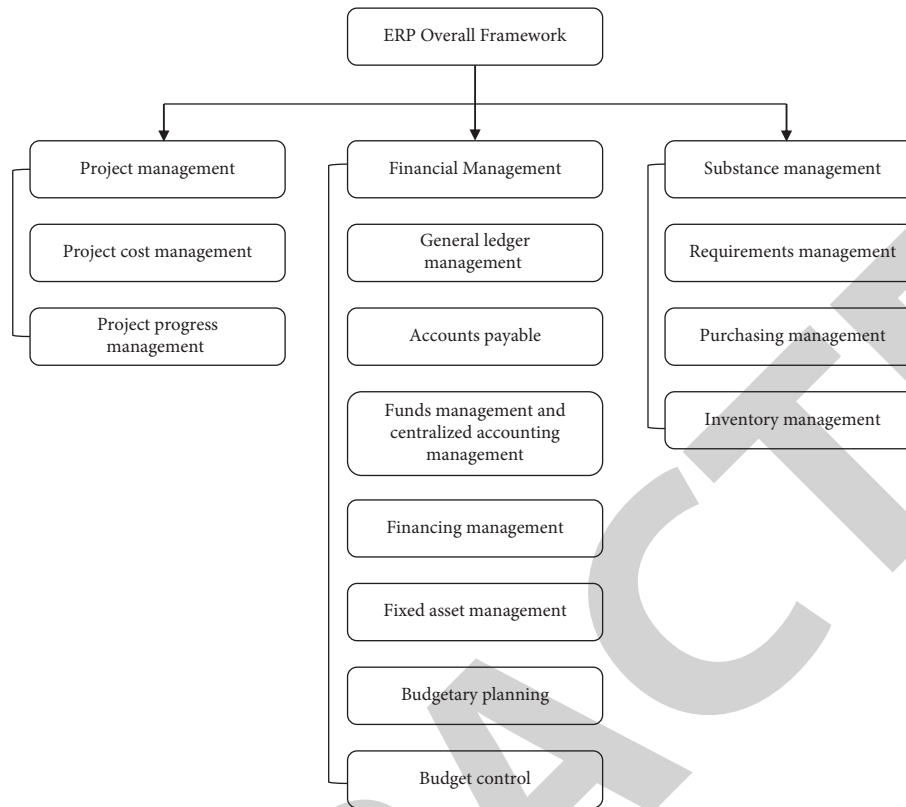


FIGURE 2: Overall framework of ERP.

human resources management; strengthen the intensive and refined management of people, finances, and materials; build a standardized and intensive management model for L Power company's projects, materials, and financial management; and provide a model for other enterprises' ERP promotion as a good reference. The overall framework of the company's ERP is shown in Figure 2.

3.2.2. Demand Analysis of the ERP Financial Management System for a Power Company. Fixed Asset Management is a comprehensive asset management system that maintains accurate asset information. Its main function is to carry out centralized value management of fixed assets and physical tracking management. In the fixed asset system, you can directly add assets manually, or you can add assets to the asset module through the project module transfer process. In the asset workbench, the staff can carry out corresponding business processing on the assets and maintain the financial information and physical management information of the assets [16]. At the same time, the system provides the standard reports for statistical analysis and tracks management of assets. The asset system is integrated with the general ledger system, and the financial information of the asset system can be transmitted to the general ledger system. The asset system is also integrated with the A/P management system. When adding assets in batches, the invoice information of the A/P system can be directly transferred to the asset module; when the project of the project module is

capitalized, asset information can also be generated and transferred to the asset module, as shown in Figure 3.

The main business scope of fixed asset management includes ① asset card increase management: manually increase assets and increase assets in batches; ② asset card depreciation management; ③ asset card adjustment management: single asset adjustment and batch asset adjustment; ④ asset transfer management: internal transfer of assets and asset transfer across account books; ⑤ asset scrap and sale management; ⑥ intangible assets and long-term amortization management; ⑦ important low-value consumables management; ⑧ asset card query and report query management; and ⑨ asset management system closing management. The main management requirements of fixed asset management are shown in Table 1.

3.3. The Design of Financial Management System of a Power Company Based on ERP. Take key flexfields as an example: Oracle standard solutions group assets by nonfinancial information; asset key flexfields can be designed to record required information. Assets can be grouped by the asset key so that the asset can be looked up without the asset number. You can define an asset key flexfield structure that meets your organization's specific needs. You can select the number of segments, the length, name, and order of each segment in the asset key flexfield. Up to ten asset key fields can be defined. This key flexfields support only one structure. As shown in Table 2.

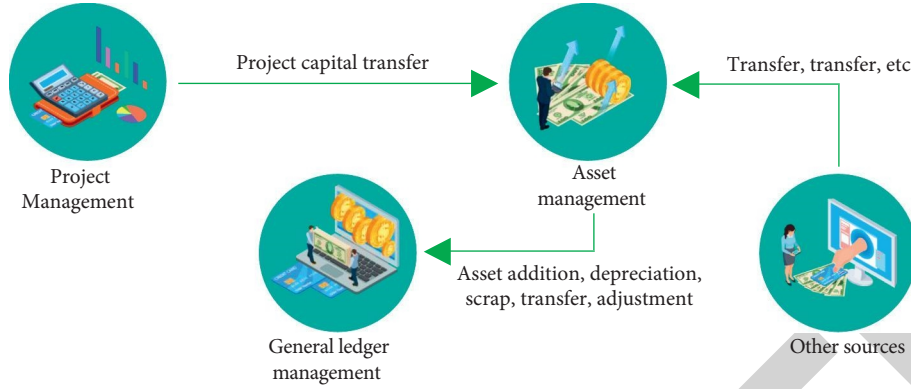


FIGURE 3: Information flow diagram of fixed asset management and other related modules.

TABLE 1: Analysis of fixed asset management needs.

Serial number	Demand category	Demand content
1	Asset book	Set up separate asset books
2	Asset base data management	Category flexfield, domain location flexfield, key flexfield, descriptive flexfield related account settings, and asset number
3	Asset business management	Asset increase, asset depreciation, asset adjustment, asset transfer, asset retirement and sale, asset inventory, asset impairment provision, important low-value consumables, intangible assets, and long-term amortization
4	Inquiries and reports	Online query and report query
5	Month-end closing and security	Run depreciation, generate documents, and close accounting periods
6	System integration	Realize the integration between different modules to ensure the flow and timely update of the information

TABLE 2: Settings of the location elastic domain of a power company.

Company	Primary location	Secondary location
A power supply company	0530L office	General manager's office
A power supply company	0530L safety inspection department	Test class
A power supply company	0530L enterprise service center	Cultural center

After the evaluation indicators are established, it is necessary to assign different weights to each indicator so that the different degrees of importance of each indicator can be clarified. The determination and distribution of weights can more objectively and truly evaluate the security benefits of enterprises. The following will use the improved analytic hierarchy process to determine the weight of each indicator. The general AHP needs to check the consistency of the judgment matrix, but when it is applied in practice, it is difficult to ensure the accuracy of this consistency check, and it needs to be adjusted many times to meet the requirements [17]. However, after improving the general AHP method by using the properties of the optimal transfer matrix, it can naturally meet the consistency requirements and directly calculate the relative weight. The steps are as follows:

3.3.1. Establishing a Judgment Matrix. Taking the element U_1 as the evaluation criterion, the same level elements below

U_1 are compared in pairs, and the judgment matrix A is constructed. When making a pairwise comparison, the line-scale method can be used to express the relative importance.

3.3.2. Solution of the Antisymmetric Matrix. Perform $b_{ij} = \lg a_{ij}$, and transform A into an antisymmetric matrix and a transfer matrix B .

3.3.3. Solution of the Optimal Transfer Matrix. Find the optimal transitive matrix of an antisymmetric matrix.

$$c_{ij} = \frac{1}{n} \sum_{i=1}^n (b_{ik} - b_{jk}), \quad i = 1, 2, \dots, n; \quad j = 1, 2, \dots, n. \quad (1)$$

It suffices to minimize $\sum_{i=1}^n \sum_{j=1}^n (c_{ij} - b_{ij})$.

Perform $W^* = 10^C$ transformation to find the Quasi-optimized consensus matrix of WW^* and the Quasi-optimized consensus matrix W^* of the judgment matrix, which

preserves the information in the judgment matrix to the greatest extent [18].

$$w_{ij}^* = 10^{c_{ij}}, \quad i = 1, 2, \dots, n; \quad j = 1, 2, \dots, n. \quad (2)$$

3.4. Financial Risk Prevention Measures

3.4.1. Rational Formulation of Corporate Financing Strategies. The capital of a power company mainly comes from debt financing, which has led to the high asset-liability ratio of the company in recent years. A power company should formulate a reasonable financing strategy to broaden its own financing channels, thereby reducing the company's asset-liability ratio and optimizing its capital structure. First, companies can change their conservative financing strategies into moderate financing strategies and use short-term financing to raise funds. Secondly, the enterprise itself can issue additional stocks to raise funds, increase equity financing, reduce debt financing, or can use the form of a "debt-to-equity swap" for related optimization, at the same time, it can also delay the enterprise's expenditure on interest, form "natural financing" and increase the utilization of funds [19]. Finally, enterprises can further optimize the industrial structure through fixed increase fundraising, actively respond to the impact of the power system reform on the traditional power business, and improve the layout of the distribution network energy-saving service business.

3.4.2. Steady Promotion of the Corporate Investment Strategy

- (1) Accelerate corporate investment and mergers and acquisitions to promote the development of power distribution and energy-saving business.

According to relevant information reports, in mid-August 2020, a power company on the listed platform of the State Grid disclosed that it planned to promote the distribution of power distribution and energy-saving business through a combination of capital raising and asset acquisition. A power company originally mainly engaged in the power supply business, since it entered the field of power distribution and energy saving, has entered the "fast lane" of business performance and growth. If this trend continues, the development of the enterprise will make great progress, the business can be further expanded, and the situation of investment losses can be reversed.

- (2) Increase investment in energy conservation of distribution network and promote the development of "dual main business" of enterprises.

After a power company participated in State Grid's distribution network energy-saving business in 2016, its performance has risen significantly, but it has also attracted the attention of provincial companies within the State Grid, and they all want to profit from it. This disrupts the energy-saving business of the

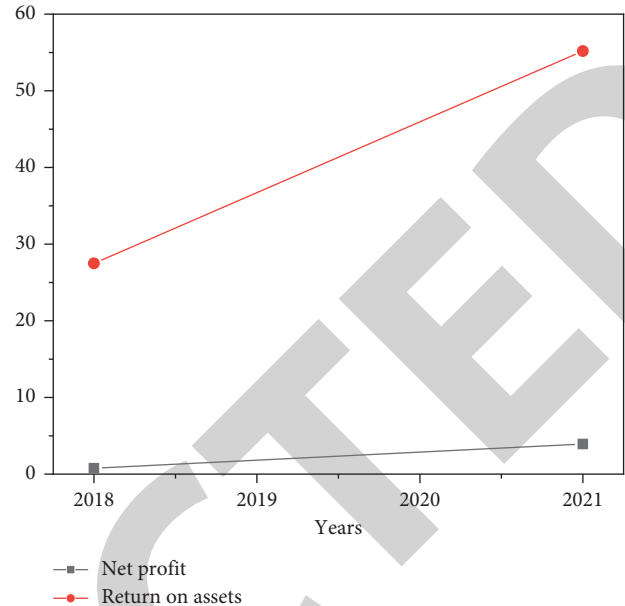


FIGURE 4: Comparison of operating performance.

State Grid that should have been developing continuously because the internal competition has become full of uncertainty [20]. Therefore, a power company must seize this opportunity, cooperate with the relevant policies of the State Grid, actively increase investment in the energy-saving business of the distribution network, and strive to achieve the goal of achieving a revenue of 80 billion yuan for the comprehensive energy service business of the State Grid in 2025.

- (3) Improve the management of accounts receivable.

A power company's accounts receivable account for a large proportion of the company's current assets, at the same time, the company's accounts receivable turnover days continue to increase; the recovery period is longer, and the company's capital flow speed has become relatively slow. This poses a certain threat to the financial status of the company, hinders the development of a power company to a certain extent, and may cause the company to not have enough funds to repay current liabilities; therefore, enterprises should formulate scientific and effective policies to improve the management of their own accounts receivable. On the one hand, a power company should pay attention to the credit level of its associated customers and their business conditions. Enterprises should maintain long-term, stable contact, and cooperation with related party customers with better management level and reduce opportunities for economic cooperation with those enterprises with more debts and poor credit status. On the other hand, the power company itself should reduce bad debts by reasonably setting credit terms and other methods, and then gradually increase the company's accounts receivable turnover rate.

4. Results and Discussion

Judging from the operating performance of a power company after the development of “dual main business,” the company will achieve a net profit of 392 million yuan in 2021, an increase of about 4 times compared with the previous 77 million yuan in 2018. The company’s return on assets has risen from 27.48% in 2018 to 55.18% in 2021, an increase of 27.7%, and profitability has continued to increase. Therefore, in order to solve the problem of competition in the energy-saving industry in the distribution network within the State Grid, a power company must play the role of a “commander,” increase investment and construction in related fields and continuously enhance the level of profitability, as shown in Figure 4.

5. Conclusion

The author proposes a method for the application of the big data and Internet of Things technology in the management of financial operating income of electric power enterprises, taking the financial management system of an electric power company based on ERP as the research object, on the basis of comprehensively considering the current situation of financial management of a power company, by focusing on analyzing the functional requirements of the three management modules of fixed asset management, financing management, and budget control management of the power company financial management system based on ERP, and taking the fixed asset management system as an example, the ERP-based financial management system of a power company is proposed a design. In order to prove that through informatization management methods, it is possible to further optimize the allocation of various resources of the enterprise, on the basis of realizing the management needs of the enterprise and ensuring the effective implementation of the long-term strategy and management objectives of the enterprise. The financial management system of L power company based on ERP is evaluated, and the evaluation results show that the financial management system of L power company based on ERP is at a good level.

Data Availability

The data used to support the findings of this study are available from the author upon request.

Conflicts of Interest

The author declares no conflicts of interest.

Acknowledgments

This work was supported by the 2020 Young Backbone Teachers’ Project of Henan Higher Vocational Schools: “Research and Practice of “TCPH” Professional Creative Integration Training Mode under the Guidance of Career Intention,” “under Project number: 2020GZGG096.”

References

- [1] S. Cohen, F. Manes-Rossi, I. Brusca, and E. Caperchione, “Guest editorial happy endings and successful stories in public sector financial management: a lesson drawing perspective,” *International Journal of Public Sector Management*, vol. 34, no. 4, pp. 393–406, 2021.
- [2] R. Zissler and J. S. Cross, “Impacts of a Japan–south korea power system interconnection on the competitiveness of electric power companies according to power exchange prices—sciencedirect,” *Global Energy Interconnection*, vol. 3, no. 3, pp. 292–302, 2020.
- [3] R. Majumdar, “Surviving and growing in the post-covid world: the case of indian hotels,” *Worldwide Hospitality and Tourism Themes*, vol. 13, no. 5, pp. 584–598, 2021.
- [4] A. Khan and S. Shireen, “Drivers of financial and operational efficiency of mfs: empirical evidences from eastern europe and central asia,” *Benchmarking: An International Journal*, vol. 27, no. 9, pp. 2679–2697, 2020.
- [5] A. Sharma and R. Kumar, “Performance comparison and detailed study of AODV, DSDV, DSR, TORA and OLSR routing protocols in ad hoc networks,” in *Proceedings of the 2016 Fourth International Conference on Parallel, Distributed and Grid Computing (PDGC)*, Wagnaghat, India, 2016.
- [6] Y. Feng, Z. Huang, Y. L. Wang, L. Wan, and X. Shan, “A soe-based learning framework using multi-source big data for identifying urban functional zones,” *IEEE Journal of Selected Topics in Applied Earth Observations and Remote Sensing*, vol. 14, 2021.
- [7] A. A. Eladl, M. A. Saeed, B. E. Sedhom, and J. M. Guerrero, “Iot technology-based protection scheme for Mt-Hvdv transmission grids with restoration algorithm using support vector machine,” *IEEE Access*, vol. 9, 2021.
- [8] A. Rk, S. Koch, C. Steinhardt, and A. K. Strauss, “A review of revenue management: recent generalizations and advances in industry applications,” *European Journal of Operational Research*, vol. 284, no. 2, pp. 397–412, 2020.
- [9] K. Oikonomou and M. Parvania, “Optimal coordinated operation of interdependent power and water distribution systems,” *IEEE Transactions on Smart Grid*, vol. 11, no. 6, pp. 4784–4794, 2020.
- [10] González-Arias, F. M. Baena-Moreno, L. Pastor-Pérez, D. Sebastia-Saez, L. M. Gallego Fernández, and T. R. Reina, “Biogas upgrading to biomethane as a local source of renewable energy to power light marine transport: profitability analysis for the county of cornwall,” *Waste Management*, vol. 137, pp. 81–88, 2022.
- [11] G. D. Lorenzo, R. Araneo, M. Mitolo, A. Niccolai, and F. Grimaccia, “Review of o&m practices in pv plants: failures, solutions, remote control, and monitoring tools,” *IEEE Journal of Photovoltaics*, vol. 10, no. 4, pp. 914–926, 2020.
- [12] D. Selva, B. Nagaraj, D. Pelusi, R. Arunkumar, and A. Nair, “Intelligent network intrusion prevention feature collection and classification algorithms,” *Algorithms*, vol. 14, no. 8, p. 224, 2021.
- [13] Y. Zhang, X. Kou, Z. Song, Y. Fan, M. Usman, and V. Jagota, “Research on logistics management layout optimization and real-time application based on nonlinear programming,” *Nonlinear Engineering*, vol. 10, no. 1, pp. 526–534, 2021.
- [14] G. P. Diller and H. Baumgartner, “Impact of adequate provision of care models and big data analysis for adults with congenital heart disease,” *Aktuelle Kardiologie*, vol. 10, no. 5, pp. 403–407, 2021.

Retraction

Retracted: Define Electronic Enterprise Financial Management Information Decision-Making Process Based on IoT and the ERP Model

International Transactions on Electrical Energy Systems

Received 19 September 2023; Accepted 19 September 2023; Published 20 September 2023

Copyright © 2023 International Transactions on Electrical Energy Systems. This is an open access article distributed under the Creative Commons Attribution License, which permits unrestricted use, distribution, and reproduction in any medium, provided the original work is properly cited.

This article has been retracted by Hindawi following an investigation undertaken by the publisher [1]. This investigation has uncovered evidence of one or more of the following indicators of systematic manipulation of the publication process:

- (1) Discrepancies in scope
- (2) Discrepancies in the description of the research reported
- (3) Discrepancies between the availability of data and the research described
- (4) Inappropriate citations
- (5) Incoherent, meaningless and/or irrelevant content included in the article
- (6) Peer-review manipulation

The presence of these indicators undermines our confidence in the integrity of the article's content and we cannot, therefore, vouch for its reliability. Please note that this notice is intended solely to alert readers that the content of this article is unreliable. We have not investigated whether authors were aware of or involved in the systematic manipulation of the publication process.

Wiley and Hindawi regrets that the usual quality checks did not identify these issues before publication and have since put additional measures in place to safeguard research integrity.

We wish to credit our own Research Integrity and Research Publishing teams and anonymous and named external researchers and research integrity experts for contributing to this investigation.

The corresponding author, as the representative of all authors, has been given the opportunity to register their agreement or disagreement to this retraction. We have kept a record of any response received.

References

- [1] H. Su, "Define Electronic Enterprise Financial Management Information Decision-Making Process Based on IoT and the ERP Model," *International Transactions on Electrical Energy Systems*, vol. 2022, Article ID 1191031, 8 pages, 2022.

Research Article

Define Electronic Enterprise Financial Management Information Decision-Making Process Based on IoT and the ERP Model

Huiling Su 

School of Economics and Management, Pingdingshan Polytechnic College, Pingdingshan, Henan 467001, China

Correspondence should be addressed to Huiling Su; 2020220170@mail.chzu.edu.cn

Received 11 August 2022; Revised 30 August 2022; Accepted 5 September 2022; Published 19 September 2022

Academic Editor: Nagamalai Vasimalai

Copyright © 2022 Huiling Su. This is an open access article distributed under the Creative Commons Attribution License, which permits unrestricted use, distribution, and reproduction in any medium, provided the original work is properly cited.

In order to realize the financial quality management of listed energy companies and realize the economical development of enterprises, the author proposes a refined evaluation method for the financial management quality of listed energy companies based on the Internet of Things and the ERP model. By introducing the concept of IoT, ERP and the financial characteristics of listed energy companies select an energy power supply enterprise as a pilot unit, combine the development strategy and the current challenges, and conducting a comprehensive analysis of the process and effect of its implementation of the financial management system, this reflects the superiority of the refined evaluation method of financial management quality of listed energy companies based on the Internet of Things and the ERP model. Pilot experiments show that, comparing before the pilot program, the financial operation status of listed companies has increased by 13.59% in total assets, positive growth achieved. The refined evaluation method of the financial management quality of listed energy companies based on the Internet of Things and the ERP model can realize the economic development of enterprises.

1. Introduction

The application of the Internet of Things and information technology is one of the effective means for enterprises to improve management; it has realistic and far-reaching significance in improving enterprise management levels and improving economic benefits. The ERP enterprise resource planning system represents the most advanced management concepts and information technology application results of today's international enterprises, its functions cover all aspects of enterprise operation and management, and it is the most complex information management system, its effective application can optimize the business process, rationally allocate resources, thereby improving economic benefits and enhancing the core competitiveness of enterprises. After decades of rapid development, ERP has been widely adopted by many large multinational companies and group companies in the world and has become an important part of enterprise information integration and business process reorganization, one of the main driving forces to speed up the process of enterprise informatization [1, 2]. Chinese

enterprises have also begun to enter the heyday of ERP popularization and comprehensive promotion and application, enterprise informatization is based on promoting enterprise innovation and upgrading, and effectively improving management level and powerful weapons as competitiveness. Needless to say, the financial management of an enterprise is an essential enterprise system, and every enterprise should be placed in the primary position of financial management. Now, financial management is more refined, and the performance of enterprises in financial management also has a more accurate and broader requirement. The ability of an enterprise is to respond quickly and in a timely manner to take the most effective measures [3]. Business managers are faced with many challenges that are unprecedented. First of all, in order to adapt to the globalization of the economy and in order to improve the fierce competition for survival, the company has more and more requirements for the amount of external information. In the entire industrial value chain, each company should be an important checkpoint and strictly related to financial management, in order to seek the profit point of growth as the fundamental

enterprise and in order to cope with the rapidly changing competitive environment [4]. Second, with the improvement of people's living standards now, there are higher requirements for the choice of enterprise products, in order to meet the growing demand and the choice of customers, enterprises are constantly changing their concepts and striving to meet the pursuit of customers' personalized needs. Therefore, companies need to change the way of production. Traditional financial management to "strengthen cost accounting and provide a reliable basis for pricing financial methods" to deal with the market's non-compliance with the requirements of modern society. As customer needs and customer capabilities change, companies must develop new compliance selection criteria that are changing. There is also manual work used by some small companies, which seriously affects the efficiency of financial services [5].

Therefore, the author, based on the IoT and ERP model, creatively proposed a refined evaluation method for the financial management quality of listed energy companies. This demonstrates the importance of the Internet of Things and the ERP model to realize the economic and economic development of enterprises.

2. Literature Review

Research on the Internet of Things ERP model financial system. Din and Paul proposed that, from the perspective of management and decision-making, the possible management problems in the application process of the ERP system are discussed, and it is emphasized that the application of the system should serve the strategy of the enterprise and adapt to the actual situation of the enterprise. This paper analyzes and studies the procurement, storage, and use of materials in the British clothing and textile industry under the environment; the management methods of enterprise inventory and materials; and the contribution of the financial management system to enterprise management are expounded from the perspective of managing the benefits [6]. Yang and Li studied the impact of interdepartmental interdependence on the use of financial information and the performance evaluation of subsidiaries from an empirical perspective. From a strategic point of view, it studies the goals and organizational environment of the centralized financial control system in system, as well as the arrangement of financial institutions [7]. Said proposed and summarized the common problems of enterprise informatization: the reuse of information is not sufficient, the degree of application of new technologies varies, and many new concepts are in a wait-and-see state. Some people put forward the use of governance theory, system theory, cybernetics, and other theories to analyze the key points of financial and accounting work in the ERP environment, and pointed out the new trend of financial management in the ERP system [8]. Manganelli et al. presented and introduced the advanced financial accounting, management accounting, and cost management thoughts embodied in the ERP financial management system. Focusing on the process of ERP system implementation, the development process of financial

management informatization, the application status of the financial modules and other submodules, and some key points and difficulties in development are discussed [9]. Hou and Yang proposed taking IT technology as the innovation environment, studying the integration of IT technology and financial management, pointing out the innovative ideas of financial management in the information technology revolution, and discussing the trend of financial management reform of group enterprises under the environment, and using typical examples represented by the company, explore its financial innovation model [10]. Kregel systematically expounded that after the implementation of ERP in group enterprises, how to establish a modern information system, how to achieve centralized financial management, and how to expound its long-term significance and profound impact [11]. Meltzer and Olin proposed an integrated information system to improve various operational decisions, control financial, and nonfinancial information requirements, and discuss its online real-time discounting and monitoring of sales, production, procurement, and financial operations through cases [12].

On the basis of the current research, the author proposes a refined evaluation method for the financial management quality of listed energy companies based on the Internet of Things and the ERP model, selects an energy power supply enterprise as a pilot unit, combines the development strategy and the current challenges, and conducts a comprehensive analysis of the process and effect of its implementation of the financial management system. Therefore, it reflects the superiority of the refined evaluation method for the financial management quality of listed energy companies based on the Internet of Things and the ERP model.

3. Research Methods

3.1. The Concept of ERP Financial System. In the management of enterprises, clear and distinct financial management is extremely important, and it is an indispensable part of the entire The ERP program [13]. ERP financial management system is different from general financial software, as part of ERP system; it has corresponding interfaces with other subsystems, and can integrate with logistics management, production control, and human resources, etc. Specifically, the financial management system is the core position of ERP and is mainly based on the following two points:

3.1.1. Provide Sufficient Management Information. The amount of business data of the enterprise occupied by any subsystem in the ERP environment cannot be as rich as the financial management system, and the business status of the enterprise can be comprehensively and comprehensively reflected through the value form. Almost all departments and all transaction processes in the business operation process are connected with the financial department. The financial department is responsible for recording, accounting, and reporting the business performance and financial status of the enterprise [14].

3.1.2. Realize Prebudgeting, In-Process Control, and Postevent Analysis. Any decision made by an enterprise must be planned in advance in order to ensure that the decisions made by enterprises meet market requirements and meet the constraints of their own capabilities. The financial management system can learn from past financial data and current market data, etc., and provides key information needed by senior managers to make correct decisions [15].

3.2. Functional Structure of ERP Financial Management System. The object of financial management is the capital flow of the enterprise, and it is the measurement and performance of the operation effect and efficiency of the enterprise, therefore, the financial management system has always been the focus of enterprises in various industries when implementing ERP [16]. Generally speaking, an ERP financial management system includes three levels of management decision-making types, namely financial business accounting management layer, financial management control layer, and financial auxiliary decision-making layer, and is integrated with the basic application environment of the organization and the information technology support environment to constitute an integrated system with functional modules corresponding to the information processing process at each level, forming a standardized financial management system. This system should be based on best business practice, integrate advanced management ideas and the best business processing mode into the ERP system, and inform flexible configuration to achieve various financial business needs. Financial management in ERP is different from general financial software, as part of the ERP system, it has corresponding interfaces with other modules in the system and can be integrated with each other, its functions revolve around the two basic functions of decision-making function and control function of financial management, the overall functional structure diagram is shown in Figure 1.

3.3. Characteristics of Financial Management of Listed Energy Enterprises

3.3.1. Large Scale of Capital Stock and Cash Flow. At present, energy power supply enterprises are in a period of rapid development, the construction of large-scale urban, rural, and county power grids by power supply enterprises has been launched. Objectively, it is required that power supply enterprises increase investment in large-scale infrastructure to adapt to economic growth and the needs of the masses. As state-owned enterprises, power supply enterprises have obvious advantages, and it is easy to obtain the support of state funds and policies, and holding a large amount of monetary funds has changed from possible to inevitable [17].

3.3.2. Centralized Financial Management and Unified Fund Management. Power supply enterprises currently adopt a financial management model of “centralized management and appropriate decentralization”. The financial rights are unified in the corporate headquarters, and at the same time,

the management method of “revenue and expenditure” is adopted, and appropriate decentralization is carried out according to the characteristics of subsidiaries and branches. For branches, under the unified management of the company headquarters, they adopt their own management modes according to different specific financial conditions. In terms of capital management, the head office manages the project funds in a unified manner, and allocates them according to the project construction progress of the branch; In terms of revenue, the head office has set up a special account for electricity revenue and collects all electricity fee income from each branch. In terms of costs and expenses, the head office manages cost units such as branches and subordinate units in a unified manner, and the finance department of the head office supervises and manages the allocation of budgets and the use of expenditures.

3.3.3. Financial Management Requires the Cooperation of Multiple Departments. As the core content of enterprise operation and management, the financial management of power supply enterprises cannot exist independently of the business activities of the enterprise. Therefore, the financial management of power supply enterprises requires close cooperation between enterprise finance and related business departments. The fund activities of power supply enterprises are wide-ranging, large-scale, diverse, and complicated. In this case, it is even more necessary for the financial and other management departments at all levels of the company (such as marketing, production planning, infrastructure, and other departments) and capital users to jointly manage.

3.3.4. There Are Risks in Investment Recovery and Capital Management. Engineering funds are an important capital expenditure item for power supply companies, every year, power supply companies have many large-scale engineering projects, for example, in 2009, and the investment in power grid construction of the State Grid Corporation of China reached 298 billion yuan, a considerable amount. Due to the large amount of the project, there are many uncertain factors in its construction, and it is difficult to control the leakage of secrets, therefore, it is easy to cause waste funds in the construction of engineering projects for power supply enterprises and even fraudulent behaviors, resulting in the difficulty of recovering investment income [18].

3.4. New Features of ERP Financial Management System

- (1) Scientific and timely, the ERP financial management system is not simple financial software; it is closely integrated with other business subsystems, and covers financial accounting, management accounting, and cost accounting. Through the implementation of the ERP financial management system, the integration of finance and ERP system can be realized, and advanced planning, control, and decision-making ideas can be perfectly combined with ERP software design, using the accounting data and financial analysis module, it is possible to carry out

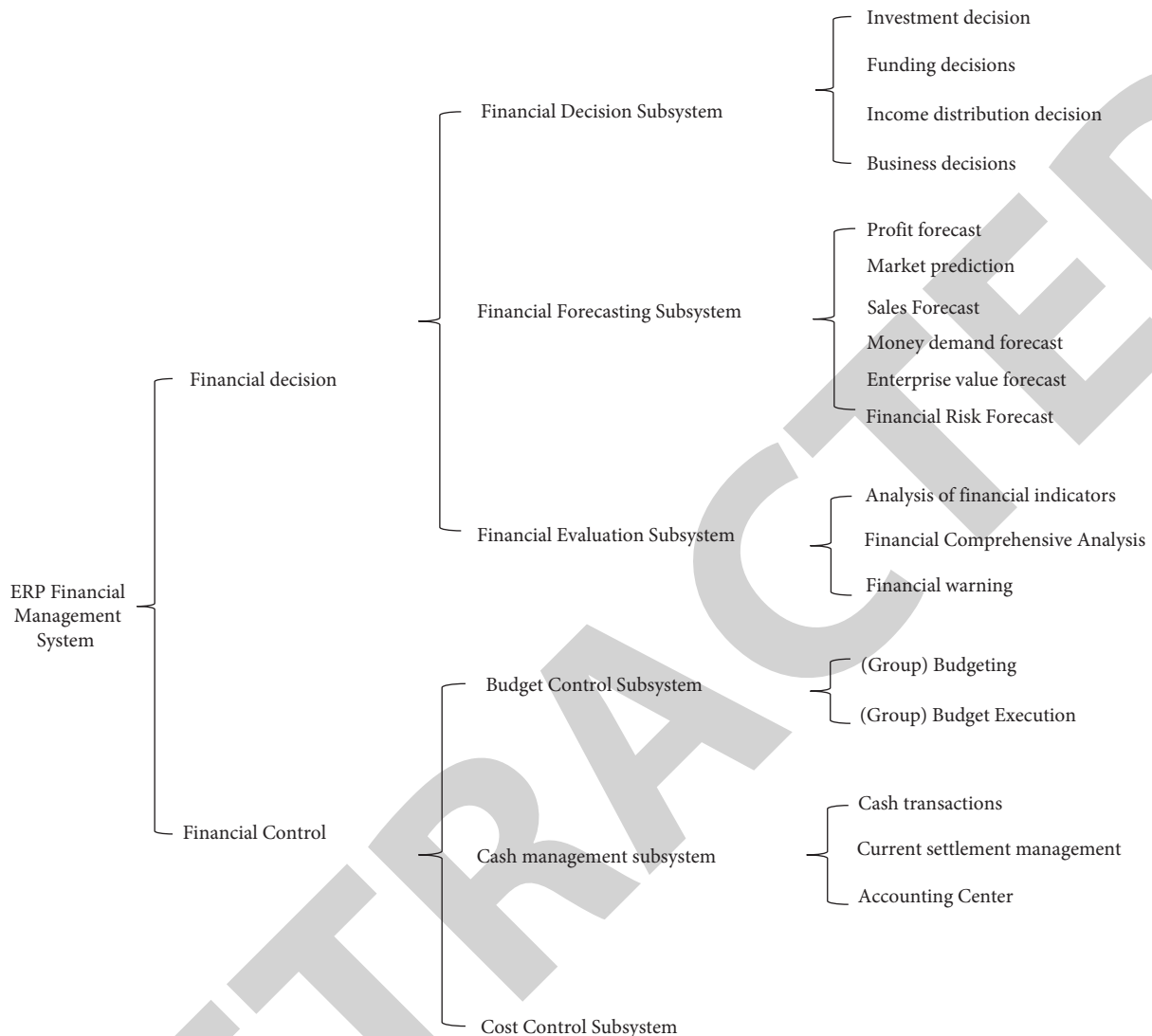


FIGURE 1: Functional structure of the financial management system.

company-level and department-level budgets and forecasts, which is helpful for enterprise management to make forward-looking and correct analysis and forecasts. Every authorized person in the ERP financial management system can grasp the real-time information at any time, and each business operation department or link of the power supply enterprise can obtain the information it needs at any time, it greatly reduces the workload of accountants, accelerates the speed of accounting work, and reduces the complexity and errors of the process, thereby greatly improving work efficiency [19].

- (2) **Comprehensiveness and integration:** the ERP system emphasizes the comprehensive combination of people, finance, materials, supply, production, and sales; it expands the meaning of enterprise resources to include plant, materials, equipment, capital, manpower, technology, reputation, and other tangible and intangible information that can be deployed and used by enterprises; it reflects advanced

management ideas and concepts. ERP financial management system is an important part of the ERP system. It is a man-machine combination system and an organic collection of resources such as people and information equipment; it is composed of accounting personnel, computer hardware, computer software, internal control systems, and other elements. It has high integration. The financial management system under the ERP environment introduces Internet technology, communication technology, and data warehouse technology into the process of financial information processing and organically integrates with other management subsystems of ERP [20].

3.5. Design and Implementation Plan of a Financial Management System for an Energy Power Supply Company

3.5.1. Accounting Level. First of all, it needs to be incorporated into the management business and economic

business settings of unified management and accounting, unifying the management and accounting of the management business and economic business of the entire enterprise group company. Provide the basis for the elimination and consolidation of group financial data. At the same time, it also reduces the workload of financial personnel and realizes the reconciliation between the upper and lower companies as well as between the subsidiary companies. Second, establish a unified subject system. Henan Company has set up first-level subjects and some detailed subjects shared by all units in the ERP financial management system and unified the subject system. By automatically summarizing the vouchers of each member company, inputting the reports in batches, and collecting the reports to generate a summary account, the “one set of accounts” management of the upper and lower companies is realized. Relieve the actual operating pressure such as adding, modifying, and deleting subjects brought by the huge subject system, which greatly reduces the workload of financial personnel. In terms of authority management, authority control is strictly carried out, and the operation process of different users in the system, the authority and data authority of different users are different, which greatly ensures the security of data. Finally, in terms of report management and accounting queries, the report templates are distributed uniformly to ensure the consistency of the report format for all units of the company. The realization of the timing function makes the summary of vouchers, batch input of reports, and report collection be completed automatically, reducing laborious manual operations and staff workload. In the implementation of the ERP financial system, the power supply company analyzed which reports can be obtained by querying premade reports in the system and which need to be obtained through customization [21].

3.5.2. Budget Management. The company formulates the budget according to the annual target indicators issued by the headquarters company and prepares the total budget with reference to the various budget preparation methods supported by the ERP system, including (setting up the organizational structure, group budget subjects, and system parameters, etc.); defining budget plans (making a unified plan for use by subordinate companies); issue budget data (mainly refers to budget subjects, managed accounting items, budget plans, etc.); system settings include budget management module settings, etc.; approval budget refers to the review and approval of the preparation of the subordinate company’s budget (that is, the secondary budget): budget issuance means that the company issues the approved information to its subordinate companies; budget execution means that the subordinate companies enter the state of budget execution: budget execution control refers to the real-time budget control of business occurrences starting from the release of budget goals, it covers the complete budget application process from budget execution and control, to budget analysis and adjustment, to budget assessment and evaluation, to achieve the purpose of real-time monitoring; budget analysis refers to the company’s budget

execution according to the subordinate secondary and grassroots units, carries out multiangle summary analysis, and the analysis methods include several fixed-format analysis reports obtained in the budget system: budget execution progress analysis Table, budget execution variance analysis Table, budget execution status Table of accounting projects, etc., you can also define personalized analysis reports through the reporting system, achieve a comprehensive analysis, it fully reflects the core management idea of comprehensive budget [22]. Figure 2.

The construction of the company’s ERP financial management system is in accordance with the requirements of centralized management of funds of the group company in terms of capital management, and strictly implements the mode of unified revenue and expenditure at the headquarters, all capital income and expenditure of subordinate companies are concentrated in the financial management department of the company headquarters, and subordinate companies do not independently set up accounts in external commercial banks, the use rights, decision-making rights, and financing rights of funds are highly concentrated [23]. In the ERP system, the collection and payment of the company’s funds are completely entrusted to the settlement center of the power supply enterprise; the settlement center gathers a lot of work and forms a payment bottleneck. Fund monitoring and approval mean that, on the basis of centralized data resources to realize unified revenue and expenditure, the approval management is carried out according to the responsibilities, authority, and process so as to realize the real-time management and online control of funds. Fund borrowing and fund analysis are done through the ERP financial management system of the bank-enterprise interconnection to finally achieve the balance of cash receipts and payments plan, control the disbursement behavior according to the budget; realize the integrated management of financial business; timely and accurate cash analysis and other fund management goals. Figure 3 [24].

3.5.3. Financial Decisions. At the level of financial decision-making, it is necessary to establish a comprehensive and complete financial analysis system, apply ERP system business intelligence and database technology, and provide effective support for company decision-making with a variety of advanced analysis, reporting, and flexible query capabilities. Provide an open application platform to meet the evolving needs of power supply companies [25]. In the original financial software, financial analysis is mainly based on reported data, the analysis method is outdated, and the timeliness and scientificity are not ideal. The financial decision-making level solution of ERP financial management system of a Power Supply Company, through the establishment of a financial decision support platform composed of a data warehouse, financial analysis system, financial audit system, comprehensive query and analysis system, in-depth financial analysis and evaluation, and timely discovery of effective information, so as to meet the decision-making needs of the management of the group company. In the ERP system, decision analysis and comprehensive query analysis

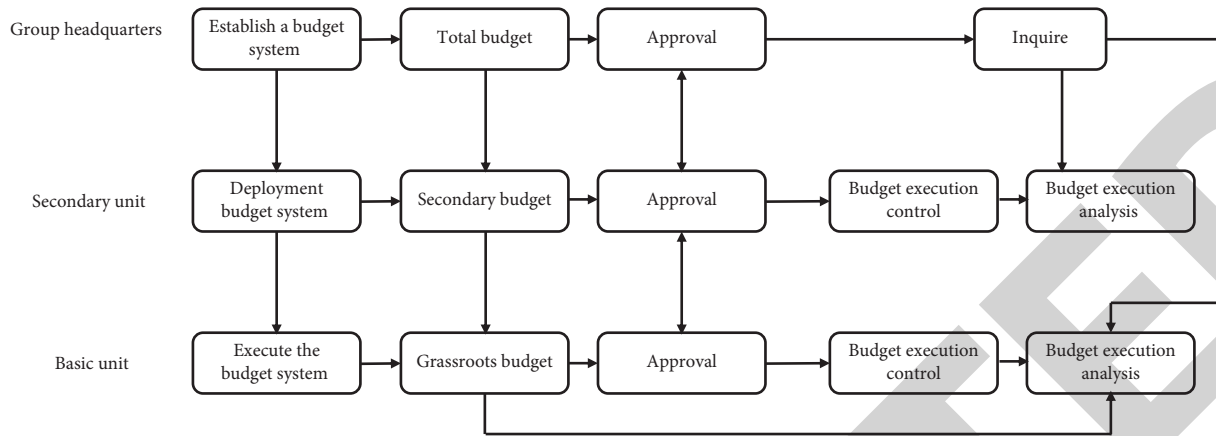


FIGURE 2: Budget management structure diagram.

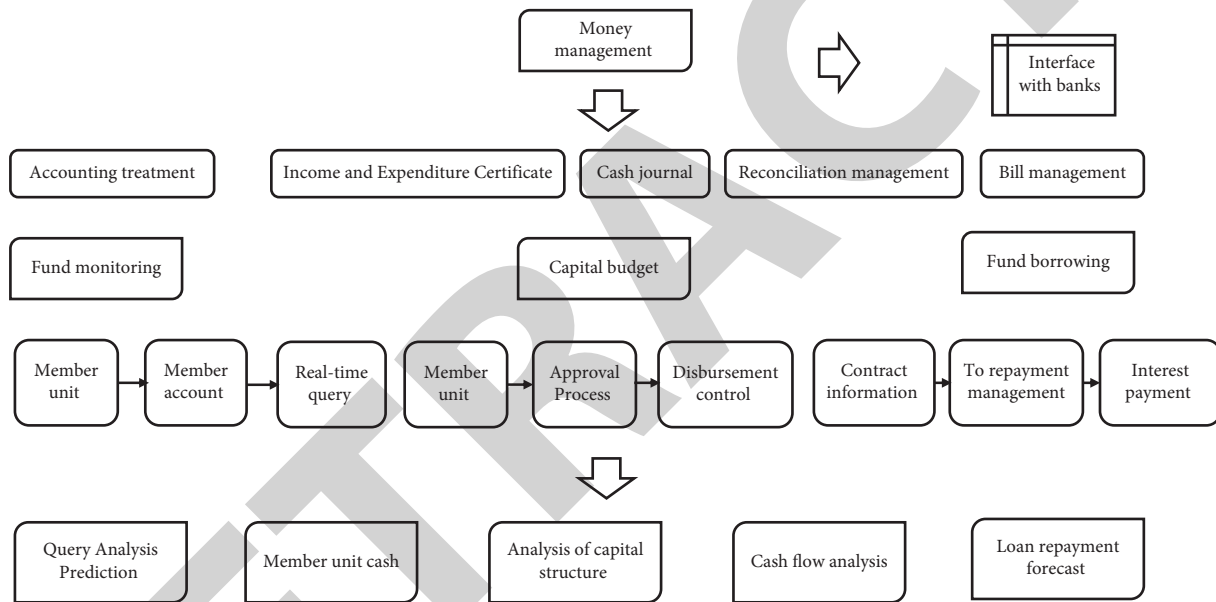


FIGURE 3: Funds centralized management mode.

are based on the centralized financial management platform and core business system. The index analysis is automated, the evaluation system is diversified, and it is seamlessly linked with other business system data. Figure 4.

4. Results Analysis

Through the implementation of the pilot, the positive effects of the company’s corporate financial management system are as follows:

4.1. Realize the Transparency of Financial Business and Realize the Dynamic Centralized Management of Funds. It mainly includes transparency of electricity bills, sales revenue, transparency of accounts receivable management, and transparency of cash flow. Real-time monitoring and management of electricity bill cash flow to speed up capital turnover and reduce financial expenses; Analyze and predict

the risk of electricity bills to provide a scientific basis for decision-making; Fundamentally solve the problems of subordinate units concealing income, fabricating accounts, man-made operations, exaggerating line losses, and misappropriating funds, etc. that are prone to occur in power supply enterprises. It has changed the situation that the traditional financial income is allocated monthly, accounts are represented by representatives, and the flow of funds is too slow. Through the real-time monitoring and management of electricity bill cash flow, the efficiency and effectiveness of the provincial company’s capital use are greatly improved. The implementation of the financial management system has realized the management of funds in a meal, and standardized the preparation, reporting, summarizing, balancing, and issuing procedures of the company’s capital plan. Establish a dynamic capital monitoring platform to dynamically monitor the company’s capital situation throughout the process to prevent capital risks.

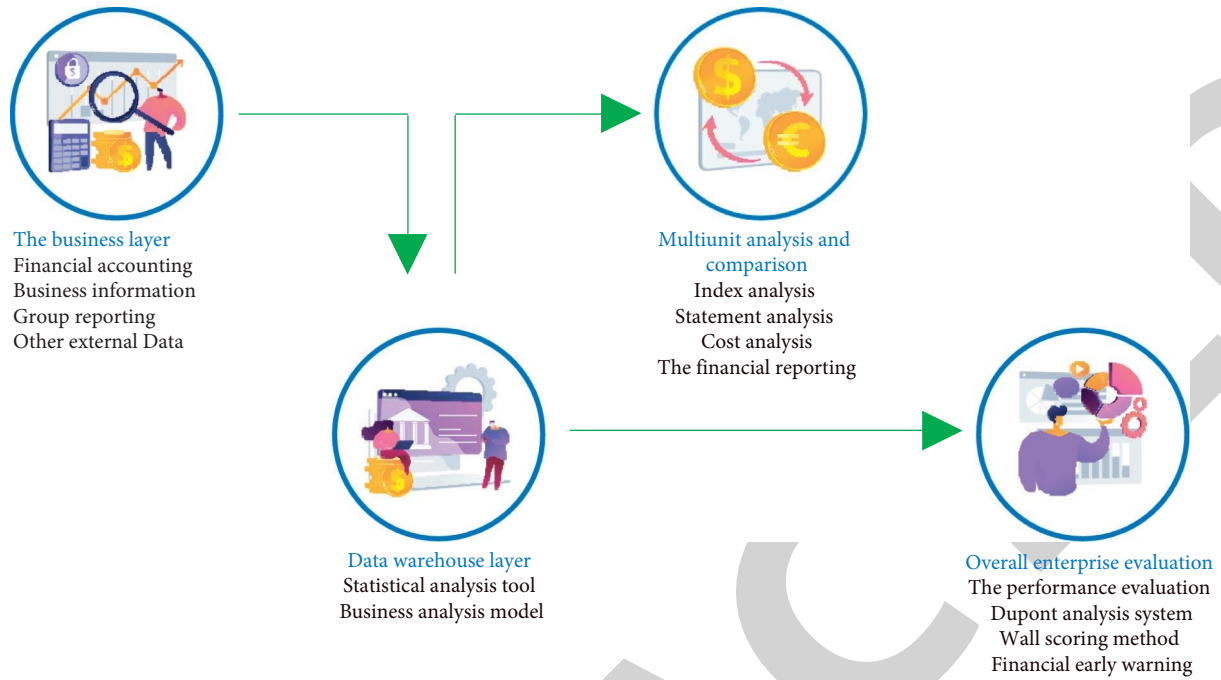


FIGURE 4: Financial decision analysis platforms (high-end).

TABLE 1: Business statements of enterprises.

Project	This reporting period	Last year
Total operating income	5,844,954,274.46	5,145,148,555.72
Operating profit	272,049,258.31	236,758,634.89
Total profit	271,850,107.55	243,704,874.25
Net profit attributable to shareholders of the company	196,838,179.44	183,963,545.32
Earnings per share (yuan)	0.85	0.79
Total assets	End of the reporting period 3,333,954,542.42	Beginning of this reporting period 2,934,954,442.32

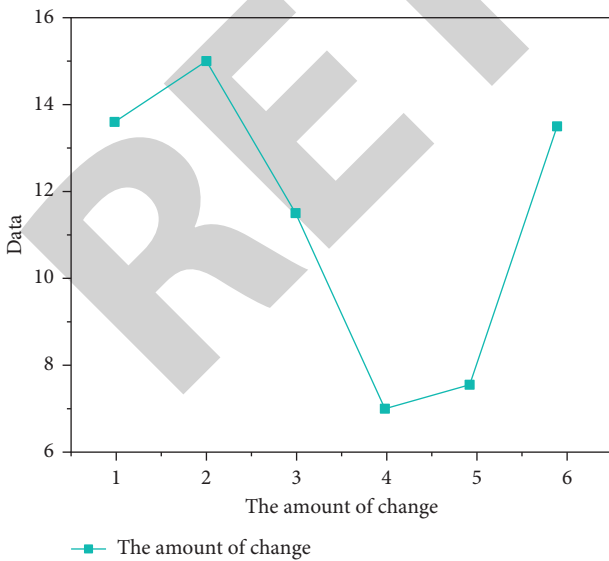


FIGURE 5: Changes in business operations.

4.2. Realize Comprehensive Budget Control and Financial Revenue Increase. The implementation of financial management systems enables managers to use the budget to

allocate, assess, and control various financial and non-financial resources of various departments and units within the company; effectively organize, and coordinate the company's business activities, control the company's key operating indicators; centralize fund management, reduce costs; and complete the established business objectives, so that the overall budget control is truly implemented. For a brief review of the financial statements, see Table 1 and Figure 5 below.

As can be seen from the chart, after conducting the pilot of a refined assessment of the financial management quality of listed energy companies based on the Internet of Things and ERP model, the increase in total assets has changed by 13.59%.

5. Conclusion

To sum up, the financial operation status of listed energy companies is higher than that before the pilot program. Total assets increased by 13.59%. This shows that the refined evaluation method of the financial management quality of listed energy companies is based on the Internet of Things and the ERP model, it can realize the economic development of the enterprise and truly improve the financial

Retraction

Retracted: Application of Laser Scanning Technology in Digital Method

International Transactions on Electrical Energy Systems

Received 19 September 2023; Accepted 19 September 2023; Published 20 September 2023

Copyright © 2023 International Transactions on Electrical Energy Systems. This is an open access article distributed under the Creative Commons Attribution License, which permits unrestricted use, distribution, and reproduction in any medium, provided the original work is properly cited.

This article has been retracted by Hindawi following an investigation undertaken by the publisher [1]. This investigation has uncovered evidence of one or more of the following indicators of systematic manipulation of the publication process:

- (1) Discrepancies in scope
- (2) Discrepancies in the description of the research reported
- (3) Discrepancies between the availability of data and the research described
- (4) Inappropriate citations
- (5) Incoherent, meaningless and/or irrelevant content included in the article
- (6) Peer-review manipulation

The presence of these indicators undermines our confidence in the integrity of the article's content and we cannot, therefore, vouch for its reliability. Please note that this notice is intended solely to alert readers that the content of this article is unreliable. We have not investigated whether authors were aware of or involved in the systematic manipulation of the publication process.

Wiley and Hindawi regrets that the usual quality checks did not identify these issues before publication and have since put additional measures in place to safeguard research integrity.

We wish to credit our own Research Integrity and Research Publishing teams and anonymous and named external researchers and research integrity experts for contributing to this investigation.

The corresponding author, as the representative of all authors, has been given the opportunity to register their agreement or disagreement to this retraction. We have kept a record of any response received.

References

- [1] F. Liu, "Application of Laser Scanning Technology in Digital Method," *International Transactions on Electrical Energy Systems*, vol. 2022, Article ID 2629688, 11 pages, 2022.

Research Article

Application of Laser Scanning Technology in Digital Method

Fangfang Liu 

Zhoukou Vocational and Technical College, Henan, Zhoukou 466000, China

Correspondence should be addressed to Fangfang Liu; 1520110207@st.usst.edu.cn

Received 14 July 2022; Revised 31 July 2022; Accepted 8 August 2022; Published 16 September 2022

Academic Editor: Nagamalai Vasimalai

Copyright © 2022 Fangfang Liu. This is an open access article distributed under the Creative Commons Attribution License, which permits unrestricted use, distribution, and reproduction in any medium, provided the original work is properly cited.

In order to improve the efficiency and accuracy of retrieval and mining of highway operation management information, a digital method research and application method based on laser scanning technology is proposed. Combined with the data storage and backup requirements of highway toll collection system, such as large amount of information, high reliability, easy management, and easy management, a complete design scheme of optical storage backup chip based on programmable logic array FPAG technology is proposed. The function, design, and simulation implementation of the write strategy subsystem and the laser power automatic control subsystem of the optical storage backup chip system are emphatically introduced. Through a lot of simulation tests, the scheme is reasonable and feasible, and its performance is stable and reliable.

1. Introduction

With the continuous improvement and operation of expressways, how to manage and use them well and give full play to their role as modern transportation infrastructure has become the most urgent issue. The collection of highway tolls is one of the essential tasks of highway operation and management. The construction and operation of the highway toll system directly affect the quality and economic efficiency of road operation and management in Chuan [1, 2].

The construction of toll roads in China began in Taiwan Province in the 1970s. The North-South Taiwan Expressway, opened to traffic in October 1978, was 373 km long and used toll reimbursement, becoming the first tolled expressway. On the mainland, since October 1988 Shanghai-Jia Expressway toll, there have been Guangfo Expressway, Shen Da Expressway, West Lin Expressway, Beijing-Tianjin-Tang Expressway, and other successive opening and implementation tolls. In addition to a few provinces such as Tibet, most areas have a varying number of toll expressways. Guangdong, Liaoning, Hubei, Shandong, and other regions have more toll roads. Because of the highway construction task and the shortage of funds, contradiction is more prominent, so constructing a toll collection system on the

highway, charging vehicle tolls will become the central theme of China's highway development in the future.

The highway toll system is an information data system, and the information of the highway includes three parts: highway personnel information [3, 4], highway activity information, and highway data information. Freeway personnel information includes toll collectors, toll management personnel, maintenance personnel, drivers and passengers, and service organization personnel. Freeway activity information includes information about the tolling process, operations related to the tolling process, and data information processing supporting business activities, such as toll monitoring and toll plaza control. Highway data information includes data generated during the tolling process, such as toll data, traffic volume data, and video information, and data issued by the toll center, including toll rates and base clocks.

Although the data is stored in hard disk memory within the specified time, the hard disk memory cannot be recovered for the data damage caused by many reasons. Therefore, while storing data in real-time, data backup storage should also be performed regularly to ensure that when data is damaged, data can be recovered quickly and correctly and that backup data is easy to keep, reliable, and economical. For the traffic information storage volume,

high information accuracy requirements, storage reliability, financial requirements, and other characteristics, we study what kind of storage backup technology to become one of the keys to the design of highway toll system.

2. Optical Storage Backup Related Technologies

2.1. Data Conversion Process of DVD. First, the data coming from the host is called master data or user data, and the master data consists of 2048 raw data bytes. At the beginning of the master data, 4 bytes of identification code ID are added to identify the sector format, track mode, reflection rate, area where the sector is located, data type, number of layers, number of sectors, etc., 2 bytes are used for ID error detection IED, and 6 bytes of RSV code, and 4 bytes of error detection code EDC are added at the end. The 2064 bytes of data are arranged in a structure of 12 rows and 172 columns, which is called a data frame or data sector.

The 2048 bytes of master data in the data frame are scrambled and encoded to obtain the scrambled data frame. Sixteen consecutive scrambled data frames are combined together to form a data block of 192 (rows) \times 172 (columns), and then, the data block is encoded with Reid Solomon error correction; that is, a 16-byte external parity Reid Solomon check code, referred to as P0, is calculated for each column of the 172 columns of the data block, and 16 new P0 rows are formed at the bottom of the ECC block. A complete ECC block can be guaranteed to correct at least 5 bytes of error on each row and 5 bytes of error on each column [5].

The ECC block is crossed in rows, and one P0 row is inserted in order every 12 rows of data, and each of the 16 P0 rows is inserted into the data rows to form a new data structure-record frame. That is, each record frame has 13 rows (including 12 rows of data and 1 row of P0) and 182 columns, and one ECC block will generate 16 record frames. This way of interpolating P0 rows to each sector facilitates the further play of error correction features.

In the process of data encoding and modulation of DVD disc data storage backup system, two techniques are applied to determine the basic form of DVD disc storage backup data, which are 8-14 enhanced modulation EFM + technique and NRZI transform technique.

2.2. EMF + Modulation. EFM+ is the abbreviation for 8-14 enhanced modulation. Optical disk storage system: the purpose of using EMF + modulation is to make the data to be stored into a physical expression suitable for storage on the media; that is, a byte of 8-bit data into 14bit channel code, the transformation from 214 types of code type selected 28 types of code type, and the selected code type should meet: in the channel code between the adjacent two, 1 must have at least 2 more than 10 below the 0. At the same time, in order to extract the synchronization signal in the readout signal, the synchronization signal in EFM + adopts 14T-14 T code type. Thus, EFM + follows the 3T~11 T, 14T rule; that is, there are 10 possible choices of 3T~11 T and 14T for the width of the notch/platform.

The reason why EFM + modulation is used is that when multiple "1s" and "0s" appear in succession when writing data, the laser beam emission will be turned on and off so frequently that the length of the pits becomes very short, which will make the manufacturing process of the optical discs complicated or even difficult. This will make the optical disc manufacturing process complicated or even difficult to achieve. When reading data, because the resolution of the channel code pit/platform is limited by the wavelength of the reading laser and the NA of the focusing lens, if the length of the pit/platform is too short, their edge detection will be difficult; a very short pit will produce unstable data for signal identification; frequent "1" will cause the servo circuit to work unstably, and frequent "0" will cause the laser beam to turn on and off. Frequent "0" will cause the voltage controlled oscillator of the decoding circuit to work unstably because there is no "1" for a longer period of time, and at the same time, long distance pits or planes will also affect the tracking ability of the reading device.

2.3. NRZI Transformation. NRZI transformation is also used before data is stored and backed up to the disc, so that the data to be stored and backed up only jumps when data "1" appears, while the previous state is maintained when data "0" is present. In this way, the data to be stored for backup corresponds to the pit and platform of the VDD, and the transformation from pit to platform or from platform to pit on the DVD disc represents binary data "1," while no transformation represents binary data "0." Figure 1 shows the NRZI conversion timing diagram.

2.4. Overall Solution for Optical Storage Backup Chip Design. The optical disk storage and backup chip is the main component of the optical disk storage and backup system, and its structure is shown in Figure 2.

The functions of each subsystem are described as follows:

- (1) The function of the optimal power control subsystem is to determine the optimal power value for reading and burning discs at all levels by conducting a test burn in the disc test burn area.
- (2) The automatic laser power control subsystem monitors the power level by closed-loop control to stabilize the power level at its optimal value when reading or burning discs.
- (3) The function of the write strategy subsystem is to generate switching control signals for each power level according to the type of disc and the burning speed.
- (4) The function of the encoding and modulation subsystem is to convert the user data in the host into the NRZI data to be recorded after a series of encoding and modulation. Coding and modulation are mainly used for error correction and data recovery.
- (5) The function of the phase-locked loop subsystem is to provide a stable and unified clock mnemonic for the reading and burning of the disc.

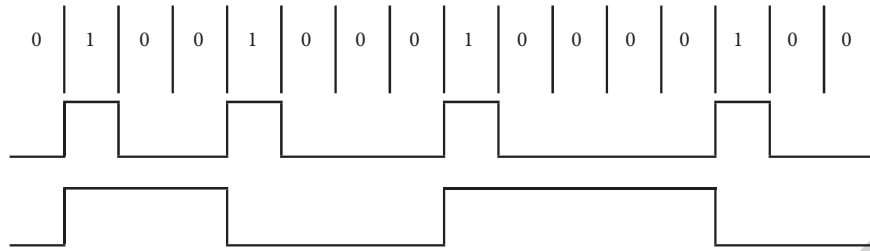


FIGURE 1: NRZI conversion timing diagram.

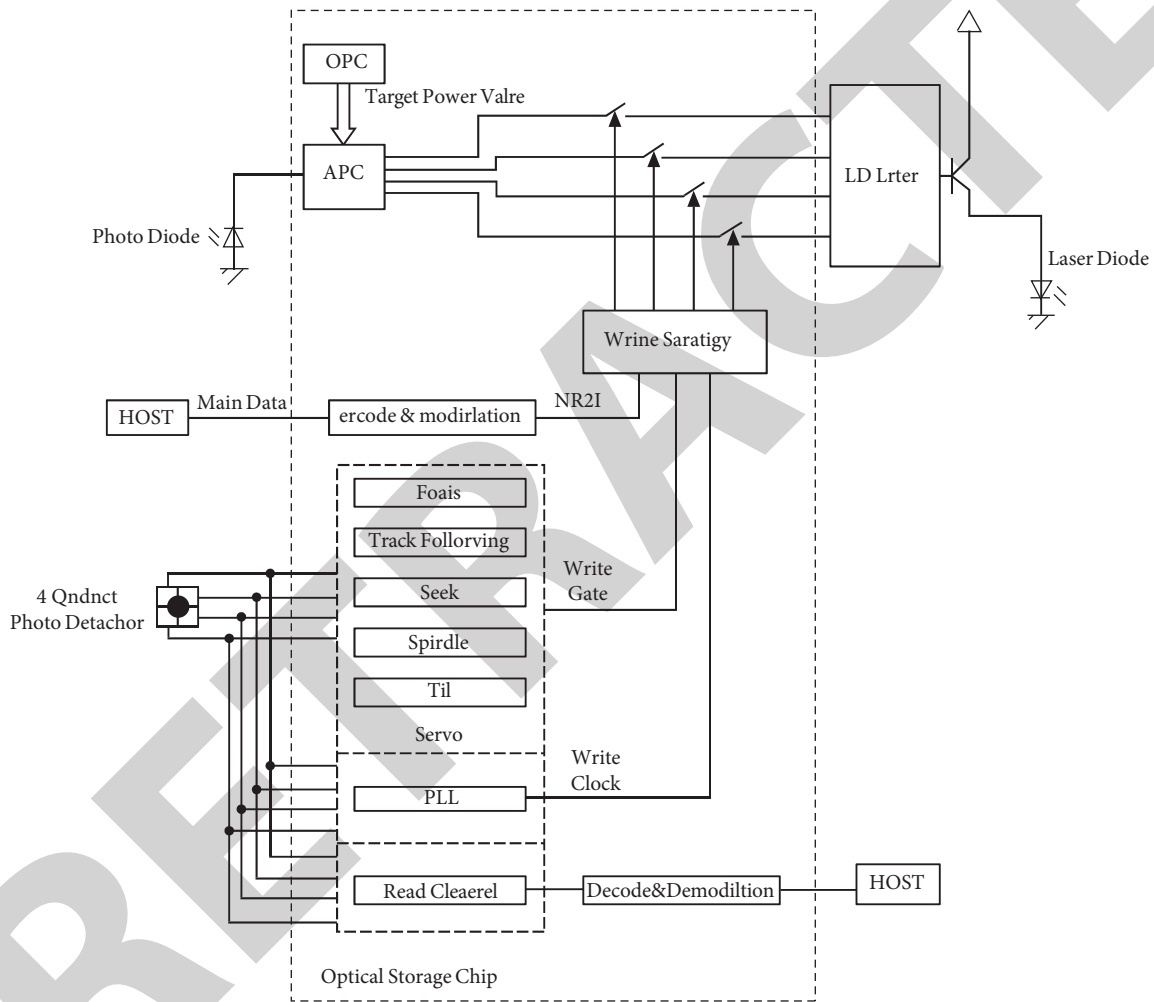


FIGURE 2: Optical disk data storage backup chip structure diagram.

(6) The function of the servo subsystem is to ensure the correct tracking scan relationship of the read/write laser spot to the track traces. The correct tracking and scanning relationship between the spot and the traces mainly includes space and time aspects. Spot in space and the trace to maintain the correct tracking relationship means: the optical head and disc for high-speed relative motion, on the one hand, must make the disc signal surface always fall in the reading beam about 2um depth of focus range, which is mainly by the tilt servo, height servo, and focus

servo to achieve it: on the other hand, to ensure that the reading spot can always be scanned on the trace, which is mainly by the tilt servo, tracking servo, and feed servo to achieve it. This is mainly achieved by the tilt servo, the tracking servo, and the feed servo. The rate of the correct scanning relationship is to ensure that the reading rate is correct, so that the playback signal and the time base of the recorded signal are consistent, which is mainly by the spindle servo and playback signal processing system to achieve it.

- (7) Read channel subsystem function is through the Partial Response Maximum Likelihood (PRML) technology, that is, the use of logic rules to analyze a set of data read out by the optical head, inducting a signal closest to the standard data method to convert the data signal RF into NRZI signal.
- (8) Decoding and demodulation subsystem is the inverse process of encoding and modulation subsystem, whose function is to recover the original data, audio, or video information burned according to the NRZI signal output from the read channel subsystem. The eight subsystems of the optical storage backup chip work in coordination to complete the read and write operation of the optical disc data together.

3. New Automatic Laser Power Control Design Scheme for Digital Information

The conventional sampling/holding analog circuit uses nonuniform sampling, which has a costly design and a complex structure that cannot accommodate more levels of power. In this paper, a new all-digital automatic laser power control design is used to depart from the conventional sample/hold circuit design introduced earlier, avoiding the generation of high-frequency nonuniformly sampled clock signals and making the structure of automatic laser power control simple and easy to implement.

3.1. New Automatic Laser Power Control Design Principle. Automatic laser control, as a closed-loop control system, is much less frequent for power detection and adjustment than the frequency of laser power signal changes [6]. Therefore, instead of using the average value of the laser power at each level as the feedback of the closed-loop control system by the power sampling value of the sampling/holding circuit, a scheme is proposed with a power adjustment frequency of 20 kHz at each level. This closed-loop control scheme using the average value of the laser power can be implemented entirely by hardware, that is, FPAG implementation, which greatly increases the design flexibility and reduces the design cost (Figure 3).

First of all, since the output-PDNI signal of the laser detection diode DP, which represents the power situation at all levels of the disc storage and recording process, is an analog signal, and the FPGA can only process digital signals, the PDIN signal is first converted into a digital power signal by a digital-to-analog converter chip ADC, and then the converted digital signal enters the FGPA according to a certain rule for classification and processing and outputs the feedback control signal for each power. The feedback control signal is used to control the laser emitter, but also it must be converted from digital signals to analog signals, and the design uses PWM plus analog low-pass filter method instead of digital/analog converter chip DAC to complete the conversion of digital signals to analog signals; the converted analog signal directly controls the laser emission of all levels of power to achieve the role of stable power. The Soc, ACP, and P delete parts in the above figure

are done in FPGA, the first-order analog low-pass filter is implemented with hardware analog circuit, and the analog/digital conversion is done with the AD/converter chip [7, 8].

3.2. New Automatic Laser Power Control FPAG Design. The new automatic laser power control FGPA design consists of three main parts, namely, Soc, ACP, and PWM. The principle of connecting the three parts is shown in Figure 4.

In the figure, Soc is the core of the whole optical memory backup chip, controlling the reset (RESET) and enable (EN) of each subsystem and providing the clock signal (CLK) for each subsystem, and it can read and write with each subsystem through the three control signals of read (RD), write (WR), and chip select (CS), the 32-bit data input bus (DINO ~ DIN31), the 32-bit output data bus (DOUTO ~ DOUT31), and 32-bit address bus (ADDRO ~ ADDR31) for read and write operations with each subsystem. For ACP subsystem, Soc mainly completes system reset and enable of ACP subsystem and PWM, provides clock for ACP subsystem and PWM, and sets control and status registers of ACP subsystem.

APC structure is the main structure of APC subsystem. There are two main functions: one is to complete the control of AD/chip, including the setting of AD/chip working mode (by setting the control register of AD/chip), the generation of control signals of AD/chip (clock signal ADCLK, enable signal ADCS, read control signal ADRD, write control signal ADWR, and receiving A/D conversion completion signal ADINT and A/D conversion result (ADD0~ADD9)); secondly, the result of AD/conversion (ADD0~ADD9) is processed to get the digital drive signal of the laser emitter, that is, laser emitting power signal read laser power, that is, RP0~RP9, write laser power WP0~WP9 erase laser power BP0~EP9, and bias laser power BP0~BP9.

The purpose of the PWM is to replace the expensive D/A converter with a digital circuit design that changes the DC component of the output by modulating the duty cycle of the square wave, and after a low-pass filter to get the desired level signal, complete the transformation of the digital signal to the analog signal. The design of the analog low-pass filter is shown in Figure 5. Each power level corresponds to a set of PWM with analog low-pass filter [9, 10].

The new all-digital makes the power level increase, and APC design scheme can be closed-loop control of each level of laser emission power; that is, it only needs to increase the APC structure, and the increase in its hardware structure is extremely limited, as well as the structure of the power signal processing and PMW junction, and there is no technical bottleneck.

3.3. New Automatic Laser Power Control Design for a/D Conversion. The analog/digital converter chip in this design is the TLV1571 chip from TI. The TLV1571 is a 10 bit single-channel analog input analog/digital converter with two internal 8-bit control registers COR and CRI to control the ADC operating modes, including software conversion or hardware conversion start selection, internal or external clock selection, and binary or binary-complement output.

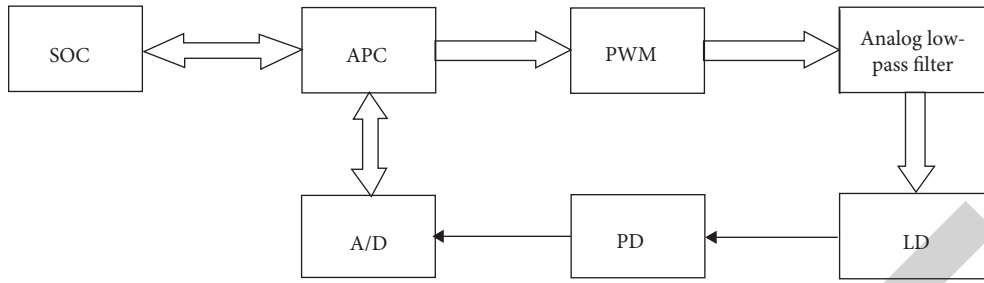


FIGURE 3: Structural block diagram of the new all-digital ACP design.

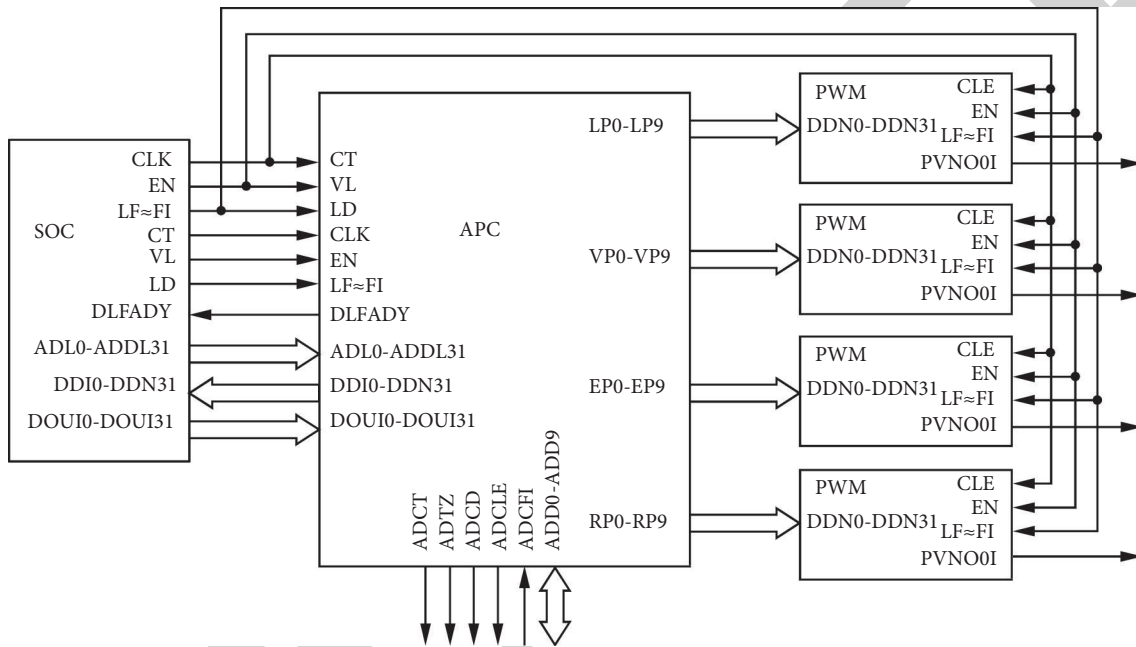


FIGURE 4: New automatic laser power control FPGA internal structure diagram.

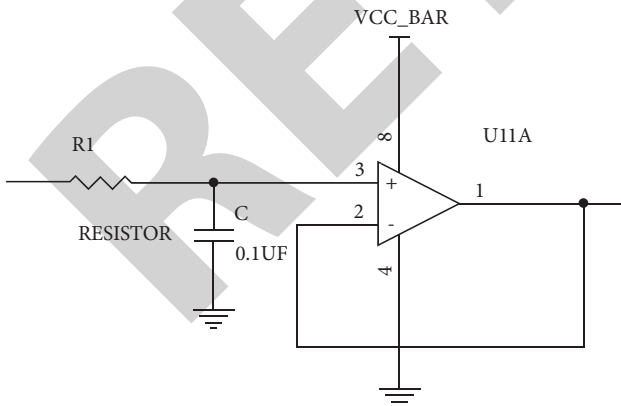


FIGURE 5: Analog low-pass filter circuit diagram.

The following diagram shows the operating modes of the TLV1571. Figure 6 shows the block diagram of the TLV1571 functional structure.

AIN is the input analog signal port of TLV1571; D0~D9 are 1b0ti tristate bidirectional data bus; when used as input,

D0~D9 is used to set two 8-bit control registers, among which D0~D7 is used as the setting value of control registers, and D8 and D9 are used as the address selection of two control registers; when used as output, D0~D9 are the result of A/D conversion output. CLK is the input clock signal port of TLV1571, and TLV1571 supports internal clock signal and external clock signal in two ways: the internal clock signal frequency range is gMHz~22 MHz, and the external allowed input clock frequency range is 1-20 MHz; RD, WR, and CSTART are the control signal input ports for A/D conversion, which control the way and time of AD/conversion.

When the TLV1571 performs A/D conversion, its AD/sampling takes 6 clock cycles, AD/conversion takes 10 clock cycles, and output data takes at least one clock cycle, so the maximum A/D conversion frequency $f=f(1/17)$. The design controls the conversion working mode by setting the two control registers of the TVL1571 to the external clock signal, and its working timing is shown in Figure 7.

When both CS and WR signals are low, the control register of TLV1571 is written. After setting the control register of TLV1571, the AD/sampling starts at the rising edge of WR, and after the sampling lasts for 6 clock cycles,

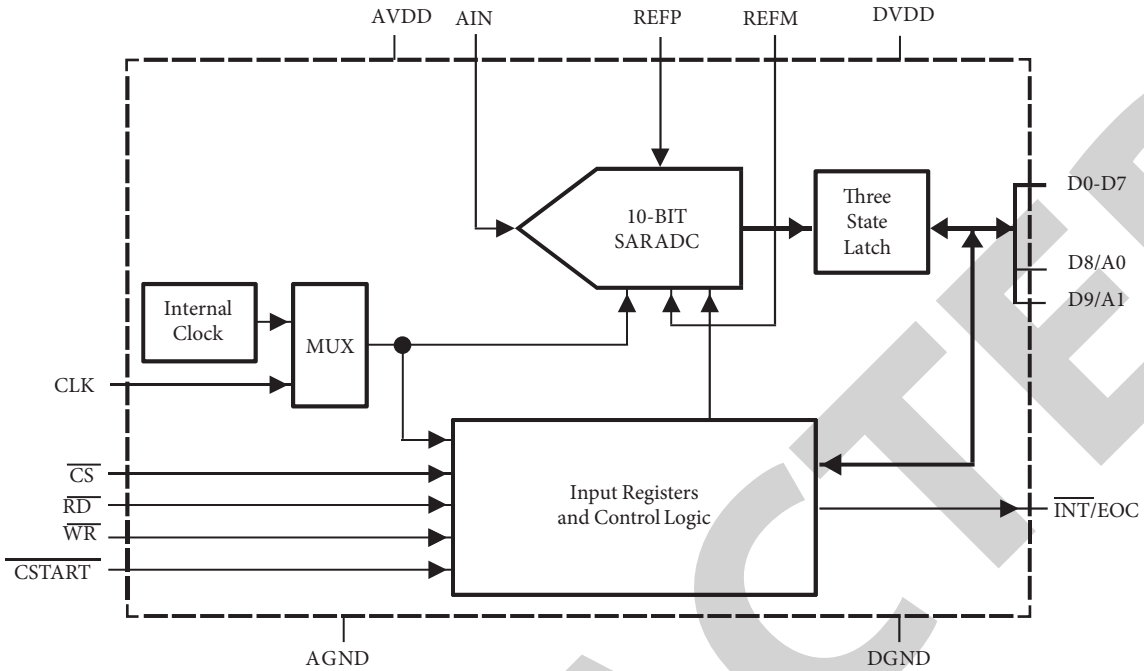


FIGURE 6: Block diagram of the functional structure of the TLV1571.

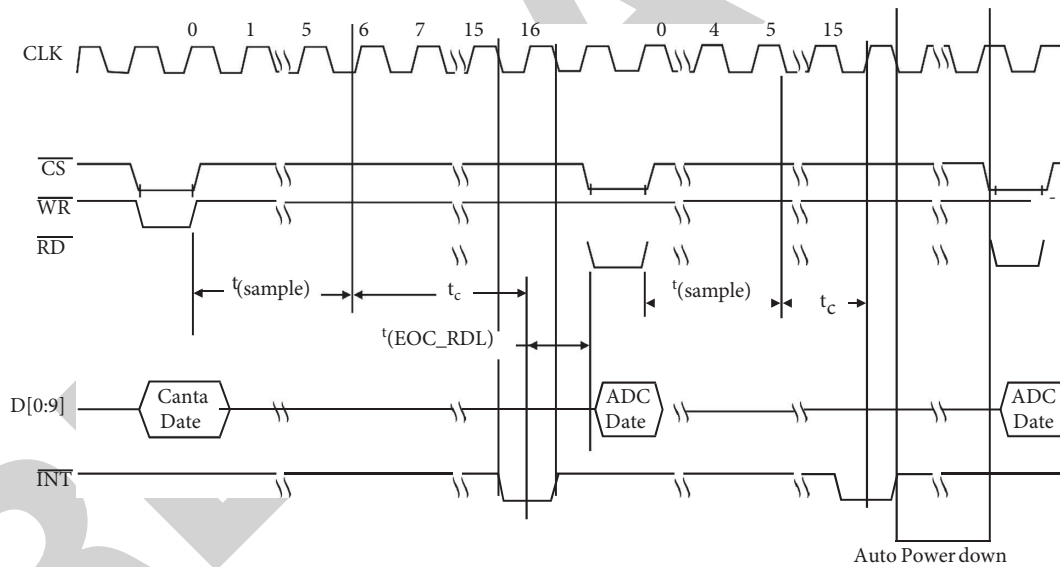


FIGURE 7: TLV1571 operating timing diagram.

the A/D conversion is automatically performed, and the conversion takes 10 clock cycles. After the conversion is completed, INT becomes low to notify the FPGA that the AD/conversion has been completed, and at the same time, the AD converted digital signals are prepared on the D0~D9 data bus, and at the falling edge of the RD signal, the data is read into the FPAG for next processing. The clock signals CKL, CS, WR, and RD of the TLV1571 are generated by the FPGA. D0~D9 are connected to the 10 bidirectional I/O ports of the FPGA for completing the two control registers of the TLV1571 settings and the transfer of AD/conversion results. Figure 8 shows the circuit diagram of TLV1571 and FPGA connection.

3.4. Advantages of the New All-Digital Automatic Laser Power Control Design. The new fully digital automatic laser power control design applies the FPGA design, which has the following advantages over the conventional sample/hold circuit design.

Hold circuit design; it has the following advantages.

- (1) The sampling frequency of the ADC is fixed and determined by the selected ADC model, so it is not necessary to use a special structure to generate the sampling clock signal, and the sampling conversion frequency of the ADC can be easily adjusted according to the actual needs.

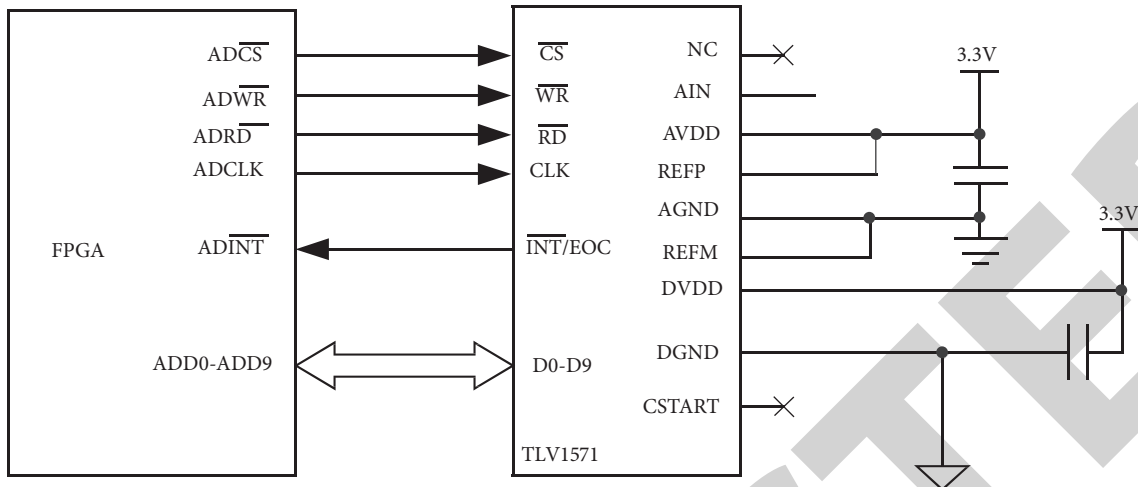


FIGURE 8: TLV1571 and FPGA connection circuit diagram.

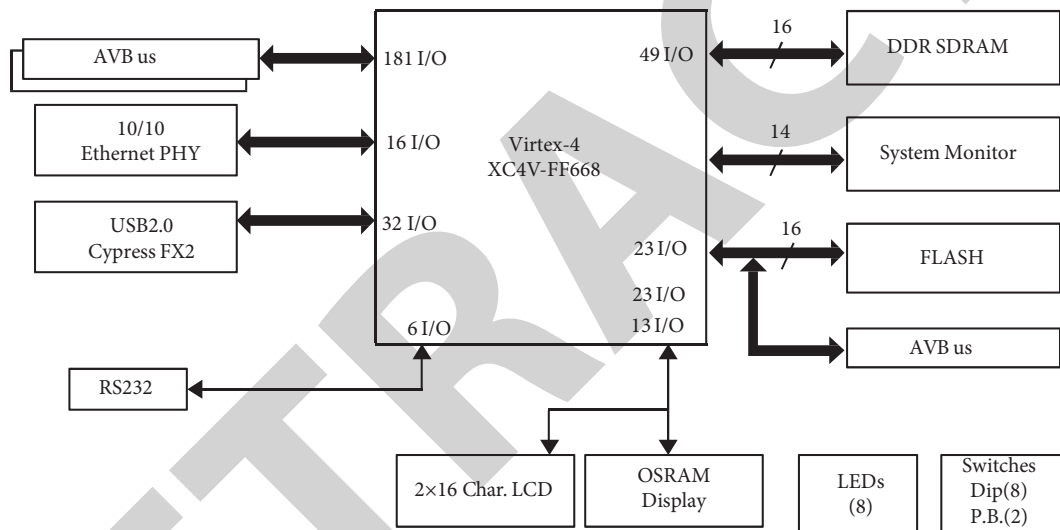


FIGURE 9: Block diagram of AVNET's XC4vLX25-FF668 FPGA evaluation board.

- (2) The sampled signal is classified into its corresponding power level (write power, read power, and erase power) by the power level classification standard, which will not generate misjudgment and misadjustment caused by missampling.
 - (3) According to the different discs, the power level classification is bound to be different. By setting the value of the corresponding power level register, the power level classification standard can be easily changed, which greatly increases the flexibility of the design.
 - (4) Through the division of the power level, avoid the sampling difficulty caused by the read/write pulse is too narrow, and use other power level to replace the judgment, for Blu-ray technology, even if the power level increases, and we only need to increase the ACP structure of the power signal processing structure and PWM structure, the increase of its hardware structure is extremely limited, and there is no technical bottleneck.
 - (5) Use the cumulative average value instead of the actual power to avoid misjudgment caused by sudden noise.
 - (6) PWM plus analog low-pass filter design instead of D/A chip greatly reduces the design and production costs.
- This greatly reduces the design and production cost.

4. Experiment and Analysis Based on FPGA

This design uses the FPGA evaluation board designed by Avnet Design Services, which uses Xilinx's XC4VLX25-FF668 type FPGA chip. Figure 9 shows the block diagram of AVNET's XC4vLX25-FF668 FPGA evaluation board structure.

In addition, there are 32 MB DDRSDRAM and SMB Intel StrataFlash, 10/100 M adaptive Ethernet interface, USB2.0 interface and RS232 serial interface, 128 × 64 OLED graphic display, 3 sets of 140-pin universal I/O connectors

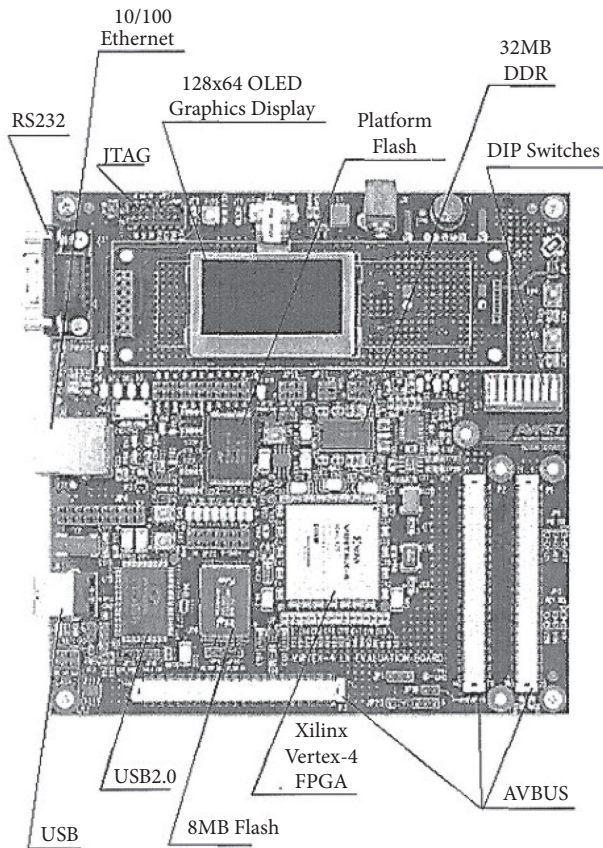


FIGURE 10: AVNET's XC4VLX25-FF668 type FPGA evaluation board.

(AvBus), and other hardware structures. Figure 10 shows AVNET's XC4VLX25-FF668 FPGA evaluation board.

The XC4vLX25-FF668 FPGA evaluation board has two types of board-level clock inputs, 50 M and 100 M, and its configuration methods include boundary-scan and serial and parallel configuration.

XC4VLX25-FF668 is a Virtex-4 series field programmable gate array (FPGA) from Xilinx, the first LX high-performance logic application solution, and platform FPGA based on the ASMBL architecture. XC4VLX25-FF668 uses 300 mm (12-inch) wafer technology and 90 nm CMOS copper process manufacturing, reducing dynamic power consumption, while we use trigate oxide layer technology to reduce static power consumption, and compared with the previous generation of FPGA, the net power consumption reduced to 50%, while compared with other competitive products using 90 nm technology, it also has the following significant advantages.

- (1) xc4vLx25 a FF668 type FPGA is 96×28 array structure, with 24,192 logic cells (Logic Cells), 10,752 Slices structure, and its maximum configurable 168 kb RAM.
- (2) With 48 XtermDSP51iecs, it provides the highest performance, the lowest power consumption, and the most functional arithmetic units, and it can implement multiply one accumulation unit or

cascade with other similar modules to achieve a larger design architecture; in addition, the DSP module can also be configured to work at 500 MHz counters, barrel shift registers, address subtractors, accumulators, and other structures. This performance and scalability can be used to implement highly integrated and performant DSP functions without taking up general-purpose logic resources.

- (3) With 72 built-in block RAMs, each block RAM can store 18 kb, and two adjacent block RAMs can be combined to form a 32 kb memory. The combination of block RAMs can be easily configured into synchronous or asynchronous SRAM, DSARM, synchronous/asynchronous FIOF, ORM, CAM, and other memory forms according to user requirements.
- (4) With eight digital clock managers (DCM), each DCM can be used to eliminate clock distribution delay, clock multiplication, frequency division, shifting, and other operations; in addition, the DCM also has clock synthesis capabilities; the most critical is as follows: DCM processing of the resulting clock signal has good timing characteristics, and the signal can be directly connected to the global clock network to improve the driving capability and reduce the clock DCM, and global clock multiplexer provides a complete solution for designing high-speed clock networks.
- (5) The Phase-Matched Clock Dividers (PMCD) module with four new phase-matched clock dividers provides 32 ps accuracy, simplifying clock synthesis and alignment. The differential clock tree is utilized to ensure minimal distortion and jitter.
- (6) With 11 input/output banks (Total I/O Banks), the most flexible I/O interfaces and XCITE serial/parallel/differential active I/O ports are supported, thus providing the highest performance, enhanced power, and better signal integrity for both single-ended and differential I/O.
- (7) With 448 user-available I/O pins.
- (8) The Generic Routing Matrix (GRM) provides an array of routing switches between each programmable part to connect the components of the XC4vLX25-FF668 to the routing matrix, and all components use the same interconnect mechanism.

The FPGA design process for this design includes several major steps: design input, functional simulation, synthesis, postsynthesis simulation, implementation, post-layout-wiring simulation, and download verification debug.

The design input usually includes schematic input, hardware description language (HDL) input, waveform input, state machine input, and a combination of several input methods. The design input for this design is VHDL hardware description language; after the design input is completed, the design should be simulated using simulation tools to verify whether the designed circuit meets the design requirements, and if not, go back to the design step and modify the original design until it meets the design

requirements. Functional simulation can identify errors in the design and speed up the design process. After the completion of the functional simulation to synthesize the design, synthesis refers to the process of converting the design input into a logic connection diagram consisting of basic logic units such as with, or, nongates, RAM, flip-flops, etc.; after the completion of the synthesis, the same is needed for postsynthesis simulation to check whether the synthesis results are consistent with the original design, as well as the synthesis in the postsynthesis simulation, and the generated delay file is backlabeled to the model of the postsynthesis simulation to check the working situation after adding the delay of the device, and if the simulation result shows that it does not match with the design requirements, it should go back to the input or synthesis stage for modification until it reaches the design requirements. Since the result of synthesis still has a certain gap with the actual configuration, the implementation step is also performed. Implementation is the process of configuring the basic logic cells generated by synthesis to specific FPGA devices, and it is composed of three substeps: translation, mapping, and layout wiring. After implementation, there is another simulation, that is, post-layout-wiring simulation. The post-layout-wiring simulation includes both device delay and delay caused by layout and wiring, which can basically reflect the actual working condition of the chip correctly. Similarly, if the result of post-layout-wiring simulation cannot meet the design requirements, the link that produces the difference should be found whether it is in the design input stage, synthesis stage, or implementation stage, and go back to the corresponding stage for modification until it meets the design requirements. When all the simulations meet the requirements, it is time to configure and verify the FPGA chip. Only the design that is successfully verified on the FPGA chip is a design that really meets the design requirements. In addition, in the synthesis and implementation process, the performance of the design can usually be improved by adding constraints, including timing constraints, pin constraints, and area constraints.

4.1. Write Policy Subsystem FPGA Design and Verification. In this paper, the top-level structure of the block-type and pulse-type write strategy subsystems are given, and the layout wiring after the design of the block-type and pulse-type write strategies are given as an example for the CD-R preheat method and the DVD-R preheat method, respectively. The real waveforms of the block-type and pulse-type write strategy designs are given in the example of CD-R preheat and DVD-R preheat.

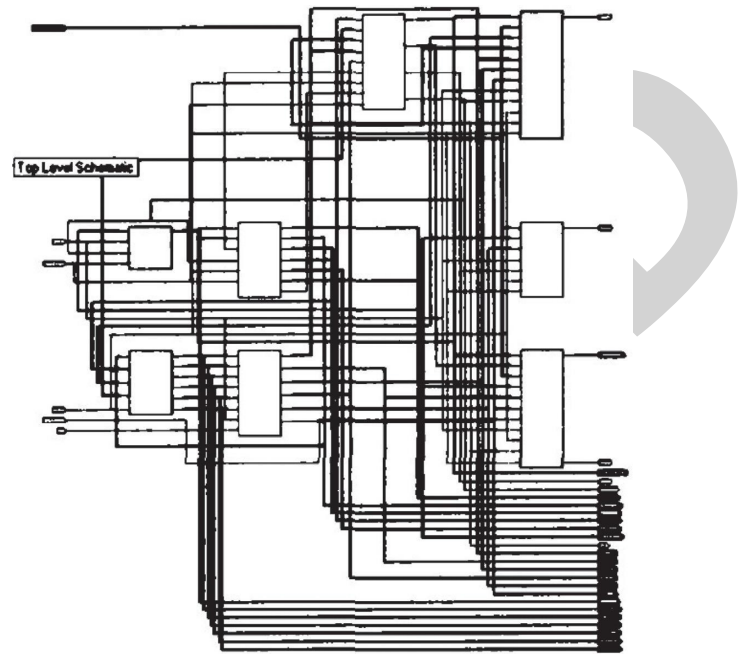


FIGURE 11: Top-level structure diagram of FPGA-designed block writing strategy.

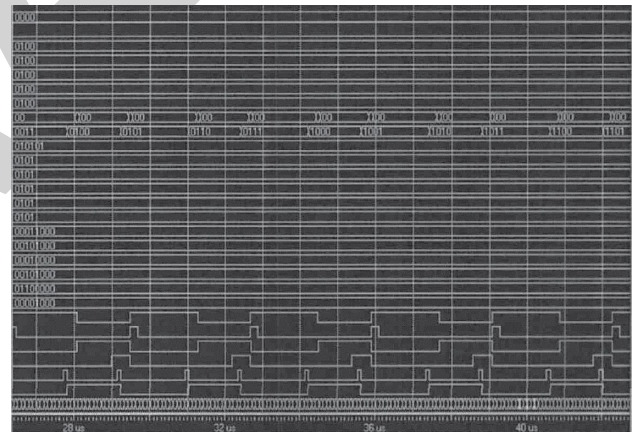


FIGURE 12: Simulation waveform after wiring the block-type write strategy layout in CD-R preheat mode.

4.1.1. Block Write Strategy FPAG Design and Verification

- (1) Top-level structure of block write strategy for FPGA design

The top-level structure of the block write strategy for FPGA design is shown in Figure 11.

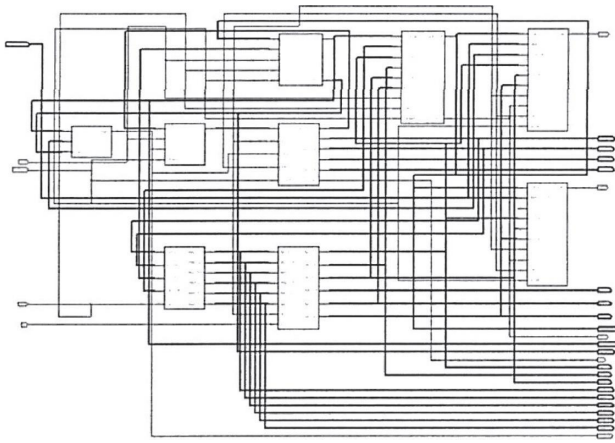


FIGURE 13: Top-level structure diagram of the FPGA-designed pulse-based writing strategy.

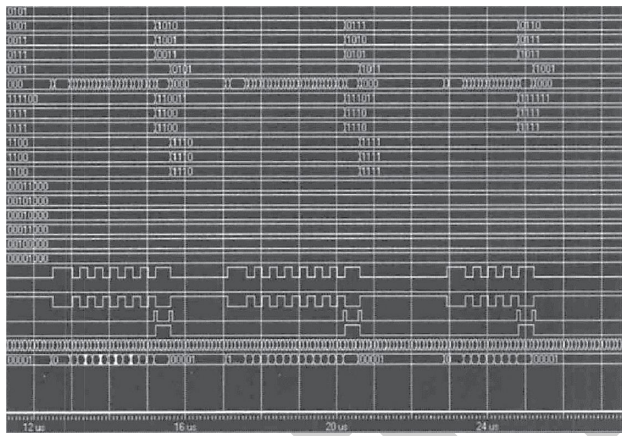


FIGURE 14: Simulation waveform after layout wiring of DVD-R preheat method with pulse-type write strategy.

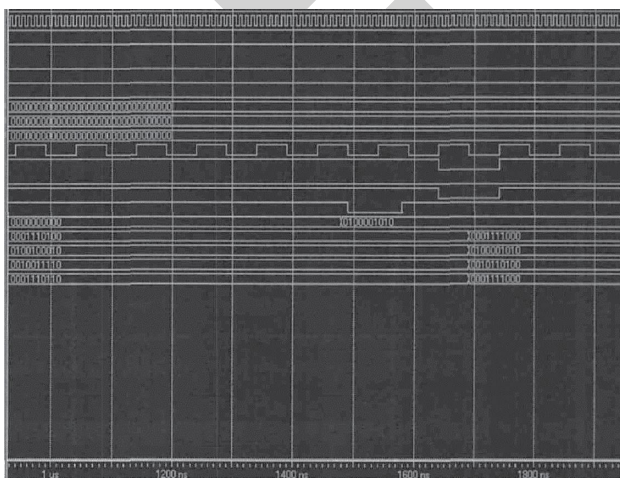


FIGURE 15: Simulation waveform of automatic laser power control subsystem after layout and wiring.

- (2) Simulation waveform after the layout and wiring of block-type write strategy in CD-R preheat mode

Figure 12 shows the simulation waveform after the layout and wiring of the CD-R preheating method with block-type write strategy.

4.1.2. Pulse Mode

- (1) Top-level structure of the FPGA-designed pulse-type write strategy

The top-level structure of the pulse-based write policy designed by FPGA is shown in Figure 13.

- (2) Simulation waveform after layout wiring of DVD-R preheat method with pulse-type write strategy

Figure 14 shows the simulation waveform after the layout and wiring of DVD-R preheat method with pulse-type write strategy.

4.2. Automatic Laser Power Control Subsystem FPGA Design and Verification. Figure 15 shows the simulation waveform of the automatic laser power control subsystem after layout and wiring.

5. Conclusion

With the rapid development of modern road traffic, the development of advanced information technology, electronic communication technology, automatic control technology, computer technology, sensor technology, and network technology, and their penetration in the field of road traffic, the storage and backup of massive traffic information have become an extremely important link in traffic transportation and management. The optical storage backup technology designed in this paper has the advantages of high recording density, large storage capacity, long service life, easy storage, low storage cost, and strong compatibility. It will replace the existing disk and tape storage backup technology and become the mainstream of traffic information storage backup in the future.

Data Availability

The data used to support the findings of this study are available from the corresponding author upon request.

Conflicts of Interest

The authors declare that they have no conflicts of interest.

References

- [1] H. Xu, X. Zhao, and K. Guan, *Theory and Application of Highway Toll Collection System*, Electronic Industry Press, Beijing, China, 2003.
- [2] W. Huang and R. Chen, *Introduction to Intelligent Transportation System (ITS)*, People's Traffic Publishing House, Nanchang, China, 1999.

Retraction

Retracted: Power Grid Intelligent Energy Dispatching Interactive System Based on Virtual Reality Technology

International Transactions on Electrical Energy Systems

Received 10 October 2023; Accepted 10 October 2023; Published 11 October 2023

Copyright © 2023 International Transactions on Electrical Energy Systems. This is an open access article distributed under the Creative Commons Attribution License, which permits unrestricted use, distribution, and reproduction in any medium, provided the original work is properly cited.

This article has been retracted by Hindawi following an investigation undertaken by the publisher [1]. This investigation has uncovered evidence of one or more of the following indicators of systematic manipulation of the publication process:

- (1) Discrepancies in scope
- (2) Discrepancies in the description of the research reported
- (3) Discrepancies between the availability of data and the research described
- (4) Inappropriate citations
- (5) Incoherent, meaningless and/or irrelevant content included in the article
- (6) Peer-review manipulation

The presence of these indicators undermines our confidence in the integrity of the article's content and we cannot, therefore, vouch for its reliability. Please note that this notice is intended solely to alert readers that the content of this article is unreliable. We have not investigated whether authors were aware of or involved in the systematic manipulation of the publication process.

Wiley and Hindawi regrets that the usual quality checks did not identify these issues before publication and have since put additional measures in place to safeguard research integrity.

We wish to credit our own Research Integrity and Research Publishing teams and anonymous and named external researchers and research integrity experts for contributing to this investigation.

The corresponding author, as the representative of all authors, has been given the opportunity to register their agreement or disagreement to this retraction. We have kept a record of any response received.

References

- [1] W. Hu, Y. Yang, B. Liu, S. Guo, and K. Zhang, "Power Grid Intelligent Energy Dispatching Interactive System Based on Virtual Reality Technology," *International Transactions on Electrical Energy Systems*, vol. 2022, Article ID 8008461, 8 pages, 2022.

Research Article

Power Grid Intelligent Energy Dispatching Interactive System Based on Virtual Reality Technology

Wenjian Hu ¹, Yang Yang ¹, Baoan Liu ¹, Siyan Guo ¹, and Kuizhong Zhang ²

¹State Grid Shijiazhuang Power Supply Company, Shijiazhuang 050200, Hebei, China

²Shijiazhuang Kelin Electric Co., Ltd., Shijiazhuang 050000, Hebei, China

Correspondence should be addressed to Kuizhong Zhang; 201903306@stu.ncwu.edu.cn

Received 22 June 2022; Revised 18 August 2022; Accepted 26 August 2022; Published 14 September 2022

Academic Editor: B. Madhavan

Copyright © 2022 Wenjian Hu et al. This is an open access article distributed under the Creative Commons Attribution License, which permits unrestricted use, distribution, and reproduction in any medium, provided the original work is properly cited.

Objective. In order to improve the intelligence of power grid energy dispatching, this study proposes an interactive system of power grid intelligent energy dispatch based on virtual reality technology. Through the introduction of the main functions of the intelligent energy dispatching visualization system and the analysis of the construction of software and hardware, as well as the application of the actual power energy dispatching real-time operation visualization system, the system is described in detail and applied. The application results show that since the application of the system, the accuracy rate of comprehensive intelligent early warning is 100%, the monthly availability rate is 100%, and the average processing time of single fault scanning is less than 2 s. **Conclusion.** The system has good application prospects and in-depth research value and provides technical support for the further development of the smart grid.

1. Introduction

In the 1990s, the marketization of power systems was developed by leaps and bounds, rapidly covering the world. With the rapid development of computer technology, the improvement of computing speed, and the efficient realization of modern computer perception technology, display ability, and drawing technology, visualization technology is also making continuous progress. Many experts and scholars have shifted their research focus to the application of visualization technology in power systems and tried to combine new computer technology with cognitive science, mine new algorithms, try new schemes, and develop a visualization platform for power system energy dispatching. From the initial single-line diagram, simple data, text, and tables are superimposed, and factors such as color, animation, time bar, geographical location, and split-screen display are gradually added. The graphics are also developed from two-dimensional to three-dimensional, forming a series of visual expressions corresponding to the power system [1]. Nowadays, with the arrival of the era of the smart grid and big data, as the core embodiment of the smart grid,

intelligent energy dispatching has gradually become an important research direction for scholars. In order to meet the needs of the smart grid, the intelligent energy dispatching system should have a more comprehensive and accurate data acquisition system, have a powerful intelligent security early warning function, and pay attention to the coordination of system security and economy in energy dispatching decision-making. When the system fails, it can quickly diagnose the fault and provide fault recovery decision-making. The visualization technology can be used to comprehensively and intuitively provide the real-time operation of the power grid to the dispatcher to assist him in judging the power grid situation, formulating the operation mode, dealing with emergencies, and so on. Visualization of intelligent energy dispatching of power systems is to use visualization technology to display various attributes of power system equipment and system operation status in the form of graphics or images after being processed by various advanced algorithms and technologies, so that system operators can understand the present system operation status more conveniently and clearly, so that their operation control measures can be more effective and targeted [2].

2. Literature Review

Zaghwan and others, based on the concept of intelligent machine dispatcher (AO) proposed by Dr. Dy-Liacco and combined with the actual situation of China's power grid energy dispatching operation, proposed and studied the data mining technology based on the power grid fine rules and automatically mined the fine power grid safe operation rules through the steps of subject definition, massive training sample generation, feature selection, and rule generation. The prototype system of AO is developed, the hardware design and software structure based on cluster computers are given; and the software functions and algorithms are introduced. The AO prototype system is tested and analyzed for a provincial power system [3]. Sang and others extended the concept of energy dispatching center, put forward the concept of modern energy control center, and focused on the transformation of control centers in informatization, automation, integration, and intelligence, including applying information theory to analyze the information flow of power systems, rebuilding the original appearance of real power systems, and improving the operating conditions of power systems. It integrates the data of the existing energy control center, establishes a data warehouse, and carries out data mining for the decision support of the control center. It realizes a higher level of automation for the routine operation of power systems and the operation of abnormal and accident handling. Through the above ways, the function of the control center has developed from a single focus on safety and stability to the coordination of safety and economy, from local control to global hierarchical control, from offline analysis to online analysis, from open-loop control to closed-loop control, and from online steady-state analysis to online transient analysis [4]. Rojas and others proposed an intelligent auxiliary decision support system for accident handling based on an expert system after discussing the intelligent fault diagnosis algorithm, the principle and implementation algorithm of fault recovery decision. The expert system realizes the information interaction with SCADA, EMS, and fault information systems by using the information integration technology and provides comprehensive fault recovery decisions, so that the dispatcher can quickly locate the fault and recover the power supply in the face of complex faults [5]. Liu and others put forward a power grid operation decision support system based on multiagent on the basis of analyzing the present situation of power system operation, designing the framework of the system, and describing the functions and decision-making process in detail [6]. Sun and others introduced multiagent technology into the power market technical support system, proposed the model and design scheme of a generalized power market technical support system based on multiagent, and discussed the key technologies of agent system development [7]. Chukkaluru and others introduced the structure of the decision support system (DSS) of the Ordos power grid and the functions of each module and described the decision-making process of the system. The system combines artificial intelligence technology such as expert systems with DSS, realizes the preliminary intelligence of power grid

dispatching systems, and can assist dispatchers to make more reasonable dispatching decisions. The intelligent energy dispatching decision support system is composed of five parts: database, model base, knowledge base, functional module, and human-computer interaction. The data part is a database system. The model part includes the model base and its management system. The knowledge base part is composed of the knowledge base management system and the knowledge inference engine. The functional module is a variety of analysis applications based on EMS. The human-computer interaction part is used to accept and test users' requests and call the system's application software for decision-making services, so as to organically unify the model operation, data call, and knowledge reasoning [8].

3. Research Methods

3.1. Power Grid Intelligent Energy Dispatching System. The power grid intelligent energy dispatching system takes the power grid energy dispatching system as the object and realizes the intelligent exchange of information in all links of power grid energy dispatching through continuous research, development, and application of new power grid control technology, information technology, and management technology [9]. It is a technical system to improve the security production guarantee ability and decision-making ability of power grid dispatching; improve the sharing and optimal allocation ability of dispatching resources; improve the standardized lean and intelligent operation and management ability of power grid dispatching; and provide support and guarantee for the safe, high-quality, and economic operation of the power grid. The equation constraint condition of a power system means that the active power and reactive power of the system are kept in real-time balance, which is expressed by the following equation:

$$\begin{aligned} \sum_{i=1}^{i=n} P_{Gi} &= \sum_{j=1}^{j=m} P_{Lj} + \sum_{k=1}^{k=l} P_{sk}, \\ \sum_{i=1}^{i=n} Q_{Gi} &= \sum_{j=1}^{j=m} Q_{Lj} + \sum_{k=1}^{k=l} Q_{sk}, \end{aligned} \quad (1)$$

where P_{Gi} and Q_{Gi} are the active and reactive power from the first power source in the system; n is the number of power supply nodes; P_{Lj} and Q_{Lj} are the active and reactive power consumed by the first load in the system; m is the number of loads in the system; P_{sk} and Q_{sk} are the active and reactive power loss of the k power transmission and transformation equipment in the system; and l is the number of power transmission and transformation equipment in the system.

At present, the development trend of large-scale and complex power grids highlights the problems of power grid security and economic operation, and the research and development of power grid intelligent energy dispatching systems has become the focus of attention [10]. From the existing research results, the research of power grid intelligent dispatching systems mainly focuses on three aspects: power grid state calculation (including prediction) method, decision-making system, and system platform construction.

3.2. Visualization Technology and Its Application in Power Grid Energy Dispatching. Visualization technology integrates many branches of computer technology, such as graphics, image processing, data management, network technology, and human-computer interface. It uses computer graphics and image processing technology to convert data into graphics or images for display on the screen, which is conducive to correctly understand the meaning of data or processes. In the present energy management system/power grid dispatcher training simulation system (EMS/DTS), in addition to a small amount of data visualization, more power system operation data are displayed in real time on the power flowchart [11]. Although the digital information display is very accurate, for a large power grid, to monitor all the information of the whole power grid in real time, the digital display alone is undoubtedly monotonous, complex, and extremely lack intuition. These data do not contain the high-level abstract information required by the dispatcher, such as global centralized representation, and the relationship between these data is not clear, and the data representation lag behind.

To sum up, simple methods such as data text display to monitor and analyze the power grid can no longer meet the needs of power grid development. There is an urgent need for some methods and tools that can comprehensively and intuitively monitor the real-time operation of the power grid, highlight the data that are critical to the operation of the power grid, identify the weak links of the system through analysis and calculation, and effectively manage and process various types of information in the power system [12]. The appearance of visualization technology provides a solution to these requirements of modern power grid operation.

3.3. Design and Implementation of the Power Grid Intelligent Energy Dispatching Visualization System

3.3.1. General Design Ideas and Principles. The existing safety monitoring and data acquisition/energy management system (SCADA/EMS) has mature theoretical basis and application experience. While learning from and inheriting its essence, it integrates many new technologies. It is necessary to put forward design ideas and principles different from the traditional ones. The main problems faced are as follows: in real-time operation systems, the interaction between the dispatcher (person) and the automation system; massive data extraction and its utility display; the validity of knowledge models and display platforms that do not completely depend on mathematical models, such as data mining methods, in the application of giant systems; and integration and opening of multisource data (real-time and historical, static, and dynamic) in many systems such as production and management [13]. In view of the above problems, this paper introduces the latest achievements in the design and research of dispatcher and automation systems and puts forward the design idea of a power grid intelligent energy dispatching visualization system with dispatcher thinking mode as the framework, visual interface as the functional model, and interactive computing as the core of the system.

The visualization system first proposes four stages of a complex man-machine system task in terms of ideas and principles: obtaining information → analysis and display → decision-making action → execution action, as shown in Figure 1.

- (1) The system inherits the effective practical experience of the original SCADA/EMS
- (2) The system effectively adopts the dispatcher's thinking mode in the actual scheduling. It can show the workflow in the order of scheduling principles and can work according to the dispatcher's intuition.
- (3) The visual interface shall be closely combined with functions to display the visually sensitive interface that the dispatcher thinks, wants to see, and operates, so as to deepen the understanding of the system's situation and solutions
- (4) The system framework is an open system, and subsequent functions can be inserted at will. The core algorithm of the system is an online algorithm with interaction and sequence coordination, which can adopt pure mathematical model algorithms, data mining algorithms, artificial intelligence algorithms, and so on.

The characteristics of the visualization system are as follows:

In the visualization system, a series of visualization interfaces and corresponding functions are designed, multiple real-time algorithms suitable for interactive computing are proposed, and the display technology of multidata source fusion is explored (Figure 2). The operation practice shows that the system performance indicators fully meet the real-time operation requirements of power grid energy dispatching, and a new way is explored for the application of the next generation SCADA/EMS.

3.3.2. Introduction to Main Functions. The visualization system is displayed in three layers according to the power grid operation status.

- (1) The first layer shows the overall operation status of the power grid, which is the most concerned by the operators. Under normal circumstances, only a small amount of information is displayed on the visualization interface of the visualization system. However, once the visualization system enters the early warning state, it will immediately give an alarm through a very intuitive graphical interface and use a variety of means to represent different alarm levels, such as through the change of color (light color indicates low-level alarm and the darker the color, the higher the alarm level) and through the change of color and size of the percentage pie [14]. The alarm level can be set through the configuration attribute of the visualization system.
- (2) The second layer shows the macrodata analysis results of problems or aspects concerned by operators. Under normal conditions, the visualization system

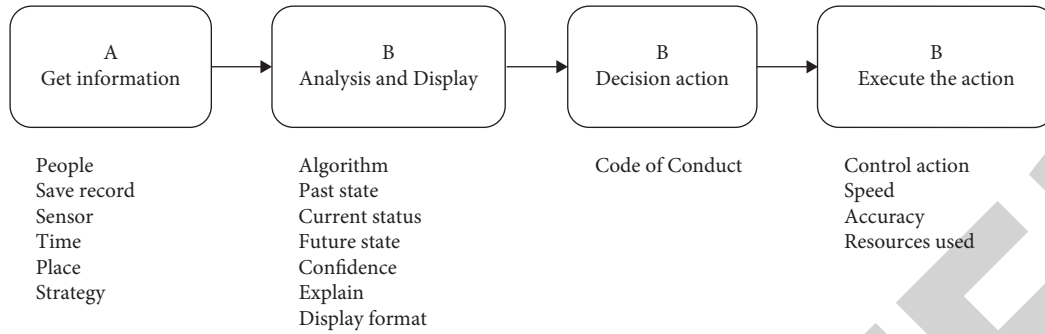


FIGURE 1: Four phases of complex man-machine system tasks.

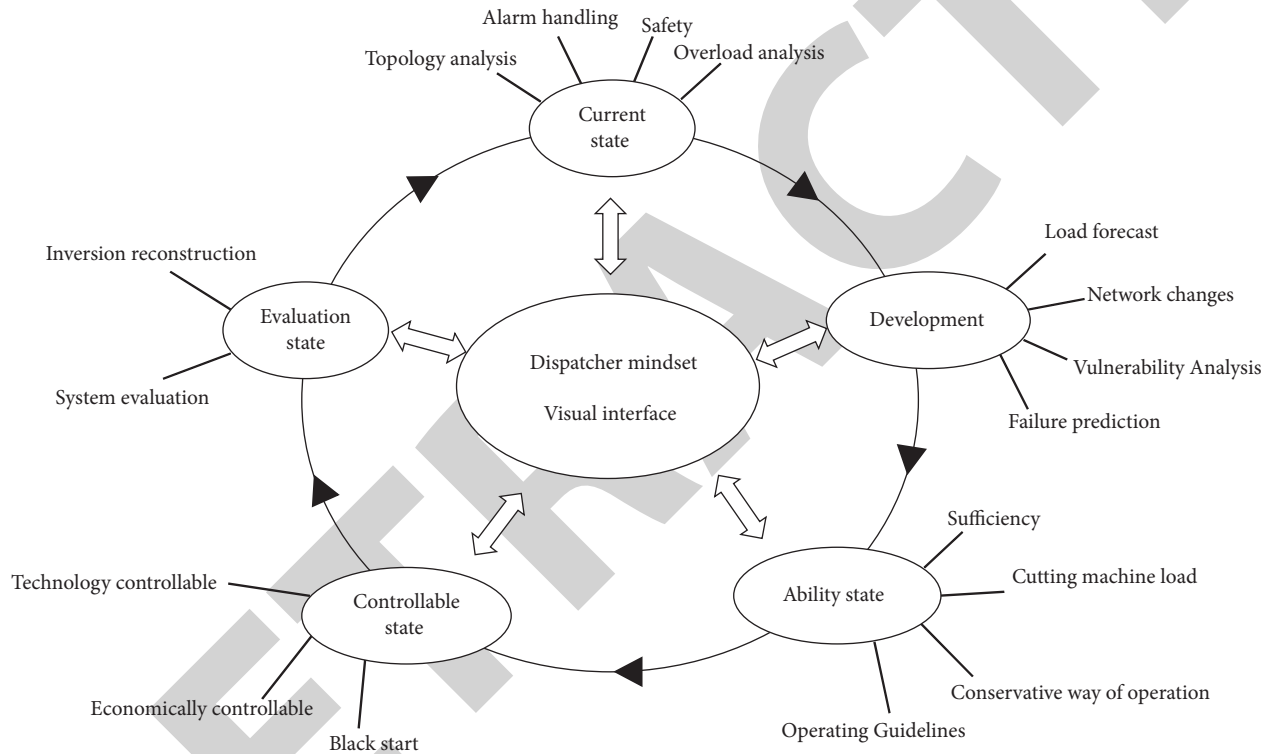


FIGURE 2: Display technology of multidata source fusion.

- can monitor the tidal current of one or more specific sections with a three-dimensional column diagram. If the power grid is in a normal safe state, the distance from the power grid to the unsafe state shall be displayed graphically. If it is in an abnormal operation state, it gives suggestions and countermeasures to remove the unsafe state. At the same time, the system “disconnection” accident is scanned and analyzed in real-time every 5 min, and the indicators of each fault’s severity are given in graphical form.
- (3) The third layer shows the specific value of the quantity of interest. The visualization system can display the monitoring data of all devices.

The visualization system realizes the following functions:

- (1) Realize the collection of real-time data of power grid and use dynamic display and two-dimensional images to visually express the real-time information of power grid lines, node voltages, and generator active and reactive power [15,16]. It mainly includes the contour of node voltage, load pie chart of line, contour of line load, dynamic generator, and dynamic power flow.
- (2) The dynamic three-dimensional images are used to visually express the real-time information of active and reactive power reserves, such as reactive power reserve, transformer temperature monitoring,

- transformer reserve, and three-dimensional rotation
- (3) The sensitivity calculation and three-dimensional sequencing display of power grid lines to generators, loads, and node voltages to reactive power equipment are realized
 - (4) Web publishing of visual graphics: integrate the visual display function, transmit data through a special isolation device, publish the web on the network, and realize cross-platform data sharing.
 - (5) Visual playback, replay, and evaluation of historical data: The visualization system has the ability to accident recall and can playback and replay historical data. Different from the general SCADA/EMS, the visual system replay is to replay the graph and data at the same time on the historical network topology, use the historical data to track the power grid loss statistics, conduct comparative analysis according to the cycle, provide optimization strategies, and visually display the real-time and historical indicators.
 - (6) Visual display of precontrol scheme depending on sensitivity [17]: Sensitivity is actually a quantity used to describe the linear relationship between the variables of the power flow equation. It can analyze how many changes will occur to other variables when some variables change.
 - (7) Visual monitoring of low-frequency oscillation mode dynamic threshold of key lines: According to the data of synchronous phasor measurement unit (PMU), real-time data detect the low-frequency oscillation of the system, calculate the oscillation frequency and amplitude of the detected line, and dynamically display them on the single-line diagram and geographical wiring diagram. If low-frequency oscillation is detected, the corresponding lines on the single-line diagram and geographical wiring diagram will be displayed in the form of an oscillation curve, and flashing, color change, sound, and others will be used for limit violation warning. Under normal conditions without low-frequency oscillation, the single-line diagram and geographic wiring diagram are displayed in the normal display mode [18]. When you want to care about the details of low-frequency oscillation of a certain line, you can locally track and amplify the details of line oscillation, so as to provide timely and visual warnings for preventing the occurrence of such faults.
 - (8) Visualization of prewarning of total power flow of any section: The system provides a display of the total power of any section combination of the line, and the results are represented by a histogram. This function greatly reduces the work intensity of dispatchers and provides powerful technical support for dispatchers to quickly and accurately evaluate the running state of the system.
 - (9) The index system of power grid operation in real-time state and the visual expression of power grid static vulnerability by virtual instrument: The real-time data transmitted by SCADA/EMS are used to classify the operating conditions of power generation systems, transmission systems, loads, and reactive power devices, and then, the weights of safety, critical state, and insecurity are determined according to their attributes. The fuzzy clustering method is used to objectively evaluate the safe operating state of the whole system, and the virtual instrument is used to display it.
 - (10) Visualization of “” fault early warning assessment of the power grid. The power grid operation situation changes the assessment brought by the “power grid.” The assessment is used to quickly sort the “power grid” faults, formulate the sorting indicators, and use the classification rules to express the nonconvergence and controllable conditions in three dimensions. Online “” analysis provides dispatchers with advanced analysis of possible faults, which is helpful for judgment and decision-making in the case of real faults.
 - (11) Visualization of intelligent energy dispatching of power grid reservoir and power generation capacity maximization: By collecting data such as generation curve, water consumption curve, and minimum water level limit of hydropower units and corresponding reservoirs, the maximum operation time of hydropower units according to the maximum, minimum, average, or user-defined generation output is calculated in real-time, and the corresponding time of hydropower unit output is expressed visually, so as to facilitate the dispatcher to fully grasp the hydropower generation capacity of the power grid.

3.4. System Application. In order to illustrate and demonstrate the specific functions and advantages of the power grid intelligent energy dispatching visualization system, the following takes the application of this system in the actual power grid energy dispatching system as an example.

3.4.1. Software Architecture. According to the previous introduction of the system functions, the software system of the corresponding visualization system for power grid intelligent energy dispatching is shown in Figure 3.

In Figure 3, CIM is the computer centralized management system, SVG is the scalable vector graphics, and DMIS is the spatial measurement interface standard.

3.4.2. Hardware Architecture. Figure 4 shows the hardware system of the power grid intelligent energy dispatching visualization system.

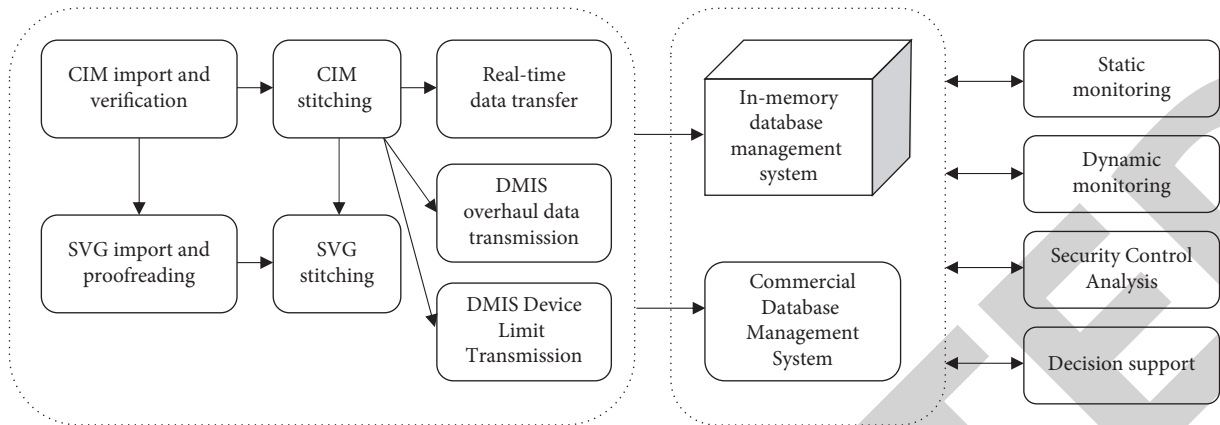


FIGURE 3: Schematic diagram of the power grid intelligent energy dispatching visualization system software system.

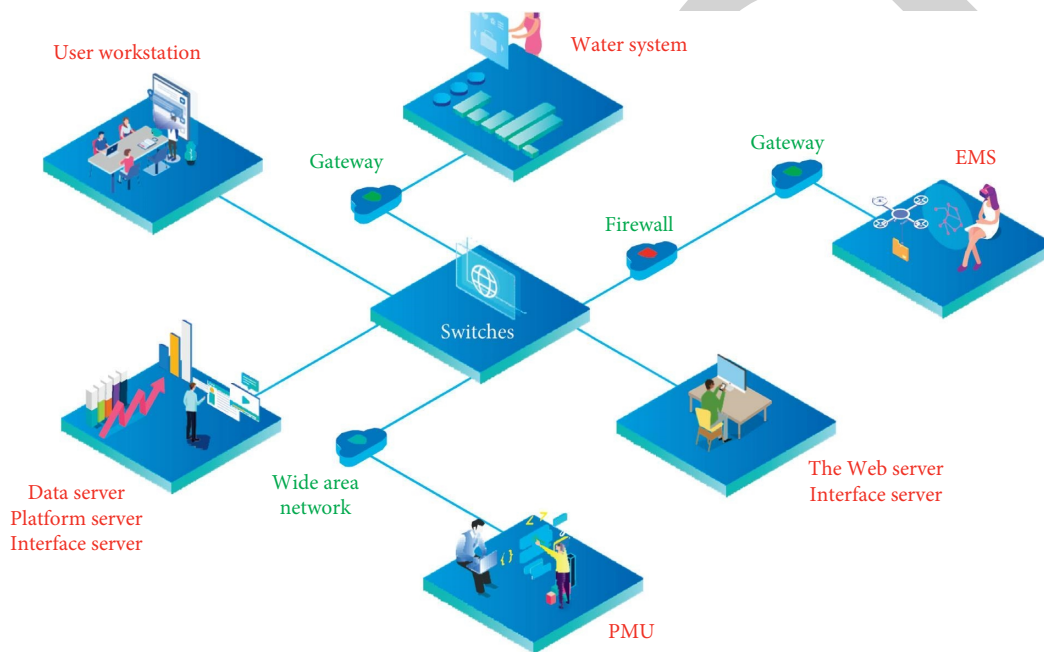


FIGURE 4: Hardware system diagram of the power grid intelligent energy dispatching visualization system.

3.4.3. *Design Route of Interactive Calculation.* The power grid intelligent energy dispatching visualization system takes the dispatcher's thoughts as the core in the design route and organically combines the power grid operation sequence, dispatcher's experience, and power system analysis functions. The visualization interface provides a platform for data display, function expression, and interactive calculation. Interactive calculation organically adds the human role to a closed-loop control system [19, 20]. This kind of interactive computing integrates the dispatcher's perception and experience and can conduct real-time computing and make corresponding verification through the interactive computing window.

3.4.4. *Characteristics of Visual Technology Support Platform.* In order to display SCADA data and EMS analysis results, there must be a strong technical support platform [21]. In

addition to the functions of the existing energy dispatching automation system, the platform also develops an intelligent support environment based on the graphical interface and adopts the open and standardized concepts supported by the computer system. It has the following characteristics:

- (1) The supporting platform emphasizes ease of use and intelligence
- (2) The implementation technology adopts the object-oriented design idea
- (3) The development of the supporting platform is carried out at different levels, that is, from the bottom hardware, operating systems, distributed database to the upper communication service, data service, application programming interface, and user interface, the platform is organized at multiple levels [22].

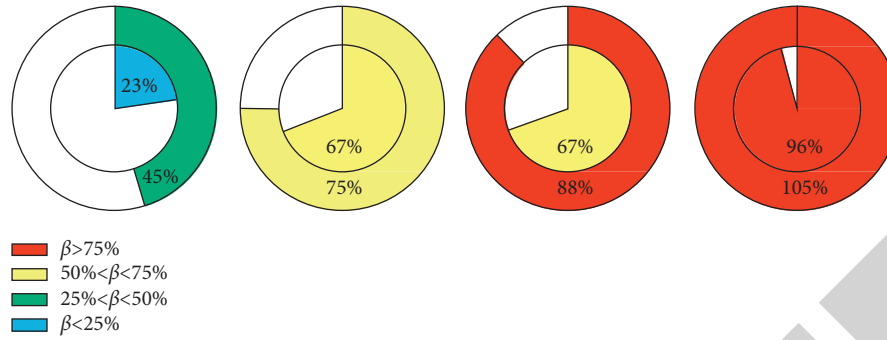


FIGURE 5: Visual diagram of the line load rate comparison.

3.4.5. Display Mode of the Power Grid Intelligent Energy Dispatching Visualization System

- (1) Dynamic display and two-dimensional images are used to visualize the real-time information of power grid lines, node voltages, and generator active and reactive power. Dynamic three-dimensional images are used to visualize the real-time information of active and reactive power reserve.
- (2) The sensitivity calculation and three-dimensional sequencing display of power grid lines to generators, loads, and node voltages to reactive power equipment are realized
- (3) Visual playback, replay, and evaluation of historical data
- (4) Visual monitoring of low-frequency oscillation mode dynamic threshold of key lines
- (5) Visualization of power flow total sum early warning of any section and "" fault early warning evaluation of the power grid
- (6) The index system of a power grid operation in real-time state and the visual expression of a power grid static vulnerability by virtual instrument

4. Result Analysis

In order to better serve the regulation and control joint duty mode under the large-scale operation system, the regulation and control center of a power supply company has set up a set of visual early warning system workstations in the energy dispatching work area and the monitoring work area [23]. As shown in Figure 5, concentric circles are used in this paper to show the comparison of line load rate before and after layout. The inner circle represents the scheme after layout, and the colored sector represents its line load rate (that is, the percentage of line load value in the rated value). The outer circle represents the scheme before layout, and the colored arc filler strip represents the line load rate. The arc-shaped filler strip extends clockwise from the top of the centerline. When the load rate is between 0 and 25%, the sector is blue, 25%–50% green, 50%–75% yellow, 75%–100% red, and more than 100% red with flashing. The larger the load rate, the larger the relative radius of the circle.

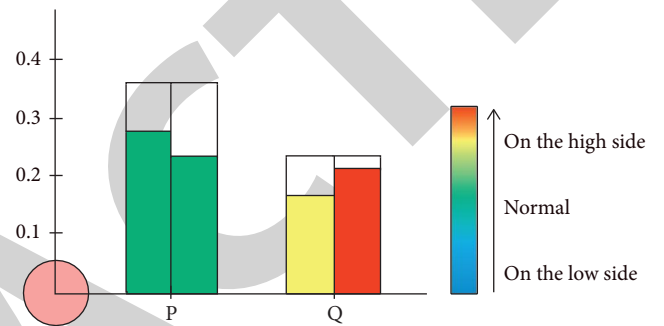


FIGURE 6: Visual diagram of comparison between the active power output and reactive power output.

As shown in Figure 6, the double bar graph is used in this study to represent the active output and reactive force of nodes before and after the layout. The left half of the double bar graph represents the scheme after the layout, and the right half represents the scheme before the layout. The white column is the historical maximum value and the current value of the colored column position. If the current value is within the normal range of the historical mean value, fill the green column. If the current value is greater than the historical mean value, fill the warm color system according to the degree of deviation. If it is less than the historical mean value, fill the cold color system according to the degree of deviation. The wide range of values can be set by experience.

The application of the system not only greatly improves the ability of the regulator to monitor the operation of the power grid and helps the regulator to effectively master the overall operation status of the power grid but also improves the safety production level of the power grid with significant social and economic benefits [24].

5. Conclusion

Power grid energy dispatching is the core content of power grid operation. Under the power grid development trend of building a strong smart grid, it is inevitable to research and develop intelligent energy dispatching systems, and visualization technology, as the key technology under the intelligent system, has become the research focus. This study analyzes the overall design idea, principles, and software and hardware system composition of the power grid intelligent

Retraction

Retracted: Improved VMD-+ACO Algorithm Navigation and Positioning Technology for Robot Electric Power Inspection

International Transactions on Electrical Energy Systems

Received 19 September 2023; Accepted 19 September 2023; Published 20 September 2023

Copyright © 2023 International Transactions on Electrical Energy Systems. This is an open access article distributed under the Creative Commons Attribution License, which permits unrestricted use, distribution, and reproduction in any medium, provided the original work is properly cited.

This article has been retracted by Hindawi following an investigation undertaken by the publisher [1]. This investigation has uncovered evidence of one or more of the following indicators of systematic manipulation of the publication process:

- (1) Discrepancies in scope
- (2) Discrepancies in the description of the research reported
- (3) Discrepancies between the availability of data and the research described
- (4) Inappropriate citations
- (5) Incoherent, meaningless and/or irrelevant content included in the article
- (6) Peer-review manipulation

The presence of these indicators undermines our confidence in the integrity of the article's content and we cannot, therefore, vouch for its reliability. Please note that this notice is intended solely to alert readers that the content of this article is unreliable. We have not investigated whether authors were aware of or involved in the systematic manipulation of the publication process.

Wiley and Hindawi regrets that the usual quality checks did not identify these issues before publication and have since put additional measures in place to safeguard research integrity.

We wish to credit our own Research Integrity and Research Publishing teams and anonymous and named external researchers and research integrity experts for contributing to this investigation.

The corresponding author, as the representative of all authors, has been given the opportunity to register their agreement or disagreement to this retraction. We have kept a record of any response received.

References

- [1] Y. Long, M. Du, X. Luo, S. Li, and X. Jiang, "Improved VMD-+ACO Algorithm Navigation and Positioning Technology for Robot Electric Power Inspection," *International Transactions on Electrical Energy Systems*, vol. 2022, Article ID 5467622, 6 pages, 2022.

Research Article

Improved VMD-+ACO Algorithm Navigation and Positioning Technology for Robot Electric Power Inspection

Yingkai Long ¹, Mingming Du ², Xiaoxiao Luo ¹, Siquan Li ¹ and Xiping Jiang ¹

¹State Grid Chongqing Electric Power Research Institute, Chongqing 401121, China

²State Grid Chongqing Electric Power Company, Chongqing 400013, China

Correspondence should be addressed to Yingkai Long; 201804202@stu.ncwu.edu.cn

Received 8 July 2022; Revised 17 August 2022; Accepted 24 August 2022; Published 12 September 2022

Academic Editor: Nagamalai Vasimalai

Copyright © 2022 Yingkai Long et al. This is an open access article distributed under the Creative Commons Attribution License, which permits unrestricted use, distribution, and reproduction in any medium, provided the original work is properly cited.

In order to meet the navigation and positioning requirements of force inspection robot, a new technology based on improved VMD- + ACO algorithm is proposed. The main content of this technology is based on the research of improved VMD algorithm and ACO algorithm, through the comparison of VMD algorithm and improved VMD algorithm. By using ACO parameter optimization design and so on, the research means of improving VMD- + ACO algorithm navigation and positioning technology of electric inspection robot is finally established through experiments and analysis. The experiment result shows the following. The minimum iteration number of the improved ACO is 112, which is 24.32% less than that of the basic ACO. The mean value of the worst value and the optimal value of the function are equal to 0. It shows that the improved ACO has higher convergence precision and the number of iterations is significantly reduced. *Conclusion.* Based on the improved VMD- + ACO algorithm, it can meet the navigation and positioning requirements of electric inspection robot.

1. Introduction

Power inspection robot is a regular or random inspection in the production and operation of products, aiming to find quality problems or operation faults of equipment in time [1]. At present, the traditional navigation solutions of inspection robot at home and abroad have certain limitations. Magnetic track and RFID tag schemes need to be embedded, which causes great damage to the ground and has high maintenance costs. GNSS schemes are easy to lose satellite signals in scenes with lots of occlusion and cannot be used indoors. The navigation errors of inertial navigation and encoder schemes will accumulate, and there will be a large error when used for a long time [2]. The visual scheme has high requirements for light and is sensitive to shadow, resulting in poor outdoor application effect.

At present, all inspection machines in substation field operation adopt the navigation and positioning mode of magnetic track guidance and RFID positioning, which requires embedding magnetic track on the running route of

robot in advance and embedding RFID tags on the location where the robot needs to dock [3].

During the operation of the robot, the magnetic sensor array on the robot detects the deviation of the robot's motion center relative to the magnetic track and controls the difference between the left and right wheels through the motion controller, so that the robot can run along the set route. When the RFID card reader detects the label buried in the path, it notifies the robot to arrive at the set position. At this time, the robot can complete the detection of parking steering acceleration and deceleration equipment under the control of the car computer. Although this method has the characteristics of high repeatability of navigation and positioning and strong anti-interference ability, it also faces some problems in practice. For example, when magnetic track is laid, the ground construction is complicated and the workload is large, the robot running route is inflexible, and the height of the robot crossing the barrier is limited by the detection distance of the magnetic sensor, etc. These problems are difficult to solve under the existing methods [4].

2. Literature Review

In the current social development, electric power inspection robot is a kind of wheeled mobile robot. It can inspect outdoor high-voltage equipment in unattended or less attended substations by autonomous or remote control, collect operating status information of power equipment, timely find thermal defects, foreign body suspension, and other equipment anomalies of power equipment, and ensure the safety of power production. In terms of navigation mode, electric power inspection robot generally adopts magnetic track navigation. The magnetic sensor array installed in the front of the robot detects the deviation of the robot relative to the magnetic track and controls the robot to run along the magnetic track by means of two-wheel differential [5]. In practice, it is found that although the navigation method has centimeter-level navigation positioning accuracy, good repeatability, and strong anti-interference ability, the short detection distance of magnetic sensor results in the low chassis of the robot, and the obstacle crossing ability is not strong. In addition, the magnetic track navigation mode cannot feed back the precise position of the robot in the substation in real time, which is not conducive to the remote monitoring of the robot operation. At present, in addition to magnetic trajectory navigation, there are also inertial navigation, laser navigation, GPS navigation, and vision navigation for mobile robots. In view of the deficiency of magnetic trajectory navigation mode, considering that the inertial navigation positioning data are obtained by integral accumulation, the navigation accuracy will decrease with the passage of time, which is not suitable for long-term accurate positioning. At the same time, the outdoor environment has adverse effects on laser and visual navigation, while GPS navigation can directly learn the absolute position coordinates of the current measurement point from the GPS receiver, and its dynamic positioning accuracy can be up to centimeter level, and there is no error accumulation, so the coordinates of any position in the substation can be accurately obtained theoretically [6].

To solve the above problems, this paper proposes navigation and positioning technology analysis and research of electric inspection robot based on improved VMD- + ACO algorithm [7, 8].

3. Research Technique

3.1. Research on Improved VMD Algorithm

3.1.1. VMD Algorithm Research. VMD is a completely non-recursive decomposition algorithm; by constructing and solving the constrained variational problem, the signal is decomposed into K centre frequencies with $\{\omega\}$ center frequency. Compared with EMD algorithm, VMD algorithm has more strict mathematical model, overcomes the defects of EMD algorithm, can effectively separate intensive modes, and has been widely used in signal analysis, fault diagnosis, time series prediction, and other fields [9]. However, the selection of decomposition parameters of VMD, such as decomposition layers K and penalty factor α , has a great

influence on the decomposition effect, and there is no clear theoretical guidance for its value.

The VMD computational complexity of the algorithm mainly depends on the iteration of the center frequency of each component and the equivalent FFT (fast Fourier transform) process, and the computational complexity of single FFT is $O(N \lg N)$. N refers to the length or sampling points of the analysis signal. Therefore, the computational complexity of decomposing a signal of length N into K components using VMD algorithm can be simply considered as the sum of the iterative consumption of the center frequency of all components and $K O(N \lg N)$ [10]. The computational complexity of EMD has been proved to be the same as FFT, both $O(N \lg N)$, which is an efficient decomposition algorithm. Therefore, VMD algorithm overcomes the inherent defects of EMD while sacrificing computational efficiency.

In addition, different from the adaptive decomposition of EMD, VMD is a completely non-recursive decomposition algorithm, whose decomposition effect is affected by the number of decomposition layers K and the value of penalty factor α [11]. If the number of decomposition layers is too much, the larger the penalty factor is, the narrower the bandwidth of the target signal will be, resulting in the redundant mode with multiple signal components belonging to the same main mode. On the contrary, if the bandwidth is too wide, the target signal will carry more noise and even contain other modal components. Too wide or too narrow bandwidth of the target signal will reduce the decomposition performance and affect the subsequent analysis results. At present, there is no clear theoretical basis for the value of decomposition parameters, which is very subjective and random.

3.1.2. Research on Improved VMD Algorithm. In order to solve the problem of VMD parameter selection, scholars at home and abroad constructed evaluation function based on envelope entropy orthogonal coefficient correlation coefficient and other parameters and used intelligent optimization algorithm to search the optimal value of decomposition layer K and penalty factor α simultaneously. Some achievements have been made in fault diagnosis and other fields. However, due to the limitation of the calculation efficiency of VMD algorithm, the optimization efficiency of large-scale hyperplane parameters is low, and the two-parameter or even multi-parameter optimization of VMD decomposition parameters will consume a lot of computing resources. The existing evaluation function of single index is not suitable for modal decomposition of vibration signals. Therefore, a new VMD optimization algorithm is proposed in this paper. The values of K and α are optimized separately, and the initialization process of the center frequency is optimized, so as to improve the efficiency of parameter optimization and give full play to the decomposition performance of VMD [12].

In the process of modal parameter identification, the accuracy of frequency identification is higher than that of damping, and even in most cases, the frequency range can be accurately estimated and the number of main modes can be judged according to the results of signal spectrum analysis

[13]. The goal of the VMD algorithm is to decompose the signal into K AM/FM signals with central frequency $\{\omega K\}$, which is essentially a narrowband filter bank with the center frequency of $\{\omega K\}$. Therefore, a simple peak method is used in this paper to determine the main modal number M and its corresponding central frequency $\{f_i, i = 1, 2, \dots, M\}$ in advance. The decomposition parameter K is assigned as $K = M$, so the original multi-parameter optimization problem is simplified to the single-parameter optimization of penalty factor α , and the ADMM convergence process is accelerated to improve the calculation efficiency of VMD.

For the single-parameter optimization of penalty factor α , the evaluation function is established first, and the value of α is modified based on the posterior information of VMD decomposition results. However, because there is no clear functional relationship between α and the signal component finally decomposed, the analytic solution of the optimal value of α cannot be obtained directly by the established evaluation function. In addition, if traditional optimization methods (such as Newton method, simplex method, and so on) are adopted, the whole search space needs to be traversed, and VMD calculation efficiency is limited, so the search cannot be completed in a short time [14]. Therefore, intelligent optimization algorithms (such as genetic algorithm and particle swarm optimization algorithm) are also used in this paper to search for the optimal value of penalty factor α in the hyperplane.

The evaluation function established in this paper can accurately reflect the characteristic that each decomposed signal component contains only a single vibration mode and has no false component and redundant mode in the ideal state. The existing evaluation function of single index, such as envelop entropy orthogonal coefficient correlation, can represent the sparsity of signal. However, in the practical application process, negative optimization is easy to occur, which leads to the situation that the value of α is too large, and a group of harmonic signal components is decomposed [15]. This is due to the narrowband filtering characteristics of VMD. The larger the penalty factor α value is, the smaller the bandwidth of the signal component is, and finally the signal degenerates into a harmonic signal. Compared with the real target signal component, the harmonic signal component can get higher evaluation in the evaluation function of the above single index, resulting in the situation of negative optimization. However, this kind of harmonic signal is a false component, which only accounts for a very small part of the energy of the original signal. In order to facilitate the solution of the optimization algorithm, the following formula is used:

$$\text{fitness} = \left(1 - \sum_{k=1}^K \frac{u_k^2}{x^2}\right) (1 - \min\{r(u_k, x)\}) \in (0, 1). \quad (1)$$

The essence of the optimization objective is to avoid false components or redundant modes, and the decomposed signal component has a large energy proportion and maintains a high correlation with the original signal [16]. Given the fitness function, the specific optimization algorithm adopted for solving the problem has little influence on

the final optimization result, and the specific process of parameter optimization within the scope discussed in this paper is not shown in Figure 1.

3.2. Research on Improved ACO Algorithm

3.2.1. Basic ACO Principle and Mathematical Model Analysis. The ACO mathematical model is as follows: $G = (C, L)$ is a directed graph, $C = \{C_1, C_2, \dots, C_n\}$ is a collection of N cities, $L = \{l_{ij} | c_i, c_j \in C\}$ is a collection of two connected cities, that is, two connected paths between cities, and d_{ij} ($i, j = 1, \dots, n$) is the distance of l_{ij} .

Ant k ($k = 1, 2, \dots, m$) is in the process of foraging; according to the probability selection formula, the following formula selects the next city.

$$\eta_{ij}(t) = \frac{1}{d_{ij}}. \quad (2)$$

The pheromone intensity Q represents the total amount of pheromones retained on the path after one cycle that affect ACO positive feedback function. ACO searches for the global optimal solution under the action of positive feedback. When Q is too large, the higher the total number of pheromones on the path is, the higher the probability that the searched path will be selected again, which will lead to the reduction of ant search range and global search ability, and ACO is prone to fall into the insufficient phenomenon of local optimal. If Q is too small, ants may enter into random path selection, which will cause ACO to fall into disordered disorder and ACO is prone to slow convergence [17].

To sum up, improper parameter setting and pheromone update lag are the reasons why basic ACO is prone to low convergence accuracy and slow convergence speed and fall into local optimal deficiency [18].

3.2.2. ACO Optimizing Design of Parameter. Improper setting of parameters such as pheromone heuristic factor α and expectation heuristic factor β leads to low convergence accuracy and slow convergence speed of basic ACO. The ACO parameter optimization design was carried out by combining the Python model and Matlab simulation calculation. Among them, TSP case base (ISPLIB) adopted Eil51 as the test library and designed variable expressions, as shown in the following formula:

$$\begin{aligned} X &= [x_1, x_2, x_3, x_4, x_5], \\ E &= \left\{ \begin{array}{l} x | x_j^i \leq x_i \leq x_j^j \\ i = 1, 2, 3, 4, 5, \\ j = 1, 2, 3, 4, 5 \end{array} \right\}. \end{aligned} \quad (3)$$

The following parameters are optimized: the design variable of N_c and L , coefficient x_1 of the relationship between the number of ants and the number of cities, pheromone heuristic factor x_2 , the expected heuristic factor x_3 , pheromone volatilization coefficient x_4 , pheromone intensity x_5 . The curves of change relationship are shown in Figures 2–5, respectively.

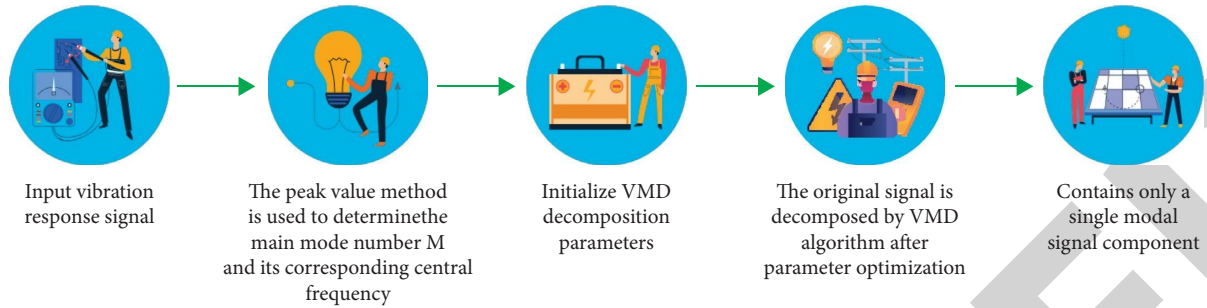


FIGURE 1: Flowchart of improved VMD algorithm.

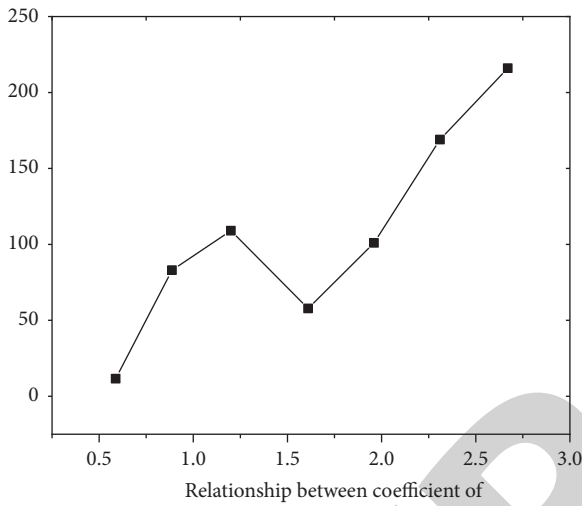


FIGURE 2: Variable ant quantity and city quantity relationship coefficient change curve.

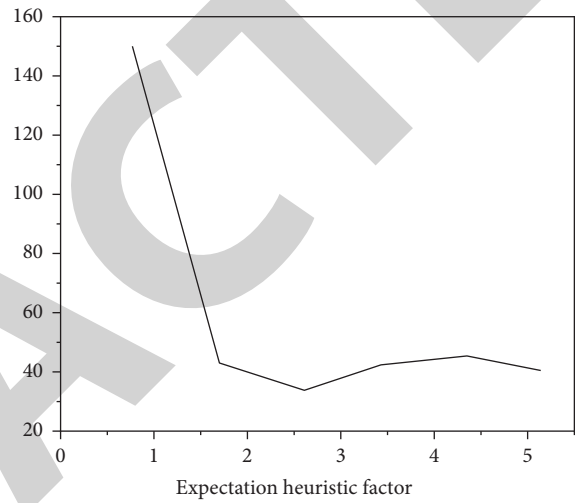


FIGURE 4: The expected heuristic factor change curve.

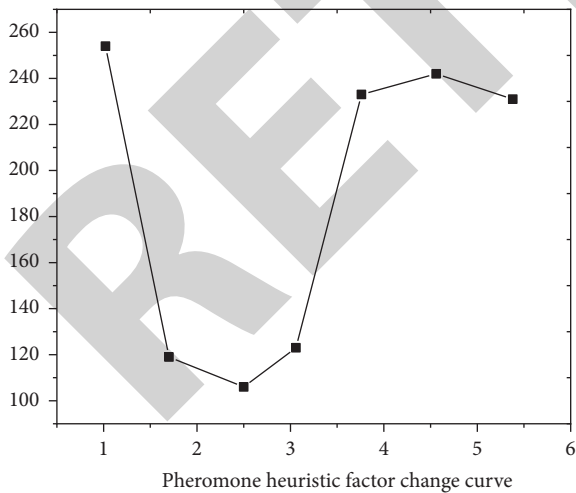


FIGURE 3: Graph of pheromone heuristic factor variation.

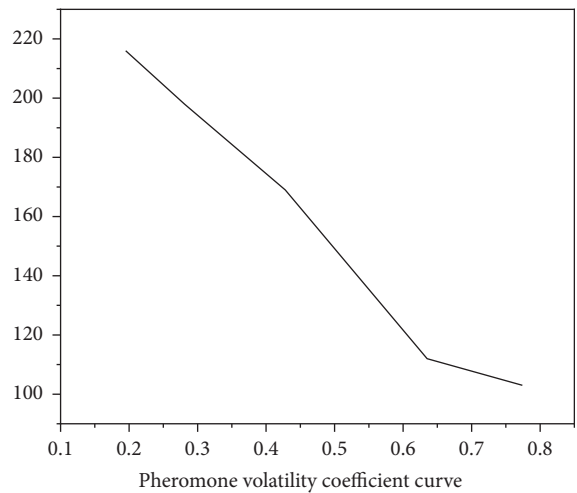


FIGURE 5: Pheromone volatilization coefficient curve.

Analysis shows that when x_1 (0.1 ~ 1.5) is set, N_C presents a downward quadratic function change trend with the increase of x_1 , and L presents a decreasing trend. When x_1 (1.5 ~ 3.0), with the increase of x_1 , N_C presents a first-order function increasing trend, and L is without significant change. Therefore, when x_1 is 1.5, N_C and L obtain the

optimal values. When x_2 is (0.0 ~ 1.0), with the increase of x_2 , N_C and L represent decreasing trend. When x_2 is (1.0 ~ 3.0), with the increase of x_2 , N_C and L have no significant change. When x_2 is (3.0 ~ 6.0), N_C represents decreasing trend, and L represents increasing trend first and then has no significant change. Therefore, when [1.0 ~ 3.0]

TABLE 1: Maximum relative error and average relative error of the two methods.

Function	Algorithm	Optimal value	Worst-case value	Mean value	Minimum number of passes
F1 (x)	Basic ACO	0.15	0.96	0.58	148
	Improved ACO	0	0	0	112
F2 (x)	Basic ACO	0.07	0.59	0.26	139
	Improved ACO	0	0	0	101

is set, both N_C and L obtain the optimal value. When x_3 is (1.0 ~ 2.0), with the increase of x_3 , N_C and L represent increasing trend. When x_3 is (2.04,0), with the increase of x_3 , N_C and L have no significant change. When x_3 is (4.0 ~ 6.0), with the increase of x_3 , N_C has no significant change, and L represents increasing trend. Therefore, when x_3 is [2.0, 4.0], N_C and L obtain the best value. When x_4 is (0.0 ~ 0.9), with the increase of x_4 , N_C and L represent decreasing trend. When x_4 is (0.5 ~ 0.7), with the increase of x_4 , N_C and L approach two parallel lines. Therefore, when x_4 is [0.5, 0.7], N_C and L obtain the best value. When x_5 is (10 ~ 1000), with the increase of x_5 , N_C and L have no significant change. When x_5 is (10009000), with the increase of x_5 , N_C represents decreasing trend, and L represents increasing trend. Therefore, when x_5 is [10, 1000], N_C and L obtain the best value.

4. Interpretation of Result

In order to verify ACO performance, two multi-peak test functions with certain searching ability, Griewank function and Ackley function, were used to compare ACO and basic ACO, respectively, and the initial value range of variable dimension of the function was the theoretical optimal value [19].

The Griewank function and Ackley function of improved ACO and basic ACO were compared and analyzed for 10 performance test experiments, respectively, and the average value of 10 experiments was taken as the final result, as shown in Table 1 [20].

By analyzing the test results of Griewank function, the minimum iteration number of basic ACO is 148. The difference between the average value of 0.58 and the optimal value of 0.15 is 0.81 and 0.43, and the fluctuation errors are 540.00% and 286.67% compared with the optimal value. It shows that the convergence accuracy of basic ACO is not high. The minimum iteration number of improved ACO is 112, which is 24.32 less than that of basic. The mean value of the worst value and the optimal value of the function are both 0, indicating that the convergence accuracy of the improved ACO is higher and the number of iterations is significantly reduced [21, 22].

5. Conclusion

In order to meet the navigation and positioning requirements of force inspection robot, a new technology based on improved VMD- + ACO algorithm is proposed. The main content of this technology is based on the research of improved VMD algorithm and ACO algorithm, through the comparison of VMD algorithm and improved VMD algorithm. By using ACO parameter optimization design and so

on, the research of improving VMD- + ACO algorithm navigation and positioning technology of electric inspection robot is finally established through experiments and analysis. The evaluation function established in this paper can accurately reflect the characteristic that each decomposed signal component contains only a single vibration mode and has no false component and redundant mode in the ideal state. Through experiments, the convergence accuracy of improved ACO is higher, and the number of iterations is significantly reduced. Based on the improved VMD- + ACO algorithm, it can meet the navigation and positioning requirements of electric inspection robot.

Data Availability

The data used to support the findings of this study are available from the corresponding author upon request.

Conflicts of Interest

The authors declare that they have no conflicts of interest.

References

- [1] B. Ye and X. Song, "Research on an intelligent electric inspection robot," *Journal of Physics: Conference Series*, vol. 2005, no. 1, Article ID 012100, 2005.
- [2] X. Yang, W. Zhao, and B. Song, "Thrust force calculation and analysis for the permanent magnet linear motor motion system considering the encoder errors," *IEEE Transactions on Industrial Electronics*, vol. 69, 2021.
- [3] Y. Tao, L. Wu, J. Sidén, and G. Wang, "Monte Carlo-based indoor rfid positioning with dual-antenna joint rectification," *Electronics*, vol. 10, no. 13, p. 1548, 2021.
- [4] N. Li, C. Zhang, S. Liu, C. Xie, and C. Li, "Design and study of intensive track laying system for single hole and double road in open cut station," *IOP Conference Series: Materials Science and Engineering*, vol. 780, no. 4, Article ID 042004, 2020.
- [5] M. V. Petrenko, S. P. Dmitriev, A. S. Pazgalev, A. E. Ossadtchi, and A. K. Vershovskii, "Towards the non-zero field cesium magnetic sensor array for magnetoencephalography," *IEEE Sensors Journal*, vol. 21, 2021.
- [6] J. Li, J. Lv, B. S. Oh, Z. Lin, and Y. J. Yu, "Identification of stress state for drivers under different gps navigation modes," *IEEE Access*, vol. 8, p. 1, 2020.
- [7] Y. Chen and N. Shang, "Comparison of ga, aco algorithm, and pso algorithm for path optimization on free-form surfaces using coordinate measuring machines," *Engineering Research Express*, vol. 3, no. 4, Article ID 045039, 2021.
- [8] J. Jia, C. Zhang, B. Yuan, Z. Chen, and J. Chen, "Development and process parameter optimization with an integrated test bench for rolling and forming strips of oolong tea," *Journal of Food Process Engineering*, vol. 44, no. 12, 2021.
- [9] L. Zhang, C. Yu, and Y. Tan, "A method for pulse signal denoising based on vmd parameter optimization and grey

Retraction

Retracted: Power Tracking and Energy Balancing of Energy Storage Systems under Unreliable Communication Network

International Transactions on Electrical Energy Systems

Received 28 November 2023; Accepted 28 November 2023; Published 29 November 2023

Copyright © 2023 International Transactions on Electrical Energy Systems. This is an open access article distributed under the Creative Commons Attribution License, which permits unrestricted use, distribution, and reproduction in any medium, provided the original work is properly cited.

This article has been retracted by Hindawi, as publisher, following an investigation undertaken by the publisher [1]. This investigation has uncovered evidence of systematic manipulation of the publication and peer-review process. We cannot, therefore, vouch for the reliability or integrity of this article.

Please note that this notice is intended solely to alert readers that the peer-review process of this article has been compromised.

Wiley and Hindawi regret that the usual quality checks did not identify these issues before publication and have since put additional measures in place to safeguard research integrity.

We wish to credit our Research Integrity and Research Publishing teams and anonymous and named external researchers and research integrity experts for contributing to this investigation.

The corresponding author, as the representative of all authors, has been given the opportunity to register their agreement or disagreement to this retraction. We have kept a record of any response received.

References

- [1] H. Cai, Y. He, and H. Gao, "Power Tracking and Energy Balancing of Energy Storage Systems under Unreliable Communication Network," *International Transactions on Electrical Energy Systems*, vol. 2022, Article ID 6550925, 9 pages, 2022.

Research Article

Power Tracking and Energy Balancing of Energy Storage Systems under Unreliable Communication Network

He Cai , Yaqi He , and Huanli Gao 

School of Automation Science and Engineering, South China University of Technology, Guangzhou 510641, China

Correspondence should be addressed to Huanli Gao; hlgao@scut.edu.cn

Received 6 August 2022; Accepted 31 August 2022; Published 12 September 2022

Academic Editor: Nagamalai Vasimalai

Copyright © 2022 He Cai et al. This is an open access article distributed under the Creative Commons Attribution License, which permits unrestricted use, distribution, and reproduction in any medium, provided the original work is properly cited.

In this paper, we consider the distributed power tracking and energy balancing problem of a general energy storage system subject to unreliable switching communication network. In order to deal with the uncertainty of the network topology, a distributed observer-based approach has been proposed. First, an adaptive distributed observer is employed to recover the reference power for the entire energy storage system for each energy storage unit. Second, based on the estimated reference power, a certainty equivalent control law is synthesized to simultaneously achieve power tracking and energy balancing. Numerical simulations are provided to validate the proposed control approach.

1. Introduction

Facing the more and more severe global warming problem due to the release of greenhouse gases generated by using fossil fuels, the legacy grid is experiencing a rapid transition to the future smart grid, which involves deeply with the renewable energy sources such as solar, wind, tidal, and so on. As an indispensable part of the smart grid, energy storage system plays a key role to deal with the intermittency of the renewable energy sources by absorbing superfluous energy during off-peak time and releasing stored energy during the peak time [1–5]. There are many types of energy storage systems, such as flywheel energy storage system [6], super-capacitor energy storage system [7], battery energy storage system [8], and hybrid energy storage system [9], just to name a few. Each type of energy storage system has its own cons and pros from the perspective of power density, energy density, lift-time, maintenance, environmental impact, power quality, etc.

There have thus far been various energy management strategies and control approaches for energy storage systems. The model predictive control [10–12] could ensure robust performance for nonlinear systems and has the ability to work at a relatively low switching frequency, but it cannot deal with uncertain system parameters. By offering minimal

steady state error at changing frequencies, repetitive control is one popular control method to be employed by energy storage unit. While, system stability is hard to be guaranteed under repetitive control [13–15]. The H_∞ control proves to be robust against system uncertainties and can offer minimal tracking errors. Nevertheless, it comes with the price of slow system response and complicated mathematical treatment [16–18]. Like the H_∞ control, the sliding mode control is also good at tackling uncertain system dynamics and parameters, which, however, is less appealing due to the chattering issues [19–21].

The control configuration for the energy storage system consisting of multiple energy storage units can be roughly categorized into three groups, namely, the centralized control, the decentralized control, and the distributed control. For the centralized control, all the commands and control decisions are made by the central controller, which thus only applies to small-scale energy storage systems and is not scalable. The decentralized control usually adopted the idea of the conventional droop control, which is easy to implement, but would result in poor voltage performance [22, 23]. To overcome this issue, many other variants of droop control have been developed, such as modified droop control featuring quick transient response [24, 25], combined droop control featuring equal power sharing [26, 27],

networked droop control featuring efficient active power allocation [28], and hierarchical droop control featuring compromise voltage and frequency regulation [29]. The distributed control relies on the infrastructure of the communication network, which can be made very sparse in contrast to the centralized control. On one hand, the information will be spread over the communication network in a distributed way in the sense that each energy storage unit can only obtain information of its neighbors over the communication network. On the other hand, the control decisions will be made locally by each energy storage unit. With the significant growth of the multiagent theory through the past two decades, the consensus algorithm-based control has found many applications for the energy management of microgrids. In Reference [30], a distributed cooperative control scheme was proposed to achieve secondary regulation of an islanded microgrid by taking use of feedback linearization. Later, by adopting the distributed observer approach, Reference [31] considered energy management problem of both the VCVSI and CCVSI interfaced microgrid. In Reference [32], by feeding the local and neighboring state-of-charge information to the controller, a consensus-based distributed integral control approach was proposed to achieve state-of-charge synchronization for battery packs. Reference [33] developed a semiconsensus mechanism for a hybrid energy storage system targeting for multiple control objectives, including power dispatch, bus voltage regulation, and state-of-charge balancing. The energy management problem for a hybrid energy storage system featuring a cascaded multiport converter was investigated in Reference [34]. To balance the power output and maintain the bus voltage, a consensus-based method was developed and validated by hardware-in-loop experiments. Reference [35] focused on small-scale energy storage system, which not only achieved frequency regulation but also fulfilled state-of-charge balancing by adopting a finite time consensus scheme for a leader-follower network.

For an energy storage system, there are two fundamental control objectives. The first one is the energy storage system as a single entity should track its reference power arranged possibly by some upper level control. The second one is to balance the energy level of all the energy storage units. Till now, there have been fruitful results for the state-of-charge balancing for batter energy storage systems on both the cell and pack level, such as References [36–38]. On the contrary, for general energy storage system, there have been few results. By utilizing the simultaneous eigenvalue placement technique, Reference [39] has considered the absolute energy balancing problem for a general energy storage system based on leaderless consensus algorithm. Later, the concept of state-of-energy was proposed by Reference [40], where a distributed control approach was proposed to solve the power tracking and energy balancing problem simultaneously. However, in Reference [40], the communication network is assumed to be static and reliable, which might not be realistic in practice due to constant communication links failure and restoration.

In this paper, we further consider the distributed power tracking and energy balancing problem of a general energy

storage system subject to unreliable switching communication network. In order to deal with the uncertainty of the network topology, a distributed observer-based approach has been proposed. First, an adaptive distributed observer is employed to recover the reference power for the entire energy storage system for each energy storage unit. Second, based on the estimated reference power, a certainty equivalent control law is synthesized to simultaneously achieve power tracking and energy balancing. By rigorous Lyapunov analysis, it is proven that the proposed control approach can work effectively in the presence of switching network topology.

The main contributions of this paper are twofold:

- (i) In contrast to the existing results of References [36–39], both the energy balancing and the power tracking control objectives are considered in this paper. By doing so, the power capacity of the energy storage system can remain maximal for all the time, and thus, the energy storage system can always be fully functional for grid supporting.
- (ii) Different from the result of Reference [40], the communication network considered in this paper is allowed to switch among different connected sub-graphs. On one hand, the communication network might not be always reliable in practice, which might lead to time-varying network topologies. On the other hand, the communication network can be designed in an intermittent manner so as to lower the communication burden. In this sense, the result of this paper is more practical than that of Reference [40].

2. Graph Notation

A graph $\mathcal{G} = (\mathcal{V}, \mathcal{E})$ is defined by a node set $\mathcal{V} = \{1, \dots, N\}$ and an edge set $\mathcal{E} \subseteq \mathcal{V} \times \mathcal{V}$. For $i, j = 1, 2, \dots, N$, $i \neq j$, $(i, j) \in \mathcal{E}$ means there exists an edge in \mathcal{E} from node i to node j . If $(i, j) \in \mathcal{E}$, then node i is called a neighbor of node j . Let $\mathcal{N}_i = \{j, (j, i) \in \mathcal{E}\}$ denote the neighbor set of node i . If $(i, j) \in \mathcal{E}$ if and only if $(j, i) \in \mathcal{E}$, then the edge (i, j) is called undirected. If all the edges of a graph are undirected, then the graph is called undirected. If \mathcal{E} contains a set of edges of the form $(i_1, i_2), (i_2, i_3), \dots, (i_k, i_{k+1})$, then the set $\{(i_1, i_2), (i_2, i_3), \dots, (i_k, i_{k+1})\}$ is called a path of \mathcal{G} from node i_1 to node i_{k+1} , and node i_{k+1} is said to be reachable from node i_1 . A graph \mathcal{G} is said to contain a spanning tree if there exists a node in \mathcal{G} such that all the other nodes are reachable from it, and this node is called the root of the spanning tree. Given a set of m graphs $\mathcal{G}_k = (\mathcal{V}, \mathcal{E}_k)$, $k = 1, \dots, m$, the graph $\mathcal{G} = (\mathcal{V}, \mathcal{E})$ with $\mathcal{E} = \cup_{k=1}^m \mathcal{E}_k$ is called the union of \mathcal{G}_k , denoted by $\mathcal{G} = \cup_{k=1}^m \mathcal{G}_k$.

A time signal $\sigma(t): [0, +\infty) \rightarrow \mathcal{S} = \{1, \dots, s\}$ for some positive integer s is called a piecewise constant switching signal with dwell time τ for some $\tau > 0$ if there exists a time sequence $\{t_k, k = 0, 1, 2, \dots\}$ satisfying, $t_0 = 0$; for any positive integer k , $t_k - t_{k-1} \geq \tau$; $\sigma(t) = p$, $p \in \mathcal{S}$, for all $t \in [t_{k-1}, t_k)$. Given a node set $\mathcal{V} = \{1, \dots, N\}$ and a piecewise constant switching signal $\sigma(t)$, define a switching

graph $\mathcal{G}_{\sigma(t)} = (\mathcal{V}, \mathcal{E}_{\sigma(t)})$ where $\mathcal{E}_{\sigma(t)} \subseteq \mathcal{V} \times \mathcal{V}$ for all $t \geq 0$. For a switching graph, let $\mathcal{N}_i(t)$ denote the neighbor set of node i at time instant t . Associated with a switching graph $\mathcal{G}_{\sigma(t)}$, the matrix $\mathcal{A}_{\sigma(t)} = [a_i(t)] \in \mathbb{R}^{N \times N}$ is called a time-varying weighted adjacency matrix of $\mathcal{G}_{\sigma(t)}$ if $a_{ii}(t) = 0$; $a_{ij}(t) > 0 \Leftrightarrow (j, i) \in \mathcal{E}_{\sigma(t)}$; and $a_{ij}(t) = 0$ otherwise. Let $\mathcal{L}_{\sigma(t)} = [l_{ij}(t)] \in \mathbb{R}^{N \times N}$ be such that $l_{ii}(t) = \sum_{j=1}^N a_{ij}(t)$ and $l_{ij}(t) = -a_{ij}(t)$ if $i \neq j$. Then, $\mathcal{L}_{\sigma(t)}$ is called the Laplacian of $\mathcal{G}_{\sigma(t)}$ associated with $\mathcal{A}_{\sigma(t)}$.

3. Problem Statement

In this paper, we consider an energy storage system consisting of M energy storage units. Suppose the energy capacities of all the energy storage units are the same, denoted by C_{e0} . In the meantime, we let $C_{ei}(t)$ denote the remaining energy of the i -th energy storage unit at time instant t . Therefore, the state-of-energy $\chi_i(t)$ of the i -th energy storage unit can be defined by

$$\chi_i(t) = \frac{C_{ei}(t)}{C_{e0}}. \quad (1)$$

The relationship between energy and power is given by

$$\dot{C}_{ei}(t) = -\wp_i(t), \quad (2)$$

where $\wp_i(t)$ denotes the power output of the i -th energy storage unit. In particular, $\wp_i(t) > 0$ means the energy storage unit is releasing energy to the grid, and $\wp_i(t) < 0$ means the energy storage unit is absorbing energy from the grid.

Then, by (1) and (2), we can obtain the dynamics of the state-of-energy of the i -th energy storage unit as follows:

$$\dot{\chi}_i(t) = -C_{e0}^{-1} \wp_i(t). \quad (3)$$

In terms of $\wp_i(t)$, the total power output of the entire energy storage system can be obtained by

$$\wp_{\text{ess}}(t) = \sum_{i=1}^M \wp_i(t). \quad (4)$$

In addition, we define the following reference generator:

$$\begin{aligned} \dot{r}_0(t) &= R_0 r_0(t), \\ \wp_{\text{ess}}^r(t) &= W_0 r_0(t), \end{aligned} \quad (5)$$

where $r_0(t) \in \mathbb{R}^n$ is the state of the reference generator and $\wp_{\text{ess}}^r(t) \in \mathbb{R}$ denotes the reference power output for the entire energy storage system. R_0 and W_0 are constant matrices, which satisfy the following assumptions.

Assumption 1. All the eigenvalues of R_0 have nonpositive real parts.

Remark 1. Assumption 1 does not lose any generality from the practical point of view since exponential divergent signals can hardly be used in practice. On the other hand, under Assumption 1, we allow the reference power signal to be the combination of multitone sinusoidal signals with

polynomial signals, which can model a large class of reference signals.

Let switching graph $\overline{\mathcal{G}}_{\sigma(t)} = (\overline{\mathcal{V}}, \overline{\mathcal{E}}_{\sigma(t)})$ model the unreliable communication network for the energy storage system as well as the reference generator, where $\overline{\mathcal{V}} = \{0, 1, \dots, M\}$ and $\overline{\mathcal{E}}_{\sigma(t)} \subseteq \{\overline{\mathcal{V}} \times \overline{\mathcal{V}}\}$. The node 0 represents the reference generator, and the node i represents the i -th energy storage unit. For $i = 0, 1, \dots, M$, $j = 1, \dots, M$, $(i, j) \in \overline{\mathcal{E}}_{\sigma(t)}$ if and only if the j -th energy storage unit can get message from the reference generator or the i -th energy storage unit at time instant t . In addition, let $\mathcal{G}_{\sigma(t)} = (\mathcal{V}, \mathcal{E}_{\sigma(t)})$ be defined by $\mathcal{V} = \{1, \dots, M\}$ and $\mathcal{E}_{\sigma(t)} = \overline{\mathcal{E}}_{\sigma(t)} \cap \{\mathcal{V} \times \mathcal{V}\}$. Moreover, define $\overline{\mathcal{A}}_{\sigma(t)} = [a_{ij}(t)] \in \mathbb{R}^{(M+1) \times (M+1)}$ as the weighted adjacency matrix of $\overline{\mathcal{G}}_{\sigma(t)}$, and let $\mathcal{L}_{\sigma(t)}$ be the Laplacian of $\mathcal{G}_{\sigma(t)}$.

Two assumptions regarding the communication graphs $\overline{\mathcal{G}}_{\sigma(t)}$ and $\mathcal{G}_{\sigma(t)}$ are listed as follows.

Assumption 2. The switching graph $\mathcal{G}_{\sigma(t)}$ is undirected and connected for all $t \geq 0$.

Assumption 3. There exists a subsequence $\{\alpha_k: k = 0, 1, 2, \dots\}$ of $\{k = 0, 1, 2, \dots\}$ satisfying $t_{\alpha_{k+1}} - t_{\alpha_k} < \nu_\alpha$ for some $\nu_\alpha > 0$, such that every node i , $i = 1, \dots, N$, is reachable from node 0 in the union graph $\cup_{l=\alpha_k}^{\alpha_{k+1}-1} \overline{\mathcal{G}}_{\sigma(t_l)}$.

Remark 2. Assumption 2 requires bidirectional communication between energy storage units, which can be implemented in practice through wired communication network. Moreover, it is further required that though the unreliable communication network topology can be switching, the connectivity of the network topology should be guaranteed. Together with Assumption 2, Assumption 3 means for the energy storage system, the information obtained from the reference generator, though not necessarily available for all the time being, should at least be frequently available with the maximal time interval less than ν_α .

Now, we are ready to state the problem considered in this paper as follows.

Problem 1. Given systems (3), (5), and the unreliable communication network $\overline{\mathcal{G}}_{\sigma(t)}$, for $i = 1, \dots, M$, design $\wp_i(t)$ such that

$$\lim_{t \rightarrow \infty} (\wp_{\text{ess}}(t) - \wp_{\text{ess}}^r(t)) = 0, \quad (6)$$

and

$$\lim_{t \rightarrow \infty} (\chi_i(t) - \chi_j(t)) = 0, \quad i, j = 1, \dots, M. \quad (7)$$

Remark 3. The control objective (6) means that the differences between the power output of the energy storage system and its reference should be regulated to zero asymptotically, and the control objective (7) means that the energy levels of all the energy storage units should keep balanced with respect to each other.

4. Main Result

In this section, we will solve Problem 1 by a distributed control law, which consists of two parts. First, an adaptive distributed observer is employed to recover the reference power for the entire energy storage system for each energy storage unit. Second, based on the estimated reference power, a certainty equivalent control law is synthesized to simultaneously achieve power tracking and energy balancing.

To begin with, we introduce the adaptive distributed observer as follows. For $i = 1, \dots, N$, design

$$\begin{aligned}\dot{R}_i(t) &= \mu_R \sum_{j=0}^M a_{ij}(t)(R_j(t) - R_i(t)), \\ \dot{W}_i(t) &= \mu_W \sum_{j=0}^M a_{ij}(t)(W_j(t) - W_i(t)), \\ \dot{r}_i(t) &= R_i(t)r_i(t) + \mu_r \sum_{j=0}^M a_{ij}(t)(r_j(t) - r_i(t)), \\ \varphi_{ess,i}^r(t) &= W_i(t)r_i(t),\end{aligned}\quad (8)$$

where $R_i(t) \in \mathbb{R}^{n_r \times n_r}$, $W_i(t) \in \mathbb{R}^{1 \times n_r}$, $r_i(t) \in \mathbb{R}^{n_r}$, and $\varphi_{ess,i}^r(t) \in \mathbb{R}$ are the estimate of R_0 , W_0 , $r_0(t)$, and $\varphi_{ess}^r(t)$, respectively. $\mu_R, \mu_W, \mu_r > 0$ are the observer gains.

For $i = 1, \dots, N$, define

$$\begin{aligned}\tilde{R}_i(t) &= R_i(t) - R_0, \\ \tilde{W}_i(t) &= W_i(t) - W_0, \\ \tilde{r}_i(t) &= r_i(t) - r_0(t), \\ \tilde{\varphi}_{ess,i}^r(t) &= \varphi_{ess,i}^r(t) - \varphi_{ess}^r(t).\end{aligned}\quad (9)$$

Then, by Theorem 4.8 of Reference [41], it follows that, under Assumptions 1–3, all $\tilde{R}_i(t)$, $\tilde{W}_i(t)$, $\tilde{r}_i(t)$, and $\tilde{\varphi}_{ess,i}^r(t)$ approach to zero exponentially for any $\mu_R, \mu_W, \mu_r > 0$. In general, the larger the observer gains are selected, the faster the estimation can be realized. However, fast convergence of the distributed observer may come at the price of large overshoot for transient response.

Remark 4. The dynamic compensator (8) is distributed since it only relies on neighboring information over the communication network. It is called an adaptive distributed observer of the reference generator (5) due to the following two reasons. First, it does not take the system matrices of the reference generator as prior knowledge but instead estimates all these matrices adaptively, and this explains why it is named ‘‘adaptive’’. Second, it recovers all the information of the reference generator, and in this sense it is called an observer of the reference generator.

Next, we show the local certainty equivalent control law as follows. For $i = 1, \dots, N$, design

$$\varphi_i(t) = -\mu_\varphi \sum_{j=1}^M a_{ij}(t)(\chi_j(t) - \chi_i(t)) + \frac{\varphi_{ess,i}^r(t)}{N}, \quad (10)$$

where $\mu_\varphi > 0$ is the control gain.

We have the following main results.

Theorem 1. *Given systems (3), (5), and the unreliable communication network $\mathcal{G}_{\sigma(t)}$, under Assumptions 1–3, Problem 1 is solvable by the control law composed of (8) and (10) for any $\mu_R, \mu_W, \mu_r, \mu_\varphi > 0$.*

Proof: Substituting (10) to (3) gives

$$\dot{\chi}_i(t) = C_{e0}^{-1} \left(\mu_\varphi \sum_{j=1}^M a_{ij}(t)(\chi_j(t) - \chi_i(t)) - \frac{\varphi_{ess,i}^r(t)}{N} \right). \quad (11)$$

Define $\bar{\mu}_\varphi = C_{e0}^{-1} \mu_\varphi$ and $\hat{\mu}_\varphi = C_{e0}^{-1}/N$. Then we have

$$\begin{aligned}\dot{\chi}_i(t) &= \bar{\mu}_\varphi \sum_{j=1}^M a_{ij}(t)(\chi_j(t) - \chi_i(t)) - \hat{\mu}_\varphi \varphi_{ess,i}^r(t) \\ &= \bar{\mu}_\varphi \sum_{j=1}^M a_{ij}(t)(\chi_j(t) - \chi_i(t)) - \hat{\mu}_\varphi \tilde{\varphi}_{ess,i}^r(t) - \hat{\mu}_\varphi \varphi_{ess}^r(t).\end{aligned}\quad (12)$$

Let (For $a_i \in \mathbb{R}^M$, $i = 1, \dots, M$, $\text{col}(a_1, \dots, a_M) = [a_1^T, \dots, a_M^T]^T$) $\chi(t) = \text{col}(\chi_1(t), \dots, \chi_M(t))$ and $\tilde{\varphi}_{ess}^r(t) = \text{col}(\tilde{\varphi}_{ess,1}^r(t), \dots, \tilde{\varphi}_{ess,M}^r(t))$. Then we have

$$\dot{\chi}(t) = -\bar{\mu}_\varphi \mathcal{L}_{\sigma(t)} \chi(t) - \hat{\mu}_\varphi \varphi_{ess}^r(t) \mathbf{1}_M - \hat{\mu}_\varphi \tilde{\varphi}_{ess}^r(t), \quad (13)$$

where $\mathbf{1}_M = \text{col}(1, \dots, 1) \in \mathbb{R}^M$.

Define $Q = [Q_1, Q_r]$ where $Q_1 = \mathbf{1}_M/\sqrt{M}$ and $Q_r \in \mathbb{R}^{M \times (M-1)}$ is selected such that Q is orthogonal. Then, $Q^{-1} = Q^T$. Furthermore, since

$$Q^T Q = \begin{bmatrix} Q_1^T \\ Q_r^T \end{bmatrix} [Q_1 \ Q_r] = \begin{bmatrix} Q_1^T Q_1 & Q_1^T Q_r \\ Q_r^T Q_1 & Q_r^T Q_r \end{bmatrix} = I_M, \quad (14)$$

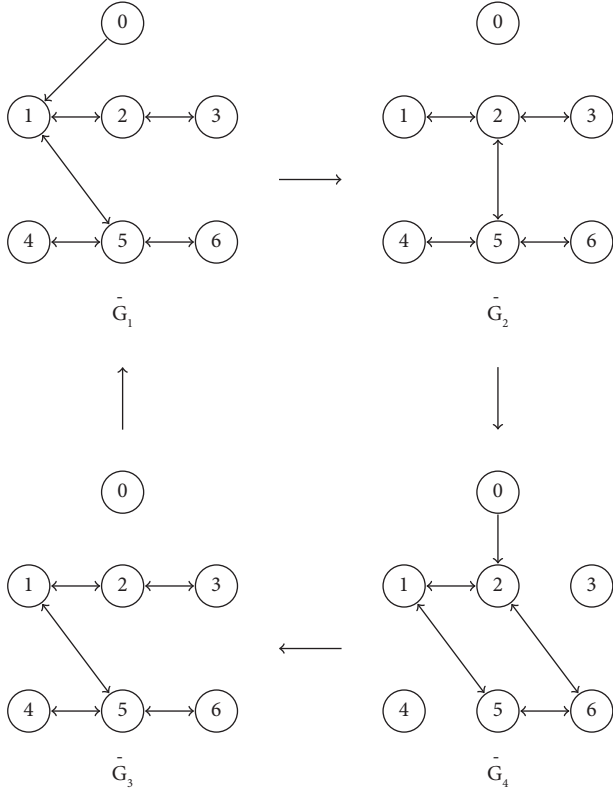
it follows that $Q_r^T Q_1 = 0$. Therefore,

$$Q^{-1} \mathbf{1}_M = \begin{bmatrix} Q_1^T \\ Q_r^T \end{bmatrix} \mathbf{1}_M = \begin{bmatrix} \sqrt{M} \\ 0 \\ \vdots \\ 0 \end{bmatrix}. \quad (15)$$

Let $\mathcal{F}_{\sigma(t)} = Q_r^T \mathcal{L}_{\sigma(t)} Q_r$. Since $\mathcal{L}_{\sigma(t)} \mathbf{1}_N = 0$ and $\mathcal{L}_{\sigma(t)}$ is symmetric for all $t \geq 0$, we have

$$\begin{aligned}Q^T \mathcal{L}_{\sigma(t)} Q &= \begin{bmatrix} Q_1^T \\ Q_r^T \end{bmatrix} [\mathcal{L}_{\sigma(t)} Q_1 \ \mathcal{L}_{\sigma(t)} Q_r] = \begin{bmatrix} Q_1^T \\ Q_r^T \end{bmatrix} [0 \ \mathcal{L}_{\sigma(t)} Q_r] \\ &= \begin{bmatrix} 0 Q_1^T \mathcal{L}_{\sigma(t)} Q_r \\ 0 Q_r^T \mathcal{L}_{\sigma(t)} Q_r \end{bmatrix} = \begin{bmatrix} 0 & 0 \\ 0 Q_r^T \mathcal{L}_{\sigma(t)} Q_r \end{bmatrix} = \begin{bmatrix} 0 & 0 \\ 0 & \mathcal{F}_{\sigma(t)} \end{bmatrix}.\end{aligned}\quad (16)$$

Then, under Assumption 2, by Theorem A.1 of Reference [41], $\mathcal{F}_{\sigma(t)}$ is symmetric and all the eigenvalues of $\mathcal{F}_{\sigma(t)}$ are positive for all $t \geq 0$. Let $\bar{\chi}(t) = Q^{-1} \chi(t)$. Then we have


 FIGURE 1: Unreliable communication network $\bar{\mathcal{G}}_{\sigma(t)}$.

$$\begin{aligned} \dot{\bar{\chi}}(t) &= -\bar{\mu}_\varphi Q^{-1} \mathcal{L}_{\sigma(t)} \bar{\chi}(t) - \hat{\mu}_\varphi \varrho_{\text{ess}}^r(t) Q^{-1} \mathbf{1}_M - \hat{\mu}_\varphi Q^{-1} \bar{\varrho}_{\text{ess}}^r(t) \\ &= -\bar{\mu}_\varphi Q^T \mathcal{L}_{\sigma(t)} Q \bar{\chi}(t) - \hat{\mu}_\varphi \varrho_{\text{ess}}^r(t) Q^{-1} \mathbf{1}_M - \bar{\zeta}(t), \end{aligned} \quad (17)$$

where $\bar{\zeta}(t) = \hat{\mu}_\varphi Q^{-1} \bar{\varrho}_{\text{ess}}^r(t)$.
Let

$$\begin{aligned} \bar{\chi}(t) &= \text{col}(\bar{\chi}_{ss}(t), \bar{\chi}_{tr}(t)), \\ \bar{\zeta}(t) &= \text{col}(\bar{\zeta}_{ss}(t), \bar{\zeta}_{tr}(t)), \end{aligned} \quad (18)$$

where $\bar{\chi}_{ss}(t), \bar{\zeta}_{ss}(t) \in \mathbb{R}$ and $\bar{\chi}_{tr}(t), \bar{\zeta}_{tr}(t) \in \mathbb{R}^{M-1}$. Then system (13) can be decomposed into the following two subsystems:

$$\dot{\bar{\chi}}_{ss}(t) = -\hat{\mu}_\varphi \varrho_{\text{ess}}^r(t) \sqrt{M} - \bar{\zeta}_{ss}(t), \quad (19a)$$

$$\dot{\bar{\chi}}_{tr}(t) = -\bar{\mu}_\varphi \mathcal{F}_{\sigma(t)} \bar{\chi}_{tr}(t) - \bar{\zeta}_{tr}(t). \quad (19b)$$

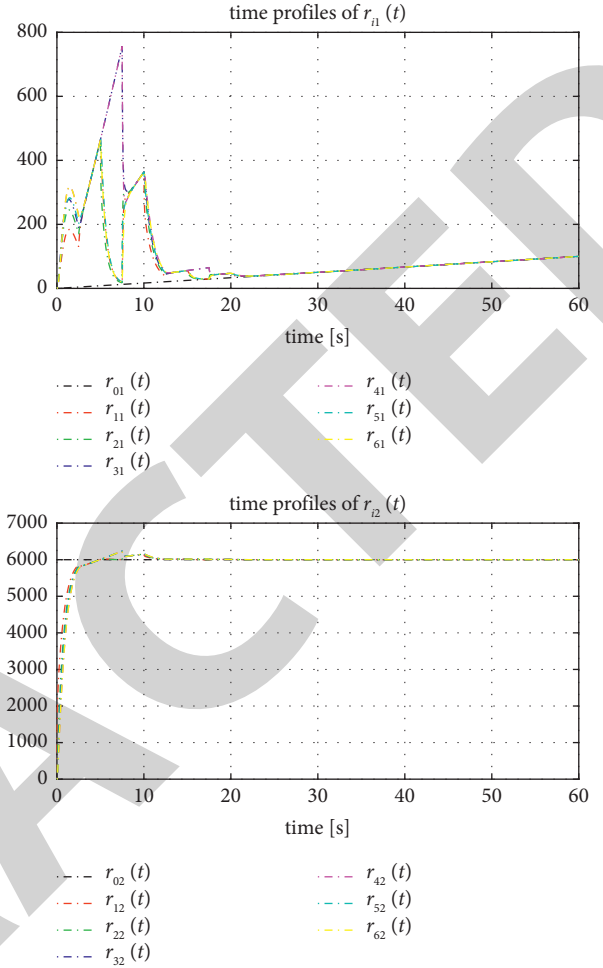
Associate with system (19b), define the following auxiliary system:

$$\dot{\theta}(t) = -\bar{\mu}_\varphi \mathcal{F}_{\sigma(t)} \theta(t), \quad (20)$$

and design the following Lyapunov function:

$$V(t) = \frac{1}{2} \theta(t)^T \theta(t). \quad (21)$$

Then, along system (20), it follows that


 FIGURE 2: Time profiles of $r_0(t)$ and $r_i(t)$ in case 1.

$$\begin{aligned} \dot{V}(t) &= -\bar{\mu}_\varphi \theta(t)^T \mathcal{F}_{\sigma(t)} \theta(t) \leq -\bar{\mu}_\varphi J_{\min} \theta(t)^T \theta(t) \\ &= -2\bar{\mu}_\varphi J_{\min} V(t), \end{aligned} \quad (22)$$

where J_{\min} is the smallest eigenvalue of $\mathcal{F}_{\sigma(t)}$ for all $t \geq 0$. By (22), $V(t)$ tends to zero exponentially, and so is $\theta(t)$ of system (20), that is, the origin of system (20) is exponentially stable. As a result, since $\bar{\zeta}_{tr}(t)$ tends to zero exponentially, by Lemma 2.8 of [41], it follows that $\bar{\chi}_{tr}(t)$ of system (19b) also tends to zero exponentially. In consequence, by noting that

$$\chi(t) = Q \bar{\chi}(t) = [Q_1 Q_r] \begin{bmatrix} \bar{\chi}_{ss}(t) \\ \bar{\chi}_{tr}(t) \end{bmatrix} = Q_1 \bar{\chi}_{ss}(t) + Q_r \bar{\chi}_{tr}(t), \quad (23)$$

it concludes that

$$\lim_{t \rightarrow \infty} \left(\chi(t) - \left(\frac{\bar{\chi}_{ss}(t)}{\sqrt{M}} \right) \mathbf{1}_M \right) = 0, \quad (24)$$

that is,

$$\lim_{t \rightarrow \infty} (\chi_i(t) - \chi_j(t)) = 0, \quad i, j = 1, \dots, N, i \neq j. \quad (25)$$

Moreover, we have

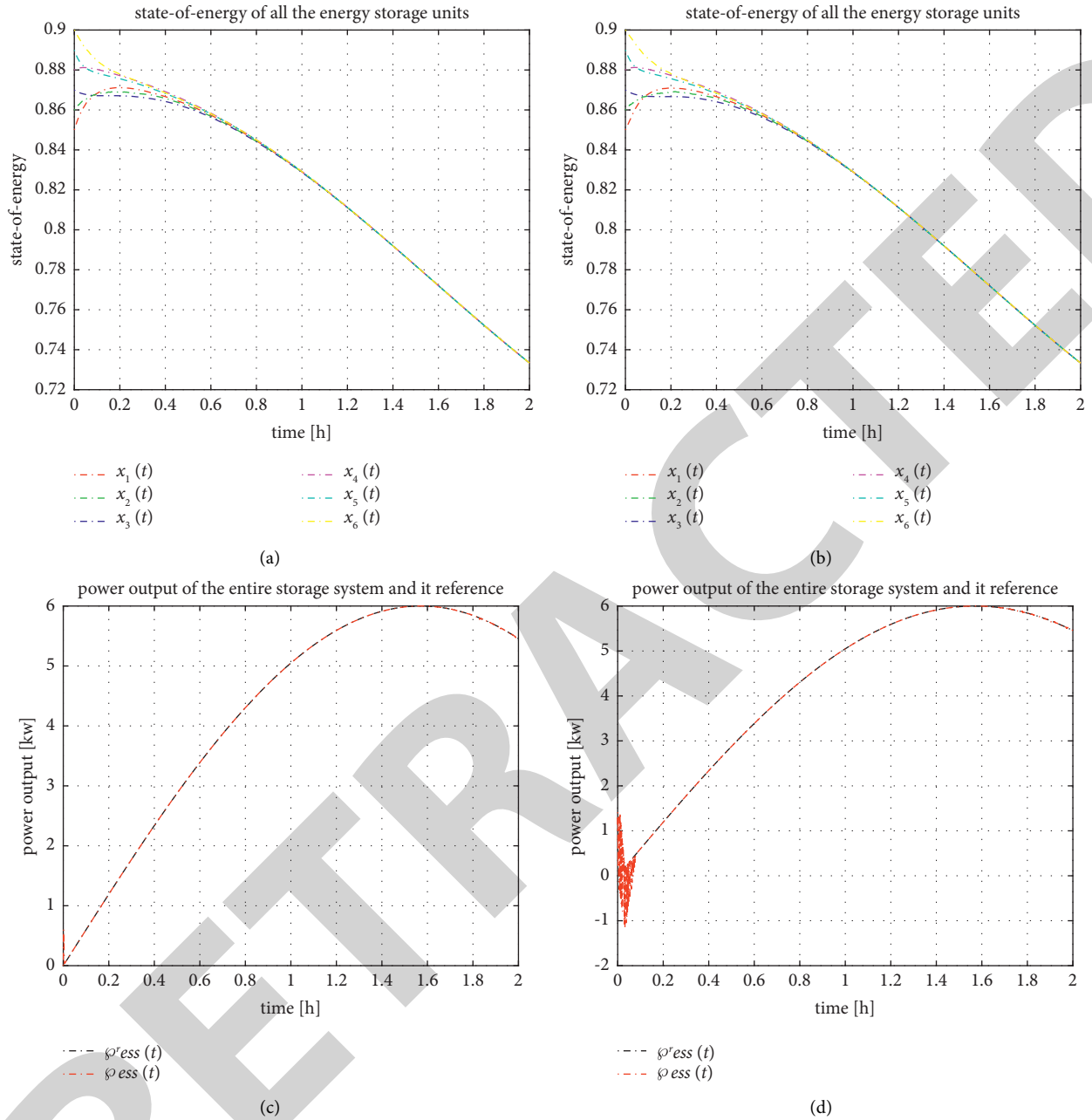


FIGURE 3: Continued.

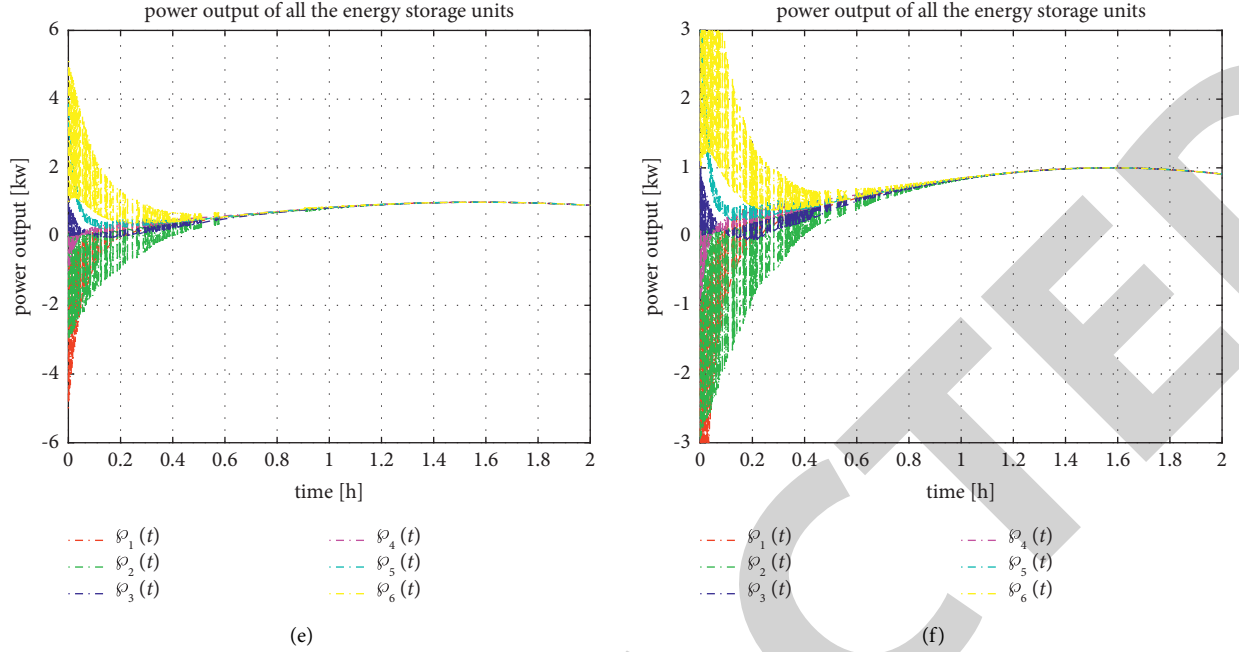


FIGURE 3: Simulation results for cases 1 and 2. (a) State-of-energy of all the energy storage units in case 1, (b) state-of-energy of all the energy storage units in case 2, (c) power output of the energy storage system and its reference in case 1, (d) power output of the energy storage system and its reference in case 2, (e) power outputs of all the energy storage units in case 1, and (f) power outputs of all the energy storage units in case 2.

$$\begin{aligned}
 \varphi_{\text{ess}}(t) - \varphi_{\text{ess}}^r(t) &= -\mu_{\varphi} \sum_{i=1}^M \sum_{j=1}^M a_{ij}(t) (\chi_j(t) - \chi_i(t)) \\
 &\quad + \sum_{i=1}^M \frac{\varphi_{\text{ess},i}^r(t)}{M} - \varphi_{\text{ess}}^r(t) \\
 &= -\mu_{\varphi} \sum_{i=1}^M \sum_{j=1}^M a_{ij}(t) (\chi_j(t) - \chi_i(t)) + \sum_{i=1}^M \frac{\tilde{\varphi}_{\text{ess},i}^r(t)}{M}.
 \end{aligned} \tag{26}$$

Hence, it follows that

$$\lim_{t \rightarrow \infty} (\varphi_{\text{ess}}(t) - \varphi_{\text{ess}}^r(t)) = 0. \tag{27}$$

The proof is thus complete.

5. Numerical Simulations

In this section, we will use a numerical example to illustrate the proposed control method. Consider an energy storage system consisting of 6 energy storage units. Suppose the energy capacity of each energy storage unit is 10 kWh.

The unreliable switching communication network is shown by Figure 1. To be more specific, the communication network is assumed to switch among four subgraphs $\overline{\mathcal{G}}_1$, $\overline{\mathcal{G}}_2$, $\overline{\mathcal{G}}_3$, and $\overline{\mathcal{G}}_4$ periodically every T_c sec. In the simulation, suppose $T_c = 10$. It can be easily verified that Assumptions 2 and 3 are satisfied. From these four subgraphs, it can also be noticed that the information of the reference generator is only available to the energy storage system for half of the time.

Suppose the reference generator is given by

$$\begin{aligned}
 \dot{r}_0(t) &= \begin{bmatrix} 0 & \omega \\ -\omega & 0 \end{bmatrix} r_0(t), \\
 r_0(0) &= \begin{bmatrix} 0 \\ 6 \times 10^3 \end{bmatrix}, \\
 \varphi_{\text{ess}}^r(t) &= [1 \ 0] r_0(t),
 \end{aligned} \tag{28}$$

where $\omega > 0$. Clearly, Assumption 1 is satisfied. In the simulation, we let $\omega = 1/3600$ rad/s and thus $\varphi_{\text{ess}}^r(t) = 6 \times 10^3 \sin((1/3600)t)$ kw.

Suppose the control gains are selected to be $\mu_R = \mu_W = \mu_r = 10$ and $\mu_{\varphi} = 10^5$. Note that μ_{φ} should be sufficiently large so that the energy balancing objective can be achieved timely.

The initial state-of-energy of all the energy storage units takes values in $[0.85, 0.92]$.

The initial values of the control laws take values in $[0, 0.5]$.

In the following, we will conduct the simulations for two cases.

5.1. Case 1: Standard Case. The simulation results for this case are shown in Figures 2 and 3. In particular, Figure 2 shows the state of the reference generator and its estimate by each adaptive distributed observer. It can be seen that the information of the reference generator has been successfully recovered within 20 seconds. Figure 3(a) shows that the balance of state-of-energy has been achieved in about 0.8

hours. While, Figure 3(c) shows that the power tracking is fulfilled very soon after initialization. Figure 3(e) shows the power outputs of all the energy storage units. Due to the switching of the communication network, there are oscillations in the transient response of the power outputs.

5.2. Case 2: Power Saturation. In this case, we consider the practical scenario that the power output of the energy storage unit is subject to saturation. Specifically, we assume the power output of each energy storage unit is limited to ± 3 kw. The simulation results are shown by Figure 3. It can be seen from Figures 3(b) and 3(d) that the power output saturation does not affect much the performance on energy balancing, but it takes a little bit longer time to achieve power tracking. Moreover, Figure 3(f) shows that all the power outputs are within the specified limits.

6. Conclusion

In this paper, the dual objectives of power tracking and energy balancing for a general energy storage system are considered and solved by a distributed control law. To make the proposed control law robust against unreliable communication links, the distributed observer approach has been adopted, which together with the local certainty equivalent control law solves the dual objective problem over the unreliable switching communication network. In the future, it would be interesting to further extend this work for a jointly connected communication network without assuming that the information exchange among energy storage units is undirected. Moreover, it would also be meaningful to consider the case of energy storage units with heterogenous power capacities.

Data Availability

The data used to support the findings of this study are available from the corresponding author upon request.

Conflicts of Interest

The authors declare that they have no conflicts of interest.

Acknowledgments

This research was supported in part by the National Natural Science Foundation of China under grant number 61803160 and in part by the Guangdong Natural Science Foundation under grant numbers 2020A1515010810 and 2021A1515012584.

References

- [1] J. Xiao, P. Wang, and L. Setyawan, "Hierarchical control of hybrid energy storage system in DC microgrids," *IEEE Transactions on Industrial Electronics*, vol. 62, no. 8, pp. 4915–4924, 2015.
- [2] M. Katsanevakis, R. A. Stewart, and J. Lu, "Aggregated applications and benefits of energy storage systems with application-specific control methods: a review," *Renewable and Sustainable Energy Reviews*, vol. 75, pp. 719–741, 2017.
- [3] A. K. Rohit and S. Rangnekar, "An overview of energy storage and its importance in Indian renewable energy sector: part II—energy storage applications, benefits and market potential," *Journal of Energy Storage*, vol. 13, pp. 447–456, 2017.
- [4] E. Dehnavi, F. Aminifar, and S. Afsharnia, "Congestion management through distributed generations and energy storage systems," *International Transactions on Electrical Energy Systems*, vol. 29, no. 6, Article ID e12018, 2019.
- [5] T. S. Babu, K. R. Vasudevan, V. K. Ramachandaramurthy, S. B. Sani, S. Chemud, and R. M. Lajim, "A comprehensive review of hybrid energy storage systems: converter topologies, control strategies and future prospects," *IEEE Access*, vol. 8, pp. 148702–148721, 2020.
- [6] S. Choudhury, "Flywheel energy storage systems: a critical review on technologies, applications, and future prospects," *International Transactions on Electrical Energy Systems*, vol. 31, no. 9, Article ID e13024, 2021.
- [7] K. Gong, J. Shi, Y. Liu, Z. Wang, L. Ren, and Y. Zhang, "Application of SMES in the microgrid based on fuzzy control," *IEEE Transactions on Applied Superconductivity*, vol. 26, no. 3, pp. 1–5, 2016.
- [8] Y. Yuan, X. Zhang, P. Ju, Q. Li, K. Qian, and Z. Fu, "Determination of economic dispatch of wind farm-battery energy storage system using Genetic Algorithm," *International Transactions on Electrical Energy Systems*, vol. 24, no. 2, pp. 264–280, 2014.
- [9] J. Li, R. Xiong, Q. Yang, F. Liang, M. Zhang, and W. Yuan, "Design/test of a hybrid energy storage system for primary frequency control using a dynamic droop method in an isolated microgrid power system," *Applied Energy*, vol. 201, pp. 257–269, 2017.
- [10] D. Hyacinthe Tungadio and Y. Sun, "Predictive controller for interconnected microgrids," *IET Generation, Transmission & Distribution*, vol. 14, no. 19, pp. 4273–4283, 2020.
- [11] C. Wu, S. Gao, Y. Liu, T. E. Song, and H. Han, "A model predictive control approach in microgrid considering multi-uncertainty of electric vehicles," *Renewable Energy*, vol. 163, pp. 1385–1396, 2021.
- [12] J. R. Nelson and N. G. Johnson, "Model predictive control of microgrids for real-time ancillary service market participation," *Applied Energy*, vol. 269, Article ID 114963, 2020.
- [13] T. Chmielewski, W. Jarzyna, D. Zieliński, K. Gopakumar, and M. Chmielewska, "Modified repetitive control based on comb filters for harmonics control in gridconnected applications," *Electric Power Systems Research*, vol. 200, Article ID 107412, 2021.
- [14] C. Xie, D. Liu, K. Li, J. Zou, K. Zhou, and J. M. Guerrero, "Passivity-based design of repetitive controller for LCL-Type grid-connected inverters suitable for microgrid applications," *IEEE Transactions on Power Electronics*, vol. 36, no. 2, pp. 2420–2431, 2021.
- [15] G. Yang, J. Yin, Z. Huang, and Y. Zhang, "A method to improve the reliability of threelevel inverter based on equivalent input disturbance and repetitive control combinations," *Microelectronics Reliability*, vol. 114, Article ID 113837, 2020.
- [16] V. Skiparev, R. Machlev, N. R. Chowdhury, Y. Levron, E. Petlenkov, and J. Belikov, "Virtual inertia control methods in islanded microgrids," *Energies*, vol. 14, no. 6, p. 1562, 2021.
- [17] B. E. Sedhom, M. M. El-Saadawi, M. A. Elhosseini, M. A. Saeed, and E. E. Abd-Raboh, "A harmony search-based

Retraction

Retracted: Electricity Network Security Monitoring Based on Bee Colony Algorithm

International Transactions on Electrical Energy Systems

Received 19 September 2023; Accepted 19 September 2023; Published 20 September 2023

Copyright © 2023 International Transactions on Electrical Energy Systems. This is an open access article distributed under the Creative Commons Attribution License, which permits unrestricted use, distribution, and reproduction in any medium, provided the original work is properly cited.

This article has been retracted by Hindawi following an investigation undertaken by the publisher [1]. This investigation has uncovered evidence of one or more of the following indicators of systematic manipulation of the publication process:

- (1) Discrepancies in scope
- (2) Discrepancies in the description of the research reported
- (3) Discrepancies between the availability of data and the research described
- (4) Inappropriate citations
- (5) Incoherent, meaningless and/or irrelevant content included in the article
- (6) Peer-review manipulation

The presence of these indicators undermines our confidence in the integrity of the article's content and we cannot, therefore, vouch for its reliability. Please note that this notice is intended solely to alert readers that the content of this article is unreliable. We have not investigated whether authors were aware of or involved in the systematic manipulation of the publication process.

Wiley and Hindawi regrets that the usual quality checks did not identify these issues before publication and have since put additional measures in place to safeguard research integrity.

We wish to credit our own Research Integrity and Research Publishing teams and anonymous and named external researchers and research integrity experts for contributing to this investigation.

The corresponding author, as the representative of all authors, has been given the opportunity to register their agreement or disagreement to this retraction. We have kept a record of any response received.

References

- [1] W. Su and B. Zhang, "Electricity Network Security Monitoring Based on Bee Colony Algorithm," *International Transactions on Electrical Energy Systems*, vol. 2022, Article ID 4533154, 8 pages, 2022.

Research Article

Electricity Network Security Monitoring Based on Bee Colony Algorithm

Wenzhi Su  and Baolong Zhang 

Jiyuan Vocational and Technical College, Jiyuan, Henan 459000, China

Correspondence should be addressed to Wenzhi Su; 1710211105@hbut.edu.cn

Received 28 June 2022; Revised 5 August 2022; Accepted 13 August 2022; Published 7 September 2022

Academic Editor: B. Madhavan

Copyright © 2022 Wenzhi Su and Baolong Zhang. This is an open access article distributed under the Creative Commons Attribution License, which permits unrestricted use, distribution, and reproduction in any medium, provided the original work is properly cited.

In order to effectively detect and discover network threats in the initial stage, this study proposes an electricity network security intrusion detection method based on feature selection. A heuristic feature selection algorithm based on the bee colony algorithm is proposed to overcome the shortcomings of existing feature evaluation methods. The algorithm uses average mutual information to measure the importance of features and more truly reflects the relationship between the selected features, the selected features, and the classification labels. Aiming at the problem that the algorithm is easy to fall into local optimization, a heuristic random search algorithm is proposed, which iteratively optimizes to generate smaller feature subsets, and improves the speed and accuracy of intrusion detection. The experimental results show that compared with the traditional algorithm, the proposed method can effectively evaluate the risk of attack path on the selected experimental data set, and the gap between the generation strategy and the optimal strategy is reduced by 71.3%, which enhances the practicability of the attack graph analysis method in a large-scale network environment. *Conclusion.* This method has good scalability and can be applied to large-scale network environments. It can effectively obtain attack paths that are more in line with the real threat situation in an acceptable time, so as to effectively find the network threats.

1. Introduction

With the wide application of cloud computing, the security problem of cloud computing has become increasingly prominent. The cloud environment not only has to face all the security threats faced by the traditional network environment, but also has the characteristics of resource virtualization, high dynamic, and sharing, which makes the cloud environment have more attack surfaces than the traditional network, so it also needs to face many new threats [1]. Network systems are faced with a variety of security threats every day, such as IP and port scanning, camouflage attacks, DDoS attacks, illegal privilege escalation, and so on. These means are not only destructive to the system but also may be used as the leading means of subsequent high-level threats, seriously endangering the system security. Therefore, effective detection and discovery of threats in the initial stage are of great significance to ensure system security.

Intrusion detection system can provide an early warning function for the system in the face of threats. Since the intrusion detection technology was proposed, it has become a common electricity network security guarantee method and an important part of the electricity network security guarantee system. For an intrusion detection system, the correct rate of identifying intrusion and the detection speed are two important indicators to evaluate its performance [2]. Anomaly-based intrusion can extract features from incoming and outgoing network packets and system logs waiting for analysis data, and judge whether the samples belong to normal or intrusion according to the features. However, the more features are extracted, the better. Too many features will seriously affect the performance of the intrusion detection system. In fact, many features do not contribute or contribute little to the identification of samples. Cloud environment electricity network security monitoring can monitor the status and behavior of physical

nodes, virtual nodes, software, users, etc. of the cloud, integrate security tools such as firewall, vulnerability detection, intrusion detection, deep packet detection, collect data for fusion analysis, and present the results in a visual form to help administrators or users effectively understand the security status of the cloud and ensure the electricity network security of the cloud environment (as shown in Figure 1).

On this basis, the research on the emerging bee colony algorithm and other technologies has enabled it to adapt to the characteristics of the network and built a basic electricity network security guarantee system, which is of great development significance to improve electricity network security [3].

2. Literature Review

For electricity network security monitoring, George and Ganesan proposed a multi granularity pub/sub mode cloud security monitoring architecture based on communication load prediction. On this basis, a multi granularity pub/sub mode cloud security monitoring architecture PSCSMA based on communication load prediction is proposed, which meets the scalability requirements of the monitoring architecture by dividing the monitoring domain, adopting the publish- or subscribe-based information interaction mode to meet the elastic requirements of the monitoring architecture, and meets the comprehensive requirements of the monitoring architecture through the multi-user characteristics of data collection agent and publish/subscribe mode [4]. Etinkaya, and others proposed a multi-granularity topic adaptive mechanism based on communication load prediction to balance the relationship between timeliness, accuracy, and adaptability of the monitoring architecture [5]. Tefek, and others proposed a method to generate an electricity network security reinforcement policy in cloud environment based on an attack graph. They put forward a risk assessment method that comprehensively considers the attack difficulty, attack consequence severity, path length, and the importance of target nodes. They search through heuristic algorithms to obtain the approximate maximum risk coefficient in the attack graph, avoiding the exponential time complexity problem of accurately searching the attack path [6]. Vajjha and Sushma proposed an electricity network security intrusion detection method in cloud environment based on feature selection. Aiming at the shortcomings of existing feature evaluation methods, a heuristic feature selection algorithm HFS-ACMI based on average conditional mutual information is proposed [7]. Wu and others proposed a regular expression grouping algorithm for efficient deep packet detection in cloud environment. After analyzing the state explosion problem of DFA merging regular expressions, the optimal grouping problem of regular expressions is reduced to the K-MAX cut problem of weighted undirected graphs [8]. Einy, and others proposed a heuristic random search algorithm for iterative optimization. Compared with other algorithms, the random search algorithm can generate a smaller feature subset, and the classifier constructed with this subset has faster detection speed and higher classification accuracy [9].

Therefore, taking into account the shortcomings of existing methods for evaluating traits, we propose an algorithm for selecting heuristic traits based on the bee colony algorithm. The algorithm uses average mutual information to measure the importance of features, and more truly reflects the relationship between the selected features, the selected features, and the classification labels. Aiming at the problem that the algorithm is easy to fall into local optimization, a heuristic random search algorithm is proposed, which iteratively optimizes to generate smaller feature subsets, and improves the speed and accuracy of intrusion detection.

3. Research Methods

3.1. Introduction to Artificial Bee Colony Algorithm. The ABC algorithm uses the location of the nectar source to represent the solution and the number of nectar source dusts to represent the fitness value of the solution [10, 11]. All bees are divided into three groups: working bees, follower bees, and research bees. Worked bees and companion bees make up half of the total bee colony. Mercenary bees are primarily responsible for finding and exchanging honey sources. The following bees are responsible for collecting honey in the hive according to the information provided by the hive bees. Exploration bees are responsible for randomly searching for new sources of honey. Replace the original honey source after leaving the honey source. Like other herd intelligence algorithms, the ABC algorithm is iterative [12]. After initiating a bee colony and nectar source, three processes are repeated to find the optimal solution to the problem: hiring bees, tracking bees, and studying bees. Each step is described as follows.

- (a) Start the herd. To start the parameters of the ABC algorithm, these parameters are the number of nectar sources SN, the number that determines the limit of discarding the nectar source, and the number of iteration ends. In the standard ABC algorithm, the number of nectar sources SN is equal to the number of working bees and the number of following bees. The formula for generating a specific nectar source is as follows:

$$x_{ij} = x_{\min j} + \text{rand}[0, 1](x_{\max j} - x_{\min j}), \quad (1)$$

where x_{ij} represents the j -th dimension value of the i -th honey source x_i , i is taken from $\{1, 2, \dots, sn\}$, and j is taken from $\{1, 2, \dots, d\}$; $x_{\min j}$ and $x_{\max j}$ represent the minimum and maximum values of dimension respectively. To initiate a nectar source, the above formula is used to assign a random value within all dimensional values of each nectar source and randomly generate the first nectar source of SN.

- (b) Employment bee stage. In the stage of employing bees, employing bees use the following formula (2) to find new honey sources:

$$v_{ij} = x_{ij} + \varphi_{ij}(x_{ij} - x_{kj}), \quad (2)$$

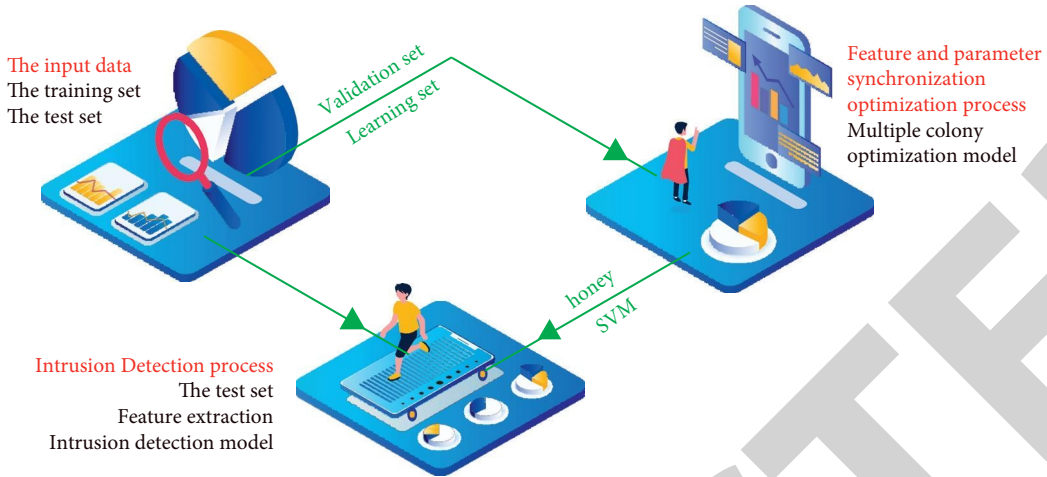


FIGURE 1: Research method of electricity network security monitoring based on bee colony algorithm.

where x_k represents the neighborhood honey source, k is taken from $\{1, 2, \dots, sn\}$, and k is not equal to i ; φ_{ij} is a random number with a value of $[-1, 1]$. After a new honey source is obtained through equation (2), the greedy algorithm is used to compare the fitness values of the old and new honey sources and select the best.

- (c) Follow the bee stage. The bee hiring phase ends and the bee compliance phase begins. At this stage, hired bees share information about the source of nectar on the dance floor. Following the bees will be more likely to analyze the data, control and extract nectar sources using a roulette strategy, and extract nectar sources of high fitness value. Following the bee extraction process is similar to hiring honey, using formula (2) to find a new source of nectar and leave a better adaptive. Nectar has a parametric test. When backing up the nectar update, the line is incremented by 0, otherwise the string is incremented by 1. Thus, the court can count how many times the source of nectar has not been renewed.
- (d) Study the bee stage. If a nectar source has not been updated after many times of mining, and the trail value is too high and exceeds the predetermined threshold limit, then the nectar source needs to be discarded and the exploration bee stage is started. This reflects the negative feedback and volatility properties of self-organization in ABC. At this stage, the bee is randomly looking for a new nectar source to replace the destroyed nectar source using the following equation:

$$x_{ij} = x_{\min j} + \text{rand}[0, 1](x_{\max j} - x_{\min j}). \quad (3)$$

- (a) ABC operation is simple and local search capabilities are weak. GA and DE are hybridized to create a new solution, but ABC is not. ABC's new solution is based solely on the original solution (the old

solution) and is simple to operate, suitable for local search frequency modulation, but it does not allow good information to spread rapidly to a population, leading to each mutation. Because it only changes one dimension of the original solution, and because the range of change is small, ABC's local optimization capabilities are weak and integration speeds are slow, especially in solving constraint policies, complex functions, and integral functions [13].

- (b) ABC has good exploration capabilities. The researcher can jump out of the original solution package and randomly find a new solution that completely replaces the old solution. This function reduces the dependence of the algorithm on the size of the herd and the impact of the initial solution package, ensures herd diversity, and prevents premature mergers, making ABC suitable for high-dimensional and multidimensional problems.
- (c) The ABC parameters are low. In addition to the maximum number of cycles and the size of the population, the ABC algorithm has only one control parameter limit. The limit value, in turn, depends on the size of the population and the size of the problem, such as the limit = $SN \times D$. Finally, ABC has two control parameters: maximum cycle number (MCN) and bee colony number (SN). For the ABC algorithm, the effects of some key parameters on the algorithm's performance are summarized as follows:
 - (a) The performance of ABC is better when the number of initial colonies is more. However, the performance of ABC algorithm will not be improved when the number of bees reaches a certain amount. When the number of the bee colony is 50~100, a better convergence rate can be obtained. ABC algorithm does not need a large number of bees in high-dimensional optimization problems, and is suitable for solving high-dimensional problems [14].

- (b) The limit control parameter of ABC is very important. Its size is inversely proportional to the frequency of the exploratory bees, so as to ensure the diversity of the population. For single-mode functions, the deployment of search bees will not affect the performance of the algorithm, but for multi-mode functions, it can effectively improve the searchability of the algorithm. At the same time, the limit cannot be set too low for small-scale bee colonies, while for large-scale populations, the impact of the limit value will be relatively reduced if the population diversity can be guaranteed. Through experimental analysis, it is concluded that $\text{limit} = \text{Sn} \times D$ is appropriate [15].

3.2. Improved Artificial Bee Colony Algorithm. The artificial bee colony algorithm is a swarm intelligence optimization algorithm proposed in, which is based on the self-organizing simulation model of bee swarm intelligence. It was successfully applied to the numerical optimization of functions at first. The algorithm has the characteristics of simplicity, strong robustness, and strong global search ability.

Artificial bee colony algorithm simulates the real honey collecting behavior of bees by dividing the colony into collecting bees, observing bees, and reconnaissance bees. The position of each honey source (the decision variable of the function to be solved) in the program algorithm represents a feasible solution of the optimization problem, and the quality of the honey source corresponds to the quality of the corresponding feasible solution. Each group of solutions $x_i (i = 1, 2, \dots, d)$ is a dimensional vector (the number of decision variables of the optimization parameters). They are evaluated at the same time when they are generated. Then, honeybees are collected to generate a new honey source location and evaluate it according to the local honey source location information. If it is better than the initially generated honey source, it will be replaced. Otherwise, the original solution will not be changed [16]. In the second step, according to the quality of the honey source, the observation bees are dispatched to select the solution with good quality of the honey source with a high probability through the set "survival of the fittest" mechanism. At the same time, a group of new honey sources is also generated according to the local information disturbance at the honey source. If the quality of the new honey source is better than the old one, it will be replaced, and vice versa. The above two steps, such as collecting bees and observing the continuous circulation of bees, gradually improve the location of the honey source. After several times of selection, if the location of some honey source is still not improved, the reconnaissance bee operation will be carried out, the honey source will be abandoned, a group of substitutes will be found, and the evaluation will be carried out as before. The whole process is executed repeatedly, and the optimal solution of each step is recorded until it stops [17].

Taking the minimum optimization problem as an example, the fitness of the nectar amount of the food source corresponding to the actual solution is the formula:

$$\text{FIT}_i = \begin{cases} \frac{1}{1 + \text{fit}_i}, & \text{fit}_i \geq 0, \\ 1 + \text{abs}(\text{fit}_i), & \text{fit}_i < 0. \end{cases} \quad (4)$$

Among them, the higher the quality of a group of honey sources, the greater the corresponding fitness. The probability of observing a bee selecting a group of honey sources is given by the following formula:

$$P_i = \frac{\text{FIT}_i}{\sum_{i=1}^n \text{FIT}_i}. \quad (5)$$

In the algorithm, roulette is used to realize the "survival of the fittest," so that the higher the fitness of the honey source, the greater the probability of being selected.

After bee collecting judges the advantages and disadvantages of the honey source, a new solution for the neighborhood is generated according to the following formula, and the evaluation is continued, which is given in the following formula:

$$x_{ij} = x_{ij} + \emptyset(x_{ij} - x_{kj}), \quad (6)$$

where \emptyset is a random number $(-1, 1)$, j is $(1, 2, \dots, d)$, and $k(1, 2, \dots, n)$ is randomly selected here, but it must be ensured that $k \neq i$. In this way, the neighborhood of the original honey source is controlled, which can make the honey sources learn from each other and shorten the distance from the optimal solution. With the gradual approximation of the optimal solution, the range of the neighborhood will be gradually reduced, and the step size will be adaptively reduced. If a honey source has not been improved after a limited number of times, give up the position and perform a reconnaissance bee operation, which is given in the following formula:

$$x_i^j = x_{\min}^j + \text{rand}[0, 1](x_{\max}^j - x_{\min}^j). \quad (7)$$

3.3. Modeling Steps of Stepwise Regression Based on Artificial Bee Colony Algorithm

Step 1: establish the dam deformation regression model according to the stepwise regression analysis model, and retain the regression load set variable factor;

Step 2: make the load set coefficient the decision variable of the objective function of the artificial bee colony, and make full use of the stepwise regression results to make the policy variable b randomly assigned in their respective definition domain $(x_{\max}^j - x_{\min}^j)$, so as to reduce the blindness of the initial population and improve the optimization speed and efficiency;

Step 3: according to the actual solution problem, the residual sum of squares is taken as the objective function, which is transformed into the optimization problem of finding the function's extreme value. If

there are s groups of observation samples, the actual displacement is y_i , and the prediction result obtained by the model is \hat{y}_i ; Then the objective function is formula:

$$\min(g) = \sum_{i=1}^s (y_i - \hat{y}_i)^2. \quad (8)$$

Since the large-scale deformation model is a minimization problem and non-negative, it is transformed into individual fitness. The smaller the target value, the higher the fitness and the greater the probability of being selected;

After the new solution is found in Step 4, the relevant statistical indicators of the model are calculated and compared with the original model. This process is repeated until the decision variables obtained from the optimization results reach satisfactory accuracy, as shown in Figure 2.

3.4. Risk Coefficient Measurement Method of Base Attack Path. Security vulnerabilities are common in the network environment, and a large number of new vulnerabilities are discovered every day, but it is often unrealistic to repair all vulnerabilities. The attack graph can well show the correlation between vulnerabilities. Through the analysis of the attack graph, it is a more practical method to select vulnerabilities with high risk and low repair difficulty to repair, so as to make the network environment have a relatively high degree of security as far as possible [18].

In order to obtain the electricity network security reinforcement strategy, we first need to know what possible attack paths the attacker has. In the attack graph, the algorithm of searching all attack paths has unavoidable exponential time complexity, and can not be applied to large-scale network environments [19]. A more practical method is to evaluate the risk of attack paths, search for attack paths that are more likely to be attacked, and block them in advance to ensure the relative security of the network.

In order to measure the attacker's willingness to attack on different attack paths, it is necessary to evaluate the severity of all vulnerabilities on the attack path. To solve this problem, CVSS will give a base score for each known vulnerability. The score is calculated by such indicators as an access method, attack complexity, authentication, confidentiality impact, integrity impact, and effectiveness impact. The higher the vulnerability risk, the higher the score. The value range is [0,10]. It can be seen that, as a general vulnerability scoring standard, the CVSS basic score comprehensively considers the attack difficulty and the severity of the consequences, which can better reflect the attacker's willingness to attack different vulnerabilities [20]. Therefore, the CVSS basic score is used as a reference to explain the calculation method of the attack path risk coefficient. In the process of attackers' multi-step attack on the network, each step of the attack corresponds to a security vulnerability. For any atomic attack a , let $r(a)$ be the risk factor of atomic attack a , then the formula can be given as:

$$r(a) = \frac{\text{CVSSBase score}(a)}{10}. \quad (9)$$

For any attack path l , $r(l)$ is the risk factor of the attack path, which is defined as the product of the risk factors of all exploits on l , then formula can be given as:

$$r(l) = \prod_{a \in l} r(a). \quad (10)$$

The risk coefficient of the attack path reflects the relative degree of the willingness of the attacker to choose the path, which provides a basis for evaluating the threat degree of the attack path.

4. Result Analysis

To verify and illustrate the effectiveness of the proposed method, a simple example network is built, as shown in Figure 3.

A network is a general office network that consists of three servers: a file server (FS), a database server (DB), and a web server (WS). The three servers are connected to the Internet via a loose firewall, making FS easily accessible to anyone with user privileges, and DB and WS are key nodes. For convenience, we call FS Host 0, DB Host 1, and WS Host 2. Network vulnerabilities are shown in Table 1.

Before using the proposed method, the attack graph should be constructed first. Since the research focus of this study is to put forward the network security reinforcement strategy through the analysis of the attack graph, the manual method is used here to build the attribute attack graph AG of the network. The key attributes in the attack graph AG are root (1) and root (2). First, add the subsequent atomic attack a_1, a_2 , $r(a_1) = r(a_2) = 1$ for root (1) and root (2) respectively, and then add a common result attribute v_k for a_1, a_2 , which turns the problem into finding the maximum risk coefficient attack path of attribute v_k in the AG. The number of iterations of the ant colony (as) algorithm T50, the number of ants $k = 4$, $\omega = 2$, and other parameter settings refer to the common settings of the ASrank model, as shown in Table 2. Where w^g is the solution constructed by greedy algorithm, and m is the number of steps of the solution.

After calculation, the maximum risk factor attack path L_{\max} in AG is (sshd BOF (1) \rightarrow a_1), and the risk factor $r_{\max} = 0.9$. Experiments show that the proposed method can effectively evaluate the risk of attack path.

Based on the above discussion, 10 groups of data are used to compare the performance of the bee colony algorithm and the weighted-greedy (WG) algorithm. Each group of data includes the number of sets m , the number of elements n , the cost of each element W_j , the elements contained in each set and the optimal solution of each group of problems [21, 22]. For 10 groups of data, WG algorithm and bee colony algorithm are used to solve them respectively. The parameters of the bee colony algorithm are set as follows: the number of iterations t is set to 100, $\alpha = 1$, $\beta = 2$, $\rho = 0.5$, $Q = 1$, $\tau_0 = w^g/m$, the result is shown in Figure 4.

Figure 4 shows the average time that the two algorithms run on each set of data. WG algorithm takes less than 1

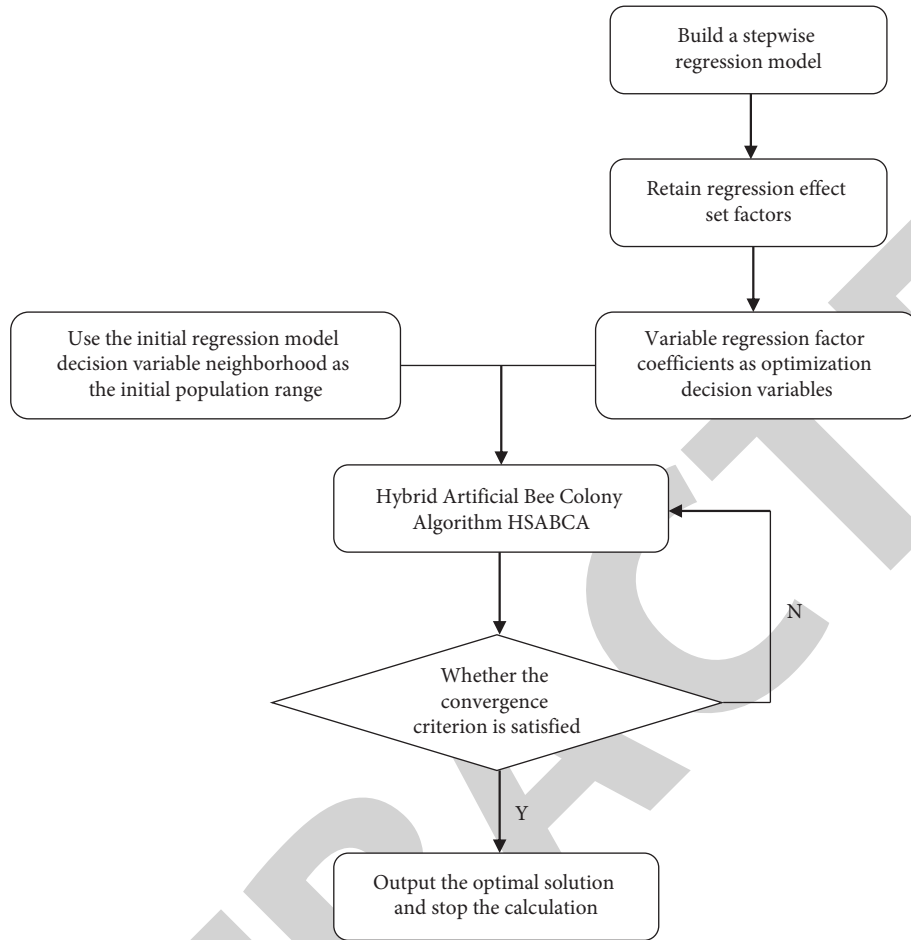


FIGURE 2: Bee colony algorithm model.

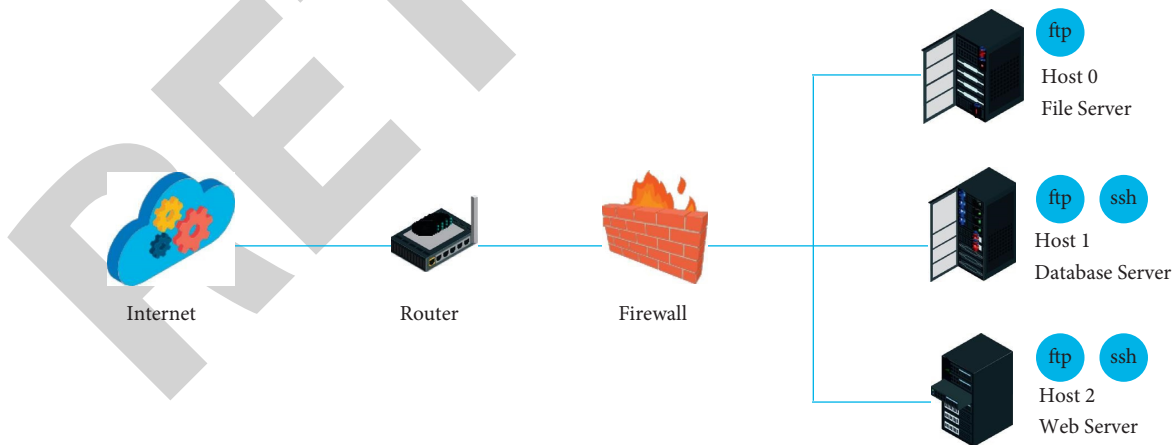


FIGURE 3: Example system.

second, which is obviously less than the bee colony algorithm. Although the running time of the bee colony algorithm is long, it is still within a reasonable range. Combined with the previous experimental results, the results calculated by the WG algorithm are not ideal. In practical application, the reinforcement strategy given by the WG algorithm will

cause greater repair costs to users, and the result of the bee colony algorithm is closer to the optimal solution, which can effectively reduce the required security reinforcement cost and obtain a better reinforcement strategy and better security guarantee in the case of limited resources. For an actual network, the time required to generate the security

TABLE 1: Vulnerabilities in the network.

CVE	Access	Protocol	CVss score	Host
CVE2012-2999	Remote	Ftp	6.8	1.2
CVE2008-3234	Remote	Ssh	6.5	1
CVE2004-1161	Remote	Ssh	7.5	2
CVE2013-4512	Local		4.7	1.2
CVE2008-6899	Remote	Ssh	9.0	1

TABLE 2: ASrank model settings.

a	β	ρ	τ_0	Q
1	2	0.5	w^g/m	1

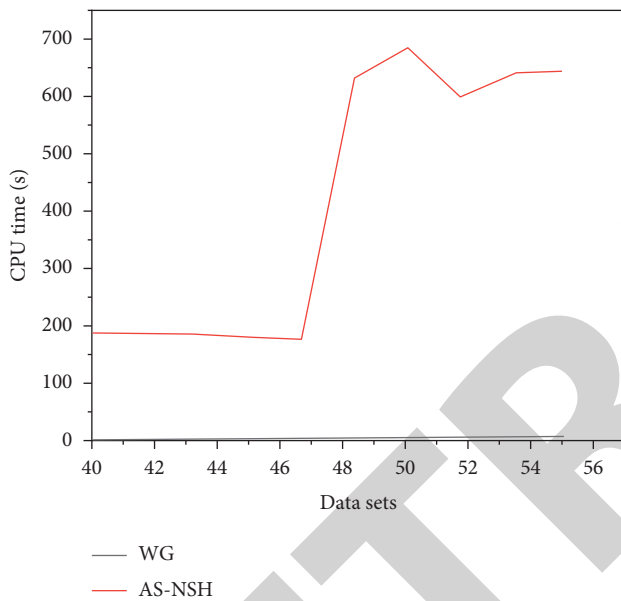


FIGURE 4: CPU running time of various algorithms under different scale attacks.

reinforcement strategy is only within a reasonable range. It is obviously more practical to be able to calculate a better solution and save the repair cost for users as much as possible. Therefore, for the network security reinforcement of a large-scale network environment, the bee colony algorithm has greater practical application value.

5. Conclusion

This article proposes an algorithm for selecting heuristic traits based on the bee colony algorithm. The algorithm uses average mutual information to measure the importance of features, and more truly reflects the relationship between the selected features, the selected features, and the classification labels. Focusing on the fact that the algorithm is easily accessible to local optimization, it offers a heuristic random search algorithm that seeks to generate subgroups of iterative functions over and over again, improving the speed and accuracy of attack detection. Combined with the

approximate maximum risk coefficient, network scale, network nature and actual demand, the danger threshold is set, the search process is limited to the threshold of danger to reduce the complexity of the algorithm. Experimental results show that this method is highly scalable and can be used in large network environments. Compared with the existing methods, it can effectively obtain attack paths that are more in line with the real threat situation in an acceptable time. On the selected experimental data set, compared with the traditional algorithm, this method reduces the gap between the generation strategy and the optimal strategy by 71.3% and enhances the practicability of the attack graph analysis method in large-scale network environments.

Data Availability

The data used to support the findings of this study are available from the corresponding author upon request.

Conflicts of Interest

The authors declare that they have no conflicts of interest.

Acknowledgments

This work was supported by (1) Training Program for Young Backbone Teachers in Colleges and Universities of Henan Province, 2020YB0655, Research on quality monitoring and evaluation of Teachers Quality Improvement Program in Higher Vocational Colleges; (2) Training Plan for Young Backbone Teachers in Colleges and Universities of Henan Province, 2018GGJS259, Development of Lingfang Yuncheng Platform Based on VUE; (3) Project of Jiyuan Vocational and Technical College, JYZY-2021-95, Construction and Research of College Network Space Security Experience Platform; and (4) 2022 Humanities and Social Science Research Project of Universities in Henan Province, 2022-ZDJH-00152, Research on Red Culture Network Communication.

References

- [1] X. Liu, J. Liang, D. Y. Liu, R. Chen, and S. M. Yuan, "Weapon-target assignment in unreliable peer-to-peer architecture based on adapted artificial bee colony algorithm," *Frontiers of Computer Science*, vol. 16, no. 1, Article ID 161103, 2022.
- [2] X. Zong, A. Liu, C. Wang, Z. Ye, and J. Du, "Indoor evacuation model based on visual-guidance artificial bee colony algorithm," *Building Simulation*, vol. 15, no. 4, pp. 645–658, 2022.
- [3] P. Lakshminarayana and T. V. Sureshkumar, "Automatic generation and optimization of test case using hybrid cuckoo search and bee colony algorithm," *Journal of Intelligent Systems*, vol. 30, no. 1, pp. 59–72, 2020.
- [4] T. George and V. Ganesan, "An effective technique for tuning the time delay system with pid controller-ant lion optimizer algorithm with ann technique," *International Journal of COMADEM*, vol. 23, no. 1, pp. 39–48, 2020.
- [5] M. B. Etinkaya and H. Duran, "A detailed and comparative work for retinal vessel segmentation based on the most

Retraction

Retracted: High Efficiency Compound Vacuum Oil Gas Separation Technology Based on Integrated Oil Filter of Ultra-High Voltage Transformer

International Transactions on Electrical Energy Systems

Received 19 September 2023; Accepted 19 September 2023; Published 20 September 2023

Copyright © 2023 International Transactions on Electrical Energy Systems. This is an open access article distributed under the Creative Commons Attribution License, which permits unrestricted use, distribution, and reproduction in any medium, provided the original work is properly cited.

This article has been retracted by Hindawi following an investigation undertaken by the publisher [1]. This investigation has uncovered evidence of one or more of the following indicators of systematic manipulation of the publication process:

- (1) Discrepancies in scope
- (2) Discrepancies in the description of the research reported
- (3) Discrepancies between the availability of data and the research described
- (4) Inappropriate citations
- (5) Incoherent, meaningless and/or irrelevant content included in the article
- (6) Peer-review manipulation

The presence of these indicators undermines our confidence in the integrity of the article's content and we cannot, therefore, vouch for its reliability. Please note that this notice is intended solely to alert readers that the content of this article is unreliable. We have not investigated whether authors were aware of or involved in the systematic manipulation of the publication process.

Wiley and Hindawi regrets that the usual quality checks did not identify these issues before publication and have since put additional measures in place to safeguard research integrity.

We wish to credit our own Research Integrity and Research Publishing teams and anonymous and named external researchers and research integrity experts for contributing to this investigation.

The corresponding author, as the representative of all authors, has been given the opportunity to register their agreement or disagreement to this retraction. We have kept a record of any response received.

References

- [1] J. Guan, X. Hu, H. Liu, and Y. Yang, "High Efficiency Compound Vacuum Oil Gas Separation Technology Based on Integrated Oil Filter of Ultra-High Voltage Transformer," *International Transactions on Electrical Energy Systems*, vol. 2022, Article ID 9989686, 6 pages, 2022.

Research Article

High Efficiency Compound Vacuum Oil Gas Separation Technology Based on Integrated Oil Filter of Ultra-High Voltage Transformer

Jin Guan ¹, Xuechao Hu ^{1,2}, Huan Liu ¹, and Yaoguo Yang ¹

¹Inner Mongolia Power (Group)Co., Ltd, Inner Mongolia Power Research Institute Branch, Hohhot 010000, Inner Mongolia Autonomous Region, China

²Inner Mongolia Enterprise Key Laboratory of High Voltage and Insulation Technology, Hohhot 010000, Inner Mongolia Autonomous Region, China

Correspondence should be addressed to Jin Guan; 1764300103@e.gzhu.edu.cn

Received 28 July 2022; Revised 12 August 2022; Accepted 23 August 2022; Published 7 September 2022

Academic Editor: Nagamalai Vasimalai

Copyright © 2022 Jin Guan et al. This is an open access article distributed under the Creative Commons Attribution License, which permits unrestricted use, distribution, and reproduction in any medium, provided the original work is properly cited.

In order to improve the filtering effect of vacuum oil purifier, the author proposes the research and application of high-efficiency compound vacuum oil-gas separation technology based on electric ultra-high voltage transformer integrated oil purifier. The author studies under the condition of constant oil temperature and flow rate, the effect of vacuum degree on the filtering effect of transformer oil vacuum oil filter. Using the research results, a frequency conversion automatic vacuum oil filter is designed, which makes the processing process have the characteristics of simple operation, high degree of automation, and high work efficiency. The test results show that if the transformer oil processed by the variable frequency automatic vacuum oil purifier is new oil, its water content is less than 45 mg/kg and the gas content is less than 12%; when the breakdown voltage is greater than 25 kV, the transformer oil index can meet the following requirements after the equipment is filtered for one cycle: breakdown voltage ≥ 75 kV; water content ≤ 5 mg/kg; and gas content $\leq 0.1\%$ (volume ratio). After one cycle (after 100 min), the variable frequency automatic (three-stage) vacuum oil filter can greatly shorten the time of transformer oil circulating and filtering. *Conclusion.* The designed frequency conversion automatic vacuum oil purifier is obviously better than other transformer oil vacuum oil purifiers.

1. Introduction

Transformer is important equipment in the power system, mainly used to change the voltage of alternating current and reduce losses during power transmission. According to different cooling methods, transformers can be divided into dry-type transformers and oil-immersed transformers. Dry-type transformers are small in size and clean in technology, and they are often used in indoor environments with high requirements for fire and explosion protection; oil-immersed transformers have large capacity, good heat dissipation, low price, and are more widely used, especially in occasions with high requirements on capacity and load [1]. Transformer oil is used as a medium for insulation and heat dissipation, and its quality will directly affect the safety and

reliability of the transformer. The impurity content is usually required to be kept at a low level to avoid corrosion of fuel tanks, wires, and insulating materials. However, during the long-term operation of the transformer, it is affected by electrical, chemical, and environmental factors, and some performance indicators of the pressure converter oil may not meet the requirements for safe operation. The traditional practice is regular manual inspections and preventive testing (Figure 1). In addition to making judgments and discovering abnormalities based on the appearance, sound, temperature, and instrument values of the equipment, the inspectors also need to conduct preventive offline (power failure) inspections on the transformers on a regular basis and filter the transformer oil that does not meet the requirements of safe operation to make the technical indicators of the

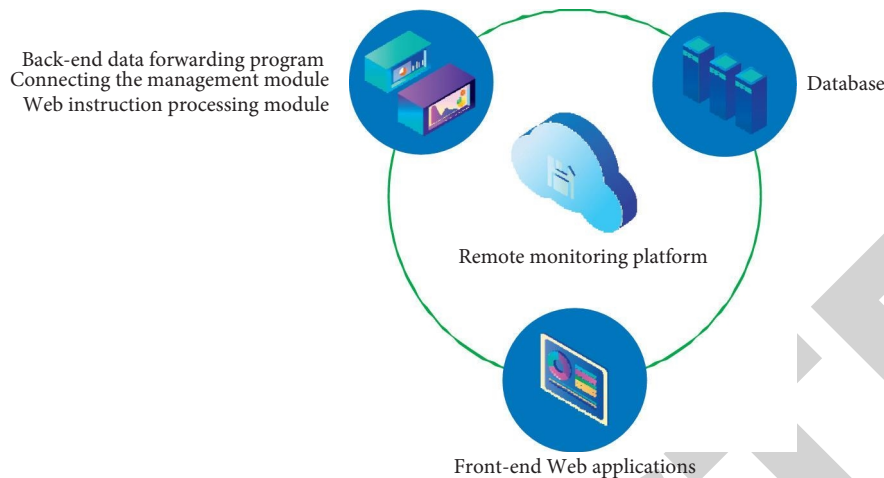


FIGURE 1: Technical route.

transformer oil return to normal [2]. Over the years, a certain proportion of transformer failures have been caused by excessive impurities in the oil. At the same time, the transformer is damp due to the aging of the seal, that is, the moisture in the transformer oil increases, which has a great impact on the electrical performance of the transformer oil, thus threatening the safe operation of ultra-high voltage transformers.

2. Literature Review

Cai et al. proposed a new filtering method, according to the mechanism of bionic glomerular filtration, the bioelectric field in the kidney-type filtration process is replaced by the “low-energy heterogeneous isoelectric field,” and the rubber-plastic composite biomaterial with variable pore size is used, it replaces glomerular filtration [3]. A high-efficiency HEP100S three-stage transformer oil vacuum oil filter was proposed by Sato et al. The oil purifier adopts three vacuum pumps, and its biggest advantages are high vacuum rate, high filtration precision, and high purification efficiency, and the transformer body can be evacuated while the transformer oil of the ultra-high voltage equipment is vacuum filtered [4]. Sharma and Chaurasia used gas chromatography to analyze the components of dissolved gases in transformer insulating oil and designed a computer fault diagnosis program: the program simplifies the calculation procedures of the chromatographic result processing and improves the reliability and accuracy of data processing and diagnosis [5]. However, due to the analysis of a single gas, and as the three-ratio method is used in the analysis process, the diagnostic error is large. Selva et al. used the neural network method to establish a prediction model for the parameters of transformer oil, such as flash point, water-soluble acid, acid value, breakdown voltage, and moisture and dissolved gas of oil, as it provides a strong basis for fault diagnosis and elimination, and the diagnostic error is further reduced, and the accuracy is high, which can ensure the safe and economical operation of the transformer [6]. Huang et al., based on

neural network theory and fuzzy theory, expounded the blackboard expert system for transformer oil and gas diagnosis, and this type of object-oriented technology reflects the characteristics of an expert system, that is, it is flexible and has outstanding performance; through the application of fuzzy theory, it can not only solve the problems existing in the process of diagnosing faults such as fuzziness, but also at the same time, based on neural network functions, modes, etc., the system as a whole has higher fault diagnosis accuracy. The problems faced in the single-method diagnosis process are thus effectively overcome, making the diagnosis of transformer insulation more accurate [7].

The author purifies the transformer oil and effectively filters out the solid particles, water, gas, etc., in it, so as to ensure the safe operation of the power grid. The degree of vacuum and the temperature of the oil are key factors in the effectiveness of oil treatment. A large number of secondary vacuum oil purifiers in operation have poor vacuum lifting capacity, and there are likely to be traces of acetylene and other impurities in the treated transformer oil, resulting in low efficiency. A three-stage vacuum oil filter with large flow rate and frequency conversion control is developed, which can adapt to UHV equipment [8].

3. Research Methods

3.1. Overall Structure Design of Vacuum Oil Filter. The vacuum oil filter is mainly composed of heating, filtering, and vacuum systems. Its working principle is as follows: under the vacuum state, due to different saturated vapor pressures of oil and water, the water in the transformer oil vaporizes and evaporates and is pumped into the atmosphere by the vacuum pump, and the water can be separated from the oil and the composition is stable. The research design strives to achieve the best matching state of vacuum and temperature.

The frequency conversion automatic vacuum oil purifier adopts a three-stage vacuum unit, which is composed of a frame, an imported pump, a heater, a filter, a vacuum system, an electrical control system, and an outlet pump.

3.1.1. Three-Stage Vacuum System Structure. The principle of frequency conversion automatic vacuum oil purifier is the following: the vacuum pump group is composed of 2 Roots pumps (008, 009) and 1 mechanical vacuum pump (010) in series, 2 frequency conversion motors control oil intake and oil discharge, and multiple switching commands of the oil level in the vacuum separation chamber control the speed of the motor [9]. The working process is as follows: after the transformer oil is filtered by the coarse filter (001), it is sent to the oil filter system under the drive of the oil inlet pump (002), then it enters the vacuum separation chamber (005) to separate the gas contained in the transformer oil, and the water contained in it is vaporized and evaporated by the Roots pump (008, 009) and the mechanical vacuum pump (010). The degassed and dehydrated transformer oil is sent to the fine filter (013) with a filtration accuracy of $0.5 \mu\text{m}$ by the oil outlet pump (012) and then enters the power transformer. When the isolation valve (006) is closed, the mechanical vacuum pump (010) and the Roots pump (008, 009) are started. In addition, as an auxiliary function, the independent vacuum circuit (007) can be used to directly vacuum the transformer body and the airtight container.

3.1.2. Vacuum System Design. The speed of evaporation and dissipation of the moisture in the transformer oil in the vacuum separation chamber determines the dehydration efficiency of the oil filter, the heated transformer oil circulates from the top of the vacuum separation chamber to the bottom by gravity, in this free fall state, and the moisture and gas in the oil escape and are quickly pumped into the atmosphere by the vacuum pump [10]. The main feature of the vacuum system of variable frequency automatic vacuum oil purifier is that in addition to the professional functions of water, gas, and particles, it can also vacuum the transformer body and airtight container and dry the windings of the transformer.

In addition to the pumping capacity of the vacuum pump itself, the vacuum degree of the vacuum separation chamber is also affected by the resistance of the pipeline to the gas.

(1) Three-Stage Vacuum System Design. Evacuate the 500 kV transformer body with a volume of 40 m^3 , from atmospheric pressure ($1.013 \times 10^5 \text{ Pa}$) to working pressure (133 Pa), and the ultimate pressure of the transformer body is kept less than 80 Pa, while the general vacuum system takes about 75 minutes to evacuate. In order to improve the efficiency, the three-stage vacuum system is designed to take less than 40 minutes to evacuate.

In order to improve the vacuuming efficiency of the vacuum unit, the high-efficiency vacuum system scheme is designed as follows: 2-stage Roots pump + 1-stage mechanical vacuum pump are connected in series, and the three-stage vacuum unit formed is used as the pumping system.

The calculation of vacuum pump selection includes the following steps: (1) according to the analogy method, choose Roots pump 008 as the main pump, and the pumping rate

$S_z = 0.278 \text{ m}^3/\text{s}$; (2) calculate the effective pumping rate $S_e = [1/4 \sim 1/2] S_z$ of Roots pump 009, pumping rate $S_z = 0.139 \text{ m}^3/\text{s}$; and (3) select mechanical vacuum pump 010 as the backing pump, and the effective pumping rate needs to be selected with reference to the multiple of Roots pump 008. Its effective pumping rate $S_q = [1/8 \sim 1/4] S_z$ and effective pumping rate $S_q = 0.056 \text{ m}^3/\text{s}$. The pumping capacity of the 500 kV transformer body vacuum pumping test is verified, and the test results are shown in Table 1.

(2) Calculate the Pumping Time of the Three-Stage Vacuum System. The pumping time is calculated as formula (1) by ignoring other influencing factors such as air leakage, pipeline, and pipeline accessories:

$$t = 2.3K_q \cdot \frac{V}{S} \cdot \lg \frac{P_i}{P}, \quad (1)$$

where t is the pumping time, s; K_q is the correction coefficient, which is related to the pressure P when the vacuum pump is exhausted (as shown in Table 2); S is the nominal pumping rate of the vacuum pump, m^3/s ; V is the volume of vacuum separation chamber, m^3 ; P is the pressure after pumping at time t , Pa; and P_i is the pressure at the beginning of the vacuum pump pumping, Pa.

The startup conditions of the vacuum pumps at all levels are different during prepumping, and the startup sequence is as follows: first start the mechanical vacuum pump (010) at normal pressure, that is, at standard atmospheric pressure; when the vacuum sensor detects that the vacuum degree in the vacuum separation chamber (005) reaches a certain value, the Roots pump (009) is started in sequence; and when the vacuum sensor detects that the vacuum degree in the vacuum separation chamber (005) increases to a certain value, start the Roots pump (008) until the vacuum degree in the vacuum separation chamber (005) reaches the set operating value [11, 12]. In the above three pumping stages, the effective pumping rates of the vacuum units are different, and the prepumping time needs to be calculated in segments, the total pumping time is composed of the sum of the three pumping times, and the time is shown in Table 3.

It can be seen from Table 3 that the total pumping time is 1 955.7 s, about 33 min. Calculations show that the pumping capacity of the three-stage vacuum unit exceeds that of the two-stage vacuum unit commonly used in the market, can meet and exceed the technical requirements, and greatly improve the working efficiency of the vacuum oil filter [13].

(3) Design Heating Power. In order to ensure the efficiency of the oil purifier, the power calculation of the heater is very important, according to the characteristics of the oil purifier and the operating environment, the empirical temperature rise can be $6^\circ\text{C}/\text{h}$ in the initial design, and 100 min is a working cycle. Set the temperature rise Δt of the transformer oil to 10°C .

Transformer oil is incompressible during repurification. Considering the constant volume thermal system during

TABLE 1: Performance index of vacuum pump (cooled by air cooling).

Project	Nominal pumping rate (m ³ ·s ⁻¹)	Maximum differential pressure (Pa)	Ultimate vacuum (Pa)	Motor power (kW)
Roots pump 008	0.556	5200	5 × 10 ⁻¹	5.5
Roots pump 009	0.278	5200	5 × 10 ⁻¹	4
Vacuum pump 010	0.084	Straight to the atmosphere	10	4

TABLE 2: Correction factors.

Correction factor	1.0~0.1	10 ¹ ~1.0	1.0 × 10 ² ~10 ¹	1.0 × 10 ³ ~1.0 × 10 ²	1.0 × 10 ⁴ ~1.0 × 10 ³	1.0 × 10 ⁵ ~1.0 × 10 ⁴
K _q	6	4	2.25	1.75	1.5	1.25

TABLE 3: Air extraction schedule for each stage (cooling by air cooling).

Project	Vacuum separation chamber volume (m ³)	Pumping rate (m ³ ·s ⁻¹)	Pressure at the start of vacuum pump evacuation (Pa)	Pressure after pumping (Pa)	Correction factor (kW)	Pumping time (s)
Mechanical vacuum pump 010	40	0.084	1 × 10 ⁵	7 × 10 ³	1.5	1 590.4
Roots pump 008	40	0.556	4 × 10 ³	1 × 10 ²	1.75	289.9
Roots pump 009	40	0.278	7 × 10 ³	4 × 10 ³	4	75.4
Total pumping time						1955.7

treatment, the heat q absorbed by 1 kg of transformer oil processed by an automatic vacuum oil purifier is expressed as the following formula:

$$q = \eta \cdot \frac{P}{(\rho Q)} = C_v \Delta t, \quad (2)$$

where η is the thermal efficiency which is taken as 0.45 in the calculation (considering that the heat loss during the oil filtering process is relatively large); P is the heating power, kW; Q is the work flow, m³/s, and the value is 0.002 498; ρ is the transformer oil density, kg/m³, which is 895; C_v is the specific heat capacity of the transformer oil constant volume, J/kg; K , the value is 2.15; and Δt is the temperature rise of the transformer oil treated by the oil filter in one cycle which is taken as 10°C.

According to formula (2), we can get the following: $P = (C_v \Delta t \rho Q) / \eta = (2.15 \times 10 \times 895 \times 0.002 498) / 0.45 = 120.15$ kW, so the power of the heater is 120 kW.

(4) *Operation Control of Frequency Conversion Automatic Vacuum Oil Purifier.* The use of frequency converter speed regulation technology is a key factor for high-quality vacuum oil purifiers, which can avoid damage to the oil inlet pump (002) or the oil supply solenoid valve (004) due to frequent opening and stopping [14]. The use of inverter power supply can weaken the starting and impact of the three-stage vacuum oil purifier, which can gradually increase the output voltage and frequency of the motor, so the starting current and impact of the motor are relatively small; thus, ensuring the performance and stability of the equipment.

The heaters are divided into three groups, temperature adjustment and control sensors are installed on the three groups of independent heaters, and make sure that the temperature of the transformer oil being processed is kept constant at around 60°C. The heater adopts fuzzy control theory, uses temperature sensor, and realizes dual control of vacuum oil purifier through fuzzy mathematical operation [15].

The circuit is equipped with the functions of interruption, overcurrent, and overtemperature alarm and protection and integrates precision filtration with high-efficiency dehydration and degassing as much as possible.

4. Analysis of Results

4.1. Test Method. Use the transformation project to carry out the necessary tests, and the transformer oil to be treated is 15 t, which is filtered by a three-stage transformer oil vacuum oil filter with a flow rate of 150 L/min, before vacuum filtering the oil, the method of adding evenly stirred pure water to the oil in the oil tank [16]. In the actual operation process, the detection instruments and detection methods are limited; in this test, the water content in the transformer oil was tracked and detected for 2 hours continuously, and the time interval was 10 minutes, and then sampling was carried out. The technical parameters of the transformer oil before treatment are shown in Table 4.

4.2. Test Items. Breakdown voltage: it is a very important indicator to test the ultimate electrical stress resistance of the transformer.

TABLE 4: Technical parameters of transformer oil before treatment.

Technical parameters before filtering	Flow/ $\text{m}^3 \cdot \text{h}^{-1}$	Water content/ $\text{mg} \cdot \text{kg}^{-1}$	Gas content/%	Initial oil temperature/ $^{\circ}\text{C}$	Dielectric strength/kV	Ambient temperature/ $^{\circ}\text{C}$
Transformer oil	9 000	48	12.05	38.4	29	24.7

TABLE 5: Test results of frequency conversion automatic (three-stage) vacuum oil filter.

Project	Working vacuum/ Pa	Breakdown voltage/ kV	Air content (volume)/%	Water content/ $\text{mg} \cdot \text{kg}^{-1}$	Ambient temperature/ $^{\circ}\text{C}$
Automatic (three-stage) vacuum oil filter	9.7	76	0.045	2.8	26

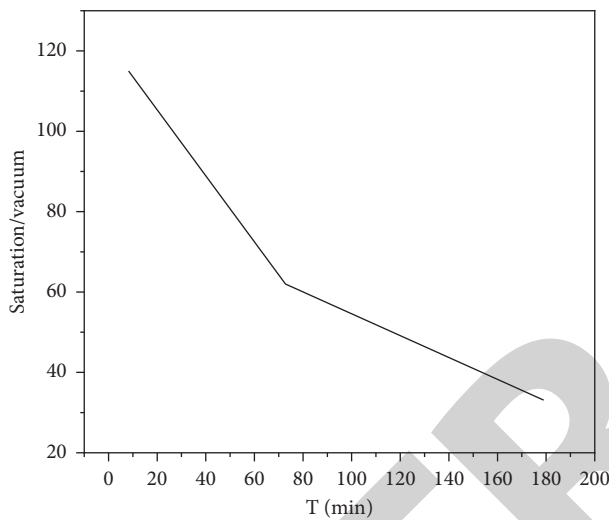


FIGURE 2: Vacuum degree and saturation curve of the variable frequency automatic vacuum oil filter.

Gas content: it is mainly used to analyze the causes of transformer failures, it can detect specific gases such as CO and CO₂ in the oil, and the dissolved gas content in the transformer oil is strictly monitored and controlled.

Water content: China's power industry stipulates that the water content in transformer oil should be less than 10 mg/kg.

If the transformer oil processed by the variable frequency automatic vacuum oil purifier is new oil, its water content is less than 45 mg/kg, the gas content is less than 12%, and the breakdown voltage is greater than 25 kV, after using the equipment for one cycle of filtration, and the transformer oil index can meet the following index requirements: breakdown voltage ≥ 75 kV; water content ≤ 5 mg/kg; and gas content $\leq 0.1\%$ (volume ratio) [17, 18].

In order to test and check the operation effect of the variable frequency automatic vacuum oil filter, firstly turn on the heater, ensure the temperature of the oil entering the vacuum separation tower, record the test data, and draw the vacuum degree and saturation curve of the three-stage vacuum oil filter (as shown in Figure 2).

It can be seen from Figure 2 that with the increase of the vacuum degree of the vacuum oil filter, the saturation of

water in the oil is significantly reduced, after 100 min (1 cycle) treatment, and the test results of the oil filter are shown in Table 5 [19, 20].

5. Conclusion

The test results show that, in one cycle (after 100 min), the variable frequency automatic (three-stage) vacuum oil purifier can greatly shorten the time of circulating and filtering transformer oil; the work efficiency is improved; the cycle of the whole project is shortened; it can meet the requirements of ultra-high voltage transformer oil treatment in China; and the treatment efficiency is improved, the equipment has high practicability and promotion value, and the market prospect is optimistic.

Data Availability

The data used to support the findings of this study are available from the corresponding author upon request.

Conflicts of Interest

The authors declare that they have no conflicts of interest.

References

- [1] J. Wang and Y. Xiong, "Research and application of high-density cementing slurry technology under the condition of oil-based drilling fluid in salt formation," *Arabian Journal for Science and Engineering*, vol. 47, no. 6, pp. 7069–7079, 2022.
- [2] S. Khodabakhshi, M. Taddei, J. A. Rudd, M. J. Mcpherson, and E. Andreoli, "Interplay between oxygen doping and ultramicroporosity improves the CO₂/N₂ separation performance of carbons derived from aromatic polycarboxylates," *Carbon*, vol. 173, no. 23, pp. 989–1002, 2021.
- [3] Z. Cai, S. Wang, Y. Wei, and Y. Wang, "Research and application status of VSP wavefields," *Geophysical Prospecting for Petroleum*, vol. 60, no. 1, pp. 81–91, 2022.
- [4] H. Sato, K. Takimoto, M. Kato, S. i Nagaoka, K. Tamura, and A. Yamagishi, "Real-time monitoring of low pressure oxygen molecules over wide temperature range: feasibility of ultrathin hybrid films of iridium(iii) complexes and clay nanosheets," *Bulletin of the Chemical Society of Japan*, vol. 93, no. 2, pp. 194–199, 2020.

Retraction

Retracted: On-Load Electromagnetic Compatibility Test and Simulation Closed-Loop of the Electric Drive System of New Energy Vehicles

International Transactions on Electrical Energy Systems

Received 19 September 2023; Accepted 19 September 2023; Published 20 September 2023

Copyright © 2023 International Transactions on Electrical Energy Systems. This is an open access article distributed under the Creative Commons Attribution License, which permits unrestricted use, distribution, and reproduction in any medium, provided the original work is properly cited.

This article has been retracted by Hindawi following an investigation undertaken by the publisher [1]. This investigation has uncovered evidence of one or more of the following indicators of systematic manipulation of the publication process:

- (1) Discrepancies in scope
- (2) Discrepancies in the description of the research reported
- (3) Discrepancies between the availability of data and the research described
- (4) Inappropriate citations
- (5) Incoherent, meaningless and/or irrelevant content included in the article
- (6) Peer-review manipulation

The presence of these indicators undermines our confidence in the integrity of the article's content and we cannot, therefore, vouch for its reliability. Please note that this notice is intended solely to alert readers that the content of this article is unreliable. We have not investigated whether authors were aware of or involved in the systematic manipulation of the publication process.

Wiley and Hindawi regrets that the usual quality checks did not identify these issues before publication and have since put additional measures in place to safeguard research integrity.

We wish to credit our own Research Integrity and Research Publishing teams and anonymous and named external researchers and research integrity experts for contributing to this investigation.

The corresponding author, as the representative of all authors, has been given the opportunity to register their agreement or disagreement to this retraction. We have kept a record of any response received.

References

- [1] X. Luo, W. Liu, and J. Li, "On-Load Electromagnetic Compatibility Test and Simulation Closed-Loop of the Electric Drive System of New Energy Vehicles," *International Transactions on Electrical Energy Systems*, vol. 2022, Article ID 9256401, 6 pages, 2022.

Research Article

On-Load Electromagnetic Compatibility Test and Simulation Closed-Loop of the Electric Drive System of New Energy Vehicles

Xinwen Luo , Weize Liu , and Jingpu Li 

Hebei Vocational University of Technology and Engineering, Xingtai, Hebei 054035, China

Correspondence should be addressed to Xinwen Luo; 20160839@ayit.edu.cn

Received 29 July 2022; Revised 12 August 2022; Accepted 23 August 2022; Published 7 September 2022

Academic Editor: Nagamalai Vasimalai

Copyright © 2022 Xinwen Luo et al. This is an open access article distributed under the Creative Commons Attribution License, which permits unrestricted use, distribution, and reproduction in any medium, provided the original work is properly cited.

In order to solve the problem of high-amplitude and high-frequency interference generated by the electric drive system of new energy vehicles, the author proposes a closed-loop research method for on-load electromagnetic compatibility testing and simulation for electric drive systems of new energy vehicles. The method includes EMC design of the electric drive system on-load test equipment, establishment of a conducted EMI simulation platform for the electric drive system under load conditions, and optimization of the conducted EMI performance of the electric drive system based on key parameters and PWM control. Experimental results show that if the parasitic inductance of the IGBT gate increases, the conducted emission level in the frequency range of 2~30 MHz will increase, and there is basically no change at the low frequency, and the position of each resonance point shifts to the relatively low frequency. The experiment was replaced with the DPWM3 modulation mode, and the conducted emission amplitude was reduced by about 2 dB μ V in the range of 200 kHz~2 MHz, and there was basically no change on the whole. *Conclusion.* It is proved that the electromagnetic compatibility closed-loop development technology of the electric drive system of new energy vehicles under load conditions can meet the development needs of new energy vehicles in the environment where energy problems and air pollution problems are becoming more and more serious.

1. Introduction

With the increasingly prominent problems of energy and air pollution, the research and development of new energy vehicles has great practical significance. Vigorously developing new energy vehicles is the only way for my country to transform from a big automobile country to a powerful automobile country, and at the same time, it is also an important measure to deal with climate problems and promote green and low-carbon development [1]. Highly autonomous vehicles realize commercial applications in limited areas and specific scenarios. New energy vehicles have added many power electronic devices, and the electric drive system as the main power source has the characteristics of high power, high voltage, high current, and high switching frequency, as shown in Figure 1. These devices will cause electromagnetic interference to other electrical systems and equipment during operation, the electromagnetic compatibility problem of new energy vehicles is becoming more and

more serious, which greatly limits the development of new energy vehicles [2]. Automotive electromagnetic compatibility refers to the ability of the entire vehicle and its components to work normally in the electromagnetic environment in which it is located, without causing undesired electromagnetic interference to other things in the environment. In order to ensure the reliability, safety, and stability of the car, it is required that the on-board electronic equipment can work normally under the interference of other power electronic equipment; it will not affect the safe and stable operation of other electronic equipment, that is, achieve electromagnetic compatibility [3]. In this big environment, the on-load electromagnetic compatibility test and simulation closed-loop research of the electric drive system of new energy vehicles, aiming at the main problems existing in the electric drive EMC on-load test system, the mechanism is analyzed, and the solutions and measures are proposed, which provide reliable, standard-compliant, and cost-effective solutions for new energy OEMs; component

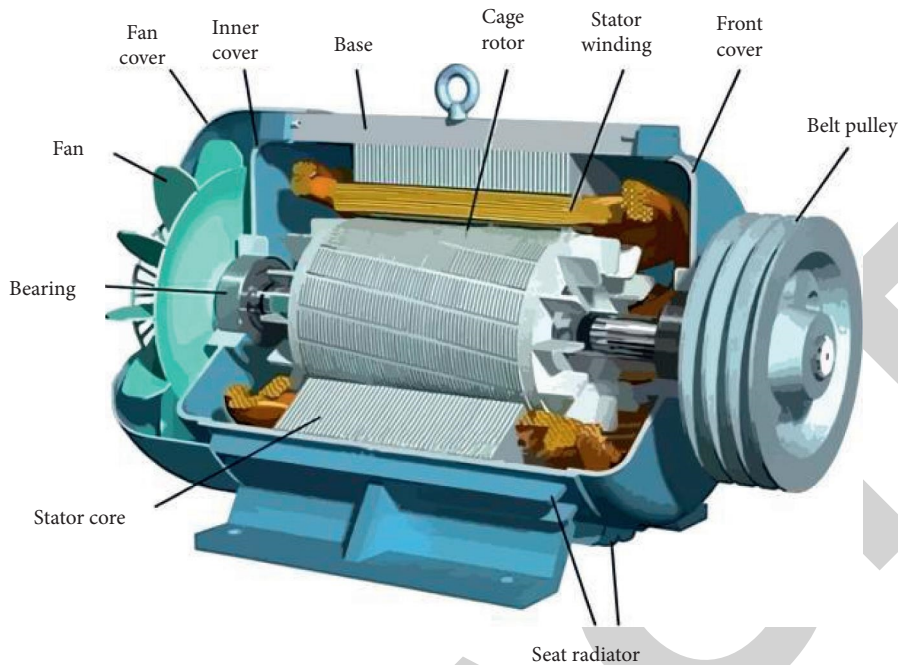


FIGURE 1: New energy vehicle electric drive system.

manufacturers and third-party testing agencies in the field of electric drive EMC on-load evaluation break the technical monopoly of the electric drive EMC on-load test system and improve China's research and development capabilities and voice in the field of automotive electronics EMC [4].

2. Literature Review

The electromagnetic compatibility of the battery system of new energy high-voltage pipe fittings is studied; in terms of common mode noise suppression, Mott and Priefer analyzed the common mode and differential mode interference in the electric vehicle drive system through experiments and proposed that the multilayer printed circuit board technology should be adopted for the differential mode interference [5]. Ajay and Jaya proposed in the literature that when the AC motor and the PWM inverter are connected by a long cable and when the transmission time of the PWM pulse in the cable exceeds 1/3 of the rise time of the PWM pulse, a total reflection will be sent at the motor end. It is verified that increasing the rise time of the PWM pulse can greatly reduce dv/dt at the motor end, thereby reducing the generation of electromagnetic interference [6]. Xie and Yuan believed that the common mode current was mainly caused by high frequency switching, used the equivalent circuit method to analyze the generation mechanism of common mode noise, and proposed a new type of a BOOST balanced switch converter [7]. This kind of a converter is active and can generate a current with the same magnitude and opposite phase as the common mode current, and in theory, it can completely suppress the generation of common mode interference. Based on a certain type of hybrid vehicle, Welti analyzed the electromagnetic environment in the vehicle and the coupling interference mechanism to the battery

management system and studied the anti-interference technology of the battery management system, focusing on improving the anti-interference ability of the battery management system, in order to realize the electromagnetic compatibility design of the battery management system [8]. Wang et al. carried out the theoretical research on the electromagnetic compatibility of the battery management system, the power line conduction of the battery management system, the modeling and simulation of the radiation interference, and the electromagnetic compatibility test analysis of the battery management system [9]. Antonov et al. determined the main interference sources and coupling paths of the high-voltage system, analyzed the influence of the interference sources generated by the motor controller and the internal switching devices of the DC/DC converter on the electromagnetic compatibility performance of the power battery, and established the power equivalent model of battery coupled interference and applied the extracted interference sources to the coupled interference model [10]. Based on the electromagnetic shielding theory and the finite element method, Dogra et al. combined numerical simulation and the Robinson equivalent model method, and the factors affecting the shielding effectiveness of the open rectangular cavity were studied [11]. The electromagnetic compatibility analysis of the battery management system has improved the electromagnetic compatibility characteristics of the battery management system to varying degrees, which has a great reference effect. On the basis of the current research, the author proposes an electromagnetic compatibility closed-loop development technology for the electric drive system of new energy vehicles under load conditions, which mainly includes three key links: the test platform focuses on the formulation and improvement of test standards and test methods and is a means to directly evaluate

the electromagnetic compatibility performance of the electric drive system; the test equipment is centered on the development of a standardized and low-cost test bench, which is the hardware support for the electromagnetic compatibility test of the electric drive system; the simulation platform focuses on the parameter design, prediction, and optimization of forward development, which is a means of controlling the EMC performance of electric drive system products in the early stage of design [12].

3. Methods

3.1. EMC Design of On-Load Test Equipment for the Electric Drive System

3.1.1. 3D Electromagnetic Modeling of On-Load Test Equipment for the Electric Drive System. According to the geometric model, block simplification processing, material property assignment, mesh division, and other operations are carried out, and a three-dimensional electromagnetic model of the electric drive system under load test equipment is established [13]. It mainly includes the end of the dynamometer motor, the shaft through the wall and its connecting parts, the parts of the end under test, and the dark room.

3.1.2. Shaft Current Simulation Analysis. In order to simulate the shaft current path generated by the dynamometer motor, the excitation of the current source is set on the axial surface of the output shaft of the dynamometer motor with an amplitude of 1A, and the direction is along one side of the anechoic chamber [14]. Set up three axial current simulation observation points, which are located at the shaft head of the shaft through the wall outside the semianechoic chamber (observation point A), the shaft head of the shaft through the wall inside the anechoic chamber (observation point B), and the position of the test piece installed inside the anechoic chamber (observation point C). The effects of different materials on the shaft current are compared and analyzed, the values of the three materials at the same observation point are compared, and the results are shown in Figures 2(a) and 2(b).

3.1.3. Shielding Effectiveness Simulation Analysis. Considering the electromagnetic field in space, current and plane wave excitations need to be applied in the excitation setup [15]. The shape of the hole through the wall is set as a circle, and the apertures of the openings in the shielding wall are 370 mm, 380 mm, 390 mm, and 400 mm, respectively. The shielding effectiveness test is carried out under these four sizes, and the results are shown in Figure 3.

From this, it can be seen that in the 9 kHz~2 MHz and 30~200 MHz frequency bands, the shielding effectiveness is generally better when the diameter of the hole through the wall is 390 mm; in the range of 2~30 MHz, there is not much difference between the diameter of 390 mm and 400 mm through the wall; in the two frequency bands of 141~157 MHz and 190~197 MHz, the shielding effectiveness is relatively good when the diameter of the through-wall hole

is 380 mm [16]. In order to protect the integrity of shielding, when designing the shielding cover, the through-wall shaft should be completely surrounded, and the electromagnetic interference in the space should not enter the semianechoic chamber as much as possible. The shaft current is suppressed by grounding, so a conductive grounding ring is installed outside the dark room of the on-load test system, on the outside of coupling, and at one end of the shaft through the wall [17].

The simulation test was carried out with the shielding cover alone, and compared with the simulation results without the shielding cover, it can be seen that after the shielding cover is installed, the overall shielding efficiency is improved; especially in the frequency bands of 9 kHz~5 MHz, 7~50 MHz, and 60~200 MHz, the shielding effectiveness is significantly improved by 14~40 dB. After the shielding case is installed, the shielding effectiveness around 6 MHz becomes poor, and further research is needed. In general, installing a shielding case is one of the effective measures to improve the shielding effectiveness [18]. After adding the shielding cover, continue to install the conductive grounding ring for the simulation test and compare the shielding effectiveness simulation test results of no shielding cover, only the shielding cover, and the conductive grounding ring; after installing the conductive grounding ring, the shielding effectiveness is improved again; at frequencies below 2 MHz, the shielding effectiveness is increased by at least 6 dB compared to the case where only the shield is installed, and the shielding effectiveness in frequency bands of 7~10 MHz, 25~30 MHz, and 50~80 MHz is significantly improved by 3~10 dB. It can be seen that the installation of the conductive grounding ring can effectively reduce the electromagnetic interference caused by the shaft current.

3.1.4. EMC Performance Evaluation of Electric Drive System On-Load Test Equipment. Using the iterative optimization of the above parameters and filter design, a set of on-load test equipment "MotorChamber" for the through-wall electric drive system that meets the standard requirements is developed, and the electrical performance specifications are shown in Table 1.

Under the working conditions of a dynamometer speed of 7000r/min and a current of 150A, the radiation emission test in the dark room was carried out to evaluate the EMC performance of the loaded test equipment [19]. The radiation emission test results of each frequency band are compared with the level 5 limit of GB/T18655-2018; the results show that the radiation emission in the darkroom is lower than the level 5 limit of GB/T18655-2018 by more than 20 dB in all frequency bands, which meets the requirements [20].

3.2. Establishment of Simulation Platform for Conducted EMI under Load Conditions of the Electric Drive System

3.2.1. Conducted EMI Model Structure of the Electric Drive System. According to the actual circuit structure of the

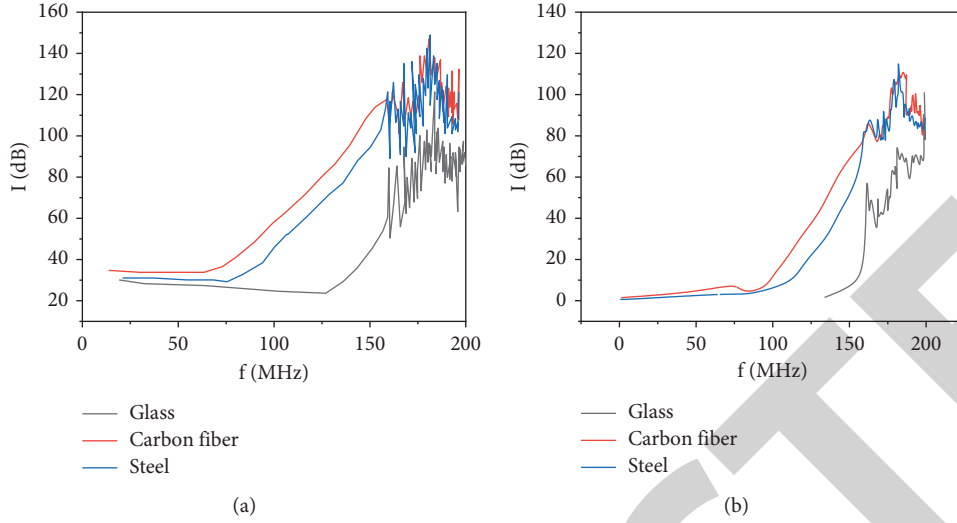


FIGURE 2: Comparison of simulation results of through-wall shafts using different materials. (a) Data comparison of the observation point B. (b) Data comparison of the observation point C.

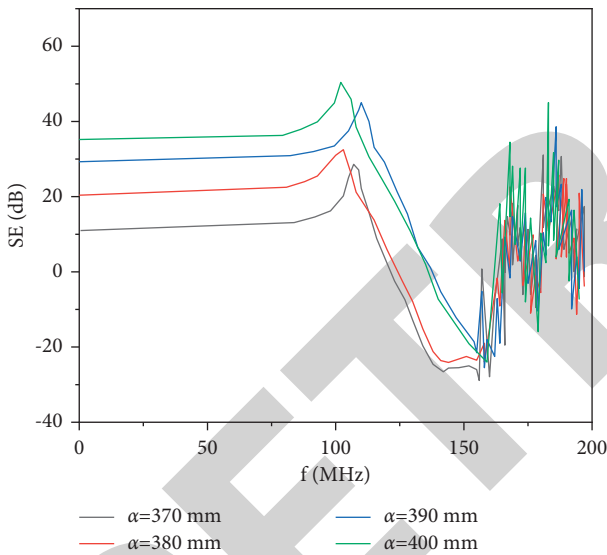


FIGURE 3: Comparison of simulation results of through-wall holes with different diameters.

TABLE 1: Test system electrical specifications.

Category	Parameter
High voltage supply voltage/V	1000
Low voltage supply voltage/V	9~200
Rated current/A	500
Stand power/kW	220
maximum speed/(r/min)	7000
highest torque/(N·m)	1000

integrated electric drive system, combined with the layout of the test standard, the time domain simulation results are converted by the established mathematical model of the EMI receiver to obtain the peak and average spectrum.

(2) The motor load model of the electric drive system establishes the electromagnetic torque equation of the on-board permanent magnet synchronous motor as shown in the following equation:

$$\begin{aligned} T_{em} &= p(\varphi_d i_q - \varphi_q i_d) = p[L_{md} i_f i_q + (L_d - L_q) i_d i_q] \\ &= p[\varphi_f i_q + (L_d - L_q) i_d i_q]. \end{aligned} \quad (1)$$

Among them, T_{em} is the electromagnetic torque, p is the number of motor pole pairs, φ_d is the flux linkage, i_d is the direct axis current, i_q is the quadrature axis current, L_d is the direct axis inductance, and L_q is the quadrature axis inductance.

In order to obtain the values of the above parameters of the motor under various working conditions, a three-dimensional electromagnetic simulation is carried out; according to the main design parameters of the motor, a three-dimensional electromagnetic model of the motor is established, and the boundary conditions are set for simulation, and the characteristic parameter curves of the motor are output. The motor needs to use the maximum torque/current control, in order to find the load characteristic parameters corresponding to the maximum torque under each working condition and establish the motor load model under each working condition. Taking the motor torque of 3000r/min and the current of 100N·m as an example, the speed and torque of the load model are shown in Figures 4(a) and 4(b).

3.2.2. Conducted EMI Model Verification of the Electric Drive System. The conducted EMI model of the electric drive system is established, where the circuit simulation step size is 2 ns, and the backward Euler solver is used to solve it. Set the intermediate frequency bandwidth (RBW) and step size of the EMI receiver according to GB/T18655-2018. The RBW in the 150 kHz~30 MHz frequency band is 9 kHz, and the step size is 4 kHz.

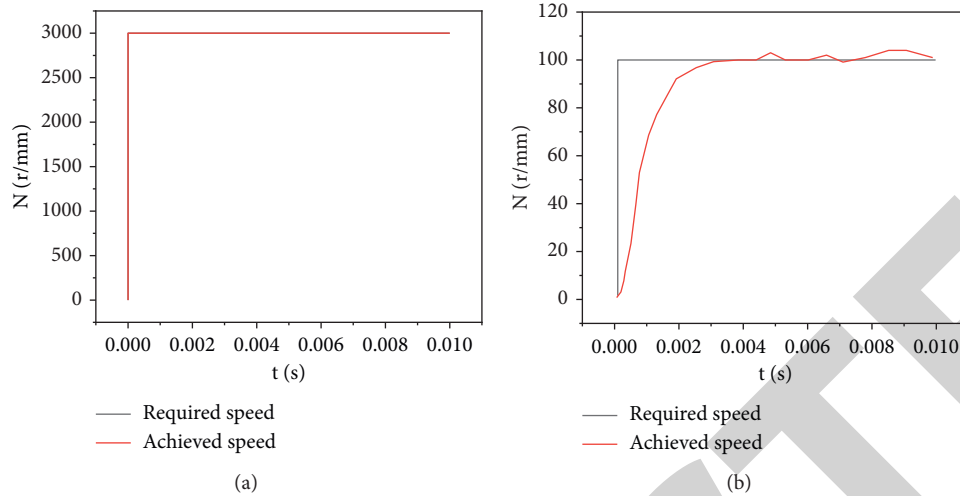


FIGURE 4: The effect of speed and torque realization of the loaded model. (a) Speed realization effect and (b) torque realization effect.

4. Results and Discussion

4.1. Validation Results of the Conducted EMI Model of the Electric Drive System. Under the working conditions of motor torque of 3000r/min and current of 50N-m, the high-voltage LISN positive and negative conduction emission (voltage method) simulation is carried out, and the comparison results with the test spectrum are shown in Figure 5.

It can be seen that in the high frequency range of 150 kHz~20 MHz, the high-risk resonance points concerned in conducted emission are basically consistent, the amplitude error of the main resonance point is less than $6\text{ dB}\mu\text{V}$, and the spectrum trend in the overall range is consistent.

4.2. Optimization of Conducted EMI Performance by the PWM Control Method. In engineering, the electric drive system generally adopts the SVPWM (space voltage vector pulse width modulation) method. Change the PWM (pulse width modulation) mode to DPWM (discontinuous pulse width modulation) and analyze its influence on the electromagnetic interference of the system. Change the modulation mode to DPWM3 for the simulation test and compare it with the simulation result of the SVPWM modulation. It can be seen from the results that by replacing the DPWM3 modulation method, in the range of 200 kHz~2 MHz, the conducted emission amplitude is reduced by about $2\text{ dB}\mu\text{V}$, and there is basically no change on the whole. Then, change the modulation mode to DPWMmin for the simulation test and compare it with the simulation results of the SVPWM method. It can be seen from this that the overall conducted emission level is reduced by replacing the modulation mode with DPWMmin, the amplitude at the 4 MHz resonance point is unchanged, and the amplitude at the 8 MHz resonance point is reduced by about $8\text{ dB}\mu\text{V}$.

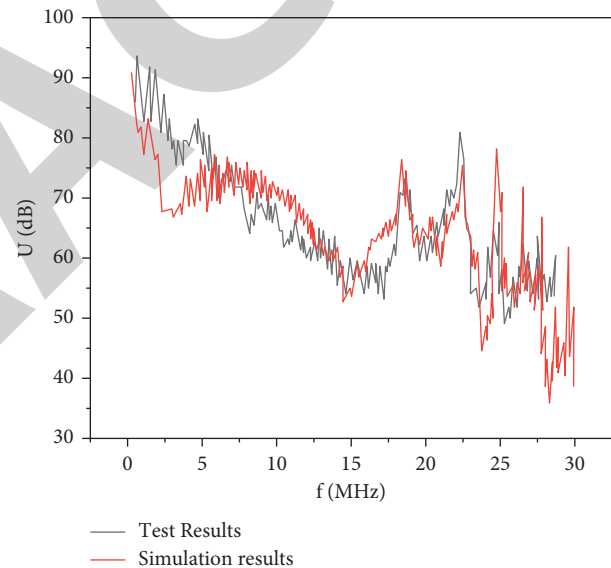


FIGURE 5: 150 kHz~30 MHz conducted emission simulation and test comparison.

5. Conclusion

The author proposes a closed-loop research method for on-load electromagnetic compatibility testing and simulation for electric drive systems of new energy vehicles. The method includes EMC design of the electric drive system on-load test equipment, establishment of a conducted EMI simulation platform for the electric drive system under load conditions, and optimization of the conducted EMI performance of the electric drive system based on key parameters and PWM control. The following conditions were observed through experiments: simulation platform based on electric drive system; IGBT gate parasitic inductor with motor torque 3000R per minute and current 100N-m under typical working conditions; the effect of IGBT and the parasitic capacitance of the heat sink on the conduction interference;

Retraction

Retracted: Realization of Single-Phase Grounding Fault Location and Recovery Technology in Distribution Network

International Transactions on Electrical Energy Systems

Received 19 September 2023; Accepted 19 September 2023; Published 20 September 2023

Copyright © 2023 International Transactions on Electrical Energy Systems. This is an open access article distributed under the Creative Commons Attribution License, which permits unrestricted use, distribution, and reproduction in any medium, provided the original work is properly cited.

This article has been retracted by Hindawi following an investigation undertaken by the publisher [1]. This investigation has uncovered evidence of one or more of the following indicators of systematic manipulation of the publication process:

- (1) Discrepancies in scope
- (2) Discrepancies in the description of the research reported
- (3) Discrepancies between the availability of data and the research described
- (4) Inappropriate citations
- (5) Incoherent, meaningless and/or irrelevant content included in the article
- (6) Peer-review manipulation

The presence of these indicators undermines our confidence in the integrity of the article's content and we cannot, therefore, vouch for its reliability. Please note that this notice is intended solely to alert readers that the content of this article is unreliable. We have not investigated whether authors were aware of or involved in the systematic manipulation of the publication process.

Wiley and Hindawi regrets that the usual quality checks did not identify these issues before publication and have since put additional measures in place to safeguard research integrity.

We wish to credit our own Research Integrity and Research Publishing teams and anonymous and named external researchers and research integrity experts for contributing to this investigation.

The corresponding author, as the representative of all authors, has been given the opportunity to register their agreement or disagreement to this retraction. We have kept a record of any response received.

References

- [1] D. Zhang, H. Tang, J. Zhu, H. Zhou, Z. Zhang, and X. Song, "Realization of Single-Phase Grounding Fault Location and Recovery Technology in Distribution Network," *International Transactions on Electrical Energy Systems*, vol. 2022, Article ID 6282843, 10 pages, 2022.

Research Article

Realization of Single-Phase Grounding Fault Location and Recovery Technology in Distribution Network

Di Zhang , Haiguo Tang , Jiran Zhu , Hengyi Zhou , Zhidan Zhang ,
and Xingrong Song 

State Grid Hunan Electric Power Company Limited Research Institute, Changsha 410007, Hunan, China

Correspondence should be addressed to Haiguo Tang; 20152600036@m.scnu.edu.cn

Received 20 July 2022; Revised 10 August 2022; Accepted 16 August 2022; Published 7 September 2022

Academic Editor: Nagamalai Vasimalai

Copyright © 2022 Di Zhang et al. This is an open access article distributed under the Creative Commons Attribution License, which permits unrestricted use, distribution, and reproduction in any medium, provided the original work is properly cited.

In order to locate the single-phase-to-ground fault in distribution network, a research method of single-phase-to-ground fault location and recovery technology in distribution network is proposed. According to the characteristics of single-phase-to-ground fault in distribution network, the fault characteristics of zero-sequence current and three-phase current transient records are extracted by generalized S transform of correlation coefficient, and multi-source redundant information is formed. Fuzzy C-means clustering analysis method is used to fuse multiple fault features online location strategy. The simulation results show that the fuzzy clustering based on FCM changes continuously with the accumulation of samples, and the sample center changes with the enrichment of the samples. When the arc suppression coil is grounded with different initial phase angle transition resistance and intermittent fault, the state of each measuring point can be correctly identified, and the accurate energization rate is 97%. The test results show that the system can achieve accurate positioning for all sections.

1. Introduction

For many years, single-phase grounding fault line selection of small current grounding system has been a research topic at home and abroad, such as zero-sequence power method, zero-sequence electricity current active component method, harmonic component method, first half wave method, negative sequence current component method, transient component method, zero-sequence admittance method, wavelet analysis method, residual current increment method, and so on. However, in practice, the line selection effect of these protection methods is not ideal. In view of the fact that there is no certain characteristic quantity that is sensitive to all kinds of small current ground faults, before the breakthrough in the research of fault feature information detection and extraction, how to break through the limitation of fault detection only at the front end of the line is the key to solve the problem.

China's medium voltage power distribution network is mainly neutral point without direct grounding. The fault of distribution network line is mainly divided into phase short circuit fault and single-phase grounding fault. If single-phase

grounding fault occurs in distribution line, it can be allowed to supply power to load for 1~2 h with fault according to regulations to improve the reliability of power supply. However, it causes the non-fault phase voltage to rise to line voltage, which can be extended to phase short circuit for long time operation with fault, which affects the safety of the power system. Therefore, the study of single-phase grounding fault section location technology has become one of the hot spots to improve the power supply reliability of distribution network [1]. With the practical application of power distribution automation main station, distribution terminals and fault indicators of various types of different manufacturers are connected to the power distribution automation main station. When single-phase grounding fault occurs, the overhead transient recording electricity fault indicator sends fault recording. Other fault indicators or power distribution terminals send fault information. Therefore, the following two problems need to be solved in locating single-phase grounding faults based on the main station of power distribution automation: (1) the fault feature extraction based on fault recording, the fault

processing strategy integrating fault feature and fault event information, and the unified fault processing in the scenario that the single-phase grounding fault turns into short circuit fault in the field equipment mixed installation; (2) Figure 1 shows how to solve the failure of locating faults caused by the loss of device installation diversity information and startup criteria in engineering applications.

2. Literature Review

Mendes et al. proposed a DC open circuit and AC tracing fault location method suitable for single-phase grounding fault of distribution network. Based on the principle of injection method, the fault point is maintained in breakdown state by applying high voltage under power failure state, and the injection signal is traced to determine the fault area or location. The S signal injection method to avoid the small current grounding system gets the influence of the coil, applicable to install two-phase current transformer power network overhead line, but the method needs to use signal injection equipment, and signal strength is restricted and the injected signal may affect the power quality, in addition to the high resistance grounding fault and intermittent fault special fault condition, such as this. The fault location effect of the method is not ideal [2]. Neiva et al. proposed a fault segment location method based on XOR operation of matrix, which multiplied the network description matrix and fault information matrix to obtain the fault discrimination matrix; then, XOR operation was performed on the elements of the fault discrimination matrix and the corresponding criteria were used to obtain the fault segment. However, this method requires matrix mathematical operation, which takes a long time when the distribution network is large in scale [3]. Almeida and Muniz improved the zero-sequence power method and used the zero-sequence active power component to determine the fault segment, which was suitable for the arc suppression coil grounding system. However, the method was interfered by the unbalanced current of the current transformer, resulting in low reliability of fault location [4]. The transient zero-mode power direction method proposed by Bhatia is used to calculate the transient zero-mode voltage and current to determine the fault direction and then the field terminal measuring equipment is used to determine the fault section. This method makes use of the characteristics of large transient signal and overcomes the influence of arc suppression coil to a certain extent [5]. Kazhekin used the expert system to establish the expert system database of the segmented switch and protection device of the circuit breaker. When the fault information occurs, the fault information set can be deduced. Finally, the fault section can be determined through the analysis of the credibility [6]. Xu and Hu applied neural network to the expert system, which made the traditional expert system have self-adaptive ability and effectively improved the accuracy of fault location [7]. Through the distribution network to establish a suitable equivalent model, Zhao et al. used ant colony algorithm to realize fault location, and fault location problem can be converted to optimization algorithm of global optimization problems.

However, it is difficult to overcome the problem of local optimal solution, which leads to the appearance of false fault segments. Depending on its own advantages, intelligent algorithm has become a hot spot in current research [8].

With the popularization and application of distribution automation, the fault indicator and distribution terminal are connected to the main distribution station, which creates conditions for the online location of the single-phase grounding fault section of the main distribution station. In view of the complexity of fault processing caused by the access of distribution terminal in engineering application of various fault indicators, this paper proposes to extract the characteristic values of the fault recording of overhead transient fault indicator (hereinafter referred to as the fault recording type) by using a variety of algorithms and fuzzy C. The mean clustering analysis method integrates all characteristic parameters to improve the strategy of single-phase grounding fault location and optimizes the fault processing process to meet the needs of engineering applications.

3. Research Method

3.1. Overall Solution for Online Single-Phase Grounding of the Main Power Distribution Station. When single-phase grounding occurs, the power distribution monitoring equipment installed on site (power distribution terminal fault indicator, etc.) collects distribution network operation information such as current, voltage, and electric field and performs single-phase grounding fault recording detection or judgment processing according to the set value and judgment conditions. Through wireless optical fiber and other communication channels, the IEC 60870-5-101/104 power communication protocol is used to communicate with the distribution master station. The master station analyzes and locates faults based on the received information (see Figure 2).

The overall structure of single-phase grounding positioning based on distribution master station is divided into distribution master station layer, communication network layer, and equipment layer.

3.1.1. Main Station Layer. Analyze the fault information and fault recording files collected by various fault indicators and distribution terminals, extract the fault characteristic quantity, and collect the real-time fault information of the topological distribution network of the main distribution station for single-phase grounding fault location and treatment.

3.1.2. Communication Layer. Through the communication channel of optical fiber wireless network, IEC 60870-5-101/104 communication protocol is used to realize the data communication between distribution monitoring equipment and distribution master station.

3.2. Single-Phase Grounding Fault Processing and Feature Extraction. When single-phase grounding occurs in distribution network, according to the selection of the State

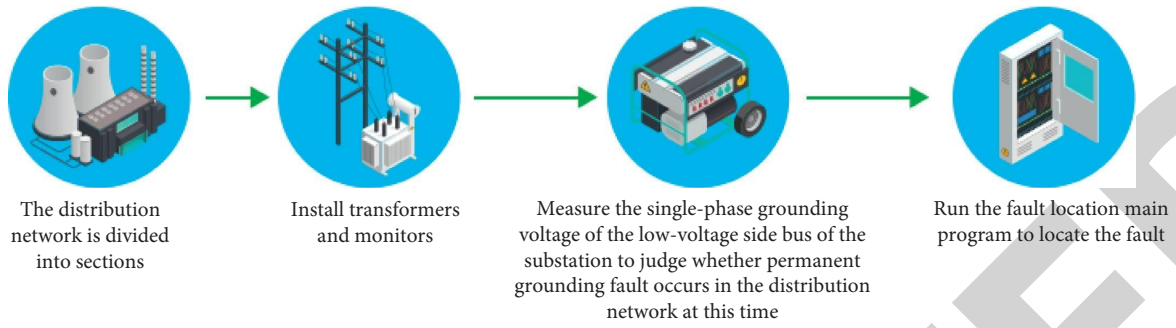


FIGURE 1: Multi-information fusion.

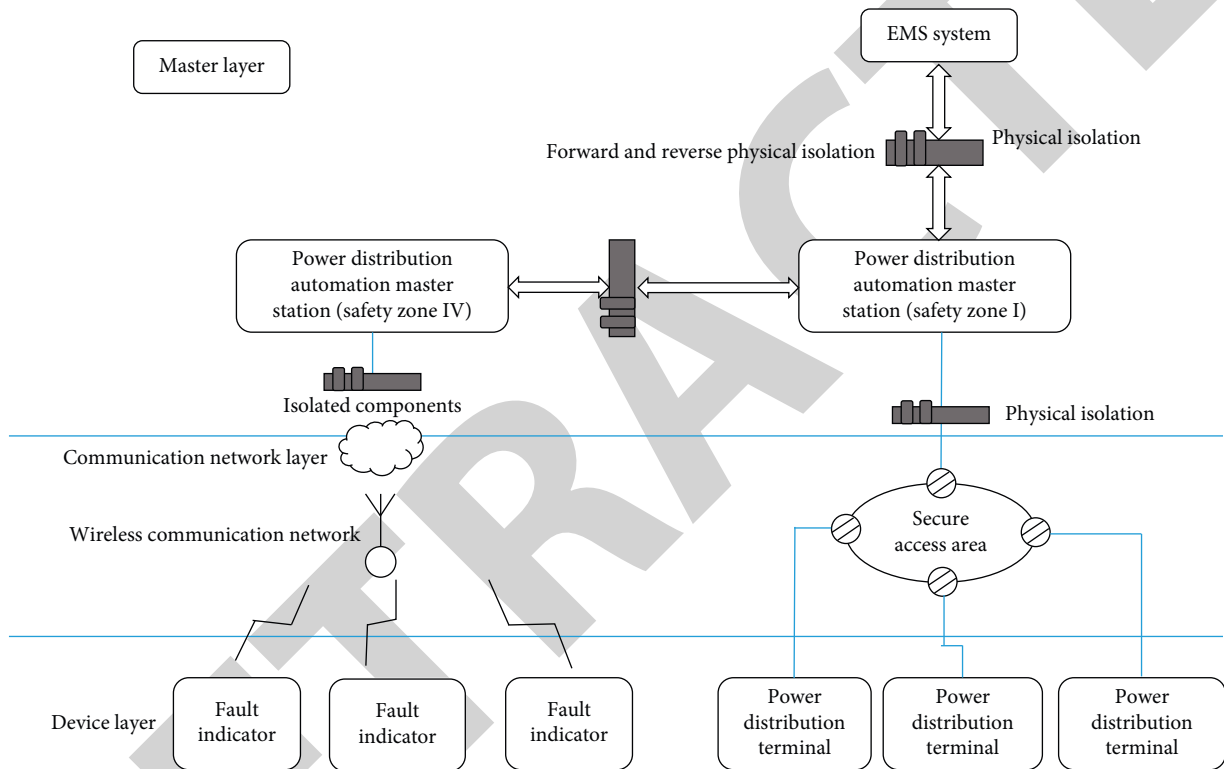


FIGURE 2: Structure diagram of single-phase ground fault location based on power distribution master station.

Grid Distribution Line Fault Indicator Technical Principle (Trial) and Distribution Automation Terminal Technical Specification (Trial) Distribution, terminals or non-overhead transient wave recording fault indicators are required to have single-phase grounding indication and send single-phase grounding fault signs. The main power distribution station can directly locate faults online according to the fault signs sent; however, the fault recording type fault indicator sends the fault recording to the distribution master station, which depends on the distribution master station to parse the fault recording and extract the fault characteristic quantity and locate the fault according to the diagram mode and topology of distribution automation [9]. As shown in Figure 3, in order to adapt to the needs of various complex application scenarios, the power distribution master station automatically detects the type of fault information when receiving it and starts different fault processes.

In engineering application, only current transformer is installed for data collection of fault indicator of wave recording type. When single-phase fault occurs, the fault phase current zero-sequence current transient wave recording file is sent to the main distribution station [10].

3.2.1. Similarity Feature Extraction of Zero-Sequence Current Waveform. When single-phase grounding fault occurs in the low-current grounding system, a virtual voltage source is added to the fault point accessory of the original system after the fault, and the characteristics of single-phase grounding zero-sequence current of the low-current grounding system are analyzed [11]. In digital signal processing, the correlation coefficient reflects the similarity of waveforms, that is, the larger the correlation coefficient is, the more similar the waveforms are, and the smaller the correlation coefficient is,

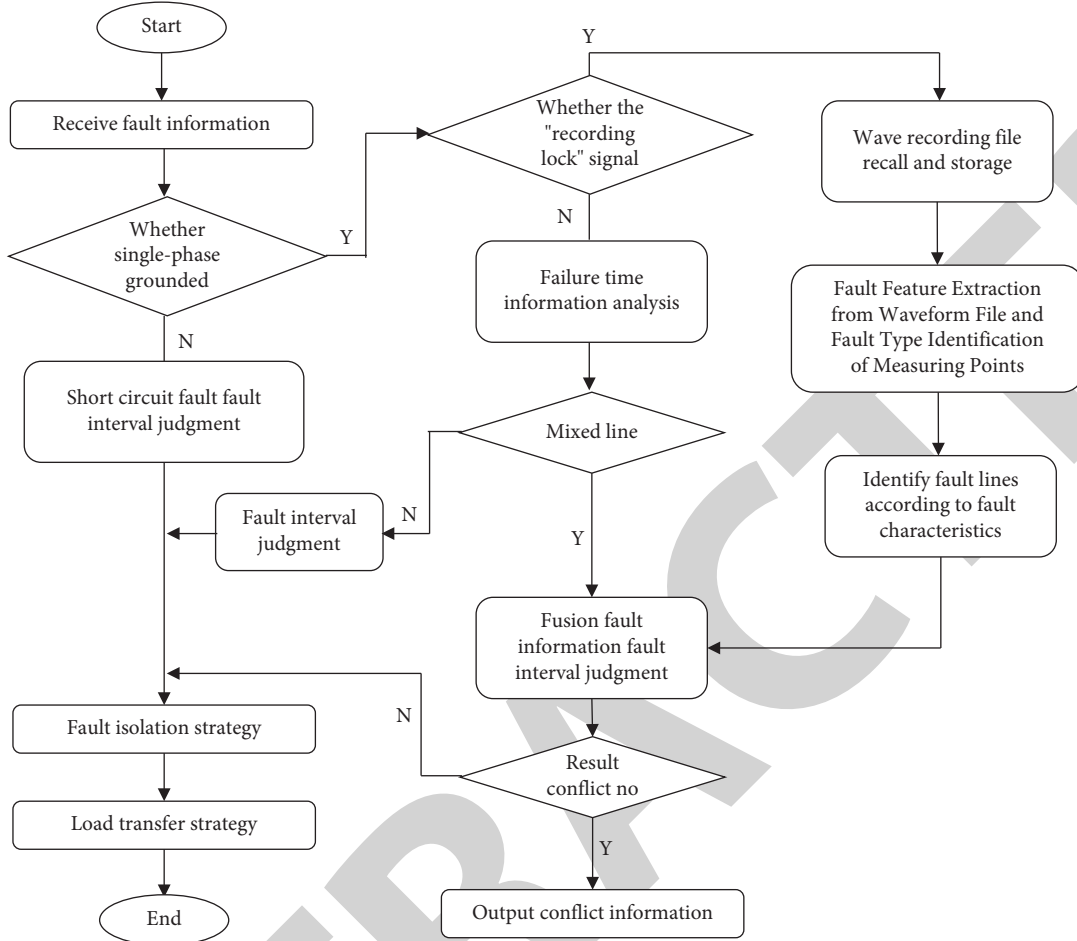


FIGURE 3: Process for troubleshooting single-phase grounding faults of the main power distribution station.

the more different the waveforms are. Therefore, fault line selection and fault location can be realized by analyzing the relation number of transient zero-sequence current recording waveforms [12]. The number of phase relation of transient zero-sequence current recording wave is calculated as follows:

- (1) The calculation formula of correlation coefficient between measuring points m and n is as follows:

$$\rho_{mn} = \frac{\sum_{i=1}^N X_{i-n} X_{i-m}}{\sqrt{\sum_{i=1}^N X_{i-n}^2 \sum_{i=1}^N X_{i-m}^2}} \quad (1)$$

- (2) Based on the correlation coefficient matrix ρ , the comprehensive correlation coefficient $E\rho_i$ of each measurement point i can be calculated, as shown in the following formula:

$$E\rho_i = \frac{1}{L-1} \left(\sum_j \rho_{ij} - \rho_{ij} \right), \quad j = 1, \dots, L. \quad (2)$$

In equations (1) and (2), N is the number of samples collected and L is the number of measurement points.

3.2.2. Feature Extraction Based on Generalized S Transform

(1) *Generalized S Transform Obtains Time-Frequency Matrix of Measuring Point.* The generalized S-transform combines the advantages of short-time Fourier transform and wavelet transform, and has good time-frequency local variation characteristics. It can effectively reflect the characteristics of the signal at each frequency and fully show the details of the fault characteristics of the signal to be analyzed. It can improve the accuracy and reliability of fault detection and has been preliminarily applied in single-phase ground fault determination [13]. The generalized S-transform discrete formula is as follows:

$$S(m, n) = \sum_{k=0}^{N-1} X(n+k) e^{2\pi^2 k^2 / n^2} e^{j2\pi mn/N} \quad (3)$$

$$= A(m, n) e^{j\theta_{mn}}, \quad n \neq 0,$$

$$S(m, n) = \frac{1}{N} \sum_{k=0}^{N-1} x(k), \quad n = 0, \quad (4)$$

$$X(n) = \frac{1}{N} \sum_{k=0}^{N-1} x(k) e^{-j(2\pi nk/N)}, \quad (5)$$

where N is the sampling number, $A(m, n)$ is the amplitude $S(m, n)$, and θ_{nm} is the phase angle of $S(m, n)$. For the collected N discrete signal points $x(k)$, S transformation is carried out by using equations (3)–(5), and the complex time-frequency matrix can be obtained, where row corresponds to frequency and column corresponds to sampling time point.

3.2.3. Zero-Mode Energy Function and Eigenvalue Extraction. The zero-mode energy function of each measuring point is the product and integral of zero-mode voltage and current within a certain time. Considering unified use of bus zero-sequence voltage, after applying S transformation, its energy function can be equivalent to: the amplitude square of $S(m, n)$ is $A(m, n)^2$, then the transient energy W_{i-n} of measurement point i at the corresponding frequency f_n is shown in the following equation:

$$W_{i-n} = \sum_m [A(m, n)]^2, \quad i = 1, \dots, L. \quad (6)$$

Only the energy function time-frequency matrix is obtained through S change transformation for signal analysis, and further extraction of its characteristic quantity is needed to directly reflect the fault characteristics.

3.2.4. Extraction of Energy Moment Characteristic Quantity in Characteristic Frequency Band. After S transformation, the energy moment analysis of its characteristic frequency band shows that the corresponding energy difference between measuring points on both sides of the fault section in the characteristic frequency band is large, and the difference between measuring points on the front and back end of the fault point and on the sound line is small [14]. The extraction process of characteristic frequency energy moment is as follows. According to formula (6), the transient energy of a measurement point f_n is obtained, and the frequency corresponding to the maximum secondary energy of a measurement point is extracted as the characteristic frequency band. The average value of the corresponding energy moment in the characteristic frequency band is taken as the energy characteristic quantity, and the energy characteristic quantity E_i of the measuring point i is shown in the following formula:

$$E_i = \frac{(W_{i-f1} + W_{i-f2})}{2}. \quad (7)$$

3.2.5. Relative Information Entropy Feature Extraction. Relative information entropy reflects the degree of information ordering. The more orderly information is, the lower the relative information entropy will be, and the higher it will be otherwise. According to the fault characteristic analysis, the difference of zero-sequence current waveform on both sides of the fault point is large, and the relative information entropy is large. The front and back end of the fault point is similar to the zero-sequence current waveform of the non-fault line, and its relative entropy is small, so the relative entropy can be used as a characteristic quantity to locate the fault segment [15]. The extraction process of the feature quantity of relative information entropy based on S transformation is as follows. After the energy function is transformed by generalized S, the weight

coefficients q_{i-n} of each measurement point can be calculated according to the transient energy f_n at frequency, as shown in the following formula:

$$q_{i-n} = \frac{W_{i-n}}{\sum_{n=1}^K W_{i-n}}, \quad (8)$$

where $\sum_{n=1}^K W_{i-n}$ is the total sum of all the measurements under frequency f_n ; according to the relative entropy theory, the relative information entropy m_{ij} between the measurement points i and the measurement points j can be calculated, and the information entropy matrix M can be obtained. According to the information entropy matrix M , the comprehensive energy entropy of the measurement points i can be calculated as follows:

$$m_{ij} = \sum_n q_{i-n} \ln \frac{q_{i-n}}{q_{j-n}}, \quad (9)$$

$$M_i = \frac{1}{L-1} \left(\sum_j M_{ij} - M_{ij} \right), \quad j = 1, \dots, L. \quad (10)$$

n in equations (9) to (10) is the corresponding frequency band; L is the total number of measurement points.

3.2.6. Correlation Analysis and Calculation of Phase Current Mutation. When a fault occurs in the small current grounding system, the system line voltage remains symmetric after the fault. It can be known from the analysis of the change of the sound phase fault current mutation before and after the fault point of the sound line and each fault line: sound line three-phase current mutation amplitude is equal, phase is the same, and waveform is the same [16]. By analyzing the correlation characteristics of phase current mutation between two phases, the correlation characteristics of phase mutation between two phases can be extracted as follows for fault interval location.

The phase current mutation is calculated in the following formula:

$$\Delta I(k) = I(k) - I(k-N), \quad (11)$$

where N represents the sampling points of power frequency cycle.

Calculate the correlation coefficient $\rho_{AB}, \rho_{BC}, \rho_{CA}$ between two phases of phase current mutation based on formula (1). Take the average of the correlation coefficient between two phases of three-phase current mutation as the comprehensive correlation coefficient of the measurement point, and the comprehensive correlation coefficient $I\rho_i$ of the measurement point i is shown in the following formula:

$$I\rho_i = \frac{\rho_{AB} + \rho_{BC} + \rho_{CA}}{3}. \quad (12)$$

3.3. Multi-Criteria Integrated Fault Location Based on Fuzzy C-Means Clustering

3.3.1. Fault Determination Process. Due to external interference of line parameters in neutral ground mode, each characteristic quantity does not necessarily have a clear

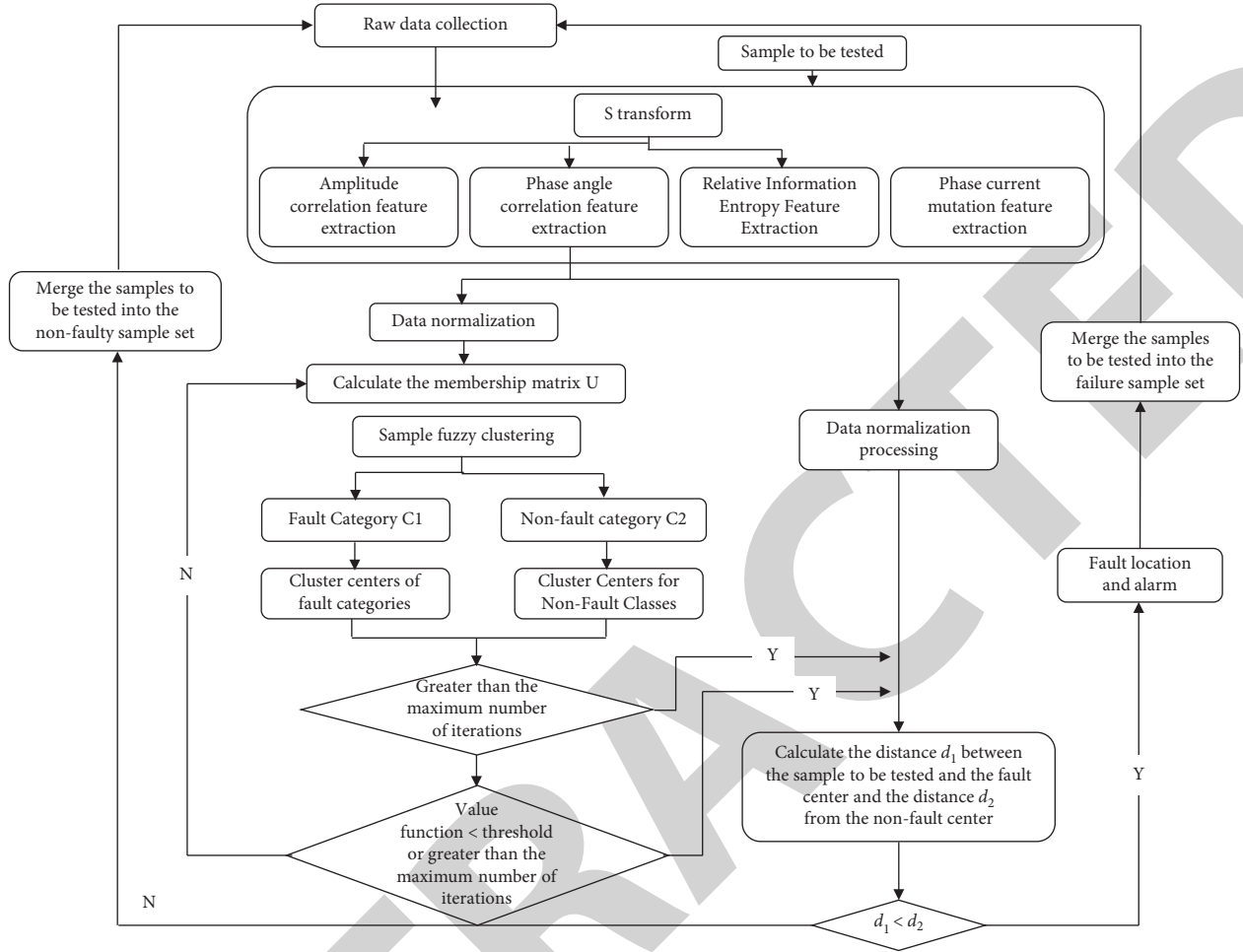


FIGURE 4: FCM fuzzy clustering flowchart.

boundary, and there may be misjudgment in fault location by using a single characteristic quantity. In order to overcome the deficiency of single location method, information fusion methods such as fuzzy theory of extreme learning machine, D-S evidence theory, fuzzy neural network clustering analysis, and other information fusion methods are used to fuse the fault characteristics to improve the correctness of single-phase grounding fault. Among them, fuzzy C-means clustering algorithm (FCM) algorithm is a data clustering method based on the optimization of the objective function. It has the characteristics of unsupervised and does not need human intervention and is the most extensive and successful in information fusion [17]. Figure 4 shows the troubleshooting process of single-phase grounding fusion based on fuzzy C-means clustering analysis.

Specific steps are as follows:

- (1) Load the fault recording file and extract its characteristic quantity according to formulas (2), (7), (10), and (13).
- (2) Considering the complex structure of distribution network, the characteristic quantity of energy

moment information entropy amplitude varies greatly between different faults, so the normalized data preprocessing is carried out for the same fault data. Keep them at the same level of quantity and reduce their influence on the conclusion. The sample set X generated by normalization is shown in the following formula:

$$X_i = \frac{x_i - x_{\min}}{x_{\max} - x_{\min}}. \quad (13)$$

- (3) Parameter setting and initialization. Set the classification number c , weighting index q , iteration number N , and convergence condition. Random numbers are generated in the interval $[0,1]$ to form the initial membership matrix U , and the initial clustering center matrix V is calculated.
- (4) The objective function of fuzzy clustering is calculated according to equation (14), and the membership matrix and clustering center matrix are updated according to equations (15) and (16).

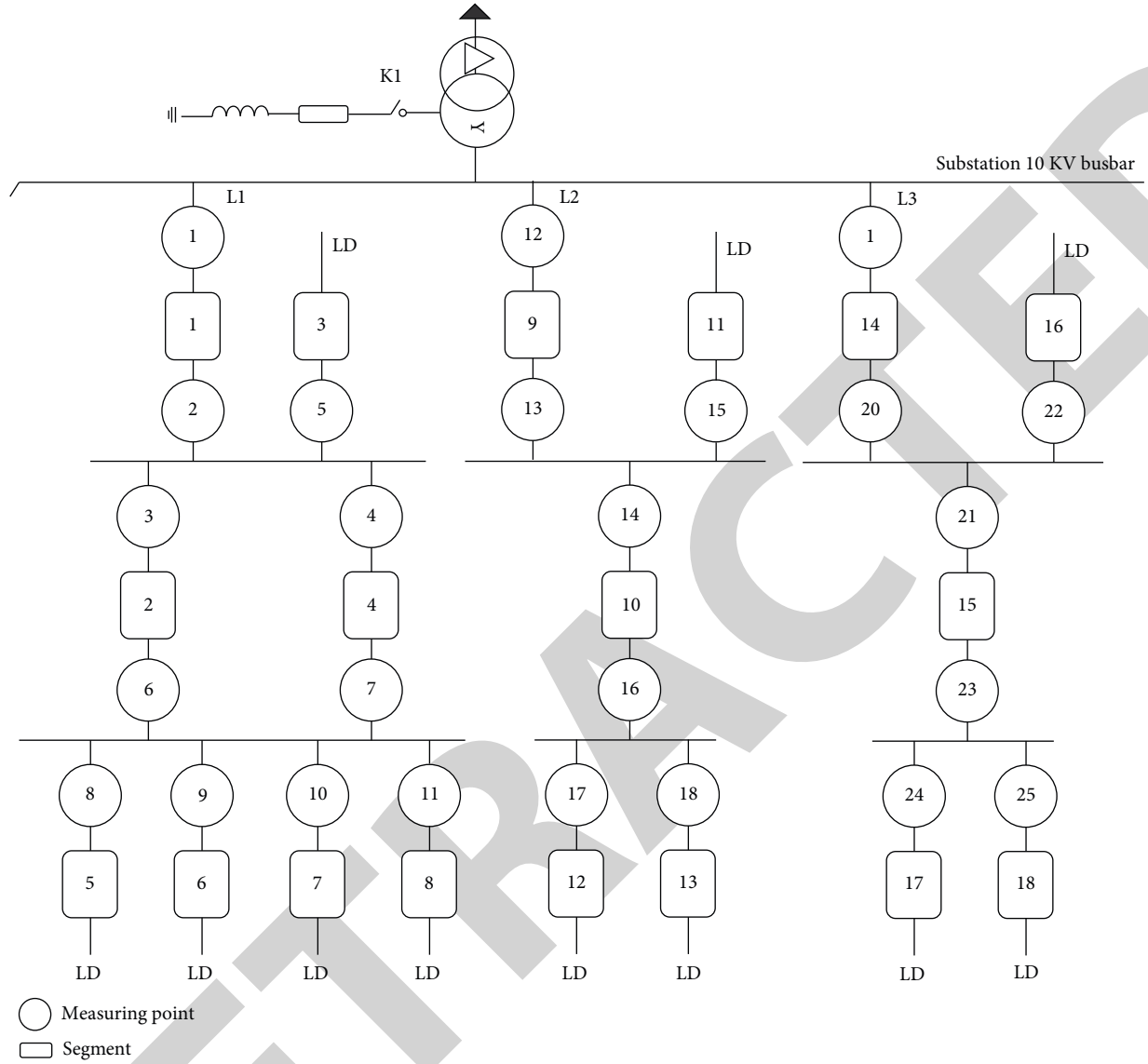


FIGURE 5: Wiring diagram of distribution network.

$$I_q(U, V) = \sum_{k=1}^N \sum_{i=1}^c (u_{ik})^q (d_{ik})^2, \quad (14)$$

$$d_{ik} = \sqrt{\sum_{j=1}^m (x_{kj} - v_{ij})^2}, \quad (15)$$

$$v_i = \frac{\sum_{k=1}^N (u_{ik})^q x_i}{\sum_{k=1}^N (u_{ik})^q}, \quad 1 \leq i \leq c, \quad (16)$$

where d_{ik} is the distance between sample x_i and the k th clustering center [18, 19].

- (5) Determine whether the objective function calculated by formula (15) is greater than the set threshold ε and the number of iterations N . If the number of

iterations N has not reached the maximum and is greater than the threshold, return (4); otherwise, turn to (6);

- (6) Output partition matrix and cluster center matrix.
- (7) The distance d_{1k}, d_{2k} between the sample data x_i to be tested and the fault clustering center and the non-fault clustering center is calculated one by one. The sum of the distance between all the feature values of the sample and the fault clustering center is d_1 , and the sum of the distance between the non-fault clustering center is d_2 . If $d_1 > d_2$, the sample is judged to belong to the non-fault category; otherwise, it is judged to be the fault category.
- (8) After the fault is determined, the sample set to be tested is stored in the database [20]. After correctly identifying the fault or non-fault state of the test

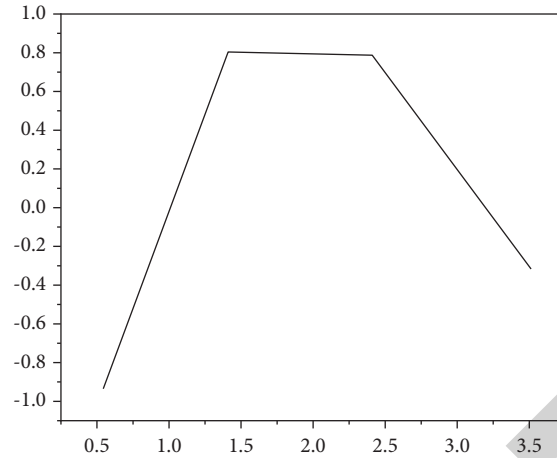


FIGURE 6: C-means clustering center where A-phase single-phase ground positioning occurs between 2–3 measuring points of line 1.

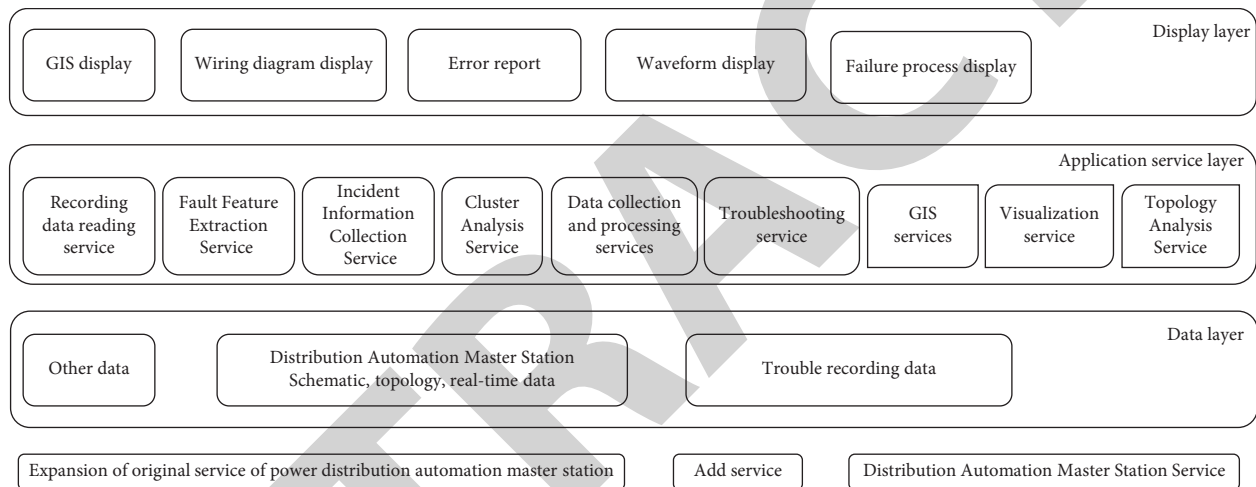


FIGURE 7: Fault location system software structure diagram.

points, the samples to be tested will be classified into the corresponding categories as historical data according to the identification results to enrich the sample database. Meanwhile, the samples will be returned to (4) and the clustering centers of various types will be re-evaluated to prepare for the next fault determination.

After FCM fuzzy clustering analysis of the fault recording files of each measuring point, it can be determined whether each measuring point belongs to the fault class or non-fault class. The output of the fault class is defined as 1, and the output of the non-fault class is defined as 0.

4. Interpretation of Result

4.1. Simulation and Verification. In order to verify the effectiveness of the algorithm, Matlab simulation software is used to build the distribution network wiring diagram model and its simulation and calculation.

The distribution network wiring diagram in Figure 5 shows a typical 110 kV/10 kV distribution network wiring.

The main transformer is triangle or star wiring, and the neutral point on the low-voltage side is controlled by a switch to determine whether it is grounded by arc suppression coil.

The simulation of distribution network without direct grounding is carried out, the grounding of distribution network through arc suppression coil is simulated, different initial phase angle, transition resistance or intermittent single-phase grounding of distribution network are also simulated (see Figure 6 for the specific simulation results).

The simulation results show that the fuzzy clustering based on FCM has the ability to learn with the accumulation of samples, and the sample center changes with the enrichment of samples. When the arc suppression coil is grounded with different initial phase angle transition resistance and intermittent fault, the state of each measuring point can be correctly identified, and the accuracy rate is 97%.

4.2. Online Positioning Software for Single-Phase Grounding Based on Distribution Automation. Based on the analysis of single-phase earthing locating technology, the online

locating software of single-phase earthing is designed [21], as shown in Figure 7.

- (1) *Data Layer*. It mainly includes event information about distribution network faults, topology information about the power distribution network, real-time operating status data of distribution network, distribution network attributes, fault records, and their analytical results.
- (2) *Application Service Layer* [22, 23]. It provides basic services, including recording data reading, fault feature extraction, event collection, data collection, and fault location. New services include fault recording, fault feature extraction, event collection, adjustment and optimization of fault location data collection, and fault processing;
- (3) *Presentation Layer*. The real-time status and fault of distribution network are displayed by graphical GIS and other visualization techniques [24, 25].

5. Conclusion

- (1) The fault characteristic quantity of transient zero-sequence current three-phase current fault recording file is extracted by digital processing method when single-phase grounding is performed. The fuzzy C-means clustering analysis method was used to fuse the feature information from multiple dimensions, effectively utilizing the complementary information between feature quantities, avoiding the inherent defects of single algorithm, and improving the adaptability of fault location accuracy.
- (2) With the field operation, a large number of single-phase grounding fault recording data are obtained. The fuzzy C-means clustering analysis method automatically updates the fault or non-fault clustering center, applies its self-adaptive and self-learning ability to reflect the single-phase grounding fault characteristics more truly, and further improves the accuracy of fault location.
- (3) With the operation of the field, the single-phase grounding fault recording data in the whole province and the national network are accessed, and the fault recording data can be automatically clustered by the fuzzy C-means clustering analysis method. Divide the types of single-phase faults such as grounding impedance and grounding fault types. The next step is to explore the application of big data technology theory fuzzy C-means clustering analysis to extract the threshold value of fault characteristic quantity for the massive recording data of single-phase grounding fault, so as to improve the accuracy of single-phase grounding fault research.

Data Availability

The data used to support the findings of this study are available from the corresponding author upon request.

Conflicts of Interest

The authors declare that they have no conflicts of interest.

Acknowledgments

This study was supported by the Science and Technology Project of State Grid Hunan Electric Power Co. LTD. (Based on the research and application of the key technology of single-phase ground fault disposal of the circuit breaker on the new power distribution primary and secondary fusion column) (project no. 5216A521003K).

References

- [1] O. I. Vasin, V. V. Novikova, A. K. Kulygin, and A. S. Avilov, "Automation of the method for construction of the radial distribution function for studying the structure of amorphous substances," *Journal of Surface Investigation X-ray Synchrotron and Neutron Techniques*, vol. 14, no. 5, pp. 1085–1091, 2020.
- [2] V. Mendes, A. Silva, and J. Costa, "Chronological monte carlo simulation for evaluating spare transformer requirements in distribution substations," *Journal of Control, Automation and Electrical Systems*, vol. 32, no. 5, pp. 1365–1376, 2021.
- [3] L. J. R. Neiva, F. C. R. Coelho, W. Peres, S. A. Flávio, and L. R. Dias, "Analysis of power flow reversiocrn in distribution transformers due to medium-voltage fault and distributed generation in secondary networks," *Journal of Control, Automation and Electrical Systems*, vol. 32, no. 6, pp. 1718–1727, 2021.
- [4] L. S. Almeida and P. R. Muniz, "Economic analysis of vegetable-oil-filled power transformers in brazilian energy distribution systems compared to mineral-oil-filled ones," *Journal of Control, Automation and Electrical Systems*, vol. 32, no. 4, pp. 1063–1070, 2021.
- [5] K. Bhatia, P. B. Darji, and H. R. Jariwala, "Assessment of mutual influence of groundings in close proximity to each other through estimation of safety parameters," *IET Science, Measurement and Technology*, vol. 14, no. 8, pp. 955–963, 2020.
- [6] I. E. Kazhekin, "Generating maximum overvoltages in ferroresonant processes during single-phase arc shorts in ship low-voltage electrical systems," *Vestnik of Astrakhan State Technical University Series Marine Engineering and Technologies*, vol. 2020, no. 1, pp. 115–124, Article ID 115124, 2020.
- [7] X. Xu and W. Hu, "Modeling and simulation of arc grounding fault of middle and low voltage distribution network based on atp-empt," *Journal of Computational Methods in Science and Engineering*, vol. 20, no. 4, pp. 1279–1288, 2021.
- [8] X. Zhao, Y. Jia, A. Li, R. Jiang, and Y. Song, "Multi-source knowledge fusion: a survey," *World Wide Web*, vol. 23, no. 4, pp. 2567–2592, 2020.
- [9] Q. Y. Xu, J. Ye, and Y. J. Lyu, "A multi-source data fusion modeling method for debris flow prevention engineering," *Journal of Mountain Science*, vol. 18, no. 4, pp. 1049–1061, 2021.
- [10] B. Wu, W. Qiu, W. Huang, G. Meng, Y. Nong, and J. Huang, "A multi-source information fusion evaluation method for the tunneling collapse disaster based on the artificial intelligence deformation prediction," *Arabian Journal for Science and Engineering*, vol. 47, no. 4, pp. 5053–5071, 2022.

Retraction

Retracted: Data Mining Algorithm for Power User Network Based on Multi-Information Fusion

International Transactions on Electrical Energy Systems

Received 3 October 2023; Accepted 3 October 2023; Published 4 October 2023

Copyright © 2023 International Transactions on Electrical Energy Systems. This is an open access article distributed under the Creative Commons Attribution License, which permits unrestricted use, distribution, and reproduction in any medium, provided the original work is properly cited.

This article has been retracted by Hindawi following an investigation undertaken by the publisher [1]. This investigation has uncovered evidence of one or more of the following indicators of systematic manipulation of the publication process:

- (1) Discrepancies in scope
- (2) Discrepancies in the description of the research reported
- (3) Discrepancies between the availability of data and the research described
- (4) Inappropriate citations
- (5) Incoherent, meaningless and/or irrelevant content included in the article
- (6) Peer-review manipulation

The presence of these indicators undermines our confidence in the integrity of the article's content and we cannot, therefore, vouch for its reliability. Please note that this notice is intended solely to alert readers that the content of this article is unreliable. We have not investigated whether authors were aware of or involved in the systematic manipulation of the publication process.

Wiley and Hindawi regrets that the usual quality checks did not identify these issues before publication and have since put additional measures in place to safeguard research integrity.

We wish to credit our own Research Integrity and Research Publishing teams and anonymous and named external researchers and research integrity experts for contributing to this investigation.

The corresponding author, as the representative of all authors, has been given the opportunity to register their agreement or disagreement to this retraction. We have kept a record of any response received.

References

- [1] S. Huang, "Data Mining Algorithm for Power User Network Based on Multi-Information Fusion," *International Transactions on Electrical Energy Systems*, vol. 2022, Article ID 2337460, 6 pages, 2022.

Research Article

Data Mining Algorithm for Power User Network Based on Multi-Information Fusion

Shutong Huang 

Department of Applied Mathematics, The Hong Kong Polytechnic University, Hong Kong 999077, China

Correspondence should be addressed to Shutong Huang; 20160627@ayit.edu.cn

Received 19 July 2022; Revised 5 August 2022; Accepted 8 August 2022; Published 6 September 2022

Academic Editor: Nagamalai Vasimalai

Copyright © 2022 Shutong Huang. This is an open access article distributed under the Creative Commons Attribution License, which permits unrestricted use, distribution, and reproduction in any medium, provided the original work is properly cited.

In order to solve the problem of accurately mining the power consumption characteristic data of power users, this paper proposes a research on power user network data mining algorithms based on multi-information fusion. In the past, the mining methods based on neural networks and cure algorithms were affected by noise data, resulting in low mining accuracy. To solve this problem, this paper proposes a user-complex power consumption feature mining method based on the K-means clustering algorithm. In the K-means clustering algorithm, the principle of mining complex power consumption characteristics of users is studied, and the data are cleaned, integrated, and preprocessed by protocol transformation to avoid noise interference. The information entropy principle is used to cluster the matrix to regularize the feature points. According to the complex power consumption characteristics, the power consumption feature points are determined through the cluster, the distance between the clusters is calculated, the power consumption feature information gain is obtained, and the user complex power consumption feature mining is completed. The experimental results show that the mining accuracy of this method is up to 99%, providing users with better quality services. *Conclusion.* The automatic control performance of the system is good, and the acquisition results are accurate and reliable.

1. Introduction

With the explosive growth of power distribution data brought about by the large-scale popularization and application of smart meters and the lean management of the power grid, accurate classification and characteristic analysis of power users have become an important task for power grid companies [1, 2]. Mastering the characteristics of user demand response helps to fully tap the potential of user demand response and improve the implementation efficiency of demand response, which is the basis for formulating a demand-side management scheme and electricity price package. With the development of economy and technology, the types and behaviors of power users are complex and diverse [3]. The obtained data of power users show the characteristics of high-dimensional and massive data, which makes it more difficult to classify users and analyze response characteristics. Therefore, efficient

processing of complex user data and accurate analysis of power consumption characteristics are very important [4–6].

At present, the research on user response characteristics is mainly divided into two categories: machine rational analysis and nonmachine rational analysis. The mechanism analysis is mainly to analyze and model the relationship between electricity price and other incentive signals and user load in a specific environment [7]. For example, analyze the power consumption characteristics and strategic bidding behavior of power users in the market environment and establish a bilateral game model between power producers and power users [8]. Taking the time-of-use price environment as an example, the self-elasticity and mutual elasticity of users with price changes are analyzed, and the user response model is established [9]. These studies can clearly explain the mechanism of electricity price and other incentive signals on user load and are well adapted to

small-scale specific users, but the modeling is complex and not suitable for users with large differences in characteristics and a large number of users [10]. Nonmachine rational analysis analyzes the effect of incentive means such as electricity price on user load through user data mining. Its core technology is clustering algorithms and data fitting, which is mainly divided into two steps: ① classify the power consumption characteristics of users through a clustering algorithm and classify the users with the same power consumption characteristics; ② use historical data to model the response characteristics of each type of user requirement.

2. Literature Review

With the rapid development of the economy, science, and technology, users' electricity consumption behavior will be more diversified, and the dimension of electricity consumption data will be higher. Clustering faces not only the problem of increasing data volume but also the problem of the high-dimension of electricity consumption data. In order to solve this problem, the nonmechanism analysis method is more concerned. Shao, Z., and others used the fuzzy c-means (FCM) clustering method to cluster power users. This method is a soft clustering algorithm, which overcomes the classification shortcomings of hard clustering. However, this method is sensitive to the initial clustering center and needs to manually determine the cluster number, so it is easy to fall into the local optimal solution [11]. Geetha, S., and others analyzed the power consumption data by using the agglomerative hierarchical clustering method, which does not need to determine the classification number, but the clustering quality is limited for the consolidation of complex data types [12]. Zhou, Y., and others considered the random characteristics of user load, proposed a user classification and behavior modeling method based on the Fourier transform method but ignored more nonprincipal factor information [13]. A self-organizing map (SOM) clustering algorithm and deep learning method are used to classify power consumption patterns of power users. These two algorithms belong to machine learning clustering methods, which can effectively process high-dimensional data but are difficult to adapt to large-scale data. HaDy, A. K., and others used piecewise linear regression to classify and model user demand responses. Although this method is simple to operate, the relationship between incentive and user power consumption is not simply linear, which makes the model less accurate [14]. Zhou, J., and others constructed an analysis model of user response behavior based on long-term and short-term memory networks and applied the equal gradient iterative learning method to obtain appropriate incentive schemes [15]. The above methods try to cluster the data after dimensionality reduction and can solve the problem of clustering some high-dimensional data, but it is difficult to deal with high-dimensional nonlinear data in the process of dimensionality reduction. Technologies such as the automatic encoder (AE) can effectively solve the problem of "dimension disaster" in the face of high-dimensional data and have been applied in engineering [16, 17].

With the increasing demand of power consumption in recent years, there are security problems in power user data [18]. Mining the complex power consumption characteristics of users plays an important role in improving the operation safety of the power system. When the power system is affected by various factors, there are certain power consumption characteristic data [19]. However, these data are mixed with normal power consumption characteristic data, and the mining of normal power consumption characteristic data is subject to a lot of interference, resulting in low mining accuracy. In the past, the mining method based on a neural network was used to generate mining feature data by preprocessing the data. The mining method based on a cure algorithm is adopted to randomly distribute the normal data and power consumption characteristic data in the same proportion and classify the data characteristics by setting different parameters [20]. Both methods can be easily broken down by noise data and have low mining risk. Given the disadvantages of these two methods, we propose a K-means-based and algorithm-based group algorithm to eliminate the complex characteristics of consumer electronics. K-means is the algorithm group that has been taught to learn in detail about the complex characteristics of electronic users.

3. Method

3.1. K-Means Clustering Algorithm. The K-means clustering algorithm takes minimizing the objective function as the optimization objective, iterates continuously, and selects K-means initial condensing points to meet the local optimal clustering effect. The combination is selected according to different initial condensing points. In the process of clustering using a k-means algorithm, different initial condensing points need to be selected many times, and then a clustering operation is carried out. Before clustering with a k-means algorithm, data preprocessing is required. Assume that the data first used as a K-cluster algorithm consists of m data examples and k -data properties. At this point, $k > 0$ is an integer. The whole K-key set includes changing the m data examples for the numbers of squares of the middle group. The formula is

$$F = \sum_{i=1}^K F_i = \sum_{i=1}^K \sum_{j=1}^m \alpha_{ij} \|A_j - B_i\|^2, \quad (1)$$

In formula (1), F represents the objective function of the sum of squares of the distance between cluster centers, A_j represents J data characteristic attributes, B_i represents i feature clustering centers, and α_{ij} represents the weight coefficient.

During clustering, it is necessary to obtain the actual value of the target function by the number of squares at a distance from the center of the group. Figure 1 shows the application process when using the K-mean algorithm group to exclude the complex characteristics of electronic users.

As the application process is shown in Figure 1, the dataset is first determined, then the average values are randomly selected, and the K-mean group algorithm is used to calculate the value of F . If the value of F changes

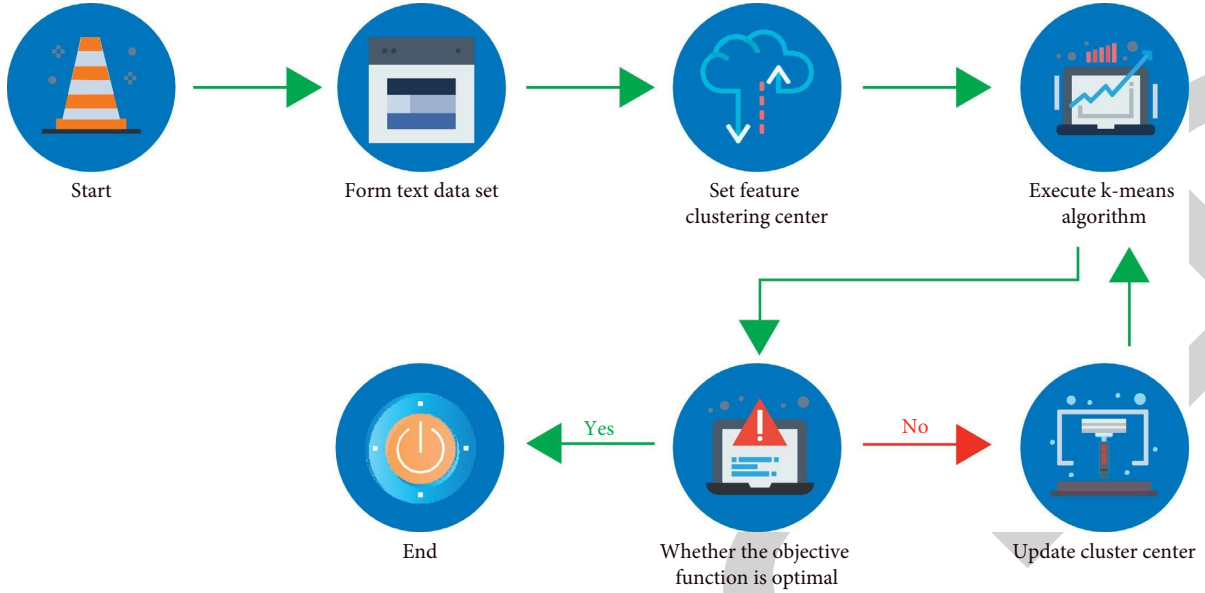


FIGURE 1: Application process of the K-means clustering algorithm.

continuously during iteration, it indicates that the agglomeration does not reach the observed mass. At this point, the subgroup needs to be modified, and the process needs to be repeated.

The calculation formula of cluster center (2) is as follows:

$$O_{ij} = \|A_j - B^{i-1}\|, \quad (2)$$

The formula of the equation (2) mainly calculates the distance from the sample data to the feature cluster center.

Based on the above given model, the steps to use the K-mean grouping algorithm are as follows:

- (1) take point K at the first condensation point first;
- (2) calculate the distance from the data structure to the location of the special groups;
- (3) K gives all the points to the group structure of K objects according to the principle of their agglomeration;
- (4) count the centroids of K-specific sites in the group;
- (5) repeat steps (2), (3), and (4) until the centroid needs to be repaired;
- (6) we use K-agglomeration.

3.2. Mining of Complex Power Consumption Characteristics of Users. The data of the characteristics of the power supply are combined with the total power consumption of the customer, and the samples are sampled, completed, and sent to the office for data collection to measure the energy consumption of consumers.

Figure 2 shows the mining principles that illustrate the combined power consumption of consumers.

According to the above-mentioned mining principles, the complex power consumption characteristics of users are mined with the support of the K-means clustering algorithm.

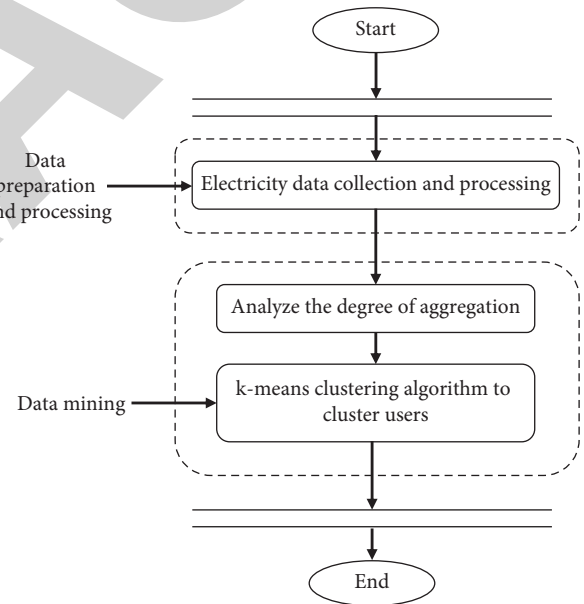


FIGURE 2: Principle of user complex power consumption feature mining.

3.2.1. Data Preprocessing. The mining data of complex power consumption characteristics of users are affected by external noise interference in the process of collection and transmission, and the mining quality is low. Therefore, it is necessary to preprocess them first.

(1) *Data cleaning.* Fill in gaps in consumer electronics, make data noise, eliminate cluster differences, and avoid unreliable data. In the missing data, the mean and intermediate data can be used for interpolation, and the value of the behavior close to the missing pattern can be found in the interpolation log. If you use constants to fill in missing values, you need to analyze the data attributes in advance to clean the data based on them.

(2) *Data integration.* During data integration, data quality should be improved first to reduce redundant data. The metadata method is used to avoid possible identification problems in the data set. In the case of data redundancies, the correlation analysis method is used to ensure the presence of redundant data and stored in different units of measurement.

(3) *Document protocol.* Consider the difference between it all, show the old file in a small space, and decide whether it is possible to create the old file after compressing the file to show the file large.

(4) *File transfer.* The files are divided into separate sections to remove clutter in the file, convert the next batch into subdivisions, and group the files.

3.2.2. *Power Consumption Feature Mining Based on the K-Means Clustering Algorithm.* According to the periodicity of users' complex power consumption characteristics, real-time analysis will be carried out based on the users' power consumption data attributes to prevent the users' complex power consumption data from changing and affecting the mining results. The x targets contained in the user's complex power consumption characteristics are randomly sampled and divided into n numbers to ensure that the user's complex power consumption characteristics are randomly sampled and can be identified with the data in each divided cluster. The regions in any segmented cluster are clustered into x/hn cluster blocks, where h represents the complex power consumption characteristics of users after segmentation for the first time.

According to the complex power consumption characteristics of each user, the power consumption characteristic points are determined through the change of information in the process of clustering. According to the principle of the minimum example method, the cluster formed by the user's complex power consumption characteristic data set is normalized to obtain the first clustering structure, which is merged with the information entropy decision. The characterization results of the distance between the two clusters are

$$d_{\min}(x_1, x_2) = \min_{h \in x_1, h_2 \in x_2} \|h - h_k\|, \quad (3)$$

In formula (3), x_1 , and x_2 , respectively, represent two cluster sets; h and h_k , represent the complex power consumption characteristics of users in the cluster set.

If we are looking for h_k data points for the complex characteristics of consumer electronics and the combination of x objectives, it is contained in the characteristics of the consumer devices. If we are looking for the strength, we count the data content and select the lowest data based on the h_k data. The combination of x targets the difficult characteristics of the effort of the consumer. At this time, the amount of information carried by the point of convergence is the largest, and a new cluster of user characteristic data is formed through this process. The user's complex power consumption characteristic information gain z of the two cluster sets is

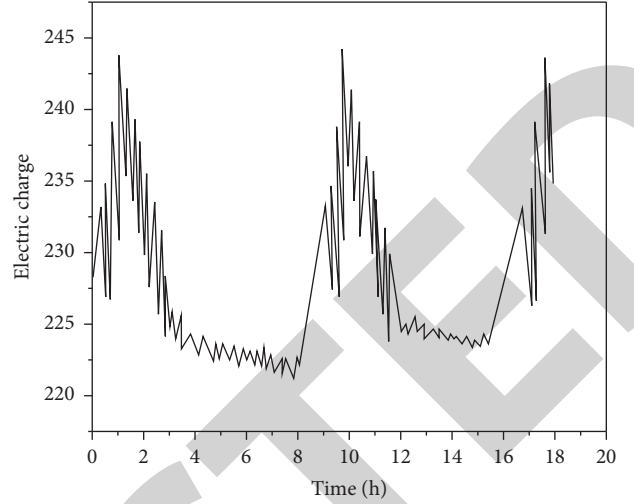


FIGURE 3: Power load characteristics of users in daytime.

$$z(x_{h_\Delta}) = z_1(x_h + x_{h_n}) - z_1(x_h), \quad (4)$$

In formula (4), z_1 represents the feature information gain of a cluster set. The clustering result represented by the maximum target point of the feature information gain z of the two clustering sets is taken as the clustering result after normalization.

After iterating the clustering feature points in any segmentation, the original clustering data in each subregion are reclustered. After calculation, a new cluster centroid is obtained, and the cluster number is marked in turn. Finally, the required number of regulatory clusters is achieved.

In the process of clustering, the processing of user characteristic data should be measured according to the clustering growth rate of user complex power consumption characteristic data. Using this method, the error data can be eliminated on time, and the result of feature data mining is more accurate.

3.3. *Experiment.* Using the Linux operating system, 200 power consumption data points of a city are selected as experimental objects to verify the effectiveness of the user-complex power consumption feature mining method based on the K-means clustering algorithm.

3.3.1. *Mining of Electricity Consumption Characteristics of Daytime Users.* For the situation of high-power consumption by users in the daytime, it is necessary to analyze the load characteristics of users, and the results are shown in Figure 3.

It can be seen from Figure 3 that when the time is 6:00/12:00/18:00, it is the peak period of user power consumption, and the highest charge is 244 c. When the time is 8:00–10:00/13:00–17:00, the user uses less power, and the load is low. According to this feature, the mining accuracy of the neural network mining method, the mining method based on the CURE algorithm, and the proposed method are compared and analyzed. The results are shown in Table 1.

TABLE 1: Accuracy Analysis of daytime feature mining by three methods.

Time/h	Neural network mining method (%)	Mining method based on the CURE algorithm (%)	Proposed method (%)
06.00	50	82	98
08.00	42	74	97
10.00	38	68	97
12.00	35	60	98
14.00	35	65	97
16.00	31	60	95
18.00	30	60	96

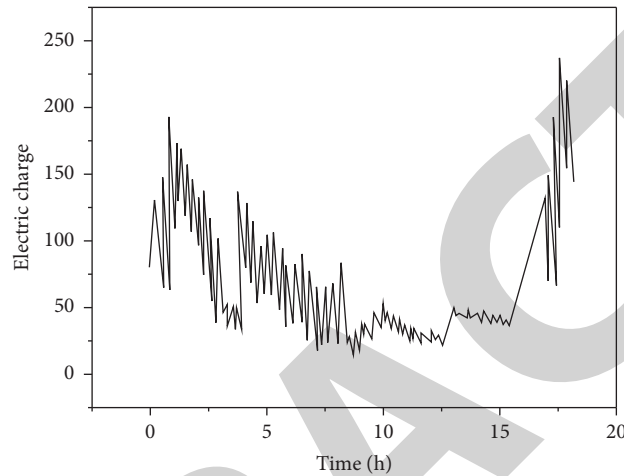


FIGURE 4: Power load characteristics of users at night.

TABLE 2: Accuracy analysis of night feature mining by three methods.

Time/h	Neural network mining method (%)	Mining method based on the CURE algorithm (%)	Methods proposed in this paper (%)
18.00	50	80	99
20.00	52	75	98
22.00	58	71	98
24.00	55	70	98
02.00	56	75	98
04.00	51	70	97
06.00	52	70	97

4. Results and Discussion

For the case of high-power consumption by users at night, it is necessary to analyze the load characteristics of users, and the results are shown in Figure 4.

It can be seen from Figure 4 that when the time is 18:00/06:00, it is the peak period of users' power consumption, while when the time is 20.00/22.00, users' power consumption is relatively large. According to this feature, the mining accuracy of the neural network mining method, the mining method based on the CURE algorithm, and the proposed method are compared and analyzed. The results are shown in Table 1 and Table 2.

It can be seen from Table 1 that the mining accuracy of the proposed K-means clustering method is high, up to 98%, while the mining accuracy of the mining method based on the CURE algorithm remains above 60%, and the mining accuracy of the neural network mining method is always

lower than 50%. It can be seen that the mining method based on the K-means clustering algorithm has high accuracy for mining the complex electricity consumption characteristics of daytime users.

It can be seen from Table 2 that the accuracy of the three methods for feature mining at night is higher than that during the day. The mining method based on the K-means clustering algorithm has a mining accuracy of up to 99%. Therefore, the mining method based on the K-means clustering algorithm has high accuracy in mining the complex power consumption characteristics of night users.

5. Conclusion

This article presents an algorithm for deleting data from electronic devices based on multiple data connections. K-means that a group algorithm is used for real-time data analysis and then for impact research to study the

Retraction

Retracted: Hazard Trend Identification Model Based on Statistical Analysis of Abnormal Power Generation Behavior Data

International Transactions on Electrical Energy Systems

Received 28 November 2023; Accepted 28 November 2023; Published 29 November 2023

Copyright © 2023 International Transactions on Electrical Energy Systems. This is an open access article distributed under the Creative Commons Attribution License, which permits unrestricted use, distribution, and reproduction in any medium, provided the original work is properly cited.

This article has been retracted by Hindawi, as publisher, following an investigation undertaken by the publisher [1]. This investigation has uncovered evidence of systematic manipulation of the publication and peer-review process. We cannot, therefore, vouch for the reliability or integrity of this article.

Please note that this notice is intended solely to alert readers that the peer-review process of this article has been compromised.

Wiley and Hindawi regret that the usual quality checks did not identify these issues before publication and have since put additional measures in place to safeguard research integrity.

We wish to credit our Research Integrity and Research Publishing teams and anonymous and named external researchers and research integrity experts for contributing to this investigation.

The corresponding author, as the representative of all authors, has been given the opportunity to register their agreement or disagreement to this retraction. We have kept a record of any response received.

References

- [1] G. Xu, X. Qian, X. Li, and W. Wu, "Hazard Trend Identification Model Based on Statistical Analysis of Abnormal Power Generation Behavior Data," *International Transactions on Electrical Energy Systems*, vol. 2022, Article ID 5463109, 7 pages, 2022.

Research Article

Hazard Trend Identification Model Based on Statistical Analysis of Abnormal Power Generation Behavior Data

Gaojun Xu ¹, Xusheng Qian ¹, Xiaodong Li ², and Weijiang Wu ¹

¹State Grid Jiangsu Electric Power Company Limited Marketing Service Center, Nanjing 210019, Jiangsu, China

²Nanjing Power Supply Company, State Grid Jiangsu Electric Power Company Limited, Nanjing 210000, Jiangsu, China

Correspondence should be addressed to Gaojun Xu; 2010412211@hbut.edu.cn

Received 13 July 2022; Revised 28 July 2022; Accepted 3 August 2022; Published 31 August 2022

Academic Editor: Nagamalai Vasimalai

Copyright © 2022 Gaojun Xu et al. This is an open access article distributed under the Creative Commons Attribution License, which permits unrestricted use, distribution, and reproduction in any medium, provided the original work is properly cited.

In order to solve the problem of abnormal data identification for key indicators with the deepening and development of power enterprise reform, this paper proposes a method of dangerous trend identification model based on a statistical analysis of abnormal power generation behavior data. The method includes a data access scheme, feature extraction scheme, and anomaly detection algorithm. The experimental results show that the proportion of users whose electricity consumption behavior conforms to the peak period electricity consumption > normal period electricity consumption > valley period electricity consumption exceeds 90%. More than 85% of users' electricity consumption behavior is in line with the proportion of electricity consumption that is less than 0.25 in millet hours. The proportion of users whose fluctuation coefficient of electricity consumption in the valley period is less than 1 exceeds 85%, and 99.9% of users' fluctuation coefficient of electricity consumption in the valley period is less than 5, which proves that abnormal power generation behavior data and abnormal power consumption data can bring early warning to some dangerous power consumption behaviors. The statistical analysis model of abnormal power generation behavior data can play a positive role in the identification of dangerous trends.

1. Introduction

Power statistical data are an important basis for the government to implement macrocontrol, strengthen professional supervision, formulate national economic planning, energy, power, and other special planning, and an important reference for studying and judging the economic and energy situation and formulating industrial policies [1]. We should attach great importance to the statistical work of power regulation. We should not only systematically collect, sort out, and share power statistical information but also use statistical information and data to carry out in-depth comprehensive analysis and special research, so as to better serve the energy and economic decision-making, industry management and supervision, and “deregulation service” reform. With the continuous deepening and development of the reform of power enterprises, energy conservation and consumption reduction in high energy-consuming industries is very important to solve energy problems and is also the fundamental guarantee to achieve the energy

conservation and consumption reduction goal of the 13th five-year plan [2]. The national energy administration and government departments attach great importance to the authenticity and effectiveness of energy conservation and consumption reduction-related indicators when conducting power supervision and statistics. As the main bodies of China's power market are relatively concentrated, the legal awareness of market subjects is relatively weak, and the market supervision system is not perfect; the market power risk has become the main risk of China's power market, showing the characteristics of many forms, difficult prevention, difficult supervision, and great influence, which greatly increases the difficulty of power market construction. The current power generation statistical model lacks an effective data quality control system, and even some power plants report false values to meet the requirements of energy conservation, consumption reduction, and carbon emission, which may form abnormal data, affecting the cognition of relevant departments and enterprises on power generation. Therefore, it is necessary to carry out abnormal data

identification for key indicators to monitor the actual operation level of the power plant. For example, the influence coefficient of a 1% change in the auxiliary power rate on coal consumption for power supply is 3.499%, and each 1% decrease in the load rate will affect the increase of the auxiliary power rate by 0.06%. Therefore, it is of great significance to take the power consumption rate of the power plant as the key index, analyze the potential law of the power consumption rate of the power plant by using the historical data, and identify whether the reported value is abnormal, so as to identify the dangerous trend in all aspects.

2. Literature Review

Chinese and foreign scholars have put forward some identification methods and preventive measures against violations in the power market. Ji and Bai and others built a regulatory index system to judge the use of market power on the generation side [3]. Kulikov and others built a framework for identifying violations in the whole process of electricity market transactions [4]. Li et al., respectively, used game theory, genetic algorithm, and joint evolutionary optimization to determine whether a single power producer participated in collusion [5]. Yang et al. used econometric methods to analyze the collusive bidding behavior between the two major power generation companies in the UK [6]. Phanab et al. proposed that anomaly detection methods for time series include frequency-based methods and machine learning-based methods [7]. The former has the advantage of high processing efficiency and can detect novel patterns in linear time and space. However, due to the use of time series discretization technology, meaningful data may be lost in the process of conversion. The basic idea of the latter is to predict the sequence and determine the abnormal value through the difference between the predicted value and the actual value. It mainly includes two categories: the support vector machine method and the neural network method. As a kind of dynamic neural network, the nonlinear active autoregressive model has the functions of memory and association of historical information and strong adaptability to the time-varying characteristics of time series. At present, it has been used in the fields of wind speed and photovoltaic power prediction. However, these studies have the following problems and shortcomings: first, they only pay attention to the establishment of market supervision indicators but do not specifically explain how to use indicators to identify abnormal trading behavior. Second, the market model has been greatly simplified, and only a small number of market members are concerned, but there is little research on dealing with large-scale datasets generated by actual market operations. At present, there is a lack of research on abnormal power consumption behavior detection based on the power consumption data of users (residents, communities, buildings, enterprises, etc.). However, the existing anomaly detection methods for equipment operation status mainly design data mining analysis algorithms and match them based on the known characteristics of equipment operation status reflected in the data. They do not use the method of automatically learning and summarizing universal laws from

massive data, so they cannot automatically identify the abnormal behavior characteristics different from universal laws or unknown [8].

Facing the big data early warning demand of social security risk, this paper studies the problem of abnormal trend identification and early warning based on the data mining and analysis of people's daily behavior (such as power consumption behavior) and puts forward the characteristic identification method and the early warning model of abnormal power consumption behavior. Combined with the structure of the power system and the characteristics of power consumption data, the schemes of data security access, distributed storage, parallel computing analysis, and visual display are designed, and the construction of power consumption anomaly analysis and early warning system is completed [9]. The technical implementation scheme of electricity behavior anomaly detection and the public security risk early warning method based on power big data analysis is as follows.

We read the user profile, electric energy representation value, electricity consumption in each period, and other data required for power consumption behavior analysis from the relational database of the power grid data acquisition system and use the security access technology to store the data in the HBase distributed database of the Hadoop platform in real time. Then, the MapReduce algorithm is designed to preprocess the data, extract the characteristics of power consumption behavior, cluster based on multi features and time series, and summarize the general laws of residential power consumption behavior [10].

3. Method

3.1. Data Item Extraction. The user profile database and power operation database are the core of the relational database in the power grid data acquisition system. In the data access stage, first, we select the data items to be read in the analysis and early warning stage, including the file data such as the meter number, user identity, and power consumption location, as well as the current positive indication value of the meter, the accumulated power consumption in each period, and other operating data. The specific initial data items to be extracted are shown in Table 1.

3.2. Construction of Intermediate Warehouse. We set up an interface server and a relational database in the power intranet. The data are synchronized from the database of the power grid data acquisition system to the intermediate database through the goldengate data synchronization technology. Among them, the archive data in the user archive database and the historical operation data in the power operation database are synchronized to the intermediate database at one time by using the data pump technology, and the newly collected power consumption data of the power grid data acquisition system are synchronously updated to the intermediate database every day [11].

3.3. Data Transmission Method. The data transmission channel adopts strong isolation technology [12]. This

TABLE 1: Description of data items extracted from the power system.

Serial number	Data item name	Data item meaning
1	Measure_id	Number of acquisition terminals
2	Date	Acquisition time
3	User_name	User registration name
4	User_id	Customer meter No
5	User_address	Address of user meter
6	Sum_cur_total	Current total electricity consumption
7	Sum_cur_peak	Cumulative power consumption during peak hours
8	Sum_cur_normal	Accumulated electricity consumption in the normal period
9	Sum_cur_valley	Accumulated electricity consumption in the valley period

technology is technology that allows the external network to access the intranet database, but the database seen by the external network is only a virtual database. At the same time, policies can be added in the strong isolation to prevent illegal access by users. The data transmission architecture is shown in Figure 1.

First, it is necessary to route through the firewall and then the Intrusion Prevention System (IPS) and Access Controller (AC) can be connected to the strongly isolated devices to realize interaccess. If the social security risk precontrol system based on abnormal electricity use behavior detection is deployed on the private network of political, legal, and public security departments, a special data transmission line is required. One end is connected to the intermediate library deployed in the power intranet and the firewall outside the IPS and other security systems through the above steps, and the other end is connected to the corresponding private network through the security access platform (dedicated to the public security network) [13]. The intermediate database is configured as the data source, and only one-way transmission of data points (intermediate database) to points (database of power abnormal analysis system) is allowed.

3.4. Distributed Data Storage. After associating the file data read from the intermediate database with the operation data according to the user ID, the historical data are stored in the HBase distributed database in the key value mode. Since the user ID of the user meter is unique, the digital string spliced between the user ID and the acquisition time (date) is used as the key, and the acquisition terminal number and the cumulative value of electricity consumption in each period are used as the column value. When new data are entered, we first generate data records in key-value format and then execute the query and insert each into the data block where the same key is located [14].

3.5. Feature Extraction Scheme. During equipment condition monitoring, clear fault characteristics can be used for anomaly identification. In contrast, there is no clear definition of abnormal power consumption behavior before. The residential electricity data collected in a city for one month (30 days) are selected as the training set, and the feature extraction scheme is as follows:

Step 1. Data preprocessing to eliminate the data with class B abnormal characteristics.

For each meter, the positive electric energy indication value of each day in a month is $Sum_cur_total_i$, where $i \in [1, 2, \dots, 30]$, and then, the daily power consumption is

$A_i = Sum_cur_total_{i+1} - Sum_cur_total_i$. If $A_i < 0$, or the sum of the indicated electricity consumption in three periods of a day is not equal to $Sum_cur_total_i$, the data of the corresponding electricity meter shall be deleted.

Step 2. Calculate the power consumption in each period of the day.

The power department divides a day into three periods according to the electricity consumption, including the peak period, normal period, and valley period. For residential power consumption, the peak period is the period with the highest power demand, generally in the early morning and at night (taking the area in Dongba district as an example, the peak period is from 6:00 to 10:00 and from 18:00 to 22:00). The valley period is the period with the lowest power demand, generally from midnight to early morning (22:00 to 6:00 in the East 8th District). Electricity demand in the normal period is between the peak period and the valley period. For each meter that is not excluded, the electricity consumption in three periods of each day is calculated as follows:

Power consumption during peak hours:

$$A_{i,peak} = Sum_cur_peak_{i+1} - Sum_cur_peak_i;$$

Electricity consumption in the normal period:

$$A_{i,normal} = Sum_cur_normal_{i+1} - Sum_cur_normal_i;$$

Electricity consumption during the valley period:

$$A_{i,valley} = Sum_cur_valley_{i+1} - Sum_cur_valley_i.$$

Step 3. Calculate the proportion of electricity consumption in each period of the day.

The proportion of peak, average, and valley electricity consumption in the total electricity consumption of the day is calculated as follows:

Proportion of electricity consumption in the peak period: $ratio_{i,peak} = A_{i,peak}/A_i$; proportion of electricity consumption in the normal period: $ratio_{i,normal} = A_{i,normal}/A_i$; proportion of electricity consumption in the valley period: $ratio_{i,valley} = A_{i,valley}/A_i$.

Step 4. Calculate the fluctuation coefficient of daily power consumption, power consumption in each period, and the proportion of power consumption in each period.

The average value of each parameter is calculated. Taking the daily power consumption as an example, the monthly average value is

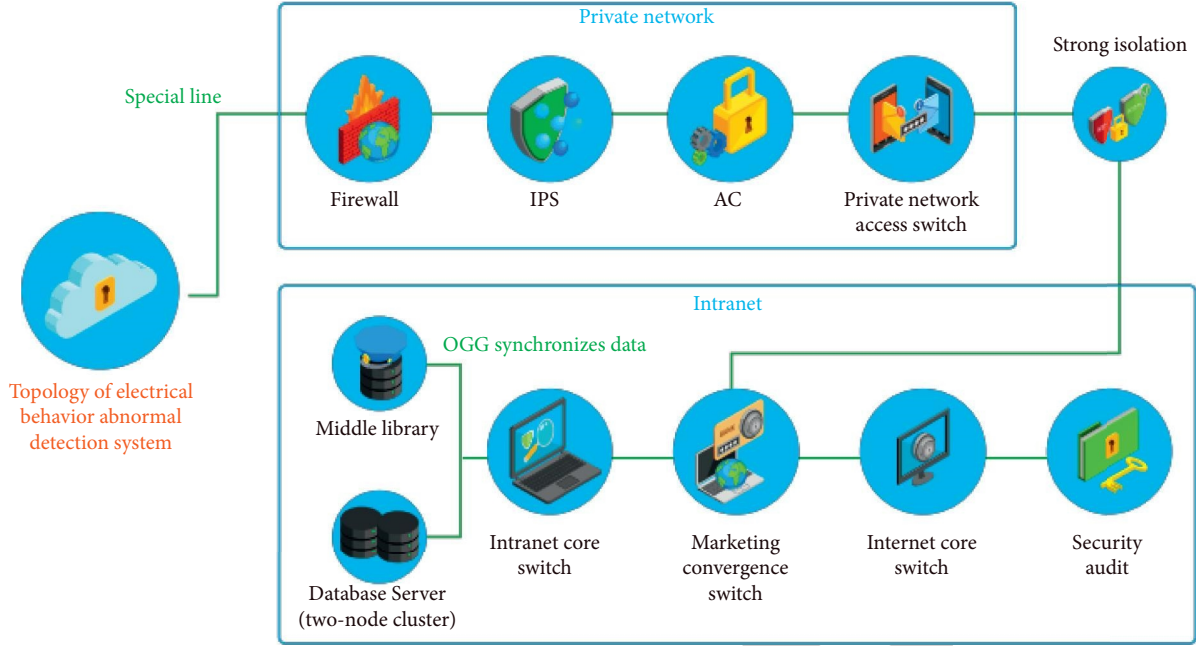


FIGURE 1: Schematic diagram of data transmission.

$$\text{mean}(A) = \sum_{i=1}^{30} \frac{A_i}{30} \quad (1)$$

The variance of each parameter is calculated, and taking the power consumption in the peak period as an example, the variance is

$$\text{var}(A_{\text{peak}}) = \sum_{i=1}^{30} [A_{i,\text{peak}} - \text{mean}(A_{\text{peak}})]^2 \quad (2)$$

The fluctuation coefficient of each parameter is calculated. Taking the proportion of electricity consumption in the valley period as an example, the fluctuation coefficient is as follows:

$$\text{cv_ratio_valley} = \frac{\sqrt{\text{var}(\text{ratio}_{\text{valley}})}}{\text{mean}(\text{ratio}_{\text{valley}})} \quad (3)$$

3.6. Anomaly Detection Algorithm. The abnormal detection process of electric behavior is divided into two parts: abnormal behavior detection and abnormal feature analysis. The former stage is used to identify abnormal power consumption behavior, and the latter stage is used to match the characteristics of abnormal power consumption behavior with those of criminals in actual cases to generate accurate early warning information.

Step 5. The MapReduce computing model is used in the abnormal behavior discovery process.

- (1) We perform two types of map tasks, respectively; that is, we calculate the daily power consumption, power consumption in each period of the day, and the

proportion of power consumption in each period of the day of each meter for the latest week and the latest month, as well as the mean value, variance, and fluctuation coefficient of these parameters in the selected period.

- (2) The reduce process performs clustering. The selected clustering features are shown in Table 2. Clustering shows that the data characteristics are different from those of most meters [15].
- (3) Using the LOF (local outlier factor) algorithm for further anomaly detection, the highest abnormal level of power consumption behavior can be found according to the score value distribution.

Step 6. In the abnormal feature analysis process, the abnormal behavior data extracted from the abnormal behavior discovery process and the existing feature database are calculated to confirm whether the abnormal power consumption behavior meets the alarm conditions and outputs the accurate early warning type [16].

- (1) We verify whether the fluctuation coefficient of night power consumption and its proportion increases sharply at the same time. As shown in Figure 2, the gang gathered at the home of a criminal for two consecutive days before the crime, and its midnight (valley time) power consumption increased sharply, while there was no significant change in the peak period and peacetime power consumption, resulting in a sudden increase in the valley time power consumption fluctuation coefficient and the valley time power consumption proportion fluctuation coefficient of the meter. The warning type generated by such an abnormal behavior is abnormal power

TABLE 2: Description of clustering features selected by the anomaly detection algorithm.

Serial number	Feature name	Feature definition
1	Cv_cur_total	Fluctuation coefficient of power consumption throughout the day
2	Cv_cur_peak	Fluctuation coefficient of power consumption in the peak period
3	Cv_cur_normal	Fluctuation coefficient of electricity consumption in the normal period
4	Cv_cur_valley	Fluctuation coefficient of electricity consumption in the valley period
5	Cv_ratio_peak	Fluctuation coefficient of electricity consumption in the peak period
6	Cv_ratio_normal	Fluctuation coefficient of electricity consumption in the normal period
7	Cv_ratio_valley	Fluctuation coefficient of electricity consumption in the valley period

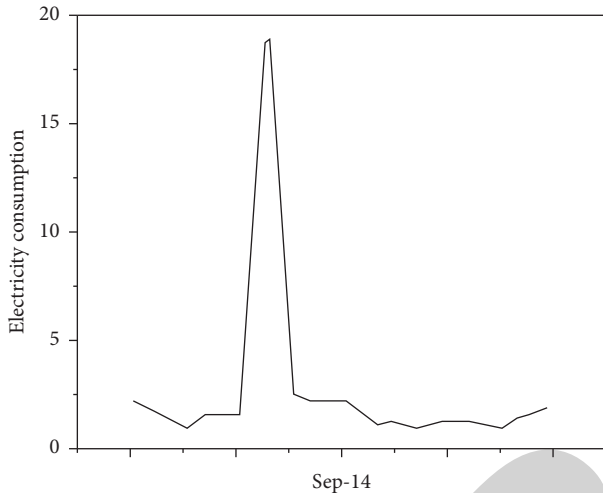


FIGURE 2: Abnormal characteristics of the sudden increase of power consumption at night.

consumption at night. The judgment conditions are as follows: for users whose fluctuation coefficient of electricity consumption in the valley period and the proportion of electricity consumption in the valley period are greater than 50%, we calculate the proportional relationship between the electricity consumption in the valley period on the day of the sudden change and the previous day and the electricity consumption in the other two periods, $A_{i, \text{valley}} / (A_{i, \text{peak}} + A_{i, \text{normal}})$. If the value on the day is greater than twice the value on the previous day, this kind of alarm information will be generated.

- (2) The fluctuation coefficient of electricity consumption in each period continues to increase. As shown in Figure 3, a criminal used high-power electrical appliances to make crime tools at home during the preparation stage. The electricity consumption in each period has increased significantly and fluctuated sharply within the time window. The warning type generated by such an abnormal behavior is the abnormal fluctuation of power consumption throughout the day [17]. The specific judgment conditions are as follows: the whole day power consumption fluctuation coefficient Cv_cur_total is calculated. If the value increases for three consecutive days and the cumulative increase exceeds 100%, this kind of alarm information will be generated.

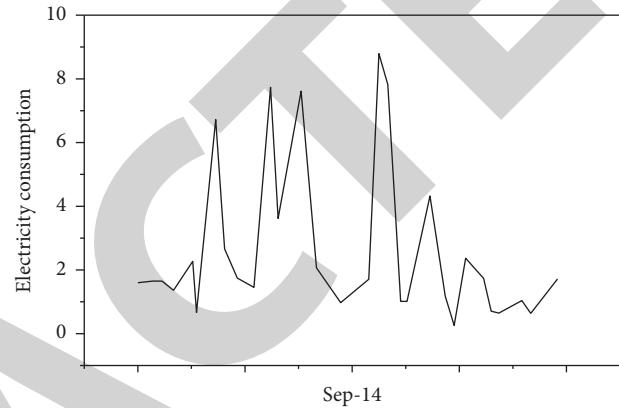


FIGURE 3: Abnormal characteristics of sudden increase and sharp fluctuation of electricity consumption throughout the day.

- (3) The electricity consumption decreases sharply (even approaches zero) and continues to rise. As shown in Figure 4, on the eve of the crime, the perpetrator left his home and joined the crime gang. Its power consumption is close to 0, and there is no fluctuation in power consumption in each period [18]. The alert type generated by such an abnormal behavior is suspected of leaving home.

3.7. Alarm Visualization Scheme. Visualization of early warning information: the visualization interface is mainly based on the application of GIS Geographic Information System. Based on the power consumption address information (place name, longitude, and latitude) in the file data, the location of the electricity meter that generates the abnormal power consumption early warning is displayed on the GIS map, and all the power consumption early warning information within the jurisdiction is displayed on the page in the form of a list. The contents displayed in the list include alarm level, user name, and alarm time. In addition, the location of the alarm is visually displayed on the map. You can click the alarm location to view the user details, alarm type, power consumption curve, and other specific information.

Visualization of regional early warning: we calculate regional abnormal electricity consumption indicators from the two dimensions of judging whether the location of abnormal electricity consumption meters is concentrated in a certain area and whether the electricity consumption of suspected personnel in each key monitoring area is

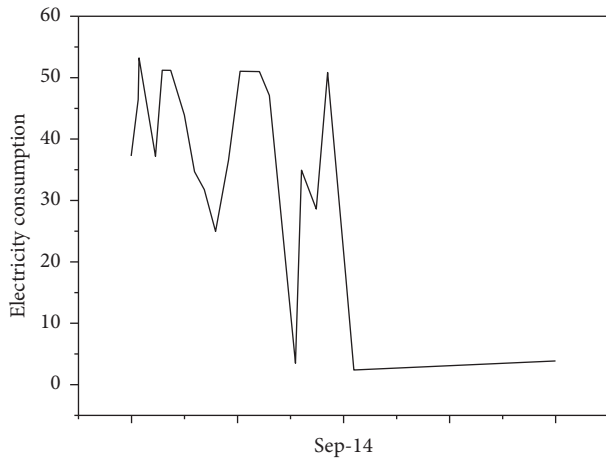


FIGURE 4: Sharp decrease in power consumption and no recovery.

abnormal [19]. The level of indicators mainly depends on the level of abnormal electricity consumption in the region and the number of abnormal electricity meters. Different colors are used to represent different regional early warning levels.

4. Results and Discussion

The distribution of electricity consumption in each period and its fluctuation coefficient were analyzed. Through the distribution of each parameter, the general law of normal electricity consumption behavior can be obtained.

The proportion of users whose electricity consumption behavior is in line with peak period electricity consumption > normal period electricity consumption > valley period electricity consumption exceeds 90%. More than 85% of the users whose electricity consumption behavior is in line with the valley period have electricity consumption proportion < 0.25.

The proportion of users whose fluctuation coefficient of electricity consumption in the valley period is less than 1 exceeds 85%, and the fluctuation coefficient of 99.9% of users' electricity consumption in the valley period is less than 5.

Obviously, if the electricity consumption and its proportion in the valley period increase significantly and the electricity consumption and its proportion in each period fluctuate violently (the value of the fluctuation coefficient is significantly greater than the value in the normal range), it belongs to abnormal electricity consumption behavior [20].

5. Conclusion

In this paper, a method of hazard trend identification model based on a statistical analysis of abnormal power generation behavior data is proposed. This method also analyzes the power consumption in each period, the proportion of power consumption in each period, and the distribution of its fluctuation coefficient, calculates the proportion of power consumption in each period of the day, and reverses the early warning of abnormal power generation behavior data on the identification of dangerous trends to prove that the

power consumption rate of the power plant is taken as the key index. It uses historical data to analyze the potential law of the power consumption rate of power plants and identify whether the reported value is abnormal. It is of great significance to identify dangerous trends in all aspects.

Data Availability

The data used to support the findings of this study are available from the corresponding author upon request.

Conflicts of Interest

The authors declare that they have no conflicts of interest.

References

- [1] S. Liao, L. Wei, T. Kim, and W. Su, *Modeling and Analysis of Residential Electricity Consumption Statistics: A Tracy-Widom Mixture Density Approximation*, IEEE Access, Piscataway, NJ, USA, 2020.
- [2] K. Giwa and O. D. Osahon, "Article average annual committed effective dose and threshold consumption rate of bovine samples collected from a government owned abattoir, ikpoba slope, Benin city, Nigeria," *Canadian Journal of Physics*, vol. 98, no. 8, pp. 742–751, 2020.
- [3] M. Ji and X. Bai, "Construction of the sponge city regulatory detailed planning index system based on the swmm model," *Environmental Technology and Innovation*, vol. 23, no. 19, 2021.
- [4] A. A. Kulikov, "Application of biometric systems in face identification technologies," *Russian Technological Journal*, vol. 9, no. 3, pp. 7–14, 2021.
- [5] X. Li, J. Liu, M. S. Obaidat, P. Vijayakumar, Q. Jiang, and R. Amin, "An unlinkable authenticated key agreement with collusion resistant for vanets," *IEEE Transactions on Vehicular Technology*, vol. 70, pp. 7992–8006, 2021.
- [6] C. Yang, W. Zhang, F. Zhang et al., "Research and dynamic analysis based on nonlinear identification of sports goods econometrics," *Journal of Physics: Conference Series*, vol. 1802, no. 2, 2021.
- [7] T. T. H. Phanab, É. P. Caillaultac, L. Alain, and A. Biganda, "Dynamic time warping-based imputation for univariate time series data—sciencedirect," *Pattern Recognition Letters*, vol. 139, pp. 139–147, 2020.
- [8] A. Hemeida, S. Alkhalaf, A. Mady, E. Mahmoud, M. Hussein, and A. M. Baha Eldin, "Implementation of nature-inspired optimization algorithms in some data mining tasks," *Ain Shams Engineering Journal*, vol. 11, no. 2, pp. 309–318, 2020.
- [9] Y. Zhou and P. Zhang, "Reachable eigenanalysis," *IEEE Transactions on Power Systems*, vol. 35, pp. 4936–4939, 2020.
- [10] S. Graham, D. Huffer, and J. Blackadar, "Towards a digital sensorial archaeology as an experiment in distant viewing of the trade in human remains on instagram," *Heritage*, vol. 3, no. 2, pp. 208–227, 2020.
- [11] K. Yuan, X. Guo, and J. Tian, "Research and implementation of clock synchronization technology based on ptp," *Journal of Physics: Conference Series*, vol. 1757, no. 1, 2021.
- [12] Y. Zhang, C. Zhang, Y. Wang, K. Yu, G. Xue, and J. Crowcroft, "Kylinx: simplified virtualization architecture for specialized virtual appliances with strong isolation," *ACM Transactions on Computer Systems*, vol. 37, pp. 1–27, 2019.

Retraction

Retracted: Application of Computer Vision and Sensor Technology in Multivariate Assessment of Ecological Environment Carrying Capacity

International Transactions on Electrical Energy Systems

Received 19 September 2023; Accepted 19 September 2023; Published 20 September 2023

Copyright © 2023 International Transactions on Electrical Energy Systems. This is an open access article distributed under the Creative Commons Attribution License, which permits unrestricted use, distribution, and reproduction in any medium, provided the original work is properly cited.

This article has been retracted by Hindawi following an investigation undertaken by the publisher [1]. This investigation has uncovered evidence of one or more of the following indicators of systematic manipulation of the publication process:

- (1) Discrepancies in scope
- (2) Discrepancies in the description of the research reported
- (3) Discrepancies between the availability of data and the research described
- (4) Inappropriate citations
- (5) Incoherent, meaningless and/or irrelevant content included in the article
- (6) Peer-review manipulation

The presence of these indicators undermines our confidence in the integrity of the article's content and we cannot, therefore, vouch for its reliability. Please note that this notice is intended solely to alert readers that the content of this article is unreliable. We have not investigated whether authors were aware of or involved in the systematic manipulation of the publication process.

Wiley and Hindawi regrets that the usual quality checks did not identify these issues before publication and have since put additional measures in place to safeguard research integrity.

We wish to credit our own Research Integrity and Research Publishing teams and anonymous and named external researchers and research integrity experts for contributing to this investigation.

The corresponding author, as the representative of all authors, has been given the opportunity to register their agreement or disagreement to this retraction. We have kept a record of any response received.

References

- [1] Z. Wang and W. Wang, "Application of Computer Vision and Sensor Technology in Multivariate Assessment of Ecological Environment Carrying Capacity," *International Transactions on Electrical Energy Systems*, vol. 2022, Article ID 5087610, 8 pages, 2022.

Research Article

Application of Computer Vision and Sensor Technology in Multivariate Assessment of Ecological Environment Carrying Capacity

Zhiguo Wang  and Wei Wang 

Suihua University, Suihua, Heilongjiang 152061, China

Correspondence should be addressed to Zhiguo Wang; 201903531@stu.ncwu.edu.cn

Received 12 July 2022; Revised 28 July 2022; Accepted 3 August 2022; Published 30 August 2022

Academic Editor: Nagamalai Vasimalai

Copyright © 2022 Zhiguo Wang and Wei Wang. This is an open access article distributed under the Creative Commons Attribution License, which permits unrestricted use, distribution, and reproduction in any medium, provided the original work is properly cited.

In order to solve the problems of low accuracy and long monitoring time of the existing ecological environment monitoring system, this study puts forward the application method of computer vision and sensor technology in the multivariate evaluation of ecological environment carrying capacity. In this method, the monitor, server, and spatial identifier are designed in the hardware area of the ecological environment monitoring system to maximize the monitoring performance according to the data memory. By analyzing the monitoring principles of RS technology and GIS positioning technology, the devices in the hardware area are reasonably called, and the workflow of the ecological environment monitoring system is summarized, so as to complete the optimization of the ecological environment monitoring system based on RS and GIS technology. The experimental results show that the monitoring accuracy of the ecological environment monitoring system proposed in this study is higher than that of the traditional monitoring system, with an average of 95.4%; the detection time is about 70 s, which is the lowest compared with other systems when the detection quantity is from 0 to 40 and the detection time is from 0 to 80. The designed monitoring system effectively improves the monitoring effect of the ecological environment and promotes the sustainable development of the ecological environment.

1. Introduction

Environmental issues are global issues in the 21st century. Environmental planning is a reasonable arrangement of space and time for human activities and the environment to make the environment, economy, and society develop in a coordinated manner [1]. Ecological environment planning is an important way to achieve the coordinated development of society, economy, and environment. The idea of the modern ecocity directly originated from Edward Howard's garden city [2]. The theory of the garden city shows people the ecological charm of the balance between city and nature. Since the 1960s, the United States, Japan, Britain, Germany, and France have taken a series of actions in environmental planning management, established environmental planning committees, and designated and implemented national, state, and urban environmental planning [3]. The timely

development of eco-environmental planning has timely alleviated the contradiction between the economy and environment. However, the research and solution of environmental problems must involve complex and open information systems. Computer information technology combines modern theories and methods in the development of environmental protection with computers. It has strong spatial and attribute analysis capabilities and can provide convenient and accurate data management and analysis means for the research of ecological environmental protection planning. Therefore, the combination of computer information technology and environmental science has great development potential [4].

Solving the problem of ecological environment monitoring is a major event related to urban environmental protection and people's health [5]. We must do a good job in ecological environment monitoring, strengthen applied

research on ecological environment monitoring, protect the urban ecological environment, and promote sustainable urban development. Modern ecological environmental monitoring has diversity and complexity. With the help of Internet of Things technology, the scientific and technological content of ecological environmental monitoring can be improved, and the efficiency of ecological environment monitoring can be improved. At the same time, it can relatively reduce the detection pressure of environmental monitoring personnel [6].

At present, with the development of the national economy, the public has higher and higher requirements for the living environment. The living environment level is mainly composed of the ecological environment and man-made environment. Among them, the man-made environment is controllable, but the ecological environment is uncontrollable. Therefore, to improve the living environment level, the protection of the ecological environment is particularly critical [7]. The function of the ecological environment monitoring system is to monitor the ecological environment status of each region, provide key analysis data for the protection of the ecological environment, and promote the sustainable development of the ecological environment. The traditional ecological environment monitoring system has a poor ability to identify potential ecological environment change factors and is not forward-looking, which makes some ecological environments unable to be treated and protected in time, resulting in irreparable losses [8]. Therefore, based on the traditional monitoring system, this study integrates RS technology and GIS positioning technology and takes the development needs of the field of ecological environment management as the core to build a new ecological environment monitoring system.

2. Literature Review

In recent years, the rapid development of computer information technology has added new blood to the traditional ecological planning theories and methods. It makes the ecological planning system expressed in the form of numbers and tables and provides convenience for information acquisition, data analysis, and scheme formulation of ecological planning [9]. Haruna and others proposed the application of remote sensing, GIS technology, and software engineering in ecological planning. Later, with the deepening of computer information technology in urban planning, architectural design, and other spatial environment design fields, GIS and virtual reality (VR) technology began to be applied in urban construction [10]. Liu and others systematically integrated the most advanced GIS and VR platforms in the world based on the urban planning and design method of GIS and VR technology, highlighted the applicability, served the production projects, greatly improved the quality and efficiency of urban planning and design, introduced virtual scenes into urban planning, visually and intuitively, generated data in urban planning, and provided conditions for the future implementation of urban planning and computer urban planning information management [11]. Yakubova and others used VR, GIS, WWW,

and other information technologies to digitally collect and store, dynamically monitor and process, comprehensively manage, and transmit and distribute various information such as geographical environment, infrastructure, natural resources, ecological environment, population distribution, social and economic status in the study area. Build a three-dimensional urban model and urban basic information platform and establish a professional application rule base, model base, and corresponding application system suitable for different functional departments. On this basis, develop a computer application system for governments at all levels to comprehensively manage cities and make macro decisions and use digital technology for ecological planning, changing the concept of planning [12]. Mai and others proposed the Yellow River Basin water based on the spatial data collection, editing, management, analysis, and mapping system, which directly provides the government departments with the query of the background data of the ecological environment and reflects the change trend and law of the ecological environment [13]. Alharthi and others used RS and GIS technology, took the TM satellite remote sensing image of the study area as the main data source, combined with the social and economic data and field investigation records of the study area in recent years, conducted scenario simulation on the ecological environment of the study area, and used env4.5 as a supporting tool to guide the development planning and ecological construction of the study area by exploring the dominant resources and contradictions in land use [14]. Khashaba and others aimed to realize dynamic monitoring and information management of the ecological environment in the research of the ecological environment information management system based on WebGIS. Based on the investigation of basic ecological environment data and the establishment of a massive spatial database, WebGIS technology is seamlessly integrated with traditional mls/oa, and the integrated "3S" technology is used to realize the management of massive ecological environment resource data in the planning area [15]. Through the extraction and mining of "3S" thematic information, it preliminarily provides auxiliary decision support for ecological environment planning and management.

3. Methods

3.1. Hardware Design of the Ecological Environment Monitoring System Based on RS and GIS. The hardware of the ecological environment monitoring system based on RS and GIS is mainly composed of a monitor, server, spatial identifier, and memory. Figure 1 shows the hardware composition of the system.

3.1.1. Monitor. The monitor is the core hardware equipment in the hardware area of the ecological environment monitoring system based on RS and GIS technology [16]. Its main function is to call RS monitoring technology and GIS technology to monitor the ecological environment according to relevant conditions through the data information fed back by the spatial identifier and memory. The sbh-98h series monitor

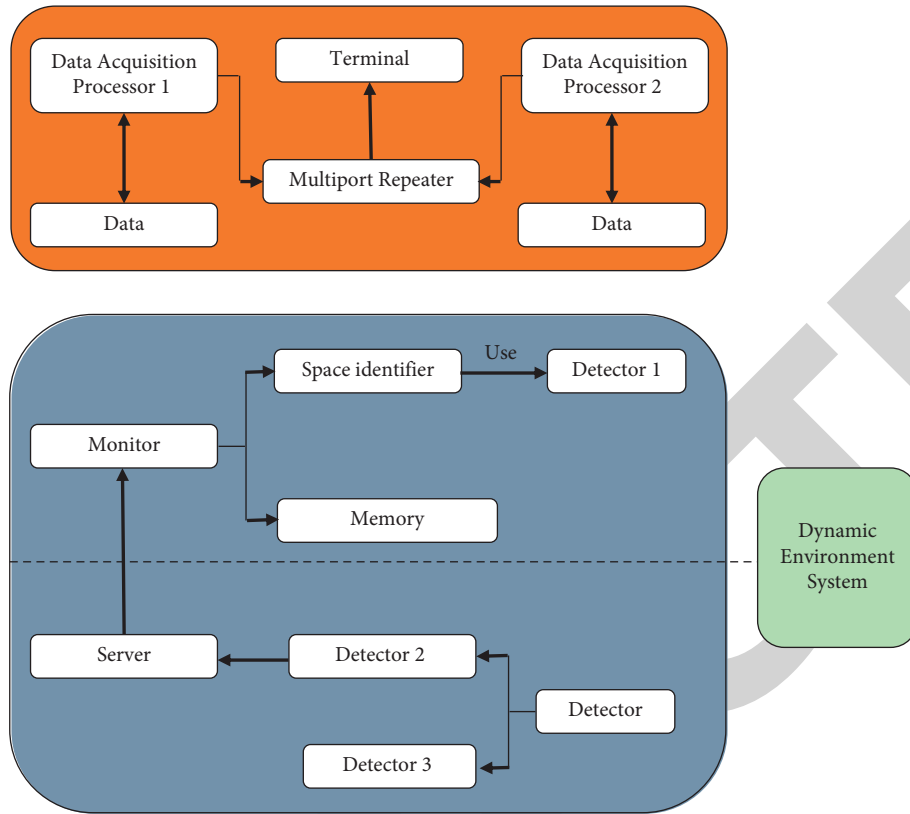


FIGURE 1: Hardware of the ecological environment monitoring system based on RS and GIS.

selected in this article has a resolution of 1296p, a lens aperture of f1.4, a monitoring visual angle of 360 degrees, and an SD card tag with the ability to track the movement of the ecological environment. The sbh-98h monitor adopts 8-channel multichannel mode and is equipped with 940 nm infrared fill light. It can also master the nighttime changes in the ecological environment. For the data collected by the monitor, the H.264 coding method is used for data conversion. In addition, the monitor has a memory comparison function. The monitoring system will submit a safety monitoring standard to the monitor. Once the environmental status of the monitor comparison area does not meet the standard, an alarm will be sent immediately.

3.1.2. Server. The function of the hardware area server is to maintain the normal operation of each hardware device in the hardware area and ensure the stable operation of the monitoring system [17]. The core of the server used in this article is the CC2530 chip, which is mainly composed of a CPU, DMA channel, controller core, and other basic devices [18]. CC2530 chip is applicable to the 2.4 GHz IEEE802.11 communication standard and provides a powerful background operation support for the ecological environment monitoring system. CC2530 chip integrates RF front-end, data converter, clock, and other modules and can also conduct environmental monitoring in areas with weak signals. In addition, the CC2530 chip has 21 programmable i/o interface units, and there is no queue cache during operation, which improves the working efficiency of the

monitoring system. The 8 km ram of the CC2530 chip has its own memory function. When conducting secondary environmental monitoring on the same area, it will call the first monitoring data and environmental change rules to simplify the monitoring process of the monitoring system.

3.1.3. Spatial Identifier. The function of the spatial recognizer is to identify the data of the ecological environment of a certain area and provide the basis for the monitoring of the ecological environment [19]. This study adopts a Kohkuo-98 spatial recognizer, which weighs 130 g. The effective distance of this spatial recognizer is 1000 km, the recognition accuracy is 40 mm, the angular resolution is 25 msec/scan, the driving current is 150 mA, and the driving current when the recognizer is turned on is 300 mA. The vibration mode of the spatial recognizer is 1.5 mm, 10–55 Hz, 2-hour double amplitude vibration mode for each axis, and its protection grade is IP65, which meets the IEC standard of the recognizer. Three groups of input and output ports are designed at the edge of the device. P1 port has 8 pins, P2 port has 5 pins, and P3 port has 10 pins, a total of 23 pins. These pins can not only identify the data of the ecological environment but also complete the configuration of the pin data transmission function of the spatial identifier.

3.1.4. Memory. This article uses the 8051 core memory, which has four 8 + 256 g storage spaces and multiple slots. When the memory detects that the storage space is not

redundant enough, it immediately inserts a temporary storage card. At the same time, the memory immediately clears up the buffer data and invalid data stored in the space and then transfers the data in the slot to the memory. The task of the memory is to store the ecological environment data for the monitoring system and call the previous environment data during monitoring, so as to simplify the monitoring process. Each storage space of the memory has a read-write function. Is memory module is set for storage, and the ecological environment data deleted in a certain period can be retrieved. The read/write storage speed of the 8051 core memory can reach 2045 mb/s, which is also scalable. It can be additionally equipped with two $d \times 517$ hard disks to expand the original 4 GB DDR4 to 32 GB, so as to improve the storage speed and call the speed of the memory.

3.2. Software Design of the Ecological Environment Monitoring System Based on RS and GIS. Remote sensing technology is based on electromagnetic wave theory. It uses a variety of card readers and sensors to identify electromagnetic waves within a certain distance and processes the collected data, so as to affect the ecological environment, apply it to different fields, and solve different problems. Remote sensing technology is used to collect data on a certain space area, simulate its environmental status, and assist ecological environment monitoring [20]. The basic principle of applying remote sensing image main analysis technology to ecological environment monitoring is to use the remote sensing effect to classify the ecological environment and then monitor according to the data of various ecological environment indicators. Figure 2 shows the RS technical idea.

When monitoring the ecological environment, the principal component analysis technology of remote sensing images is used to determine the ecological environment level according to the remote sensing ecological environment indicators. The principal component analysis of remote sensing images was used to monitor the ecological environment of air quality and soil dryness. Its eco-environmental indicators include ground humidity, air humidity, ground temperature, and green plant coverage. Using remote sensing technology for monitoring, first, collect the above ecological environment indicators, normalize the collected data, and calculate the correlation matrix of each indicator. The monitoring system automatically simulates the regional ecological environment and analyzes the ecological environment level of the region in combination with the geographic location information detected by GIS technology. The specific normalization calculation formula is as follows:

$$RSE = 1 - \{PCI[a, b, c, d, e]\}, \quad (1)$$

$$D = \frac{(RSE - RSE_{0MIN})}{(RSE_{0MAX} - RSE_{0MIN})}, \quad (2)$$

where a is the soil moisture; b represents air quality; c represents the air humidity component; d is the surface temperature; e refers to green plant coverage. The fluctuation

range of the normalized value is between 0 and 1. The closer the value is to 1, the better the ecological environment is. On the contrary, the worse the ecological environment is.

GIS is also called geographic information technology. The task of this technology is to integrate information science and geographic science. It is a comprehensive geographic information technology based on cybernetics, information theory, artificial intelligence, spatial analysis, and other disciplines. It is used to collect data related to geographic information. With the development of the network field, the biggest advantage of geographic information technology in the field of ecological environment monitoring is visualization and real-time, which makes the results of ecological environment monitoring highly accurate. The principle of geographic information monitoring is to call the geographic information of the area to be monitored in the geographic information system through the network to provide the analysis data basis for the identification of the ecological environment level and then combine the regional ecological environment simulation imaging formed by GIS technology to carry out a visual geospatial analysis. Figure 3 shows the implementation path of GIS technology.

In the ecological environment monitoring system, the main work of GIS technology is to collect, analyze, and monitor the geographical information of the monitoring environment and the surrounding area. Once there is a fluctuation in the geographical area within the monitoring area that can affect the monitoring area, GIS technology will identify it for the first time and make countermeasures to maintain the development of the ecological environment.

Based on the performance analysis of the equipment in the hardware area of the ecological environment monitoring system and the analysis and discussion of the monitoring principle of RS technology and GIS technology, this study summarizes the workflow of the ecological environment monitoring system based on RS technology and GIS technology. Figure 4 shows the specific work steps.

3.3. Experimental Study. In order to verify the ecological environment monitoring system based on RS and GIS, a comparative experiment is designed. The selected comparative systems are the ecological environment monitoring system based on high score images and the ecological environment monitoring system based on the fuzzy analytic hierarchy process. Setting the ecological index mainly includes ecol index (ID), with the data type of Int. Corresponding to the ecological quality grade, the data type is Int; area occupied by grade, the data type is double; the percentage of grade area in the total area, the data type is double. According to the above experimental parameters, a comparative experiment was carried out. Table 1 provides the accuracy of monitoring results.

4. Results and Discussion

According to Table 1, the accuracy of the monitoring results of the ecological environment monitoring system proposed in this study is higher than that of the traditional monitoring

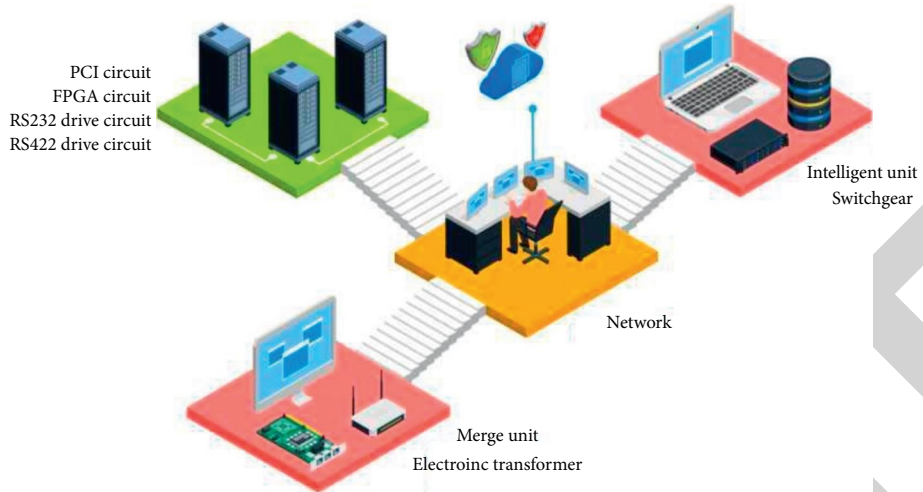


FIGURE 2: RS technical idea.

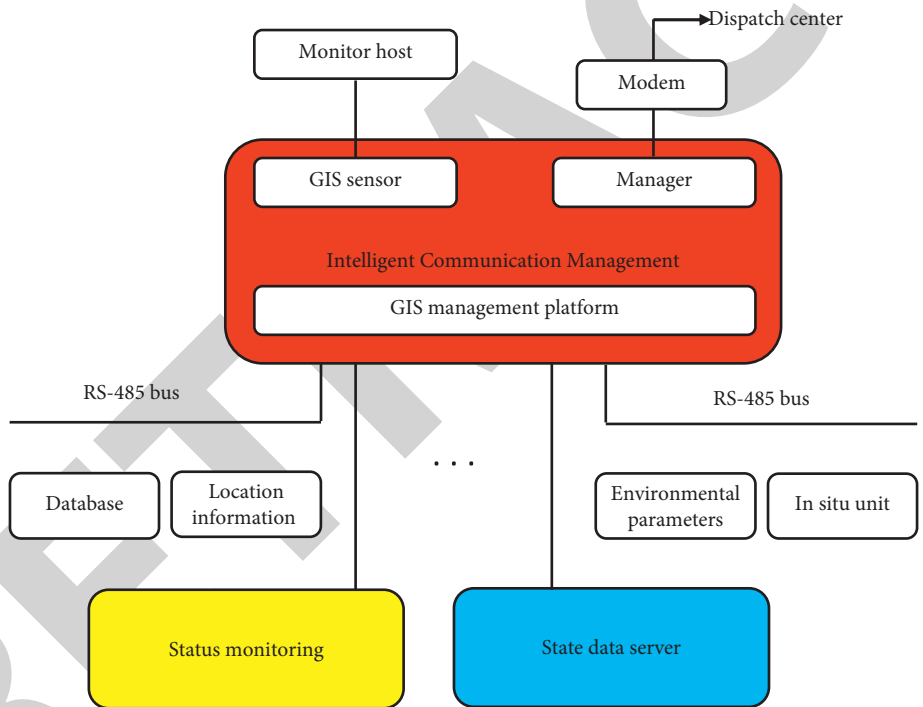


FIGURE 3: Implementation path of GIS technology.

system, with an average of 95.4%. The remote sensing technology based on GIS, combined with its own advantages, uses GIS technology to manage, analyze, and map spatial data while extracting urban ecological index information, so as to realize the quantitative evaluation of the urban ecological environment. It can be used in monitoring, PM2.5 spatial interpolation classification, thematic mapping, and other integrated system environments.

Figure 5 shows the test results of monitoring time. According to Figure 5, the monitoring system proposed in the article has a shorter monitoring time and better monitoring effect. With the increase in monitoring data, the monitoring time of the article system and the

traditional system is getting longer and longer. However, the monitoring time of the monitoring method proposed in the article is always lower than that of the traditional system. Through the analysis and implementation of the existing technology, it can more objectively reflect the advantages and guarantee mechanism of the existing technology and provide ideas for the improvement of the overall function and application function of the environmental monitoring system in the future. The detection quantity of this system increases from 0 to 40, and the detection time increases from 0 to 80. Compared with other systems, the detection time is the lowest, about 70 s. This study focuses on the design and analysis of an air

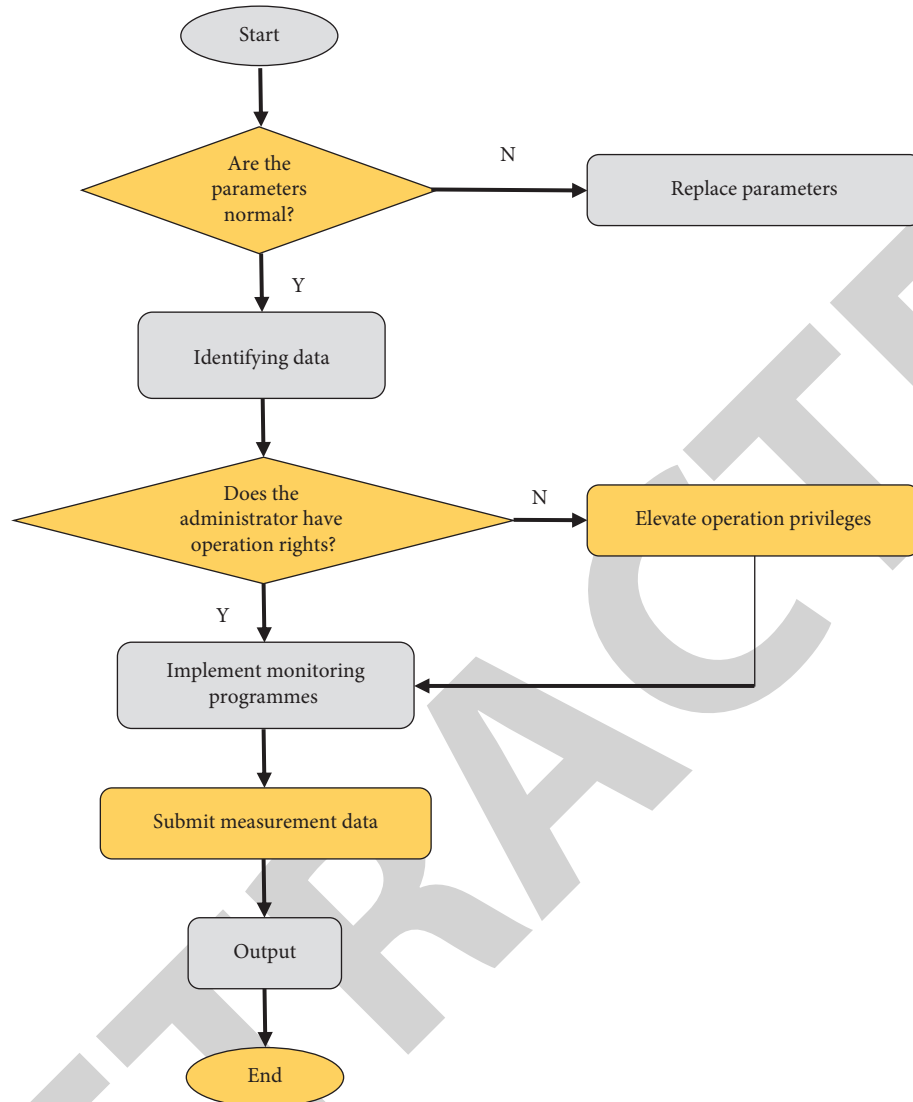


FIGURE 4: Software workflow of an ecological environment monitoring system based on RS and GIS.

TABLE 1: Accuracy of monitoring results.

Number of experiments	Accuracy %		
	Ecological environment monitoring system based on high-resolution image	Ecological environment monitoring system based on the fuzzy analytic hierarchy process	Ecological environment monitoring system based on RS and CIS
1	82.55	84.55	92.48
2	87.64	86.93	95.44
3	80.33	87.64	98.22
4	82.15	89.37	92.48
5	83.39	90.60	94.77
6	84.33	87.00	94.33
7	87.14	86.31	97.25
8	82.17	85.69	95.13
9	80.05	84.21	98.31
10	82.69	88.23	95.44

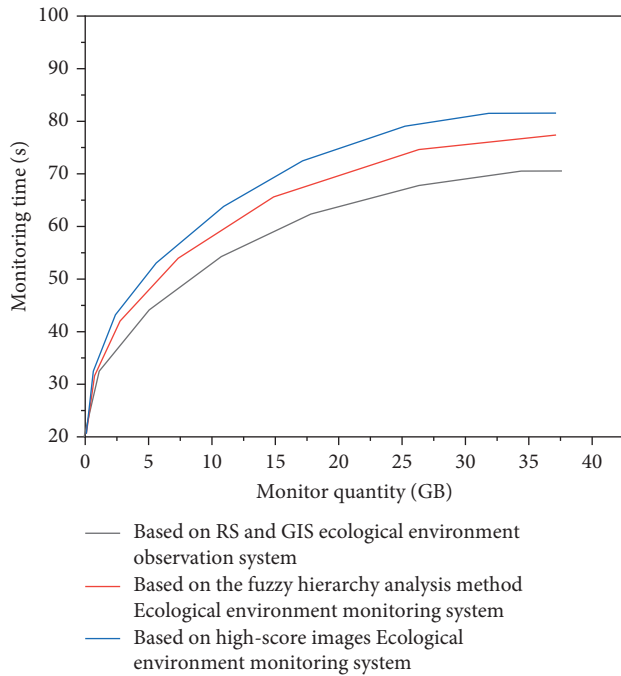


FIGURE 5: Monitoring time test results.

environment monitoring system. Through the structure and analysis characteristics of this system, the accuracy of monitoring results is enhanced.

5. Conclusion

This study puts forward the application of computer vision and sensor technology in the multivariate evaluation of ecological environment carrying capacity. In order to improve the environmental monitoring accuracy of the ecological environment monitoring system, including hardware and software, this study puts forward the system development scheme. Combined with RS, GIS technology, AE, and IDL language, the correct and feasible idea of design and development is realized. The urban ecological environment monitoring and evaluation functions involved in the system can be realized on the same interface, which has the characteristics of comprehensive functions and simple operation. The RI method is used to evaluate the ecological environment, which overcomes the problems of a single evaluation index and incomplete conclusions in the past. In addition, the system can quickly monitor and evaluate the regional ecological status, which is operable, objective, and progressiveness. The experimental results show that the ecological environment monitoring system based on RS and GIS proposed in this study has a shorter monitoring time, higher monitoring accuracy, and stronger monitoring ability.

Data Availability

The data used to support the findings of this study are available from the corresponding author upon request.

Conflicts of Interest

The authors declare that they have no conflicts of interest.

Acknowledgments

This study was supported by the scientific research project of the Heilongjiang Provincial Education Department in 2016 (2016-KYYWF-0936).

References

- [1] D. A. Konyaev, E. B. Popova, A. A. Titov, N. M. Agarkov, and V. V. Aksenov, "The prevalence of eye diseases in the elderly population is a global problem of modernity," *Zdravookhranenie Rossiiskoi Federatsii/Ministerstvo zdravookhraneniia RSFSR*, vol. 65, no. 1, pp. 62–68, 2021.
- [2] W. Deng, A. Cheshmehzangi, Y. Ma, and Z. Peng, "Promoting sustainability through governance of eco-city indicators: a multi-spatial perspective," *International Journal of Low Carbon Technologies*, vol. 15, no. 2, pp. 1–12, 2020.
- [3] M. Worku, T. B. Taw, and M. Tarekegn, "Economic valuation of local environmental amenities: a case study of bahir dar city, amhara regional state, Ethiopia," *African Journal of Hospitality Tourism and Leisure*, vol. 10, pp. 698–711, 2021.
- [4] S. B. Nyuysoni, J. M. Mutua, and P. G. Home, "Mathematical model development and 3d printing of cylindrically shaped biofilm carrier media from recycled plastic waste for wastewater treatment," *Journal of Environmental Protection*, vol. 13, no. 01, pp. 15–31, 2022.
- [5] Y. Zhang, L. Zhao, K. Niu, and A. Manlike, "Environmental monitoring in northern aksu, China based on remote sensing ecological index model," *Open Journal of Applied Sciences*, vol. 12, no. 05, pp. 757–768, 2022.
- [6] Z. Liu and J. Kan, "Effect of basketball on improving the health of obese people under the monitoring of internet of things technology," *Mobile Information Systems*, vol. 2021, Article ID 9525062, 8 pages, 2021.
- [7] X. Zhan, Z. H. Mu, R. Kumar, and M. Shabaz, "Research on speed sensor fusion of urban rail transit train speed ranging based on deep learning," *Nonlinear Engineering*, vol. 10, no. 1, pp. 363–373, 2021.
- [8] C. Tan and X. Lu, "Research on user security authentication method of eco-environmental monitoring database," *Arabian Journal of Geosciences*, vol. 14, no. 11, pp. 986–1011, 2021.
- [9] C. Zhang, C. Liu, H. Gong, and J. Teng, "Research on the protection and development of traditional villages from the perspective of ecological wisdom—taking yanfang ancient village in ji an as an example," *Open Journal of Social Sciences*, vol. 10, no. 05, p. 11, 2022.
- [10] M. Haruna, M. K. Ibrahim, and U. M. Shaibu, "Assessment of land use and vegetative cover in kano metropolis (from 1975–2015) employing GIS and remote sensing technology," *Nigerian Journal of Basic and Applied Sciences*, vol. 27, no. 2, pp. 1–7, 2020.
- [11] X. Liu, "Three-dimensional visualized urban landscape planning and design based on virtual reality technology," *IEEE Access*, vol. 8, 2020.
- [12] G. Yakubova, R. O. Kellems, B. B. Chen, and Z. Cusworth, "Practitioners' attitudes and perceptions toward the use of augmented and virtual reality technologies in the education of students with disabilities," *Journal of Special Education Technology*, vol. 37, no. 2, pp. 286–296, 2022.

Retraction

Retracted: Application of Big Data Technology in Environmental Pollution Control in Energy Ecological Economic Zone

International Transactions on Electrical Energy Systems

Received 19 September 2023; Accepted 19 September 2023; Published 20 September 2023

Copyright © 2023 International Transactions on Electrical Energy Systems. This is an open access article distributed under the Creative Commons Attribution License, which permits unrestricted use, distribution, and reproduction in any medium, provided the original work is properly cited.

This article has been retracted by Hindawi following an investigation undertaken by the publisher [1]. This investigation has uncovered evidence of one or more of the following indicators of systematic manipulation of the publication process:

- (1) Discrepancies in scope
- (2) Discrepancies in the description of the research reported
- (3) Discrepancies between the availability of data and the research described
- (4) Inappropriate citations
- (5) Incoherent, meaningless and/or irrelevant content included in the article
- (6) Peer-review manipulation

The presence of these indicators undermines our confidence in the integrity of the article's content and we cannot, therefore, vouch for its reliability. Please note that this notice is intended solely to alert readers that the content of this article is unreliable. We have not investigated whether authors were aware of or involved in the systematic manipulation of the publication process.

Wiley and Hindawi regrets that the usual quality checks did not identify these issues before publication and have since put additional measures in place to safeguard research integrity.

We wish to credit our own Research Integrity and Research Publishing teams and anonymous and named external researchers and research integrity experts for contributing to this investigation.

The corresponding author, as the representative of all authors, has been given the opportunity to register their agreement or disagreement to this retraction. We have kept a record of any response received.

References

- [1] X. Jin and X. Jin, "Application of Big Data Technology in Environmental Pollution Control in Energy Ecological Economic Zone," *International Transactions on Electrical Energy Systems*, vol. 2022, Article ID 1569905, 7 pages, 2022.

Research Article

Application of Big Data Technology in Environmental Pollution Control in Energy Ecological Economic Zone

Xinxue Jin ¹ and Xinxin Jin ²

¹Department of Culture Management, Shanghai Publishing and Printing College, Shanghai 200093, China

²Department of Electronic and Information Engineering, Bozhou University, Bozhou, Anhui 236800, China

Correspondence should be addressed to Xinxin Jin; 3100501017@caa.edu.cn

Received 15 July 2022; Revised 1 August 2022; Accepted 8 August 2022; Published 30 August 2022

Academic Editor: Nagamalai Vasimalai

Copyright © 2022 Xinxue Jin and Xinxin Jin. This is an open access article distributed under the Creative Commons Attribution License, which permits unrestricted use, distribution, and reproduction in any medium, provided the original work is properly cited.

In order to solve the problem of environmental pollution control in the energy ecological economic zone, this paper proposes a technology to realize environmental pollution control by using big data. The main content of this technology is based on the characteristics and application of big data technology; through the collection of online monitoring data of ecological environment pollution, the construction of the online monitoring data quality model of ecological environment pollution, and finally through the experiments in the simulation environment, the feasibility of big data technology is obtained. The experimental results show that the average quality factor data of the quality control model in the environmental scientific data supervision is 2.16, the average quality factor data of the Internet of things in the marine pollution monitoring is 5.88, and the average quality factor data of the model in the ecological environment pollution online monitoring based on the big data technology is 8.64. Big data technology has good applicability. It is proven that the research of big data technology can meet the needs of environmental pollution control in the energy ecological economic zone.

1. Introduction

With the acceleration of economic development and urbanization, the problems of resource shortage and environmental degradation are becoming more and more serious. People gradually realize the importance of coordinated development of the economy and environment. While developing the economy, paying attention to environmental protection has become a topic of common concern to the whole society [1]. Economic development and resources and the ecological environment restrict and promote each other. In the past 30 years, human living standards and material conditions have been greatly improved with the continuous development of social productivity. However, with the continuous development of productivity and science and technology, the environmental pollution problem of globalization has become increasingly prominent and has become the most serious problem facing mankind (Figure 1). Its main manifestations are air pollution, marine pollution, urban environment, and

other problems directly caused by land desertification and forest vegetation destruction. Various pollution phenomena have caused serious damage to the global ecosystem and affected the normal life of human beings. Natural or man-made addition of certain substances to the environment, which exceeds the self-purification capacity of the natural environment, is generally called environmental pollution. The scope of environmental pollution generally includes air pollution, water resource pollution, soil geological pollution, noise pollution, and various radioactive element pollution. Environmental pollution control mainly refers to the specific means and measures to control the discharge of various pollutants. At present, it mainly includes two main aspects: pollutant emission control technology and pollutant emission control policy. It should be noted that the formulation of specific policies for pollution control is the basic function of the government. The process of policy formulation is determined according to the environmental quality and economic development of the country or region [2].

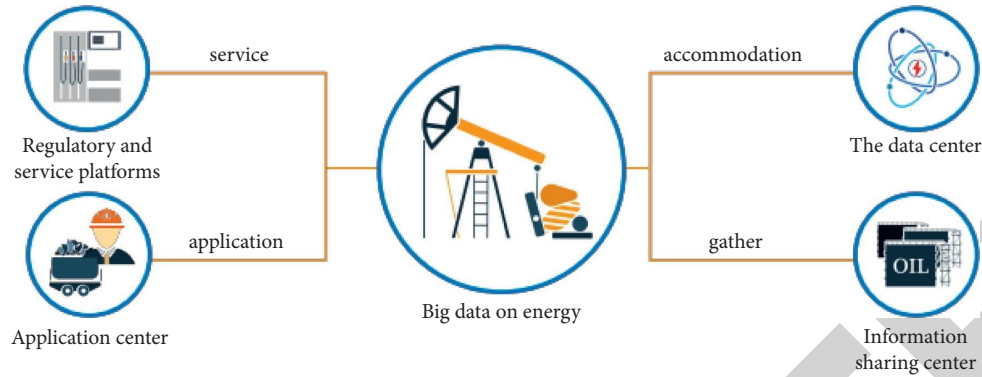


FIGURE 1: Application of big data technology in environmental pollution control in the energy ecological economic zone.

For a long time, the extensive development mode continued by China's rapid economic prosperity has resulted in the waste and depletion of resources and the destruction and deterioration of the ecological environment. People are not only gradually feeling the increasingly rich material and cultural life but also personally feel the increasingly severe environmental protection situation. As the global climate change problem continues to heat up, it is facing increasing pressure from the international community to reduce emissions. Developed countries continue to put pressure on China to commit to emission reduction obligations [3]. In view of this, the effective implementation of environmental pollution control policies is not only effectively promoting the sustainable development of the economy and society but also, as a responsible big country, China is showing its image as a responsible big country to the international community.

2. Literature Review

With the vigorous development of the country's current economy, under the current background, the acceleration of urbanization and industrialization has exacerbated environmental problems and posed a great threat to people's production, life, and health. Under the traditional extensive development strategy, the problems of environmental pollution and ecological damage cannot be recovered in a short time, and the impact on the natural ecological balance cannot be estimated. Traditional environmental monitoring and diagnosis rely more on manual methods. The work under the manual operation mode is intensive, stressful, and time-consuming. With the increasingly serious environmental problems and the arrival of the information age, we should pay attention to the application of big data monitoring and diagnosis technology to promote the reform of environmental protection work. With the increasing attention to environmental protection around the world, more and more human, material and technology have been invested in environmental protection, and the scope and content of environmental protection monitoring have become more and more extensive. This trend has exacerbated the difficulty of environmental protection, monitoring, and diagnosis. For example, taking environmental monitoring as an example, it is necessary to conduct real-time and dynamic

monitoring of air, water, soil, noise, and other pollution. Once it is found that harmful substances or gases exceed the normal standard through corresponding monitoring, the local environmental protection department should immediately formulate corresponding treatment countermeasures according to the degree and type of pollution. Therefore, big data technology provides technical support for environmental monitoring, enabling the orderly progress of environmental monitoring. In the process of promoting environmental protection, the state has successively issued corresponding environmental protection policies. The introduction and implementation of various environmental protection policies have made environmental pollution under certain control, which is in line with the overall strategic goal of sustainable development. The application of big data technology in environmental monitoring and intelligent diagnosis is an inevitable requirement in the information age. In the corresponding environmental work, the application of big data technology can effectively provide corresponding data support for the formulation of environmental protection policies [4].

In view of the above problems, this paper proposes the application of big data technology in environmental pollution control in the energy ecological economic zone [5]. The main content of this technology is based on the characteristics and application of big data technology; through the collection of online monitoring data of ecological environment pollution, the construction of online monitoring data quality model of ecological environment pollution, and finally through the experiments in the simulation environment, the feasibility of big data technology is obtained. Big data technology is used to collect online monitoring data of ecological environment pollution. By setting the online monitoring frequency of ecological environment pollution, the online monitoring data quality model of ecological environment pollution is constructed.

3. Research Methods

3.1. Research on Big Data

3.1.1. Big Data. The global research institute first gave such a definition to big data. Big data is a kind of data aggregation, and its scale far exceeds the storage, management, analysis,

and application capabilities of traditional data technologies [6]. There is a large amount of data involved in big data. Using some conventional software tools, it has been unable to mine its most valuable information in a very limited time, and there are certain difficulties in management and in-depth processing. Therefore, it is necessary to develop more advanced big data technology to provide services for solving practical problems. This definition emphasizes the role and value of big data from another level. It points out the main characteristics of big data and emphasizes its importance to the five in one construction of economic, political, cultural, social, and ecological civilization. Although there is no unified definition of big data, it has become a global focus and an important force to promote the development of modern society.

With the development of informatization, big data has accumulated certain resources in many industries and fields. The Internet industry is the first field that has achieved fruitful research results. The application of big data in finance, government affairs, retail, industry, medical and health care, and other fields has also shown a step-by-step growth [7]. In the research released by the Big Data Industrial Innovation Research Institute, 100 enterprises with high market popularity and obvious differentiated competitive advantages were collected. Through the reclassification and summary of the industry fields corresponding to these cases, the statistical results are shown in Figure 2.

3.1.2. Build a Smart Environmental Protection Platform Based on Environmental Protection Big Data. As far as environmental protection is concerned, it involves many work contents and a wide range. As far as environmental monitoring is concerned, it involves the monitoring contents of air quality, water quality, soil, meteorology, and so on. In the process of promoting the routine environmental protection work, there are relatively many departments involved in the environmental protection work. The work of different departments is relatively independent and scattered, and they are responsible for different types of data. It is difficult to achieve unified processing for various types of data collection, analysis, and processing. With the arrival of the information age, in the process of promoting environmental protection, people gradually realize the advantages of information technology and intelligent technology and actively apply big data technology in environmental monitoring and intelligent diagnosis [8].

The construction idea of the environmental protection big data sharing platform is shown in Figure 3. The relevant environmental work departments need to build not only a professional data processing platform but also an information database consistent with the platform. Through the effective cooperation between the data platform and the database, the integration and utilization of environmental information data are fully guaranteed [9]. Taking a city as an example, its investment in big data monitoring and intelligent diagnosis of environmental protection has increased. Through special research on environmental protection, the platform has many functions, such as monitoring,

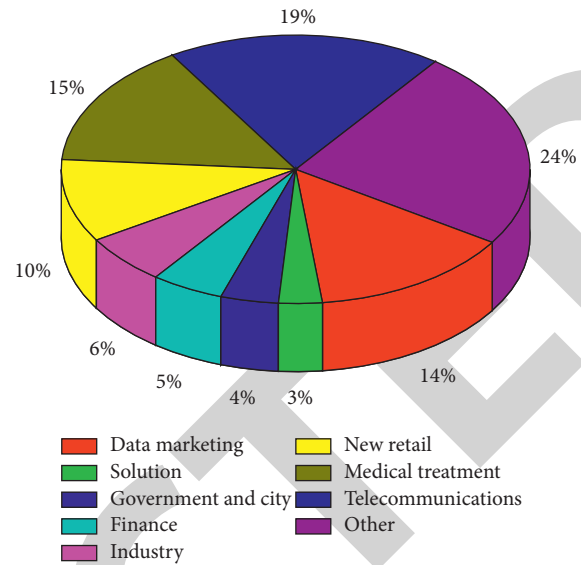


FIGURE 2: Classification of big data application fields.

monitoring, early warning, video monitoring, intelligent analysis, environmental supervision, and decision support; after the platform was put into use, the environmental work has ushered in major changes. Once the corresponding environmental indicators exceed the normal standards, the intelligent early warning module in the platform will immediately start the corresponding early warning to remind the relevant departments.

3.2. Design of the Data Quality Model for Online Monitoring of Ecological Environment Pollution

3.2.1. Collect Online Monitoring Data of Ecological Environment Pollution. Taking advantage of big data technology, the collection method of online monitoring data of ecological environment pollution is optimized. Considering the impact of industrial wastewater discharge and industrial waste gas, the ecological environment pollution sensor data collection is carried out by using chips with low cost and power consumption. Through the collected online monitoring data of ecological environment pollution, the types of ecological environment pollution are counted [10]. The CC2430 chip is used to calculate the computing unit. The MCU 8051 single chip is used as the controller, the ADC channel is used to connect with the data acquisition unit, and the standard comparison method in big data technology is introduced to judge whether there is pollution in the node field. The standard comparison method is to establish a pollution-free ecological environment curve function, which is expressed as

$$Z = \lim_{0 \rightarrow \infty} Q_n \prod_{i=1}^n X_i f! \quad (1)$$

Based on the ecological environment curve function, the online monitoring data of ecological environment pollution are obtained by relying on the sensor data acquisition unit, and the online monitoring curve function is established [11], specifically expressed as

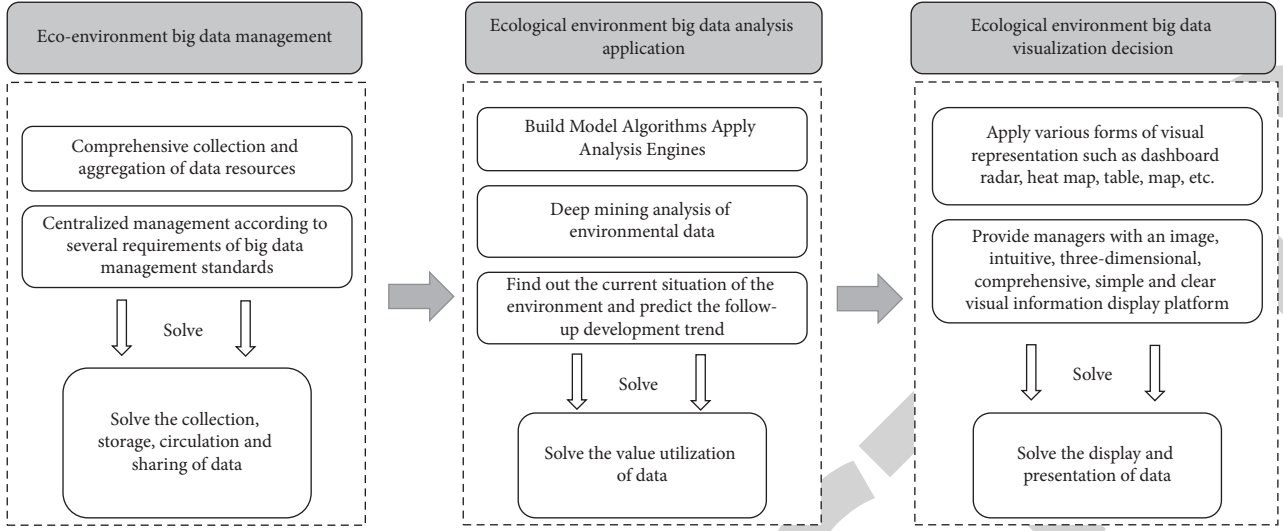


FIGURE 3: Construction idea of environmental protection big data sharing platform.

$$C = Z\gamma_i + W_0 \frac{\partial^2 q_k dx}{S}. \quad (2)$$

In formula (2), Z represents the ecological environment curve function without pollution, γ_i represents the eco-environmental adaptation coefficient, W_0 represents the online monitoring time, q_k represents the online monitoring data of eco-environmental pollution, and S represents the online monitoring distance. Perform the difference operation between formula (2) and formula (1), and the difference operation formula is

$$f(x) = \Delta C - \Delta Z. \quad (3)$$

If the difference of formula (3) is zero, it indicates that ecological environment pollution has occurred. If the difference of formula (3) is larger, it indicates that the degree of ecological environment pollution is more serious [12].

The period flux in big data technology is used to set the online monitoring frequency of ecological environment pollution. Period flux refers to the pollution degree of the ecological environment within the specified time. According to the ecological environment pollution, the calculation formula of period flux is divided into tidal period flux and nontidal period flux. The calculation formula of tidal period flux is

$$W_t = \int_0^t Q_i \frac{C_i}{dt}. \quad (4)$$

Based on the calculation of ecological environment pollution, determine the online monitoring frequency of ecological environment pollution according to the ecological environment pollution and provide judgment basis for the online monitoring data quality model of ecological environment pollution [13].

3.2.2. Construction of the Data Quality Model for Online Monitoring of Eco-Environmental Pollution. According to the setting results of online monitoring frequency of

ecological environment pollution, online monitoring data of ecological environment pollution can be obtained. Based on the quality of online monitoring data of ecological environment pollution, the quality information of online monitoring data of ecological environment pollution can be fused. The main purpose of online monitoring data quality information detection and fusion of ecological environment pollution based on big data technology is to fuse online monitoring data quality information by using multisensors in big data technology [14].

As the online monitoring system for ecological environment pollution is composed of multiple sensors, distributed data fusion mainly includes two structural modes, as shown in Figure 4 and Figure 5.

According to the above process, each node in the cluster is configured with its corresponding decision-making task to fuse the quality observations of the online monitoring data of ecological environment pollution of each information fusion node and transmit them to the cluster head node. The cluster head node will make the final decision and judgment on the quality information of the online monitoring data of ecological environment pollution according to the local decisions on the quality of the online monitoring data it receives [15]. Formula of fusion processing is

$$P_d = \sum_{j=k}^N \sum_{n/w} \prod_t^{n_i} (1 - P_d^i)^{1-i}. \quad (5)$$

In equation (5), k represents the online monitoring data quality information fusion processing threshold, N represents the number of observations of the online monitoring data quality information, P represents the likelihood function, d represents the detection rate of the online monitoring data quality information of the sensor, i represents the false detection probability of the online monitoring data quality information, o represents the false alarm probability, and j represents the fusion criteria of the online monitoring data quality.

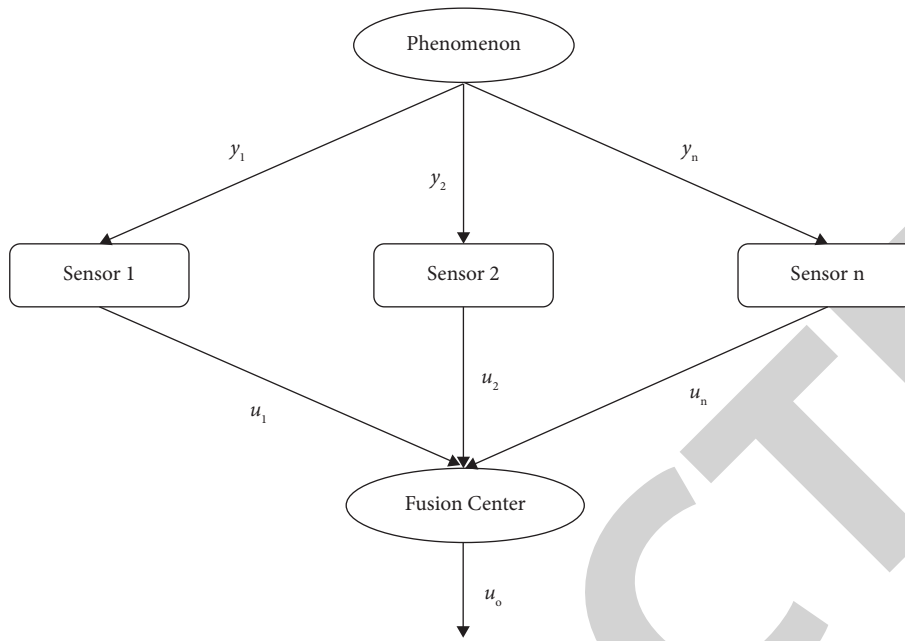


FIGURE 4: Distributed data fusion mode, fusion model A.

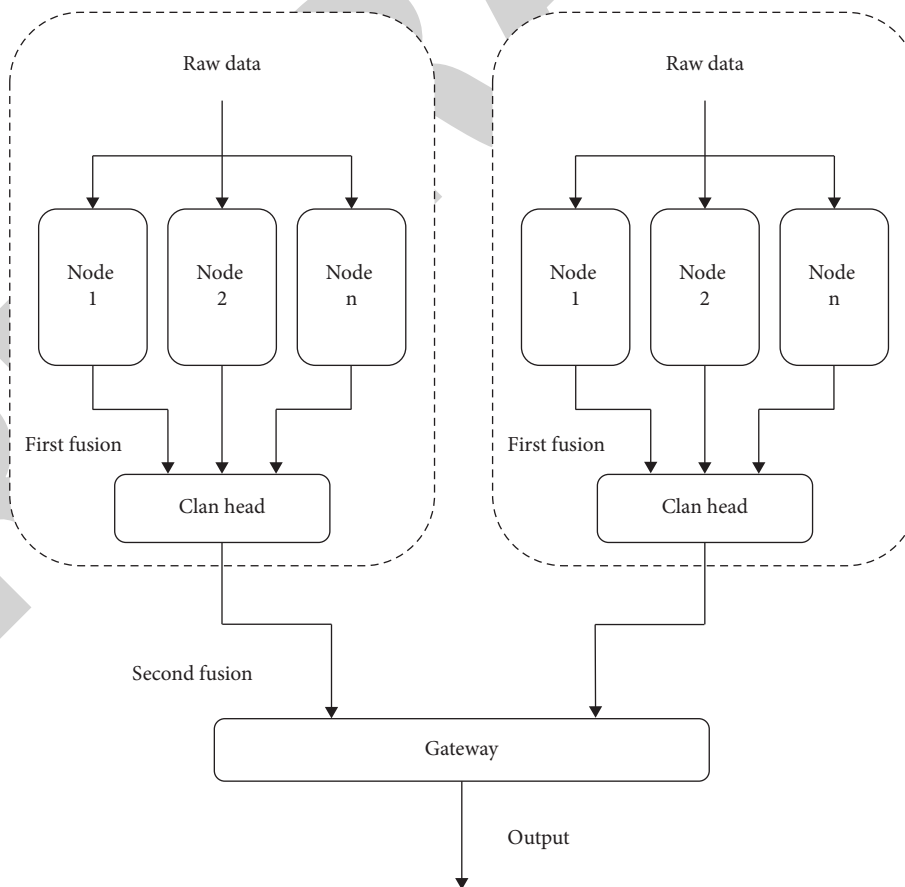


FIGURE 5: Distributed data fusion mode, fusion model B.

TABLE 1: Quality test results of online monitoring data of ecological environment pollution.

Quality control model in scientific data supervision under environment		The model of internet of things technology in marine pollution monitoring		Online monitoring model of ecological environment pollution based on big data technology	
Iterations/time	Quality factor	Iterations/time	Quality factor	Iterations/time	Quality factor
1	2.2	1	6.0	1	9.0
2	3.3	2	6.6	2	8.3
3	1.0	3	5.3	3	9.2
4	2.7	4	6.2	4	8.5
5	1.6	5	5.3	5	8.2
Mean value	2.16	Mean value	5.88	Mean value	8.64

In the distributed data fusion mode, formula of centralized information fusion is

$$\hat{X} = \sum_{i=1}^N \alpha_i Y_i. \quad (6)$$

In equation (6), X represents the weighted estimation value of centralized information fusion, α represents the weighting factor of the data quality information node of the online monitoring of ecological environment pollution, and Y represents the output value of the clustering node t .

According to the setting results of the online monitoring frequency of ecological environment pollution, the online monitoring data of ecological environment pollution are obtained. By using the distributed information fusion mode, the final decision and judgment are made on the online monitoring data quality information of ecological environment pollution, and the online monitoring data quality model of ecological environment pollution is established [16].

4. Result Analysis

In order to verify the performance of the data quality model for online monitoring of ecological environment pollution based on big data technology, a simulation environment is constructed [17]. The quality control model in environmental scientific data supervision and the model of Internet of things in marine pollution monitoring are used for comparison. The test results are as follows [18]. Table 1 shows the test results of online monitoring data quality of ecological environment pollution of the three online monitoring data quality models of ecological environment pollution. The average quality factor data of the quality control model in the environmental scientific data supervision is 2.16, the average quality factor data of the Internet of things in the marine pollution monitoring is 5.88, and the average quality factor data of the ecological environment pollution online monitoring model based on the big data technology is 8.64. Big data technology has good applicability [19].

5. Conclusion

In order to solve the problem of environmental pollution control in the energy ecological economic zone, a technology using big data was proposed. The main content of this

technology is based on the characteristics and application of big data technology; through the collection of online monitoring data of ecological environment pollution, the construction of online monitoring data quality model of ecological environment pollution, and finally through the experiments in the simulation environment, the feasibility of big data technology is obtained. Big data technology is used to collect online monitoring data on ecological environment pollution. By setting the online monitoring frequency of ecological environment pollution, the online monitoring data quality model of ecological environment pollution is constructed. The simulation results show that the data quality factor of this model is much higher than that of the other two methods in many iterations, which shows that the method designed in this paper can ensure the data quality of online monitoring of ecological environment pollution.

Data Availability

The data used to support the findings of this study are available from the corresponding author upon request.

Conflicts of Interest

The authors declare that they have no conflicts of interest.

Acknowledgments

This study was funded by Anhui Province Quality Engineering Mixed Online and Offline Courses (2021xsxxkc181), Key Program of Humanities and Social Science of Anhui Province (SK2019A0342), Double Reduction Program for Basic Education (2021SJZX092), and Industry-University-Research Cooperation Project of Bozhou University (BYC2021Z01).

References

- [1] M. A. Vasilenko, E. L. Kuzina, V. A. Galkin, and N. A. Drozdov, "Managing the development of the environmental protection system in transport companies," *IOP Conference Series: Earth and Environmental Science*, vol. 666, no. 6, Article ID 062079, 2021.
- [2] B. Surya, H. Hamsina, R. Ridwan, B. Baharuddin, and E. S. Rasyidi, "The complexity of space utilization and environmental pollution control in the main corridor of Makassar City, South Sulawesi, Indonesia," *Sustainability*, vol. 12, 2020.

Retraction

Retracted: Modeling and Optimization of Ship Waste Heat Utilization System Based on Genetic Algorithm and Sensing

International Transactions on Electrical Energy Systems

Received 3 October 2023; Accepted 3 October 2023; Published 4 October 2023

Copyright © 2023 International Transactions on Electrical Energy Systems. This is an open access article distributed under the Creative Commons Attribution License, which permits unrestricted use, distribution, and reproduction in any medium, provided the original work is properly cited.

This article has been retracted by Hindawi following an investigation undertaken by the publisher [1]. This investigation has uncovered evidence of one or more of the following indicators of systematic manipulation of the publication process:

- (1) Discrepancies in scope
- (2) Discrepancies in the description of the research reported
- (3) Discrepancies between the availability of data and the research described
- (4) Inappropriate citations
- (5) Incoherent, meaningless and/or irrelevant content included in the article
- (6) Peer-review manipulation

The presence of these indicators undermines our confidence in the integrity of the article's content and we cannot, therefore, vouch for its reliability. Please note that this notice is intended solely to alert readers that the content of this article is unreliable. We have not investigated whether authors were aware of or involved in the systematic manipulation of the publication process.

Wiley and Hindawi regrets that the usual quality checks did not identify these issues before publication and have since put additional measures in place to safeguard research integrity.

We wish to credit our own Research Integrity and Research Publishing teams and anonymous and named external researchers and research integrity experts for contributing to this investigation.

The corresponding author, as the representative of all authors, has been given the opportunity to register their agreement or disagreement to this retraction. We have kept a record of any response received.

References

- [1] L. Lyu, "Modeling and Optimization of Ship Waste Heat Utilization System Based on Genetic Algorithm and Sensing," *International Transactions on Electrical Energy Systems*, vol. 2022, Article ID 9917212, 8 pages, 2022.

Research Article

Modeling and Optimization of Ship Waste Heat Utilization System Based on Genetic Algorithm and Sensing

Long Lyu 

College of Marine&Electrical Engineering, Jiangsu Maritime Institute, Nanjing 211112, Jiangsu, China

Correspondence should be addressed to Long Lyu; 202014000722@hceb.edu.cn

Received 12 July 2022; Revised 30 July 2022; Accepted 8 August 2022; Published 29 August 2022

Academic Editor: Nagamalai Vasimalai

Copyright © 2022 Long Lyu. This is an open access article distributed under the Creative Commons Attribution License, which permits unrestricted use, distribution, and reproduction in any medium, provided the original work is properly cited.

In order to solve the optimization problem of ship waste heat utilization system, the modeling and optimization method of ship waste heat utilization system based on genetic algorithm and sensing is proposed. The 6S50ME-C8.2 volume method model was established based on Matlab/Simulink simulation platform. According to the test data of the 6S50ME-C8.2 diesel engine, the simulation value is very close to the test value, which verifies the accuracy of the simulation model. The experimental results show that the thermal efficiency of high-power medium and low-speed two-stroke diesel engines is high, the exhaust temperature of the main engine is generally maintained at about 230°C, and the energy content of exhaust gas is relatively low. If no other measures are taken, the waste gas is directly channeled into the waste heat boiler, which cannot effectively recover the heat in the waste gas. *Conclusion.* The model can well simulate the actual working condition of the diesel engine, and the exhaust temperature has reached 298°C. The energy quality of waste gas at the inlet of the waste heat boiler is improved to meet the requirements of the waste heat recovery system.

1. Introduction

Up to now, the progress of science and technology and the development of the economy cannot be separated from the promotion of energy. Energy is a necessary condition for the survival of human society. Take China as an example. BP World Energy Statistical Yearbook statistics show that by 2015, China's energy consumption has accounted for 23% of the global total, and the net growth of energy consumption has accounted for 34% of the global total growth, surpassing other developed countries and becoming the largest energy consumption country in the world. By 2035, China's energy consumption is expected to reach or exceed 25 percent of the world's total. Worldwide, the use of fossil fuels has caused serious environmental pollution. Therefore, optimizing energy structure, improving energy efficiency, and reducing pollution emissions have become an important research topic in China and even the world.

2. Literature Review

Wang et al. said that energy is the material basis for human survival and development. Energy is closely related to our work, production and life, and our future living environment, which promotes the rotation of machines. The combination of machine and man has formed advanced productive forces, which have promoted the continuous development of human society [1]. Tang et al. said that throughout the development history of human civilization, every major change of human civilization was accompanied by the improvement and replacement of energy [2]. Koshevyi et al. said that with the rapid development of the social economy, human's demand for energy is also increasing, especially for the exploitation and utilization of oil resources, which is far beyond the tolerable range of nature, and oil resources are on the verge of exhaustion [3]. Kauko et al. said that since the energy supply failed to catch up with the increase of demand, two world oil crises broke out

successively in the 1970s. The rise of oil prices led to global economic recession and social unrest [4]. Martinez Cesena et al. said that in the middle of this century, with the exhaustion of fossil fuel resources, the surge of energy demand for economic development and the change of energy consumption structure will inevitably lead to a global energy crisis again and ultimately destroy the whole modern market economy [5]. Kamminana et al. said that the energy crisis, a worldwide problem, is attracting more and more attention and strong concern from governments of all countries [6]. In the era of economic globalization, the trade between countries is frequent. Huang et al. said that due to the huge advantages of sea transportation, the transportation volume of sea transportation has accounted for 90% of the total amount of international trade, and all countries rely on sea transportation for trade, resulting in a sharp increase in the holding and tonnage of large ships [7]. Yong et al. said that with the rise of international oil prices, the uncontrolled development of ships in the golden age of shipping, and the significant impact of the economic crisis, excess shipping capacity was caused, and shipping enterprises had to strive to reduce shipping costs and improve the economy of ships [8]. Singh et al. stated that when a ship is running normally at sea, the ship's main engine, as the ship's main propulsion device, needs to operate continuously for 24 hours, consuming 70%–90% of the ship's total fuel [9]. Nandan et al. said that in order to meet the normal operation of the ship and the daily life of the crew, the ship is also equipped with various auxiliary equipment to provide the electricity and heat needed by the ship, consuming 10–30% of the ship's fuel [10]. When the ship's main engine is running, the fuel is burned in the combustor and the chemical energy is mainly converted into mechanical energy and heat energy. About half of the energy is used in the propulsion device, and part of the remaining half of the energy is recycled for the preheating of the fuel tank. A large portion of the energy enters the atmosphere through diesel exhaust, while the rest is released to the environment in a variety of ways. Taking MAN 12K98ME/MC low-speed two-stroke diesel engine as an example, the main engine consumes fuel to drive the ship sailing at the specific fuel consumption rate of 171 g/kWh. The modeling diagram of the ship waste heat utilization system is shown in Figure 1.

3. Methods

At present, considering the complexity of ship owners and shipyards to the scheme of ship waste heat recovery and utilization system and the actual power consumption of ships in operation, the following three different types of ship waste heat recovery schemes are provided: this is the simplest and most economical scheme of ship waste heat recovery. The power turbine is driven by exhaust gas that bypasses the turbocharger and runs a generator through a gearbox to generate electricity. Power supply and parallel operation power supply are provided for the ship. The specific power generation depends on the bypass exhaust flow, and the waste heat recovery rate of 3–5% can be achieved [11]. Steam is used for power generation by

installing steam turbine generators [12]. With a steam turbine generator (STG) system, it is possible to recover 5–8% of the energy, depending on the host model, output power, and ambient conditions. For ships with high-power requirements, such as container ships, this combined system is an option. The power turbine and steam turbine are built on the same chassis and connected to the generator through a reduction gearbox. The system can meet the total power demand of the ship in a variety of circumstances, significantly reduce the fuel cost of the ship, and recover about 8–11% of the energy [13, 14]. When evaluating whether a waste heat utilization system should be installed in a new ship project, the payback period of system installation is always involved. To calculate the payback period of the project, a key factor that must be considered is the expected operating characteristics of the new vessel. The operating characteristics of ships vary according to ship types. Bulk carriers and tankers typically operate at sea at a set speed, while large container ships, which consume more fuel a day, have a more diversified operation model. When calculating the return on investment period of the waste heat recovery scheme according to the operation characteristics of the ship, the main engine load and its running time should be taken into account. The following takes a large container ship of 14000TEU as an example. According to its operating characteristics and WHRS output power, the investment return period of different waste heat recovery schemes of ships is calculated. The operating characteristics and WHRS output power of this container ship are shown in Figure 2.

The investment return cycle of different waste heat recovery schemes is shown in Table 1.

As can be seen from Table 1, the combined WHRS waste heat recovery scheme has a return on investment period of 4.3 years, but the ship owner may be more interested in his ship's 20 years of operation. Using the combined WHRS waste heat recovery solution can save \$36 million in fuel costs over the same ship life. The exhaust temperature of the 6S50ME-C8.2 waste heat main engine studied in this essay is about 298°C. On this basis, about a 5°C pipe temperature drop is subtracted, that is, the inlet flue gas temperature of the waste heat boiler is 293°C. According to the data, the main steam temperature of the waste heat boiler mainly depends on the exhaust temperature of the waste heat host, and the temperature difference between the hot end refers to the temperature difference between the exhaust temperature of the host and the main steam temperature. Lowering the temperature difference of the hot end can get higher superheat, so as to improve the quality of superheated steam. However, decreasing the temperature difference at the hot end will also reduce the logarithmic average temperature difference of the superheater, increase the heat transfer area of the superheater, and increase the metal consumption. The temperature difference at the hot end of the existing waste heat boiler is generally between 20°C and 40°C. By selecting several temperatures to calculate, the preferred main steam temperature is 270°C. Increasing the main steam pressure of waste heat boiler can improve the power capacity and increase the power generation. But by the boiler equipment cost and steam pressure itself and other factors, the main

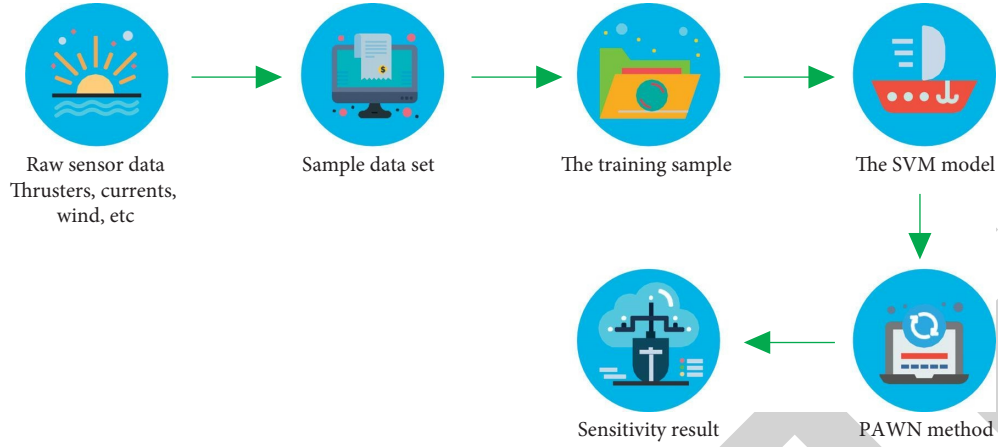


FIGURE 1: Modeling diagram of ship waste heat utilization system.

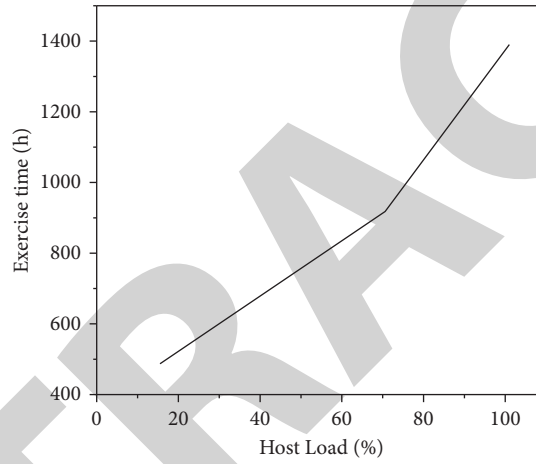


FIGURE 2: Operation characteristics and WHRS output power of large container ships.

TABLE 1: Calculation table of investment return period of waste heat scheme of large container ships.

	Modular generating unit	Steam turbine generating unit	Power turbine generating unit
Total fuel cost savings per year (\$)	2,617,674	1,577,689	937,069
Additional fuel required per year (\$)	284,954	284,954	284,954
Total investment cost of waste heat scheme (\$)	10,000,000	7,500,000	2,300,000
Actual payback period/year	4.3	5.8	3.5

steam pressure cannot be increased indefinitely, so there is an extreme value of the main steam pressure. Based on the discriminant method of stable flow entropy equation, this essay determines the extreme value of the main steam pressure of the waste heat boiler [15, 16]. It is assumed that the heat exchange process of the waste heat boiler is a stable flow process, without considering the heat absorption of the furnace body itself, and the heat released by the waste gas of the main engine flowing through the waste heat boiler is all used for heating water supply. Therefore, exhaust gas, water supply, and steam constitute an open heat system. Let the mass flow through waste heat boiler exhaust gas be m_s , and the specific heat capacity be c_p . The temperature drops from

T_{s1} to T_{s2} , the steam flow rate of superheated steam is T_{s2} , the temperature is T_1 , the ambient temperature and the feedwater temperature are T_0 , and the corresponding feedwater enthalpy is h_0 and entropy is s_0 according to the table of thermodynamic properties of water and steam. The enthalpy of superheated steam is h_1 , the entropy is s_1 , and the heat loss coefficient of the boiler is η . The steady flow entropy equation of the thermodynamic system is shown in the following formula:

$$\sum (ms)_{\text{out}} - \sum (ms)_{\text{enter}} - \frac{Q}{T_0} \geq 0. \quad (1)$$

Entropy change of flue gas in waste heat boiler is shown in the following formula:

$$\Delta S_s = \int_1^2 \frac{\delta Q}{T} = m_s c_p \ln \frac{T_{s2}}{T_{s1}}. \quad (2)$$

The entropy change from feed water to superheated steam is shown in the following formula:

$$\Delta S_v = m_v (s_1 - s_0). \quad (3)$$

Entropy change caused by heat dissipation from the thermal system to the external environment is shown in the following formula:

$$\Delta S_e = \frac{Q}{T_0} = \frac{\eta m_s c_p (T_{s1} - T_{s2})}{T_0}. \quad (4)$$

According to the energy balance, the amount of steam is shown in the following formula:

$$m_v = \frac{(1 - \eta) m_s c_p (T_{s1} - T_{s2})}{h_1 - h_0}. \quad (5)$$

The results of the above types are shown in the following formula:

$$\frac{(s_1 - s_0)}{h_1 - h_0} \geq \frac{\ln(T_{s2}/T_{s1})}{(1 - \eta)(T_{s1} - T_{s2})} + \frac{\eta}{T_0(1 - \eta)}. \quad (6)$$

According to formula (6), when the equal sign is established, it is a reversible process, corresponding to the limit steam parameter of the actual heat exchange process of the waste heat boiler. The heat loss coefficient on the right side of the inequality is determined by experience, and the inlet and outlet temperature of boiler flue gas has been determined, so the right side of the inequality can be considered as a constant value. So when you choose the vapor pressure on the enthalpy entropy diagram, you can choose a point on the isotherm as long as you make sure that this formula is satisfied. When both sides of formula (6) are equal, the corresponding steam pressure is the theoretically desirable limit pressure. Referring to the structure size of the waste heat boiler that has been determined, according to the basic principle of heat transfer, the heat transfer coefficient of the waste heat boiler is calculated to determine its design value. Flue gas heat release is shown in the following formula:

$$Q = C_p G_z (T_{in} - T_{out}), \quad (7)$$

where C_p is the specific heat of flue gas at constant pressure, J/(kg·K); G_z is the diesel engine exhaust mass flow, kg/s; T_{in} is the inlet flue gas temperature, K; and T_{out} is the outlet flue gas temperature, K.

The countercurrent temperature difference is shown in the following formula:

$$\Delta t = (\Delta t_j - \Delta t_x) \ln \frac{\Delta t_d}{\Delta t_x}, \quad (8)$$

where Δt_d is the temperature difference between flue gas and steam inlet, K and Δt_x is the temperature difference between the flue gas and steam inlet, K.

The flow rate of flue gas is shown in the following formula:

$$w = \frac{G_z (t + 273)}{3600 F^* 273 \gamma_y}, \quad (9)$$

where t is the flue gas temperature, K; F is the flue gas circulation area, m²; and γ_y is the flue gas severity, kgNm³.

The convection heat transfer coefficient of flue gas is shown in the following formula:

$$\alpha_d = 0.15 C_z C_s \frac{\lambda^*}{s} \left(\frac{d}{s}\right)^{-0.54} * \left(\frac{h}{s}\right)^{-0.14} * \left(\frac{ws}{v}\right)^{0.65}, \quad (10)$$

where λ is the thermal conductivity of average temperature of airflow, kW/(m²·C); C_z and C_s are tube row correction coefficient; S is the equivalent radiation thickness, m; d is the tube diameter, m; h is the fin height, m; and v is the Actual kinematic viscosity of flue gas, m²/s.

4. Experiment and Analysis

The simulation modeling of the marine diesel engine involves a wide range of fields and is very complicated, so modular modeling is adopted, that is, a complex diesel engine model is divided into many sub-modules. Models are established for all sub-modules, and each sub-module is finally encapsulated [17]. In general, the whole model can be divided into the in-cylinder working process model and a dynamic model when the volume method is used to model the diesel engine. Comparatively speaking, the modeling of dynamics is relatively simple, and the modeling of diesel engine in-cylinder working process is extremely complex, including multiple working processes, which need to be further refined [18]. At the same time, in order to ensure the dynamic operation of the model, the electronic control unit module and load module are further added. Generally speaking, the model is composed of three parts, namely the diesel module, load module, and ECU module. ECU module is the electronic control unit. The load module is used to calculate the propeller by adjusting the circulating fuel injection amount and timing of a single cylinder. These two modules are relatively simple [19, 20]. The diesel module describes the whole working process of diesel engine, its model is extremely complex, and is the core of the whole model. The module contains multiple layers of modules nested layer by layer. The diesel module can be divided into the MCylinder module, the intake module, exhaust module, InterCooler module, turbocharger module, and kinetics module. In addition, the exhaust gas bypass module and power turbine module are added after exhaust module in the exhaust heat main engine of the ship waste heat utilization system. MCylinder module describes the calculation process of 6 cylinders of diesel engine. In fact, it is based on the calculation data of one cylinder and multi-cylinder superposition calculation, that is,

the output of the diesel engine single cylinder model is calculated, and then superposition calculation is carried out according to the ignition sequence of the diesel engine and the crankshaft Angle is delayed successively, and finally the simulation data of the whole diesel engine is obtained. The SYN module and Syntotime module are used to realize the superposition of six cylinders [21]. This method cannot investigate the influence of the performance change of one or several cylinders on the performance of the whole diesel engine. Because the main content of this essay is the simulation calculation of exhaust temperature and performance of the waste heat utilization system of a low-speed two-stroke diesel engine, it is not necessary to consider the influence of the performance change of a cylinder on the performance of the whole diesel engine. Therefore, this method can greatly reduce the workload of calculation and speed up the calculation. In the simulation of the diesel engine, the crankshaft angle is the independent variable of the calculation inside the cylinder, and the time is the independent variable of the calculation outside the cylinder. Therefore, these parameters with crankshaft rotation angle as independent variable need to be converted from angle domain to time domain, and then delay stacking, such as mass flow, heat flow, and these variables are stacked with Syntotime module. Some state variables, such as the pressure and temperature in the cylinder, do not need to be converted and can be directly delayed by the SYN module. In this essay, the heat release law of diesel engine combustion in a cylinder is simulated using a double web curve. In the process of simulation, the parameters of diesel engine such as speed, structure size, fuel injection timing, working medium state in the cylinder at the compression end point, and excess air coefficient have a certain influence on the shape of fuel combustion heat release rate curve, and the calculation is complicated [22]. When the diesel engine is running according to the propulsion characteristics, the diffusion combustion cycle is short. In the case of the variable load operation, there is little change, and generally the value of rated operating condition is calculated. When diesel engine is running under stable conditions, θ is determined by fuel injection timing, which directly affects the law of combustion heat release. The premixed combustion lead Angle τ and the number of diffused combustion fuel Q can be determined from the measured indicator plots, and the parameter values under variable conditions can be calculated by linear interpolation as shown in Table 2.

For the simulation model of a marine large low-speed two-stroke diesel engine, the volume method is usually used to build the model, as shown in Figure 3.

In the ship waste heat recovery system, there are many kinds of waste heat recovery devices with different utilization effects. Comparatively speaking, the utilization of Marine diesel engine exhaust gas energy is very necessary and the effect is good. There are two ways to recover the exhaust gas energy of the main engine. One is to use the exhaust gas of the main engine to directly drive the power turbine to do work. The other is to recover the heat energy in the exhaust through the waste heat boiler to generate steam to drive the steam auxiliary, drive the turbine generator set to generate electricity, and integrate it into the ship power station. At

present, most of the schemes about ship waste heat recovery systems are based on the integration and improvement of these two schemes. The heat efficiency of high-power medium and low-speed two-stroke diesel engines is high. The exhaust temperature of the main engine is generally maintained at about 230°C. The energy contained in the exhaust gas is relatively low. In order to improve the energy utilization rate of the waste heat boiler, it is necessary to adopt appropriate methods to raise the exhaust temperature of the main engine to above 290°C and increase the heat of waste gas at the inlet of the waste heat boiler. Taking 6S50ME-C8.2 diesel engine as the target engine, the method of exhaust gas bypass was adopted to improve the exhaust temperature based on the simulation model of the standard main engine above. However, compared with the standard host, the exhaust gas bypass method reduces the turbine flow capacity, and the flow through the compressor decreases. Because the turbine efficiency remains unchanged, the compressor efficiency also remains unchanged according to the power balance, and the boosting pressure increases and scavenging pressure gradually increases. As the turbine flow capacity decreases, the amount of air entering the cylinder decreases, the fuel combustion is insufficient, and the exhaust temperature after the cylinder is high, which leads to the rise of the exhaust temperature after the turbine. Therefore, the exhaust gas bypass method can raise the exhaust temperature of the main engine to about 290°C, thus improving the energy quality of waste heat boiler exhaust gas and meeting the limit of acid dew point temperature parameters of waste heat boiler. However, as the intake flow of the diesel engine is reduced, the excess air coefficient in the cylinder of the diesel engine becomes smaller, which leads to an increase in fuel consumption rate, the increase in the maximum burst pressure, the increase in heat load, etc., and reduces the working performance of the diesel engine [23]. Therefore, it is necessary to take new measures to ensure the power and economy of diesel engines. Taking all things into consideration, the 6S50ME-C8.2 diesel engine should rematch turbocharger and reduce fuel consumption rate and maximum combustion pressure by adjusting fuel injection timing and exhaust timing. However, with the increase of injection advance Angle, the pressure and temperature in the cylinder will increase, which is conducive to the generation of NO_x. NO_x is the main emission of Marine diesel engines. According to the decision of the 58th MEPC (Committee for Marine Environmental Protection) meeting, engines built and shipped after 2011 must meet the IMO-Tier II emission standard, that is, the engine NO_x emission is reduced to 14.4 g/kWh. In order to meet the emission requirements, it is not expected that the injection advance Angle is too large, so the injection advance Angle directly affects the economic performance and emission performance of diesel engine. In the selection of injection advance Angle, these two factors should be considered comprehensively. In addition, the injection advance Angle has a great influence on the maximum explosion pressure in the cylinder of diesel engine, which should be taken into consideration [24, 25]. This is because when the diesel engine runs at high working conditions, the maximum explosion pressure will increase with

TABLE 2: Parameters of combustion heat release law.

Rotational speed (r/min)	Load (%)	Fuel injection timing θ_z ($^{\circ}CA$)	Premixed combustion lead angle r ($^{\circ}CA$)	Diffused combustion fuel fraction Q_f
128	100	-1.5	25	0.16
120.4	84	-2.6	17	0.17
116.4	76	-4.3	19	0.22
100.8	50	-3.4	15	0.18

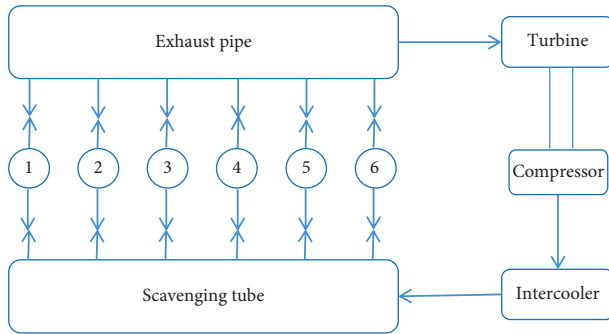


FIGURE 3: Schematic diagram of volumetric method model of large marine low-speed two-stroke diesel engine.

the increase of injection advance Angle, resulting in a great increase in the pressure and temperature in the cylinder. This will not only increase the mechanical and thermal load of the cylinder to bear, but also the increase of the pressure rise rate will lead to more rough combustion, and the diesel engine combustion noise will also increase. This will put forward higher requirements for material strength and noise control of diesel engine. In low working conditions, even if the injection advance Angle is increased, the combustion temperature in the cylinder does not change much, and the exhaust pressure is basically unchanged. Because the temperature and pressure in front of the turbine remain roughly constant, the efficiency of the turbine does not change much. The turbine power capacity is basically in a low state, and the exhaust temperature behind the turbine does not increase. To sum up, in order to meet the requirements of WHR engine fuel consumption rate, cylinder implosion pressure, and TierII emission standard, an appropriate injection advance Angle must be selected. The 6S50ME-C8.2 diesel engine adopts a variable fuel injection timing mechanism and is selected under different working conditions. Different injection advance Angle is used to meet the requirements of the economy, power performance, and TierII emission standard of diesel engine. Through simulation calculation, the injection advance Angle selected in each working condition is shown in Table 3:

In the working process of diesel engine, the opening time of the exhaust valve directly affects the scavenging process of diesel engine, and the scavenging ability determines the combustion performance of diesel engine. Therefore, exhaust timing has a great influence on diesel engine performance. In order to increase the maximum combustion pressure and improve the economy of diesel engine, the exhaust valve is opened in advance at the rated working conditions. This prolongs the diesel engine-free exhaust

TABLE 3: Injection advance angle of WHR main engine.

Working condition	100%	95%	85%	75%	65%	50%
Injection advance angle ($^{\circ}CA$)	-1.5	-1.8	-2.3	-3.4	-4.5	-4

process, reduces the scavenging resistance, and increases the charging efficiency, fuel, and air mix fully, and combustion is good. However, the increase of temperature and pressure in the cylinder is beneficial to NOx generation, which affects the emission performance of diesel engine. In order to reduce NOx emissions and meet Tier II emission indicators, the opening time of the exhaust valve is delayed. This increases the pressure in the cylinder when the scavenging port is open, which is not conducive to fresh air entering the cylinder. After the scavenging process, the residual exhaust gas in the cylinder of the diesel engine increases. Because of its inertia, this part of the residual exhaust gas delays the combustion process and slows down the pressure formation process in the cylinder. The combustion temperature in the cylinder decreases, the combustion quality decreases, and the fuel consumption rate increases. As the exhaust temperature of the cylinder decreases, the temperature of the rear turbine decreases [26]. With the development of social science and technology, equipment manufacturing technology has been improved. At present, the efficiency of the designed turbocharger has reached a very high level, and the power capacity of the turbine has been significantly enhanced. Because the exhaust volume of a large low-speed Marine two-stroke diesel engine is very large in high working conditions, even if part of the exhaust gas is bypassed, it can meet the work needs of the turbocharger. Therefore, the turbocharger used by the marine two-stroke diesel engine will have a bypass valve at the turbine end. When the main engine runs in high working conditions, exhaust gas bypass is adopted to drive the power turbine to do work; When running under low working conditions, due to the small exhaust volume of the main engine, in order to ensure the intake gas of the diesel engine under low working conditions, the bypass valve is closed, and the exhaust gas is all passed into the turbine to meet the working performance of the supercharger under low working conditions. When the main engine runs in high working conditions, the exhaust gas bypass is adopted to reduce the exhaust volume flowing through the turbine and the power emitted by the turbine. According to the flow and power balance between the compressor and the turbine, the power capacity of the compressor decreases. The amount of air entering the cylinder decreases, resulting in a lower excess air coefficient in the cylinder and a higher diesel exhaust temperature. The

exhaust gas temperature after the turbine will also rise, which is conducive to the recovery of exhaust heat from the waste heat boiler and the increase of steam. However, if the side flux is too large, the pressure ratio of the compressor is reduced, and the joint operation point of the turbocharger moves to the surge line, which is likely to cause the compressor surge. The simulation model of the 6S50ME-C8.2 low-speed two-stroke diesel engine is established by Matlab/Simulink. By setting the parameters of injection timing, exhaust timing, and combustion starting point, the volumetric model of the diesel engine can not only calculate the characteristic parameters of diesel engine under steady-state conditions, but also simulate the variation of performance parameters in the dynamic process when the diesel engine load speed changes. Under the rated working condition, the calculated cylinder pressure curve is in good agreement with the test value and reflects the real situation of the pressure change in the cylinder [27, 28]. According to the established simulation model of the whole machine, according to the propulsion characteristics of the simulation calculation, and compared with the test value. The results show that the propulsive characteristics of the diesel engine are basically consistent with the experimental values, which indicates that the simulation model of the 6S50ME diesel engine is accurate and reliable, and can well simulate the steady-state characteristics of the diesel engine. In the step response of the model, the dynamic change process of the model accords with the actual situation of diesel engine and can reflect the instantaneous change of parameters such as turbine exhaust temperature and instantaneous speed. The diesel engine simulation model has good dynamic simulation ability. In order to improve the thermal efficiency of the WHR waste heat utilization system and improve the energy utilization rate of the waste heat boiler, a simulation model of the WHR main engine was established by matching tCA-55 turbocharger and adding a waste gas bypass module on the basis of standard main engine model, and to reduce fuel consumption rate and maximum combustion pressure of WHR engine by adjusting fuel injection timing and exhaust timing. When the steady-state and dynamic performance of the WHR engine are simulated, the simulation results show that the model is accurate and reliable except that the fuel consumption rate increases slightly. The exhaust temperature of the WHR main engine has reached 298°C, and the energy quality of waste gas entering the waste heat boiler has been improved to meet the requirements of the waste heat recovery system.

5. Conclusion

Based on the detailed analysis of the working process in the cylinder of the diesel engine, the 6S50ME-C8.2 volume method model was established based on Matlab/Simulink simulation platform, and the propulsion characteristics of the model were verified and calculated according to the test data of 6S50ME-C8.2 diesel engine. The simulation value was very close to the test value. Thus, the accuracy of the simulation model is verified. In order to improve the thermal efficiency of the marine waste heat utilization system, the

simulation model of the standard main engine was improved and the exhaust gas bypass module was added under the condition of ensuring the dynamic performance of the Marine diesel engine. The main engine model of the ship waste heat utilization system was established by adjusting the timing of fuel injection, exhaust timing, and exhaust gas flux, and the steady-state operation and transient working conditions were simulated. The results show that the model can well simulate the actual operation of the diesel engine, the exhaust temperature has reached 298°C, and the energy quality of waste gas at the inlet of the waste heat boiler has been improved, which meets the requirements of waste heat recovery system.

Data Availability

The data used to support the findings of this study are available from the corresponding author upon request.

Conflicts of Interest

The author declares that there are no conflicts of interest.

References

- [1] F. Wang, L. Wang, H. Zhang, L. Xia, and J. Yuan, "Design and optimization of hydrogen production by solid oxide electrolyzer with marine engine waste heat recovery and orcycle," *Energy Conversion and Management*, vol. 229, Article ID 113775, 2021.
- [2] E. Tang, J. Ding, and J. Lu, "Heat transfer and energy utilization of waste heat recovery device with different internal component," *Energy and Power Engineering*, vol. 12, no. 2, pp. 88–100, 2020.
- [3] O. Koshevyi, D. Levkivskiy, V. Kosheva, and A. Mozharovskiy, "Computer modeling and optimization of energy efficiency potentials in civil engineering," *Strength of Materials and Theory of Structures*, vol. 106, pp. 274–281, 2021.
- [4] H. Kauko, D. Rohde, A. Hafner, and E. Scubba, "Local heating networks with waste heat utilization: low or medium temperature supply?" *Energies*, vol. 13, no. 4, p. 954, 2020.
- [5] E. A. Martinez Cesena, E. Loukarakis, N. Good, and P. Mancarella, "Integrated electricity-heat-gas systems: techno-economic modeling, optimization, and application to multienergy districts," *Proceedings of the IEEE*, vol. 108, pp. 1392–1410, 2020.
- [6] R. Kamminana and V. Kambagowni, "Modeling and optimization of process parameters of friction stir welding of al-li alloy aa2050 by response surface methodology," *International Journal of Engineering Trends and Technology*, vol. 69, no. 5, pp. 208–227, 2021.
- [7] W. Huang, N. Zhang, Y. Cheng, J. Yang, Y. Wang, and C. Kang, "Multienergy networks analytics: standardized modeling, optimization, and low carbon analysis," *Proceedings of the IEEE*, vol. 108, no. 9, pp. 1411–1436, 2020.
- [8] L. Yong, J. Qingsong, L. Zhongyao et al., "Lake eutrophication responses modeling and watershed management optimization algorithm: a review," *Journal of Lake Sciences*, vol. 33, no. 1, pp. 49–63, 2021.
- [9] R. Singh and R. Bhatia, "Experimental and modeling process optimization of lead adsorption on magnetite nanoparticles via isothermal, kinetics, and thermodynamic studies," *ACS Omega*, vol. 5, no. 19, pp. 10826–10837, 2020.

Retraction

Retracted: State Diagnosis and Monitoring Method of Robot Electric Power Equipment Based on Data Mining

International Transactions on Electrical Energy Systems

Received 19 September 2023; Accepted 19 September 2023; Published 20 September 2023

Copyright © 2023 International Transactions on Electrical Energy Systems. This is an open access article distributed under the Creative Commons Attribution License, which permits unrestricted use, distribution, and reproduction in any medium, provided the original work is properly cited.

This article has been retracted by Hindawi following an investigation undertaken by the publisher [1]. This investigation has uncovered evidence of one or more of the following indicators of systematic manipulation of the publication process:

- (1) Discrepancies in scope
- (2) Discrepancies in the description of the research reported
- (3) Discrepancies between the availability of data and the research described
- (4) Inappropriate citations
- (5) Incoherent, meaningless and/or irrelevant content included in the article
- (6) Peer-review manipulation

The presence of these indicators undermines our confidence in the integrity of the article's content and we cannot, therefore, vouch for its reliability. Please note that this notice is intended solely to alert readers that the content of this article is unreliable. We have not investigated whether authors were aware of or involved in the systematic manipulation of the publication process.

Wiley and Hindawi regrets that the usual quality checks did not identify these issues before publication and have since put additional measures in place to safeguard research integrity.

We wish to credit our own Research Integrity and Research Publishing teams and anonymous and named external researchers and research integrity experts for contributing to this investigation.

The corresponding author, as the representative of all authors, has been given the opportunity to register their agreement or disagreement to this retraction. We have kept a record of any response received.

References

- [1] H. Guo, Z. Meng, H. Yu, R. Chen, L. Li, and L. Cheng, "State Diagnosis and Monitoring Method of Robot Electric Power Equipment Based on Data Mining," *International Transactions on Electrical Energy Systems*, vol. 2022, Article ID 4272364, 7 pages, 2022.

Research Article

State Diagnosis and Monitoring Method of Robot Electric Power Equipment Based on Data Mining

Haifeng Guo , Zhaojun Meng , Huimin Yu , Rui Chen , Ling Li , and Li Cheng 

College of Electrical and Information Engineering, Liaoning Institute of Science and Technology, Benxi, Liaoning 117004, China

Correspondence should be addressed to Haifeng Guo; 20180025@ayit.edu.cn

Received 22 June 2022; Revised 3 August 2022; Accepted 8 August 2022; Published 29 August 2022

Academic Editor: B. Madhavan

Copyright © 2022 Haifeng Guo et al. This is an open access article distributed under the Creative Commons Attribution License, which permits unrestricted use, distribution, and reproduction in any medium, provided the original work is properly cited.

In recent years, with the continuous improvement of system networking, the use of robot electric power equipment is becoming more and more extensive, so it is very necessary to diagnose and monitor its status. Therefore, a diagnosis and monitoring system based on the data mining algorithm is constructed. This study mainly uses the gray prediction algorithm and discrete prediction algorithm; the results showed that after the combination of gray prediction has a certain degree of increase, through the analysis, we can draw the reason for this is that gray prediction algorithm to check the failure data is no longer as input data in the detection of outliers, thereby reducing the noise of the data set, so that the performance of outlier detection algorithm can achieve a great progress. In terms of the running time of outlier detection, the running time of outlier detection using K-Mean algorithm and DBSCAN algorithm increases to a certain extent because the algorithm combines gray prediction and increases the algorithm process.

1. Introduction

In recent years, with the continuous improvement of the system network degree and the rapid development of the field real-time data storage and communication technology, the data volume in the system database is increasing. However, at this stage, one can only have a very limited use and analysis of these data, such as basic data query or device working state statistics. This phenomenon, in which a large portion of the system's data are underutilized, is often described as data-rich, but information-poor. In fact, behind a large number of historical data, a lot of important information is often hidden. It is not until system decision does the comprehensive analysis of the information behind the data that historical data can be converted to directly used knowledge, which makes people urgently need an approach to dig out huge amounts of hidden knowledge of historical data. In this context, data mining (DataMining, DM) technology gradually developed, which is a new tool generated from information science and technology, whose development and the development of a new generation of information systems such as data warehouse are inseparable [1].

Data mining is the discovery of unknown and potential application patterns or information from its own and large number of data (data warehouse or database). See Figure 1.

In general, the basic process of human discovery of knowledge can be divided into the following steps:

- (1) Observe and understand the objective world through various means such as people's own feelings, and sensors, and collect the original data from the objective world, sort out, archive them, and input them into the database.
- (2) Change the collected raw data, remove noise and a series of data preprocessing work.
- (3) Further refine the preprocessed data and screen out the useful information for people.
- (4) After in-depth research and analysis of string information, summarize and extract more useful information, which can help human beings to understand the mode of the operation of objective things, namely, knowledge
- (5) From the accumulated large amount of knowledge, summarize the principles and laws that can guide people's action and form wisdom.

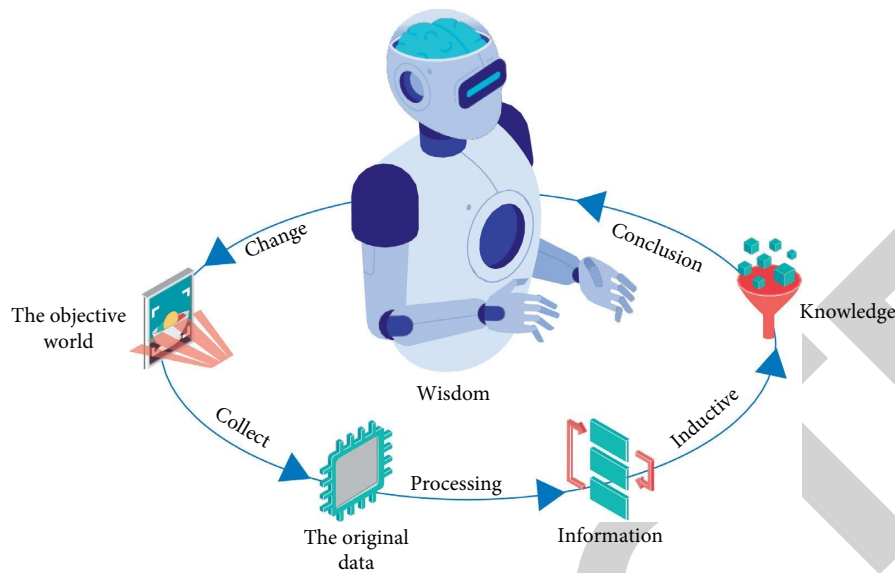


FIGURE 1: Process of finding the basic knowledge.

- (6) Using wisdom, engaged in productive labor, human beings can change the objective world according to their own will.

In the process of the above knowledge discovery, data mining plays an important role in steps (2) to (4), mining useful knowledge that can be understood from a large amount of incomplete data. Need is the mother of invention. In recent years, data mining has been boosting at home and abroad and has been widely used in scientific research, government project management, enterprise financial decision-making, industrial production line production, Chinese and western medicine, and other fields. In terms of machine learning and artificial intelligence, the data mining technology that comprehensively uses statistics, pattern recognition, visualization technology, database, numerical analysis, and other subject knowledge has also become a research hot spot [2].

With the development of fault diagnosis technology, various fault diagnosis methods can be roughly divided into large categories of mathematical model-based methods, artificial intelligence-based methods, and data-driven methods.

The diagnostic idea of the mathematical model-based method is diagnosed through the analysis of the residual sequence, but the precise mathematical model of the diagnosed system must be established first. According to the different modes of residual production, it can be divided into state estimation-based diagnostic method, parameter estimation-based diagnostic method, and equivalent space method [3]. Among them, the method based on parameter estimation needs to find a one-to-one correspondence between model parameters and physical parameters to facilitate the separation of faults. Methods for linear parameter estimation can be implemented using well-established parameter identification techniques such as least squares and a Kalman filter. However, the most studied parameter estimation methods for nonlinear systems are the strong

tracking filter method [4]. Its biggest feature is that using a strong tracking filter to estimate the model parameters is robust to the model uncertainty. See Figure 2.

Artificial intelligence-based method is a common fault diagnosis method based on nonanalytical model which includes expert system-based diagnostic method, neural network-based diagnostic method, fuzzy logic-based diagnostic method, pattern recognition-based diagnostic method, and graph theory-based diagnostic method. Expert application in the medical diagnostic system has been extended to electric power equipment maintenance and diagnosis, industry, agriculture, business, and other industries. The diagnostic method based on the neural network is divided into two categories. One is the neural network as the output estimator and replaces the traditional observer; the other is the neural network for classification and pattern recognition [5].

2. Literature Review

In fault diagnosis with a modern, networking, integrated, and electric power equipment complicated system, the system of real-time running state data is very large and inevitably contains noise, incomplete and isolated points, etc. The traditional fault diagnosis method is difficult to meet the requirements of the system fault diagnosis speed, and effectiveness, where electric power equipment monitoring and knowledge acquisition has bottleneck problems. Generally, the composition structure of data mining-based fault diagnostic systems is shown in Figure 3.

The application of data mining technology in fault diagnosis belongs to a knowledge-based intelligent fault diagnosis method developed in the late 1980s. By using the powerful knowledge acquisition ability unique to data mining technology, it can effectively solve the problems such as the difficulty to establish the traditional expert diagnosis system model, the effective use of failure history data, the

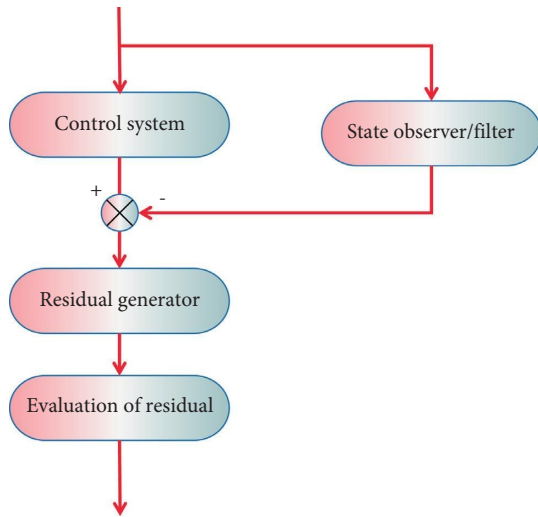


FIGURE 2: Schematic diagram of the fault diagnosis based on the mathematical model.

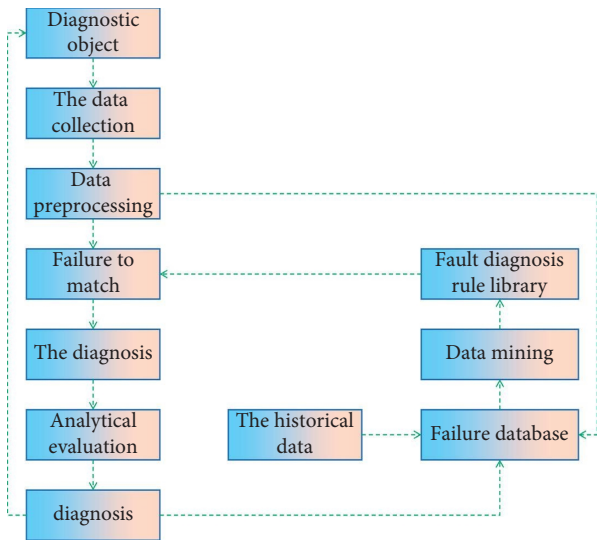


FIGURE 3: Schematic diagram of the fault diagnosis system based on data mining.

failure of the system, and the failure detection system. At the same time, to a certain extent, the use of data mining technology can improve the lack of self-learning ability in the fault diagnosis method and that the knowledge base cannot be updated and so on [6].

Cheng et al. CASSIOPEE mass quantity control system is based on data mining technology. The main application of this system is the fault diagnosis and fault prediction of the Boeing 737 aircraft, which achieves satisfactory fault diagnosis results in some practical projects and brings a considerable economic benefit [7]. According to the intelligent fault diagnosis problem of steam turbine, a TIGE civilian diagnosis system based on data mining technology is developed by Zhang et al. and the actual application effect meets the requirements of steam turbine system diagnosis [8]. ROSETTA, a data mining toolkit based on the coarse set theory, was developed to summarize and extract specific

discriminant rules for each fault from many vibration signal characteristic parameters by Lv et al [9]. The KATE data mining software by Zhang et al. was developed to mine implicit knowledge from large amounts of data through inductive methods and automatically generate decision trees to provide strong support for electric power equipment fault diagnosis decisions. The system has now been used in a Boeing aircraft manufacturing [10]. After Afrash et al. applied data mining technology to loans and other business monitoring, the company's credit card utilization rate increased by 10%–15% [11].

In China, due to the late start of data mining technology research, the research mainly focuses on theoretical and method discussion and simulation verification; thus, there are practical applications in only a few fields. In recent years, many scientific research institutions and high research institutes attach great importance to the research of data mining methods. Relevant studies in China are as follows:

Li et al. has studied the improvement direction of decision tree algorithm, analyzed the shortcomings of feature discretization, improved the Fayyad boundary point decision theorem, and studied the sample incremental learning problem of decision tree [12]. Zhou et al. designed a comprehensive diagnosis method based on simulation which is designed to form the fault detection and diagnosis process, which can improve the speed and accuracy and effectively improve the automation and intelligence of system fault diagnosis [13]. Zhou et al. introduced time series data mining technology into spacecraft telemetry data analysis and processing, system state feature extraction, fault diagnosis and identification, to promote the development of spacecraft fault diagnosis technology, improve the reliability and safety of satellite orbit operation, and extend the service life of satellite, which has great significance, which also proves that data mining in the field of spacecraft fault diagnosis has broad application prospects [14]. For association rule algorithm, Jiang et al. combined with the fuzzy clustering method and made it possible that association rule algorithm can not only mine Boolean attribute rules but can also be extended to the field of mining numerical properties [15]. For the decision tree algorithm, an improved algorithm combined with the ant colony algorithm is proposed to fundamentally improve the efficiency of the decision tree. Zhang taking full-attitude combined top TQZ-1A as the research object and using Clementine data mining tool and CRISP-DM industry standard, constructed, and improved C5.0 classification model based on two-stage clustering. It verifies the good predictability of the model evaluation index [16].

3. Methods

3.1. Gray Prediction Algorithm. The first-order linear gray model $G_m(1, 1)$ is the basic prediction model of gray system theory. It takes differential fitting as the kernel and finds out the change law between the data according to the data characteristics of the system. The $G_m(1, 1)$ gray prediction model modeling process is as follows:

Raw data preprocessing is as shown in formula (1):

$$x^{(1)}(k) = \sum_{i=1}^k x^{(0)}(i), \quad k = 1, 2, \dots, n. \quad (1)$$

The defined form predicted by Gm (1, 1) gray is shown in formula (2):

$$x^{(0)}(k) + az^{(1)}(k) = b, \quad k = 1, 2, \dots, n, \quad (2)$$

where $z(k)$ is the adjacent generation of $x(k)$, namely, $z(k) = 0.5x(1)(k) + 0.5x(1)(k-1)$, a is the development coefficient, and b is the gray action amount. The whitening

differential equation for this system is obtained: as shown in formula (3):

$$\frac{dX^{(1)}}{dt} + aX^{(1)} = b. \quad (3)$$

Using least squares, solve a, b as shown in formula (4):

$$[a, b]^T = (B^T, B)^{-1} B^T Y. \quad (4)$$

Taking together formulas (2) and (3), it is as shown in formula (5):

$$\left\{ \begin{aligned} \hat{x}^{(1)}(k+1) &= \left(\hat{x}^{(0)}(1) - \frac{b}{a} \right) e^{-ak} + \frac{b}{a} \hat{x}^{(0)}(k+1) \\ \hat{x}^{(1)}(k+1) &= \hat{x}^{(1)}(k+1) - \hat{x}^{(1)}(k). \end{aligned} \right. \quad (5)$$

Furthermore, the predicted value of time point $K+1$ can be found as shown in formula (6):

$$\hat{x}^{(0)}(k+1) = \left(x^{(0)}(1) - \frac{b}{a} \right) (1 - e^{-ak}). \quad (6)$$

The running state of the electric power robot is affected by the surrounding environment and changes all the time. If only the Gm (1, 1) static prediction model is used, the prediction accuracy of the real-time data of the electric power robot system will gradually decrease with the change of the electric power robot state. Therefore, the gray prediction algorithm applied to the robot system should be able to actively discard the old data to the historical moment, constantly introduce the new data from the current moment, and establish a real-time dynamic prediction model. The method of dynamic prediction is to establish the Gm (1, 1) model, introduce the continuous data of L group in the time window, that is, from the current moment to the past L group data, which constantly updates the sample data of Gm (1, 1) model [17].

As shown in formula (7):

$$X^0_{\text{new}} = \{x^{(0)}(k-L+1), x^{(0)}(k-L+2), \dots, x^{(0)}(k)\}. \quad (7)$$

With the complex underwater working environment of AUV, as well as many external interference, the nonlinearity and uncertainty of its own system is strong, which requires that the fault diagnosis method of the AUV system should have high accuracy and stability and can meet the real-time requirements of independent control of the system [18]. To this end, this paper first adopts the gray dynamic prediction method, to select real-time and continuous K data $X^{(0)} = \{x^{(0)}(1), x^{(0)}(2), \dots, x^{(0)}(k)\}$ obtained by AUV sensor, and then get the gray prediction $X^{(1)} = \{x^{(1)}(1), x^{(1)}(2), \dots, x^{(1)}(k)\}$ after pretreating these data by first-order accumulated generating operation. Eventually, $x(k+1)$ is obtained as the output expected value of $k+1$, and then the residual difference of the output value is calculated as shown in formula (8):

$$\varepsilon(k+1) = y(k+1) - x(k+1), \quad k = 1, 2, 3, \dots \quad (8)$$

According to the abovementioned principle, using the dynamic gray prediction algorithm, the system fault can be quickly determined and the fault judgment rules are as shown in formula (9):

$$\varepsilon(k+1)^2 \begin{cases} > \varepsilon_{\theta}, & \text{NO,} \\ \leq \varepsilon_{\theta}, & \text{YES,} \end{cases} \quad (9)$$

Where θ is the fault threshold set based on the system history failure data.

3.2. Outliers Detection Algorithm. In general, the fault diagnosis method based on outlier detection is based on the historical data of the system. Without the need of obtaining the system accurate model, it analyzes the hidden information implied in these data through data mining and obtains the fault rules to achieve the fault diagnosis. There are many methods for outlier detection, such as statistical-based, proximity-based, cluster-based, and classification-based, and so on [19]. Among them, the cluster-based outlier detection method determines the outlier points by examining the relationship between objects and clusters. Each outlier is an object, which belongs to a small remote cluster, or does not belong to any cluster. The fault diagnosis method is based on outlier detection has the following advantages. First, it is an unsupervised fault diagnosis method, effective for many types of data; second, after comparing other objects with the obtained cluster, the object can be decided whether it is outlier from in a rapid speed, and then fault diagnosis will be made [20]. The advantages of this kind of detection method are very suitable for the fault diagnosis requirements of the electric power robot system. Therefore, a cluster-based outlier detection method was used.

The effectiveness of clustering-based outlier detection is highly dependent on the clustering method. Improper selection of the clustering method will directly lead to poor clustering effect and even clustering failure. Therefore, it is necessary to find a clustering method with high clustering accuracy and good timeliness for the fault diagnosis based on outlier detection [21]. An improved clustering algorithm with DBSCAN kernel and kernel idea, iterative density-

based clustering algorithm IKD, and iterative density-based spatial clustering algorithm with noise application combining K-mean) are proposed [22].

By analyzing the various steps of the IKD algorithm, it is seen that the IKD algorithm is an unsupervised clustering party rebellion without any prior knowledge. In order to evaluate the effect of the IKD algorithm clustering method, clustering evaluation parameter H is used. Assuming that the data objects are clustered into K clusters, H is defined as shown in formula (10):

$$H = \frac{A}{B} = \frac{\sum_{s=1}^{K_r} \sum_{p \in C_s} |p - m_s|}{\sum_{s=1}^{K_r} |m_s - m|}, \quad s = 1, 2, 3, \dots, K_r. \quad (10)$$

Compared with the original clustering algorithm, the IKD algorithm has the following advantages;

- (1) First of all, after the first DBSCAN clustering, the outlier is temporarily deleted, which is ready for the next K-mean clustering, and completes the data pretreatment, so as to greatly overcome the disadvantage of using K-mean clustering algorithm in the process of clustering, but also the advantage of that DBSCAN algorithm can handle noise points has been fully utilized;
- (2) Second, on the basis of the DBSCAN algorithm, the IKD algorithm combines with K-mean clustering algorithm, which through the change in the algorithm process, fundamentally and effectively solves two problems: one is that K-mean algorithm needs to give the number of clusters K of clusters to be generated in advance; the other is that W and clustering effect is excessively dependent on the private random selection in the initial;
- (3) Third, the final step of the IKD algorithm is to use the improved DBSCAN algorithm combined with the ISODATA algorithm for clustering, so the algorithm completely inherits the advantages of density-based clustering method, and can find clusters of any shape or clusters with great differences in the number of data objects, which is difficult for other clustering algorithms to do this;
- (4) Finally, the IKD algorithm can automatically merge the clusters obtained in the clustering process, and through repeated iterative operation it can independently decide whether to terminate the cluster according to the cluster evaluation parameter H , so as to obtain the objective and correct clustering.

By using this AUV fault diagnosis method based on gray prediction and IKD algorithm, the efficiency of fault diagnosis of robot system is significantly improved, and the accuracy of diagnosis is basically unchanged when using DCD based on $D C D$ algorithm alone [23].

4. Experimental Results and Discussion

The 500 sets of data in the electric power robot propeller system are test data. See Figures 4–7.

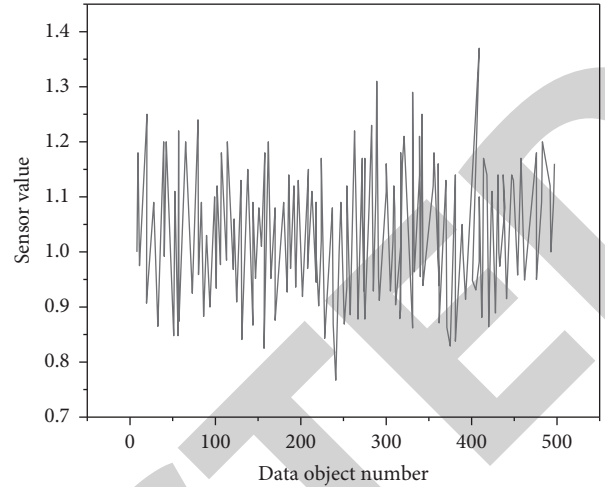


FIGURE 4: Raw data.

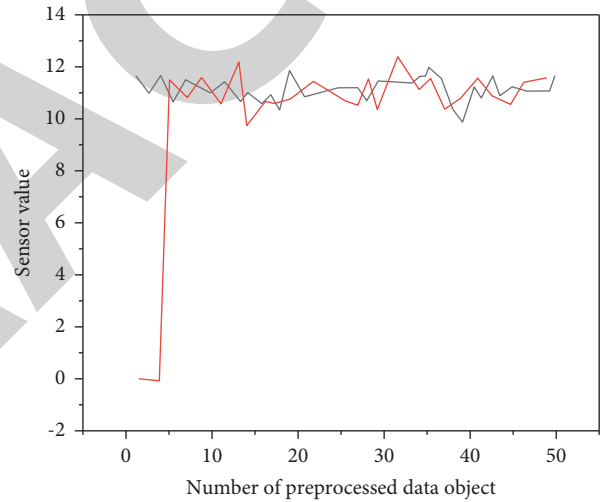


FIGURE 5: Comparison of clever evidence and predicted knot harvest after pretreatment.

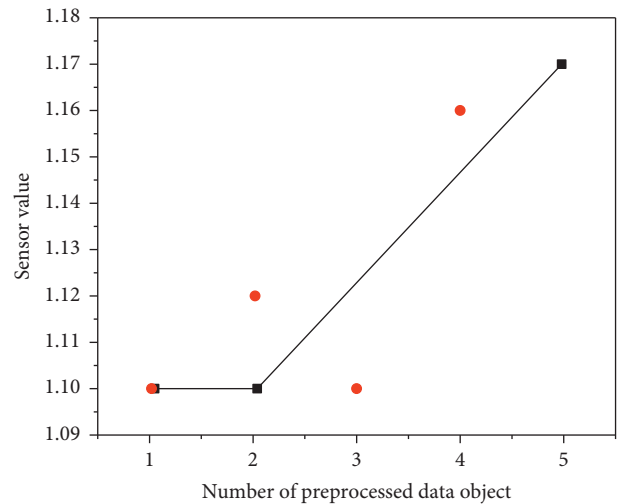


FIGURE 6: Results of predicting the model running.

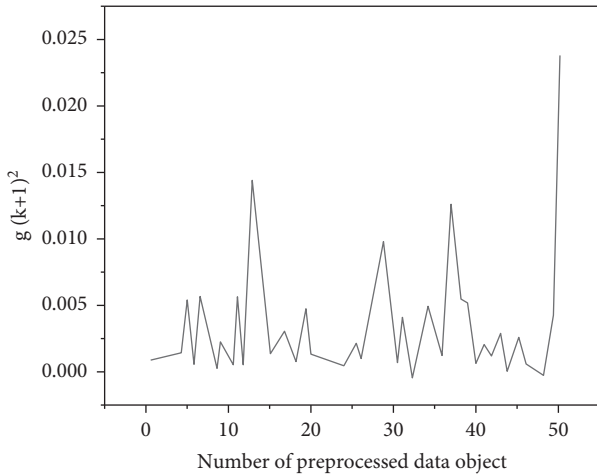


FIGURE 7: Operation curve diagram.

In the test, the real-time operation data collected by the sensor are preprocessed. The specific method is to get the average from 10 sets of data to represent the sensor value.

It can be seen from the test results that the Gm (1, 1) predicted the model accurately, and the residual square $\varepsilon(k+1)^2$ did not exceed 0.03. If the fault width set in the fault diagnosis system based on gray prediction is 0.05, it can be diagnosed that the electric power robot system has not failed [24].

The reason why the first four predictions are 0 is that the sensor data of the first four gray predictions are used as the observation value of the initial moment in the algorithm, so the predicted value is only available from the fifth time on. From the comparison of preprocessed data and prediction data, the prediction curve well fits the actual measurements of the sensor, which verifies that the electric power robot fault diagnosis based on gray prediction is feasible [25].

Finally, the test and analysis based on gray prediction and improved outlier detection are summarized. In addition to detecting hard faults in the system, another main purpose of introducing gray prediction methods is to improve the timeliness of outlier detection based on the IKD algorithm. As with the test set above, in the experiment, the number of iterations of ISODATA algorithm and IKD algorithm were still set at 5 times, and the same data pre-processing and gray prediction operations were performed before running the four cluster-based outlier tests.

- (1) In the use of four algorithms outlier detection, combined with the gray prediction, the accuracy of result has a certain degree of improvement. Through analysis, it can be concluded that the fault data checked out by gray prediction algorithm is no longer used, thus reducing the noise in the data set, which in turn makes the outlier detection algorithm performance give full play;
- (2) The running time of outlier detection using K-mean algorithm and DBSCAN algorithm increases to a certain extent, because the algorithm combines gray prediction and increases the algorithm process;

- (3) It is worth noting that the running time of outlier detection using ISODATA algorithm and IKD algorithm is reduced to a certain extent. Among them, the time of diagnosis using IKD algorithm is reduced by 29.79%, which verifies that the fault diagnosis method based on gray prediction and outlier detection is feasible and improves the timeliness of fault diagnosis based on outlier detection.

5. Conclusion

This paper presents a diagnosis and monitoring method based on data mining. It analyzes the K-mean algorithm, the DBSCAN algorithm, and the ISODATA algorithm, respectively, and tests the improved IKD clustering algorithm in outlier detection. The verification results show that the outlier detection method based on data mining IKD algorithm is feasible. By comparison, it was found that the detection accuracy obtained by using the IKD algorithm was significantly higher than that obtained with other clustering algorithms, but with slightly less timeliness. To solve this problem, a gray prediction model is introduced in the fault detection of the electric power robot, and the test data show that this method works well and improve the speed of fault detection to some extent. Finally, the detected fault data completes the fault diagnosis of the underwater electric power robot propeller system.

In the future data mining, the visualization means have been greatly enriched and improved. This advanced technology is very suitable for being applied to the fault diagnosis of complex systems. If this difficulty is overcome, the function of the fault diagnosis system in human-computer interaction will be greatly improved.

Data Availability

The data used to support the findings of this study are available from the corresponding author upon request.

Conflicts of Interest

The authors declare that they have no conflicts of interest.

Acknowledgments

This work was supported by the basic scientific research project of Liaoning Provincial Department of Education, Research on Key Technologies of Health Assessment Of High Safety Equipment Based On Deep Learning (Project No. LJKZ1061).

References

- [1] S. N. Mohammed and A. Karim, "A novel facial emotion recognition scheme based on graph mining," *Defence Technology*, vol. 16, no. 5, pp. 1062-1072, 2020.
- [2] Z. Lv and L. Qiao, "Deep belief network and linear perceptron based cognitive computing for collaborative robots," *Applied Soft Computing*, vol. 92, Article ID 106300, 2020.
- [3] Z. Lv, Y. Han, A. K. Singh, G. Manogaran, and H. Lv, "Trustworthiness in industrial IoT systems based on artificial

Retraction

Retracted: Application of Internet of Things Technology in Optimization of Electronic Assembly Process Parameters

International Transactions on Electrical Energy Systems

Received 19 September 2023; Accepted 19 September 2023; Published 20 September 2023

Copyright © 2023 International Transactions on Electrical Energy Systems. This is an open access article distributed under the Creative Commons Attribution License, which permits unrestricted use, distribution, and reproduction in any medium, provided the original work is properly cited.

This article has been retracted by Hindawi following an investigation undertaken by the publisher [1]. This investigation has uncovered evidence of one or more of the following indicators of systematic manipulation of the publication process:

- (1) Discrepancies in scope
- (2) Discrepancies in the description of the research reported
- (3) Discrepancies between the availability of data and the research described
- (4) Inappropriate citations
- (5) Incoherent, meaningless and/or irrelevant content included in the article
- (6) Peer-review manipulation

The presence of these indicators undermines our confidence in the integrity of the article's content and we cannot, therefore, vouch for its reliability. Please note that this notice is intended solely to alert readers that the content of this article is unreliable. We have not investigated whether authors were aware of or involved in the systematic manipulation of the publication process.

Wiley and Hindawi regrets that the usual quality checks did not identify these issues before publication and have since put additional measures in place to safeguard research integrity.

We wish to credit our own Research Integrity and Research Publishing teams and anonymous and named external researchers and research integrity experts for contributing to this investigation.

The corresponding author, as the representative of all authors, has been given the opportunity to register their agreement or disagreement to this retraction. We have kept a record of any response received.

References

- [1] X. Song, "Application of Internet of Things Technology in Optimization of Electronic Assembly Process Parameters," *International Transactions on Electrical Energy Systems*, vol. 2022, Article ID 2375521, 7 pages, 2022.

Research Article

Application of Internet of Things Technology in Optimization of Electronic Assembly Process Parameters

Xianghui Song 

Jari Electronics, Lianyungang, Jiangsu 222061, China

Correspondence should be addressed to Xianghui Song; 1612022210008@hainanu.edu.cn

Received 28 June 2022; Revised 23 July 2022; Accepted 2 August 2022; Published 29 August 2022

Academic Editor: B. Madhavan

Copyright © 2022 Xianghui Song. This is an open access article distributed under the Creative Commons Attribution License, which permits unrestricted use, distribution, and reproduction in any medium, provided the original work is properly cited.

In order to meet the demand of the Internet of things in the intelligent power monitoring system, this paper proposes a method to build an intelligent power monitoring system by combining 4G technology, the Android operating system, and other technologies closely related to the Internet of things. This method is evaluated by building an intelligent monitoring system and a transit node system and observing the test speed in the coco data set and the Pascal VOC data set. The experimental results show that the accuracy of animals measured by this method can reach up to 81%; the accuracy of humans can reach up to 76%; and the accuracy of vehicles can reach up to 87%. *Conclusion.* The application of Internet of things technology in the optimization of electronic assembly process parameters can quickly and effectively reflect the information in practical applications, so as to achieve the goal of seamless link and information exchange between things and people, and accurately manage and control the physical world in real time on the basis of scientific decisions.

1. Introduction

With the development of the third scientific and technological revolution, the Internet of things technology has played a promoting role in all walks of life [1]. The Internet of things technology, in short, is a technology that uses sensor equipment to realize the network transmission of information resources and exchange and share information through the corresponding information media, so as to realize the function of intelligent management. With the support of Internet of things technology, information transmission and exchange are more safe, efficient, energy-saving, and environmentally friendly, and they truly realize the intelligitization of network flow transmission [2]. It has always been a world leader in R & D and innovation in the field of Internet of things technology. In recent years, colleges and universities have attached importance to talent development and industry technology leadership and have made many achievements internationally. The Internet of things technology has the same advantages and has an important influence in the world. At the same time, in the field of global sensor networks,

China is also one of the leading countries in the formulation of international standards. However, at present, the development of the smart grid is common all over the world and is still in its infancy. However, many professionals have realized the great value potential that the smart grid brings to mankind.

The smart grid, under the Internet of things technology, plays an important role in the sustainable development of the social economy. Compared with the traditional power grid and power equipment, the smart grid based on the Internet of things technology can effectively protect the environment, achieve the development of environment-friendly industries, and reduce greenhouse gas emissions. It can also realize the optimization of the power industry structure and make the power allocation more efficient. It can also improve the efficiency of energy transportation and use and enhance the security and stability of power grid operation. At the same time, it can continuously promote technological development and innovation in the field of animal networking and the power grid industry to drive social and economic development.

2. Literature Review

Robinaugh, D. J., and others put forward a formal theory that can diagnose specific equipment exceptions based on redundant information. In this way, the status of equipment can be observed and monitored, so that equipment exceptions can be detected and eliminated in time [3]. Li et al. and others gave a comprehensive overview of abnormal diagnosis techniques through the literature [4]. The development of the abnormal diagnosis of mechanical equipment has gone through a long process. The general stage is divided into three stages. The first stage is a period of relatively low productivity. During this period, mechanical equipment with a simple structure and working principle is produced, and the existence of abnormalities is detected through the inspection and experience of professional technicians. In the second stage, after the development of high-efficiency productivity, special anomaly detection equipment based on sensing technology was produced, and the equipment was detected through scientific detection equipment. We obtain the operation status information of the system, analyze and determine specific abnormalities through analysis and comparison, and formulate a more scientific and effective abnormal maintenance plan according to the obtained equipment status information so as to improve the elimination of abnormalities and ensure the reliable operation of mechanical equipment. The third stage is to create intelligent technology in the context of greatly improved productivity. Inference engines and expert systems are developed by intelligent technology and traditional sensor signal acquisition methods. Expert knowledge is required to analyze and classify other diagnostic methods, as well as to diagnose and analyze abnormal information throughout the diagnosis process. The early economic and technological development of a certain place lags behind many advanced countries in the world, so the research and theoretical practice of mechanical equipment diagnosis are relatively late. With the development of technology and applications, the connotation of the Internet of things has undergone a major funding project: the funding of NSFC projects has changed. According to the Internet report released by the International Telecommunication Union, the current three major networks, including the Internet, telecommunication network, and radio and television network, are the basis for the realization and development of the Internet of things, which is an extension and expansion of the basis of the three networks. We examine and evaluate the current state of smart device-based energy management based on current research and complete the use of Internet technology in accordance with the should-do intelligent energy system. As a result, intelligent power management based on Internet technology has been achieved [5]. As a large group of aircraft knowers, the system can record and send a variety of data to the top application using a variety of communication interfaces for intelligent control and identification to support smart levels of energy.

3. Method

3.1. Intelligent Power Monitoring System Architecture Based on Internet of Things Technology. Based on the Internet of things technology, this paper makes an in-depth and detailed analysis of the actual functions and internal architecture of the intelligent power monitoring system, fully integrates some functional modules that are closely related to the Internet of things technology into the system, and develops the intelligent power monitoring system based on the scientific and advanced Internet of things technology. The research focuses on the development and utilization of equipment for video monitoring.

3.1.1. Structure of the Intelligent Power Monitoring System. Taking the internal technical framework as the standard, the IOT technology can be divided into three different levels: perception layer, network layer, and application layer (as shown in Figure 1). The sensing layer realizes the collection of relevant data through a series of terminal devices, base stations, and other infrastructure. The sensing layer is at the lowest level of the IOT system in the overall structure and is an essential part to help the IOT to carry out comprehensive sensing. The network layer is based on the Internet and related LAN and other network systems to transmit the collected relevant data in real time and accurately. Its existence has greatly improved the reliability of the Internet of things on the original basis. The role of the application layer is to use scientific and intelligent methods to process relevant data and then design corresponding personalized services according to the actual needs of customers [6, 7].

3.1.2. Research on the Intelligent Power Monitoring System. With the accelerating development of the modern power industry, large units, large capacity power equipment, and related power facilities have occupied the vast majority, resulting in stricter technical requirements for their normal operation. The failure rate is increasing on the original basis, and the time required for maintenance and treatment of related failures is also increasing, resulting in unnecessary economic losses. In order to ensure that the power transmission and transformation system can be in a safe and stable operation mode for a long time, the international power industry has also successively introduced more stringent relevant standards [8].

In power facilities, many factors, such as excessive load-bearing and failure to timely heat dissipation, can cause damage to cable joints, knife switch contacts, and other important node connections, thus causing the equipment to fail to operate normally. Therefore, the smart integration of scientific and reasonable Internet of things technology into the intelligent maintenance system can greatly improve the actual effect of monitoring and early warning functions, timely find potential faults, and repair them.

Because many important points in the power equipment are in a dangerous environment with high voltage and continuous electromagnetic interference, the temperature monitoring methods used in the past have been unable to

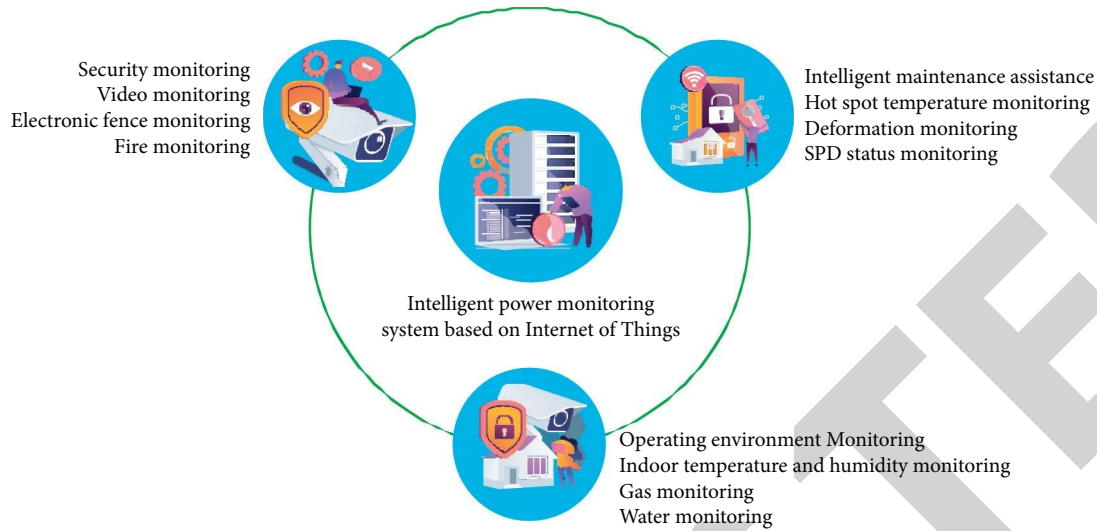


FIGURE 1: Functional framework of the intelligent power monitoring system.

meet the current actual needs [9]. At the same time, the number of hot spots is large and the price needs to be controlled within a reasonable range. Therefore, when selecting the most appropriate temperature monitoring method, it is necessary to comprehensively consider the voltage, the specific price of the equipment, and other factors. At present, the international research on real-time temperature monitoring of some important points of power equipment mostly focuses on the means of real-world temperature measurement. Common measuring tools mainly include:

(1) *Infrared Thermal Imager*. This technology mainly draws relevant images based on the differential response of the relevant parts of different objects to the infrared thermal radiation intensity, and then finds the location of the target according to the actual temperature difference between the target and its background [10]. It can span a long distance and can be monitored without contact. It has superb characteristics but is expensive. Therefore, it is mainly used in large transformers at present.

(2) *Optical Fiber Temperature Sensor*. The working principle of the optical fiber temperature sensor is to use its internal multiple optical fibers to realize the rapid and accurate transmission of temperature signals. Optical fibers have an incomparable insulation effect compared with other materials and can play a good isolation role for the high voltage in high-voltage equipment. Because of their isolation effect, they can be installed on the surface of high-voltage equipment [11]. However, the optical fiber is also prone to fracture and cannot withstand high temperatures. In the actual installation process, strict requirements are put forward for the surrounding environment, which is also the reason that restricts its further wide application. At the same time, it often needs to invest more money in the manufacturing process, which also limits the development of optical fiber to a certain extent.

(3) *Digital Wireless Temperature Sensor*. [12]. The principle of this sensor is to lay several independent temperature sensing modules on the surface of the equipment in turn, collect the real-time temperature of the equipment, and send this temperature data to the receiving end in real-time by means of wireless communication for further processing. The great advantage of the digital wireless temperature sensor lies in its good insulation effect and moderate price.

(4) *Video Analysis*. The research focus of video surveillance is how to extract information and alarm violations in the video. Currently, video surveillance is mainly used through end-node and cloud video analysis and processing. The Internet of things is an obvious successful demonstration of the extensive use of wireless communication in relevant end nodes [13].

3.1.3. Deep Convolution Neural Network Training Algorithm.

Figure 2 shows the training steps of a deep convolution neural network. In essence, this training is a cycle from feedforward propagation to response propagation. From the input layer, the image data is transmitted to the convolution layer and the hidden layer in turn. In this process, it is analyzed and processed until it reaches the output layer and the final output result. Forward propagation refers to this output process [14]. Once the forward propagation is over, the output results will be compared with the data accuracy, and the network state will be evaluated in the form of error comparison. The purpose of backpropagation is to transmit the error to the upper layer, and all units in the previous layer can update their own weights.

Training process learning can effectively explain the conduction mode and calculation in the training process. For example, the Softmax classifier is connected based on the Softmax classifier, the deep convolution neural network can classify and process specific target objects, and the logistic regression model is popularized based on the classification, so the Softmax regression is obtained. The marked m samples constitute the logistic regression training set [15].

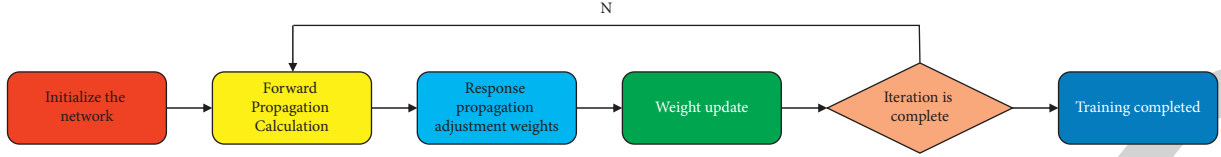


FIGURE 2: Training flow chart of a deep convolution neural network.

$\{(x^{(1)}, y^{(1)}), \dots, (x^{(m)}, y^{(m)})\}$, where $x^{(i)} \in R^{n+1}$ is the input characteristic. $N + 1$ is the x dimension of the eigenvector, and $x_0 = 1$ corresponds to the intercept term. Because binary classification is the goal of logistic regression, there is $y^{(i)} \in \{0, 1\}$. The following functions exist:

$$h_{\theta} = \frac{1}{1 + \exp(-\theta^T x)}. \quad (1)$$

In essence, the training model parameters are functions that can minimize the loss.

$$J(\theta) = -\frac{1}{m} \left[\sum_{i=1}^m y^{(i)} \log h_{\theta}(x^{(i)}) + (1 - y^{(i)}) \log(1 - h_{\theta}(x^{(i)})) \right]. \quad (2)$$

The number of y (category label) values is different from k , which is mainly because it needs to deal with a multi-classification problem. So, for $\{(x^{(1)}, y^{(1)}), \dots, (x^{(m)}, y^{(m)})\}$, there is a class $(i) \in \{1, 2, \dots, k\}$ marker. For the sample input (given) X , the occurrence probability $p(y = i|x)$ of each classification result can be expressed by a k -dimensional vector output.

3.1.4. Structure of the Intelligent Power Monitoring System. The monitoring system structure of wireless sensor network is shown in Figure 3.

The system includes many nodes and transfer nodes arranged at the end of the security monitoring network [16]. In the figure, the camera module and the front-end image processing module contained in the end node are hidden on the device, in which the sensor network is wired with the front-end image processing module; the equipment in the transfer node is placed in a more hidden place about 10 meters away from the end node. The dotted line in the figure represents WiFi wireless communication, and the solid line represents 4G network communication. The end node detects the data from the temperature sensor and other operating environment monitoring and intelligent maintenance auxiliary sensors in real-time and sends an alarm signal to the transfer node in case of any abnormality. When pedestrians and vehicles pass by, the front-end image processing module detects objects in the video captured by the camera in real-time and sends the detection results to the transfer node. The transfer node compresses the pictures, integrates the information with other end nodes connected to the transfer node, and finally transmits them to the Internet monitoring management system through the 4G wireless network [17]. On the contrary, the transfer node also receives instructions from the monitoring management system through the 4G network, takes photos, and uploads them through the control end node.

Through the construction of a power grid energy efficiency management system based on the Internet of things, the selected neural network optimization algorithm is simulated and analyzed by a computer to process the data of a power grid energy efficiency management system. Using MATLAB simulation software, the corresponding genetic algorithm is designed to optimize the line loss and line loss rate in the power grid system, and the change of line loss rate before and after optimization can be obtained.

According to the change in the line loss rate in Figure 4, the average line loss rate in the power grid energy efficiency management system is reduced by 48% after genetic optimization using MATLAB simulation software. Therefore, the grid energy efficiency management technology based on the Internet of things can better realize the optimization of grid energy efficiency in the system by using genetic algorithms.

3.1.5. Transit Node System Design

(1) *Hardware Design of Transfer Node.* The platform hardware used by the transit node in this study is an Android mobile phone with a long standby time. The main modules of this system include the main processor, a 4G wireless module, and a WiFi module. The hardware structure of the system is shown in Figure 5. In the experiment, the Android mobile phone of the transfer node is placed in a hidden place 10 meters away from the end node.

(2) *Workflow of Transfer Node.* First, the transfer node receives the picture by sending a request from the end node. If the data sent by the end node is really valid picture data rather than an interference signal, the transfer node will automatically store the picture in the storage medium of the transfer node when it receives the information sent by the end node and compress the picture on the hardware platform of the transfer node. The algorithm used is the wavelet transform compression algorithm. Then the management system server successfully establishes socket communication and transmits the processed pictures to the management system server through the 4G wireless network. At the same time, it notifies the designated user to obtain the pictures. After receiving the picture, the server of the management system saves it, and then automatically decompresses the file to get the picture in its normal format. As long as the monitoring personnel want to display the picture in the middle of the page, they can directly click the "get picture" button to browse the picture. In addition, the server side of the management system can also take "remote photos." After receiving the set of words, you can click the button to send a

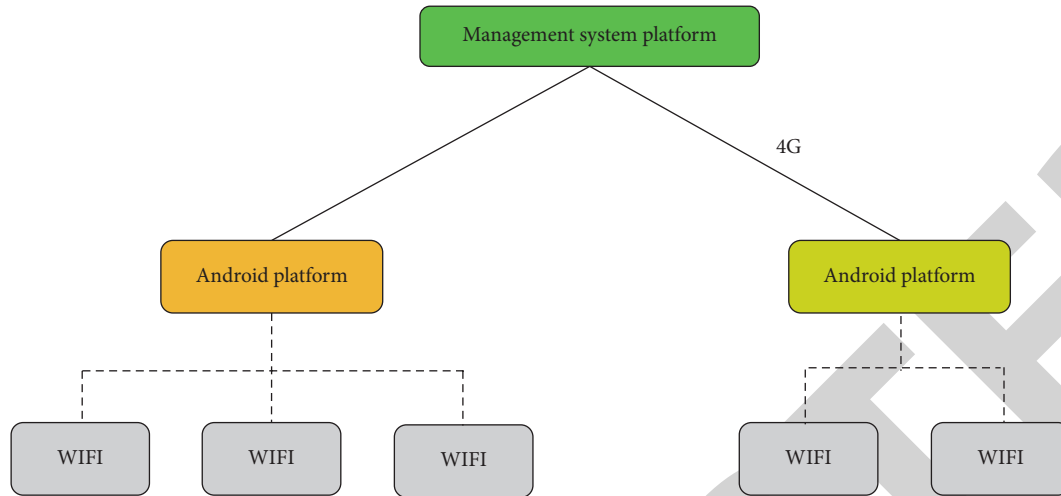


FIGURE 3: Structure diagram of an intelligent power monitoring system.

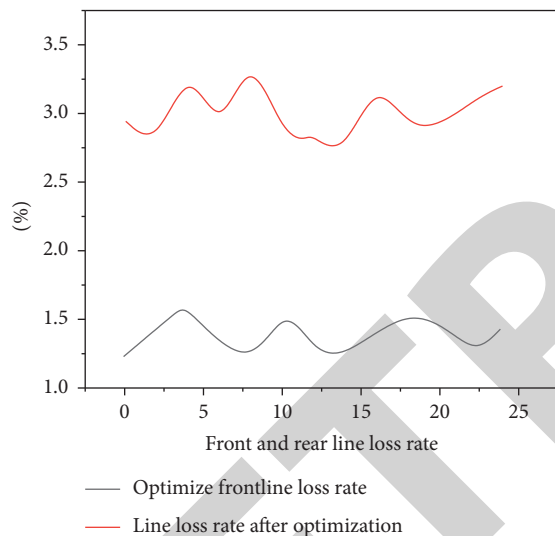


FIGURE 4: Line loss rate changes before and after genetic algorithm processing.

photo request to the end node, and then repeat the node photo-taking process. If the server side of the management system wants to cancel the monitoring of socket links, it only needs to press the “stop listening” button, and the end node will shut down the monitoring system by itself.

(3) *Function Design of Transfer Node.* The client program design should complete the following parts: Open the monitoring system to automatically capture pictures and information of human beings and vehicles within the monitoring range; Then, the camera function is used to complete the picture acquisition, filter and compress the collected pictures, transmit them to the front-end server at the same time, and finally wait for the call instruction from the server. These parts should not only complete their own work independently but also complement each other, cooperate with each other, and “help” each other. For example, the trigger signal of the waiting end node and the command sent by the waiting management

system server are carried out in the same time period. When uploading pictures, the management system server not only accepts the upload work but also monitors whether it receives the server’s command and the next round of opening instructions. Therefore, a thread concept commonly used in the Android system is involved [18].

(4) *End Node Object Detection Effect.* Object detection mainly uses neural networks for training. Before the work of the neural network begins, it is necessary to update the training model parameters, that is, the new weights after initialization. The update method is to first evaluate the network training through the cross mutual loss function and then update the weights with the random gradient descent [19]. Figure 6 is the calculation flow chart. First, use the trained learning model to initialize the parameters. Then, the neural network starts to read the data set, selects the object detection model from the training set, and gradually calculates the network output through the forward propagation network.

Coco data sets have developed rapidly in recent years. It is sponsored by Microsoft and has powerful functions. It has a wide range of image annotation information, including category, location, and even text information. Moreover, coco data sets provide great help for image segmentation semantics and achieve a high level of results. In recent years, many image semantic understanding algorithms use it as an evaluation standard [20].

4. Results and Discussion

Randomly select a test sample from the test set as the input of the neural network, then start forward propagation through the neural network, calculate layer by layer, and obtain the output of the neural network. Then compare the selected test samples with the output of the neural network, judge whether the results are correct, and sort out the results. Finally, judge whether all the tests are completed. If they are completed, stop the network test. If not, continue working until all tests are completed. Due to the advantages of various types of coco data sets, the internal scenes of their pictures

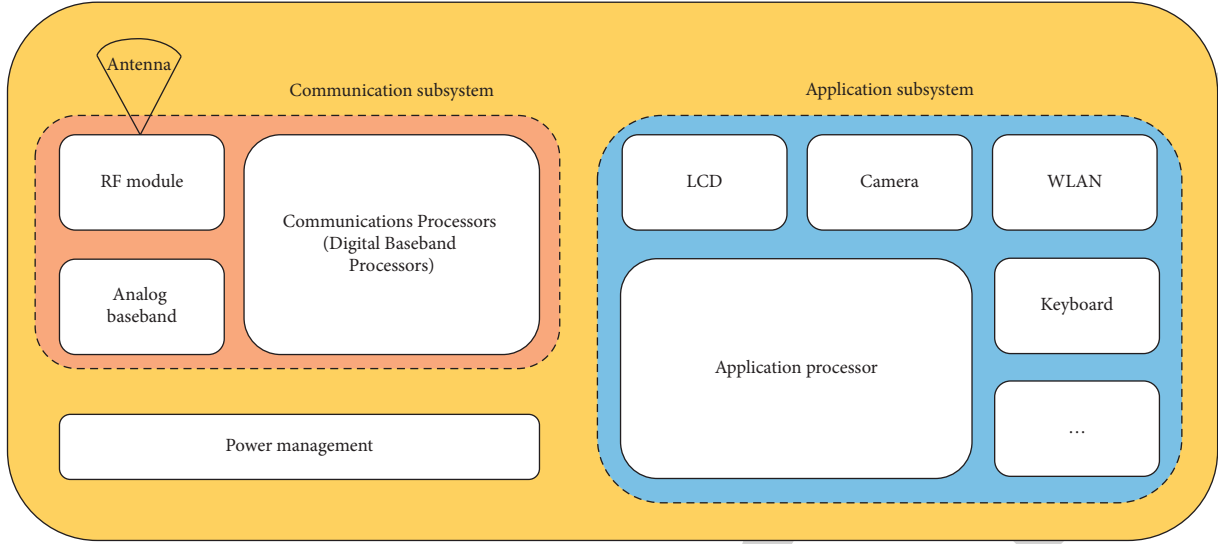


FIGURE 5: Android system hardware of the transit node.

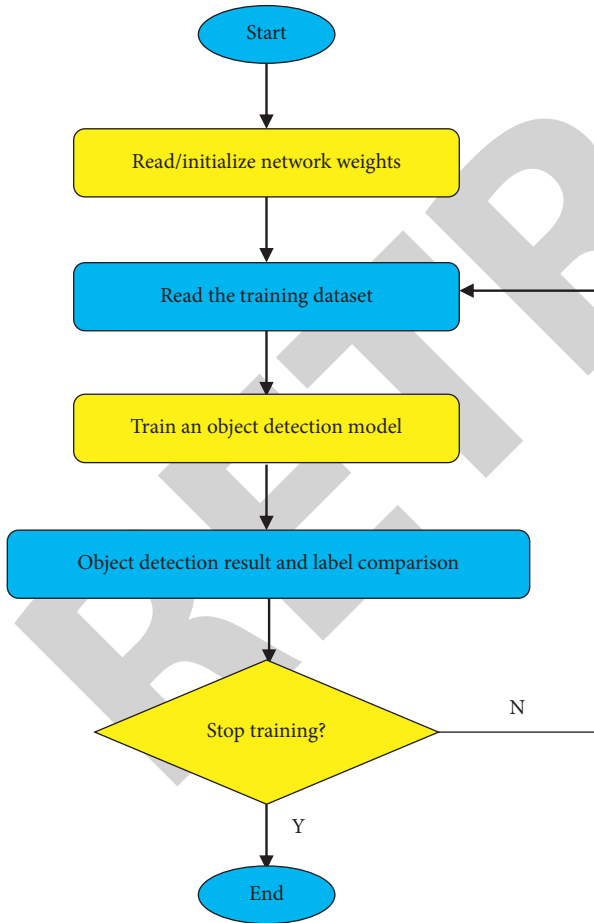


FIGURE 6: Object detection training process.

are also extremely complex. Therefore, compared with the Pascal VOC data sets, the neural network is trained with coco data sets, and then the new network weights are fine

TABLE 1: SSD300 test accuracy.

Category	Animal	Human beings	Vehicle
Accuracy	0.81	0.76	0.87

tuned. Then, the neural network is trained with the Pascal VOC data sets. Finally, after the training is completed, the comparison model is selected and the performance is evaluated under the test set. According to the scenes involved in this study, objects are classified into three categories: animals, humans, and vehicles. The test accuracy of an SSD300 is shown in Table 1.

The accuracy of animals measured by this method can reach up to 81%; human accuracy can reach 76% at most. The accuracy of the vehicle can reach up to 87%, and the detection effect of end node objects can reach a high accuracy under the neural network, so that the scheme of the perception layer of the Internet of things can be realized, so that the Internet of things can work well in its complex environment with excellent anti-interference, simple and convenient application, and high-cost performance.

This research discards the bandwidth limitation problem encountered in the video transmission process of traditional power monitoring system-related technologies, carries out image recognition and processing in the front end, only uploads useful picture data, greatly reduces the amount of data, and applies it to the smart grid monitoring system through the Android mobile phone operating system. At the same time, it also realizes the full-automatic call function in this system, with low development cost and simple technology.

5. Conclusion

This paper presents a method for an intelligent power monitoring system based on the Internet of things technology based on the current social development needs. Then,

Retraction

Retracted: Application of Data Mining Algorithm in Electric Power Marketing Inspection Forecast Analysis

International Transactions on Electrical Energy Systems

Received 19 September 2023; Accepted 19 September 2023; Published 20 September 2023

Copyright © 2023 International Transactions on Electrical Energy Systems. This is an open access article distributed under the Creative Commons Attribution License, which permits unrestricted use, distribution, and reproduction in any medium, provided the original work is properly cited.

This article has been retracted by Hindawi following an investigation undertaken by the publisher [1]. This investigation has uncovered evidence of one or more of the following indicators of systematic manipulation of the publication process:

- (1) Discrepancies in scope
- (2) Discrepancies in the description of the research reported
- (3) Discrepancies between the availability of data and the research described
- (4) Inappropriate citations
- (5) Incoherent, meaningless and/or irrelevant content included in the article
- (6) Peer-review manipulation

The presence of these indicators undermines our confidence in the integrity of the article's content and we cannot, therefore, vouch for its reliability. Please note that this notice is intended solely to alert readers that the content of this article is unreliable. We have not investigated whether authors were aware of or involved in the systematic manipulation of the publication process.

Wiley and Hindawi regrets that the usual quality checks did not identify these issues before publication and have since put additional measures in place to safeguard research integrity.

We wish to credit our own Research Integrity and Research Publishing teams and anonymous and named external researchers and research integrity experts for contributing to this investigation.

The corresponding author, as the representative of all authors, has been given the opportunity to register their agreement or disagreement to this retraction. We have kept a record of any response received.

References

- [1] W. Wu, G. Xu, X. Qian, and C. Chu, "Application of Data Mining Algorithm in Electric Power Marketing Inspection Forecast Analysis," *International Transactions on Electrical Energy Systems*, vol. 2022, Article ID 9229415, 7 pages, 2022.

Research Article

Application of Data Mining Algorithm in Electric Power Marketing Inspection Forecast Analysis

Weijiang Wu ¹, Gaojun Xu ¹, Xusheng Qian ¹, and Chengbo Chu ²

¹State Grid Jiangsu Electric Power Company Limited Marketing Service Center, Nanjing, Jiangsu 210019, China

²Nanjing Power Supply Company, State Grid Jiangsu Electric Power Company Limited, Nanjing, Jiangsu 210019, China

Correspondence should be addressed to Gaojun Xu; 20160628@ayit.edu.cn

Received 14 July 2022; Revised 28 July 2022; Accepted 12 August 2022; Published 28 August 2022

Academic Editor: Nagamalai Vasimalai

Copyright © 2022 Weijiang Wu et al. This is an open access article distributed under the Creative Commons Attribution License, which permits unrestricted use, distribution, and reproduction in any medium, provided the original work is properly cited.

In order to improve the accuracy of power load forecasting and deal with the challenge of insufficient stand-alone computing resources brought by the intelligent power system, data extraction algorithms are used in energy market analysis. Preliminary weather performance algorithms are optimized online based on the nature of the power load data. In order to improve the accuracy of the computational algorithms, the concept of classification and various agents was introduced. The MapReduce cloud computing programming framework is used simultaneously to improve design algorithms to improve the ability to process large amounts of data. The actual electronic data provided by EUNITE was selected as a sample analysis and a complete experiment of the 32-node cloud computing group. The results of the experiment show that the load data provided by EUNITE was expanded into four different data sets: 1000 times, 2000 times, 4000 times, and 8000 times. Works on older data and the cloud. Platforms with groups of 4, 8, 16, and 32 nodes are designed to calculate acceleration ratios and scale speeds. The acceleration ratio of a perfectly parallel system algorithm can reach 1. However, in practical applications, as the number of cluster nodes increases, so does the transmission cost of the node network. *Conclusions.* Accuracy assumptions based on this model are better than the general evaluation of supported vector regression prediction algorithms and neural network algorithms, and the planning process is well underway.

1. Introduction

In recent years, the power system accumulated tens of thousands or even hundreds of millions of pieces of data information in the database, and there are many useful information in the database data. This information is of great help to leaders in making decisions. Nowadays, information technology is so advanced that the use of these data resources provides technical support. People also try to find the possible internal laws from these data resources. If appropriate information technology is adopted to process these data, power enterprises can better serve people. Electric power is an industry related to national economy and people's livelihood. The quality of its service greatly affects people's quality of life. The data could also help power companies cut costs and boost profits. By studying the law of market change, China's electric power enterprises

represented by State Grid Corporation are implementing informatization [1]. It also includes research on how to extract useful information from this vast amount of data through effective information technology. China is now a socialist market economy; the power enterprise information is also to serve the market economy. How to make the power enterprises and customers between the win-win is the problem that China's power enterprises face. The market orientation replaces the original production orientation, improves efficiency and reduces costs internally, improves service level externally, and expands the market [2]. Therefore, it puts forward new requirements for the functions of electric power marketing system of enterprises. Electric power industry is a basic industry, which affects all sectors of society. Whether electric power forecast is accurate or not has great influence on society and electric power enterprise itself. For example, China has experienced

a serious shortage of power supply due to insufficient investment in power facilities due to insufficient prediction of future electricity demand, which has a great negative impact on the development of the 11th Five-Year Plan [3]. The importance of power demand forecasting can be seen. Demand forecasting is a key component of electric power marketing system. The forecast of electricity demand plays a key role in the construction of electric power facilities, the formulation of electric power marketing strategy, and the decision and subordinate of electric power production schedule tracking. So, how to improve the accuracy of electricity demand prediction becomes an important topic.

2. Literature Review

Tai et al. developed the concept of using smart decision-making technology in the field of electronics and developed the “DSS + problem-solving + knowledge base” smart decision-making process (IDSS) to fulfill decision-making tasks [4]. In studying the principles and algorithms of systems to support decision-making in the energy sector based on data mining [5], Wolf et al. integrated the real issues of the energy market in China. Based on a view of the nature and multidimensionality of big data in different data mining models, a power system decision-making system design process model was developed that combines neural network structure and spatial selection algorithms for data mining and organically integrates problem solving and interpretation functions [6]. In a short-term load hypothesis based on an uncertain neural network, Wang et al., in the study of short-term prediction, the BP algorithm was introduced using a neural network, and a holiday model was developed to calculate the specific holiday load. Based on the data from the analysis of the power plant in Guangxi, the concept of energy load calculation based on the neural network was well received [7]. Sharma conducted research on topics related to power decision-making support system in recent years, for example, support for decision-making in the energy sector based on data warehousing technology, forecasting of electricity production load, use of group research in the sector, use of electricity, structural research, use of electrical decision-making industry, etc. Some research progress has been made [8]. Shafiei Chafi and Afrakhte developed a three-stage DSS system: a language system (LS), a problem system (PPS), and a knowledge system (KS). This model is “problem-solving,” “conscious,” and in some cases has consequences [9].

Aiming at the actual application scenarios of power load prediction, this article proposes a distributed extreme learning machine power load prediction algorithm based on MapReduce, which applies online sequence optimization extreme learning machine to power load prediction, and introduces cloud computing technology and multiagent technology to improve its ability to process massive high-dimensional data and improve the accuracy of load prediction [10]. The parallel performance and load prediction accuracy of the improved algorithm were tested on a cluster built in the laboratory, and an example was used to analyze the real power load data.

3. Research Methods

3.1. Cloud Computing. The Hadoop cloud computing platform developed by the Apache Foundation is a fully open-source application that supports the MapReduce framework and data exchange. MapReduce is a sample program that processes large files in batches. This was the first request from Google to address the issue of distribution and counting [11]. The MapReduce framework makes it easy to use by protecting the content from being used. In large groups, complex parallel computations are abstracted into two user-written functions, the Map and the Reduction function.

The specific explanation is as follows:

- (1) *Access.* The input file is first read from the fragmented file and then truncated. The MapReduce framework allocates data slices to each worksheet.
- (2) *Schedule.* The MapReduce framework fixes the data format as a set of Content and Value pairs, runs, and executes framework shared key-value (key, value) processes according to user-defined operating system requirements [12]. Finally, a new pair of averages (Key, Value) is created.
- (3) *Competition.* At this stage, it takes more time to convert a mean-value pair from a Map node to a Reduced node, depending on bandwidth and CPU speed, rather than Map and Reduce. At this stage, the intermediate values corresponding to the same average concept are combined and generated (main, list of results), and the values are determined.
- (4) *Reduction.* Performs the user-written reduce function. Repeat all intermediate values and their intermediate keys or product names, run user processing data, and generate new content and double values. [13].
- (5) *Output.* Export the reduced output to a distributed file system.

3.2. Extreme Learning Machine Algorithm

3.2.1. Description of Extreme Learning Machine Algorithm. Cloud learning technology algorithms are different from traditional direct feedback neural network education. The team does not require repetition and carefully selects and adjusts difficult techniques and procedures to conceal injustice. To minimize training errors, the weight concealment procedure is defined by an algorithm [14]. The special weather training algorithm is described as follows.

N arbitrary data (x_i, t_i) , where $x_i = [x_{i1}, x_{i2}, \dots, x_{in}]^T \in R^n$ and $t_i = [t_{i1}, t_{i2}, \dots, t_{im}]^T \in R^m$ contain Nn hidden layer nodes and the regression model of extreme learning machine whose excitation function is GG can be expressed as

$$f_{\overline{N}} = \sum_{i=1}^{\overline{N}} \beta_i G(\mathbf{a}_i, b_i, \mathbf{x}_j) = \mathbf{t}_j, \quad j = 1, \dots, N, \quad (1)$$

where $\mathbf{a}_i = [a_1, a_2, \dots, a_n]^T$ is the weight vector of the i th hidden node and the input node; $\beta_i = [\beta_1, \beta_2, \dots, \beta_n]^T$ is the weight vector of the i th hidden layer node and the output node. b_i is bias of the i th hidden layer node; \bar{N} is the number of hidden layer nodes. Formula (1) can be abbreviated as

$$\mathbf{H}\beta = \mathbf{T}, \quad (2)$$

$$H(\mathbf{a}_1, \dots, \mathbf{a}_{\bar{N}}, b_1, \dots, b_{\bar{N}}, \mathbf{x}_1, \dots, \mathbf{x}_N) = \begin{bmatrix} G(\mathbf{a}_1, b_1, \mathbf{x}_1) & \cdots & G(\mathbf{a}_{\bar{N}}, b_{\bar{N}}, \mathbf{x}_1) \\ \vdots & \vdots & \vdots \\ G(\mathbf{a}_1, b_1, \mathbf{x}_N) & \cdots & G(\mathbf{a}_{\bar{N}}, b_{\bar{N}}, \mathbf{x}_N) \end{bmatrix}_{N \times \hat{N}}, \quad (3)$$

$$\{\beta = [\beta_1^T \cdots \beta_{\bar{N}}^T]_{\bar{N} \times m}^T, T = [t_1^T \cdots t_N^T]_{N \times m}\}, \quad (4)$$

where H is the output matrix of the hidden layer, and the i th column of H corresponds to the output vector of the i th hidden layer of input x_1, x_2, \dots, x_n . The weighted output can be obtained by solving the least-squares solution of the linear equation.

$$\|H\beta - T\| = HH^T T - T = \min_{\beta} \|H\beta - T\|. \quad (5)$$

The least squares solution is

$$\beta = H^{\dagger} T, \quad (6)$$

where H^{\dagger} is the general Moore–Penrose inverse of the output matrix of H hidden layers.

3.2.2. Disadvantages of Extreme Learning Machine Algorithm. Although the ELM training algorithm is superior to the SVM and BP algorithms in regression policy in terms of counting, accuracy, training algorithms, and time-tested performance, the ELM training algorithm has been introduced into energy prediction and improved weather performance. However, the ELM training algorithm is a package training algorithm, and online optimization is very important as it is not completely suitable for the power load prediction scenario in the actual power load calculation. The online optimization ELM algorithm does not need to be repeated to add new data to the learning process [15]. In addition, the ability to generate large data of the adjustment algorithm using cloud computing technology and multi-agent distribution technology has been improved to prevent discrepancies between data values and high-dimensional data of electronic information, and the accuracy of load calculations has been improved. This algorithm is called MapReduce based on MapReduce weighted online sequential extreme learning machine, Noyon, OSELM-WA.

3.3. Design MR-OSELM-WA Algorithm Based on Cloud Computing

3.3.1. Online Sequential Extreme Learning Machine Algorithm. The steps of the online education system are as follows:

- (1) Initial phase: part of the data set is defined as the initial training, and the number of nodes in the hidden stage \bar{N} is set manually. Let $k = 0$. Firstly, weight vector $\mathbf{w}_i = [w_1, w_2, \dots, w_n]^T$ of the i th hidden layer node and input node and parameters of excitation function are generated randomly [16]. Then, the initial hidden the layer output matrix H_0 is calculated. Compute the initial output weight vector β_0 .

$$P_0 = (H_0^T H_0)^{-1}, \quad (7)$$

$$\beta^0 = P_0 H_0 T_0, \quad (8)$$

where $T_0 = [t_1, t_2, \dots, t_N]$ is the output vector of the target value.

- (2) Online elementary education: when the new training data arrives, it is considered as the $k + 1$ sample of the entire training process.

Firstly, calculate the output matrix of the new hidden layer:

$$H_{k+1} = [G(a_1, b_1, \mathbf{x}_k), \dots, G(a_L, b_L, \mathbf{x}_{k+1})]. \quad (9)$$

Then, let $T_{k+1} = [\mathbf{t}_{(\sum_{j=0}^k N_j)+1}, \dots, \mathbf{t}_{(\sum_{j=0}^k N_j)+j}]^T$.

- (3) Through the following formula, calculate the output weight vector $\beta_0^{(k+1)}$:

$$\begin{cases} P_{k+1} = P_k - P_k H_{k+1}^T (I + H_{k+1} P_k H_{k+1}^T)^{-1} H_{k+1} P_k, \\ \beta^{(k+1)} = \beta^{(k)} + K_{k+1}^{-1} H_{k+1}^T (T_{k+1} - H_{k+1} \beta^{(k)}). \end{cases} \quad (10)$$

- (4) Set $k = k + 1$, go back to step 1, and continue to train the next training data.

3.3.2. MR-OSELM-WA Algorithm Based on Cloud Computing

(1) MR-OSELM-WA Algorithm Idea. As the power of intelligence deepens, the power of data transport increases geometrically, and the use of online sequential extreme learning machine (OSELM) algorithms for power failure prediction is not enough [17]. As the smart grid cloud computing model continues to mature, this paper uses the multiagent concept and cloud computing to develop a hyperlearning algorithm.

The idea of MR-OSELM-WA algorithm is that the multiagent runs the weight balance of OS-ELM to execute, and the OSELM node with higher prediction accuracy should get higher weight when calculating the final predicted value. The OSELM predicted value of each node is calculated by weighted average to get the final predicted value. The weight of each node is

$$\bar{y} = \frac{\sum_{k=1}^K \alpha_k y_k}{\sum_k \alpha_k}. \quad (11)$$

\bar{y} , y_k , and α_k are, respectively, the final predicted value, the predicted value of the k th OSELM, and the predicted weight of the k th OSELM. The predicted weight is calculated by standard error function E and gradient rise method:

$$E = \frac{1}{2}(t - \bar{y})^2, \quad (12)$$

where t is the target value of the input training set of each OSELM agent. According to the gradient ascent strategy, α_k is

$$\Delta\alpha_k = -\left(\frac{\eta}{\partial\alpha_k} \frac{\partial E}{\partial\alpha_k}\right) = -\eta \left(\frac{\partial E}{\partial\bar{y}}\right) \cdot \left(\frac{\partial\bar{y}}{\partial\alpha_k}\right), \quad (13)$$

where η is the learning rate; set $\eta = 0.1$. According to equation (14), it can be concluded that

$$\Delta\alpha_k = \eta(t - \bar{y}) \left[\frac{y_k}{\sum_{i=1}^K \alpha_i} - \frac{\sum_{i=1}^K \alpha_i y_i}{\left(\sum_{i=1}^K \alpha_i\right)^2} \right], \quad (14)$$

where α_k can be updated by $\alpha_k \leftarrow \alpha_k + \Delta\alpha_k$.

(2) *Detailed Steps of MR-OSELM-WA Algorithm.* The main idea of the MapReduce programming framework is to use the parallel structure by writing the corresponding text and Reduce functions. The average results of the MR-OSELM-WA algorithm are stored in the HBase data distribution and distribution cache. The distributed MR-OSELM-WA prediction and decision model based on MapReduce is shown in Figure 1:

- (1) Large instructional packages can be read from the data distribution on the cloud computing platform, and different learning sessions can be obtained by segmenting training packages through a simple process of the MapReduce programming system [18]. Number is the number of map locations in a cloud group.
- (2) Subpackage training is taught in parallel according to the step logic of the map function, such as the logic of OS-ELM training machine learning algorithm, which is equivalent to machine training which is different.
- (3) The benefits of working in the diagram, which is an estimate of the importance of different training systems, were passed from the Shuffle phase of the MapReduce programming frame to the Reduced phase, and the weight of the estimated values generated by the MapReduce function was determined accordingly. According to the above weight calculation method, the predicted value weight of each Map operation output is determined, and then the final predicted value is calculated.
- (4) Learn the routine procedure for estimating average and long-term loads along the specified axis, slide as required, and return to step 1. Estimate the next day behind the load data on a regular basis.

4. Result Analysis

4.1. *Experimental Preparation Stage.* The newly built Hadoop platform has 32 nodes, each with Intel (R) Core

(TM) I5-2400 4-coreCPU@2.60 GHz, 4 GBRAM, and 100 Mbit/s network bandwidth. Hadoop version is 0.20.2.

4.1.1. *Example Analysis Data Set.* The actual regional load data for 1997-1998 were selected from a 2001 Medium-Term Load Prediction Test developed by the European Smart Technology Network (EUNITE). The data sample provided by EUNITE is the power load collected every 0.5 hours from 1997 to 1998; the mean daily temperature from 1995 to 1998, and the holiday dates from 1997 to 1999 [19]. The objective of the load forecasting is to predict the maximum power load for 31 days in January 1999 from the above data samples.

4.1.2. *Evaluation Indicators.* The accuracy rate of load prediction adopts MAPE as the test index:

$$M_{APE} = 100 \left[\sum_{i=1}^n \left| \frac{(L_i - \hat{L}_i)/L_i}{n} \right| \right], \quad n = 31, \quad (15)$$

where L_i and \hat{L}_i are the true and predicted the power load value of day i , respectively; n is the number of days in the month forecast. In the power load forecasting, the smaller M_{APE} value is, the more accurate the load forecasting is.

The relative acceleration and expansion ratios were used to evaluate the performance of the MR-OSELM-WA algorithm. The evaluation is used to compare the execution time of the algorithm—again the large group, again the large data—with the original data.

4.1.3. *Load Forecasting Training Set Design.* The input sample includes three feature vectors, and the training set is composed of [date D , temperature T and historical load L]. Seven binary numbers are used to represent date information, respectively. The predicted daily temperature was expressed by decimal number and normalized. $L = [L_{i-7}, L_{i-6}, L_{i-5}, L_{i-4}, L_{i-3}, L_{i-2}, L_{i-1}]$ indicates the maximum load value of 7 days before the forecast date.

The objective of the experiment is to predict the maximum power load on January 1999. Through a large number of experiments, temperature is correlated with power load. In order to improve the accuracy of prediction, the sample data range is set as part of the winter data from November to April. The output of the training set is $y_i = L_i$, that is, the maximum power load value of the predicted day.

4.2. Example Analysis

4.2.1. *Prediction Accuracy of MR-OSELM-WA.* In this experiment, the MR-OSELM-WA algorithm is compared with the support vector regression (SVR) algorithm and functional networks algorithm of generalized neural networks. SVR prediction algorithm and functional neural network algorithm show excellent prediction ability in EUNITE competition. Compared with these two algorithms, the performance of the proposed MR-OSELM-WA algorithm for power load prediction is tested.

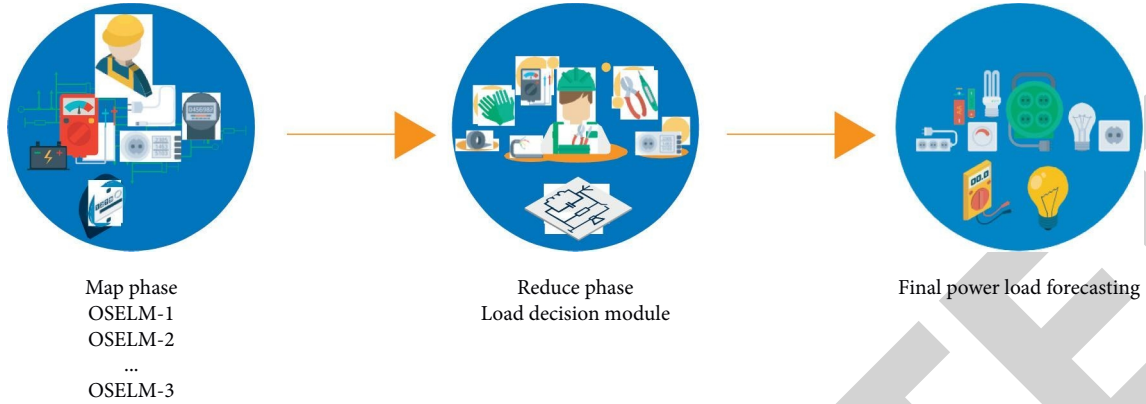


FIGURE 1: Distributed MR-OSELM-WA predictive decision model based on MapReduce.

Formula (15) for calculating the value of MAPE according to the target function was obtained, and the approval of our standard algorithm was obtained by 10-fold cross-validation. The inconsistencies of each algorithm have been taken for granted, and MR-OSELM-WA, network algorithm performance, and SVR algorithm have been reported as training packages between 1997 and 1998. The historical data of 1997 and 1998 were used as the training set; MR-OSELM-WA uses a one-by-one online sequential learning model to predict the power load values in January 1999. In order to ensure that the results were positive, 50 tests were completed and the mean was considered as the final test. MAPEs of our energy load estimation algorithms are shown in Table 1 [20]. As shown in Table 1, the MR-OSELM-WA proposed in this article received the lowest MAPE value for the load estimate, i.e., the MR-OSELM-WA algorithm has the correct high in estimated strength. Load estimates perform better than SVR and functional neural networks. In addition, SVR prediction algorithm and functional neural network prediction algorithm is a set of training. The larger the training package, the greater the memory required to complete the algorithm in the training package type. If the memory space exceeds the limit, the efficiency of the algorithm will be greatly reduced. However, the above situation is not easy to occur because MR-OSELM-WA's one-on-one online sequential learning mode training package (or half mode) is smaller than the ELM training mode.

Figures 2 and 3 show the comparison between the actual power load value and the estimated power load value of the MR-OSELM-WA algorithm, SVR algorithm, and network operation algorithm in January 1999.

4.2.2. MR-OSELM-WA Parallel Performance. To reflect the performance of the MR-OSELM-WA algorithm, the sample load data provided by EUNITE is divided into four groups: 1000 times, 2000 times, 4000 times, and 8000 times, different time records. They work on cloud platform with 4, 8, 16, and 32 nodes in a group to calculate acceleration ratios and scale ratios. The acceleration ratio of a perfectly parallel system

TABLE 1: MAPE predicted on the training set based on MR-OSELM-WA, functional network, and SVR.

Prediction algorithm	MAPE
MR-OSELM-WA	1.949 8
Functional neural networks	3.430
SVR	2.149 8

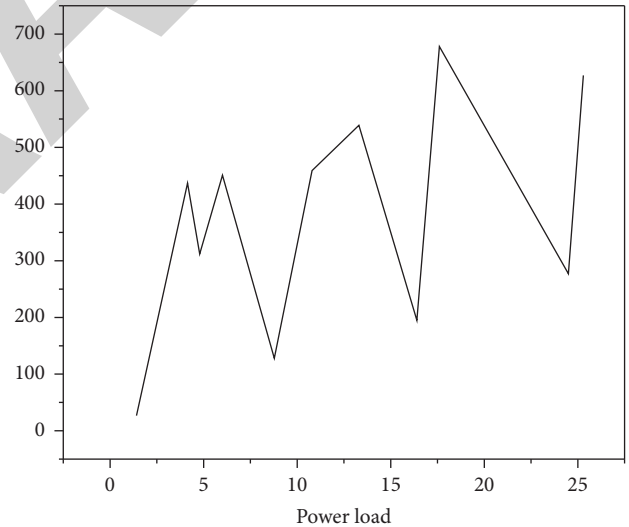


FIGURE 2: Comparison of power load value in January 1999 with the predicted value of MR-OSELM-WA algorithm and SVR algorithm.

algorithm is close to 1, but in practical use, as the number of cluster nodes increases, network forwarding nodes are used, and the linear acceleration ratio is very large, as shown in Figure 4, and hard to reach. Figure 4 shows that the acceleration ratio of MR-OSELM-WA increases linearly with the growth of data scale, especially for large files. In practice, the more the data, the better the comparison of MR-OSELM-WA, that is, MR-OSELM-WA can meet the requirements of the calculation of large data of electronic equipment.

In a perfectly parallel system, the clock speed is constant at 1, but it is not possible to complete the application. As the

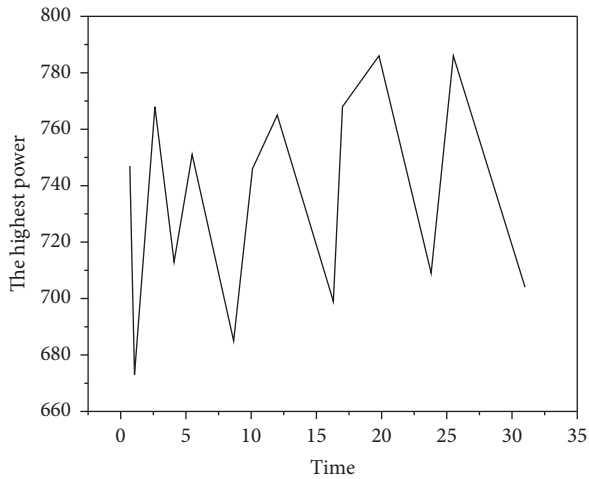


FIGURE 3: Comparison of power load value in January 1999 with the predicted value of MR-OSELM-WA algorithm and functional networks algorithm.

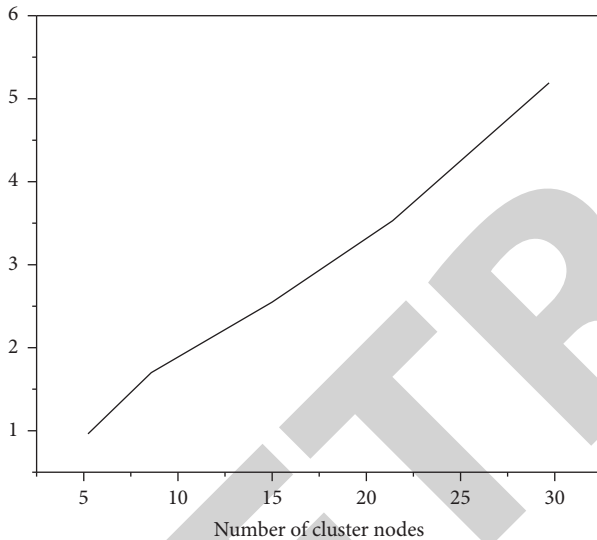


FIGURE 4: MR-OSELM-WA acceleration ratio.

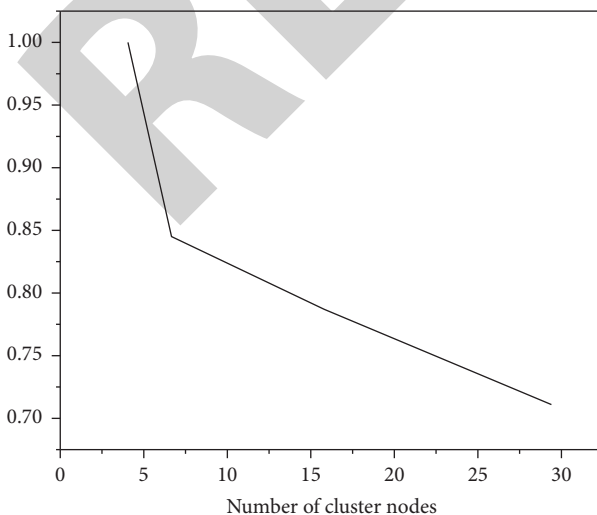


FIGURE 5: MR-OSELM-WA expansion rate.

configuration data increase, the speed of the interconnect system gradually decreases. The test results are shown in Figure 5. The measurement speed of the MR-OSELM-WA algorithm is better because the measurement height of the MR-OSELM-WA algorithm decreases when the data setup is large.

5. Conclusion

The deepening of the degree of power intelligence, power system data quantization, high dimensional trend is unstoppable. The load forecasting algorithm represented by support vector regression widely used in power load forecasting has high computational complexity. Under the massive high-dimensional data load prediction, a single machine cannot bear such a huge consumption of computing resources. In recent years, the popular large data processing technology is an effective method to solve this problem, and the algorithm parallelization caused by it has become a research direction of load forecasting in recent years. In this article, an extreme learning machine power load prediction algorithm based on cloud computing is proposed, which can not only shorten the training time and reduce the consumption of computing resources but also significantly improve the accuracy of power load.

Data Availability

The data used to support the findings of this study are available from the corresponding author upon request.

Conflicts of Interest

The authors declare that they have no conflicts of interest.

References

- [1] Y. Guo and Y. Guo, "Intelligent network office system based on cloud computing and machine learning," *Mobile Information Systems*, vol. 2021, no. 2, 14 pages, Article ID 5868261, 2021.
- [2] W. Tang, Q. Yang, X. Hu, and W. Yan, "Deep learning-based linear defects detection system for large-scale photovoltaic plants based on an edge-cloud computing infrastructure," *Solar Energy*, vol. 231, pp. 527–535, 2022.
- [3] W. Jianbo and X. Cao, "Factors affecting the evolution of advanced manufacturing innovation networks based on cloud computing and multiagent simulation," *Mathematical Problems in Engineering*, vol. 2021, no. 1, 12 pages, Article ID 5557606, 2021.
- [4] W. L. Tai, Y. F. Chang, and W. H. Huang, "Security analyses of a data collaboration scheme with hierarchical attribute-based encryption in cloud computing," *International Journal on Network Security*, vol. 22, no. 2, pp. 212–217, 2020.
- [5] M. Nazari Jahantigh, A. Masoud Rahmani, N. Jafari Navimirour, and A. Rezaee, "Integration of internet of things and cloud computing: a systematic survey," *IET Communications*, vol. 14, no. 2, pp. 165–176, 2020.
- [6] F. Wulf, M. Westner, and S. Strahringer, "Cloud computing adoption: a literature review on what is new and what still needs to be addressed," *Communications of the Association for Information Systems*, vol. 48, no. 1, pp. 523–561, 2021.

Retraction

Retracted: Optimal Pricing Model of Environmental Quality Index Futures from the Perspective of Green Finance

International Transactions on Electrical Energy Systems

Received 19 September 2023; Accepted 19 September 2023; Published 20 September 2023

Copyright © 2023 International Transactions on Electrical Energy Systems. This is an open access article distributed under the Creative Commons Attribution License, which permits unrestricted use, distribution, and reproduction in any medium, provided the original work is properly cited.

This article has been retracted by Hindawi following an investigation undertaken by the publisher [1]. This investigation has uncovered evidence of one or more of the following indicators of systematic manipulation of the publication process:

- (1) Discrepancies in scope
- (2) Discrepancies in the description of the research reported
- (3) Discrepancies between the availability of data and the research described
- (4) Inappropriate citations
- (5) Incoherent, meaningless and/or irrelevant content included in the article
- (6) Peer-review manipulation

The presence of these indicators undermines our confidence in the integrity of the article's content and we cannot, therefore, vouch for its reliability. Please note that this notice is intended solely to alert readers that the content of this article is unreliable. We have not investigated whether authors were aware of or involved in the systematic manipulation of the publication process.

Wiley and Hindawi regrets that the usual quality checks did not identify these issues before publication and have since put additional measures in place to safeguard research integrity.

We wish to credit our own Research Integrity and Research Publishing teams and anonymous and named external researchers and research integrity experts for contributing to this investigation.

The corresponding author, as the representative of all authors, has been given the opportunity to register their agreement or disagreement to this retraction. We have kept a record of any response received.

References

- [1] J. Che, S. Zhou, R. Shan, H. Jia, and Z. Liu, "Optimal Pricing Model of Environmental Quality Index Futures from the Perspective of Green Finance," *International Transactions on Electrical Energy Systems*, vol. 2022, Article ID 6951040, 8 pages, 2022.

Research Article

Optimal Pricing Model of Environmental Quality Index Futures from the Perspective of Green Finance

Junwen Che ¹, Shenghe Zhou ², Rui Shan ¹, Hui Jia ¹ and Zheng Liu ¹

¹Yantai Nanshan University, Longkou, Shandong 265713, China

²ShandongNanshan Aluminum Co, LTD., Longkou, Shandong 265713, China

Correspondence should be addressed to Rui Shan; 3100502016@caa.edu.cn

Received 14 July 2022; Revised 29 July 2022; Accepted 3 August 2022; Published 28 August 2022

Academic Editor: Nagamalai Vasimalai

Copyright © 2022 Junwen Che et al. This is an open access article distributed under the Creative Commons Attribution License, which permits unrestricted use, distribution, and reproduction in any medium, provided the original work is properly cited.

In order to establish the optimal price of low-carbon products and set the optimal target carbon emissions in the production cycle so as to maximize profits, this paper proposes the optimal pricing model of environmental quality index futures from the perspective of green finance. This paper mainly studies the optimal pricing and carbon emission strategy of low-carbon products of a single enterprise under the carbon trading system based on the quota system. When enterprises join the carbon trading system, how to optimally determine their target carbon emissions in the production cycle and the optimal price of their low-carbon products in order to maximize their own profits, based on the carbon emission quotas freely allocated by the government in the face of exogenous carbon trading prices and different consumer preferences for low-carbon products in the market, is discussed in detail. The experimental results show that the low marginal cost of emission reduction will urge enterprises to implement low-emission strategies as much as possible, and the marginal cost of a specific size will enable enterprises to implement low-carbon policies with low emissions, and the optimal emissions will decline with the increase of carbon prices. However, from the perspective of 50–300 carbon trading prices, the profits generated are less than those of the minimum emission strategy, and the difference between the two is generally one order of magnitude. Therefore, if the internal conditions permit and the external carbon trading price is reasonable, enterprises should reduce carbon emissions as much as possible. The properties obtained from the model analysis and the numerical conclusions given in the example part reflect the relationship between the enterprise product pricing, the marginal cost of emission reduction, and the target emission decision-making and draw some valuable information for the enterprise and the government decision-making.

1. Introduction

International carbon futures trading originated from the spot trading of carbon emission rights. In 2003, the Chicago Climate Exchange (CCX) was established. Based on “quota and trade,” it became the world’s first legally binding greenhouse gas emission registration, voluntary emission reduction, and trading platform based on international rules [1, 2]. In 2005, the EU established the EU Emissions Trading System (EUETS), which has become the largest total carbon emission control and trading system in the world. Since then, the European Climate Exchange (ECX), the French electricity exchange, the BlueNext trading market, the European energy exchange (EEX), the Italian electricity exchange (IPEX), and the UK emission rights exchange under

the EU Emission Rights Trading System have been gradually established. Driven by the government’s policy of low-carbon economic transformation and the promotion of relevant financial institutions, the carbon spot trading market has developed rapidly, and the trading volume is rising day by day.

In April 2005, the European Climate Exchange launched the first EU carbon emission quota (EUA) futures and operated on the electronic futures trading platform of the London International Petroleum Exchange (IPE). The Chicago Climate Exchange, the European Climate Exchange, and the European energy exchange (EEX) have successively launched certified emission reduction (CER) futures contracts. Once the carbon futures contract was launched, it was sought after by many investors, and the

trading volume increased rapidly. At present, the main carbon futures products in the global carbon finance market include the European Climate Exchange carbon finance contract (ECXCFI), emission index futures (EUAFutures), certified emission reduction futures (CERFutures), and the Chicago Climate Exchange carbon trading financial futures (CCXCFIFutures) [3]. Figure 1 shows the organizational structure of the green industry fund.

2. Literature Review

In response to this research problem, Lee et al. took the carbon emission trading pilot as the background, considered that when there was dual pressure of emission reduction policy and low-carbon demand, they introduced the manufacturer's carbon emission per unit product decision variables, and analyzed the manufacturer's optimal pricing and optimal emissions by constructing the manufacturer's simplified decision model [4]. Wu et al. studied the optimal pricing and carbon emission strategy of low-carbon products for a single enterprise under the carbon trading system based on the quota system. In the carbon trading environment, the government allocates a certain carbon emission quota to enterprises for free. Facing the carbon trading price given by the carbon trading market and the different preferences of consumers on the low-carbon degree of products in the product market, it provides solutions on how to optimally determine the target carbon emissions within the production cycle of enterprises and the optimal price of low-carbon products produced so as to maximize their own profits [5]. CSS et al. pointed out in their research on the establishment of an emission rights market in China that carbon taxation, a Pigou mean, and carbon emission rights trading, a Coase mean, are based on internalizing the external effects of environmental problems and combining policy intervention with market mechanisms to affect enterprises' emission and pollution control behavior. However, carbon tax mostly relies on government intervention, while carbon emission rights trading focuses on using market mechanisms to solve environmental problems [6]. Pan et al. pointed out that the carbon tax is levied on the carbon content of energy consumption products, which is conducive to the realization of carbon emission reduction. However, the carbon tax will have an impact on the competitiveness, distribution, and environment of enterprises' products, so some enterprises are reluctant to adopt it [7]. Yu et al. found that if the marginal emission reduction cost (MAC) and marginal loss and other cost and benefit functions of enterprises can be clearly defined, carbon trading and carbon tax can achieve the optimal goal of carbon emission reduction through appropriate pricing [8]. Yang et al. found that when other conditions remain unchanged, the optimal environmental economic means can be selected by comparing the size of the marginal management cost and marginal transaction cost. When the degree of marketization is low, the carbon tax means are more appropriate [9].

The problem we need to solve is how to set the optimal low-carbon product price and set the optimal target carbon emissions in the production cycle in the face of the

established carbon emission allocation quota and customers with different low-carbon preferences in the market so as to maximize profits. Enterprises need to balance the following issues: reducing emissions will gain carbon trading benefits and will positively affect the market demand for products due to better low-carbon performance, but at this time, enterprises will bear higher emission reduction input costs. On the contrary, if the enterprise relaxes the control on emission reduction, the cost will be relatively reduced, but on the one hand, it may not get the carbon trading income. On the other hand, it will have an adverse impact on product sales due to poor environmental performance and a negative corporate image [10]. In this paper, carbon emissions are directly taken as decision variables. The main reasons for this assumption are (1) it can clearly reflect the relationship between enterprise emissions, the trading market, the carbon quota, and the government's low-carbon policy; (2) as an indicator or task, emissions have a very intuitive guiding significance in the actual production process. We think this assumption is also reasonable from the perspective of enterprise production because carbon emissions mainly come from energy consumption. Enterprises can change the energy input structure or use efficiency to reduce carbon emissions under the condition of ensuring a certain output. For example, some agricultural product production enterprises' CDM projects change the power access from thermal power to wind power or biogas power generation, which will not affect the final production. Another example is the energy-saving projects related to cement production.

3. Research Methods

3.1. Symbol Description. The symbols used in this article are explained one by one:

p : Low carbon product market pricing, as a decision variable;

e_c : The total carbon emission in the production cycle of the enterprise, which is a decision variable;

$D(p, e_c)$: The market demand of the final product, which is the function of the above two decision variables, and the demand will decrease with the increase of price or carbon emission;

e_l : Minimum possible carbon emission, i.e., the minimum emission that the enterprise can achieve within its production cycle with all efforts;

e_m : Maximum carbon emission refers to the total carbon emission generated during the production cycle of an enterprise without any emission reduction technology;

p_0 : The market price of general products, an exogenous variable, is the market-accepted price of similar but nonlow-carbon products;

c_0 : Marginal production cost without emission reduction technology input;

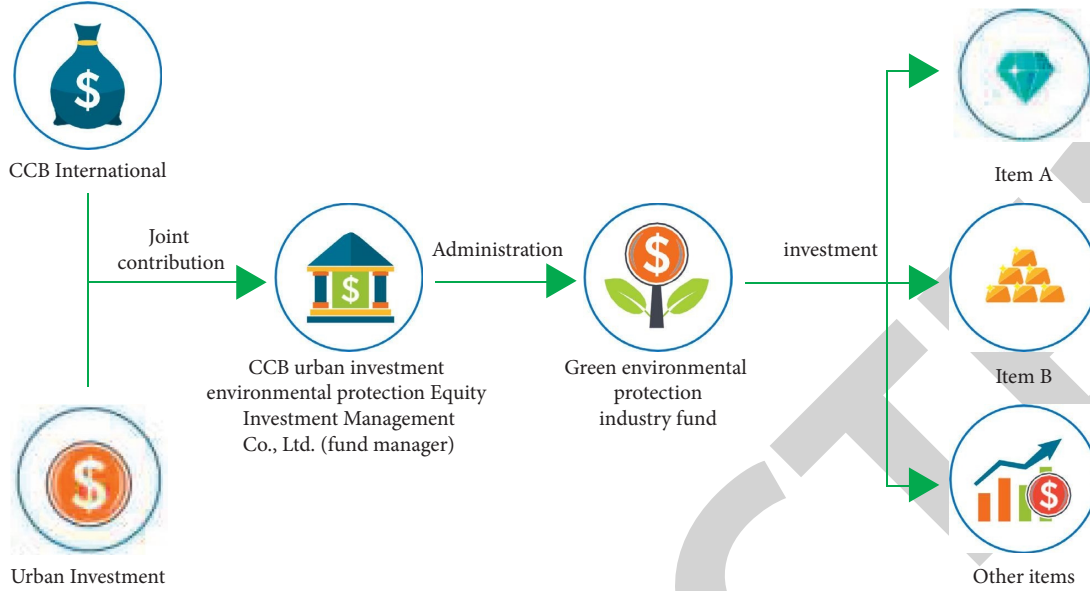


FIGURE 1: Organizational structure of the green industry fund.

$c_d(e_c)$: Low carbon input cost, set as the convex increasing function of the enterprise's target carbon emissions;

β : Emission reduction coefficient;

\bar{e} : The carbon emission limit for specific enterprises shall be allocated by the government free of charge;

ε : Carbon trading price;

δ : Low carbon preference of consumers;

t : Government subsidy coefficient for low-carbon products;

M : The total market capacity of the same type of low-carbon products and general products of the enterprise.

3.2. Enterprise Decision. After the carbon emission quota is known, the enterprise must make the optimal target carbon emission and product pricing decisions before the start of its production cycle to maximize its profits after the production cycle. The objective function is as follows:

$$\begin{aligned} \max_{p, e_c} \Pi &= D(p, e_c)(p - c_0) - c_d(e_c) + \varepsilon(\bar{e} - e_c), \\ \text{s.t. } e_l &\leq e_c \leq e_m, \end{aligned} \quad (1)$$

where if $\bar{e} - e_c$ is positive, it means that the enterprise can sell the carbon quota, and if it is negative, it means that the enterprise should purchase the quota from the outside; c_d will use the classic AJ model for reference and set the emission reduction cost as the quadratic form $c_d = \beta(e_m - e_c)^2$. Compared with previous models, the differences and innovations of this paper are as follows:

- (1) The construction of this model takes carbon emissions as the cornerstone and adds the positive and negative benefits generated by the carbon trading process to the profits;

- (2) Considering the government subsidy to the market rather than the low-carbon subsidy to enterprises because the government policy orientation in this paper focuses on the market rather than administrative means, and a corresponding part of the profits of enterprises will come from carbon trading rather than the subsidy amount.

The subsidy to the market is to stimulate consumption and improve citizens' awareness of environmental protection [11].

3.3. Product Demand. Suppose that consumers' cognition of low-carbon products (or environmental satisfaction) in the market obeys the uniform distribution on $[\underline{\delta}, \bar{\delta}]$. $\bar{\delta}$ means that for consumers who will buy any low-carbon products, $\underline{\delta}$ is a customer who has no low-carbon awareness and is only willing to buy general products. Set the government subsidy amount for consumers to purchase low-carbon products as $t(e_m - e_c)$, which indicates that the low-carbon degree is based on the maximum carbon emission of enterprises. The government can adjust the subsidy coefficient t to change the subsidy amount, which is an exogenous variable [12, 13]. Here, for the convenience of analysis, we assume that consumers' information on the carbon emissions of enterprises is complete. At the same time, in practice, e_m and e_c are generally large, so t should be a small number in reality. For consumers, whether they buy low-carbon products of the enterprise depends on whether their consumption utility is less than that of purchasing similar to nonlow-carbon products. Considering such marginal customers, their low-carbon awareness is δ , and they hold an "indifferent" attitude towards whether to buy low-carbon products, that is, for them, the utility of buying two types of products is the same, i.e., $p - p_0 = k(\delta - \underline{\delta}) + t(e_m - e_c)$, where k is a normal

number, indicating the utility coefficient of consumers' low-carbon awareness.

The following equation is obtained:

$$\delta = \frac{p - p_0 - t(e_m - e_c) + k\underline{\delta}}{k}. \quad (2)$$

Meanwhile, the market demand for such low-carbon products is as follows:

$$D(p, e_c) = M \int_{\underline{\delta}}^{\bar{\delta}} \frac{1}{\delta - \underline{\delta}} dx = M \left(1 + \frac{t(e_m - e_c) + p_0 - p}{k(\bar{\delta} - \underline{\delta})} \right). \quad (3)$$

3.4. Optimal Pricing. Considering that the enterprise makes the pricing decision first, for a given EC, there is the following formula:

$$\begin{aligned} \max_p \Pi = & M \left(1 + \frac{p_0 + t(e_m - e_c) - p}{k(\bar{\delta} - \underline{\delta})} \right) (p - c) \\ & - \beta(e_m - e_c)^2 + \varepsilon(\bar{e} - e_c). \end{aligned} \quad (4)$$

The optimal solution obtained from formula (4) F.O.C is as follows:

$$p^* = \frac{1}{2}(c + p_0 + t(e_m - e_c) + k(\bar{\delta} - \underline{\delta})). \quad (5)$$

The following conclusions can be drawn:

Conclusion 1. The higher the government subsidy, the higher the product pricing of enterprises. This can be directly observed from equation (5). Therefore, government subsidies to consumers can indirectly help enterprises that implement low-carbon production to make profits.

Conclusion 2. Under the same target emission level, the greater the maximum carbon emissions of enterprises, the higher the product price. Obviously, the larger e_m shows the characteristics of higher energy consumption in the industry [14]. The difference between e_c and EC essentially reflects the efforts of enterprises to reduce emissions.

Conclusion 3. The higher the target carbon emissions, the lower the product price. From equation (5), it can be seen that without considering the emission reduction cost and other factors, the increase in carbon emissions will affect consumers' preference for environmental protection products through $\bar{e} - e_c$ [15]. When the emissions increase, some customers with strong environmental awareness will not choose such products, and the market demand will decline. At this time, enterprises will have to reduce the product price.

Conclusion 4. The stronger the consumers' awareness of low-carbon δ , the higher the price of low-carbon products. This conclusion is not only tenable in the model but also logical in practice because the improvement of low-carbon awareness will bring more sales.

3.5. Optimal Carbon Emissions. Substitute (5) into (4) to obtain

$$\begin{aligned} \max_{0 \leq e_c \leq e_m} \Pi = & M \left(1 + \frac{p_0 + t(e_m - e_c) - 1/2(c + p_0 + t(e_m - e_c) + k(\bar{\delta} - \underline{\delta}))}{k(\bar{\delta} - \underline{\delta})} \right) \\ & \left(\frac{1}{2}(c + p_0 + t(e_m - e_c) + k(\bar{\delta} - \underline{\delta})) - c \right) - \beta(e_m - e_c)^2 + \varepsilon(\bar{e} - e_c) \end{aligned} \quad (6)$$

Formula (6)

$$\max_{0 \leq e_c \leq e_m} \Pi = \varepsilon(\bar{e} - e_c) - \beta(e_m - e_c)^2 + \frac{M(c - p_0 + te_c - te_m - h\bar{\delta} + h\underline{\delta})^2}{4k(\bar{\delta} - \underline{\delta})}.$$

Find the second derivative of e_c for (6) and obtain the following equation:

$$\frac{\partial^2 \Pi}{\partial e_c^2} = \frac{Mt^2}{2k(\bar{\delta} - \underline{\delta})} - 2\beta. \quad (7)$$

When looking for the optimal carbon emission e_c^* , we take $Mt^2/4k(\bar{\delta} - \underline{\delta})$ as the threshold and discuss it in three

cases according to the marginal cost of emission reduction of different sizes.

Case 1. $\beta = Mt^2/4k(\bar{\delta} - \underline{\delta})$

At this time, the profit function has a linear relationship with the decision variable e_c . The following properties can be obtained:

Property 1. When $\beta = Mt^2/4k(\bar{\delta} - \underline{\delta})$, the lowest emission will be the best choice for the enterprise.

3.5.1. Nature 1: Certification. Finding the first-order partial derivative of e_c for π_{e_c} yields $\partial\Pi/\partial e_c = Mt((c - p_0) - k(\bar{\delta} - \delta))/2k(\bar{\delta} - \delta) - \varepsilon \leq 0$, (6) is a monotonic nonincreasing function of e_c . Obviously, when $e_c = e_l$, the profit reaches the maximum. The certificate is completed.

The following conclusions are drawn:

Conclusion 5. When the marginal cost of enterprise emission reduction is equal to a certain value, the larger the carbon emission, the smaller the profit. Property 1 illustrates this problem, and at this time, the enterprise should reduce emissions as much as possible [16].

4. Result Analysis

The established model and its related properties and conclusions are analyzed with examples. For different marginal costs and carbon prices, we discuss the optimal decision under specific examples according to the basic properties of the objective function. The specific values are set as follows:

$$\begin{aligned} M = 500, e_m = 250, e_l = 100, t = 0.2, k = 0.1, \bar{\delta} = 10, \\ \underline{\delta} = 0, c = 10, p_0 = 20, \varepsilon = 50, \bar{e} = 200 \end{aligned} \quad (8)$$

4.1. Linear Objective Function. At this time, $\beta = Mt^2/4k(\bar{\delta} - \underline{\delta})$ and $\partial\Pi/\partial e_c = Mt((c - p_0) - k(\bar{\delta} - \delta))/2k(\bar{\delta} - \delta) - \varepsilon \leq 0$ are used to analyze the impact of target emissions on profits, as shown in Figures 2 and 3.

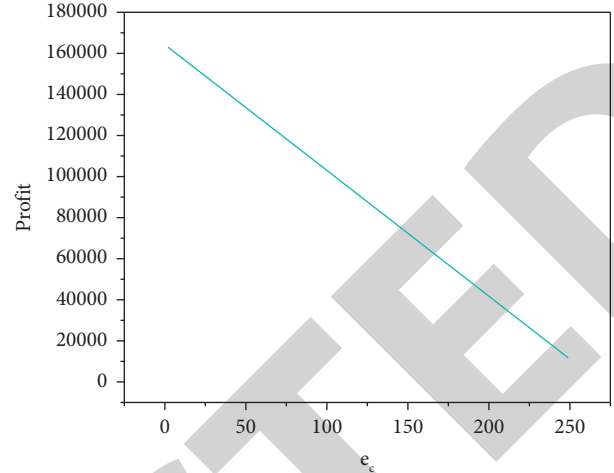
As can be seen from Figure 2, when the target emissions increase, the profits decrease rapidly. It is obvious from Figure 3 that the increase in carbon trading prices will improve the overall profit level. Figure 4 analyzes the sensitivity of profit to the carbon price. As stated in conclusion 6, higher prices will increase the absolute value of the slope of profits to emissions, that is, when the carbon price is higher, the profits of enterprises will decline faster with the increase of emissions. At this time, if enterprises loosen the control of emissions, on the one hand, they will encounter lower market demand; on the other hand, they will bear the opportunity cost of carbon trading [17].

4.2. Nonlinear Objective Function. Combining the carbon price and the marginal cost of emission reduction, we analyze it based on inference 4.

Known by

when $Mt^2/4k(\bar{\delta} - \underline{\delta}) = 5 < \beta \leq kMt(\bar{\delta} - \underline{\delta}) + 2k\varepsilon(\bar{\delta} - \underline{\delta}) - Mt(te_l - te_m - p_0 + c)/4k(e_m - e_l)(\bar{\delta} - \underline{\delta}) = 6.26$, the change of profit to marginal cost is analyzed in Figure 5. It is found that when other conditions remain unchanged, the profit will rapidly decline with the increase of emission reduction marginal cost.

When $\beta \geq kMt(\bar{\delta} - \underline{\delta}) + 2k\varepsilon(\bar{\delta} - \underline{\delta}) - Mt(te_l - te_m - p_0 + c)/4k(e_m - e_l)(\bar{\delta} - \underline{\delta}) = 6.26$, we analyze the impact of



— The impact of targeted emissions on profits

FIGURE 2: $\varepsilon = 50, \bar{e} = 200, e_c \in [0, 250]$.

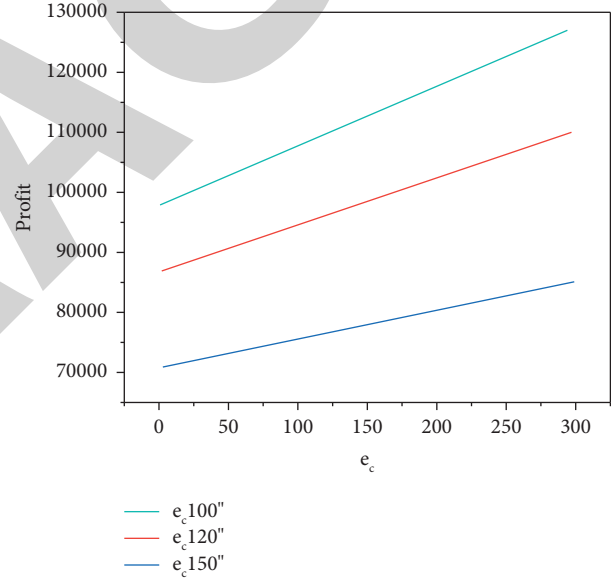


FIGURE 3: $\varepsilon \in [0, 300], \bar{e} = 200, e_c = 100$.

the marginal cost of emission reduction on the optimal carbon emission, and Figure 6 is obtained. The results show that when the marginal cost of emission reduction increases, the decision-maker will increase the target carbon emissions, and the graph is concave to β and takes the maximum emission of 250 as the limit value. This shows that the positive impact of the marginal cost of emission reduction on carbon emissions is limited by the capacity of enterprises.

Figure 6 analyzes the impact of the corresponding optimal emissions on profits when $\beta \in [6.3, 20]$. Compared with Figure 4, it is found that when the emission reduction cost is large, the overall profit level decreases significantly, and the impact of cost on profit is also different. The former is linear in a limited range, whereas the latter is nonlinear, and its influence degree varies from large to small [18].

Figure 7 analyzes the sensitivity of profit to carbon price under the concave function ($\beta = 6.3$). From the change

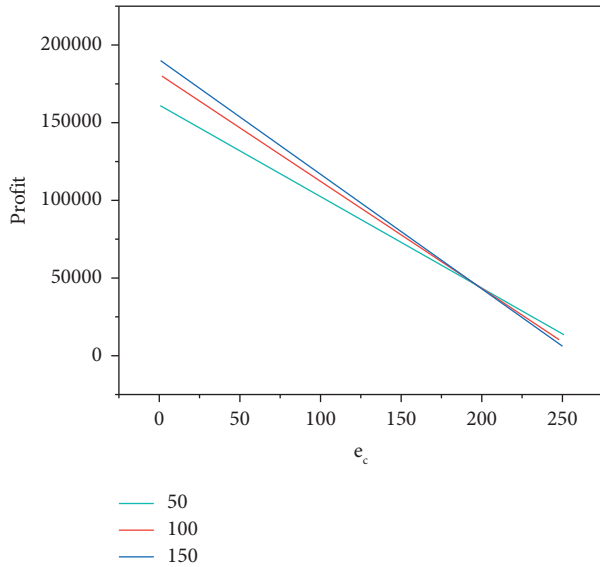


FIGURE 4: $\varepsilon = 50, 100, 150, e_c \in [0, 250]$.

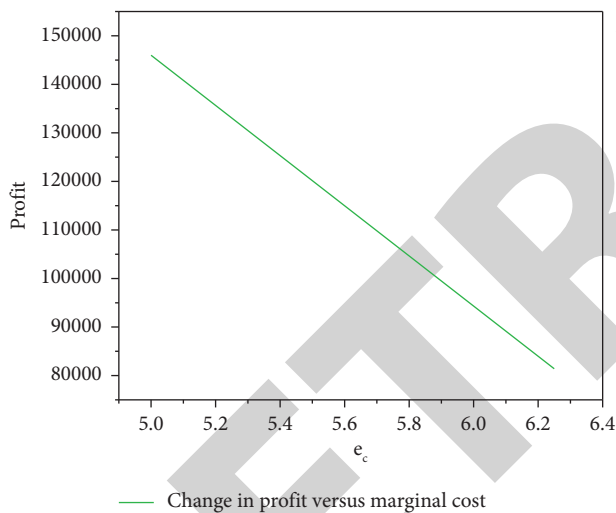


FIGURE 5: $e_c = 0, \beta \in [5, 6.3]$.

track of the stable point, a higher carbon price will enable enterprises to obtain the global optimal profit with less emissions. At the same time, if enterprises expand emissions, their profits will decline faster [19, 20]. When $e_c = 200$, the enterprise profits under the four carbon prices are the same, and beyond this point, the enterprise profits under the higher carbon prices will be lower [21].

The low marginal cost of emission reduction will urge enterprises to implement low emission strategies as much as possible. The marginal cost of a specific size will enable enterprises to implement low-carbon policies with low emissions, and the optimal emissions will decline with the increase in carbon prices. However, from the perspective of 50–300 carbon trading prices, the profits generated are less than those of the minimum emission strategy, and the difference between the two is generally one order of magnitude. Therefore, if the internal conditions permit and the

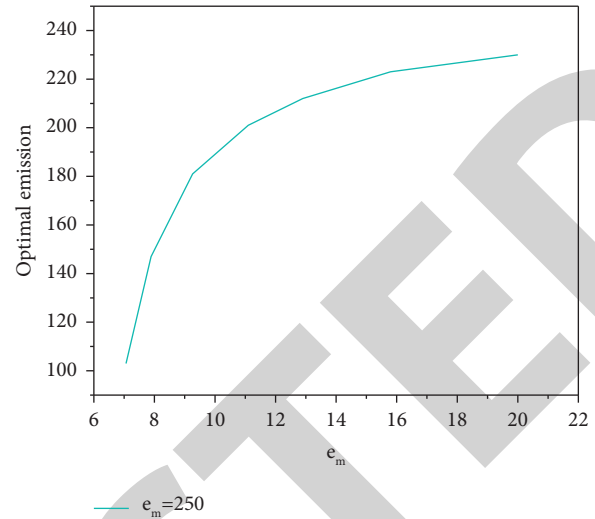


FIGURE 6: $\beta \in [6.3, 20]$.

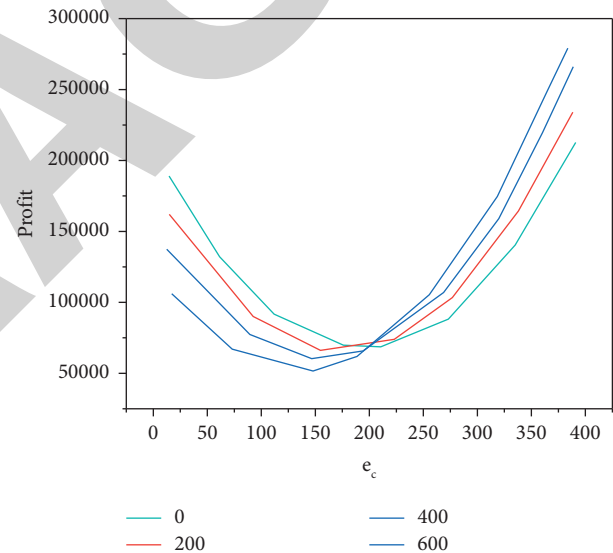


FIGURE 7: $e_c = [0, 400], \varepsilon = 0, 200, 400, 600$.

external carbon trading price is reasonable, the enterprise should reduce carbon emissions as much as possible [22].

5. Conclusion

This paper discusses how enterprises make the optimal price of low-carbon products and emission reduction strategies under the carbon trading system.

In terms of carbon emission decision-making, we first analyze different decisions based on linear, concave, and convex objective functions according to the size of enterprise marginal cost and obtain some valuable information combined with numerical examples. For example, when there is a linear relationship between corporate profits and carbon emissions, profits will decrease with the increase of carbon emissions, and this trend will intensify with the rise in the carbon trading prices. Under the nonlinear function, when

the price of carbon trading market rises, the larger marginal cost of emission reduction will lead to lower optimal target emissions. When the marginal cost of emission reduction is within a certain range, enterprises will try their best to reduce carbon emissions. In addition, when the carbon price is higher, lower carbon emissions will enable enterprises to obtain higher profits, and at this time, the opportunity cost of increasing emissions will be greater. In general, the overall profit level of a convex function (lower marginal cost of emission reduction) is larger than that of a concave function.

Based on the above discussion, we further analyzed the carbon trading price and obtained some valuable information for enterprises and government decision-making. For example, for enterprises, if their marginal cost of emission reduction is low in the carbon trading environment, they should try to reduce their carbon emissions in the production cycle. In particular, when the carbon price rises, emission reduction becomes a top priority for enterprises because there will be a large profit space in the trading market at this time. As far as the government is concerned, it should try to increase the carbon price if its capacity permits, such as through administrative intervention, so as to stimulate the enthusiasm of enterprises to voluntarily reduce emissions. If the local government does not have the ability to affect the carbon price, it should appropriately adjust the subsidies for low-carbon products to indirectly change the cost structure of enterprises and encourage enterprises to implement emission reduction.

The limitation of this paper is that carbon emissions can indeed be measured, and the production environment indicators of consumers and enterprises can also be obtained through some of the ways described in this paper, but the marginal price of consumers' willingness to pay for low-carbon products is a difficult value to measure. The value of different consumers is different and should change over time, but the description of low-carbon awareness in this paper is more abstract. Second, this paper assumes that the carbon emission quota for a certain enterprise is an exogenous variable, but in practice, if the enterprise or group is large, its industrial energy consumption level will affect the government's formulation of carbon trading quota.

Data Availability

The data used to support the findings of this study are available from the corresponding author upon request.

Conflicts of Interest

The authors declare that they have no conflicts of interest.

Acknowledgments

This study is funded by The Youth Fund Project of Yantai Nanshan University (Humanities and Social Sciences) in 2021 (Humanities and Social Sciences) and Practical research on Transformation and Innovation of Cultural Industry with Digital Empowerment of Shandong Province (Project number: 2021QSK05).

References

- [1] M. Song, X. Zhao, Y. Shang, and B. Chen, "Realization of green transition based on the anti-driving mechanism: an analysis of environmental regulation from the perspective of resource dependence in China," *The Science of the Total Environment*, vol. 698, no. Jan.1, pp. 134317.1–134317.12, 2020.
- [2] X. Zhou, X. Tang, and R. Zhang, "Impact of green finance on economic development and environmental quality: a study based on provincial panel data from China," *Environmental Science and Pollution Research*, vol. 27, no. 16, 2020.
- [3] A. Shokri and G. Li, "Green implementation of lean six sigma projects in the manufacturing sector," *International Journal of Lean Six Sigma*, vol. 11, no. 4, pp. 711–729, 2020.
- [4] J. H. Lee and K. S. Im, "Effect of in-situ silicon carbon nitride (sicn) cap layer on performances of algan/gan mishfets," *IEEE Journal of the Electron Devices Society*, vol. 9, no. 99, pp. 728–734, 2021.
- [5] S. Wu and Z. Huang, "Coordination of an environmentally responsible supply chain with cost disturbance under carbon price fluctuations," *Mathematical Problems in Engineering*, vol. 2020, no. 3, pp. 1–17, 2020.
- [6] A. C. S. A. R. D. B. L. F. Q. P. M. and A. Cap, "Electrodeposited cobalt hydroxide in expanded carbon graphite electrode obtained from exhausted batteries applied as energy storage device - sciencedirect," *Arabian Journal of Chemistry*, vol. 13, no. 1, pp. 3448–3459, 2020.
- [7] J. Pan, W. Zhong, Z. Gao et al., "N, S-doped silicon oxy-carbide-driven carbon/amorphous ball-flower-like NiO as high performance electrode in asymmetric supercapacitors," *Ceramics International*, vol. 47, no. 19, pp. 27833–27842, 2021.
- [8] H. Yu, S. Bai, and D. Chen, *An Optimal Control Model of the Low-Carbon Supply Chain: Joint Emission Reduction, Pricing Strategies and New Coordination Contract Design*, IEEE Access, no. 99, p. 1, NJ, USA, 2020.
- [9] Y. Yang, M. Zhao, Z. Cao, Z. Ge, Y. Ma, and Y. Chen, "Low-cost and scalable carbon bread used as an efficient solar steam generator with high performance for water desalination and purification," *RSC Advances*, vol. 11, no. 15, pp. 8674–8681, 2021.
- [10] S. Xia, F. Lin, Z. Chen, C. Tang, Y. Ma, and X. Yu, "A bayesian game based vehicle-to-vehicle electricity trading scheme for blockchain-enabled internet of vehicles," *IEEE Transactions on Vehicular Technology*, vol. 69, no. 7, pp. 6856–6868, 2020.
- [11] X. Ji, Z. Yin, Y. Zhang, H. Gao, X. Zhang, and X. Zhang, "Comprehensive pricing scheme of the ev charging station considering consumer differences based on integrated ahp/dea methodology," *Mathematical Problems in Engineering*, vol. 2020, no. 3, pp. 1–11, 2020.
- [12] Y. Tao, J. Qiu, S. Lai, J. Zhao, and Y. Xue, "Carbon-oriented electricity network planning and transformation," *IEEE Transactions on Power Systems*, vol. 36, no. 2, pp. 1034–1048, 2021.
- [13] A. Yi, W. A. Hui, B. Dc, G. B. Lin, W. C. Xin, and J. A. Xian, "Achieving thermally stable and anti-hydrolytic sr2si5n8: eu2+ phosphor via a nanoscale carbon deposition strategy - sciencedirect," *Ceramics International*, vol. 47, no. 3, pp. 3244–3251, 2021.
- [14] W. Liu, X. Wu, X. Du, G. Xu, and S. Wang, *Tension Networked Control Strategy for Carbon Fiber Multilayer Diagonal Loom*, IEEE Access, no. 99, p. 1, NJ, USA, 2020.
- [15] X. Xu, Q. Yang, L. Fang, Y. Du, and Y. Fu, "Anion-cation dual doping: an effective electronic modulation strategy of ni₂p

Retraction

Retracted: Mathematical Modeling Method of the Improved Genetic Algorithm for Random Power Fluctuation

International Transactions on Electrical Energy Systems

Received 3 October 2023; Accepted 3 October 2023; Published 4 October 2023

Copyright © 2023 International Transactions on Electrical Energy Systems. This is an open access article distributed under the Creative Commons Attribution License, which permits unrestricted use, distribution, and reproduction in any medium, provided the original work is properly cited.

This article has been retracted by Hindawi following an investigation undertaken by the publisher [1]. This investigation has uncovered evidence of one or more of the following indicators of systematic manipulation of the publication process:

- (1) Discrepancies in scope
- (2) Discrepancies in the description of the research reported
- (3) Discrepancies between the availability of data and the research described
- (4) Inappropriate citations
- (5) Incoherent, meaningless and/or irrelevant content included in the article
- (6) Peer-review manipulation

The presence of these indicators undermines our confidence in the integrity of the article's content and we cannot, therefore, vouch for its reliability. Please note that this notice is intended solely to alert readers that the content of this article is unreliable. We have not investigated whether authors were aware of or involved in the systematic manipulation of the publication process.

Wiley and Hindawi regrets that the usual quality checks did not identify these issues before publication and have since put additional measures in place to safeguard research integrity.

We wish to credit our own Research Integrity and Research Publishing teams and anonymous and named external researchers and research integrity experts for contributing to this investigation.

The corresponding author, as the representative of all authors, has been given the opportunity to register their agreement or disagreement to this retraction. We have kept a record of any response received.

References

- [1] F. Zhu, "Mathematical Modeling Method of the Improved Genetic Algorithm for Random Power Fluctuation," *International Transactions on Electrical Energy Systems*, vol. 2022, Article ID 1889952, 7 pages, 2022.

Research Article

Mathematical Modeling Method of the Improved Genetic Algorithm for Random Power Fluctuation

Fu Zhu 

Department of Basic Courses, Shangqiu Polytechnic, Shangqiu, Henan 476100, China

Correspondence should be addressed to Fu Zhu; 11231522@stu.wxlc.edu.cn

Received 10 July 2022; Revised 24 July 2022; Accepted 2 August 2022; Published 25 August 2022

Academic Editor: Nagamalai Vasimalai

Copyright © 2022 Fu Zhu. This is an open access article distributed under the Creative Commons Attribution License, which permits unrestricted use, distribution, and reproduction in any medium, provided the original work is properly cited.

In order to solve the problem that the traditional genetic algorithm has a slow search speed and is easy to fall into the local optimal solution, a mathematical modeling method of an improved genetic algorithm in random power fluctuation is proposed. Drawing on the idea of a genetic algorithm (GA) and using the randomness and stability trend of cloud droplets of the normal cloud model, the author proposes a new genetic algorithm, cloud genetic algorithm (CGA). CGA is implemented by the Y-condition cloud generator of the normal cloud model to realize the cross operation, and the basic cloud generator realizes the mutation operation. Finally, the power function optimization experiment and the IIR digital filter optimization design are carried out, and the standard GA, NQGA, CAGA, and LARES algorithms are carried out compared. The experimental results show that the IIR digital filter designed by CGA has the smallest maximum ripple (A_p) in the passband, which is 0.342, and the largest minimum attenuation (A_s) in the stopband, which is 34.27. It can be observed that the overall performance is better. The validity of the algorithm is proved, and it has a certain reference and application value.

1. Introduction

The evolutionary process of a disease is usually the result of crossovers and mutations of chromosomes. Based on the principles of genetics and evolution in nature, many scientists have developed various types of coding to provide solutions and have to create and use different types of genetics to simulate it. Many different genetic operators have been developed to mimic the genetic properties of organisms in different environments. In this way, different encodings and different genetic operators create different genetic algorithms [1].

Genetic algorithms are a global and advanced scientific method that follows the theoretical process of mutation in the body. During the research process, you can gain and compile knowledge of the research area and refine and manage the search process to achieve a good solution. The function of the genetic algorithm is based on the principle of optimal survival, and of the various solutions, a set of optimal solutions is developed [2]. At each stage of the genetic algorithm, the value of identity is based on the value of the

physical body in the problem, and the process of reconstruction provided by natural genetics then creates a new approximate concept. These processes lead to the evolution of the population, and new individuals will adapt to a new environment rather than the old one, just as changes in nature.

The genetic algorithm is a global research heuristic algorithm used to solve the best performance in the field of computer science and is a kind of mutation that can be overcome. The quality of the process is always there which easily falls into the minimum values. Figure 1 shows the flow of the genetic algorithm. Genetic algorithms are widely used in bioinformatics, phylogeny, Chinese science, engineering, economics, chemistry, manufacturing, mathematics, physics, pharmacometrics, and other fields [3].

2. Literature Review

In practical applications, the standard genetic algorithm has many defects in maintaining population diversity, convergence accuracy, and convergence speed, which limit the

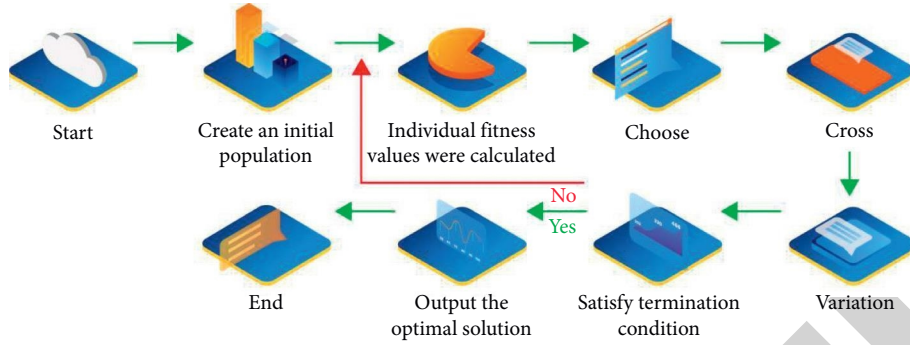


FIGURE 1: Genetic algorithm flow.

development and application of genetic algorithms. Therefore, researchers have improved the genetic algorithm from the aspects of parameter improvement and optimization, scheme adjustment, hybrid genetic algorithm, and neighborhood topology improvement. In terms of parameter improvement and optimization and scheme adjustment, Cao, Y. et al. proposed a new improved genetic algorithm, its fitness function can change with the individual state, at the same time, the mutation operation is adjusted in the genetic algorithm, and it is found that the performance of the improved genetic algorithm has been significantly improved [4]. Duan, Li et al. deal with the large dimension of the optimization problem, and an improved genetic algorithm is proposed [5]. Peng, D. et al. optimized and adjusted the operation operator of the genetic algorithm and adaptively processed the crossover and mutation operations in the genetic algorithm, at the same time, the corresponding formula is adjusted reasonably, and the elite retention strategy is optimized to adopt a more reasonable and effective scheme [6]. In the research on combining with other algorithms, Liu, Q. et al. combined the standard genetic algorithm with the particle swarm algorithm, the improved algorithm is specially reserved for the excellent individuals, and the particle swarm algorithm further optimizes the excellent individuals; the experiment found that the combination of the two algorithms can effectively improve the performance of the algorithm [7]. Yan, F. et al. proposed a new hybrid algorithm, the algorithm combines the genetic algorithm with the adaptive particle swarm algorithm and adjusts the selection strategy reasonably, at the same time, the operation operator of the genetic algorithm and the particle update rule of the adaptive particle swarm optimization algorithm are integrated, and the design method of the fitness function is improved; the experimental results show that the improved algorithm greatly improves the solution efficiency of the optimization problem [8].

3. Research Methods

3.1. Cloud Theory. Cloud models are models of variations of the uncertainty of the positive terms expressed in key words and their data representations, which often involve uncertainties and uncertainty of the context in the target world or human data. And the two are completely integrated together

for the qualitative and quantitative combination of information processing provides a powerful means [9].

3.1.1. Basic Concepts

Definition 1. Let T be the language value on the universe u and map $C_T(x): u \rightarrow [0, 1], \forall x \in u, x \rightarrow C_T(x)$, then the distribution of $C_T(x)$ on u is called the membership cloud of T or cloud for short. When $C_T(x)$ obeys a normal distribution, it is called a normal cloud model.

The normal cloud model is a random number set that follows the normal distribution law and has a stable tendency and is characterized by three values: expected value Ex , entropy En , and superentropy He . Expected value Ex : the point in the number domain space that can best represent this qualitative concept, reflecting the position of the cloud's center of gravity. Entropy En : on the one hand, it reflects the acceptable range of language values in the number domain space; on the other hand, it also reflects the probability that a point in the number domain space can represent the language value and the randomness of cloud droplets representing qualitative concepts. It reveals the correlation between ambiguity and randomness. Hyperentropy He : it is the uncertainty measure of entropy, namely the entropy of entropy, which reflects the cohesion of the uncertainty of all points representing the language value in the number domain space, that is, the cohesion of cloud droplets [10].

3.1.2. Basic Cloud Generator. **3.1.3. X Condition Cloud Generator.** Given the three digital features (Ex, En, He) of the cloud and a specific value x_0 on the universe of discourse u , a cloud droplet drop (x_0, μ_i) is generated, this kind of a cloud generator is called the X-condition cloud generator.

3.1.4. Y-Condition Cloud Generator. Given the three digital features (Ex, En, He) of the cloud and a certain degree of certainty μ_0 , a cloud droplet drop (x_i, μ_0) is generated, and such a cloud generator is called a Y-conditional cloud generator.

3.2. Cloud Genetic Algorithm. In the continuous variable space, there is a neighborhood around the global optimal solution. In this neighborhood, with the optimal solution as


```

INPUT: {Ex, En, He}, n //Numerical features and cloud droplet count
OUTPUT: {(x1, μ1), . . . , (xn, μn)} // n cloud droplets
FOR i = 1 to n
  //Generate a normal random number with expected value En and variance He
  En' = RANDN (En, He)
  xi = RANDN (Ex, En')
  μi = e-(xi-Ex)2/2(En')2
  drop (xi, μi) //Generate the i-th cloud drop

```

ALGORITHM 1: Basic normal cloud generator.

```

INPUT: {Ex, En, He}, n, x0
OUTPUT: {(x0, μ1), . . . , (x0, μn)}
FOR i = 1 to n
  En' = RANDN (En, He)
  μi = e-(x0-Ex)2/2(En')2
  drop (x0, μi)

```

ALGORITHM 2: X Condition Cloud Generator.

the center, the value of the objective function approaches the value from far to near. When the fitness of the current solution is large, the search should be carried out in a smaller neighborhood; otherwise, it should be searched in a larger neighborhood [11]. In this way, the region where the optimal solution is located can be positioned step by step, and finally, the optimal solution can be approached. Taking the search for the “black box“ of an aircraft as an example, the density of the aircraft wreckage is regarded as fitness. On the contrary, the smaller the scattering density of debris (the smaller the fitness), the smaller the range, and the black box is less likely to exist and should be searched in a larger range [12].

Combined with the idea of a genetic algorithm, the cloud genetic algorithm follows the concept of crossover and mutation operation of GA, the crossover operation is realized by the Y-condition cloud generation algorithm of the normal cloud model, and the mutation operation is realized by the basic cloud generation algorithm. Since the normal cloud model has the characteristics of randomness and stability tendency, randomness can maintain the diversity of individuals to avoid the search falling into the local extremum, while the stable tendency can also protect the superior individual and then adaptively locate the global optimal value. The CGA is encoded with real numbers and is individually updated by the cloud model [13].

In formula (1), x_f and x_m are the parent and parent of the crossover operation, respectively; F_f and F_m correspond to their fitness, respectively. This means that the Ex in the crossover operation is determined by the weighted fitness of both parents and moves closer to the one with the larger fitness [14].

3.3. Parameter Influence and Performance Analysis. From the normal cloud generator, we know that the normal cloud is a pan-normal distribution with the characteristics

of “more in the middle and less at both ends. “From $En' \sim N(En, He^2)$, It is understood that $EX = Ex + \sqrt{-2 \ln \mu} En$, standard deviation $D = \sqrt{-2 \ln \mu} He$. Therefore, the changes of parameters Ex and En affect the horizontal position and steepness of the cloud model, respectively, while He is proportional to the dispersion degree of cloud droplets, and μ is inversely proportional to it, that is, the larger the He is, the greater the degree of dispersion is, and the smaller the μ is (for the position of the cloud, the closer to the foot of the mountain), the more dispersed the cloud droplets are. All cloud droplets fluctuate randomly around the expected curve, and the magnitude of the fluctuation is controlled by [15].

3.3.1. Certainty. The degree of certainty in 4.1 of Algorithm 4 is discussed first. The larger the μ , the closer the cloud droplets are to the top, and the narrower the variable is searched for. In accordance with the finding of the black box phenomenon described in the introduction, we adapt the μ value to the fitness and gradually locate the optimal value. Here, two methods are introduced; one is a deterministic method using a linear function, and the other is a stochastic method using the X-condition cloud generator [16, 17].

Algorithm 5. Deterministic Linear Function Method

$$\mu = \mu_{\max} - \frac{F_{\max} - F'}{F_{\max} + F_{\min}} (\mu_{\max} - \mu_{\min}), \quad (1)$$

where F_{\max} and F_{\min} represent the global “maximum“ and “minimum“ fitness values of the contemporary population, respectively, F' is the larger of the fitness of the crossover of two parent individuals, μ_{\max} and μ_{\min} are the maximum and minimum values of the artificially specified degrees of certainty, such as $\mu_{\max} = 0.95$ and $\mu_{\min} = 0.2$.

```

INPUT: {Ex, En, He}, n,  $\mu_0$ 
OUTPUT:  $\{(x_1, \mu_0), \dots, (x_n, \mu_0)\}$ 
FOR  $i = 1$  to  $n$ 
   $En' = \text{RANDN}(En, He)$ 
   $x_i = Ex \pm En' \sqrt{-2\ln(\mu_0)}$ 
  drop  $(x_i, \mu_0)$ 

```

ALGORITHM 3: Y Condition Cloud Generator.

```

(1) Initialize the population
(2) Calculate fitness
(3) Select operation
(4) Cross
(4.1) Randomly generated or artificially specified degree of certainty  $\mu$ 
(4.2)  $Ex = F_f/F_f + F_m x_f + F_m/F_f + F_m x_m$  (1)
(4.3) En variable search range/  $c_1$ 
(4.4)  $He = En/c_2$ 
(4.5) Generate a pair of children by Algorithm 3
(5) Variation
(5.1) Ex takes the original individual
(5.2) En = variable search range/  $c_3$ 
(5.3)  $He = En/c_4$  (Note:  $c_{1-4}$  is the control coefficient)
(5.4) Execute Algorithm 1, and generate a random number Temp, when  $\mu > \text{Temp}$ , update the individual (6) Go to (2) until the stopping condition is met

```

ALGORITHM 4: Cloud Genetic Algorithm.

Algorithm 6. Randomness X Conditional Cloud Generator Method

$$\begin{aligned}
 Ex &= F_{\max}, \\
 En &= \frac{(F_{\max} - F_{\min})}{c_5}, \\
 He &= \frac{En}{c_6}, \\
 En' &= \text{RANDN}(En, He), \\
 \mu &= e^{-(F' - Ex)^2 / 2(En')^2}.
 \end{aligned} \tag{2}$$

According to Algorithms 5 and 6, individuals with greater fitness have a narrower search range, which is conducive to protecting the pattern of better individuals; at the same time, the individual with the largest fitness has a certainty of 1, and the two subindividuals generated after the crossover operation are both Ex in formula (1), which is not conducive to population diversity. To this end, we add a constraint: when $\mu \geq 0.95$, $\mu = 0.95$. In order to protect the optimal individual, we introduce an optimal retention strategy in the selection operation. According to the “3 σ ” rule, c_5 takes a value slightly less than 3, and we take $c_5 = 2.8$. At the same time, it is suggested that $5 \leq c_6 \leq 15$, we take $c_6 = 10$.

3.3.2. *En and He.* The larger the En, the larger the horizontal width of cloud coverage so that the individual search range is larger during crossover and mutation operations. According to the “3 σ ” rule, combined with the speed and accuracy of the evolutionary algorithm, $6 \leq c_{13} \leq 3 \times p$ (p is the population size) in Algorithm 4 is recommended. As the evolutionary algebra increases, a larger value can be taken [18]. If the He is too large, the “stable tendency” will be lost to a certain extent; if the He is too small, the “randomness” will be lost to a certain extent. It is recommended that $c_{2,4}$ be within the range of 5 to 15.

At the same time, in order to expand the search range in the early stage of evolution and improve the search accuracy in the later stage of evolution, parameters can be adaptively and dynamically adjusted according to algebra and fitness. For example, c_{1-4} is given by the sigmoid function or linear function (monotonically increasing) of evolutionary algebra while overcoming the inconvenience of artificial specification. Although En and He are important parameters of the cloud model, in CGA, changes in both can produce the same evolutionary results through changes in Ex and certainty. Therefore, after several generations of evolution, the randomness of Ex and certainty partially masks the difference in evolutionary results caused by their different values [19]. Therefore, different values of c_{1-4} within a certain range will not have a significant impact on the final evolutionary performance, but evolutionary differences may always exist, so

TABLE 1: Performance comparison of CGA with NQGA and CAGA.

Function	Reference	Best value			Average value			Mean algebra		
		NQGA	CAGA	CGA	NQGA	CAGA	CGA	NQGA	CAGA	CGA
F1	0	$8.1080e-005$	$4.3368e-017$	$1.3147e-009$	0.000527	$4.3368e-017$	$1.4949e-007$	17.80	26.13	3.60
F2	0	0.00003541	$6.3056e-012$	$9.6253e-009$	0.00043370	$3.4925e-011$	$2.5749e-008$	67.89	161.70	39.97
F3	3	3.000121	3.000000	3.000000	3.00058551	3.000000	3.000000	190.13	75.5	40.43
F4	0	$1.8627e-005$	$1.1369e-012$	$2.2204e-016$	0.00024215	$1.7896e-06$	$1.3174e-007$	329.13	535.80	80.23
F5	-1.0316	1.031581	-1.031628	-1.031628	-1.0313833	-1.031628	-1.031628	79.82	83.54	57.43

TABLE 2: Performance comparison of GA, LARES, CAGA, and CGA.

Function	Reference	Best value				Average value			Mean algebra	
		GA	LARES	CAGA	CGA	CAGA	CGA	CAGA	CGA	
F2	0	0.00103	0.00051	$6.3056e-012$	$9.6253e-009$	$3.49251e-011$	$2.5749e-008$	161.70	39.96	
F3	3	3.03713	3.00000	3.00000	3.00000	3.00000	3.00000	75.5	40.43	
F6	0.998	1.24888	1.13103	0.998004	0.998004	0.998004	0.998004	116.2	109.83	
F7	0	9.423925	0.00032	$5.9009e-004$	$8.9394e-006$	$7.4938e-004$	$1.4909e-005$	41015.62	37249.8	
F8	7	7.00144	7.00064	7.00000	7.00000	7.00000	7.00000	19.18	19.37	
F9	-186.73	-185.588	-186.604	-186.7309	-186.7309	-186.6914	-186.6267	8663.4	8906.53	
F10	1	1.00559	1.00786	1.00000	1	1.00150	1.000584	7374.9	2482.37	
F11	0	0.01058	0.00247	$2.4399e-009$	$1.4891e-010$	$3.6361e-007$	$5.8789e-009$	987.2	526.1	
F12	0	0.00079	0.00064	$2.3842e-006$	$3.4605e-005$	$2.3842e-006$	0.00014	340.9	10746.37	
F13	0	0.00153	0.00153	$1.1921e-005$	$4.1921e-005$	$1.1921e-005$	0.00013	194.7	10642.73	
F14	0	0	0	$1.7217e-019$	$1.1809e-017$	$3.3200e-017$	$2.5825e-017$	23.6	77.67	
F15	0	0.19275	0.08927	0.15315	$3.5051e-008$	0.19605	0.01170	200000	170477.1	
F16	0	14.53298	4.9654	3.28032	$5.1994e-007$	8.40576	$1.8529e-006$	200000	15027.3	

the selection of parameters requires further research in the future. The author's experiment takes $c_{1,3} = 3 * p$, $c_{2,4} = 10$.

4. Results Analysis

4.1. Typical Electric Power Function Optimization. 16 typical functions are used for electric power function optimization experiments. F1–F5 are used to verify the new quantum genetic algorithm (NQGA) proposed by the author, and F2, F3, F6–F16 are used to verify the LARES algorithm proposed by the author. At the same time, it is compared with the cloud adaptive genetic algorithm (CAGA) proposed for edge cloud joint resource allocation based on ant colony optimization and the genetic algorithm [20].

The comparison between F1–F5 and NQGA is shown in Table 1 (100 independent experiments), and the comparison between F2, F3, F7–F14, and the LARES algorithm (30 independent experiments) and the results are shown in Table 2. Table 1 shows the optimization results of the NQGA algorithm, and Table 2 shows the optimization results of the GA and LARES algorithms. The average algebra refers to the difference between the current optimal fitness and the reference optimal fitness, which is less than the average of multiple independent experiments of evolutionary algebra at 10^{-3} [21].

CGA uses a population-based variation of the system and method of homogeneity and randomization of weather patterns [22]. The stability tendency can protect the better individuals and realize the adaptive positioning of the optimal value. The stochastic performance preserves individual diversity, which improves the ability of the algorithm to

prevent falling into local extremum, and enables CGA to better maintain the balance between exploration and production. CGA can control “research” and “control”. As can be observed from Tables 1 and 2, CGA significantly outperforms NQGA and LARES algorithms in evolution speed, robustness, and ability to avoid getting stuck in local optima [23]. Since both NQGA and LARES algorithms outperform the traditional GA, improved genetic algorithm (IGA), and optimal preserving genetic algorithm (OMGA), CGA is better than GA, IGA, and OMGA. Compared with CAGA, CGA achieves better accuracy for the rest of the functions except for the average solution accuracy of F1, F2, F9, F12, and F13. Except for F8 and F12–F14, the convergence speed of CGA for other functions is significantly faster than that of CAGA. Therefore, the overall performance of CGA is better than that of CAGA [24].

4.2. IIR Digital Filter Optimization Design. The following uses CGA to directly optimize the design of the IIR digital filter in the frequency domain.

The IIR digital filter adopts the cascade structure of the second-order section, that is, the following formula:

$$H(z) = A \prod_{k=1}^N \frac{1 + a_k z^{-1} + b_k z^{-2}}{1 + c_k z^{-1} + d_k z^{-2}}. \quad (3)$$

Example 1. Design a 6th-order band-pass IIR digital filter with the following formula:

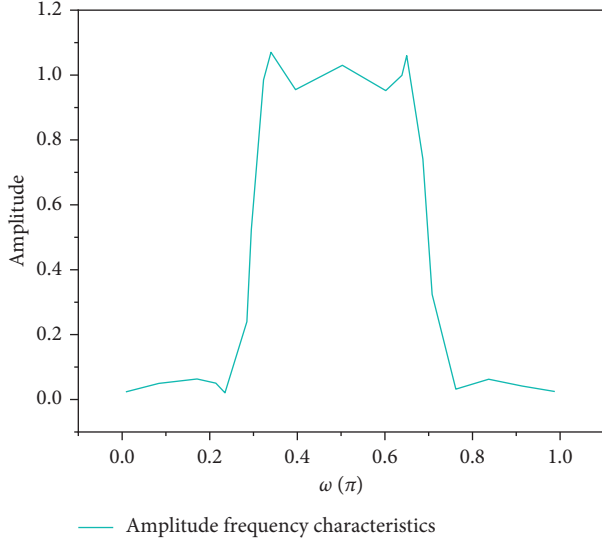


FIGURE 2: Amplitude-frequency characteristic of the IIR digital filter.

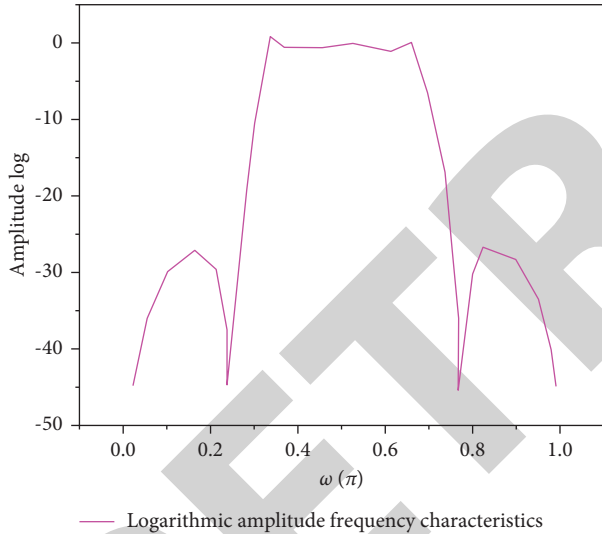


FIGURE 3: Logarithmic amplitude-frequency characteristics of the IIR digital filter.

$$\left| H_d e^{j\omega} \right| = \begin{cases} 0, & 0 \leq \omega \leq 0.28\pi, 0.72\pi \leq \omega \leq \pi, \\ 1, & 0.32\pi \leq \omega \leq 0.68\pi. \end{cases} \quad (4)$$

The IIR digital filter designed by CGA is shown in formula (5), and its frequency response is shown in Figures 2 and 3.

$$H(z) = 0.12116 \times \frac{1 + 1.4745z^{-1} + z^{-2}}{1 - 0.94906z^{-1} + 0.83404z^{-2}} \times \frac{1 - 1.4731z^{-1} + z^{-2}}{1 - 0.00073464z^{-1} + 0.45374z^{-2}}. \quad (5)$$

Table 3 compares the performance of CGA with the other four algorithms. As can be observed from Table 3, the

TABLE 3: Filter performance of each algorithm design.

Algorithm	OMGA	IGA	Iqga	NQGA	CGA
Ap/dB	0.647	0.5764	0.732	0.3546	0.342
As/dB	24.00	31.23	28.395	33.58	34.27

IIR digital filter designed by CGA has the smallest passband maximum fluctuation (Ap) of 0.342 and the largest stopband minimum attenuation (As) of 34.27, which shows that the overall performance is better [25].

5. Conclusion

The author uses the randomness and stable tendency of cloud droplets of the normal cloud model, combined with the idea of crossover and mutation of the genetic algorithm, the cross operation is realized by the cloud model's Y-condition cloud generation algorithm, the basic cloud generator algorithm realizes the mutation operation, and the evolution process is skillfully completed, and a new cloud genetic algorithm is proposed. CGA utilizes the advantages of cloud structure to create security, randomness, and population-based transformations. One way to better sustainability is to protect people, be aware of the changing nature of the best value, and preserve self-diversity, thus improving the process's ability against local rates. Population-based changes in integrated processes, some of the most common weather patterns, have resulted in strong research in small communities and people with small-scale research in large communities. Therefore, CGA can better maintain the balance between "exploration" and "mining" and has better search performance. Through the electric power function optimization experiment, it can be observed that the CGA algorithm is not only feasible but also outperforms GA, IGA, OMGA, NQGA, LARES, and CAGA. Not only the evolutionary generation is small, the evolution speed is improved, but the ability to obtain the optimal value is also strong, and the average value of multiple experiments is closer to the optimal value, so it has better robustness. The results of the optimal design of the IIR digital filter also prove that the algorithm has good application value. Subsequent work has focused on theoretical evidence of algorithmic integration, parametric analysis, algorithm improvement, and other applications of engineering optimization.

Data Availability

The data used to support the findings of this study are available from the corresponding author upon request.

Conflicts of Interest

The author declares that there are no conflicts of interest.

References

- [1] L. Shen and G. Zhang, "Optimization design of civil engineering construction schedule based on genetic algorithm," *Journal of Physics: Conference Series*, vol. 1852, no. 3, Article ID 032055, 8 pages, 2021.

Retraction

Retracted: Precise Positioning of Redundant Robot Motion Energy-Saving Control Based on Sensing Technology

International Transactions on Electrical Energy Systems

Received 3 October 2023; Accepted 3 October 2023; Published 4 October 2023

Copyright © 2023 International Transactions on Electrical Energy Systems. This is an open access article distributed under the Creative Commons Attribution License, which permits unrestricted use, distribution, and reproduction in any medium, provided the original work is properly cited.

This article has been retracted by Hindawi following an investigation undertaken by the publisher [1]. This investigation has uncovered evidence of one or more of the following indicators of systematic manipulation of the publication process:

- (1) Discrepancies in scope
- (2) Discrepancies in the description of the research reported
- (3) Discrepancies between the availability of data and the research described
- (4) Inappropriate citations
- (5) Incoherent, meaningless and/or irrelevant content included in the article
- (6) Peer-review manipulation

The presence of these indicators undermines our confidence in the integrity of the article's content and we cannot, therefore, vouch for its reliability. Please note that this notice is intended solely to alert readers that the content of this article is unreliable. We have not investigated whether authors were aware of or involved in the systematic manipulation of the publication process.

Wiley and Hindawi regrets that the usual quality checks did not identify these issues before publication and have since put additional measures in place to safeguard research integrity.

We wish to credit our own Research Integrity and Research Publishing teams and anonymous and named external researchers and research integrity experts for contributing to this investigation.

The corresponding author, as the representative of all authors, has been given the opportunity to register their agreement or disagreement to this retraction. We have kept a record of any response received.

References

- [1] Y. Lu, "Precise Positioning of Redundant Robot Motion Energy-Saving Control Based on Sensing Technology," *International Transactions on Electrical Energy Systems*, vol. 2022, Article ID 6367598, 8 pages, 2022.

Research Article

Precise Positioning of Redundant Robot Motion Energy-Saving Control Based on Sensing Technology

Yaping Lu 

Department of Mechanical and Industrial Robotics, Applied Technology College of Soochow University, Suzhou 215325, Jiangsu, China

Correspondence should be addressed to Yaping Lu; 11231549@stu.wxica.edu.cn

Received 12 July 2022; Revised 29 July 2022; Accepted 3 August 2022; Published 25 August 2022

Academic Editor: Nagamalai Vasimalai

Copyright © 2022 Yaping Lu. This is an open access article distributed under the Creative Commons Attribution License, which permits unrestricted use, distribution, and reproduction in any medium, provided the original work is properly cited.

In order to provide intelligent drinking water service for human beings, an intelligent indoor positioning water delivery system is proposed. The system can realize the functions of automatic filling water and so on. Based on the UP Squared processor, the system extends the UWB positioning Zigbee wireless transmission gyroscope manipulator and other functional modules. Based on the UP Squared processor, the system extends the UWB positioning Zigbee wireless transmission gyroscope manipulator and other functional modules. MPU6050 module was used to sense the rotation angle, and PID algorithm was used to control the rotation of redundant robot. The position of water cup is sensed based on current magnetic effect and electromagnetic induction law. Ultrasonic module is used to detect the rising height of the outlet and the water level in the cup. Several parameters of the system, such as orientation, distance adjustment, and power consumption, and the whole process of water delivery are tested through experiments. The experimental results show that the designed robot has a measurement accuracy of 1 cm, a total of static power of 5.35 W, and a total of dynamic power of 13.6 W. *Conclusion.* The system has the characteristics of accurate positioning, fast and smooth steering, and low power consumption, which can meet the technical requirements of practical application in indoor intelligent positioning water delivery.

1. Introduction

With the increasing popularity of indoor robot applications, the demand for high-precision and low-cost positioning system is increasing. UWB is a carrierless communication technology that transmits data through very narrow pulses (nanosecond or picosecond magnitude or less), enabling high temporal resolution when receiving or sending data. In general, high-precision positioning can be achieved through distance difference calculation, but, in practical applications, positioning errors and even errors often occur due to clock error, non-line-of-sight multipath, and other reasons [1]. Because of its own limitations, a single sensor is often unable to meet the changing environmental requirements and generally needs to be combined with other sensors for positioning.

However, as UWB applications have just begun to be commercialized in recent years, applications based on UWB positioning are mainly concentrated in low power

applications, which cannot meet the positioning requirements of indoor robots [2, 3]. The positioning requirements of indoor robots mainly include high-precision positioning data, relatively high positioning update frequency, low delay, a certain amount of positioning tag base station capacity, and ease of use and deployment. However, there is no mature UWB positioning system that can be applied in the field of indoor robot positioning.

In the process of acquiring UWB original location information, traditional methods based on bidirectional ranging, arrival angle, arrival time, difference arrival time, and so on cannot well meet the application scenarios of indoor robots. In view of the application of indoor robots, it is necessary to develop a set of requirements for high-precision networking communication and other functions. UWB technology can be used for communication, which can achieve other positioning functions such as visual laser radar inertial navigation that cannot be achieved.

Due to the existence of non-line-of-sight multipath and other factors, a single UWB positioning system under the interference of these conditions often needs to do a lot of optimization work before it can be applied in practical applications. It is of great significance to analyze the causes of these environmental interference factors to reduce the side effects brought by them. At the same time, a single sensor is often unable to meet the changeable environmental requirements due to its own limitations, and generally needs to be combined with other sensors for positioning. Through some algorithms, such as extended Kalman filter to combine UWB and AHRS navigation, it is of great significance to reduce the impact of interference on the environment, which is more conducive to the promotion of indoor robot positioning applications.

2. Literature Review

Bae et al. discussed IMU-based nonlinear vision detection and distance measurement combined with the EKF algorithm to reduce NLOS errors in the UWB environment [4]. Therefore, Li et al. and Zhang et al. developed the interior design space, a system based on a combination of INS and UWB. First, a standard error model has been developed for the combined navigation system INS and UWB, which includes the equivalent of INS and UWB. Based on the error model of the two sub-systems, the concept of heavy melting was prepared and the integrated navigation system was adjusted to the static state. The error system is stable within 20 cm [5,6]. To connect the 6th track, build assembly stations at the UWB base station. In the work of Zhang and Yan, the sun melts UWB and IMU data within EKF to improve the positioning accuracy of mobile robots in a nonlinear environment [7]. Therefore, Li, Z. proposed a pedestrian navigation algorithm combining UWB and INS. On the one hand, the location calculation was combined with the UWB-based state particulate filter algorithm, and, on the other hand, the INS-based zero-velocity correction algorithm was used to solve the data navigation. Within the error equation of the INERTIAL navigation system, a combination of the navigation data of the two systems is implemented. In an easy-to-walk environment, the average accuracy of UWB and INS is 53.8% higher than that of UWB alone and 40% higher than that of INS alone. Based on the stable walking distance of the household, the average location accuracy of UWB and INS is 39.7% higher than that of UWB alone and 37.5% higher than that of INS alone [8]. This unit integrates IMU and UWB and has an extended Kalman filter (EKF) and an odorless Kalman filter (UKF) to improve integration robustness and accuracy. In order to facilitate the transmission of the central station, the relationship between the geometric distribution of the base station and the actual attenuation is considered. The simulation results suggest that the preliminary data provided by the IMU may affect the error analysis of the UWB [9].

This course can be used to learn and develop knowledge of Internet-based home plumbing, which performs water placement, control, automatic filling, and other functions, and can be used for smart drinking water services in offices, hospitals, households, and other places.

3. Research Method

3.1. Overall System Framework. This paper adopts four mechanical modules driven by DC motors, and the water pouring module adopts mechanical arm to deliver water. The control system includes UP Squared processor, motor drive module STM32F103x (MCU), Zigbee wireless module, UWB positioning module, manipulator module, power supply, and voltage regulator system. Mechanical system includes transportation and water pouring system through the close cooperation of mechanical system and control system to ensure the stability of movement and functional reliability. The following steps are performed:

- (1) When the user needs the robot for service, he only needs to press the button switch and send the command to the UP Squared development board of the robot's general control center through wireless transmission of Zigbee module. The development board issues marching commands to start the robot and move forward. The auxiliary control of the robot is realized through the minimum module of MCU [10].
- (2) The robot relies on the UWB positioning module to monitor the positioning information in real time, identify the target location, and calculate the required rotation angle and travel distance to reach the target. Through the L298N module driving motor operation to achieve the robot forward and backward position adjustment and other operating state controls and through the MPU6050 module sensing forward angle, the forward direction is constantly adjusted.
- (3) When the robot reaches the target, it stops moving and uses the voltage of the magnetic coupling resonant coil to change with the space distance to achieve accurate positioning of the target water cup, so that the water outlet accurately aligns with the water cup and begins to discharge water. The water quantity of the cup is monitored in real time by ultrasonic rangefinder to ensure that the water in the cup will not overflow [11].
- (4) After the mission, the robot can return to its original position and wait.
- (5) When two or more targets send signals at the same time, the robot should respond respectively according to the time sequence of receiving signals to complete the water-pouring task.

The system scheme is shown in Figure 1.

3.2. UWB Module. The water delivery system must reach the position of the water cup quickly and accurately in order to realize the function of delivering water in a short time after receiving the water delivery request. Many common positioning methods do not meet the requirements.

Indoor environment is relatively complex, and infrared ranging positioning depth camera positioning and other

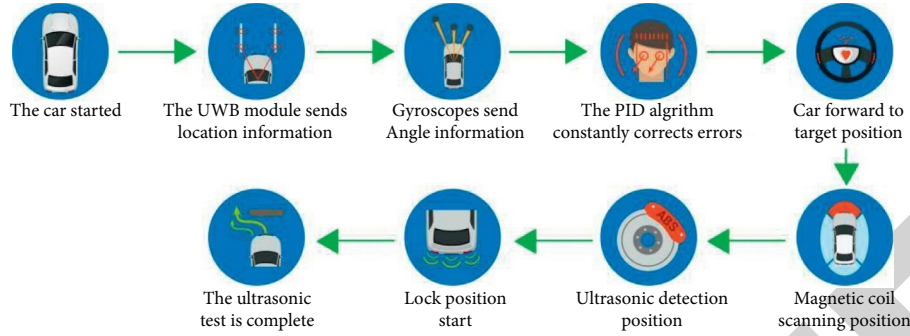


FIGURE 1: System work block diagram.

positioning methods do not have high accuracy. Moreover, the glass must be within the robot's visual range, but, in fact, due to the presence of factors such as shielding of indoor people's activities on the table, this condition is often not met.

- (1) Indoor positioning has high accuracy requirements. The accuracy of GPS, WIFI, Bluetooth, and other positioning methods is mostly at meter level, which cannot meet the requirements of high-precision positioning.
- (2) The signal transmission of Zigbee and other positioning modes is greatly affected by multipath effect and movement, and the accuracy depends greatly on hardware and environment.
- (3) The slow response of ultrasonic positioning will increase the working delay of the system.

The UWB positioning adopts very narrow pulse data transmission, fast data transmission speed, positioning accuracy up to centimeter level, and strong anti-interference ability and has the advantages of low power consumption and high security. It can better meet the requirements of the system, so we use UWB module in the system for positioning.

The DWM1000 chip is an ultrawideband wireless transceiver chip, which has stronger anti-interference ability against multipath weakness and can also carry out reliable communication in high weakness environment. It is very easy to integrate into real-time location system (RTLS) and wireless sensor network (WSN).

In this paper, the communication method using double-sided bidirectional ranging algorithm only needs 5 times of communication to measure the distance between the label and the three base stations.

3.3. Perception Principle of Angle of Target Direction. The movement of water supply system, such as forward, left turn, arc, and retreat, can be divided into two orthogonal parts, namely, straight and turn [12]. In fact, it solves the problem of the angle and direction that the robot needs to rotate to reach the target position.

3.3.1. Angle Measurement. In Figure 2, point A is the position of the starting point, and three points S_0 , S_1 , and S_2 correspond to three positioning base stations. Through UWB module for

ranging and positioning, the distance from the starting point to the third base station can be known. When the tag receives the signal from the target base station S_0 , the main controller controls the robot to travel a short distance in the initial direction to obtain the real-time position information of A. V_1 is the vector of the robot's forward direction, and V_2 is vector from real-time position to target point direction. Move V_2 to point A' for analysis, and then the angle that the robot needs to turn to the target point is the included angle θ of V_1 and V_2 [13]. The rotation angle of the robot can be calculated according to formula (1) under the condition that V_1 and V_2 are known:

$$\cos \theta = \frac{|\vec{v}_1 \cdot \vec{v}_2|}{|\vec{v}_1| \cdot |\vec{v}_2|}. \quad (1)$$

Figure out angle θ that the robot needs to turn.

3.3.2. Angle of Perception. After calculating the angle that the robot needs to turn, it also needs to tell the robot whether it should turn left or right. In the experiment, given vectors V_1 and V_2 with the same starting point, there are two cases:

- (1) When $\theta_1 > \theta_2$:
 - (a) When judgement condition is $\theta_1 - \theta_2 - \theta < 0.5^\circ$, we judge that $\theta_1 - \theta_2$ is the angle θ that the robot needs to turn, and the robot should turn right at this point.
 - (b) When $\theta_1 - \theta_2 - \theta > 0.5^\circ$, we judge that $\theta_1 - \theta_2$ is not the angle θ that the robot needs to turn, and the robot should turn left at this point.
- (2) When $\theta_2 > \theta_1$: it is contrary to the condition when $\theta_1 > \theta_2$. Because errors exist in label positioning, robot rotation control is not completely accurate; therefore, a single calculation may not allow the robot to accurately reach the target point [14]. Let the robot return to its rotation angle. When it is inconsistent with θ , the water supply system will constantly detect distance D between the real-time position (x_1, y_1) of the robot and the target point (x_2, y_2) , as shown in the following formula:

$$D = \sqrt{(x_2 - x_1)^2 + (y_2 - y_1)^2}. \quad (2)$$

When the minimum distance between the robot and the target point is less than 10 cm, the robot is stopped; that is, it

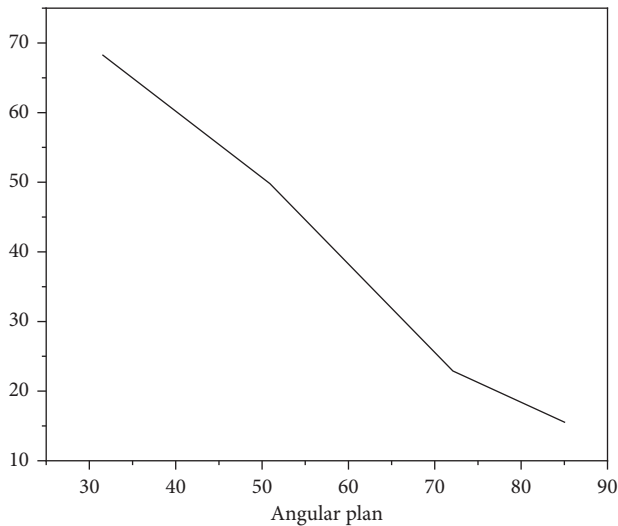


FIGURE 2: Angular plan.

is regarded as reaching the end point. If the minimum distance between the robot and the target point is greater than 10 cm, angle calculation and angle perception need to be conducted again after the robot stops. After obtaining a new angle, the robot moves forward until it reaches the destination [15]. Through this algorithm, the precision of robot addressing is greatly improved.

3.4. Direction Adjustment Algorithm. Through the calculation of the angle perception of the target direction, the direction that the robot needs to adjust is obtained. Next, the MPU6050 module is used to detect the angle of the robot rotation. The rotating speed of the robot is related to the energy output of the power supply. The situation when the power supply energy drops is different from that when the power is full, but the simple control strategy is prone to long rotation time or system shock. Therefore, we use PID control to improve the anti-interference ability of rotation process.

PID control is controlled according to Proportional Integral Differential of the deviation. In this system, the accumulation of errors is small, and there is no need to predict the arrival of the difference in advance to advance the response, so the scaling coefficient is mainly set [16]. By testing the system response under different proportions of parameters, the appropriate parameters are selected.

3.5. Precise Positioning of Outlet. After the water delivery system reaches the water cup accurately, it needs to accurately control the outlet valve to the top of the cup mouth. Considering the stability of the system, this paper adopts the magnetic coupling resonant radio transmission device for precise positioning. The main components of the magnetic coupling resonant radio transmission device include the following:

- (1) Magnetic coupling resonance section: The resonant body is composed of resonant capacitor in series by

the resonant coil, and the transmitting and receiving coils generate and receive magnetic field energy, respectively, which is the coupling medium of circuit and magnetic field. Transmitting coil adopts 1.3 mm enameled wire, cylindrical winding method $N=3$ turns, diameter is 10 cm, and receiving coil and transmitting coil size winding method is completely consistent, to ensure that the natural frequency of receiving and transmitting coil is consistent [17]. Increasing the resonance frequency and mutual inductance between the two coils can effectively improve the transmission efficiency, but the increase of the resonance frequency and the increase of the coil diameter and the number of turns will bring about great coil loss resistance, affecting the transmission efficiency. Therefore, it is necessary to increase the coil diameter and reduce the number of turns. Under the condition that the inductance of the coil remains unchanged, this method can improve the transmission efficiency more effectively than increasing the coil turns and reducing the diameter. Finally, the resonant frequency is determined at 1.3 MHz.

- (2) Magnetic field drive source: Including power supply and high frequency excitation circuit, the function of this part is to convert the DIRECT current of the DC power supply into the high frequency current in the coil, which is used to drive the magnetic coupling resonant part to generate resonant magnetic field and provide high-frequency energy to achieve radio transmission.

We designed an excitation coil placed below the water cup and fed it with pulse signals to stimulate the changing magnetic field in the surrounding space. An induction coil was placed near the water outlet of the robot, and the peak voltage in the coil was detected at the control end [18]. When the robot arrives at the specified position, the stepper motor can be first controlled to find the maximum angle of the emf peak value of the induction coil in a horizontal plane. It can be foreseen that this direction is the direction of the excitation coil. Then control the outlet vertical rise appropriate distance; control the stepper motor to move the water outlet to the direction of the excitation coil until the induction coil peak value reaches the maximum; at this time the water outlet will accurately reach the top of the water cup.

3.6. HC-SR04 Module Realizes Water Injection Control. In addition to accurately finding the position of the cup in the horizontal plane, it is also necessary to control the appropriate distance of the outlet rise in the vertical plane and complete the perception of the water level in the cup. The method of ultrasonic ranging is used in the experiment. The principle of ultrasonic ranging is to use the transmission speed of ultrasonic wave in the air as known, measure the time when the sound wave meets the obstacle after transmitting, and calculate the actual distance from the transmitting point to the obstacle according to the time difference between transmitting and receiving [19].

Ultrasonic ranging module HC-SR04 has the advantages of stable performance, accurate measurement distance, high-precision module, small blind area, and so on. It is widely used in the field of public security object ranging. The ranging steps are as follows:

- (1) IO port is used to trigger ranging, and a high level signal of 10 is issued at the control port.
- (2) The module automatically sends 8 40 kHz square waves and automatically detects whether there is a signal returned.
- (3) If a signal is returned, a high level is output through the IO port. The duration of the high level is the time from the transmission to the return of the ultrasonic wave.
- (4) When a signal returns, the timer is used to time the signal, and the value of the timer can be read when the receiver interface becomes low level. The distance can be calculated by obtaining the ranging time. Constant test can reach the value of the moving measurement.

The key to going up the right distance in the vertical plane is what does the feed system perceive as the right position. After analysis, it is found that when the height of the outlet has not exceeded the cup, there is a solid medium near the front of the outlet (cup). When the height exceeds the mouth of the cup, solid medium (wall) begins to appear in the far front of the outlet. Therefore, we can place an ultrasonic ranging module near the water outlet and stop rising after the distance exceeds the threshold value by setting a reasonable distance threshold value.

After the outlet reaches the specified position, control the relay. Start the water outlet. When the ultrasonic module detects that the water level in the cup reaches an appropriate position, a signal is uploaded to the controller to stop the water outlet and complete the corresponding work.

3.7. Zigbee Communication Module Data Interaction.

After pressing the button of the pager, the intelligent indoor positioning water delivery system receives the water pouring request and starts to work. Because not all indoor environments are covered with WIFI signals, Bluetooth transmission is limited by distance and is vulnerable to interference, so Zigbee communication module with simple networking and long transmission distance is used for wireless data transmission. DL-20 wireless transmitting and receiving module is a wireless serial module based on Zigbee technology, which can connect two or more serial ports in wireless state to configure DL-20 module in point-to-point mode. Point-to-point mode has two data transfer ports: A end and B end. Data sent by the serial port A end is received by the serial port at the B end, and vice versa. In point-to-point mode, only two nodes on a channel can communicate with each other.

In the process of data transmission, transparent transmission mode is adopted. The user only needs to encapsulate the data according to the Zigbee protocol frame format and

then send the data once. Finally, the data is received in sequence at the receiving end. In practical application, the baud rate is 9600, and two Zigbee communication modules are installed on the pager and robot, respectively.

4. Interpretation of Result

Intelligent indoor positioning water delivery system requires accurate positioning, strong adaptability to complex environment, and rapid and accurate angle adjustment and can better adapt to the change of induction coil in the moving experiment. The following parts are tested.

4.1. UWB Positioning Accuracy Test. In order to test the accuracy of UWB module in environments of different complexity levels, we conducted intensive reading tests in empty classrooms and classrooms with lots of shelters, such as desks and chairs. The specific methods are as follows:

- (1) After the base station was arranged, 6 points were randomly selected indoors.
- (2) Meter ruler was used to measure the distance between these points and base station 0, and the mean value was measured for three times, which was approximately regarded as the standard distance between point and base station 0.
- (3) Place label 0 at each of the six points.
- (4) At each point, the distance between the label and the base station is continuously measured 10 times.
- (5) The error is represented by the mean of the difference between the measured data and the standard distance [20].

We found that the distance between the base station and the tag had no significant influence on the ranging accuracy, and the data error obtained by each measurement was within 10 cm. The error of ranging in complex environment is slightly higher than that in open environment, but it can still ensure high measurement accuracy. After taking the average value of the measurement for many times, the direction finding error is reduced to less than 1%, which can meet the requirements of the system for accuracy.

This is determined by the fact that UWB relies on very narrow pulses to transmit data. Theoretically, after passing through obstacles such as desks, narrow pulses will not produce significant attenuation. Therefore, even if there are many obstacles in the environment, the impact on the ranging accuracy is very small, which is consistent with our test results.

4.2. Direction Adjustment Algorithm Test. For reasonable PID parameter selection, while improving the rotation speed of the robot, the system should have good stability, that is, low shock degree, and strong adaptability when the power energy changes, that is, always have good reaction speed and high stability.

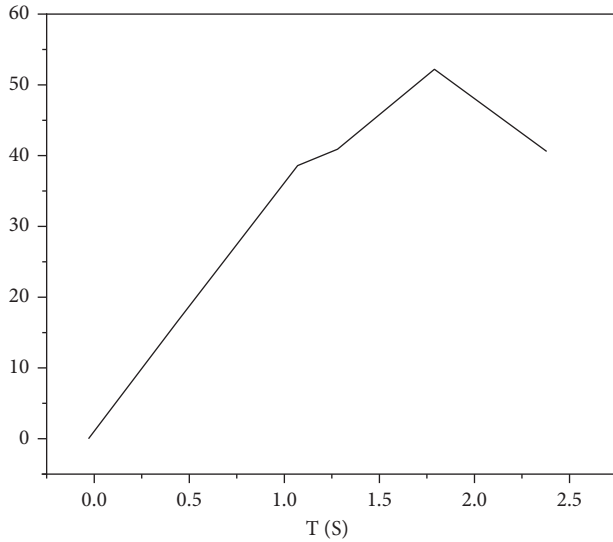


FIGURE 3: PID test data in the format of 1000-4.

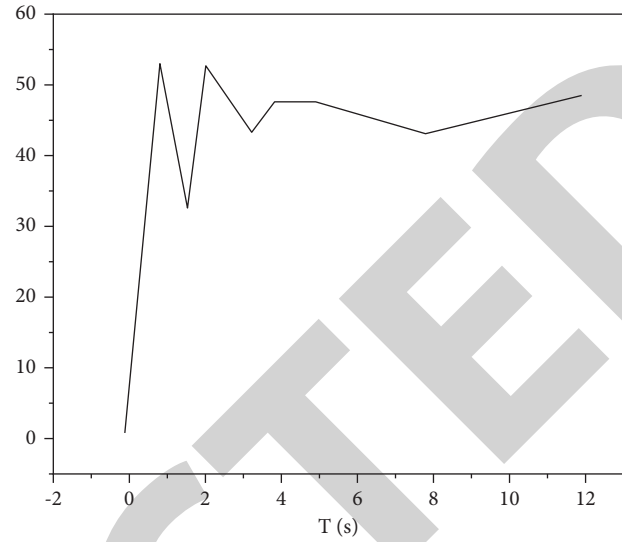


FIGURE 4: PID test data in the format of 1200-4.

Set the robot rotation target to 45, control the robot rotation, and upload the robot rotation angle to the control end in real time through the serial port. The angle changes obtained by different PID parameters were plotted into curves. After repeated tests, the curves obtained by selecting the best parameters are shown in Figures 3–5.

The first parameter of PID represents the overall speed of the system. The second parameter indicates the speed of response to instructions. After analysis, the overall speed of the first measurement is high, but the response time is long, the system vibration is serious, and the time to reach stability is long. The second group had less oscillation after the overall speed was going down. In the third group, after the overall speed is reduced, the oscillation is eliminated, so the parameters of the third group are more reasonable. PID parameters set after multiple attempts can make robots have quicker reaction while keeping the stable status. Moreover, it has strong adaptability under different power sources.

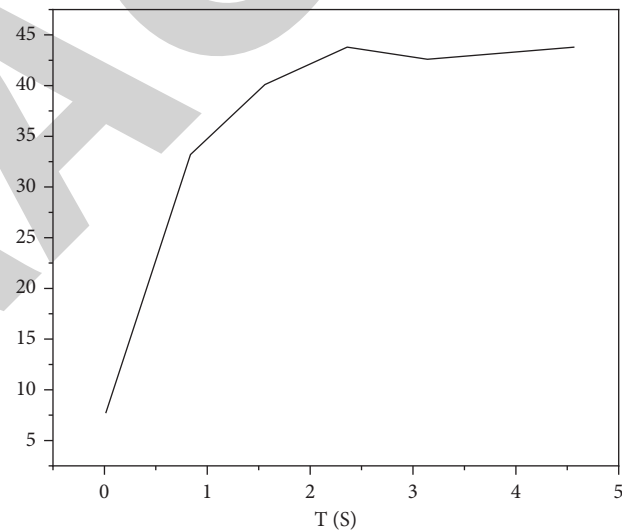


FIGURE 5: PID test data in the format of 1500-5.

4.3. Accurate Positioning Test of Outlet. In this paper, the extreme value of the induced electromotive force in the induction coil is used to determine the relative position of the water cup and the water outlet, which requires the obvious existence of the extreme value of the induced electromotive force and low detection delay.

Move the induction coil in horizontal plane and vertical plane respectively, and read the electromotive force in the induction coil, draw it into a curve, and observe the extreme value.

Because of the response delay, it is not easy to detect directly, so we detect the difference between the position of the electromotive force extreme value in the induction coil read by the system and the theoretical position, so as to describe the response delay of the system indirectly. The induction coil rotates at different angles in the

horizontal plane, and the output voltage value obtained is shown in Figure 6. There is a voltage peak value at the position nearest to the transmitting coil, and its induction voltage value is the maximum.

HC-SR04 ultrasonic ranging module can provide 2~400 cm noncontact distance sensing function; the measurement accuracy can reach 3 mm. By analyzing the above measurement results, it can be concluded that the measurement accuracy of the ultrasonic ranging module used by the designed robot is 1 cm.

According to the power test of each module, the static power is mainly concentrated in the UP Squared processor, but the overall power is relatively low, with a total of 5.35 W, and the dynamic power is 13.6 W, about 2.5 times of the static power. It is found that the robot consumes very little power under static condition and can support data

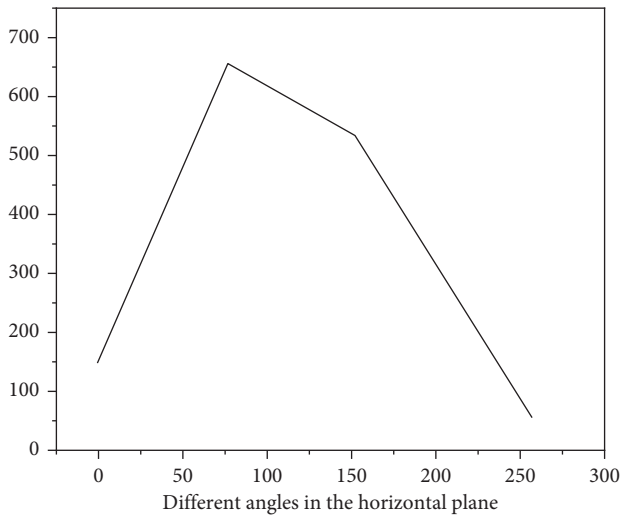


FIGURE 6: Induction electromotive force test data.

monitoring for a long time. It also has good endurance in cruise pouring mode.

5. Conclusion

The system designed in this paper uses Zigbee module to carry out data interaction between the pager and the robot; UWB module is used for precise positioning indoors. MPU6050 module is used to sense the rotation angle, and PID algorithm is used to control the rotation of the robot; the position of water cup is sensed based on current magnetic effect and electromagnetic induction law; ultrasonic module is used to detect the rising height of the outlet and the water level in the cup. It can well realize the two functions of water transport and water pouring, and the stability of the positioning accuracy movement and the reliability of the function have been well guaranteed; the function of intelligent indoor positioning water delivery is fully realized, to meet the technical requirements of practical application in indoor intelligent positioning water delivery.

Data Availability

The data used to support the findings of this study are available from the corresponding author upon request.

Conflicts of Interest

The author declares that there are no conflicts of interest.

References

- [1] S. Li, S. Guo, J. Chen, X. Yang, and H. Yang, "Multiple targets localization behind l-shaped corner via uwb radar," *IEEE Transactions on Vehicular Technology*, vol. 70, no. 99, p. 1, 2021.
- [2] B. Biswas and A. Karmakar, "Electrical equivalent circuit modelling of various fractal inspired uwb antennas," *Frequenz*, vol. 75, no. 3-4, pp. 109–116, 2021.
- [3] D. Kalra, M. Kumar, A. Shukla, L. Singh, and Z. A. Jaffery, "Design analysis of inductorless active loaded low power uwb lna using noise cancellation technique," *Frequenz*, vol. 74, no. 3-4, pp. 137–144, 2020.
- [4] J. Bae, H. W. Kim, I. H. Kang, and J. Kim, "Dual-field plated β -Ga₂O₃ nano-FETs with an off-state breakdown voltage exceeding 400 V," *Journal of Materials Chemistry C*, vol. 8, no. 8, pp. 2687–2692, 2020.
- [5] Q. Li, Y. Sun, and H. Fang, "Compact acs-fed uwb mimo antenna with dual band notches," *Applied Computational Electromagnetics Society*, vol. 36, no. 1, pp. 55–60, 2021.
- [6] P. Zhang, X. Ren, and Z. Zhang, "An efficient self-motion scheme for redundant robot manipulators: a varying-gain neural self-motion approach," *Robotica*, vol. 39, no. 10, pp. 1897–1908, 2021.
- [7] Z. Zhang and Z. Yan, "An adaptive fuzzy recurrent neural network for solving the nonrepetitive motion problem of redundant robot manipulators," *IEEE Transactions on Fuzzy Systems*, vol. 28, no. 4, pp. 684–691, 2020.
- [8] Z. Li, F. Xu, D. Guo, P. Wang, and B. Yuan, "New p-type rmpc scheme for redundant robot manipulators in noisy environment," *Robotica*, vol. 38, no. 5, pp. 775–786, 2020.
- [9] W. Luo, L. Shi, W. Xu, W. Chen, Y. YangYang, and Y. Ren, "High gain dielectric resonance antenna array for millimeter wave vehicular wireless communication," *Progress In Electromagnetics Research C*, vol. 108, pp. 63–78, 2021.
- [10] J. Huang, C. X. Wang, H. Chang, J. Sun, and X. Gao, "Multi-frequency multi-scenario millimeter wave mimo channel measurements and modeling for b5g wireless communication systems," *IEEE Journal on Selected Areas in Communications*, vol. 38, no. 9, pp. 2010–2025, 2020.
- [11] G. Zhu, D. Liu, Y. Du, C. You, J. ZhangZhang, and K. Huang, "Toward an intelligent edge: wireless communication meets machine learning," *IEEE Communications Magazine*, vol. 58, no. 1, pp. 19–25, 2020.
- [12] J. B. Padhy and B. Patnaik, "Co-ofdm and dp-qpsk based dwdm optical wireless communication system," *Journal of Optical Communications*, vol. 42, no. 2, pp. 311–323, 2021.
- [13] J. YiYi, Z. W. Liu, and W. Q. Zeng, "Isothermal extrusion speed curve design for porthole die of hollow aluminium profile based on pid algorithm and finite element simulations," *Transactions of Nonferrous Metals Society of China*, vol. 31, no. 7, pp. 1939–1950, 2021.
- [14] J. Z. Shi, "A fractional order general type-2 fuzzy pid controller design algorithm," *IEEE Access*, vol. 8, pp. 52151–52172, 2020.
- [15] R. Huang and X. Yang, "Analysis and research hotspots of ceramic materials in textile application," *Journal of Ceramic Processing Research*, vol. 23, no. 3, pp. 312–319, 2022.
- [16] M. Fan and A. Sharma, "Design and implementation of construction cost prediction model based on svm and lssvm in industries 4.0," *International Journal of Intelligent Computing and Cybernetics*, vol. 14, no. 2, pp. 145–157, 2021.
- [17] J. Jayakumar, B. NagarajNagaraj, S. ChackoChacko, and P. Ajay, "Conceptual implementation of artificial intelligent based E-mobility controller in smart city environment," *Wireless Communications and Mobile Computing*, vol. 2021, pp. 1–8, 2021.
- [18] J. Chen, J. Liu, X. Liu, X. Xu, and F. Zhong, "Decomposition of toluene with a combined plasma photolysis (cpp) reactor: influence of uv irradiation and byproduct analysis," *Plasma*

Retraction

Retracted: Reconstruction and Utilization of Energy Economy Information Resources against Humanistic Background

International Transactions on Electrical Energy Systems

Received 19 September 2023; Accepted 19 September 2023; Published 20 September 2023

Copyright © 2023 International Transactions on Electrical Energy Systems. This is an open access article distributed under the Creative Commons Attribution License, which permits unrestricted use, distribution, and reproduction in any medium, provided the original work is properly cited.

This article has been retracted by Hindawi following an investigation undertaken by the publisher [1]. This investigation has uncovered evidence of one or more of the following indicators of systematic manipulation of the publication process:

- (1) Discrepancies in scope
- (2) Discrepancies in the description of the research reported
- (3) Discrepancies between the availability of data and the research described
- (4) Inappropriate citations
- (5) Incoherent, meaningless and/or irrelevant content included in the article
- (6) Peer-review manipulation

The presence of these indicators undermines our confidence in the integrity of the article's content and we cannot, therefore, vouch for its reliability. Please note that this notice is intended solely to alert readers that the content of this article is unreliable. We have not investigated whether authors were aware of or involved in the systematic manipulation of the publication process.

Wiley and Hindawi regrets that the usual quality checks did not identify these issues before publication and have since put additional measures in place to safeguard research integrity.

We wish to credit our own Research Integrity and Research Publishing teams and anonymous and named external researchers and research integrity experts for contributing to this investigation.

The corresponding author, as the representative of all authors, has been given the opportunity to register their agreement or disagreement to this retraction. We have kept a record of any response received.

References

- [1] L. Du, "Reconstruction and Utilization of Energy Economy Information Resources against Humanistic Background," *International Transactions on Electrical Energy Systems*, vol. 2022, Article ID 2301322, 7 pages, 2022.

Research Article

Reconstruction and Utilization of Energy Economy Information Resources against Humanistic Background

Lan Du 

Dazhou Vocational and Technical College, Dazhou 635001, Sichuan, China

Correspondence should be addressed to Lan Du; 1700210525@stu.sqxy.edu.cn

Received 14 July 2022; Revised 29 July 2022; Accepted 3 August 2022; Published 25 August 2022

Academic Editor: Nagamalai Vasimalai

Copyright © 2022 Lan Du. This is an open access article distributed under the Creative Commons Attribution License, which permits unrestricted use, distribution, and reproduction in any medium, provided the original work is properly cited.

In order to explore the problem of reconstruction of energy economic information resources, the author proposes a reconstruction of energy economic information resources based on the background of digital humanities. This method recommends key technical problems and solutions based on information represented by the digital humanities background and explores research on the reconstruction of economic information resources. The research has shown that the reconstruction of energy and economic information resources based on the background of digital humanities is about 30% more efficient than traditional methods. The concept of sustainable energy development is a continuation of the concept of “sustainable development,” emphasizing the improvement of energy efficiency and using it as a way to improve overall economic efficiency and reduce energy-related environmental costs, so that economic development will not harm the environment, and future generations have equal opportunities for development.

1. Introduction

At the turn of the century, mankind is undergoing an industrial revolution that fundamentally changes the way of production, working, life, and learning [1]. In the future, the focus of competition in the world economy will be on the emerging information industry, because it not only is a new bright spot in the economic development of various countries, but also will become a new driving force for sustainable economic development through integration with traditional industries [2]. The ever-changing information technology has made the economic development of all countries in the world more closely linked. The flow of information resources that breaks the limitations of time and space makes the progress and development of human society closely related [3].

Resources are divided into social resources and natural resources [4]. Social resources include manpower, knowledge, information, science, and technology, as well as accumulated capital and social wealth. Their greatest feature is variability. Natural resources include natural environment, land, forests, grasslands, precipitation, rivers, lakes, energy, and minerals. Their essential feature is being limited.

In nature, any form of material that can be provided to human life and production needs can be called a natural resource, and it is the basis for human survival [5]. For example, solar radiation, atmosphere, water, organisms, land, various minerals, and energy are natural resources [6]. Those that have economic value to human life and production are called natural resources; for example, at a conference held by the United Nations Environment Programme in Kenya, natural resources were defined as “resources that can generate economic value under certain time and space conditions to improve human beings, elements and conditions of the natural environment for present and future well-being.” With the development of human society and the progress of technology and economy, human beings continue to expand the scope of resource utilization and continue to seek and develop new resources to meet their growing needs.

Agile manufacturing is an enterprise that adapts to the rapidly changing market needs, being the enterprise model strategy chosen for maximum competitiveness [7].

In modern enterprises, the bridge between the two is the economic information related to the enterprise, so the information becomes an important resource for managing the

enterprise [8]. On the other hand, the revolution of information technology has made a huge impact on modern enterprises, and technological innovation will inevitably lead to organizational innovation, including the emergence of a series of new production management systems such as real-time manufacturing systems and flexible production systems, as shown in Figure 1.

2. Literature Review

Okafor et al. said that at present all countries in the world attach great importance to the development of advanced manufacturing technology and related production model technologies, and many multinational companies have applied them to achieve the integration of design, manufacturing, marketing, and after-sales service, strengthening the monopoly in the international market [9]. According to Sindi, in the development of Boeing 777 airliner, due to the use of advanced product development and design technology [10], the development cycle was shortened by more than 40% from the past 8 to 9 years to 4.5 years, the cost was reduced by 25%, the error rework rate was reduced by 75%, and the user satisfaction was also greatly improved. Hou stated that, by applying modern integrated manufacturing system technology, the car development cycle has been shortened from the original 48 months to 24 months, the number of crash tests has been reduced from the original hundreds to dozens, and the application of e-commerce technology has reduced the cost of sales by 10% [11]. Fu mentioned that, after the application of advanced comprehensive automation technology, the enterprise benefit was increased by 5% to 8%, and the labor productivity was increased by 10% to 15% [12].

The core technology of robotics and automation process equipment has always been valued by countries all over the world. Special robots such as underwater robots, micro robots, medical robots, and human-injuring robots for future services; ultraprecision machining equipment for national defense, aviation, and aerospace; intelligent large-scale construction machinery for infrastructure construction; and high-precision, high-efficiency, low-cost, and high-flexibility basic manufacturing equipment for manufacturing have become the focus of current international manufacturing research and development.

Since the 1990s, the process of globalization has accelerated significantly, and it has become the most prominent feature of today's world. Erdoğan et al. believe that there is currently no unified definition of the concept of "globalization" [13]. Ma et al. believe that the more popular ones come from authoritative institutions such as the International Monetary Fund (IMF) and some well-known Western scholars [14]. In an article published in the Spring 1998 issue of *Foreign Policy*, Harvard University economist Jeffrey Sachs argued that globalization has the following four levels of meaning: (1) promotion of faster economic growth; (2) impact on macroeconomic stability; (3) impact on income distribution; (4) impact on national and international politics. The above viewpoints are quite representative,

reflecting the understanding of the "orthodox" theory of Western scholars on globalization.

Today, the globalization of various sectors and activities of human economic society is driven by two forces: one is information technology, and the other is trade liberalization. Informatization and globalization are closely linked, and globalization in the nineteenth century was driven by falling transportation costs, and now it is driven by falling communication costs. With the rapid decline in the cost of communication and data processing and the natural barriers of time and space that divide countries' markets, inexpensive and efficient communication networks allow companies to locate different parts of their production process in different countries, while keeping the parts together in close contact. As described by Melnyk, exponentially increasing information and communication networks enable the establishment of various international and transnational networks and associations, which often lead to the formation of more substantive organizational structures and the huge flow of information resulting in thousands of global business enterprises, international organizations, and intergovernmental organizations [15].

The process of market exchange is the flow of people, money, goods, and information, so people's commercial exchange activities depend on the means of transportation and information transmission. In a market economy, people make judgments and actions based on market information, and the degree, method, and scope of market information display and transmission directly affect the role of the market mechanism. When the information system is underdeveloped, the market as a whole must be a black box for individual subjects, and the subject's understanding of the market can only rely on perceptual, superficial, and fragmented and unsystematic understanding. This leads to the spontaneity of market regulation and the blindness and shortsightedness of the behavior of market players. That is, information technology makes the market more transparent and reduces the need for face-to-face contact between producers and consumers. Of course, market players must ultimately allocate resources rationally to ensure sustained and stable economic growth. This means that to realize the free flow of production factors in the market, especially in the international market, on the one hand, various institutional and artificial obstacles must be removed, and on the other hand, there must be technical guarantees. The development of the information industry has continuously opened up the possibility of realizing this kind of mobility in technology, making it adapt to the needs of the development of productive forces in modern society, enabling market entities to better actively adapt to changes in the market environment, and improving the ability to resist economic fluctuation risks.

3. Methods

3.1. The Game Theory Model of Agile Resource Selection. Based on taking manufacturing resource nodes as isolated individuals, many academic fields combine agent technology with game theory tools and use game models to describe

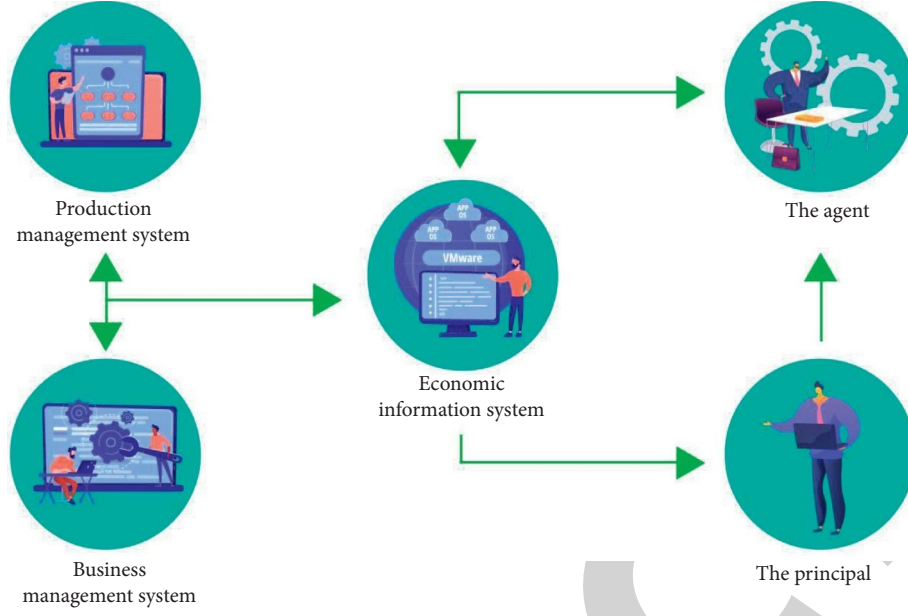


FIGURE 1: Economic information flow in modern enterprise management.

resource selection and reconstruction problems [16]. The basic concepts of game theory include players, actions, information, strategies, payoffs (utilities), outcomes, and equilibria, where players depend on choosing actions (or strategies) to maximize their level of payoffs (utility), the “rational man” hypothesis.

The division of game theory can be carried out from two different perspectives. The first perspective is the sequence of actions of the participants. From this point of view, the game can be divided into static game and dynamic game. The second angle of dividing the game is the player’s knowledge about the characteristics, strategic space, and payoff function of other players (opponents). From this perspective, the game can be divided into complete information game and incomplete information game. Combining the divisions of the two angles, we obtain four different types of games and their corresponding equilibrium concepts, as shown in Table 1.

For the convenience of studying the problem, think of resource reduction as a device or work center. The resource agent logically reconstructs local and remote resources according to the processing needs of subtasks, and the generated feasible strategy set is expressed as follows:

$$Fi = \left\{ Fi' : \delta' \leq 1 - \sum_{i \neq 1} \delta_{iki} \right\}, \quad (1)$$

where k is the resource index ($k = 1, \dots, M$), M is the total number of candidate resources, t is the time slot index ($t = 1, \dots, T$), and T is the number of planning cycles for task completion, as in the following equations:

$$\delta_{ikt} = 1, \text{ subtask } i \text{ is assigned to } k \text{ at time } t, \quad (2)$$

$$\delta_{ikt} = 0, \text{ other.} \quad (3)$$

The payout function is shown in the following equation:

$$ui = \left\{ u' : ui' = - \sum_{i=1}^r (\lambda_{ikt} + \pi_{ikt}) \right\}, \quad (4)$$

which is shown in the following equations:

$$\lambda_{ikt} = f(i, k), \quad (5)$$

$$\lambda_{ikt} = 0. \quad (6)$$

The unit transportation cost (T2, T3) from k to resource $k+1$ satisfy the equation (7)-Equation (10)

$$\delta_{dz} = 0, \quad (7)$$

$$t < t_1,$$

$$\delta_{dz} = 1, \text{ other,} \quad (8)$$

$$\delta_{i(k+1)t} = 0, \quad (9)$$

$$t < t_3,$$

$$\delta_{i(k+1)t} = 1, \text{ other.} \quad (10)$$

3.2. Evaluation Index System. A specific requirement M must be realized in a certain manufacturing system S [17]. If there is no enterprise alliance, the enterprise undertaking this task must be a specific enterprise in S , Sz , etc. or beyond the legal concept of enterprise; instead, it is a manufacturing subsystem constructed by some selected resource elements, such as the “independent manufacturing island” proposed by Zhang Shu Jiaotou of Tongji University. The ability of the corresponding manufacturing resources E , Ez , etc. to realize the requirement M can be evaluated and calculated from 7 indicators. The hierarchical structure of the elements is shown in Table 2 and Table 3.

TABLE 1: Types of games and their equilibria.

Information	Sequence of actions	Static	Dynamic
Full information		Complete information static game	Complete information dynamic game
Incomplete information		Incomplete information static game	Incomplete information dynamic game

TABLE 2: Structural layering.

Put into production/P		Production/S		Transport/r		Quality/Q
Time/T	Cost/C	Time/T	Quality/Q	Time/T	Cost/C	Quality/Q

The evaluation of manufacturing resources covers a wide range, far beyond these seven evaluation indicators; in practice, according to specific evaluation requirements, n evaluation indicators are set. The index system is layered, which is a classification mainly based on the degree of relevance and importance, and establishes a category relationship. The number of hierarchical layers will generally increase with the increase of indicators, and it can also be continuously expanded. In theory, it can also be extended to nondeterministic integer layers, such as n layers.

Since the cost index of quality compliance is a possible additional cost of quality compliance, which is different from the normal cost of production, it is taken out as an independent indicator [18]. The vector method establishes the agility evaluation of manufacturing resources; the original data must be accurately and quantitatively obtained from the objective reality of the manufacturing resources themselves; and most of them are reflected on the basis of time, cost, and other values that are easier to quantify and have units of measurement. They are difficult to conceptualize and descriptive indicators of manufacturing resources that require abstract judgment are used as raw data.

As can be seen in Table 4, the competitiveness of manufacturing subsystems covers a wide range, these seven evaluation indicators can be surpassed, n evaluation indicators are set according to specific evaluation requirements, n importance weights are assigned, and finally a more precise G value can be obtained. For a specific market demand, G is a relative index, reflecting the market competitiveness of each manufacturing subsystem in the manufacturing system. In the absence of network alliances, it reflects the agility and competitiveness of manufacturing enterprises; the closer G to 1, the stronger the ability of the enterprise to meet a certain market demand; if G is closer to 0, it shows that the company's ability to meet a certain market demand is weaker.

3.3. Energy Forecast. According to the period length of the energy forecast, it can be divided into long-term forecast, medium-term forecast, and short-term forecast [19]. Long-term energy forecasts are forecasts for long-term planning and strategic decision-making. The forecast period generally refers to 10 to 15 years or more. The results of long-term forecasts of supply and demand, while less precise or accurate, can raise extremely important strategic questions. Long-term energy forecasting is of great significance for

formulating long-term energy development plans, arranging energy construction projects in advance, and meeting social needs.

Medium-term energy forecast refers to the forecast of the development of energy supply and demand in the medium term, which serves for the formulation of medium-term planning and decision-making [20]. The forecast period is generally 5 to 10 years, and the accuracy of the mid-term energy forecast is higher than that of the long-term forecast, but the factors affecting energy supply and demand in the mid-term forecast are difficult to accurately grasp; therefore, energy supply and demand forecasts always come with various assumptions.

Short-term forecast of energy refers to the forecast of the development of energy supply and demand in the short term [21]. The forecast period is generally 1 year to 5 years. Such forecasts are the scientific basis for formulating five-year plans and annual plans. Because the forecast time is relatively short, the possible development and changes of the national economy are relatively clear, and the energy structure is unlikely to change greatly, the results of energy supply and demand forecasts need to have high precision or accuracy. This prediction result directly affects the current planning arrangement and has a direct guiding role for the development of energy and national economy.

Macro-energy forecast refers to the forecast of the energy supply and demand prospects of a country or region [22]. Macro-energy forecasting is to take the general blueprint of social and economic development as the object of investigation and predict the total demand and supply of energy. Sometimes, for a certain need, a specific energy product can be forecasted, such as forecasting the total demand and total supply of raw coal—for example, the various possibilities of the development of energy supply and demand and their impact, and the policies or decisions currently determined and to be implemented. When conducting qualitative energy prediction, it is mainly through the analysis of historical data and the study of future energy supply and demand conditions, with the forecaster's rich experience and logical reasoning ability, in order to speculate and judge the nature of energy supply and demand in the future.

Quantitative forecasting of energy refers to the determination of the future quantitative performance of energy supply and demand, such as the forecast of total energy production and total demand. Energy supply and demand forecasts are based on historical data, statistics, and other information; using mathematical or other analytical

TABLE 3: Element hierarchy.

Time/T			Cost/C			Quality/Q
Put into production/P	Production/S	Quality/Q	Put into production/P	Production/S	Transport/R	Quality/Q

TABLE 4: Two-layer weights.

Ap		As		Ay		Aq
At1	Ac1	At2	Ac2	At3	Ac3	Aq1
A1	A2	A3	A4	A5	A6	A7

techniques, build a model that can represent the quantitative relationship, and use it to calculate the quantity that energy supply and demand may represent in the future. Commonly used quantitative forecasting techniques include exponential smoothing forecasting method, unit output value and output energy consumption forecasting method, energy elasticity coefficient forecasting method, input-output forecasting method, sectoral analysis comprehensive forecasting method, and some other methods of econometrics [23].

Energy timing forecast refers to the determination of the future performance time of energy supply and demand, for example, the time when a new energy source (such as solar energy) can be applied to production, the time for product replacement, and the time for a certain decision to achieve the expected effect. Energy timing prediction generally relies on people's logical reasoning and judgment. Therefore, the methods applied to energy forecasting are mainly various survey analysis methods and analogy methods. The "growth" curve method can be used when making timed forecasts for the replacement of energy enterprises' products.

The target constraints of energy forecasting can be divided into normative forecasting and exploratory forecasting. The principle of the system means that when forecasting energy supply, we should regard energy supply and factors that affect energy supply, such as economic development, energy resources, transportation capacity, and ecological environment, as a system. We regard both the energy supply system and the energy demand system as having specific functions, a whole composed of elements that are organically connected to each other. Through comprehensive investigation and research, we propose alternative solutions to build predictive models. This way, it is possible to analyze the problem comprehensively, overcome one-sidedness, and improve the scientificity of prediction [24].

3.4. Theoretical Methods for Comprehensive Energy Forecasting. The grey forecasting method is a loose systematic method, which abandons the link of system structure analysis; by directly accumulating the original data of energy supply and demand, the overall law of the seeking system is generated, and an exponential growth model is constructed. This method can construct different prediction models according to the different characteristics of the original data, such as the grey topology model applied to the data with changing growth rate or noise data and the model containing multiple consumption factors; therefore, the prediction range of this method is very wide, both long-term

and short-term predictions can be used, the amount of data required is not large, and it can also be used when data is lacking.

Artificial neural network (Ann) is a complex network system which is widely connected by a large number of simple artificial neurons to imitate the human brain neural network. It establishes the nonlinear input and output model of the system on the basis of a given large number of input and output signals and parallel processing of data; in essence, it is to give a large amount of data to an artificial neural network constructed according to a certain structural form and excitation function for learning, and then given a future input, the computer judges the expected output based on past "experience." This method is actually a black-box simulation of the system, which is suitable for dynamic consumption forecast values and dynamic training systems, and obtains high forecasting accuracy, because its "black-box operation" is more helpful for formulating policies and improving utilization; therefore, this method is suitable for long-term and short-term consumption forecasting [25].

The system dynamics method regards the object under study as a dynamic system with a complex feedback structure and changes with time and draws a system flow chart representing the system structure and dynamics through system analysis; then, the relationship between the variables is quantified, and the structural equation of the system is established, so that the computer can be used for simulation experiments to predict the future of the system. The application effect of this method is closely related to the forecaster's professional knowledge, practical experience, and system analysis and modeling ability. Through analysis and establishment of system model, the system can be whitened, and the hidden law of the system can be found out through computer dynamic simulation. This method can not only predict the long-term forecast objects, but also find out the influencing factors and function relationships of the system, which is beneficial to system optimization. However, the system analysis process is complex, the workload is large, and the ability of analysts is relatively high, so it is not suitable for short-term forecasting. For long-term forecasting, its advantages are very obvious.

4. Results and Analysis

The evaluation of social welfare adopts the traditional cumulative discounted utility method, and the cumulative discounted utility value is reflected in the discount of the population and the benchmark individual utility value in time. When the time preference rate $\rho > 0$, both the population L and the benchmark personal utility value U are positively related to the CDU, and the size of ρ at this time reflects whether people prefer the current situation or the future situation. The larger ρ is, the more people are willing

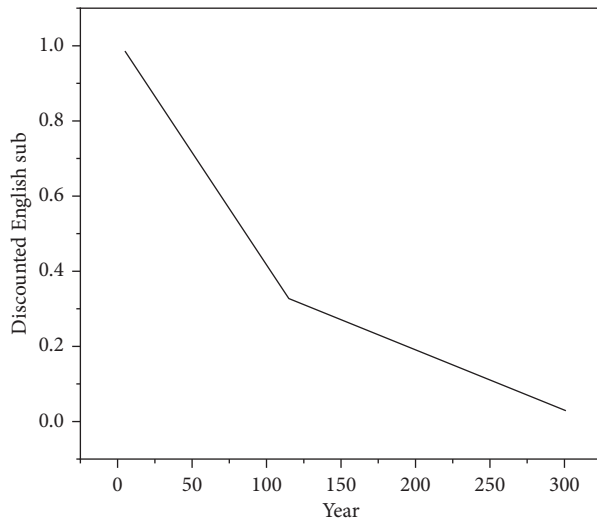


FIGURE 2: The effect of time preference rate.

to enjoy the present life and ignore the future; the smaller the ρ , the more the attention people pay to the future; that is, the future utility value has a higher discount today, as shown in Figure 2.

As an intermediary link connecting energy production and consumption, energy distribution plays an important role in social reproduction [26]. Scientific and reasonable distribution of energy products is of great significance to the smooth progress of social reproduction and the stable development of national economy. The distribution of energy products is an important part of the distribution of total social products. Through the distribution and redistribution of the total social product, three social funds are finally formed: the compensation fund, the consumption fund, and the accumulation fund. From the perspective of social reproduction, the three major funds are closely related to the two major departments of material production, and they are exchanged in accordance with the principles of material replacement and value compensation, so that products can enter the field of consumption from the production field, and social reproduction can be repeated and continuously carried out.

5. Conclusion

In the past ten years, with the wide application of information technology, people's ability to use information technology to produce and collect data has been greatly improved, and a large number of databases have been used in business management, government offices, and scientific research. People are eager to get more information that can help decision-making by analyzing data. Although the current database system can efficiently realize data entry, query, statistics, and other functions, due to the huge amount of data and the serious lack of analysis methods in the database system, it is impossible to discover the hidden interconnections in the data, and it is also impossible to predict the future development trend based on current and historical data.

Data Availability

The data used to support the findings of this study are available from the corresponding author upon request.

Conflicts of Interest

The author declares that there are no conflicts of interest.

Acknowledgments

This study was funded by Exploration and Practice of Aesthetic Education in Vocational Education System under the Background of "Double High School," 2022DZYKY16.

References

- [1] P. Stallinga, "On the energy theory of value: economy and policies," *Modern Economy*, vol. 11, pp. 1083–1120, 2020.
- [2] H. Fuhr, "Geopolitical economy of energy and environment. China and the European Union. edited by amineh, mehdi p. & Yang Guang," *Comparative Sociology*, vol. 19, no. 1, pp. 151–153, 2020.
- [3] I. A. Olanrele, A. I. Lawal, E. Osen et al., "Assessing the impacts of contemporary development in biofuel on agriculture, energy and domestic economy: evidence from Nigeria," *International Journal of Energy Economics and Policy*, vol. 10, no. 5, pp. 469–478, 2020.
- [4] R. I. Corazza and P. S. Fracalanza, "Setting the field of international political economy of energy," *Context to International*, vol. 42, no. 1, pp. 203–207, 2020.
- [5] R. R. Bora, R. Wang, and F. You, "Waste polypropylene plastic recycling toward climate change mitigation and circular economy: energy, environmental, and technoeconomic perspectives," *ACS Sustainable Chemistry & Engineering*, vol. 8, no. 43, pp. 16350–16363, 2020.
- [6] Y. Ziabina, T. Pimonenko, and L. Starchenko, "Energy efficiency of national economy: social, economic and ecological indicators," *SocioEconomic Challenges*, vol. 4, no. 4, pp. 160–174, 2020.
- [7] E. F. E. Atta Mills, K. Zeng, and M. A. Baafi, "The economy-energy-environment nexus in imf's top 2 biggest economies: a ty approach," *Journal of Business Economics and Management*, vol. 21, no. 1, pp. 1–22, 2019.
- [8] L. Karbovska, I. Yakushik, E. Feshchenko, I. Kalina, and A. Kozlova, "Sustainable development of the economy and increasing energy security based on the use of res: problems and prospects," *Financial and Credit Activity Problems of Theory and Practice*, vol. 2, no. 37, pp. 438–446, 2021.
- [9] C. Okafor, C. Madu, C. Ajaero, J. Ibekwe, and F. Otunomo, "Situating coupled circular economy and energy transition in an emerging economy," *AIMS Energy*, vol. 9, no. 4, pp. 651–675, 2021.
- [10] H. F. Sindi, A. Ul-Haq, M. S. Hassan, A. Iqbal, and M. Jalal, "Penetration of electric vehicles in gulf region and its influence on energy and economy," *IEEE Access*, vol. 9, p. 1, 2021.
- [11] J. Hou, M. Wang, and P. Liu, "Can sharing economy mode advance the transition of China's energy sector effectively: a case of pv technology transition?" *Energy Reports*, vol. 7, no. 15, pp. 502–514, 2021.
- [12] Y. Fu, M. C. Zhou, X. Guo, L. Qi, and K. Sedraoui, "Multiverse optimization algorithm for stochastic biobjective disassembly sequence planning subject to operation failures," *IEEE*

Retraction

Retracted: Energy Conservation Optimization and Numerical Simulation of Urban Green Space Landscape Pattern

International Transactions on Electrical Energy Systems

Received 3 October 2023; Accepted 3 October 2023; Published 4 October 2023

Copyright © 2023 International Transactions on Electrical Energy Systems. This is an open access article distributed under the Creative Commons Attribution License, which permits unrestricted use, distribution, and reproduction in any medium, provided the original work is properly cited.

This article has been retracted by Hindawi following an investigation undertaken by the publisher [1]. This investigation has uncovered evidence of one or more of the following indicators of systematic manipulation of the publication process:

- (1) Discrepancies in scope
- (2) Discrepancies in the description of the research reported
- (3) Discrepancies between the availability of data and the research described
- (4) Inappropriate citations
- (5) Incoherent, meaningless and/or irrelevant content included in the article
- (6) Peer-review manipulation

The presence of these indicators undermines our confidence in the integrity of the article's content and we cannot, therefore, vouch for its reliability. Please note that this notice is intended solely to alert readers that the content of this article is unreliable. We have not investigated whether authors were aware of or involved in the systematic manipulation of the publication process.

Wiley and Hindawi regrets that the usual quality checks did not identify these issues before publication and have since put additional measures in place to safeguard research integrity.

We wish to credit our own Research Integrity and Research Publishing teams and anonymous and named external researchers and research integrity experts for contributing to this investigation.

The corresponding author, as the representative of all authors, has been given the opportunity to register their agreement or disagreement to this retraction. We have kept a record of any response received.

References

- [1] L. Wang, "Energy Conservation Optimization and Numerical Simulation of Urban Green Space Landscape Pattern," *International Transactions on Electrical Energy Systems*, vol. 2022, Article ID 5324854, 7 pages, 2022.

Research Article

Energy Conservation Optimization and Numerical Simulation of Urban Green Space Landscape Pattern

Lan Wang 

Environmental Design Department, Jilin College of the Arts, Changchun, Jilin 130000, China

Correspondence should be addressed to Lan Wang; 201701340238@lzpcc.edu.cn

Received 14 July 2022; Revised 31 July 2022; Accepted 3 August 2022; Published 25 August 2022

Academic Editor: Nagamalai Vasimalai

Copyright © 2022 Lan Wang. This is an open access article distributed under the Creative Commons Attribution License, which permits unrestricted use, distribution, and reproduction in any medium, provided the original work is properly cited.

In order to alleviate the urban heat island effect, absorb harmful gases, reduce temperature, and increase humidity, a method of energy conservation optimization and numerical simulation of urban green space landscape pattern is proposed. Based on the theory of landscape ecology, green wedge, green belt, green road, park, and other types of green space with different ecological functions are designed in Shenyang, and an optimization scheme of urban green space network spatial structure of “four belts, three rings, seven wedges, and network connection” is formed. Combined with remote sensing (RS) and geographic information system (GIS) spatial analysis technology, the atmospheric environment effect under the influence of green space landscape optimization pattern in summer based on computational fluid dynamics (CFD) numerical simulation technology is analyzed, and the corresponding optimization strategies of urban green space planning are put forward. The simulation results show that in the bottom wind speed field of 1.5 m, the area ratio of 0~0.375 m/s wind speed is 15.87%, and the area ratio of 2.625~3 m/s wind speed is 32.06%. In the bottom concentration field of 1.5 m, the spatial diffusion capacity of SO₂ pollutants is enhanced, and the concentration of pollutants is relatively low. The area ratio of SO₂ concentration is 10.06% in the range of 0.1292~0.1551 mg/m³, and the area ratio of SO₂ concentration is 68.08% in the range of 0~0.05169 mg/m³. It is concluded that the spatial diffusion of wind speed, SO₂, and temperature is closely related to the urban spatial layout. The optimal spatial layout of urban green space can effectively alleviate the urban heat island effect, promote the spatial diffusion of SO₂, and better form the urban ventilation corridor. The research on atmospheric environmental effects of urban green space based on CFD can effectively simulate and evaluate the optimization measures and conceptual design of urban green space system planning, and also provide new ideas for the quantitative planning of urban green space system.

1. Introduction

City is the main place for human settlement and living; that is, human beings make use of and transform the natural environment according to their living needs to form a high-level artificial living environment. As the urban population density increases year by year and the available land decreases year by year, the city is facing a huge crisis and its sustainable development is seriously threatened. The harmonious coexistence of human beings and environment has become a hot issue. Urban ecologist Richard Regist once compared a city to a ship. He said, “A city is like a ship setting out on the future journey of mankind. The better its structure and function are, the more normal the sailing will

be.” Urban ecosystem is highly dependent on the external environment [1].

Green space (Figure 1), representing nature and life, is called “lung of the city.” The concept of green space in Ci Hai refers to the selection of trees, shrubs, and herbs suitable for planting on the basis of the existing environment, so as to form a certain range of green areas. Urban green space is the area in which the natural landscape is maintained or restored in the city, which comprehensively reflects the natural landscape and cultural landscape in the city. With the acceleration of urbanization and the continuous deterioration of urban environment, people no longer pay attention to the aesthetic effect of green space, but also begin to pay attention to its structure and function [2, 3]. If the urban green space

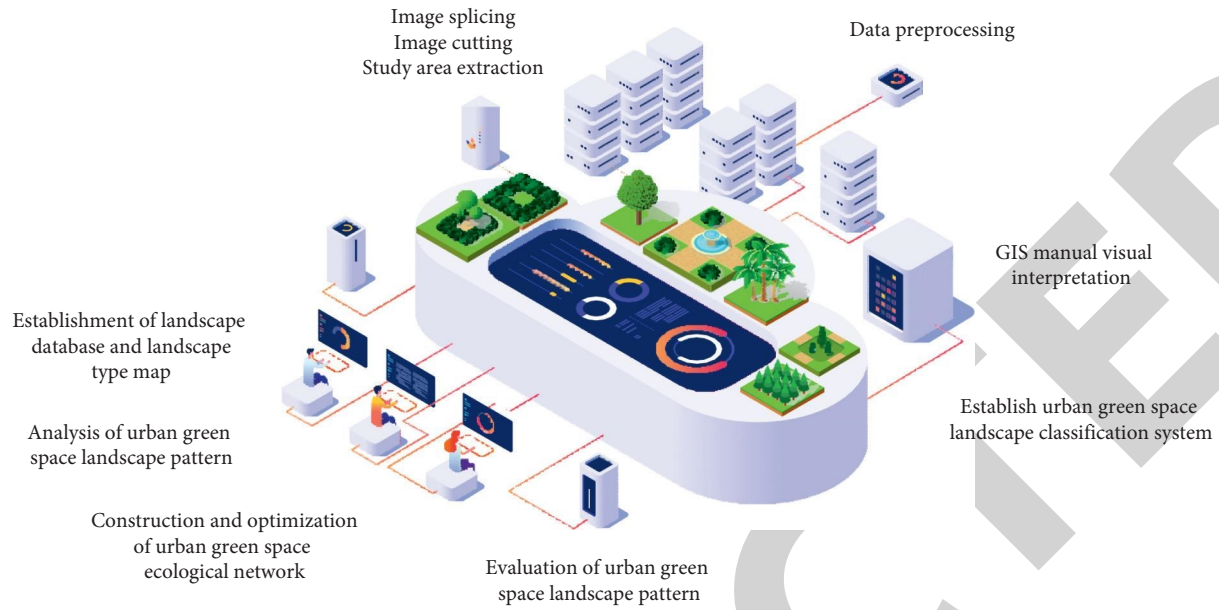


FIGURE 1: Green landscape.

cannot form a reasonable green space system structure, it is difficult to give full play to its ecological value. In order to realize the sustainable development of urban and improve the increasingly prominent urban ecological problems, the integration of multidisciplinary and multifield theories should be realized, and new planning concepts and technical means should be adopted to explore the reasonable content and layout of urban green space in the rigidly constrained urban space, so as to effectively utilize the ecological function of green space and realize the sustainable development of the city.

2. Literature Review

Liu et al. planned and studied a wide range of open space by applying the principles of landscape ecology and combining landscape structure and landscape function. Moreover, foreign research studies on the construction of urban green space system from the perspective of landscape ecology mostly focused on the ecological network, greenway, and green line, and regarded them as new planning parameters of man and nature [4]. Hou et al. mainly studied the ecological and social role of "green line" in urban landscape [5]. Su and Yu put forward some suggestions on the development of green space system in New York from the aspects of ecological principles such as ecological content, dynamic mechanism, heterogeneity, and hierarchy [6]. Ji et al. proposed a universal model for applying ecological knowledge to landscape and the urban planning [7].

Since the 1990s, people have paid more and more attention to the role of urban green space system in urban sustainable development strategy and urban biodiversity protection. Luo et al. proposed the theory and method of landscape ecological pattern internationally for the first time, and applied it to urban green space planning [8]. Miszczak et al. first discussed the reasonable basis for the

existence of artificial corridors and natural corridors in urban landscape based on the corridor effect theory, and proposed the alternate distribution of artificial and natural corridors in Beijing to form an organic dispersed landscape pattern [9]. Wang et al. also proposed the urban spatial layout with green veins as the precursor [10]. Zuo et al. discussed the relationship between landscape ecology and urban landscaping, expounded the concentric circle model of urban spatial structure and the planning and design principles of green space landscape ecology, and proposed the methods, approaches, and quantitative measurement indexes of planning and design combined with its principles [11].

Taking the urban area within the third ring road of a city in summer as the research object, in the urban scale, RS, GIS spatial analysis technology, and CFD numerical simulation technology were used to comprehensively analyze the urban atmospheric environmental effects under the influence of the urban green space landscape pattern optimization scheme. The interaction between the planning scheme and wind speed, temperature, and SO_2 concentration was explored, the urban green space layout and functional division were determined and guided according to the evaluation results, and the rationality of the green space layout of the scheme was evaluated. In the planning, the optimization measures and conceptual design of urban green space system planning can be simulated and evaluated, so as to provide a certain reference for the optimization of urban green space landscape pattern [12].

3. Research Methods

In the urban green space system planning, first of all, according to the related theory of landscape ecology, qualitative and quantitative methods are used to optimize the urban green space planning design. Secondly, combining

the RS, GIS, and CFD simulation technology for the urban atmospheric environment under the influence of the green space optimization effect, the numerical simulation analysis is performed in the evaluation of the rationality of the green space optimization scheme. Finally, corresponding planning strategies are proposed according to the evaluation results, so as to form a multiobjective, multilevel, and comprehensive ecological network structure of urban green space [13].

3.1. The Optimization Design of Urban Green Space Landscape. In order to exert the ecological function of urban green space ecological network structure efficiently, a green space network spatial structure of “four belts, three rings, seven wedges and network connection” is formed by combining centralized and decentralized layout mode.

At the municipal level, five green wedges of “ventilation corridors” are established in a certain city. Under the guidance of the dominant urban wind, the lower temperature air in the suburbs can be introduced into the urban interior with high-building density, so as to reduce the poor thermal environment in a city in summer and strengthen the connection between the surrounding area and the urban area. Two ecological green wedges can be established in the north and northeast of the site in order to connect with the surrounding mountains and farmland, so as to achieve the purpose of “introducing nature into the city.”

On the urban scale, the green space vegetation area should be increased in the low-lying area of the urban high-building density area, and the urban ventilation corridor should be formed. Urban ventilation corridors shall be established in or along urban roads in areas where urban wind speed is not impeded. Relatively large green spaces should be established near new buildings. The construction of green belt around the city should be carried out around three main ring roads, and the construction of green belt around the city water system should be strengthened to improve the quality of urban air environment [14]. At the neighborhood scale, the greening structure is optimized according to the local spatial pollution of the city [15].

3.2. Simulation of Urban Atmospheric Environmental Effects Based on Remote Sensing and CFD

3.2.1. Establishment of Urban Digital Module. In the numerical simulation, considering the urban wind speed, temperature, humidity, solar radiation, and other meteorological parameters, the spatial layout of various landscape elements in the city, building density, floor area ratio, population density, vegetation coverage and topographic characteristics, and other factors will have different impacts on the urban atmospheric environment effect. Therefore, It is necessary to establish an accurate and reasonable CFD urban digital model [16]. In the process of city classification, city classification is carried out based on the spatial information of underlying surface and comprehensive consideration of building density, vegetation coverage degree, floor

area ratio, surface temperature, SO₂ pollution degree, and population density in the region.

3.2.2. Setting of CFD Simulation Parameters. Calculation of watershed is determined. In CFD simulation, a zoom of urban space is first created, and the length, width, and height of zoom in CFD are determined, which should generally be appropriately larger than the whole city model for CFD simulation environment simulation. In the research, a 1:1 model was used to conduct research, and the zoom scale of the digital model of a city was 50,000 m × 50,000 m × 200 m.

Setting of initial conditions is as follows. After establishing the model in CFD, it is necessary to input the basic information data of a city as the initial conditions of simulation, such as latitude and longitude, calculation time, and parameters related to solar radiation. The air inlet and air outlet are established at the corresponding position of the geometric model. Under the influence of the south wind, the dominant wind direction in a city in summer, the average wind speed of the city is 3 m/s, and the average daily temperature is 29°C [17]. According to the analysis and conversion of relevant climate data, the relevant parameters of wind speed and temperature in CFD, as well as the initial parameters of air inlet and air outlet in the simulation boundary, are set to accurately simulate the climate environment of the urban digital model in CFD. The initial temperature and pollution source concentration of different modules are set according to the surface temperature and emission concentration of main pollution sources obtained from the field monitoring, remote sensing analysis, and GIS interpolation analysis.

3.2.3. The Calculation Process of CFD Model. After the parameters are set, the model can be calculated. It will simulate the spatial operation of urban wind speed, SO₂, temperature, and other atmospheric environmental factors under the spatial layout of urban green space.

(1) *Grid Division.* For the research of urban scale, appropriate grid accuracy should be selected according to the spatial form and structural composition of urban modules, and local grid encryption should be carried out in areas with relatively complex module structure. The finer the grid division, the higher the calculation accuracy [18].

(2) *Calculation Principle.* The basic formulas of the non-compressible and nonisothermal flow field simulated by the CFD model are shown in the following formulas:

$$\frac{\partial(u_i)}{\partial x_i} = 0, \quad (1)$$

$$\frac{du}{dt} = -\frac{1}{\rho} \frac{\partial P}{\partial x_j} + \frac{\partial(v(\partial(u_i)/\partial x_j))}{\partial x_j} - g\beta\Delta\theta, \quad (2)$$

$$\frac{d\theta}{dt} = \frac{\partial(\alpha(\partial\theta/\partial x_i))}{\partial x_j}, \quad (3)$$

$$\frac{\partial(C_i)}{\partial t} + \frac{\partial(u_i)(C_i)}{\partial x_i} = \frac{\partial}{\partial x_i} \left(D \frac{\partial(C_i)}{\partial x_i} - (u_i C_i) \right). \quad (4)$$

where u_i is the instantaneous velocity (m/s); x_i , the space coordinate (m); t , the time (s); ρ , the density (kg/m^3); P , the instantaneous pressure (N/m^2); ν , the molecular kinematic viscosity (m^2/s); g , the acceleration of gravity (m/s^2); β , the volume expansion coefficient ($^\circ\text{C}^{-1}$); θ , the instantaneous temperature ($^\circ\text{C}$); θ_0 , the temperature ($^\circ\text{C}$); and α , the molecular thermal diffusion coefficient (m^2/s).

(3) *Convergence*. In numerical simulation analysis, the basic formulas need to be repeatedly calculated, and the operation can be completed only when the operation factor tends to be stable or the calculation structure reaches a certain range, which is called convergence. If the convergence effect is not ideal, the model parameters need to be adjusted for the convergence problem.

(4) *Analysis of Calculation Results*. When the calculated results reach the ideal state, the results can be displayed in terms of wind speed, SO_2 , temperature, and other factors. The horizontal and vertical direction of the numerical display chart can be chosen, and it reflects the atmospheric environment of the city generally according to the numerical results in accordance with different colors.

4. Result Analysis

With the increase in urban height, urban building density and floor area ratio decrease continuously, and the resistance of urban wind speed, temperature, and SO_2 spatial diffusion decrease, and the resistance of spatial diffusion is inversely proportional to the diffusion height. In different height ranges of 0~200 m, the height range of 0~10 m (including 10 m) is defined as the bottom effect field, the height range of 10~50 m (including 50 m) is defined as the middle effect field, and the height range of 50~200 m is defined as the top effect field [19].

4.1. Simulation Analysis of Urban Wind Speed Field at Different Heights. From the diffusion analysis of urban wind speed at different vertical heights, it can be seen that the urban wind speed tends to increase with the increase in height, and the area covered by the maximum wind speed in the city keeps increasing. But the trend of the spatial diffusion range gradually increases is not obvious, and the ventilation condition of the city is relatively good. In the bottom wind speed field of 1.5 m, the area ratio of 0~0.375 m/s wind speed in urban inner space is 15.87% and that of 2.625~3 m/s wind speed is 32.06%. Areas with high wind speed in the city are still mainly distributed in some areas on the windward side. It will be conducive to urban spatial diffusion of pollutants in the air. At the same time, the urban ventilation corridors in the southwest and southeast directions are formed in the whole city, while under the influence of building density urban ventilation corridor's sphere of influence with attenuation effect, but it is

important for the spread of the urban air pollutants and the high-temperature area [1].

In the bottom wind speed field of 10 m, the buildings have a great influence on the urban wind speed. Compared with the bottom wind speed field of 1.5 m, the wind speed between 2.625 m/s and 3 m/s has a great improvement, and the area ratio increases from 32.06% to 56.64%. In the middle wind speed field (30 m, 50 m), the maximum wind speed of the city also increases, and the area ratio increases from 56.64% to 77.72%. In the top wind speed field of 100 m, the area ratio of the maximum wind speed of the city increases to 79.71%.

4.2. Simulation Analysis of Spatial Diffusion of SO_2 Concentration Field at Different Heights. From the diffusion analysis of urban SO_2 concentration at different vertical heights, it can be seen that with the continuous increase of urban height, the concentration of SO_2 gradually decreases with the increase in height. At the same time, under the influence of urban wind speed, the spatial diffusion capacity of SO_2 is significantly enhanced, and the urban air pollution environment has been further improved. In the bottom concentration field of 1.5 m, the spatial diffusion ability of SO_2 pollutants is enhanced, and the concentration of pollutants is relatively low. The area ratio of SO_2 concentration value of 0.1292~0.1551 mg/m^3 is 10.06%; the SO_2 concentration value is mostly concentrated in the concentration range of 0~0.05169 mg/m^3 ; and the area ratio is 68.08%.

With the increase in height, the area ratio of concentration values below 0.05169 mg/m^3 reaches 60.07% in the bottom concentration field of 10 m, 69.13% in the middle concentration field of 50 m, and 75.4% in the top concentration field of 100 m. In the bottom concentration field of 1.5 m, the maximum concentration value is 0.1551~0.1809 mg/m^3 , and the area ratio is 5.36%. In the middle concentration field of 50 m, the maximum concentration value is 0.1292~0.1551 mg/m^3 , and the area ratio is 7.3%. In the top concentration field of 100 m, the maximum concentration value is 0.1034~0.1292 mg/m^3 , and the area ratio is 6.4%. From the perspective of the whole city, under the guidance of urban wind environment, pollutants can effectively diffuse to the periphery of the city, and the spatial layout of urban green space can promote the diffusion of air pollutants to a certain extent, and the air environmental quality of the whole city has been improved to a certain extent [20].

4.3. Simulation Analysis of Spatial Diffusion of Urban Temperature Field at Different Heights. From the diffusion analysis of urban temperature field at different vertical heights, it can be seen that with the increase in height, temperature presents a trend of gradual decrease, and its diffusion ability gradually increases with the increase in urban wind speed. In the bottom temperature field of 1.5 m, the high-temperature area of a city can well spread to the outer part of the city under the influence of urban wind speed, and the high-temperature phenomenon will not have a great influence on the city. In other areas of the city, the

urban high-temperature phenomenon is not obvious, and the heat island effect in the central urban area is effectively alleviated. In the whole city, urban green space, Hun River, and surrounding green space and other water bodies have an obvious effect on urban temperature regulation, which is of great significance to alleviate the urban heat island effect. In the bottom temperature field of 1.5 m, the highest temperature is between 42.75°C and 46°C, and the area ratio is 0.56%. In the middle-temperature field of 50 m, the highest temperature of urban temperature is mainly concentrated between 39.5°C and 42.75°C, and the area ratio reaches 4.72%. In the top temperature field of 100 m, the urban temperature is mainly concentrated between 39.5°C and 42.75°C, and the area ratio is only 2.07%. In the bottom temperature field of 1.5 m, the lowest temperature is between 29.75°C and 33°C with an area ratio of 7%. In the middle-temperature field of 50 m, the lowest temperature is between 26.5°C and 29.75°C with an area ratio of 0.95%. In the top temperature field of 100 m, the lowest temperature is between 26.5°C and 29.75°C. The area ratio is 1.01%. Therefore, although the area ratio of the minimum temperature increases with the increase of the height of the city and the temperature of the whole city gradually decreases in the scheme, the operation of the urban thermal environment is relatively good.

4.4. Verification of CFD Simulation Results. The accuracy of the CFD numerical simulation results is verified by domestic and foreign scholars. In the research, the validation data are mainly used in a variety of monitoring data. The data verification points are mainly distributed in city residential area, within the scope of the third industrial park, park green space, and commercial and culture area. And 30 monitoring stations are selected to validate the results of model simulation. The results show that the relative errors between the simulated wind speed, SO₂ concentration, and temperature and the measured values are small, which meet the accuracy of urban scale numerical simulation (Figures 2~6). Therefore, CFD is feasible to simulate the effect of the atmospheric environment.

4.5. Optimization Strategies of Urban Green Space Landscape Planning. Based on the CFD simulation analysis of the atmospheric environment effect of urban green space optimization scheme, it can be seen that there is a one-to-one correspondence between the urban ventilation corridor area in the optimization scheme and the urban ventilation area in the CFD numerical simulation analysis, indicating that the ventilation corridor in the optimization scheme is reasonable, which can blow the low-temperature air in the suburbs into the high-temperature area inside the city, and can effectively alleviate the urban heat island effect. Under the influence of the dominant wind direction of the city, the area with high concentration of SO₂ continuously diffuses to the periphery, and the concentration gradually decreases. With the increase in height, the maximum concentration value also decreases accordingly. The optimization scheme of urban green space system plays an obvious role in improving

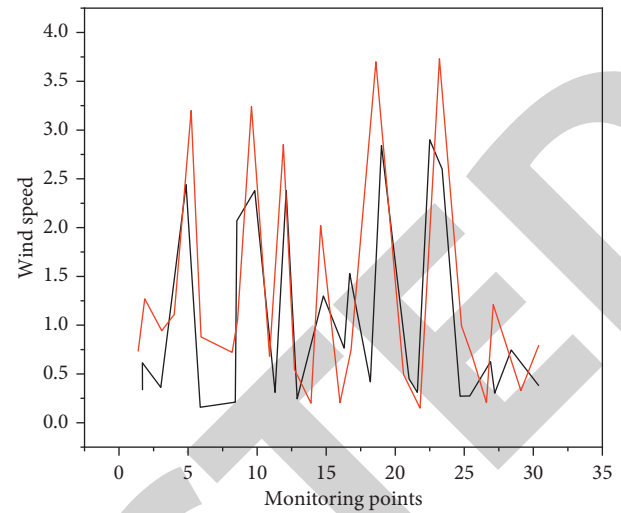


FIGURE 2: Simulation wind speed.

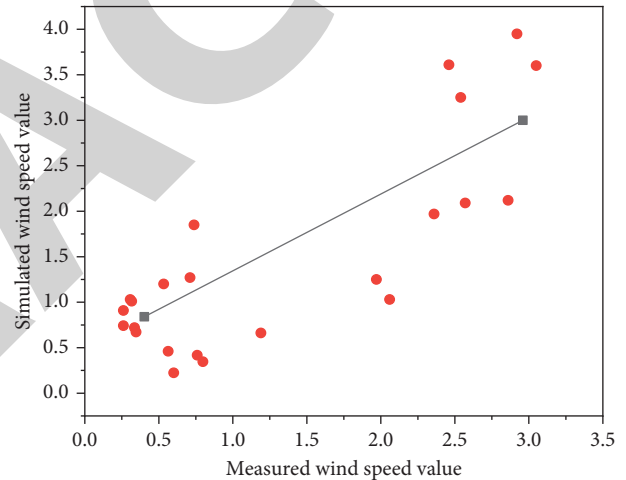
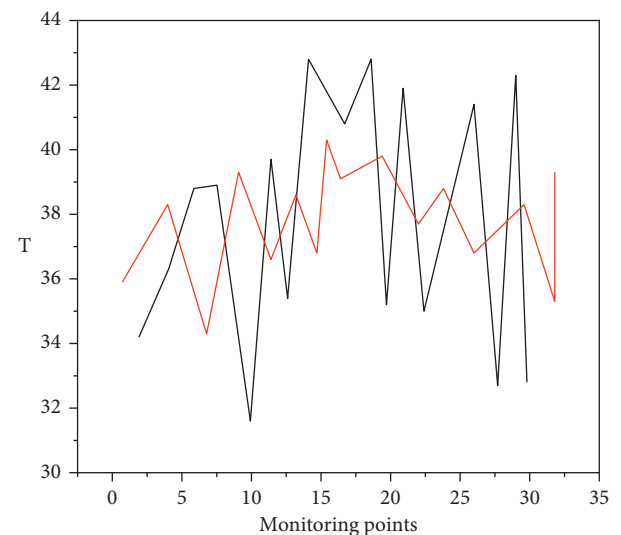


FIGURE 3: Measured wind speed.

FIGURE 4: Simulated SO₂ concentration monitoring.

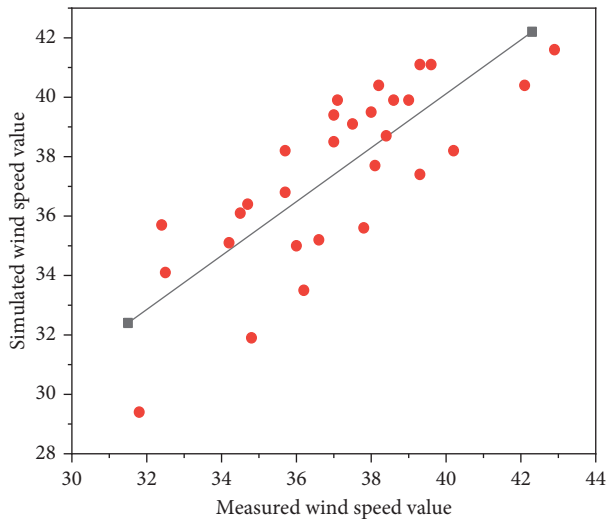


FIGURE 5: Measured SO₂ concentration.

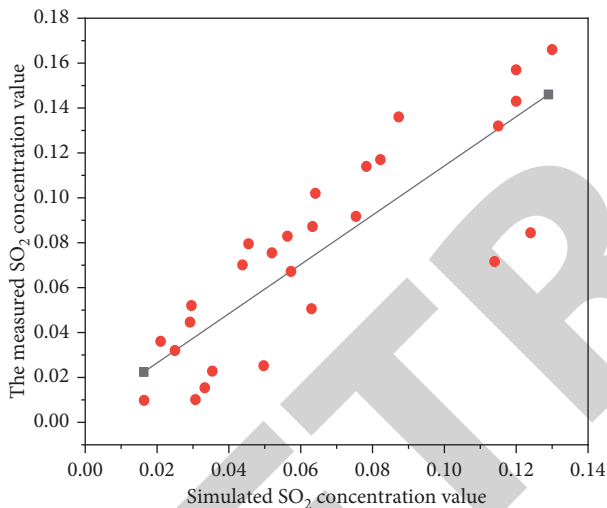


FIGURE 6: Comparison trend between simulated and measured temperature values.

urban atmospheric environment, and the scheme has certain rationality. Therefore, in green space system planning, according to the numerical simulation analysis results of green space optimization scheme, corresponding quantitative analysis methods can be used to adjust the optimization scheme at different scales and a systematic ecological network of urban green space is formed, so as to give full play to the maximum ecological efficiency of green space.

5. Conclusions

Based on the principles of landscape ecology and green space layout method, the urban green space network spatial structure optimization scheme is put forward. By using the CFD model, the simulation analysis is carried out on the optimization of atmospheric environment effects, and the rationality of its spatial layout is evaluated. At the same time,

based on the simulation analysis results, the corresponding strategy of urban green space system planning is put forward. The results show that the optimization scheme of green space in a city has a good effect on the formation of urban ventilation corridors and promoting the diffusion of SO₂ pollutants. Although there are many high-temperature areas in the diffusion of urban temperature field, the spatial diffusion capacity of the optimization scheme is relatively strong. Considering the urban wind environment, thermal environment, and the spatial diffusion capacity of SO₂ air pollutants, the layout of urban green space under the optimization scheme is relatively reasonable. Therefore, in the spatial layout planning of urban green space, the spatial layout of urban green space can be optimized at the scale of urban area, city, and block neighborhood from a systematic perspective. At the municipal scale, RS, GIS, CFD numerical simulation technology, green ecological infrastructure construction and evaluation system, and other methods are coupled to identify ecological factors, historical factors, cultural factors, and recreational factors that affect the quality of urban air environment so as to jointly build a multiobjective and comprehensive urban green space ecological network. At the urban scale, numerical simulation and other techniques are used to identify potential ventilation corridors, green belts, and other landscape elements in different functional areas, so as to alleviate urban atmospheric environment problems by forming urban ecological protection green network. At the neighborhood scale, the scale, location, form, spatial structure, and vegetation composition of green space should be reasonably planned, and the rational spatial structure layout of green space should be found by combining multiscenario plan simulation analysis to guide the spatial diffusion of pollutants and slow down the urban heat island effect, so as to improve the quality of urban environment.

Data Availability

The data used to support the findings of this study are available from the author upon request.

Conflicts of Interest

The author declares that there are no conflicts of interest.

References

- [1] P. Kowe, O. Mutanga, and T. Dube, "Advancements in the remote sensing of landscape pattern of urban green spaces and vegetation fragmentation," *International Journal of Remote Sensing*, vol. 42, no. 10, pp. 3797–3832, 2021.
- [2] J. Ji, S. Wang, Y. Zhou, W. Liu, and L. Wang, "Spatiotemporal change and landscape pattern variation of eco-environmental quality in jing-jin-ji urban agglomeration from 2001 to 2015," *IEEE Access*, vol. 8, Article ID 125534, 2020.
- [3] W. Song, Z. Yunlin, X. Zhenggang, Y. Guiyan, H. Tian, and M. Nan, "Landscape pattern and economic factors' effect on prediction accuracy of cellular automata-Markov chain model on county scale," *Open Geosciences*, vol. 12, no. 1, pp. 626–636, 2020.

Retraction

Retracted: A Fault-Tolerant Structure for Nano-Power Communication Based on the Multidimensional Crossbar Switch Network

International Transactions on Electrical Energy Systems

Received 19 September 2023; Accepted 19 September 2023; Published 20 September 2023

Copyright © 2023 International Transactions on Electrical Energy Systems. This is an open access article distributed under the Creative Commons Attribution License, which permits unrestricted use, distribution, and reproduction in any medium, provided the original work is properly cited.

This article has been retracted by Hindawi following an investigation undertaken by the publisher [1]. This investigation has uncovered evidence of one or more of the following indicators of systematic manipulation of the publication process:

- (1) Discrepancies in scope
- (2) Discrepancies in the description of the research reported
- (3) Discrepancies between the availability of data and the research described
- (4) Inappropriate citations
- (5) Incoherent, meaningless and/or irrelevant content included in the article
- (6) Peer-review manipulation

The presence of these indicators undermines our confidence in the integrity of the article's content and we cannot, therefore, vouch for its reliability. Please note that this notice is intended solely to alert readers that the content of this article is unreliable. We have not investigated whether authors were aware of or involved in the systematic manipulation of the publication process.

Wiley and Hindawi regrets that the usual quality checks did not identify these issues before publication and have since put additional measures in place to safeguard research integrity.

We wish to credit our own Research Integrity and Research Publishing teams and anonymous and named external researchers and research integrity experts for contributing to this investigation.

The corresponding author, as the representative of all authors, has been given the opportunity to register their agreement or disagreement to this retraction. We have kept a record of any response received.

References

- [1] J. Luo and B. Liao, "A Fault-Tolerant Structure for Nano-Power Communication Based on the Multidimensional Crossbar Switch Network," *International Transactions on Electrical Energy Systems*, vol. 2022, Article ID 4783847, 8 pages, 2022.

Research Article

A Fault-Tolerant Structure for Nano-Power Communication Based on the Multidimensional Crossbar Switch Network

Jun Luo  and Boxun Liao 

Guangzhou College of Technology and Business, Guangzhou, Guangdong 510850, China

Correspondence should be addressed to Jun Luo; 2020020544@stu.cdut.edu.cn

Received 14 July 2022; Revised 26 July 2022; Accepted 1 August 2022; Published 24 August 2022

Academic Editor: Nagamalai Vasimalai

Copyright © 2022 Jun Luo and Boxun Liao. This is an open access article distributed under the Creative Commons Attribution License, which permits unrestricted use, distribution, and reproduction in any medium, provided the original work is properly cited.

In order to realize fault tolerance and further reduce the transmission delay, a fault-tolerant structure design method for nano-power communication based on a multidimensional crossbar switch network is proposed. The TSV router is designed as a double crossbar structure, namely the master crossbar (MasterCrossbar) and the slave crossbar (SlaveCrossbar). Each input port of the TSV router is divided into two subports. The port connected to the master crossbar has no input buffer, and the port connected to the slave crossbar has an input buffer. Master crossbar is the first choice for data transmission, and slave crossbar is selected when it is busy to reduce the transmission delay of data packets and reduce power consumption. Dual crossbar switches can also realize the fault tolerance of crossbar switches. The experimental results show that the author's fault-tolerant scheme, without incorporating the double crossbar switch, still has a much smaller transmission delay than the reference because the author realizes fault tolerance for defective TSVs by adding bidirectional TSVs to replace faulty TSVs. Therefore, when there is a TSV failure, the reference transmission delay increases with the number of failures, but the author's design allows packets to be transmitted in the network without being affected; the author's bidirectional TSV fault-tolerant design is combined with the double crossbar design. After that, the transmission delay is smaller than the original, and the maximum transmission delay is about 40% faster than the reference. The authors' design is superior and improves the reliability of the 3DNoC system.

1. Introduction

3DNoC is a multilayer wafer (die) interconnection through through-hole via (TSV) and uses the network structure to interconnect the interconnection of resource nodes. Common 3DNoC topology structures include 3DMesh, 3DToms, 3D stacked Mesh, and others, among them, and the structure widely studied by many scholars is 3DMeshtW. The traditional 3DMesh structure is a regular 3D network structure formed by stacking regular 2DNoCs up and down, and each layer realizes interlayer power communication through TSV. At present, most of the research on 3DNoC is based on this regular 3DMesh topology [1].

However, in today's industrial design, it is usually necessary to place modules that implement different functions on different layers of a 3D chip, for example, the CPU core is placed on the top layer, RAM and ROM are placed on

the middle layer, and communication modules are placed on the bottom layer. Due to the huge difference in the area and function of the devices in each layer, it is difficult for such a design to achieve the same layout of network nodes on each layer; it is possible to have a network structure with $n * n$ on a certain layer and a network structure with $m * m$ ($m \neq n$) on the upper layer, and as a result, some routing nodes have upward or downward channels, that is, TSVs are connected, while some nodes do not have vertical channels [2]. Such a structure makes it difficult to use traditional 3D routing algorithms to achieve the purpose of transmitting data packets.

Today, the chip manufacturing process has entered a level below 65 nanometers, the process is becoming more and more complex, and the manufacturing difficulty is becoming more and more difficult. The size of TSV is only about 10 microns, and the current TSV manufacturing

technology is not mature enough, the manufacturing cost is high, and it is easy to cause voids, fractures, misalignment, and so on in the manufacturing process, resulting in TSV failure. The yield of TSVs has become one of the decisive factors affecting the yield of the entire chip, and when the number of TSVs reaches a certain order of magnitude, the yield of chips will decline exponentially. The data show that for a silicon chip manufactured by using 65 nm CMOS process technology, 46%–65% of the cost overhead is used in the processing of TSV. Therefore, under the premise of ensuring chip communication, the number of TSVs should be as small as possible [3].

2. Literature Review

The fusion of 3D technology and NoC technology brings new opportunities for the development of integrated circuit technology and at the same time brings new challenges. One of them is TSV failure due to physical defects, which affects 3DNoC yield. In order to solve the yield problem of 3D chips, TSV fault tolerance research has gradually been reported in recent years, arousing the attention of researchers at home and abroad. Guennoc, T. et al. first proposed a circuit model for vertical channels and then proposed a fault-tolerant technology for TSV redundancy, which improved the yield from 66% to 98% [4]. Xiao, Y. et al. proposed a fault-tolerant approach based on multichannel, which can improve reliability and throughput at the same time [5]. Afterward, researchers aimed at the process differences and scales of different chips, and many TSV fault tolerance mechanisms are designed to meet the performance requirements of the chip. Zhang, X. et al. proposed that when the TSV failure rate is too high, using serial power communication and signal remapping, remap the communication channel to the fault-free channel, thereby ensuring the smoothness of the vertical channel which is shown in Figure 1 as a communication method based on the binary molecular communication model [6]. Some domestic universities and research institutes have designed circuits including TSV fault self-detection function and fault-tolerant function and also proposed several redundant circuits based on chain structure, high yield can be guaranteed when the number of TSVs is small, and the number of redundant TSVs can be optimized to the greatest extent; Gao, H. et al. proposed a bidirectional redundant fault-tolerant design, which enables redundant channel clusters to dynamically configure direction and interconnection with low latency and high throughput [7]. Zhang, Y. et al. proposed a fault-tolerant routing algorithm based on local fault blocks, which uses extended local reliability information to guide fault-tolerant routing of 3D mesh/torus networks and classifies fault-free nodes within each plane, which greatly improves the system's performance. Computing power and system performance [8]. Chakrabarti, A. et al. proposed a deadlock-free three-dimensional dynamic routing algorithm, based on the traditional 2D NoC parity-turn model, the 3D routing

space is divided into 8 quadrants, and the corresponding routing strategy is determined for each elephant limit so as to avoid deadlock [9]. Yang, S. et al. proposed a fault-tolerant routing algorithm based on cache reuse of faulty links, the algorithm adds 4 self-transmitting channels to each power communication node and adopts a transparent transmission mechanism based on cache reuse, by multiplexing the normal buffers and channels at both ends of the faulty link to transparently transmit the data packets on the faulty channel, and the probability of using the optimal output port for the data packets is improved [10]. Wang, H. et al. proposed a virtual channel-free fault-tolerant routing algorithm for node failures in 3DmeshNoC, which is based on 3D defense areas. The 3D defense area can provide the location information of the faulty body, and according to the location information of the faulty body provided by the defense area, the algorithm can find the fault location in advance and change the forwarding port so as to achieve fault tolerance and avoid introducing deadlock [11].

In 3DNoC, if two sets of unidirectional TSVs connecting adjacent routers fail, data cannot be transmitted through this channel. In order to achieve fault tolerance and further reduce transmission delay and power consumption, the author designs the TSV router in 3DNoC as a double crossbar switch structure, and each input port is divided into two subports without input buffer (buffer) and with input buffer; it is connected with the two-stage crossbar Master-Crossbar and SlaveCrossbar, respectively. Compared with reference, experiments show that by organically combining the improved redundant TSV fault-tolerant design and the design of double crossbar switches, the average delay of the network can be reduced, the area overhead of the buffer in the chip is reduced, the power consumption is reduced, and the system reliability is improved.

3. Research Methods

3.1. Overview of Crossbar Fault Tolerance. In the structure of the 3DNoC router, the crossbar is the core component, and under the cooperative operation of the arbiter and the control module, it can process data from different input ports and select the corresponding output port to output. If the crossbar fails, it will greatly affect the performance of the router power. Therefore, the fault tolerance of the crossbar switch needs to be considered [12].

There is a fault-tolerant scheme that adds a bypass mechanism to bypass the faulty crossbar, and in this scheme, if the crossbar fails, data are transferred through the bypass. Alternatively, between each input and output port on either side of the crossbar, an error detection module for cyclic redundancy check (CRC) is added, and if a data error is detected, the data will be discarded or retransmitted. All unidirectional TSVs in 3DNoC are configured as bidirectional TSVs, which have certain fault tolerance; however, when the unidirectional TSVs between adjacent TSV routers all fail, fault tolerance cannot be achieved.

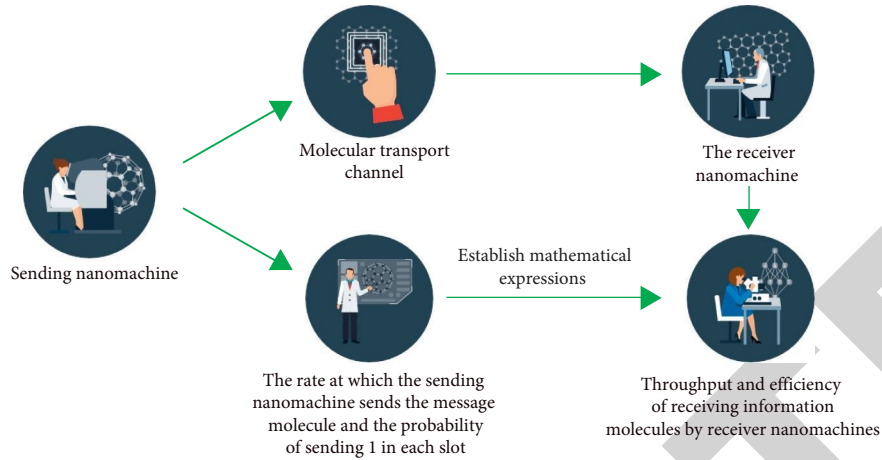


FIGURE 1: A communication method based on the binary molecular communication model.

In addition, the delay and power consumption problems faced in 2DNoC are also problems that 3DNoC hopes to solve. Its delay and power consumption are mainly distributed among the link, crossbar, and input buffer. The power consumption of the input buffer accounts for 46% of the total power consumption [13]. Some researchers reduce the input buffer or remove the buffer, but this will reduce the performance of the network [14].

The author modified the fault-tolerant design of redundant bidirectional TSVs, reducing the original two subinput buffers, and at the same time, combining with the design of the double crossbar switch of the router, the TSV router in the 3DNoC architecture is designed as a double crossbar switch architecture, which can reduce power consumption and delay while realizing fault tolerance.

3.2. Bidirectional TSV Fault Tolerant Architecture. The author has 3DNoC communication architecture, where every four 2D routers share a TSV router. When data packets require interlayer communication, the XYZ routing algorithm is used. First, the data packet is routed on the same plane to reach the cluster corresponding to the cluster where the destination node is located, and then the data packet is transmitted to the TSV router for transmission along the Z direction through TSV.

The author's bidirectional TSV fault-tolerant design structure is shown in Figure 2, which is perfected and modified on the basis of redundant bidirectional TSV fault-tolerant design. The structure design reduces the buffer area and at the same time removes the package assembly module in the original design so that the overall design is more concise and the area cost is smaller. Because the buffer is the component that occupies the largest area and consumes the largest power consumption in the entire router, reducing the use of the buffer can save resources to a large extent. If you want the structure to transmit two flits at the same time to achieve high-speed data transmission, you can perform flit-level acceleration processing on the data packets, such as using

the flit-level acceleration mechanism of the virtual channel, combined with the control module of the bidirectional link, in order to realize the flit-level acceleration high-speed transmission [15].

3.3. TSV Router Architecture

3.3.1. Design and Fault Tolerance of Double Crossbar. In order to further reduce the transmission delay of the network, realize the fault tolerance of the crossbar switch, and improve the performance of the whole 3DNoC system, the author designs the TSV router power in 3DNoC as double crossbar switch architecture.

In the cluster-based 3DNoC architecture, which commonly used TSV routers without virtual channels, each TSV router has 6 input and output ports, namely east-north (EN), west-north (WN), east-south (ES), west-south (WS), up (UP), and down (DW). These six ports are, respectively, responsible for the power communication with the four 2D routers in different directions in the same cluster and the TSV routers in the upper and lower adjacent layers. In order to prevent out-of-order crosstalk of data packets during transmission, the author's data packets are only designed in the format of a data flit.

In 3DNoC, data packet transmission must go through the crossbar switch, and the data packet can transmit data smoothly only after being assigned to the crossbar switch. When there are multiple data packets requesting transmission, the data packets that cannot be allocated by the crossbar switch and cannot be transmitted in time will be buffered in the input buffer and wait, as well as packets cannot be transmitted until the crossbar arbiter responds and assigns the crossbar. If there are many data packets communicated in the network and the network load is large, the data packets buffered in the input buffer will become more and more arriving, and the transmission delay will also increase with the increase of the waiting time of the data packets, which will seriously affect the network performance of 3DNoC. In order to reduce the transmission delay, the author redesigned the architecture of the TSV router in

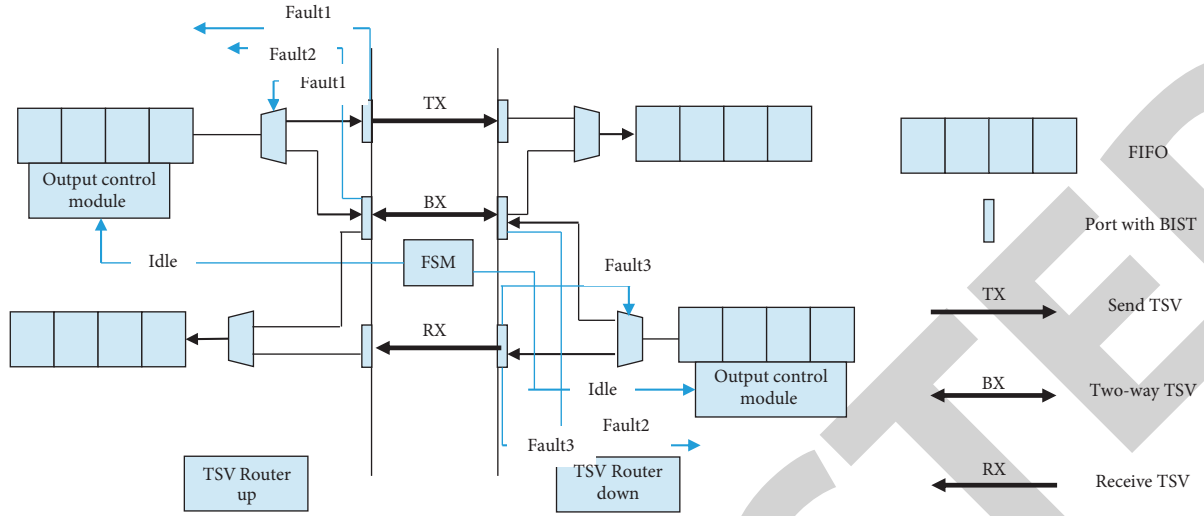


FIGURE 2: Bidirectional TSV fault-tolerant design.

3DNoC by using the architecture of the dual crossbar router in 2DNoC proposed in [16].

The designed crossbar consists of a master crossbar and a slave crossbar. Each input port of the TSV router is divided into two subports by a data distributor (Demultiplexer, DMUX), which are respectively connected to the master crossbar and the slave crossbar. There is no input buffer on the path connected to the master crossbar, and there is an input buffer on the path connected to the slave crossbar; each output port is set with a data selector (Multiplexer, MUX) connected to the master crossbar and the slave crossbar, respectively [17].

The master crossbar has higher priority than the slave crossbar. As long as there is data input from the port of the TSV router, the master crossbar is preferentially selected for transmission; only when the master crossbar is occupied, the slave crossbar is selected for transmission, and the data passing through this path must pass through the input buffer cache [18]. If there is a new data request for transmission at this time, as long as the master crossbar is idle, the master crossbar is preferred; otherwise, it must be cached in the buffer and then transmitted through the slave crossbar.

When data packets are transmitted through the master crossbar path, there is no need to buffer the data, the data can be transmitted directly through the link, and the delay and power consumption of the link are much smaller than that of the buffer; this is the main reason why the author designed the TSV router power as a dual crossbar. On the other hand, the design of the double crossbar switch also has the function of fault tolerance. In the traditional design, there is only one crossbar switch, if a hardware failure occurs in this crossbar switch, the entire TSV router cannot complete the routing and forwarding of data packets, and the entire router will be scrapped, resulting in a great waste of resources. In the author's dual crossbar TSV router, the original crossbar has been replaced by the current two crossbars, the master

crossbar and the slave crossbar, which can help each other and complement each other [19].

Define $1M_{\text{fault}}$ to represent the fault condition of MasterCrossbar,

$$M_{\text{fault}} = \begin{cases} 0, & \text{No trouble,} \\ 1, & \text{failure.} \end{cases} \quad (1)$$

Define $2S_{\text{fault}}$ to represent the fault condition of Slave Crossbar,

$$S_{\text{fault}} = \begin{cases} 0, & \text{No trouble,} \\ 1, & \text{failure.} \end{cases} \quad (2)$$

The fault-tolerant mechanism of double crossbar switches detects whether the master and slave crossbars are faulty at the same time through BIST and feeds back the detected M_{fault} and S_{fault} signal values to the crossbar arbiter (SA). After receiving the feedback signal from the BIST, the SA knows whether the crossbar switch of the router is faulty according to the value of the feedback signal and then allocates the crossbar switch according to the fault condition. If $M_{\text{fault}} = 0$ and $S_{\text{fault}} = 0$, then a single data packet preferentially selects the master crossbar of the router to transmit data and only selects the slave crossbar for transmission when the master crossbar is occupied; if multiple data packets are requested at the same time, the master crossbar and slave crossbar can be used to transmit data at the same time under the principle of two-level crossbar priority.

If one of the feedback signals has a value of 1, which indicates that one of the double crossbars is faulty, the data packet can only select the crossbar whose fault signal value is 0 in the router for transmission [20]. There are two cases for this, which are as follows:

- (1) When $M_{\text{fault}} = 1$ and $S_{\text{fault}} = 0$, the master crossbar is faulty, and the data packet can only select the slave crossbar to transmit data.
- (2) When $M_{\text{fault}} = 0$, $S_{\text{fault}} = 1$, the slave crossbar is faulty, and the data packet can only select the master crossbar to transmit data.

Therefore, the structure of the double crossbar switch can realize fault tolerance. In the event of a failure of one of the two crossbar switches, data can be passed through the other faultless crossbar switch without being blocked.

If the main crossbar fails, our original intention of reducing power consumption and delay will not be realized, but data can still be transmitted through the slave crossbar and become a traditional router transmission. If the slave crossbar fails, the data packets can still be transmitted through the master crossbar, but the master crossbar does not have an input buffer, which reduces power consumption and delay and also reduces the throughput of the system, as well as the performance of 3DNoC will decrease accordingly. It is clear that although in the double crossbar design, there is a failure in the system performance which will be affected; however, another one can be used to achieve fault tolerance so that data can be transmitted smoothly. Moreover, the TSV router can still work, and the whole router will not be disabled due to the failure of the crossbar switch, thus saving router resources.

3.3.2. TSV Router Pipeline Segment. In the 3DNoC architecture designed by the author, all 2D routers adopt the four-stage pipeline shown in Figure 3(a). (a) The figure shows the 4-stage basic pipeline of a TSV router without virtual channels. When the data packet arrives at the TSV router, it is first buffered in the buffer, that is, the write buffer (BufferWrite, BW); then, through routing calculation (routing computation, RC), the routing information of the data packet is obtained; after determining the next-hop address of the data packet, the cross switch allocation (switch allocation, SA) is performed; the cross switch determines which port to output the data packet from according to the result of route calculation and cross switch allocation, that is, the cross switch transmission (Switch Transmission, ST); after going through four basic pipelines, the data packets are transmitted through the link (link transmission) and routed to the next-hop TSV router. This is a traditional router pipeline that does not use virtual channels.

The design of the TSV router adopts the forward routing strategy to further reduce the pipeline segment, and after the TSV router adopts the design of the double crossbar switch, the master crossbar switch and the slave crossbar switch can transmit data packets at the same time, so SA and ST can be in the same segment of the pipeline [21]. Moreover, the data packets passing through the main crossbar switch do not need to be written to the buffer BW. Therefore, the pipeline can be reduced by two stages at most, as shown in Figure 3(b), which is the optimal delay. If the data packet is transmitted from the crossbar switch, it is necessary to increase the BW pipeline after the RC, and the overall

pipeline segment is only reduced by one segment, as shown in Figure 3(c). Since the pipeline segment of each data packet is reduced, the transmission delay of the whole network of 3DNoC is also reduced [22].

4. Results Analysis

The experimental tool for network simulation analysis uses OPNET simulation software to build a $4 \times 4 \times 3$ 3DmeshNoC model. In the process model modeled by OPNET, the router-related routing algorithm is set well, and the author's experimental communication still adopts a convincing random power communication mode. In the simulation experiment, under different packet injection rates, comparing the network performance between the author's proposed scheme and the communication architecture proposed in the literature, the transmission delay of data packets in the network is used as a technical indicator.

Before completing the experiment, first introduce two nouns: the Manhattan distance and the hop count.

- (1) Manhattan distance refers to the subtraction of the corresponding X , Y , and Z coordinates of two resource nodes in the 3DNoC network, and the sum of their absolute values is taken; this sum is the Manhattan distance. For example, the coordinates of the source node are (X_s, Y_s, Z_s) , and the coordinates of the destination node are (X_d, Y_d, Z_d) , which is the Manhattan distance between the source node and the destination node as follows:

$$\text{diff} = |X_s - X_d| + |Y_s - Y_d| + |Z_s - Z_d|. \quad (3)$$

- (2) Hop count refers to the sum of the number of routers separated by the source node and the destination node in the X and Y directions.

The delay of data packet transmission is mainly affected by the location and routing algorithm of the source resource node and destination resource node in 3DNoC. If the Manhattan distance between two resource nodes is far away, the number of routing hops will increase when they communicate between them, and the transmission delay will increase with it [23]; on the contrary, the number of hops will be very small, and the delay will be very small. The power communication between resource nodes is completed according to the corresponding routing algorithm; if the efficiency of the routing algorithm is relatively low, the short Manhattan distance needs to be detoured to reach it, and the transmission delay will increase [24, 25].

The author's experimental results are shown in Figures 4–7, and the results show that when the author's fault-tolerant scheme is not combined with the double crossbar switch, the transmission delay is still much less than that of the literature because the author realizes fault tolerance for the faulty TSV by adding a bidirectional TSV to replace the faulty TSV. Therefore, when there is a TSV failure, the transmission delay increases with the increase in the number of failures, but the author's design can make the data packets transmitted in the network without being affected.

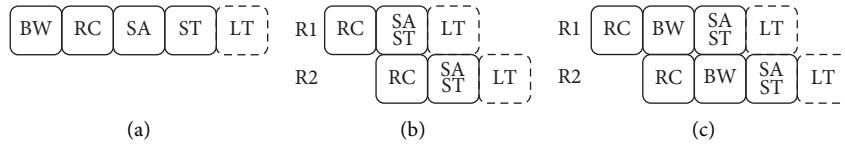


FIGURE 3: Router pipeline segment. (a) No virtual channel. (b) The main crossbar switch. (c) From the crossbar.

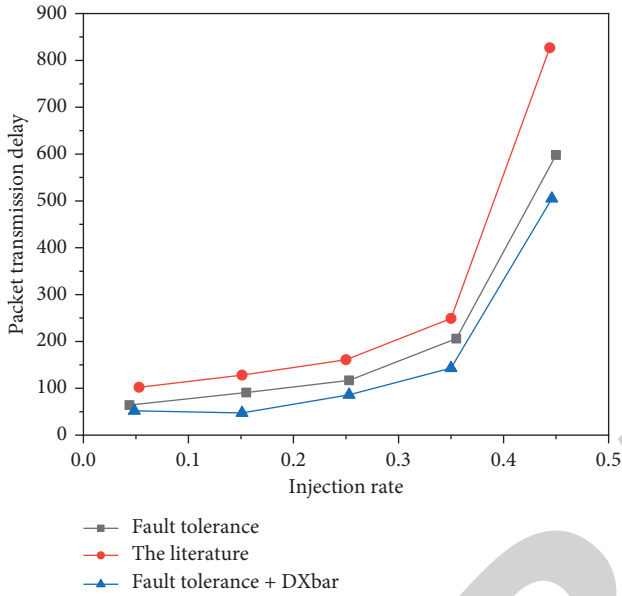


FIGURE 4: Comparison of packet transmission delays when there is no number of faulty TSVs.

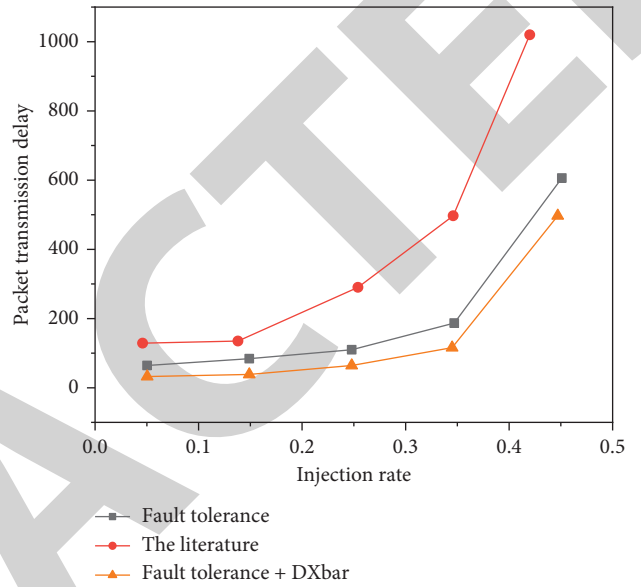


FIGURE 6: Comparison of packet transmission delay with two groups of faulty TSVs.

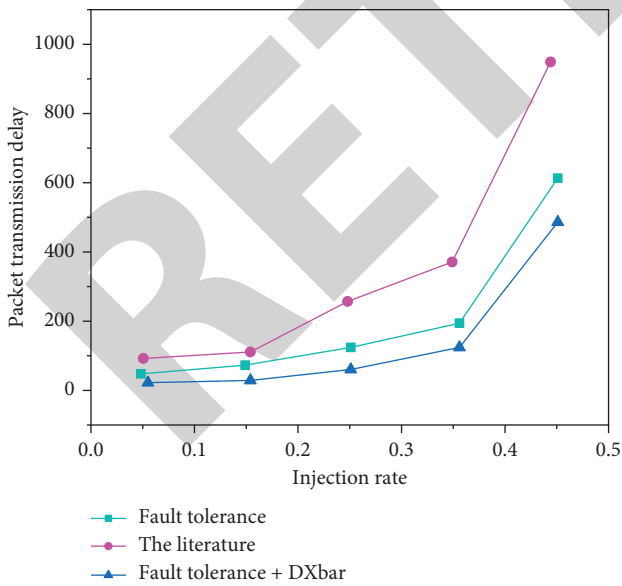


FIGURE 5: Comparison of packet transmission delays when a group of faulty TSVs is counted.

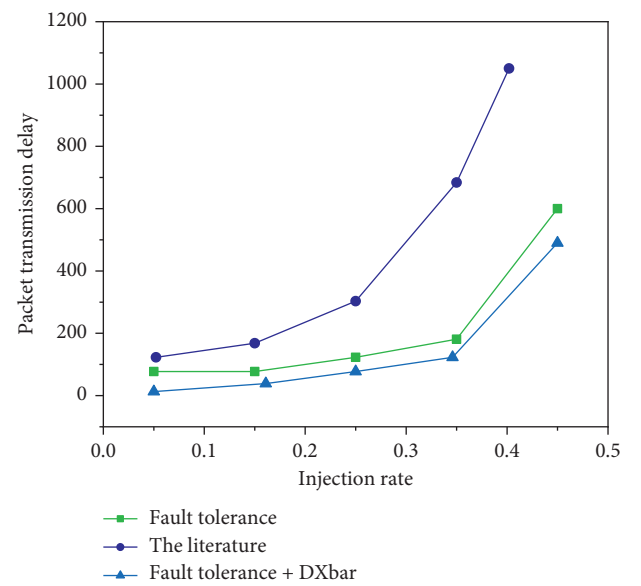


FIGURE 7: Comparison of packet transmission delays with three groups of faulty TSVs.

5. Conclusion

In order to ensure the reliability of the 3DNoC architecture, realize fault tolerance, and reduce the transmission delay of data packets, the author proposes that on the basis of the redundant bidirectional TSV design, the TSV router is designed as a double crossbar switch architecture, which realizes the fault tolerance of the original TSV and further reduces the network delay and power consumption. Moreover, the author adopts the design of double crossbar switches, which can be fault-tolerant to the crossbar switches, and the failure of any crossbar switch will not affect the transmission of data packets. The experimental results show that the author's design scheme is superior and improves the reliability of the 3DNoC system.

Data Availability

The data used to support the findings of this study are available from the corresponding author upon request.

Conflicts of Interest

The authors declare that they have no conflicts of interest.

Acknowledgments

This study is funded by the Construction of Electronic Information Experimental Teaching Demonstration Center Project of the Guangdong Undergraduate University Teaching Quality and Teaching reform project in 2020, (2020SY19).

References

- [1] E. Khodadadi, B. Barekatin, E. Yaghoubi, and Z. Mogharrabi-Rad, "Ft-pdc: an enhanced hybrid congestion-aware fault-tolerant routing technique based on path diversity for 3d noc," *The Journal of Supercomputing*, vol. 78, no. 1, pp. 523–558, 2021.
- [2] F. Al-Obaidy and F. A. Mohammadi, "Predictions optimal routing algorithm based on artificial intelligence technique for 3d noc systems," *Microsystem Technologies*, vol. 27, no. 9, pp. 3313–3323, 2021.
- [3] K. Balamurugan, B. Subrahmanyeswara Rao, and M. Vijayaraj, "Performance analysis of optad-noc: a novel optimized routing algorithm and intelligent router for 3d network-on-chip," *Wireless Personal Communications*, vol. 121, no. 4, pp. 2511–2528, 2021.
- [4] T. Guennoc, J. B. Doc, and S. Félix, "Improved multimodal formulation of the wave propagation in a 3d waveguide with varying cross-section and curvature," *Journal of the Acoustical Society of America*, vol. 149, no. 1, pp. 476–486, 2021.
- [5] R. Li, Y. Xiao, P. Yang, W. Tang, M. Wu, and Y. Gao, "Uav-aided two-way relaying for wireless communications of intelligent robot swarms," *IEEE Access*, vol. 8, no. 99, pp. 56141–56150, 2020.
- [6] X. Zhang, J. Tan, J. Wu, and W. Chen, "Event-triggered-based fixed-time adaptive neural fault-tolerant control for stochastic nonlinear systems under actuator and sensor faults," *Nonlinear Dynamics*, vol. 108, no. 3, pp. 2279–2296, 2022.
- [7] H. Gao, W. He, Y. Zhang, and C. Sun, "Adaptive finite-time fault-tolerant control for uncertain flexible flapping wings based on rigid finite element method," *IEEE Transactions on Cybernetics*, vol. 2, no. 99, pp. 1–12, 2021.
- [8] Y. Zhang, M. Liu, and C. Zhang, "Robust fault-tolerant h_∞ output feedback control of active suspension and dynamic vibration absorber with finite-frequency constraint," *IET Intelligent Transport Systems*, vol. 14, no. 14, pp. 1935–1945, 2021.
- [9] A. Chakrabarti, A. Saha, and S. K. Biswas, "Winding open-circuit fault-tolerant operation of single DC-link dual-inverter fed three-phase open-end induction motor drive...ink dual inverter fed three-phase open-end induction motor drive," *IET Power Electronics*, vol. 14, no. 7, pp. 1256–1270, 2021.
- [10] S. Yang, H. Wang, and Q. Chen, "An improved algorithm based on deep learning network for road image redundancy removal," *The Journal of Supercomputing*, vol. 78, no. 8, pp. 10385–10404, 2022.
- [11] H. Wang, L. Z. Ge, R. Li, Y. Gao, and C. Cao, "Motion optimization of humanoid mobile robot with high redundancy," *Assembly Automation*, vol. 41, no. 2, pp. 155–164, 2021.
- [12] R. A. Beardsworth, "Is this research still relevant six years on?" *BMJ*, vol. 22, no. 2, pp. 229–239, 2020.
- [13] M. Kule, H. Rahaman, and B. B. Bhattacharya, "Function-mapping on defective nano-crossbars with enhanced reliability," *Journal of Computational Electronics*, vol. 19, no. 2, pp. 555–564, 2020.
- [14] B. Tang, X. Wang, C. T. Nguyen, B. Ye, and S. Lu, "Construction of subexponential-size optical priority queues with switches and fiber delay lines," *IEEE/ACM Transactions on Networking*, vol. 28, no. 1, pp. 336–346, 2020.
- [15] Z. Zhang, A. Chen, G. Ma et al., "Controllable functional layer and temperature-dependent characteristic in niobium oxide insulator-metal transition selector," *IEEE Transactions on Electron Devices*, vol. 67, no. 7, pp. 2771–2777, 2020.
- [16] G. Li, F. Liu, A. Sharma et al., "Research on the natural language recognition method based on cluster analysis using neural network," *Mathematical Problems in Engineering*, vol. 2021, Article ID 9982305, 13 pages, 2021.
- [17] D. Selva, B. Nagaraj, D. Pelusi, R. Arunkumar, and A. Nair, "Intelligent network intrusion prevention feature collection and classification algorithms," *Algorithms*, vol. 14, no. 8, p. 224, 2021.
- [18] J. Chen, J. Liu, X. Liu, X. Xu, and F. Zhong, "Decomposition of toluene with a combined plasma photolysis (cpp) reactor: influence of uv irradiation and byproduct analysis," *Plasma Chemistry and Plasma Processing*, vol. 41, no. 1, pp. 409–420, 2020.
- [19] R. Huang, S. Zhang, W. Zhang, and X. Yang, "Progress of zinc oxide-based nanocomposites in the textile industry," *IET Collaborative Intelligent Manufacturing*, vol. 3, no. 3, pp. 281–289, 2021.
- [20] M. K. A. Kaabar, V. Kalvandi, N. Eghbali, M. E. Samei, Z. Siri, and F. Martínez, "A generalized ML-hyers-ulam stability of quadratic fractional integral equation," *Nonlinear Engineering*, vol. 10, no. 1, pp. 414–427, 2021.
- [21] L. Liu, J. Li, Y. Deng, Z. Yang, K. Huang, and S. Zhao, "Optimal design of multi-layer structure composite containing inorganic hydrated salt phase change materials and cement: lab-scale tests for buildings," *Construction and Building Materials*, vol. 275, no. 11, Article ID 122125, 2021.
- [22] D. Szalai and T. Horvath, "Design of multi-layered building structures using bim method," *IOP Conference Series: Materials Science and Engineering*, vol. 1218, no. 1, Article ID 012055, 2022.

Retraction

Retracted: Simulation of Multisensor Energy Data Fusion Transformer Acquisition System Based on FPGA

International Transactions on Electrical Energy Systems

Received 3 October 2023; Accepted 3 October 2023; Published 4 October 2023

Copyright © 2023 International Transactions on Electrical Energy Systems. This is an open access article distributed under the Creative Commons Attribution License, which permits unrestricted use, distribution, and reproduction in any medium, provided the original work is properly cited.

This article has been retracted by Hindawi following an investigation undertaken by the publisher [1]. This investigation has uncovered evidence of one or more of the following indicators of systematic manipulation of the publication process:

- (1) Discrepancies in scope
- (2) Discrepancies in the description of the research reported
- (3) Discrepancies between the availability of data and the research described
- (4) Inappropriate citations
- (5) Incoherent, meaningless and/or irrelevant content included in the article
- (6) Peer-review manipulation

The presence of these indicators undermines our confidence in the integrity of the article's content and we cannot, therefore, vouch for its reliability. Please note that this notice is intended solely to alert readers that the content of this article is unreliable. We have not investigated whether authors were aware of or involved in the systematic manipulation of the publication process.

Wiley and Hindawi regrets that the usual quality checks did not identify these issues before publication and have since put additional measures in place to safeguard research integrity.

We wish to credit our own Research Integrity and Research Publishing teams and anonymous and named external researchers and research integrity experts for contributing to this investigation.



The corresponding author, as the representative of all authors, has been given the opportunity to register their agreement or disagreement to this retraction. We have kept a record of any response received.

References

- [1] L. Luan and D. Hu, "Simulation of Multisensor Energy Data Fusion Transformer Acquisition System Based on FPGA," *International Transactions on Electrical Energy Systems*, vol. 2022, Article ID 7612674, 7 pages, 2022.

Research Article

Simulation of Multisensor Energy Data Fusion Transformer Acquisition System Based on FPGA

Lan Luan ¹ and Dan Hu ²

¹College of Computer Science and Information, Guizhou University of Commerce, Guiyang 550025, China

²School of Big Data and Information Engineering, Guizhou University, Guiyang 550025, China

Correspondence should be addressed to Lan Luan; 201903528@stu.ncwu.edu.cn

Received 10 July 2022; Revised 30 July 2022; Accepted 4 August 2022; Published 23 August 2022

Academic Editor: Nagamalai Vasimalai

Copyright © 2022 Lan Luan and Dan Hu. This is an open access article distributed under the Creative Commons Attribution License, which permits unrestricted use, distribution, and reproduction in any medium, provided the original work is properly cited.

In order to solve the problems of small signal acquisition range and poor acquisition accuracy of the existing multichannel acquisition system, a multisensor energy data fusion transformer acquisition system simulation method based on FPGA is proposed, and key hardware functions are designed and implemented. The system uses FPGA to control the core logic, synchronously collects and controls the energy data of the CCD camera and the laser rangefinder, organizes and uses an external large-capacity SDRAM group for buffering, and uses a dedicated PCI interface chip PLX9656 to achieve high-speed data transmission. Two pieces of sensor energy data and PCI bus energy data are stored in real time using a large-capacity disk array composed of multiple SATA hard disks. The function and performance of the energy data acquisition and storage system were tested. After the actual system test, the experimental results show that the transmission speed of the system through the PCI bus exceeds 200 MB/s, the writing speed of the continuous disk array is 240 MB/s, and the real-time acquisition and recording speed is 100 MB/ss. *Conclusion.* The system effectively solves the problems of high-speed data acquisition and storage and large capacity data transmission of key sensor nodes.

1. Introduction

In the research of aerospace, geological exploration, satellite navigation, and other fields, it is necessary to collect and record some important energy data parameters for energy data analysis and research, which has important reference value for the next experiment improvement and result analysis and is also more important for the result analysis of scientific research energy data. Therefore, the research and design of energy data acquisition memory is of great significance for these fields [1]. The main application of data acquisition memory in these fields is to collect and record the data collected by various sensors during the working process of aircraft, such as vibration signal, noise signal, image signal, and other key data. These energy data play a key role in the monitoring of aircraft operation status, fault analysis, environmental energy data acquisition, and so forth; it is very important to accurately collect and record

energy data. With the increase of the amount of energy data to be tested and the types of test energy data, it is necessary to collect and store multiple energy data signals at the same time, which puts forward higher requirements for the performance of the energy data acquisition and storage system. Because FPGA can process a large amount of parallel data at the same time, the current mainstream data acquisition memory design schemes use FPGA as the control module, write logic circuit programs in FPGA to control, receive the data signals sent from the outside, and save them in the memory. In recent years, with the rapid development of semiconductor technology and the maturity of production technology, energy data acquisition memory has ushered in new development. As the main control module of energy data acquisition memory, large-scale integrated circuits such as PGA and single chip microcomputer make energy data acquisition and storage more complex and functional by software programming. The products

developed in recent years have made great progress in multichannel energy data acquisition, large-capacity storage, high-speed storage, and so forth [2].

Therefore, it is of great significance to improve the collection and storage of real-time energy data by using emerging technologies.

2. Literature Review

For real-time energy data collection and storage, Miao et al. proposed realizing feeder automation FA by building distribution automation system (DAS) [3]. The meaning of feeder automation is to monitor the status of current, voltage, interconnection switch, and section switch on the feeder remotely. Yarlagadda et al. proposed updating the solid-state storage technology in the aerospace energy data storage system, changed the previous method of using tape storage, and improved the stability and reliability of the energy data storage technology [4]. Kumar et al. proposed the integration of FPGA technology and ASIC technology, so as to reduce its disadvantages of large volume, insufficient capacity, and larger power consumption than ASIC and then optimize energy data transmission [5]. He et al. proposed that FPGA chip is the core device, and online driving fatigue detection can be realized only by matching with appropriate digital image algorithm. The design omits the DSP control chip and expands the memory to form a simplified minimum system. Reprogrammable features and highly integrated features can greatly reduce the design cycle and design cost [6]. Tappari proposed designing the internal logic circuit of FPGA and creating the firmware program of FX3. It realizes the receiving and storage of LVDS energy data and the reading of energy data in memory by computer [7]. Kowalczyk et al. proposed using multiple hard disks to form a RAID array (cheap redundant disk array). High-end storage functions and redundant energy data security were provided for large servers. Raid combines multiple independent hard disks (physical hard disks) in different ways to form a hard disk group (logical hard disk), thus providing higher storage performance than a single hard disk and providing energy data redundancy technology.

According to the requirement of real-time energy data acquisition and storage of key sensor nodes, this paper proposes a solution of real-time energy data acquisition and high-speed storage based on FPGA and designs and implements the key hardware functions. The system uses FPGA for core logic control, synchronously collects and controls the energy data of CCD camera and laser rangefinder, sorts out and uses external large capacity SDRAM group for cache, uses a special PCI interface chip PLX9656, realizes the high-speed transmission of two pieces of sensor energy data and PCI bus energy data, and uses a large capacity disk array composed of multiple SATA hard disks for real-time storage. The function and performance of the energy data acquisition and storage system are tested to prove the real time, stability, and efficiency of the real-time energy data acquisition and storage of key nodes.

3. Research Methods

3.1. Main Functions and Technical Indicators. In the measurement system, in order to accurately measure the jitter of the flexible baseline and the change of the relative attitude of the two antennas in real time, it is necessary to select a CCD camera with high frame rate and large array and a high-precision laser rangefinder for combined measurement, which will produce a large amount of high-speed image energy data and distance energy data output by the laser rangefinder [8]. Therefore, the main function of the high-speed acquisition and storage system designed in this paper is to control the time synchronization between the measurement sensors, complete the real-time energy data acquisition of each sensor, and shunt the collected energy data. One channel of energy data is stored at high speed; another channel of energy data is output to another real-time processing system. According to the requirements of flexible baseline measurement system, the system in this paper should be able to collect and store the measurement energy data of two sensors in real time. The technical indicators to be achieved mainly include continuous acquisition speed, continuous storage speed, and minimum storage capacity. The CCD camera in the system adopts a high-resolution, high frame rate area array digital camera, the image resolution is 1608 columns \times 1208 rows, and the maximum frame rate of the camera is 30 Hz. The AD sampling of the camera energy data is 10 bits, and the energy data acquisition is only 8 bits high, so the energy data volume generated by the CCD camera per second is about 55.57 MB [9]. LRFS-0040-2 laser rangefinder is used as the laser rangefinder. The measurement rate can reach 50 Hz at most. RS422 interface is used as the energy data interface, and the amount of energy data generated is 9.6 kB/s. The energy data volume of the two sensors per second is about 56 MB/s, so the continuous acquisition speed of the acquisition system must be greater than 56 MB/s before real-time energy data acquisition of the two sensors can be carried out. Only when the continuous storage rate is greater than the acquisition speed can the energy data be stored in real time and accurately. Therefore, the continuous storage speed should be greater than 56 MB/s, and the maximum theoretical read-write speed of SATA hard disk can reach 150 MB/s. Using multiple SATA hard disks to form a RAID array can provide higher storage performance than a single hard disk. According to the requirements of the flexible baseline measurement system, the longest continuous working time of the acquisition storage system is about 2 h, and the minimum storage capacity required is about 390.76 GB [10]. According to the demand analysis of the above energy data acquisition system and considering the scalability of the system and the needs of actual energy data transmission and terminal processing, it is required that the energy data acquisition and recording speed should reach 70 MB/s, the continuous disk array writing speed should reach 120 MB/s, and the storage capacity should reach 2 TB. For the 32-bit/33 MHz PCI bus, it can generally reach 80 MB/s in actual use. The energy data in and out of the system memory must pass through the PCI bus, which will reduce the efficiency of the bus by half. The

acquisition speed of the system must be greater than 56 MB/s, so the 64-bit/66 MHz PCI bus is selected, and the peak speed of energy data transmission can reach 528 MB/s. The existing system shows that the actual transmission speed of the 64-bit/66 MHz PCI bus can reach more than 200 MB/s, so the transmission speed of the PCI bus fully meets the system requirements [11].

The whole system is mainly composed of CCD camera, laser rangefinder, PCI energy data acquisition card, SATA disk array, and computer. The PCI image acquisition card is mainly composed of sensor energy data interface, FPGA logic control chip, cache, and PCI interface chip. The principle of the scheme is as follows: Firstly, the host sends commands to configure the CCD camera and laser rangefinder. After the configuration is completed, the acquisition is started. The high-speed image energy data output by the CCD camera and the synchronous control signal are sent to the FPGA and cached in the FPGA. The energy data of the laser rangefinder is also sent to the dual-port RAM of the FPGA through the serial port for caching. After the FIFO is half full, the energy data of the CCD camera and the laser rangefinder are shunted under the control of the FPGA, one of which is sent to the external SDRAM group for caching. After the SDRAM is stored in the set image frame number, it is sent to the PCI for interruption. The host responds to the interruption, reads the data from the SDRAM to the memory for processing, and writes the data to the hard disk to complete real-time storage. The other way is sent to the relevant real-time processing system for processing. The block diagram of the whole design scheme is shown in Figure 1.

The design of data real-time acquisition and storage system applied to flexible baseline measurement system includes the following key technologies: CameraLink interface technology, multisensor synchronization technology, real-time acquisition and cache of multisensor data, and real-time storage of multisensor data.

3.2. Key Design and Implementation of Real-Time Energy Data Acquisition and Storage System. The experimental camera adopts CameraLink standard interface, and the basic configuration adopts standard MDR26 connector output. The system uses FPGA as the main control chip of the acquisition card, and the i/o standard supported by FPGA is LVCMOS/LVTTL signal [12]. The main function of DS90CR288A is to complete the conversion from LVDS to TTL level signals and the conversion of serial signals into parallel signals. In order to set parameters and trigger control of the camera, it is necessary to convert the camera control signals (CC1-CC4) and signal SerTC (serial to camera) output from FPGA into LVDS signals through level conversion chip ds90lv047 and send them to the receiver. In order to receive the response signal (SerTFGserial-to-frame-grabber) sent by the camera to the acquisition card, ds90lv048 is used to convert the LVDS signal into TTL signal, which is sent to FPGA and sent to the host for display.

The system adopts 64-bit/66 MHz PCI bus to realize high-speed energy data transmission. PCI interface is the

communication interface between PCI bus and external bus to realize the communication between them. In this system, PLX9656 is used to design high-speed PCI card to realize the functions of setting camera parameters, setting laser ranging parameters, setting sampling parameters, reading image energy data, and so on. PLX9656 is the PCI interface controller with the highest performance at present. It has the performance of 66 MHz and 64 bits at PCI end and 66 MHz and 32 bits at local end and conforms to PCIV2.2 specification. The key point of PCI interface design in this system is the setting and implementation of PLX9656 local bus working mode and energy data transmission mode. The local bus of PLX9656 can be set to three modes: M mode, C mode, and J mode. According to the characteristics of the system, C mode can be selected, and the working mode of C mode can be realized by pulling down the pins of mode1 and mode0. In C mode, the energy data transmission mode is divided into master mode operation, slave mode operation, and DMA operation. The DMA working mode can realize the fast transmission between high-level peripherals and memory without CPU intervention, so it is more suitable for the transmission of CCD camera energy data and laser rangefinder energy data. The DMA transmission mode can be realized by setting dmamode0/1 and PCICR of the internal registers of PLX9656 [13].

3.3. FPGA Core Logic Control

3.3.1. Sensor Trigger Setting. In this design, the working modes of the two sensors are set through the host terminal, the mode setting string is transmitted to the FPGA through the PCI bus, and the communication with the camera and the laser rangefinder is realized through the serial port controller, so as to complete the configuration of the camera and the laser rangefinder. After the camera and the laser rangefinder receive the configuration command, the response information is also transmitted to the FPGA through the serial port controller and then transmitted to the host through the PCI bus. In order to realize the synchronous control with the laser rangefinder, the camera selects the software external trigger mode. In this mode, an EXSYNC trigger signal with a frequency of 20 Hz needs to be generated in the FPGA and sent to the CCD camera for exposure reading energy data. The low-level width of EXSYNC is 10 μ s, and the exposure time of the camera is set by the host terminal.

3.3.2. Energy Data Synchronization Control. The EXSYNC trigger signal is sent to the laser rangefinder and camera at the same time to realize the output synchronization of the two sensors. Because the measurement speeds of the two sensors are different, the output frame rate of the camera is 20 frames/s, and the output frequency of the laser rangefinder is 50 Hz, so the key to the design of data synchronization is how to record the single frame image data and the laser rangefinder data at the same time. The timing diagram of the synchronous acquisition of the two sensors is shown in Figure 2(a). Clk100 Hz is the least common multiple of

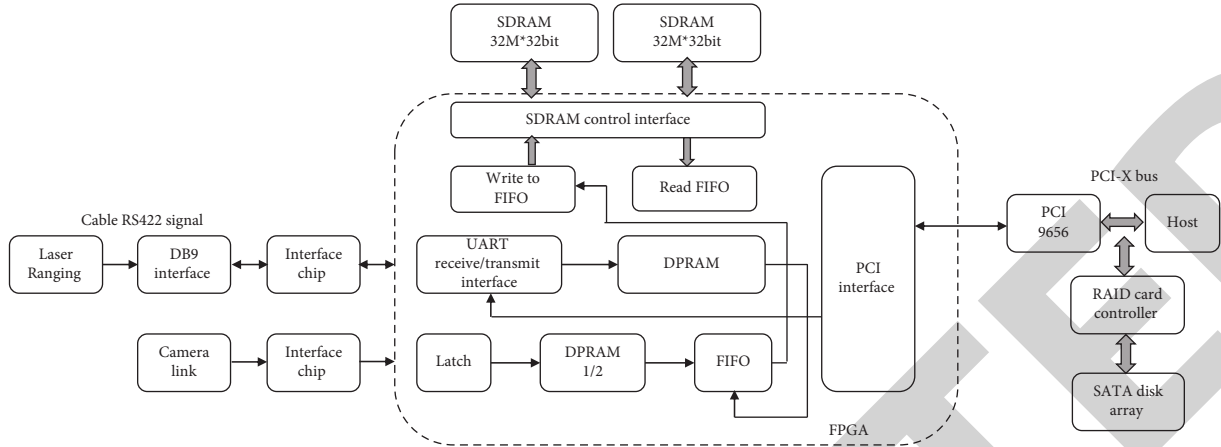


FIGURE 1: Design scheme block diagram of real-time energy data acquisition and storage system.

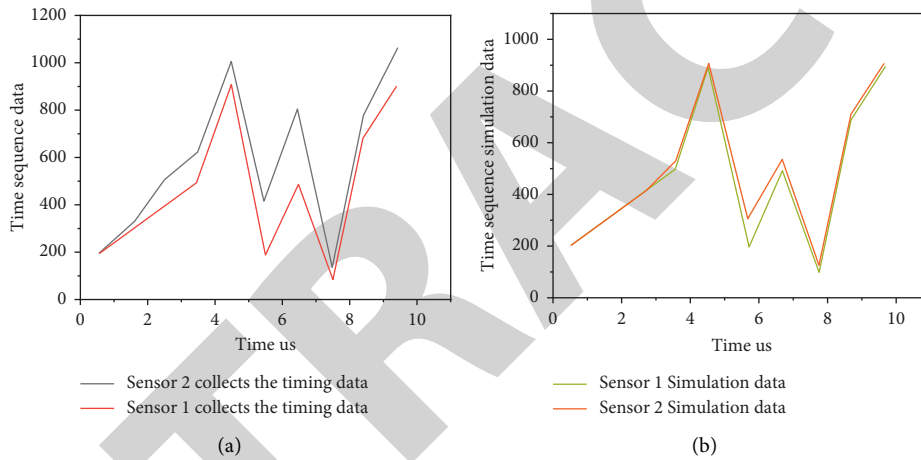


FIGURE 2: Synchronous acquisition design and simulation sequence diagram of CCD camera and laser rangefinder. (a) Collect energy data. (b) Simulation energy data.

two frequencies, which can be set according to the internal resource usage of FPGA. energy data_lrf_sel is the selected laser energy data, where I indicates that the energy data at this time is invalid, and V indicates that the energy data at this time is valid [14]. The energy data synchronization scheme is that after the camera energy data enters the FPGA, it is sorted and cached in two dual-port RAM, and the laser rangefinder sends the energy data into the FPGA through the serial port receiver. The serial port receiver of this design has FIFO cache, and the energy data is sent to the dual-port RAM for further cache after caching. The write enable Wen signal of the dual-port RAM is generated according to the timing diagram shown in Figure 2(a), and the laser energy data is written at this time into the dual-port RAM when the Wen signal is valid. When the read enable signal is valid, first the laser rangefinder energy data in the dual-port RAM is read into FIFO, and then the image energy data of the corresponding frame is read into FIFO. After the FIFO is half full, the laser rangefinder energy data and camera energy data are sent to the external SDRAM for further caching. The

simulation sequence diagram is shown in Figure 2(b) [15]. According to the simulation results in Figure 2, the synchronization design scheme in this paper can effectively reduce the delay between the two sensors and collect the relative synchronization energy data of the two sensors. Although it is not strictly synchronous, it can meet the requirements of the flexible baseline measurement system.

3.3.3. Energy Data Caching and Collation. The caching scheme adopted in this system is to firstly latch the image energy data and control signal at three levels, because the image energy data output by the experimental camera is the energy data of two taps, and the energy data of the two taps are, respectively, sent to the two dual-port RAM inside the FPGA for caching. The energy data of the left tap is stored according to the sequential address, and the energy data of the right tap is stored according to the reverse address, so as to splice the energy data of the two taps into a complete image. When the enable signal is valid, the data of the two dual-port RAM is sent to FIFO for further caching. When

the FIFO data is half full, the FIFO data is sent to the external SDRAM memory through the SDRAM interface controller.

3.3.4. PCI Logical Interface. The system completes the communication between FPGA and PLX9656 through PCI local logic interface. After the system is powered on, the internal register of PLX9656 is reset by the RST. At the same time, PLX9656 outputs local reset signal LRESET and checks whether EEPROM exists [16]. If the local DMA mode is used for control, the whole handshake process is as follows: First, when the energy data in the SDRAM cache reaches the set value, the signal is valid, and the PLX9656 sends an interrupt request signal to the host. If the CPU responds to the interrupt, it will issue the DMA read command, the number of bytes to be read, and the address information in the corresponding program of the interrupt. PLX9656 applies for the local bus to make the LHOLD signal valid. Once again, the FPGA effective ready signal is enabled, and the SDRAM control interface read enable effective signal is enabled, and the energy data begins to appear on the LD energy data bus. When the last byte of energy data starts to be transmitted, the PLX9656 drives the blast signal to be valid, and the FPGA has no ready signal [17]. Finally, the SDRAM read enable signal is made invalid, PLX9656 drives LHOLD to be invalid, the local bus is released, and then FPGA also drives LHOLDA to be invalid, ending the primary energy data transmission. The design of DMA transmission is shown in Figure 3.

3.4. Cache Design and Real-Time Cache Design. Because the internal cache capacity of PCI interface chip is too small, the cache must be used to cache the energy data in the process of real-time collection and then sent to the host through PCI bus to improve the transmission speed and performance of the system [18]. Large-capacity and high-speed SDRAM is easy to buy and the price is moderate. The system uses SDRAM for caching. Windows is a multithreaded and preemptive operating system. In order to reduce the interruption of threads due to the end of CPU occupation time, the interruption interval should be greater than the maximum thread execution time of 20 ms, so the cache capacity should be at least $20 \text{ ms} \times 70 \text{ MB/s} \times 2 = 2.8 \text{ MB}$. The caching scheme adopted by the system is to connect 2 groups of 32 m * 32-bit SDRAM to FPGA, which is configured by 4 pieces of SDRAM, and is used for energy data buffering from camera to PCI. The SDRAM is encapsulated into the FIFO interface through the controller, the camera energy data is written into the FIFO, the interrupt is sent to PCI according to the set number of images, and then the camera energy data is read by PCI, thus overcoming the shortcomings of complex SDRAM structure and difficult switching control circuit [19, 20].

Real-time streaming disk has always been the biggest bottleneck of high-speed energy data acquisition technology, which directly restricts the real-time storage capacity of acquisition and storage devices [21]. The system adopts PCI-X bus motherboard supporting 66 MHz, 100 MHz, and 133 MHz/64 bits. It consists of 8 high-speed SATA hard

disks with a capacity of 1 TB, which are configured into raid0 mode through raid card to maximize disk access rate and form a high-speed and large capacity storage device. The design block diagram of the entire digital camera energy data acquisition and storage device is shown in Figure 4. The system uses the interface chip PLX9656 to send the energy data output from the real-time acquisition module to the system memory through the PCI bus and then writes the energy data in the memory into the SATA hard disk array through the PCI bus under the control of the raid card. The theoretical continuous disk writing speed can reach more than 400 MB/s [22].

4. Result Analysis

In the experiment, the function and performance of the system are tested, respectively. Performance test mainly includes real-time acquisition and recording speed test, continuous disk array writing speed test, and stability test. For the function test of the system, the simulation image and the actual image energy data acquisition test are carried out, respectively. The analog image is the energy data with regular circulation generated in FPGA, and the corresponding image is the stripe image. The function of the acquisition system is verified according to whether the collected energy data is correct. Then switch to the actual energy data source and collect the moving image of the cooperative target. The test results of simulated and measured image energy data show that the system can collect and store energy data correctly without image dislocation, which verifies the correctness of the system function.

The test method for the real-time acquisition and recording speed of the system is as follows: because the output frequency of the sensor in the system is limited, it cannot reflect the maximum acquisition and recording speed of the system. Analog images of different frequencies are generated in FPGA, real-time acquisition and disk writing are carried out through the system, and the image is played back by the upper computer software to check whether there is frame loss and dislocation. The measured results show that when the output frequency exceeds 50 Hz, if only the image is collected and not saved, the image acquisition is correct, but when the disk is saved at the same time, the image dislocation and frame loss begin to occur. There are two main reasons: One is that when the frequency is greater than 50 Hz and the amount of energy data is greater than 100 MB/s, the theoretical reading and writing speed of the external cache of the system is 133 MHz. Because the FIFO interface is made to read while writing, the transmission speed is halved, which may lead to the cache energy data not being read in time, resulting in image dislocation and loss. The other is that the read and write of the system in the host memory is a thread, which reads and writes energy data at the same time, resulting in the rate falling behind. To sum up, the acquisition and recording speed of the system can reach 100 MB/s, meeting the index requirements of 70 MB/s.

The speed test method of continuous writing disk array is to use a special hard disk read-write speed test software to write energy data of different capacities from the host

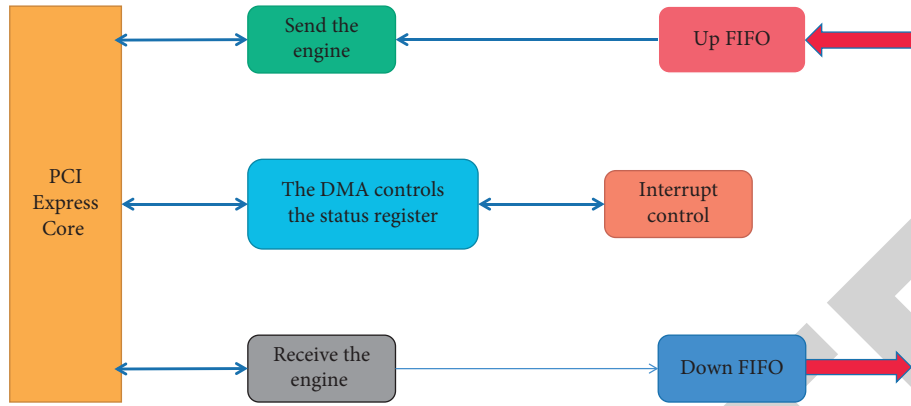


FIGURE 3: DMA transmission design.

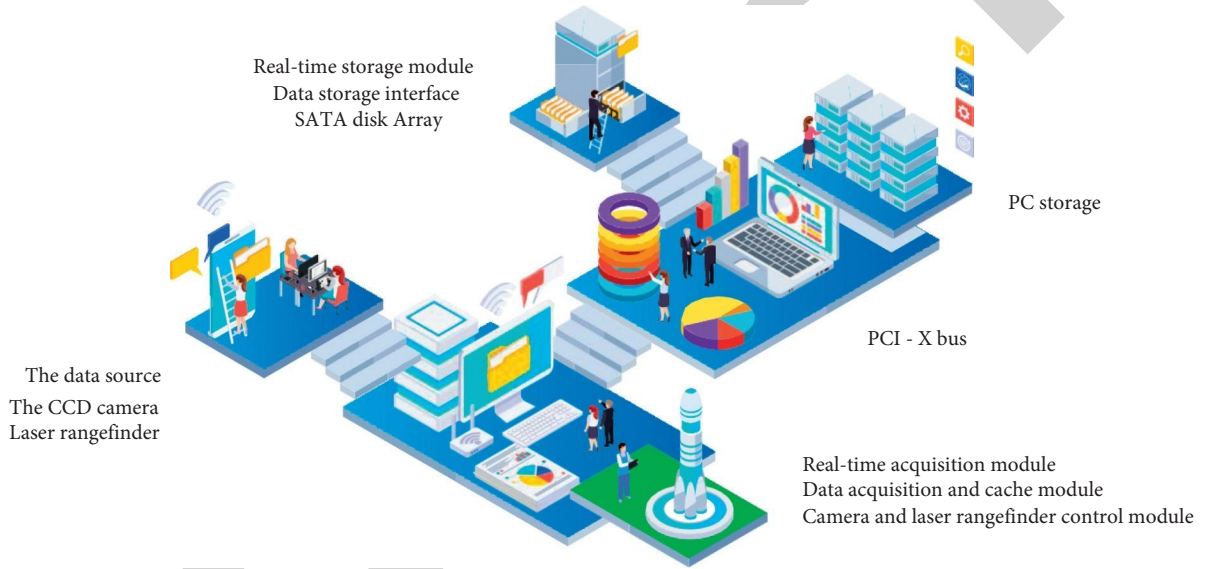


FIGURE 4: Design of real-time high-speed storage scheme.

TABLE 1: System stability test results.

Working hours (h)	2	2	4	4	6	6
Operating mode	Free running	Software external trigger	Free running	Software external trigger	Free running	Software external trigger
Frame loss rate (%)	0	0	0	0	0.03	0.01

memory to the disk array and average the speed of software statistics. The measured results show that the real-time storage speed of the system can reach more than 240 MB/s in different acquisition times, meeting the requirements of the system index of 120 MB/s. In addition, the system uses 8 1 TB SATA hard disks, with a total recording capacity of 8 TB, which meets the index requirement of 2 TB minimum recording capacity of the system.

The stability test method of the system is as follows: under different working modes, collect the energy data of two sensors for many times, verify the energy data packet header counter through the verification program, count the number of energy data lost frames, and then calculate the

frame loss rate of the system. The actual test results are shown in Table 1. It can be seen from Table 1 that, within the required working time of the system, the system has no frame loss under different modes, and the performance is very stable. Even if the working time is 3 times the required time, the maximum frame loss rate of the system is only 0.03%, which can meet the requirements of the measurement system.

5. Conclusion

Based on FPGA + PCI energy data acquisition and storage hardware design, this paper adopts a high-speed storage